R-06-70

Hydrogeochemical evaluation

Preliminary site description Laxemar subarea – version 2.1

Svensk Kärnbränslehantering AB

December 2006

Svensk Kärnbränslehantering AB
Swedish Nuclear Fuel
and Waste Management Co
Box 5864
SE-102 40 Stockholm Sweden
Tel 08-459 84 00
+46 8 459 84 00
Fax 08-661 57 19
+46 8 661 57 19

ISSN 1402-3091
SKB Rapport R-06-70

Hydrogeochemical evaluation

Preliminary site description
Laxemar subarea – version 2.1

Svensk Kärnbränslehantering AB

December 2006

Preface

This work forms part of the initial site investigation stage of the hydrogeochemical evaluation carried out at the Simpevarp area leading to a Hydrogeochemical Site Descriptive Model version 2.1 of the Laxemar subarea. SKB's ChemNet, consisting of independent consultants and university personnel, carried out the modelling during the period July 2005 to August 2006. The INSITE and SIERG review comments on the earlier model versions of Simpevarp and Forsmark were considered when possible in this work. Several groups within ChemNet were involved and the evaluation was conducted independently using different approaches ranging from expert knowledge to geochemical and mathematical modelling including also transport modelling. During regular ChemNet meetings the results were presented and discussed. The ChemNet members contributing to this report are (in alphabetic order):

David Arcos, Enviros, Appendix#6

Luis Auqué, University of Zaragoza, Appendix#3

María Gimeno, University of Zaragoza, Appendix #3

Jordi Guimerà, Enviros, Appendix#6

Javier Gómez, University of Zaragoza, Appendix#3

Ioana Gurban, 3D-Terra, Montreal, Appenix#4

Lotta Hallbeck, Vita vegrandis, Göteborg, Appendix#2

Marcus Laaksoharju, Geopoint AB, Stockholm, Appendix#4

Jorge Molinero, University of Santiago de Compostela, Appendix#5

Luis Moreno, KTH, Appendix#7

Juan Raposo, University of Santiago de Compostela, Appendix#5

John Smellie, Conterra AB, Stockholm, Appendix#1

Eva-Lena Tullborg, Terralogica AB, Gråbo, Appendix#1

Nicklaus Waber, University of Bern, Appendix#1

Marcus Laaksoharju

ChemNet leader and editor

Summary

Siting studies for SKB's programme of deep geological disposal of nuclear fuel waste currently involves the investigation of two locations, Simpevarp area and Forsmark situated on the eastern coast of Sweden, to determine their geological, hydrogeochemical and hydrogeological characteristics. Present work completed has resulted in Model version 2.1 for the Laxemar subarea which represents the fourth evaluation of the available Simpevarp area groundwater analytical data collected up to July, 2005 (i.e. the fourth "data freeze" for the Simpevarp area).

Model version 2.1 focusses on improving the methodology and tools used for evaluating the hydrochemistry combined with a sensitivity and uncertainty analysis of the available data. The major goal has been to consolidate groundwater geochemical understanding and the models used for site description, and to provide feedback to the site investigation programme concerning further sampling and analyses and to address key review issues by INISTE and SIERG.

The ChemNet group had access to new and old samples from boreholes in the Laxemar subarea. The Laxemar 2.1 data freeze involved data from eight cored boreholes and 34 percussion boreholes from the Laxemar subarea, three cored boreholes and 4 percussion boreholes from the Simpevarp penninsula, and two cored boreholes and 10 percussion boreholes from Ävrö island.

The complex groundwater evolution and patterns in the Simpevarp area are a result of many factors such as: a) the present-day topography and proximity to the Baltic Sea, b) past changes in hydrogeology related to glaciation/deglaciation, land uplift and repeated marine/lake water regressions/transgressions, and c) organic or inorganic alteration of the groundwater composition caused by microbial processes, water/rock interactions or mixing. The sampled groundwaters reflect to various degrees processes relating to modern or ancient water/rock interactions and mixing.

The groundwater flow regimes in the Laxemar/Simpevarp subareas are considered local and extend down to depths of around 600–1,000 m depending on local topography. Close to the Baltic Sea coastline where topographical variation is small, groundwater flow penetration to depth will subsequently be less marked. In contrast, the Laxemar subarea is characterised by higher topography resulting in a much more dynamic groundwater circulation which appears to extend to at least 500–600 m depth in most boreholes. The marked differences in the groundwater flow regimes between the Laxemar and Simpevarp subareas are reflected in the groundwater chemistry were four major hydrochemical groups of groundwaters (types A–D) have been identified:

TYPE A: Shallow (< 200 m) at the Simpevarp subarea but deeper (down to ~ 800 m) at the Laxemar subarea. Groundwater of low salinity (< 2,000 mg/L Cl; 0.5–3.5 g/L TDS); $\delta^{18}O$ = –11 to –8‰ SMOW. Mainly meteoric and Na-HCO_3 in type.

TYPE B: Shallow to intermediate (150–600 m) at the Simpevarp subarea but deeper (~ 500–950 m) at the Laxemar subarea. Brackish groundwater (2,000–10,000 mg/L Cl; 3.5–18.5 g/L TDS); $\delta^{18}O$ = –14 to –11‰ SMOW: Meteoric, mainly Na-Ca-Cl in type; Glacial/Deep saline components: Meteoric, mainly Na-Ca-Cl in type but some Na-Ca(Mg)-Cl(Br) types (± marine, e.g. Littorina); Glacial/Deep saline components.

TYPE C: Intermediate to deep saline groundwaters (~ 600–1,200 m) at the Simpevarp subarea but deeper (900–1,200 m) at the Laxemar subarea. Saline (10,000–20,000 mg/L Cl; 18.5–30 g/L TDS); $\delta^{18}O$ = ~ –13‰ SMOW. Dominantly Ca-Na-Cl in type at the Laxemar subarea but Na-Ca-Cl changing to Ca-Na-Cl only at the highest salinity levels at Simpevarp subarea; increasingly enhanced Br/Cl ratio and SO_4 content with depth at both Simpevarp and Laxemar subareas; Glacial/Deep saline mixtures.

TYPE D: Deep highly-saline groundwaters (> 1,200 m) only identified at the Laxemar subarea. Highly saline (> 20,000 mg/L Cl; to a maximum of ~ 70 g/L TDS); $\delta^{18}O$ = > –10‰ SMOW. Dominantly Ca-Na-Cl with higher BrCl ratios and a stable isotope composition that deviates from the GMWL when compared to Type C groundwaters; Deep saline/brine mixture; Diffusion dominant mixing process.

In this report the models and the site understanding have been consolidated. The models have been updated and further understanding achieved concerning the spatial variability, origin, evolution and major reactions of the groundwaters, in addition to the microbial contents and their depth variation, and the contents of colloids and gases. Moreover, pore water composition and its interaction with fracture groundwaters has been further quantified and uncertainties in the mixing calculations identified. The studies of fracture fillings and especially on the isotopic signatures in calcite are lending support to the conceptual understanding of the Laxemar subarea. Furthermore, the detailed mineral investigations are used as direct input to the hydrogeochemical modelling.

A more robust Hydrogeochemical Site Descriptive Model version 2.1 for the Laxemar subarea has evolved. The resulting description has improved compared to the Laxemar 1.2 version by producing a more detailed process modelling for the dilute groundwater system and ultimately for the whole subarea. The microbial characterisation gives direct support to the redox modelling. Coupled transport modelling has addressed questions relating to transport processes which are of importance for the site understanding. Further integration with the hydrogeological modelling has been initiated for the Laxemar 2.2 modelling phase. The different modelling approaches applied on the same data set and the similarities in the results gave added confidence to the modelling results presented in this report.

Contents

1 Introduction

1.1 Scope and objectives

The work presented here from the Laxemar subarea forms part of the hydrogeochemistry initial site investigation stage 2.1 based on measured data from the site investigation programme. As the investigations progress over the next years, two updated model versions (versions 2.2 and 2.3) will be based on supplementary analytical data and groundwater samples from new boreholes and repeated sampling of existing boreholes.

The aim of the site modelling is to develop a hydrogeochemical Site Descriptive Model (SDM) according to the strategy described in /Smellie et al. 2002/. The first such model for the Simpevarp area was the "version 0" model /SKB 2002/ followed by Simpevarp 1.1 /SKB 2004/, Simpevarp 1.2 /SKB 2005/ and Laxemar 1.2 /SKB 2006/. The "Simpevarp area", include 1) the "Simpevarp subarea" (including the "Simpevarp penisula" (Simpevarp), the "Ävrö island" (Ävrö)) and the Hålö island (Hålö), 2) the "Laxemar subarea", and 3) the Äspö island (Äspö) (see Figure 3-1).

The model presented in this report is the Laxemar 2.1 model version which represents the second evaluation of the available Laxemar subarea groundwater data collected up to July 2005 (i.e. the time of the "data freeze").

SKB's ChemNet (a technical group made up of independent consultants and university personnel) had access to water samples collected from the surface (i.e. streams, lakes and sea) and subsurface (i.e soil pipes in the overburden) environments, together with samples collected from drilled boreholes in the Simpevarp subarea and new and old boreholes from the Laxemar subarea. The earlier and deepest samples collected from the Laxemar subarea reflect conditions down to about 1,700 m and the new samples to conditions down to about 1,000 m depth.

The Laxemar 2.1 model version, presented here, focuses on: a) updating and consolidation of models constructed during the Laxemar 1.2 stage, b) feedback to the site investigation programme concerning further sampling, c) detailed hydrogeochemical modelling, d) establishing the fluid composition in the bedrock matrix, and e) further integration with hydrogeological modelling. The report summarises the most important findings of the Laxemar subarea with the detailed and comprehensive background information to the modelling performed documented in Appendices 1–7.

1.2 Methodology

The main objectives of the Hydrogeochemical Site Descriptive Model for the Laxemar subarea are to describe the chemistry and distribution of the groundwater in the bedrock and overburden and the processes involved in its origin and chemical evolution. The SKB hydrogeochemistry programme /Smellie et al. 2002/ is intended to fulfil two basic requirements: 1) to provide representative and quality assured data for use as input parameter values in calculating long-term repository safety, and 2) to understand the present undisturbed hydrogeochemical conditions and how these conditions will change in the future due to excavation. Parameter values for safety analysis include pH, Eh, S, SO_4, HCO_3, PO_4 and TDS, together with colloids, fulvic and humic acids, other organics, bacteria and dissolved gases. These values will be used to characterise the groundwater environment at, above and below repository depths. When the hydrogeochemical environment has been fully characterised, this knowledge, together with an understanding of the past and present groundwater evolution, should provide the basis for predicting future changes. The site investigations will therefore provide important source material for safety analyses and the environmental impact assessment of the Simpevarp region.

The hydrogeochemical evaluation approach being used at the Forsmark and Laxemar-Simpevarp subareas is based on some 25 years of collective experience within the SKB waste management programme. During this time sampling procedures, analytical methods, hydrochemical concepts

and model development have evolved through a continuous process of modification and refinement, a process which carries on to the present time. Several key issues addressed over the years which have helped steer the direction of the on-going hydrogeochemical evaluation include:

- Understanding the post-glacial evolution of the Swedish east coastal margin and the Baltic Sea. For example, to bear in mind the possibility of finding residual groundwater components in the bedrock introduced during the Quaternary period, in particular during Holocene times. Groundwater components may include glacial melt water introduced during ice degradation and retreat, and the introduction of marine/non-marine waters during periodic transgressions driven by the isostatic recovery of the landmass.
- The use of fracture mineral phases as potential palaeomarkers was recognised /e.g. Bath et al. 2000, Milodowski et al. 2005/. Calcite is especially used in order to detect interaction with groundwaters of different types (Meteoric, Marine and Brine type) and also to detect evidence for various interactions with biogenic carbon. The redox front is detected using mineralogy, mineral geochemistry and U-series analyses.
- Because of the successive introduction of different water types into the bedrock during the Holocene and their subsequent complete or partial removal by flushing out later introduced water types, groundwater mixing tends to dominate over water/rock reactions in the upper 250–500 m. The mixing depths are dependent on local hydrological conditions.
- Based on this concept early modelled simulations initially considered a simple 2-component mixing system based on the use of chloride as a conservative parameter (see below).
- Mixing was believed to be a major mechanism to explain present groundwater chemistry and distribution, and it led to the development of the M3 modelling approach (see below).

Many of the evaluation and modelling steps used within the ChemNet group are focused on differentiating between effects of reactions and transport by using different modelling approaches. It was realised at an early stage that this dual approach was more successful in the evaluation of fractured granitic bedrock groundwaters where different water types had been recently introduced, rather than relying on the more traditional geochemical equilibrium reaction approach for sedimentary/aquifer rock environments. /Laaksoharju 1990/.

The fundamental concept in the mixing approach is:

Measured groundwater composition = mixing + reactions

This leads to the need to solve the problem of mixing before the effects from reactions can be described. The first attempt was to construct a simple two end-member mixing mass-balance model and was described by /Laaksoharju 1990/ and used in /Smellie and Laaksoharju 1992, Banwart et al. 1995/. The main aim of the model was to differentiate in the groundwater between what is due to mixing/transport and what is due to water/rock reactions by using one variable, such as Cl, as a conservative tracer to create an ideal mixing model between two extreme waters. The model was used to predict concentrations for the other groundwater elements. A deviation between the predicted and measured value was interpreted as sink or source associated with reactions. No deviation for an element was taken to be an indication that transport and mixing determine that particular element concentration. However, the model seemed to have limitations when tracing a more complex system involving several end-members.

The subsequent groundwater modelling concept was named M3 (Multivariate Mixing and Mass-balance calculations) /Laaksoharju and Skårman 1995, Laaksoharju et al. 1999b/. In M3 modelling the assumption is made that the groundwater is always a result of mixing and reactions. Initially, the method evaluates the contribution from the flow system i.e. mixing. Subsequently, contributions from reactions are considered. The model is an opposite approach to many other standard models, which use reactions rather than mixing to determine the groundwater evolution.

Figure 1-1, a–d shows the different approaches to model groundwater using Na versus Cl as an example. The task is to model the reactions which had to take place to obtain the measured Na content. In Model#1 (Figure 1-1, b) the water composition is a result of reactions, for example the sample with about 0.85 mol/kg Cl and indicated with an arrow, has gained about 0.28 mol/kg Na due to reactions. There is no flux or mixing in the system since the system is closed. In Model#2

(Figure 1-1, c) the water composition is a result of mixing with two end-members (indicated with dashed black line); here the sample has gained about 0.07 mol/kg, Na. The water composition is described as a result of two component mixing by reactions where Na is gained. In Model#3 (Figure 1-1, d) the water composition is described as a result of mixing with several end members; here the sample has gained no Na since it plots on the mixing line (black dashed line). The water composition is described as result of multi-component mixing and the Na is a result of pure mixing/transport. If a sample plots above the mixing line it indicates gain of Na and below the line it indicates loss of Na.

From the above it is clear that the description of the groundwater system will be very different depending on the model selected. Model#1 describes the total amount of reactions taking place to obtain the Na measured in the sample. It does not describe where and when the reactions took place; for example, reactions taking place outside the bedrock to form sea water are not differentiated. Model 2 and Model 3 describe the water composition in relation to the end-member composition so it can be used to calculate the mixing proportions of the end members. These can be used to indicate the origin and also the possible residence time in the bedrock which is useful information when, for example, integrating the results with the hydrogeological modelling. To construct Model 2 is generally relatively easy, however the risk of applying Model 2 is that the system is oversimplified and hence there is a risk of overestimation of the effects from reactions and underestimation of the effects from transport. Model 3 can provide the most realistic description but the risk is that model uncertainties (such as uncertain end-member compositions and mathematical uncertainties in the model applied) can still lead to erroneous conclusions concerning the gain/losses of element concentrations. The accuracy of the Model 2 and 3 can be easily tested by, for example, plotting the predicted Cl content versus the measured one. A deviation from a perfect correlation will then indicate the model uncertainties /Laaksoharju 1999/.

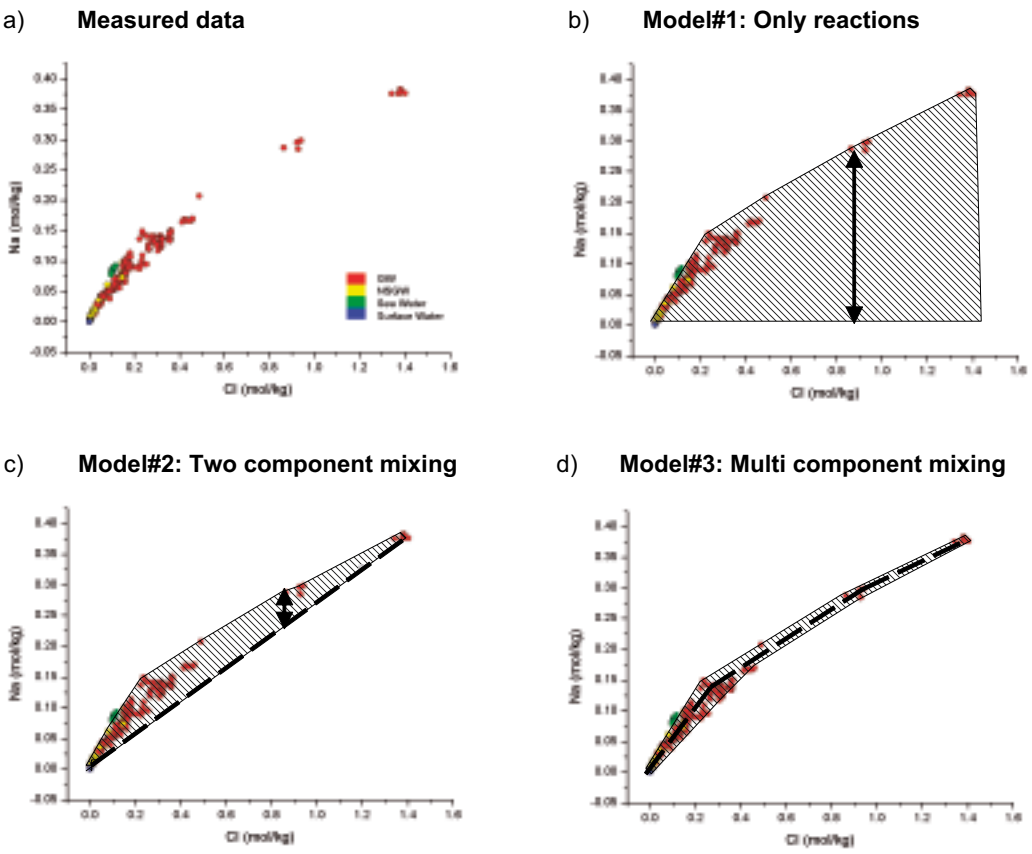

Figure 1-1. *Different schematic models are used to describe the processes behind the measured Na content. The arrow indicates the amount of reactions taking place for a particular sample, the grey dashed area indicates samples affected by reactions and the black dashed line indicates the mixing line: a) Measured Na versus Cl, b) Model based on reactions, c) model based on mixture of two end-members and, d) model based on several end-members.*

In scientific literature Models 1 and 2 are sometimes used simultaneously for site description where Model 1 is employed when, for example a Na/Cl plot is used to describe the effects from reactions and another plot (O^{18}/Cl) is used to describe the origin of the water. The modeller may by this type of approach fail to understand that the descriptions are not comparable. The first plot describes all the reactions that ever took place to form the sample, whilst the second plot describes the water conservative parameters as a result of mixing, i.e. the same system is described but from different aspects. If the difference is not understood the modeller may get the wrong impression that transport is fast and there are many reactions taking place, when the truth may be the opposite.

The reason that mixing models appear to be successful is:

- The palaeo and present climate have a huge impact on the hydrogeology and hence mixing of water and hydrochemistry in Fennoscandia.
- The temperature in the rock (11C°at –200 m, the gradient is 1.6 C° per 100 m) is relatively low and therefore the water rock interaction processes are slow.
- The flow is faster than the reactions so that the origin of the water is not concealed.

The mixing modelling can be used in performance assessment (PA) and safety assessment (SA) in the following ways:

- Provide understanding of water movement and timescales for calculating the dose and validation of hydrogeological models.
- Water types can indicate presence of hazardous species (e.g. HS, CH_4, U and high Cl) in areas with little or no sampling.
- Mixing models can be used within PA and SA to indicate changes of concentrations with time.
- Confirmation and calibration of processes of importance for PA and SA.
- Site understanding builds confidence in the site.

In theory, thousands of chemical reactions could be written involving the water, solids and gases in regional aquifers such as those presently being investigated in Sweden. There are eight main categories of reactions and processes that control the chemistry of most groundwaters: precipitation-dissolution, acid-base, complexation, substitution-hydrolysis, oxidation-reduction, ion-filtration-osmosis, dissolution and exsolution of gases and sorption/desorption. Worldwide site modelling has revealed that the actual number of reactions that dominate the groundwater chemistry is quite small /Alley 1993/. The major processes and reactions that affect the groundwater in Fennoscandia are:

- Climate.
- Flow/mixing.
- Reactions with the rock and microorganisms in the groundwater:
  - Introduction of CO_2 gas in the unsaturated zone.
  - Dissolution and precipitation of calcite.
  - Cation exchange.
  - Incongruent dissolution of primary silicates with formation of clays.
  - Oxygen consumption: organic carbon respiration, oxidation of iron minerals such as sulphides and biotite.
  - Reduction of nitrate, oxidised iron and manganese and sulphate with anaerobic oxidation of organic compounds (DOC and CH4), with production of nitrogen gas, ferrous iron, manganese (II) and sulphide.
  - Hydrogen oxidation with production of acetate and methane: organic fermentation or carbonate reduction.

Of the above reactions many can be indicated by using mixing modelling although a multidisciplinary approach such as employed by ChemNet, where explorative analysis in combination with various modelling approaches are used, is the key to avoid misunderstandings of the site.

2 Evolutionary aspects

The first step in the groundwater evaluation is to construct a working conceptual postglacial scenario model for the area based largely on known palaeohydrogeological events from Quaternary geological investigations (for details see, /SKB 2006/). This model can be helpful when evaluating data since it provides constraints on the possible groundwater types that may occur. Interpretation of the glacial/postglacial events that might have affected the Simpevarp area is based on information from various sources including /Westman et al. 1999, Påsse 2001, SKB 2002/. This recent literature provides background information which has been combined with more than 10 years of accumulated groundwater chemical and isotopic information from sites in Sweden and Finland, together with the results of various hydrogeological modelling exercises of postglacial hydrogeological events /Svensson 1996, Laaksoharju and Wallin 1997, Pitkänen et al. 1998, Luukkonen 2001/. The presented model is therefore based on Quaternary geological facts, hydrodynamic modelling, fracture mineralogical investigations and hydrochemical observations. These data have been used: a) to describe the possible palaeo-events that may have affected the groundwater composition in the bedrock, and b) to provide the basis for constructing the 2-D hydrogeochemical conceptual model for the Simpevarp area.

3 Bedrock hydrogeochemistry

Evaluation of the hydrogeochemical data has been carried out by considering not only the samples from the Laxemar subarea, but also in relation to those from the Simpevarp subarea, Äspö and, in some cases, also related to the entire Fennoscandian hydrochemical dataset. Information from hydrogeochemical model versions based on previously investigated sites in Sweden and elsewhere, and information from ongoing geological and hydrogeological modelling in the Laxemar subarea, were included in the evaluation when possible.

The evaluation and modelling of the hydrogeochemical data consist of visualisation of the groundwater properties, explorative analysis which involves manual evaluation and expert judgment, and mathematical modelling, all of which must be combined when evaluating groundwater information.

The results of the detailed hydrogeochemical modelling described in this present chapter are used to produce an updated hydrogeochemical site descriptive model. The modelled outcome is used in, for example, hydrogeological modelling, transport modelling and safety assessment modelling.

The results presented herein represent the collective effort made by the ChemNet Analysis Group; details of the modelling are described in Appendicies 1–7.

3.1 Hydrogeochemical data

To date, site characterisation at the Laxemar subarea has included the drilling of up to 34 percussion drillholes (HLX01–34) to vertical depths varying from approx. 70–200 m, and eight cored boreholes (KLX01–08) of which KLX01 extends to 1,078 m, KLX02 to 1,705 m, KLX03, KLX04, KLX05 and KLX08 to about 1,000 m, KLX06 to 850 m, and KLX07 to 830 m. Boreholes KLX01 and KLX02 are subvertical whereas KLX03 is inclined at 75°, KLX05, KLX06, KLX07 at 65° and KLX08 at 60°. Of all these boreholes, percussion boreholes HLX01–08, 10, 14, 18, 20, 22, 24, 28 and 34, and cored boreholes KLX01, 02, 03, 04, 05, 06, 07 and 08, are included in the Laxemar 2.1 data freeze database. The borehole sampling locations are shown in Figure 3-1.

The analytical programme included: major cations and anions (Na, K, Ca, Mg, Si, Cl, HCO_3^- SO_4^{2-}, S^{2-}), trace elements (Br, F, Fe, Mn, Li, Sr, DOC, N, PO_4^{3-}, U, Th, Sc, Rb, In, Cs, Ba, Tl, Y and REEs) and stable (^{18}O, ^{2}H, ^{13}C, ^{37}Cl, ^{10}B, ^{34}S) and radioactive-radiogenic (^{3}H, ^{226}Ra, ^{228}Ra, ^{222}Rn, ^{238}U, ^{235}U, ^{234}U, ^{232}Th, ^{230}Th and ^{228}Th) isotopes, microbes, gases and colloids (cf. Appendix 8). The selected pH and Eh values correspond to available downhole data (cf. Appendicies 1, 3 and 8).

The samples evaluated in the version 2.1 "data freeze" for the Laxemar subarea include (for details see, Appendices 1 and 8):

- 152 groundwater samples from the Äspö subarea of which 25 are representative samples
- 123 Groundwaters from the Ävrö subarea, 6 representative samples. Four new samples were included in the Laxemar 2.1 data freeze.
- 592 Groundwaters from the Laxemar subarea (37 representative), and 51 Near-surface groundwaters (near-surface groundwaters; 45 representative). 53 samples from percussion boreholes. 285 samples including tube samples, samples taken during drilling, and samples for the pore water experiments. 118 of them were included in the Laxemar 2.1 data freeze. 254 samples from cored boreholes and taken between packers. 68 of these were included in the Laxemar 2.1 data freeze. 51 shallow groundwater samples from soil pipes.
- 282 Groundwaters and near-surface groundwaters, 1,271 surface waters and 56 precipitation samples from Simpevarp. 171 groundwater samples (5 representative) and 111 near-surface groundwaters (32 representative); 22 samples from percussion boreholes. 99 samples including tube samples, samples taken during drilling, and samples for the pore water experiments. 51 samples from cored boreholes and taken between packers. 111 shallow groundwater samples from soil pipes. 53 of them were included in Laxemar 2.1 data freeze.

Figure 3-1. *Groundwater sampling locations in the Simpevarp area and location of hydrogeochemically prioritised boreholes, KLX01, KLX02, KLX03, KLX04, KLX05, KLX06, KLX07 and KLX08 in the Laxemar subarea. Also indicated are the percussion boreholes (HLX01–33), many of which are included in the Laxemar v.2.1 evaluation. The figure shows the outlines of Laxemar (left hand) and Simpevarp (right hand) subareas.*

- 1,271 surface water samples: 363 sea water samples (161 representative). 46 of them were delivered in Laxemar 2.1 data freeze. 249 lake water samples (167 selected as representative samples). 24 of them were delivered in Laxemar 2.1 data freeze. 659 stream water samples (297 selected as representative samples). 75 of them were delivered in Laxemar 2.1 data freeze.

56 samples of precipitation (13 selected as representative samples). 17 of them were delivered in Laxemar 2.1 data freeze.

Altogether, there are 1,200 groundwater samples (deep and near-surface groundwaters), 243 of them included in the Laxemar 2.1 data freeze, and 1,271 surface water samples, 145 of them were included in this data freeze.

3.2 Explorative analysis

A commonly used approach in groundwater modelling is to commence evaluation by explorative analysis of different groundwater variables and properties. The water type, degree of mixing, the type of reactions and the origin and evolution of the groundwater can be indicated by applying such analyses. Also of major importance is to relate, as far as possible, the groundwaters sampled to the near-vicinity geology and hydrogeology.

3.2.1 Visualisation of sampled boreholes

An important tool for site understanding (i.e. in constructing a conceptual model and for integration of the results with hydrogeology) is the spatial representation and visualisation of available data. A specific visualisation application has been developed with the aim of representing "objectively" (i.e. without interpolation) the available hydrochemical information. The visualisation tool has been programmed using the IBM Open Visualisation environment, known as OpenDX (cf. Appendix 5).

As examples, Figure 3-2 shows a view of the location of the main cored boreholes (from the point of view of the number of representative samples) available in the Laxemar and Simpevarp subareas, and Figure 3-3 shows all the available representative chloride data in the bedrock samples.

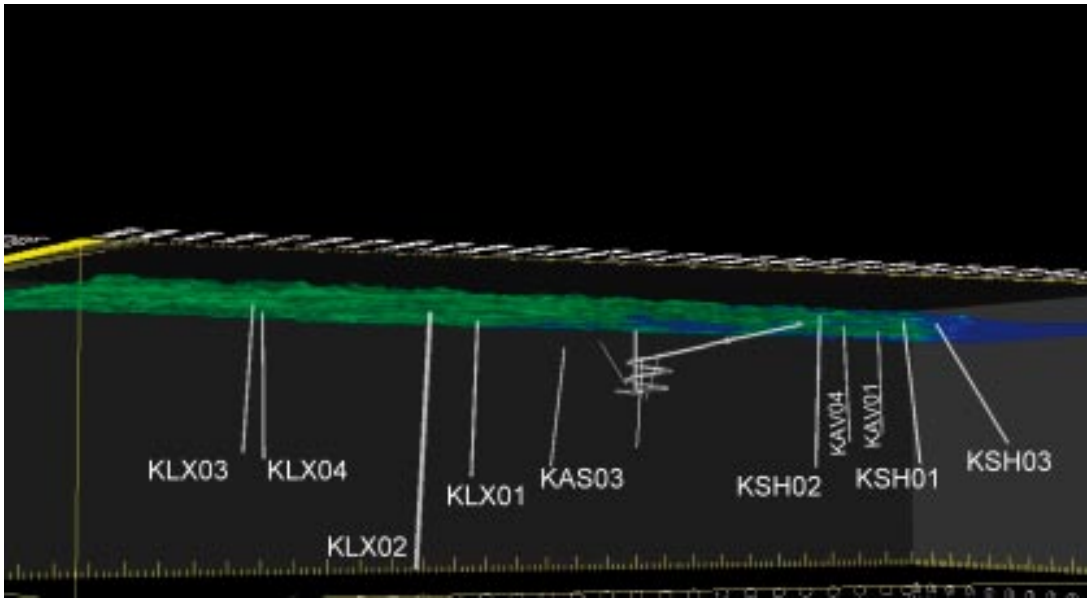

Figure 3-2. *3D-view (from the southwest) of the Laxemar and Simpevarp subareas. Some of the main cored boreholes in the Laxemar 2.1 data freeze, as well as the Äspö tunnel, have been included as geographical references in the visualisation.*

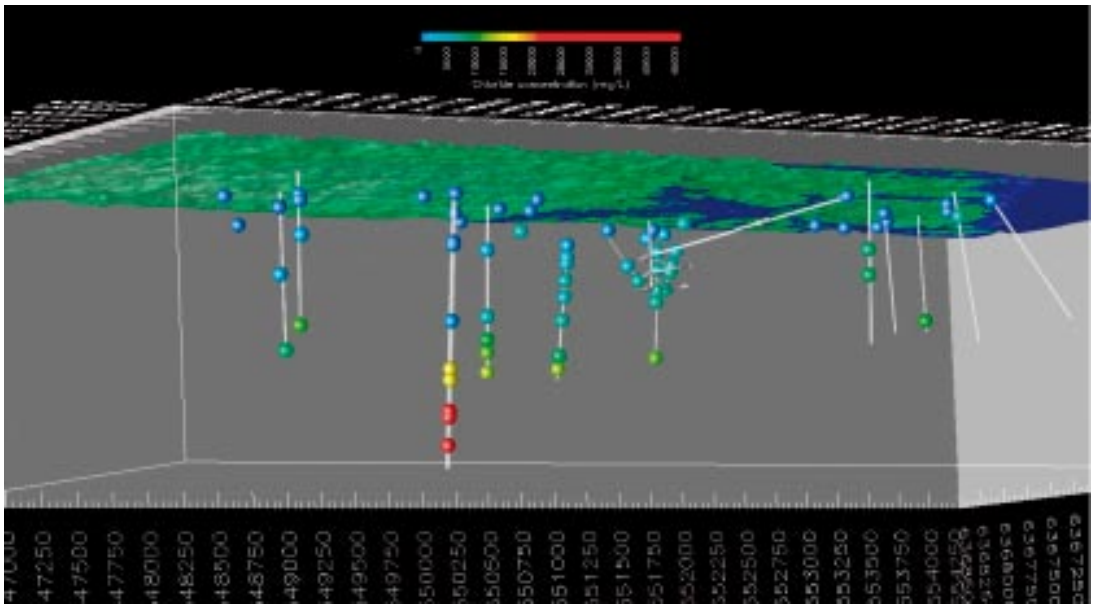

Figure 3-3. *Distribution of chloride concentrations in the bedrock under the Laxemar and Simpevarp subareas. Blue indices low, green medium and yellow and red high chloride concentration value.*

Figure 3-3 shows the occurrence of brine-type (red symbol) groundwater at depth in the Laxemar subarea detected in borehole KLX02 at a depth greater than 1,100 m. The difference in salinity between the groundwater of the Laxemar and Simpevarp subareas is immediately noticeable. The Laxemar subarea represents a continental (inland) hydrogeological environment with a thick fresh water body reaching depths of nearly 1,000 m. In contrast the Simpevarp subarea represents a coastal hydrogeological environment where fresh water bodies are confined to the upper 100–200 m of the bedrock.

3.2.2 Major groundwater features

The major results from the hydrogeochemical explorative analysis are described in detail in Appendix 1 and summarised in this chapter.

The new Laxemar 2.1 data freeze information has served to further support the Laxemar 1.2 evaluation /SKB 2006/. The interpretation of major ion trends and the main environmental isotopes tritium, oxygen-18, deuterium and carbon-13/14. is based on quality assured data and have been strengthened. There is now a good understanding of the origin and evolution (e.g. mixing processes) of the different groundwater groups characterising the Simpevarp area. Additional isotope data of sulphur and strontium isotopes have added further knowledge of water/rock interactions and, specifically from sulphur, the local influence of microbial activity on groundwater redox conditions and chemistry.

A marine component can be distinguished based on slightly higher Mg values, lower Br/Cl ratios and marine $\delta^{34}S$ values in the groundwaters with Cl values < 6,500 mg/L from the Simpevarp subarea and from KLX01 in the Laxemar subarea. In the remainder of the Laxemar subarea, in contrast, no marine signatures can be identified. The marine component at the Simpevarp subarea is, however, much less prominent than at the Forsmark area.

The Cl versus depth trend for Laxemar indicated in model version L 1.2 is further supported in Figure 3-4 and underlines the fact that the very sharp transition between fresh and very saline waters in borehole KLX02 is probably not representative of the Laxemar subarea. However, fresh to brackish groundwaters (Cl < 5,000 mg/L) seem to dominate down to 600 to 700 m depth. A detectable glacial component (^{18}O below –12‰) is found even deeper, at least down to 900–950 m.

Significant bicarbonate production is recorded in the near-surface groundwaters (upper 200 m) in the Laxemar subarea, and both the carbon and sulphur isotope ratios support the interpretation that this due to microbial activity, although some contribution from calcite dissolution has probably also taken place at shallow depth.

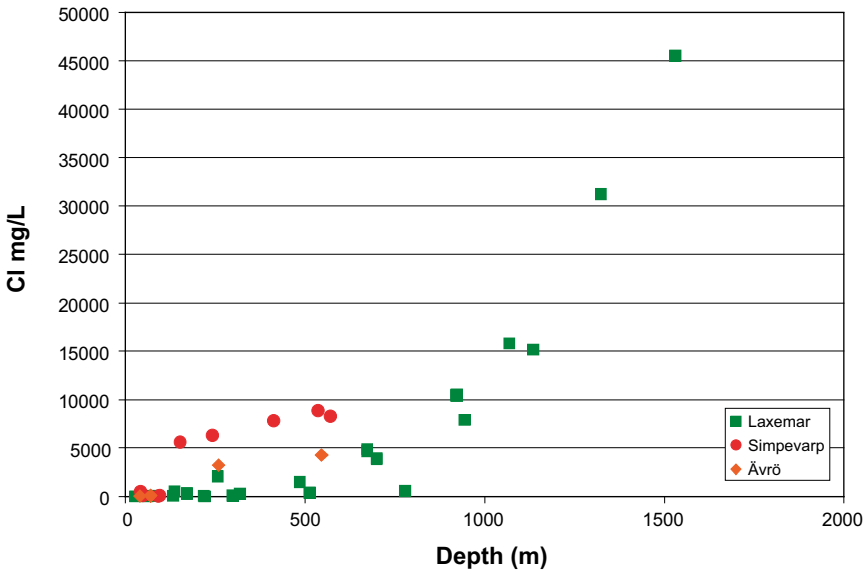

Figure 3-4. Depth variation of chloride in the Simpevarp and Laxemar subareas.

However one area of caution concerns the interpretation of the tritium (and carbon-14) values. Detailed examination of data at and close to the overburden/geosphere interface suggests that some emissions from the nearby nuclear power plant have contributed to the amounts of tritium and carbon-14 analysed in the surface and near-surface groundwaters. Figure 3-5 clearly illustrates this hydrochemical sequence from the overburden to deep bedrock environments. A rapid decrease of tritium can be observed in the groundwaters from recharge values close to the surface (10–18 TU) to values levelling out close to zero (less than ± 2 TU) around 200 m depth and remaining constant down to around 1,000 m. This indicates that despite the possible contamination from drilling water, it is clear that large portions of modern meteoric water is not affecting groundwaters below 200 m depth.

The new hydrochemical data support the 2-D integrated Laxemar 1.2 conceptual model of the Simpevarp area (see Chapter 4), and no significant change of the various groundwater types is necessary (cf. section 3.2).

3.2.3 Microbes

Microorganisms are abundant in Fennoscandian Shield groundwater from the surface down to at least 1,500 m /Pedersen 1993, Haveman et al. 1999/. To understand the present undisturbed hydrobiogeochemical conditions the following parameters are of interest: pH, E_h, S^{2-}, S^0, SO_4^{2-}, HCO_3^-, HPO_4^{2-}, Fe^{2+}, Mn^{2+} nitrogen species and TDS together with colloids, fulvic and humic acids, dissolved organic compounds and microorganisms. In addition, the concentrations of dissolved gases are of importance for a complete model since many microorganisms consume and/or produce different gases. Furthermore, for a full understanding it is necessary to be able to predict how changing conditions, during the construction of a repository and during the following phases of repository evolution, will influence microbes in the groundwater and *vice-versa.*

In energy harvesting reactions, microbes use available energy-rich compounds as electron donors and various electron acceptors from groundwater and fracture minerals. Thus microbes are intimately coupled to the redox conditions in the groundwater system.

Microbial parameters of interest are the total number of cells and the presence of different metabolic groups of microorganisms /Pedersen 2001/. These data indicate the activity of specific microbial populations at a certain location and how they interact with the geochemistry. The groups cultured for the microbial part of the site investigation were iron-reducing bacteria (IRB), manganese-reducing bacteria (MRB), sulphate-reducing bacteria (SRB), auto- and heterotrophic methanogens (AM and HM) and auto- and heterotrophic acetogens (AA and HA).

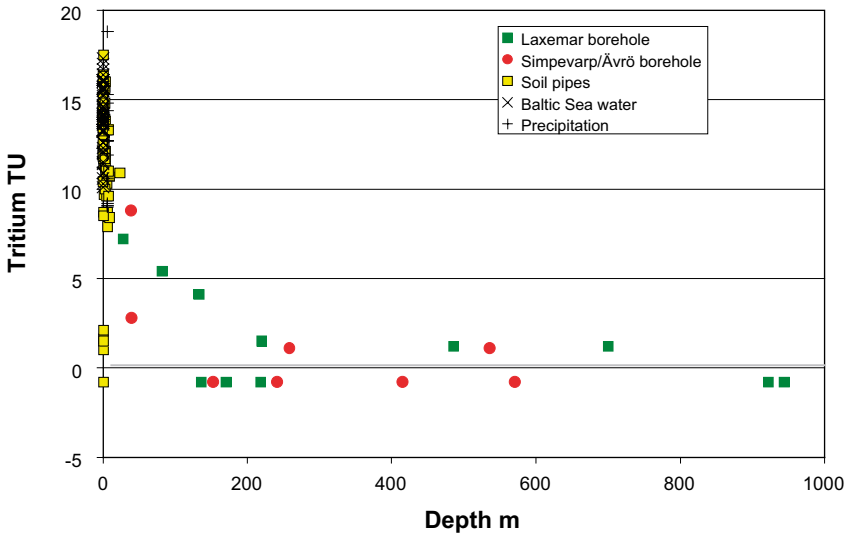

Figure 3-5. *Tritium vs depth for the Simpevarp and Laxemar subareas.*

Microbes have been evaluated from the Simpevarp area (Appendix 2). There are still rather few data from the Laxemar subarea and therefore the model reflects only the regional scale of the Simpevarp area. The model predicts (Figure 3-6) that the dominating respiring microbial process in 'The anaerobic subsurface zone' is heterotrophic sulphate reduction; this zone is found at depths from 100 to 500 metres. 'The deep sulphate reducing zone' is found at about 600 to 900 metres and 'The deep autotrophic zone' is found from 1,000–1,400 m. Here there are indications of ongoing iron- and manganese reduction and heterotrophic acetogenesis. The origin of carbon dioxide and hydrogen gas in this zone from 'The deep chemosphere' also requires to be verified with stable isotope studies of dissolved gas in the groundwater.

3.2.4 Colloids

Colloid compositional data have been evaluated from the Simpevarp area (Appendix 2). Particles in the size range 10^{-3} to 10^{-6} mm are regarded as colloids; their small size prohibits settling and renders them as a potential radionuclide transport mechanism in groundwater. The aim of the colloid study was to quantify and determine the composition of colloids in groundwater from boreholes, and to include the results in the hydrochemical modelling of the site.

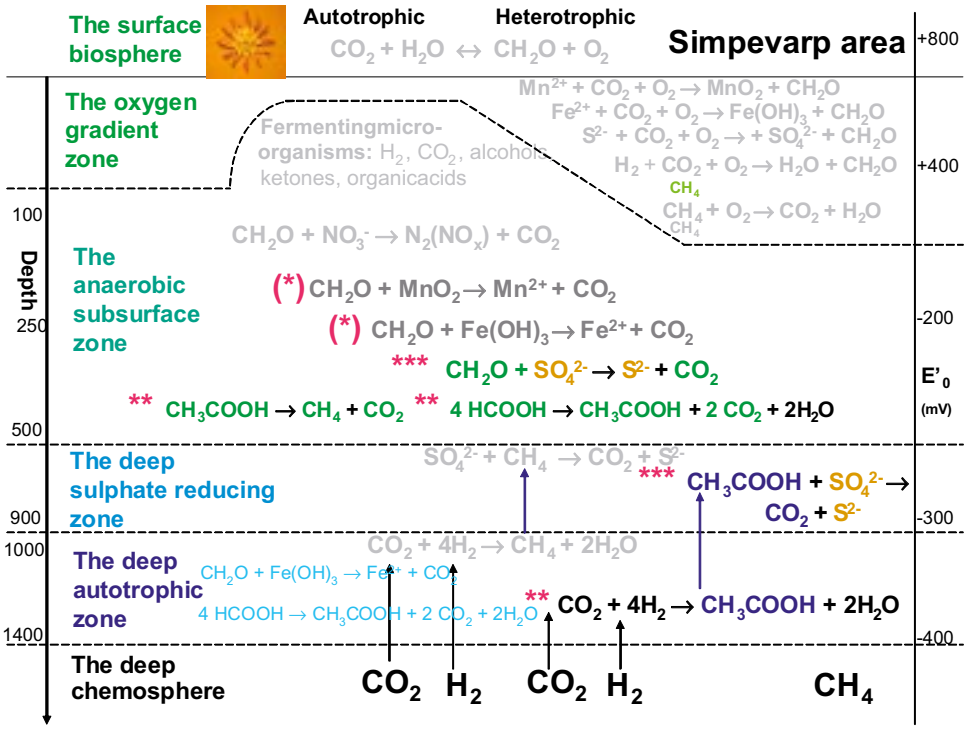

The colours in the model are used as listed below:

- , light grey: The process is not yet studied.
- , dark grey: The process is present but without influence
- , green: The carbon compounds originate from the surface biosphere
- , blue: The carbon compounds originate from the deep autotrophic zone
- ,black: Compounds from the deep chemosphere
- ,turquoise: Processes found but not anticipated and not yet confirmed

The starsymbols in the figureillustratethe MPN valuesand influenceby the microbialgroupson the geochemistry.

(*)	1–10 ml^{-1}	Present without influence
*	11–50 ml^{-1}	Present with putative influence if growth promoting changes occur
**	51–1000 ml^{-1}	Present with influence
***	> 1000 ml^{-1}	Dominating with high influence

[1]influence here means that the organism group has an effect on the geochemistry of the ground water

Figure 3-6. *The microbial model of the Simpevarp area based on data available at the time of the Laxemar 2.1 data freeze. The star symbols before the reactions depict the significance of the reaction.*

Generally, the average amount of colloids in this study (cf. Appendix 2) was 23.1 ± 7.14 µg L^{-1} if the value from KLX01: 458.5 m is omitted. These values agree very well with data reported from other colloid studies in Sweden (20–45 ug/L) and Switzerland (30 ± 10 and 10 ± 5 µg L^{-1}) /Degueldre 1994/ but about ten times lower than reported from Canada (300 ± 300 µg L^{-1}) /Vilks et al. 1991/. The possibility that some of the iron and sulphur colloids might occur as iron sulphides has to be further investigated. Particle counting could increase the value of colloid analyses by making it possible to calculate the amount of binding sites for radionuclides in the different colloid fractions.

3.2.5 Gases

The amounts of gas data are limited and therefore exclude any considerable analysis of the impact of gases on geochemistry and microbiology; there is, however, a clear trend with increasing volumes of gas towards depth.

The available gas data for the Laxemar subarea (cf. Appendix 2) show that the gas content is of the same order of magnitude as in most of the Nordic sites studied. The site-specific features are:

- Nitrogen is the dominating gas at all depths.
- Helium increases with depth.
- Highest amounts of methane were found above 400 m in KLX03, suggesting that it is biologically produced.
- The amounts of hydrocarbons increase with depth.
- The gases are probably mostly mantle-generated.
- Gases are probably oversaturated in relation to atmospheric pressure but this is not the case at depth.

3.2.6 Hydrochemical suitability criteria

There are new representative samples at repository depths from the Laxemar subarea. The representative samples from KLX03: 408–415.3 m and KLX04: 510–514 m were used to check if they meet the SKB chemical suitability criteria for Eh, pH, TDS, DOC, Colloids and Ca+Mg /Andersson et al. 2002/. Table 3-1 shows that these samples can meet the SKB suitability criteria for the analysed parameters.

3.2.7 Pore water composition in the rock matrix

Determination of pore water composition

In crystalline rocks the pore water resides in the low-permeability zones (rock matrix) between principal water-conducting zones related to regional or local fracture networks. Depending on the residence time of water in these hydraulically active zones, interaction with water present in the pore space of the low-permeability zones might become significant. In addition, the pore water present in the low-permeability zones will be the first to interact with any artificial construction made in such zones (i.e. the repository). For safety assessment considerations it is therefore important to know the composition of such pore water. The pore water studies so far carried out for the Laxemar subarea are described in detail in Appendix 1.

Table 3-1. The hydrochemical suitability criteria defined by SKB are satisfied by the analysed values of samples KLX03: 408–415.3 m (sample no: 10091) and KLX04: 510–514 m (sample no: 7776).

	Eh (mV)	pH (units)	TDS (g/L)	DOC (mg/L)	Colloids (mg/L)	Ca+Mg (mg/L)
Criterion	< 0	6–10	< 100	< 20	< 0.5	> 40
KLX03: 408–415.3 m	–275	7.9	2.9	2.2	~ 0.02	245
KLX04: 510–515 m	n.a.	7.8	2.8	2.2	n.a.	241

n.a. = not analysed.

In borehole KLX08 (Figure 3-7), pore water concentrations of less than 1 g/kgH_2O are obtained for the shallower depths down to about 500–600 m where there is a high frequency of hydraulically conductive fractures and a corresponding increase in transmissivity (up to 10^{-5} m^2s^{-1}). Furthermore, the pore water chloride increases significantly towards the transition between the Ävrö granite and quartz-monzodiorite, coinciding with transmissivities down to $10^{-8.5}$ m^2s^{-1} and less. From here there is a steady increase to salinities of 10.5 g/kgH_2O at a vertical depth of 851 m below surface (983 m borehole length).

In comparison with borehole KLX03 /Waber and Smellie 2006b/ the pore water chloride profile in KLX08 shows exactly the same general pattern, i.e. dilute water in the Avrö granite until the boundary with quartz-monzodiorite, followed by a strong increase to the top of the quartz-monzodiorite and then a decrease, and finally a strong increase at maximum depth. In contrast, the chloride pore water concentrations below about 750 m are significantly higher than the highest chloride concentrations observed in borehole KLX03.

In general, pore waters characterised by direct and indirect methods from low-permeable crystalline rocks from the Laxemar (and Forsmark) subareas have a distinct chemical and isotopic composition. Pore water compositions differ from those of fracture groundwaters depending on the distance between the location of the pore water sample in the rock matrix and the nearest water-conducting fracture, and the time period of constant composition of the fracture groundwater. Combined with measured and experimentally-derived hydraulic properties, these compositional differences support diffusion-dominated solute transport in the low-permeable rock mass. From the present investigations it can be concluded that in such a rock mass the diffusion-accessible porosity extends over significant distances (at least metres to tens of metres).

The methods applied minimise experimental disturbances and effects induced by drilling activities and/or stress release effects and the obtained pore water compositions have well definable uncertainties. For example there is a general agreement between the two independent methods

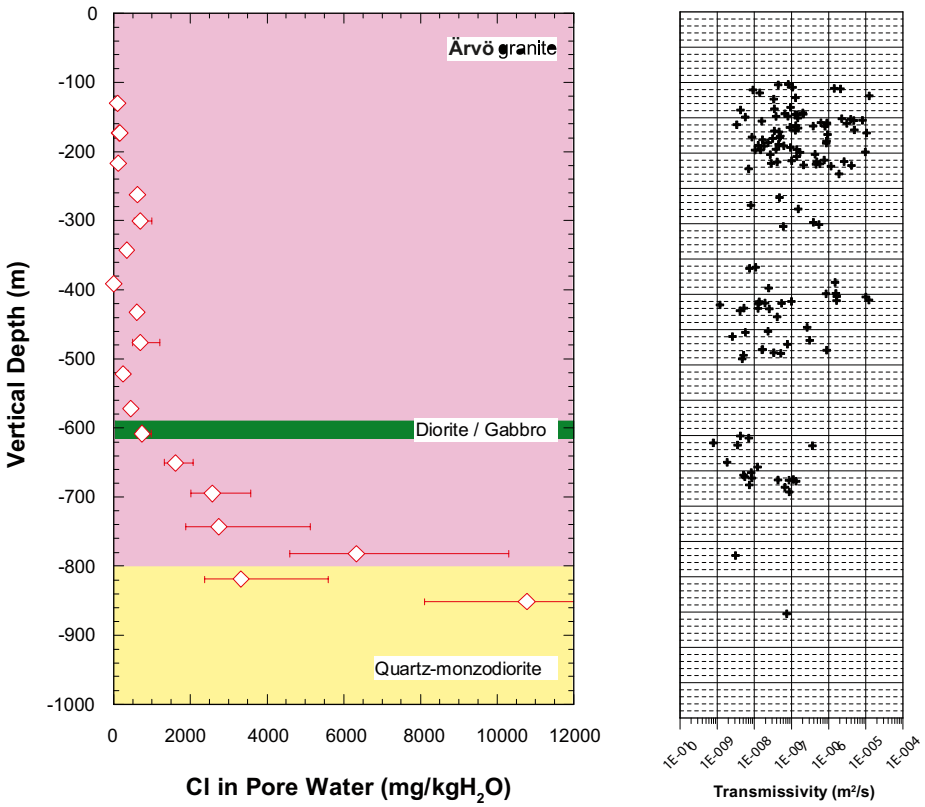

Figure 3-7. *Borehole KLX08: Chloride concentration in pore water as a function of vertical depth compared to fracture transmissivity.*

for water contents derived for drillcore samples from deep boreholes at Laxemar (and Forsmark) supporting: a) the saturated state of the sample upon arrival in the laboratory, and b) no detectable influence of drilling fluid within the present precision of the applied methods because desaturation and drilling fluid contamination would each affect the two methods in opposite ways. This argues against a significant disturbance of the drillcore samples by the drilling process and/or the creation of access pathways for drilling fluid and/or groundwater penetration into the core samples by immediate stress release. This is further supported by: a) the decrease of the water content with depth, b) a more homogeneous distribution of the water content at larger depth, and c) the absence of a systematic perturbation of the chemical and isotopic composition of out-diffusion experiment solutions as a function of depth. All this would be expected due to the increase in contact time with the drilling fluid and also rock stress perturbations. In addition, the chloride profiles of the out-diffusion experiments, which can be interpreted as diffusion profiles, greatly limit the exchange with drilling fluid. Within the overall uncertainty (about ± 10%) the obtained values for the water content and water-content (connected) porosity appear to represent in situ conditions. Additional methodological improvements are, however, required to reduce further these uncertainties.

Pore water compositions derived by indirect methods from drillcore samples from the Laxemar (and Forsmark) sites can be interpreted within a larger palaeohydrogeological framework. The pore water chemical and isotopic compositions show distinct trends correlating with rock type and with depth, becoming more saline with increasing depth at both sites. Concentration gradients established between pore water and fracture groundwaters coincide with higher fracture frequency and increased transmissivity in the host rocks, where the location of the pore water sample is closer to water-conducting fractures. Differences developed in the attainment of steady-state conditions between pore water and fracture water between the Laxemar and Forsmark sites support a different hydrogeological, and therefore hydrogeochemical evolution, at least during Holocene times.

Modelling of interaction beween fracture water and pore water in the matrix

The interaction between the ions dissolved in pore water in the rock matrix and those ions dissolved in flowing water in the fractures is studied in Appendix 7. The ions may migrate from the water flowing in the fracture into the pores in the rock matrix but also in the opposite direction. Migration of the ions takes place by diffusion in the matrix pores and its direction is determined by the concentration gradient. To simulate the effect of fresh water intrusion into a zone with saline water, several calculations were performed with increasing level of complexity.

In the first set of calculations the evolution of the concentration in the matrix is studied for the case where the concentration in the adjacent fractures is negligible. The results may be directly applied to the case of salinity depletion from the rock matrix into a fracture with negligible salinity. Three different geometries were modelled: a) fracture matrix interaction with diffusion perpendicular to the fracture plane, b) a narrow channel embedded in a large rock mass (Figure 3-8), and c) a rock block surrounded by conductive fractures. The results show that the time for salinity depletion is of the order of hundreds to thousands of years for a distance of one metre in the matrix.

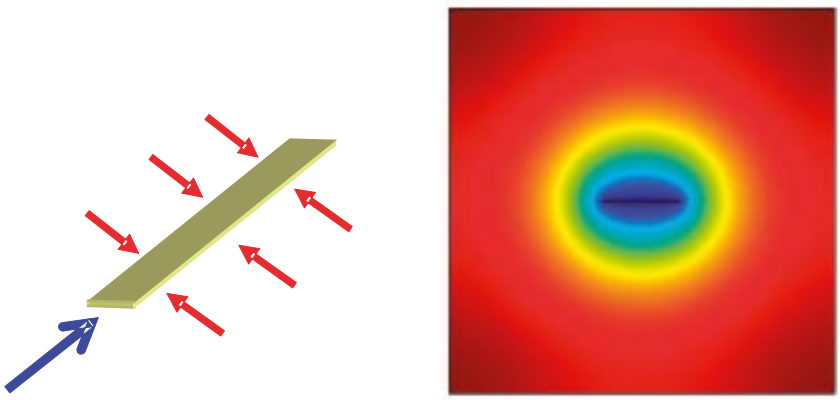

Figure 3-8. *A schematic view of diffusion into a channel/fracture surrounded by an infinite rock mass (left) and concentration profiles at the rock mass (right).*

In a second set of calculations the evolution of the concentration in water in the fracture was taken into account. The time to deplete the salinity in the matrix may then be strongly increased. The time to deplete the salinity in the fracture depends on the surface contacted by the fresh water along its path and the water-flow rates. Actually, it depends on the Σ(FWS/Q) where FWS = Flow Wetted Surface and Q = Flow rate in the channel. For small values of this term (e.g. large water-flow rate) the concentration in the fracture decreases very rapidly. However, for large values of the term Σ(FWS/Q), the salinity depletion in the fracture may be very long, i.e.thousands of years.

Finally, simulations were carried out to determine the paths followed by the water from the point of intrusion to the zone under study. These simulations were made using the Channel Network Model /Gylling et al. 1999/. Particle tracking was used to determine (ΣFWS/Q) for the several water parcels travelling through the channel network. The results show that fractures with large transmissivity collect water that has travelled through paths with ΣFWS/Q varying in a wide interval. Moreover, most of water parcels were collected by the fractures with large transmissivity. Therefore, the evolution of concentration in the fracture with time is weakly related to the transmissivity of the fracture.

3.2.8 Studies of fracture fillings

General characteristics

Fracture minerals are determined macroscopically (Appendix 1, /SKB 2006/) and are mapped within the Boremap system. However, since many of the minerals are difficult to identify and small crystals are easily overlooked, fracture mineral analyses have been carried out on additional samples for quantitative identification. This information is crucial, for example for hydrogeochemical mass-balance calculations. Fracture samples have also been selected because they can provide information on the sequence of events that have resulted in fracturing and fracture mineralisation in the area. A number of samples have been taken from boreholes KLX02, KLX03, KLX04 and KLX06 for microscopy, in most cases including SEM/EDS, chemical analyses and stable isotope analyses of calcites. Results from these studies are reported in /Drake and Tullborg 2005/. The abundance of different fracture minerals in open fractures is listed in Appendix 1.

The sequence of minerals identified in the Simpevarp and Laxemar subarea drillcores is very similar to earlier observations made at the Äspö HRL /Landström and Tullborg 1995, Andersson et al. 2002/. However, the order of frequency and the amounts of certain minerals can vary considerably throughout the Simpevarp area. Another reason for variation in the Boremap data between the Simpevarp and Laxemar subareas is the increased certainty in the core mapping. For example, it is suspected that clay minerals were underestimated in the earlier Simpevarp area drillcore characterisation.

Valid for the entire region is the sequence of minerals which change from epidote facies, in combination with ductile deformation, over to brittle deformation and breccia sealing during prehnite facies, and subsequently zeolite facies with a further mineral formation series at decreasing temperature. This indicates that most of the fractures were initiated early in the geological history of the host rock and have been reactivated during several different periods of physiochemical conditions.

The locations of the hydraulically conductive fractures are mostly associated with the presence of gouge-filled faults produced by brittle reactivation of earlier ductile precursors or hydrothermally sealed fractures. The outermost coatings along the hydraulically conductive fractures consist mainly of clay minerals, usually illite and mixed layer clays (corrensite = chorite/smectite and illite/smectite) together with calcite and minor grains of pyrite.

Hydrochemical indicators

From the perspective of groundwater chemistry, the presence of the four minerals, calcite ($CaCO_3$), gypsum ($CaSO_4$), barite ($BaSO_4$) and fluorite (CaF_2), is worth attention as their solubility has an impact on or controls the behaviour of some major ions (Appendix 1).

Calcite is the most common of these minerals. It occurs frequently at all depths except in the upper tens of metres and below approx. 1,000 to 1,100 m where it is less common. A number of calcite generations have also been identified ranging from hydrothermal to possibly recent /Bath et al. 2000, Drake and Tullborg 2004/. The stable isotope ratios, expressed as $\delta^{18}O$ and $\delta^{13}C$ are plotted against

depth in Figure 3-9 and Figure 3-10, respectively. The. $\delta^{18}O$ versus depth plot shows that the highest values, representing possible Baltic Sea water precipitates, are found in the upper 500 m at the Simpevarp and Äspö subareas. The Laxemar subarea, in contrast, has generally lower $\delta^{18}O$ values. Calcites with low $\delta^{18}O$ (< –15‰ PDB) are found at all depths except for the near-surface 50 m. Such values are expected in calcite precipitated from a groundwater with a large glacial component.

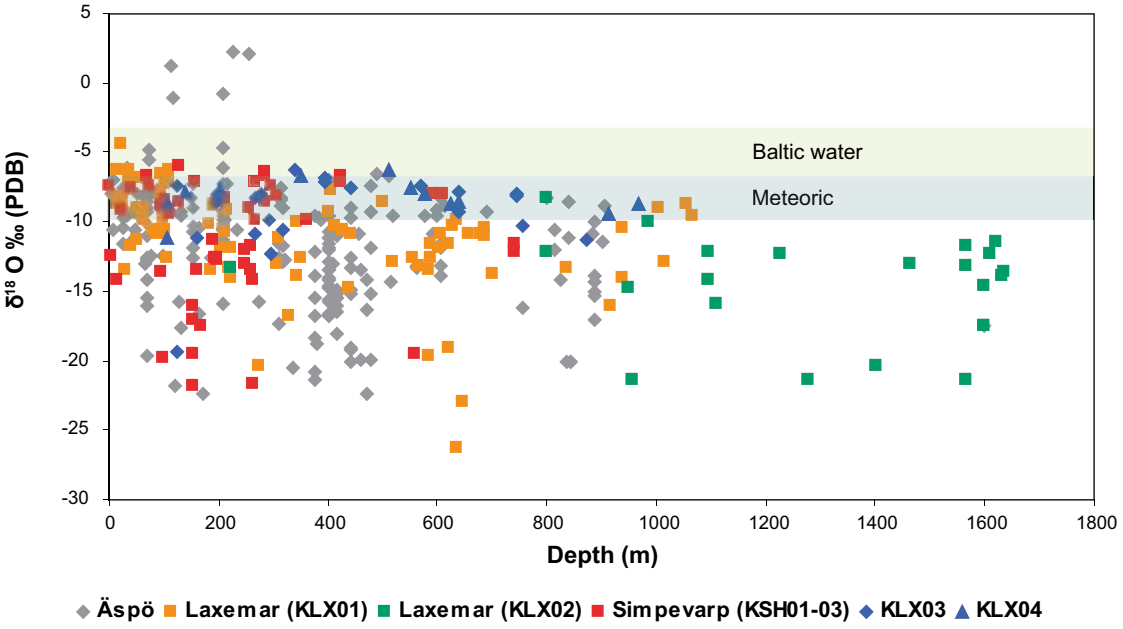

Figure 3-9. *Plot of $\delta^{18}O$ (PDB) vs depth for calcite with samples from KLX03 and KLX04 along with calcite from Äspö, Simpevarp and Laxemar (KLX01 and KLX02) (from /Drake and Tullborg 2004 in manuscript, Milodowski 2005/). The range of calcite precipitates from Baltic Sea water and meteoric water at ambient temperatures is indicated*

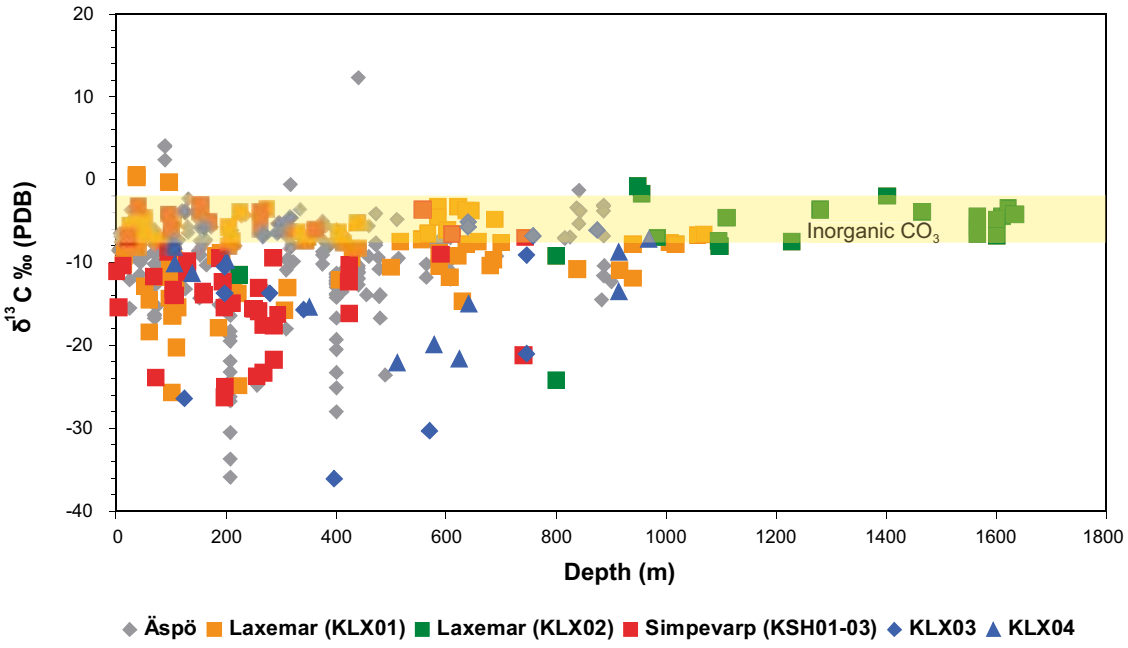

Figure 3-10. *Plot of $\delta^{13}C$ (PDB) vs depth for calcite with samples from KLX03 and KLX04 along with calcite from Äspö, Simpevarp and Laxemar (KLX01 and KLX02) (from /Drake and Tullborg 2004, 2006, Milodowsk 2005/). The range of inorganic CO_3 is indicated.*

Mineral paragenesis, trace element compositions and Sr isotope studies reveal, however, that the low $\delta^{18}O$ calcites are older and have been precipitated during increased temperatures. The carbon isotopes show large variation and extremely low values ($\delta^{13}C < -25‰$ PDB) have been observed down to 800 m depth. Such low values are probably produced by in situ microbial activity causing extreme local disequilibria. On average the $\delta^{13}C$-values are lower in the upper 500 m indicating a larger input of organic carbon. The few samples below 1,000 m are all higher than –10‰ PDB supporting more stagnant conditions at depth with no sign of exchange with organic material contributed from the surface.

Barite occurs as very small grains but is relatively frequently observed (microscopically; not during the core logging) together with calcite, pyrite and the Ba-zeolite, harmotome. In saline groundwater samples with very low SO_4 contents anomalously high Ba contents have been identified. For example, this was the case for the deepest saline groundwater from the KOV01 borehole at Oskarshamn, pointing towards a possible barite solubility control on the Ba and SO_4 content in the groundwater. Solubility has an impact or controls the behaviour of some major ions.

Fluorite occurs in several hydrothermal mineral associations; together with epidote and the later prehnite, but also together with the lower temperature (150°C) generation comprising calcite, barite and pyrite (Figure 1-8). Fluorite can be assumed to partly control the F content in the groundwaters.

Gypsum is relatively rare but has been identified in several boreholes in the Laxemar subarea. The gypsum-containing fractures are usually located in borehole sections showing a low degree of fracturing and low (or not measurable) transmissivity. Groundwater modelling /SKB 2004/ suggests dissolution of gypsum as an explanation for the relatively high SO_4 contents in the more saline Laxemar subarea groundwaters. Although gypsum has not been identified during the extensive work in the Äspö HRL, it's possible presence can not be be ruled. If present, it is probably restricted to some of the low transmissive, relatively unfractured parts of the rock.

3.3 Hydrogeochemical modelling

3.3.1 Reactive modelling

Dilute groundwater

The geochemical modelling presented in Appendix 6 considers speciation-solubility calculations, reaction path modelling and redox system analysis. The numerical calculations have been conducted using the PHREEQC code and the M3 code.

The methodology used in this analysis, though simple, aims at setting the basis for achieving a proper understanding of some of the main water-rock interaction processes acting in the upper part of the groundwater system, where the mixing process with saline water is thought to be of minor importance or it has no substantial effects on the chemical composition of groundwaters (i.e. only diluted groundwaters are considered, despite their origin).

The existing hydrochemical data for dilute groundwaters indicate that there are two relatively independent hydrogeologically active systems, one corresponding to near- surface groundwaters and other represented by the underlying granitic bedrock. For near-surface groundwaters there is a clear evolution driven by calcite and/or dolomite dissolution (dolomite is not found in fracture fillings), increasing the concentration of both aqueous calcium (and magnesium) and carbonate and increasing the pH. In the granitic aquifer, the increase in pH can not be attributed to the dissolution of calcite but it seems that silicate weathering plays a major role on the observed pH increase. This increase in pH can be properly reproduced by a geochemical model simulating the silicate weathering process through a theoretical flow line (cf. Appendix 6). The model can also reproduce the decrease in calcium and magnesium associated with the water-rock interaction processes (see, Figure 3-11).

However, the detailed geochemical model fails to reproduce the aqueous carbonate behaviour, most probably due to the oxidation of organic matter, which would induce an increase in water alkalinity.

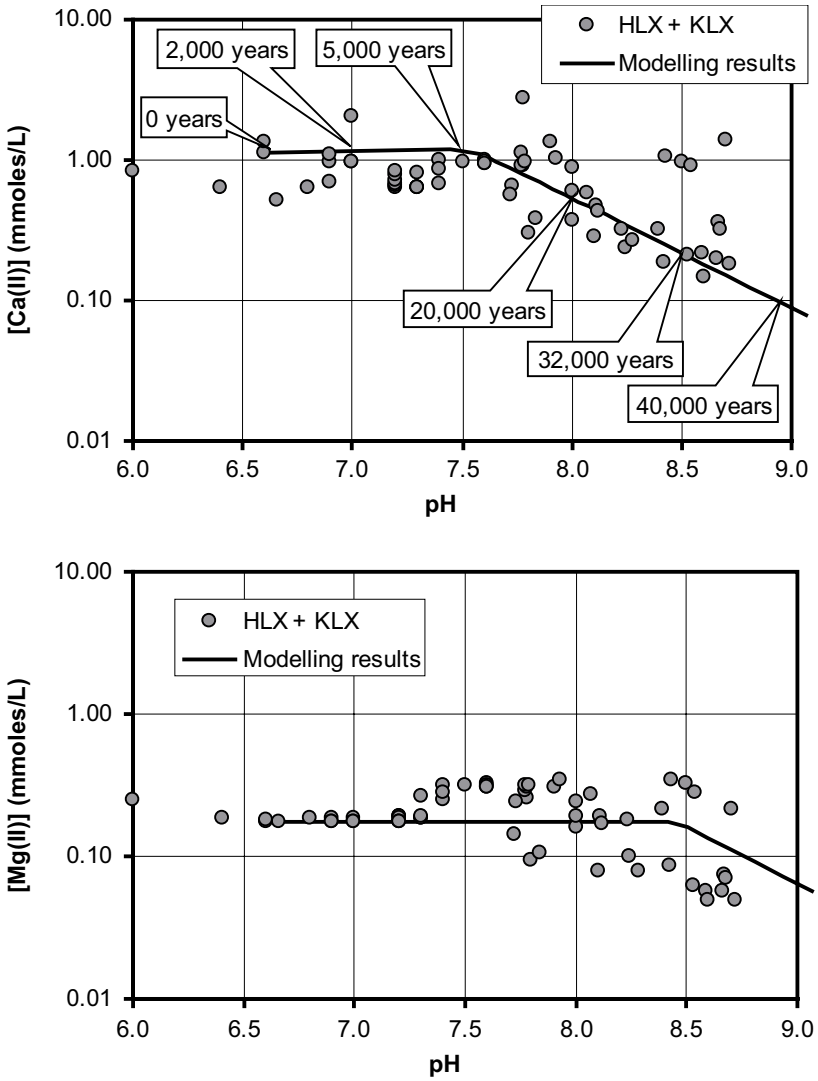

Figure 3-11. *pH-Ca(II) and pH-Mg(II) diagrams showing the analytical data for deep boreholes together with the modelling results. In the upper plot the simulation time is also indicated for the modelling results.*

All groundwaters

In parallel, complete site-specific reactive hydrogeochemical modelling has been carried out with PHREEQC /Parkhurst and Appelo 1999/ using the WATEQ4F thermodynamic database. The main goal of the modelling was to investigate the processes that control water composition at the Simpevarp area. The main conclusions from this work (cf. Appendix 3) are summarised below.

Shallow groundwaters are mainly controlled by "pure" water-rock interaction (infiltration water) with minor influence of mixing with older waters. They lack a clear thermodynamic control; if there is any, it is by fast chemical reactions (ionic exchange, surface complexation reactions, calcite dissolution-precipitation, etc.) coupled to several irreversible processes (mineral dissolution, decomposition of organic matter, etc.). Major ions show a constant increase as reactions proceed. The dissolution of calcite and silicates (see, Appendix 3) controls alkalinity and pH until equilibrium is attained, as they evolve towards the more saline and deeper groundwaters.

Chemical contents of deep groundwaters (especially for Cl concentrations higher than 10,000 mg/L) are mainly controlled by mixing with a brine end member. Most of the major ions are controlled by mixing, with minor influence from reactions (even Ca and sulphate in spite of calcite equilibrium). Alkalinity is low because it has been consumed by calcite precipitation. Calcite reaches equilibrium or keeps slightly oversaturated. The pH is mainly controlled by calcite equilibrium and, possibly, by aluminosilicate reactions which keep pH values higher than what calcite equilibrium would impose (see Appendix 3).

The potentiometrically measured Eh ranges from –210 to –380 mV. Sulphur redox pairs and the iron pair calibrated by /Grenthe et al. 1992/, show, in general, good agreement with the measured Eh (see, Figure 3-12).

Apart from this analysis and comparison, the speciation-solubility calculations have shown a clear equilibrium with amorphous iron monosulphides in most of the groundwaters from this area. This fact implies important sulphate-reducing bacterial (SRB) activity at present (in agreement with the microbiological information (cf. Appendix 2), and an iron source (in agreement with the mineralogical information, in Appendix 2). An additional conclusion is that pyrite is presently formed from monosulphide precursors (isotopic values of pyrite seem to support this).

In summary, the redox state of groundwaters in the Laxemar subarea appears to be well described by sulphur redox pairs in agreement with some previous studies in this area /Glynn and Voss 1999, SKB 2004/ and in other sites from the Fennoscandian Shield /Nordstrom and Puigdomenech 1986, Laaksoharju et al. 2004b, Pitkänen et al. 2004/. The presence of sulphate-reducing bacteria widely distributed in the Äspö and Simpevarp subareas can be related to this description and supports the idea that sulphur redox pairs could be controlling the microbiologically-mediated redox state.

However, in agreement with /Grenthe et al. 1992/, the work presented in (Appendix 3) also supports the conclusion that the iron system contributes to the redox control in some of the groundwaters through different oxide-oxyhydroxides. The plausible explanation to this is that the sulphur system governs the redox state for most of the groundwaters, and that the iron system is controlled by the microbially mediated sulphate-sulphide ratio. Hence the concentration of ferrous iron is controlled by the kinetically fastest Fe(II)/Fe(III)-oxide and sulphide phases.

The coupling between the iron and sulphur systems occurs via sulphate-reducing bacteria and sulphide mineral precipitation. Several lines of reasoning indicate that this process is effective at different depths in the Laxemar subarea. For instance, pyrite coatings have been identified on fracture fillings, which is additional evidence of the active participation of sulphur redox pairs.

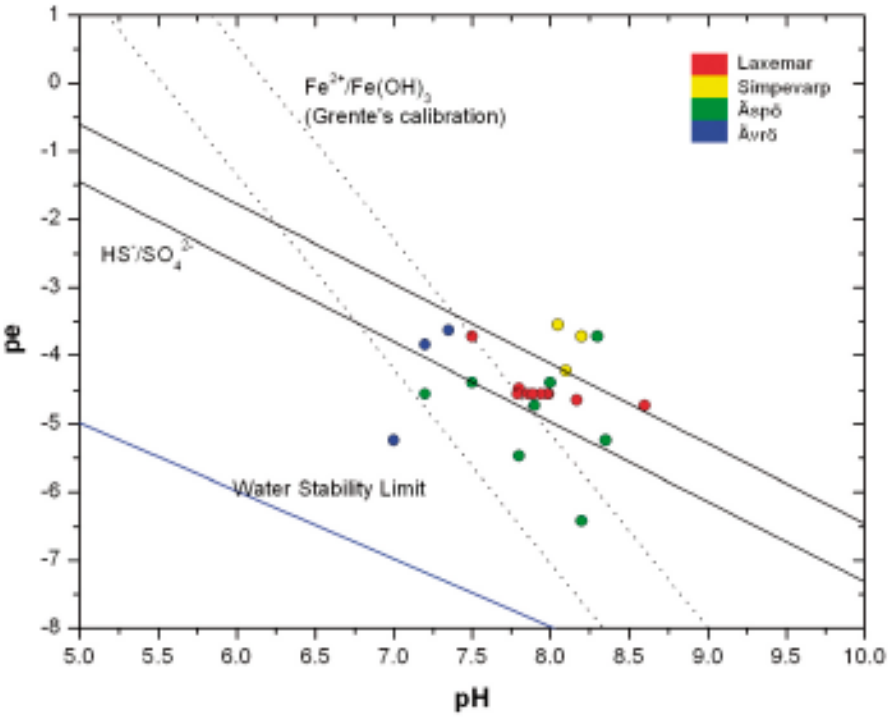

Figure 3-12. *Eh-pH diagram showing the measured Eh and pH of the selected samples in the Laxemar subarea. Boundaries for $Fe^{2+}/Fe(OH)_3$ and SO_4^{2-}/HS^- (dotted and solid black lines, respectively) are also shown for the range of pH, Fe^{2+} and S_2^- concentration in the Laxemar subarea groundwaters. Data for the $Fe^{2+}/Fe(OH)_3$ are from /Grenthe et al. 1992/ and data for the SO_4^{2-}/HS^- are from the WATEQ4F database included in PHREEQC /Parkhurst and Appelo 1999/.*

The good results obtained using the monosulphides saturation indices as tracers of SRB activity in Scandinavian groundwaters indicate that the methodology is useful in these types of systems. It can solve the common problems related to the absence of any correlation between SRB occurrence and its effects (dissolved S^{2-}) on the geochemistry of waters /Pedersen 2000/.

Finally, in the framework of repository safety assessment, the precipitation of monosulphides can have important consequences: (1) it is a process not considered (up to now) in the geochemical evolution of these kinds of systems (2) it can affect the canister integrity and the stability of colloids, and (3) a more reliable thermodynamic value for their equilibrium constant has been deduced and it should be included in the databases commonly used in safety evaluations.

3.3.2 Mixing modelling

The need for additional M3 uncertainty tests was identified during the Laxemar 2.1 modelling phase. Issues such as the use of tritium as a variable in PCA calculations and the use of different end members were addressed in Appendix 4. The PCA model, which employs all the samples including major elements (Na, K, Ca, Mg, SO_4, HCO_3, Cl), isotopes ^{2}H, ^{3}H, ^{18}O with the end members: Littorina, Brine, Glacial and Meteoric, provide the most robust mixing calculations for the Laxemar 2.1 dataset. This model was suggested as the final model.

The M3 code has been updated to include the option to calculate the mixing proportions in multi-variate space which decreases the uncertainties /Gómez et al. 2006/. Tests shows that the new code works properly and reduces the uncertainties especially for the dilute groundwaters. The results were delivered to the hydogeological group for comparison with independent hydrogeological mixing fraction calculations.

3.4 Coupled modelling

The aim of coupled modelling of flow and reactive transport is to support the hydrogeochemical interpretation of field data (cf. Appendix 5). It is expected that reactive transport modelling will provide a quantitative framework for testing alternative hydrochemical hypotheses and conceptual models of key hydrochemical processes.

The SUTRA /Voss and Provost 2003/ and CORE /Samper et al. 2000/ codes were used to integrate current hydrogeological and hydrogeochemical data and knowledge of the site. After calibration, it has been possible to reproduce the salinity fields corresponding to the current hydrogeological pseudo steady-state flow field. The numerical model has been calibrated assuming a heterogeneous equivalent porous media approach, and calibrated values of hydraulic conductivity are consistent with measurements within the range of field-derived values.

Contrary to what it was expected, the distribution of most major dissolved species (see, Figure 3-13) could be predicted by using the calibrated model, showing a conservative behaviour similar to the TDS distribution. The reason for such an apparent conservative behaviour is due to the large concentration contrast existing between fresh meteoric and deep saline waters. Thus, small amounts of mixing (by hydrodynamic dispersion) induce mass transfers much larger than those produced by active geochemical processes, which are eventually masked.

The reactive transport model accounts for mineral dissolution/precipitation processes under both local equilibrium and kinetic conditions. Taking into account silicate weathering processes under kinetic conditions leads to a better agreement between modeled results and field observations in terms of dissolved silica and pH. The reactive transport model fails at reproducing measured bicarbonate concentrations, most probably because of the occurrence of microbially-mediated respiration of dissolved organic matter present in the fresh groundwater of meteoric origin. These kinds of processes should be further studied in the near future by incorporating the simulation of microbially-catalysed processes and by using actual hydrogeological models according to /Hartley et al. 2005, 2006/ of the site.

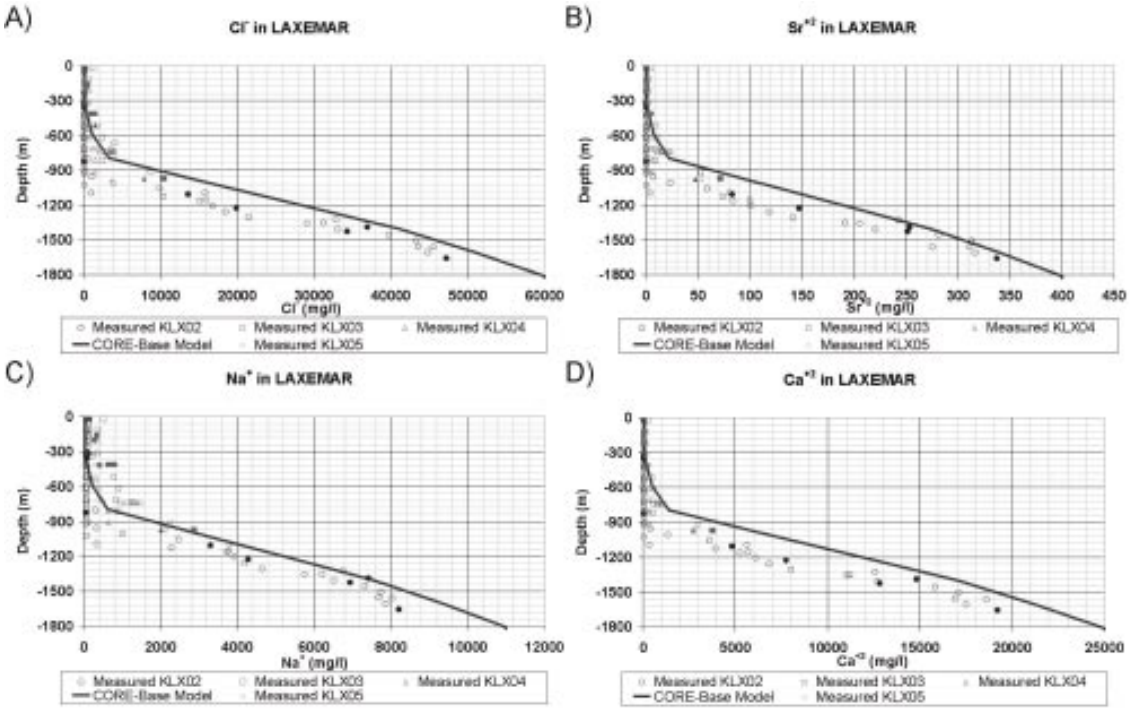

Figure 3-13. *Comparison of measured values (symbols) and computed results (solid line), plotted against depth, of: A) Chloride, B) Strontium, C) Sodium, and D) Calcium, at the Laxemar subarea. Filled symbols correspond to representative samples.*

3.5 Evaluation of uncertainties

During every phase of the hydrogeochemical investigation programme – drilling, sampling, analysis, evaluation, modelling – uncertainties are introduced which have to be accounted for, addressed fully and clearly documented to provide confidence in the end result, whether it will be the site descriptive model or repository safety analysis and design /Smellie et al. 2002/. Handling the uncertainties involved in constructing a site descriptive model has been documented in detail by /Andersson et al. 2002/. The uncertainties can be conceptual uncertainties, data uncertainties, spatial variability of data, chosen scale, degree of confidence in the selected model, and error, precision, accuracy and bias in the predictions. Many of the uncertainties are difficult to judge since they result from different steps ranging from expert judgement to mathematical modelling, and not the result of a single model such as in hydrogeology. Some of the identified uncertainties recognised during the modelling exercise are discussed below.

The following data uncertainties have been estimated, calculated or modelled for the Laxemar subarea data based on models used for the 1.2 model versions and also based on the Äspö modelling where similar uncertainties are believed to affect the present modelling:

- temporal disturbances from drilling may be ± 10–70%,
- effects from drilling during sampling is < 5%,
- sampling; may be ± 10%,
- influence associated with the uplifting of water may be ± 10%,
- sample handling and preparation may be ± 5%,
- analytical errors associated with laboratory measurements are ± 5% (the effects on the modelling were tested in Appendix 1 in /SKB 2004/),
- mean groundwater variability during groundwater sampling (first/last sample) is about 25%,
- M3 model uncertainty is ± 0.1units within the 90% confidence interval (the effects on the modelling were tested in Appendix 4 in /SKB 2004/.

Conceptual errors can occur in, for example, the palaeohydrogeological conceptual model. The occurrence and influence of old water end members in the bedrock can only be indicated by using certain element or isotopic signatures. The uncertainty therefore generally increases with the age of the end member. The relevance of an end member participating in groundwater formation can be tested by introducing alternative end- member compositions or by using hydrodynamic modelling to test if old water types can reside in the bedrock during prevailing hydrogeological conditions. In this model version, a measure of validation is obtained by comparison with results of the hydrogeological simulations.

Uncertainties in the PHREEQC code depend on which code version is being used. Generally the analytical uncertainties and uncertainties concerning the thermodynamic data bases are of importance (in speciation-solubility calculations). Care also is required to select mineral phases which are realistic (even better if they have been positively identified) for the systems being modelled. These errors can be addressed by using sensitivity analyses, alternative models and descriptions. A sensitivity analysis was performed concerning the calculations of activity coefficients in waters with high ionic strength. This analysis and also the uncertainties of the stability diagrams and redox modelling are discussed in Appendix 3.

The uncertainties were evaluated using the inverse modelling approach used in PHREEQC, and by investigating the compositional variability of end members and by checking the effects of chemical reactions on the mixing proportions calculated by M4. The test showed that PHREEQC is sensitive to the selection of end-member compositions in contrast to M3 which is less sensitive. M3 showed sensitivity to effects resulting from reactions /SKB 2006/.

The uncertainty due to 3D interpolation and 2D/3D visualisation depends on various aspects, i.e. data quality, distribution, model uncertainties, assumptions and limitations introduced. The uncertainties are therefore often site specific and some of them can be tested such as the effect of 2D/3D interpolations. The site-specific uncertainties can be tested by using quantified uncertainties, alternative models, and comparison with independent models such as hydrogeological simulations.

The discrepancies between different modelling approaches can be due to differences in the boundary conditions used in the models or in the assumptions made. The discrepancies between models should be used as an important opportunity to guide further modelling, including validation efforts and confidence building. In this work the use of different modelling approaches, starting from manual evaluation to advanced coupled modelling, can be seen as a combined tool for confidence building. The same type of process descriptions, independent of the modelling tool or approach, increases confidence in the modelling.

4 Resulting description

The results of the hydrogeochemical modelling have been used to support and consolidate the hydrogeochemical site descriptive model presented in the Laxemar 1.2 evaluation /SKB 2006/. The conceptual hydrochemical model of the Simpevarp area summarises most of the important findings. The approach to construct the conceptual model is described in Appendix 1 in /SKB 2006/. Based on existing geological and hydrogeological information and in collaboration with the site hydrogeologists and geologists, schematic manual versions of these transects were produced to facilitate illustrating the most important structures/deformation zones and their potential hydraulic impact on groundwater flow. This hydraulic information was then integrated with the results of the hydrogeochemical evaluation and modelling results to show the vertical and lateral changes in the groundwater chemistry. The identified water types A–D have the following features:

Type A

Shallow (< 200 m) at the Simpevarp subarea but deeper (down to a maximum of ~ 800 m) at the Laxemar subarea. Low saline groundwater (< 2,000 mg/L Cl; 0.5–3.5 g/L TDS); $\delta^{18}O$ = –11 to –8‰ SMOW. Mainly meteoric and Na-HCO_3 in type. **Redox:** Marginally oxidising close to the surface, otherwise reducing (no Eh values available). **Main geochemical reactions:** Weathering; ion exchange (Ca, Mg); dissolution/precipitation of calcite; redox reactions (e.g. precipitation of Fe-oxyhydroxides); **Main geomicrobial reactions**: organic carbon oxidation with oxygen reduction, acetogenesis, sulphate reduction in Simpevarp subarea and iron-and manganese reduction in Laxemar subarea**. Mixing processes:** Mainly meteoric recharge water at the Laxemar subarea; potential mixing of recharge meteoric water and a modern sea component at the Simpevarp subarea; localised mixing of meteoric water with deeper saline groundwaters at the Laxemar and Simpevarp subareas.

Type B

Shallow to intermediate (150–600 m) at the Simpevarp subarea but deeper (to ~ 500–950 m) at the Laxemar subarea. Brackish groundwater (2,000–10,000 mg/L Cl; 3.5–18.5 g/L TDS); $\delta^{18}O$ = –14 to –11‰ SMOW. B_L – Laxemar subarea: Meteoric, mainly Na-Ca-Cl in type; Glacial/Deep saline components. B_S – Simpevarp subarea: Meteoric mainly Na-Ca-Cl in type but some Na-Ca(Mg)-Cl(Br) types (± marine, e.g. Littorina); Glacial/Deep saline components. **Redox:** Reducing (~ –275 mV). **Main geochemical reactions:** Ion exchange (Ca, Mg); precipitation of calcite; redox reactions (e.g. precipitation of pyrite). **Main geomicrobial reactions**: acetogenesis and methanogenesis, sulphate reduction in Simpevarp subarea and iron-and manganese reduction together with sulphate-reduction in Laxemar subarea. **Mixing processes:** Potential residual Littorina Sea (old marine) component at the Simpevarp subarea, more evident in some fracture zones close to or under the Baltic Sea; potential glacial component at the Simpevarp and Laxemar subareas; potential deep saline (non-marine) component at the Simpevarp and at Laxemar subareas.

Type C

Intermediate to deep (~ 600–1,200 m) at the Simpevarp subarea but deeper (900–1,200 m) at the Laxemar subarea. Saline (10,000–20,000 mg/L Cl; 18.5–30 g/L TDS); $\delta^{18}O$ = ~ –13‰ SMOW. Dominantly Ca-Na-Cl in type at the Laxemar subarea but Na-Ca-Cl changing to Ca-Na-Cl only at the highest salinity levels at the Simpevarp subarea; increasingly enhanced Br/Cl ratio and SO_4 content with depth at both the Simpevarp and Laxemar subareas; Glacial/Deep saline mixtures. **Redox:** Reducing (~ 220 mV). **Main geochemical reactions:** Calcite precipitation, Ion exchange (Ca). **Main geomicrobial reactions:** Acetogenesis and methanogenesis. **Mixing processes:** Poential glacial component at the Simpevarp and Laxemar subareas; potential deep saline (i.e. non-marine) and an old marine component (Littorina?) at shallower levels at the Simpevarp subarea; Deep saline (non-marine) component at the Laxemar subarea.

Type D

Deep (> 1,200 m) only identified at the Laxemar subarea. Highly saline brine-type (> 20,000 mg/L Cl; to a maximum of ~ 70 g/L TDS); $\delta^{18}O$ = > –10‰ SMOW. Dominantly Ca-Na-Cl with higher BrCl ratios and a stable isotope composition that deviates from the GMWL when compared to Type C groundwaters; Deep saline/brine mixture; Diffusion dominant transport process. **Redox:** Reducing (~ 300 mV). **Main geochemical reactions:** Water/rock reactions under long residence times. **Main geomicrobial reactions:** unknown. **Mixing processes:** Probably long term mixing of deeper, non-marine saline component driven by diffusion.

Figure 2-12 (in Appendix 5), shows a visualisation of the spatial distribution of the four groundwater types in the Laxemar and Simpevarp subareas (cf. Appendix 5). It can be seen that low saline groundwaters (Type A) extend deeper at inland Laxemar subarea locations when compared to the Laxemar subarea coastal locations and the Simpevarp subarea, where they are only found at very shallow depths in the bedrock. In contrast, brackish and saline groundwaters (Types B and C) are predominant at the Laxemar subarea coastal areas (KLX01) and at the the Simpevarp subarea. Within the Simpevarp subarea, saline waters (Type C) are found at much shallower depths under the Simpevarp Peninsula than under the islands of Äspö and Ävrö.

Most dissolved species show qualitative trends very similar to chloride. This could be taken as an indication of the important role of physical transport processes (dispersion-diffusion; i.e mixing) in the hydrochemical evolution of bedrock groundwaters in the Laxemar and Simpevarp subareas.

There is no convincing evidence of a Littorina Sea component in the hydraulic rock domains of the Laxemar subarea. The presence of such old marine waters, and additional waters with a glacial melt water component, may be preserved as lenses/pockets along dead-end fractures and/or within rock masses of low transmissivity, but as yet the drilling campaign has not revealed such sources. Since the focus has been to quantify the structural understanding of the site, most of the boreholes, and subsequently the groundwater samples, are associated with major water-conducting zones where preservation of palaeowaters would be least expected.

Borehole KLX08 has also confirmed the strong recharge environment generally represented by the Laxemar subarea, with deep penetration of meteoric waters. At depth mixing with a cold climate component is sometimes observed.

The marked differences in the groundwater flow regimes between the Laxemar and Simpevarp subareas are reflected in the groundwater chemistry. Along the main WNW-ESE transect Figure 4-1 (cf. Appendix 1) shows the four major recognised groups of groundwaters and their interpreted spatial extent, denoted by A–D. The 'B' type groundwaters are subdivided into 'B_L' and 'B_S' types referring to Laxemar and Simpevarp respectively.

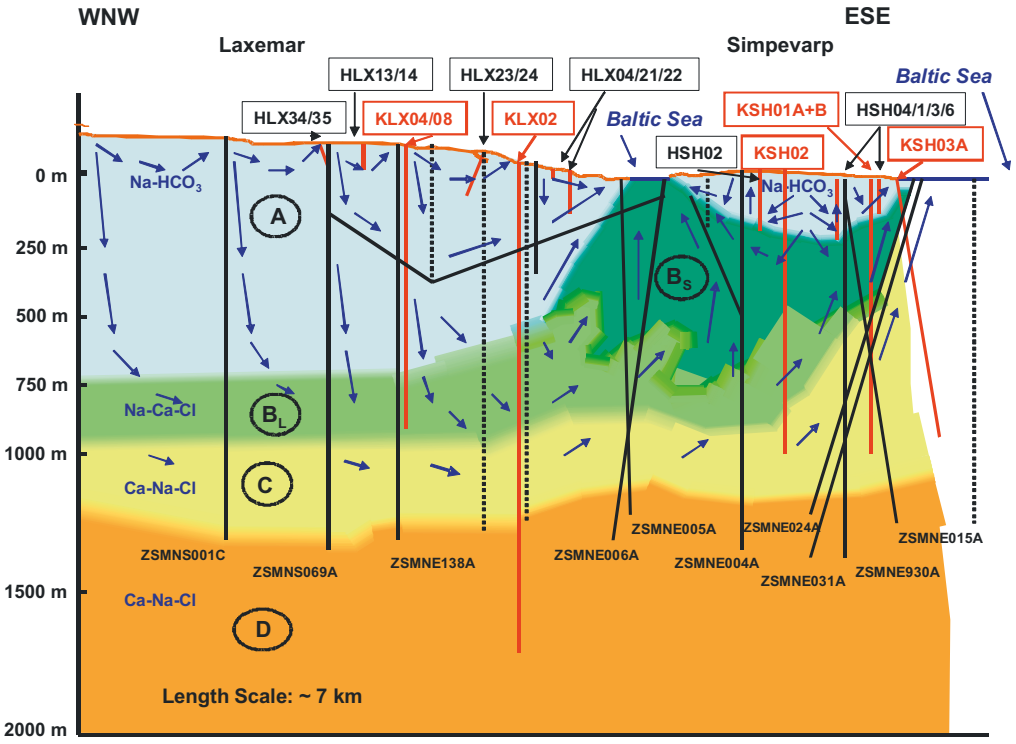

Figure 4-1. *Schematic 2-D visualisation along the WNW-ESE transect integrating the major structures, the major groundwater flow directions and the variation in groundwater chemistry from the sampled boreholes. Sampled borehole sections are indicated in red, major structures are indicated in black (full lines = confident; dashed lines = less confident), and the major groundwater types A–D are also indicated. The blue arrows are estimated groundwater flow directions.*

5 Comparison of hydrogeological and hydrogeochemical models

The present 2.1 modelling has further developed the comparison and integration between hydrochemistry and hydrogeology. Measured hydrogeochemical data, end-member compositions and their variability, M3 mixing calculations using the 2D and the new multispace option, and conceptual understanding, were delivered to the hydrogeological group.

As an example of the integration work, Figure 5-1 and Figure 5-2 (cf. Appendix 5) show two examples of combining hydrogeologic computed results (the hydrogeological model used is the L 1.2 /SKB 2006, Hartley et al. 2005/) and chloride measurements. It can be seen that there is a good qualitative agreement between modelled results and measurements in terms of a conservative tracer such as chloride. The hydrogeological model takes into account the structural geology, hydrogeological properties etc. and calibrates the model with some chemical components, e.g. measured salinities, in some boreholes. The hydrogeological model can generally be regarded as fairly independent from models based on hydrochemistry alone. The hydrogeological model mainly depends on the geology and the hydrogeological properties, but some model parameters. e.g porosity, may be calibrated due to get a better match with chemical data. However, in some cases the chemical data may signal that major revision of the hydeogeological model has to be made. A comprehensive comparison and integration between hydrochemistry and hydrogeology will be conducted for the Laxemar 2.2 modelling stage.

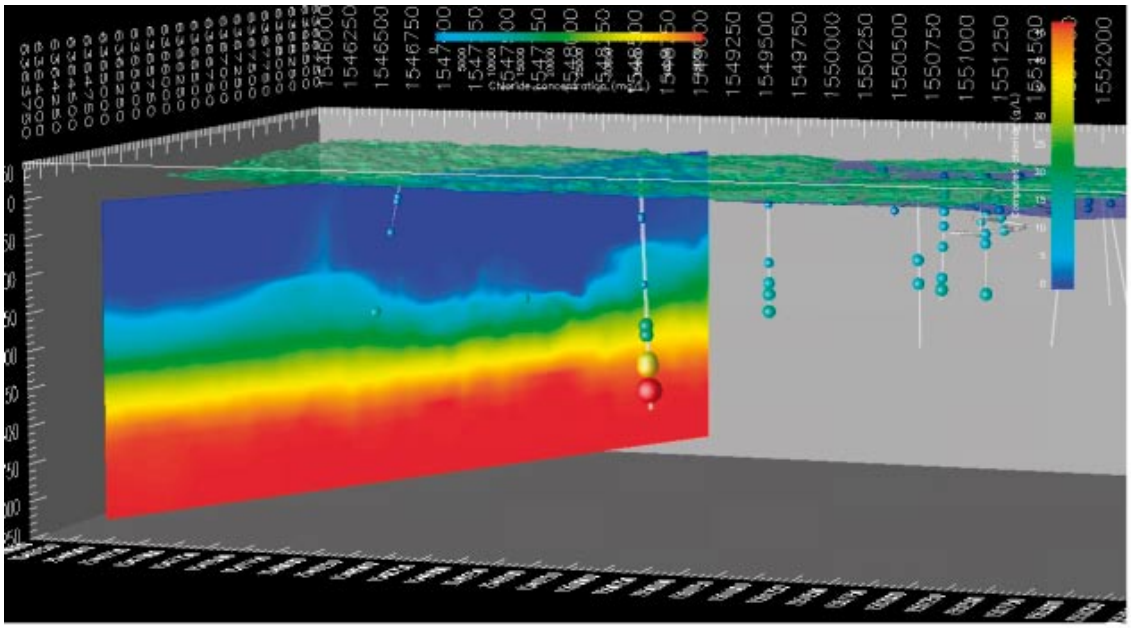

Figure 5-1. *3D view of computed and measured chloride distributions. Computed results /Hartley et al. 2005/ correspond to the second NW-SE cross-section. Colour scale is the same for both computed and measured chlorides.*

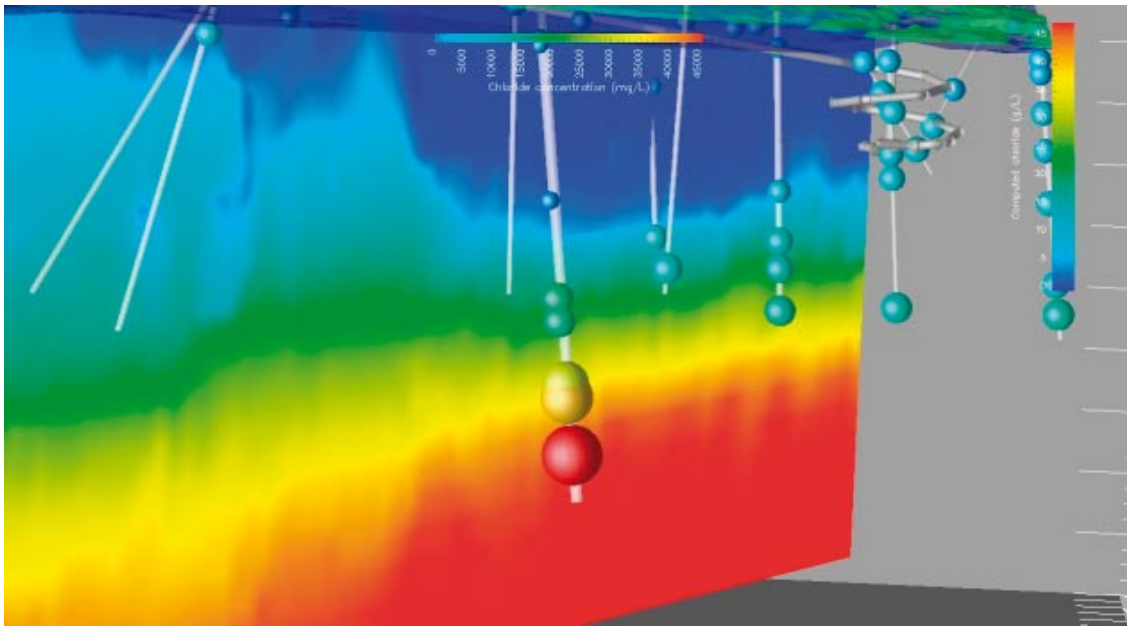

Figure 5-2. *Close-up view of /Hartley et al. 2005/ computed and measured chloride distributions. Computed results correspond to the first NW-SE cross-section. Colour scale is the same for both computed and measured chlorides.*

6 Conclusions

6.1 Overall changes since previous model version

In this report the models and the site understanding have been consolidated. The models have been updated and further understanding achieved concerning groundwater spatial variability, origin, evolution, major reactions, microbial depth variation, colloids, gases, pore water composition and its interaction with fracture water, and uncertainties in the mixing calculations. The studies of fracture fillings and especially the isotopic signatures in calcite, are lending greater support to the conceptual understanding of the site. The detailed mineral investigations are used directly in the hydrogeochemical modelling.

A more robust Hydrogeochemical Site Descriptive Model version 2.1 for the Laxemar subarea has evolved. The resulting description has improved compared to the 1.2 version for the Laxemar subarea by producing more analytical data and a more detailed process modelling for the dilute groundwater system and ultimately for the whole site. The microbial characterisation gives direct support to the redox modelling. The coupled transport modelling can address questions concerning transport processes which is of importance for the site understanding. Further integration with the hydrogeological modelling group has been initiated for the 2.2 modelling phase of the Laxemar subarea.

6.2 Overall understanding of the site

The overall understanding of the area describes the major processes taking place at the surface and to depth which includes the expected repository levels. The confidence in this description is relatively high since independent model approaches were utilised in the work. The origin, the postglacial evolution and the major reactions in the waters are fairly well understood. However the confidence concerning the spatial variation is low due to relatively few observations at depth. The continuation of the ongoing sampling programme at the Laxemar subarea will provide better spatial information and thus will increase confidence.

6.3 Implication for further modelling

Comparison and integration between geological and hydrogeological models and hydrogeochemical input in this model version was based on the hydrostructural model, fracture mineralogy, postglacial scenario models, concentrations of chloride, oxygen-18 and tritium, and mixing proportion calculations. The integration and comparison with hydrogeology should continue and the results compared using 3D visualisation techniques. This will provide efficient support for the production of conceptual models of the area but also should be used for describing the spatial variability of the chemistry at the site.

The use of independent modelling approaches within the ChemNet group provided the possibility to compare the outcome of the different models and to use discrepancies between models to guide further modelling efforts. The many similarities resulting from the ChemNet modelling have given confidence in the results obtained. The use of independent but also new modelling approaches, such as modelling of the interaction between pore water chemistry and fracture groundwater and detailed hydrogeochemical and coupled modelling helps the understanding of the complex groundwater system.

The major recommendation to the site investigation programme was to collect more high qualitative groundwater samples from repository depths in order to increase the confidence of the hydrogeochemical models.

7 Acknowledgements

This study forms part of the SKB site investigation programme, managed and supported by the Swedish Nuclear Fuel and Waste Management Company (SKB), Stockholm. The support and advice from Anders Ström, SKB and Anders Winberg, Conterra AB are acknowledged. The helpful comments by the internal reviewer Mel Gascoyne, GGP Inc. and Bill Wallin, Geokema AB improved the work. The helpful interaction with the site chemists Liselotte Ekström and Isabel Hedqvist are acknowledged.

8 References

Alley W M (ed.), 1993. Regional groundwater quality. ISBN 0-442-00937-2. Van Nostrand Reinhold, New York, USA, pp 634.

Andersson J, Berglund J, Follin S, Hakami E, Halvarson J, Hermanson J, Laaksoharju M, Rhén I, Wahlgren C-H, 2002. Testing the methodology for site descriptive modelling, Application for the Laxemar area. SKB TR-02-19, Svensk Kärnbränslehantering AB.

Banwart S (ed.), Laaksoharju M, Skårman C, Gustafsson E, Pitkänen P, Snellman M, Landström O, Aggeryd I, Mathiasson L, Sundblad B, Tullborg E-L, Wallin B, Pettersson C, Pedersen K, Arlinger J, Jahromi N, Ekendahl S, Hallbeck L, Degueldre C, Malmström M, 1995. Äspö Hard Rock Laboratory. The Redox Experiment in Block Scale. Final reporting of results from the three year project. SKB PR 25-95-06, Svensk Kärnbränslehantering AB.

Bath A, Milodowski A, Ruotsalainen P, Tullborg E-L, Cortés Ruiz A, Aranyossy J-F, 2000. Evidences from mineralogy and geochemistry for the evolution of groundwater systems during the quaternary for use in radioactive waste repository safety assessment (EQUIP project). EUR 19613 EN, Luxembourg.

Degueldre C, 1994. Colloid properties in groundwater from crystalline formation. Paul Scherrer Institute, Villigen, Switzerland.

Drake H, Tullborg E-L, 2004. Oskarshamn site investigation. Fracture mineralogy and wall rock alteration. Results from drill core KSH01A+B. SKP, P-04-250, 120 p, Svensk Kärnbränslehantering AB.

Drake H, Tullborg E-L, 2005. Oskarshamn site investigation. Fracture mineralogy and wall rock alteration. Results from drill cores KAS04, KA1755A and KLX02. SKB, P-05-174, 69 p, Svensk Kärnbränslehantering AB.

Glynn P D, Voss C I, 1999. SITE-94. Geochemical characterization of Simpevarp ground waters near the Äspö Hard Rock laboratory. SKI Report 96-29, SKI, Stockholm, Sweden, 210 p.

Grenthe I, Stumm W, Laaksoharju M, Nilsson A C, Wikberg P, 1992. Redox potentials and redox reactions in deep groundwater systems. Chem. Geol., 98, 131–150.

Gylling B, Moreno L, Neretnieks I, 1999. The Channel Network Model – A tool for transport simulation in fractured media, Groundwater 37, 367–375.

Hartley L, Hock A, Hunter F, Marsic N, 2005. Regional hydrogeological simulations – Numerical modelling using ConnectFlow. Preliminary site description Simpevarp subarea – version 1.2. SKB R-05-12, Svensk Kärnbränslehantering AB.

Hartley L, Hunter F, Jackson P, McCarthy R, Gylling B, Marsic N, 2006 (in prep). Regional hydrogeological simulations – Numerical modelling using ConnectFlow. Preliminary site description, Laxemar subarea – version 1.2. SKB R-06-23, Svensk Kärnbränslehantering AB.

Haveman S A, Pedersen K, Ruotsalainen P, 1999. Distribution and Metabolic Diversity of Microorganisms in Deep Igneous Rock Auifers of Finland. Geomicrobiology Journal 16, 277–294.

Laaksoharju M 1990. Measured and predicted groundwater chemistry at Äspö. SKB Progress Report 25-90-13, Svensk Kärnbränslehantering AB.

Laaksoharju M, Skårman C, 1995. Groundwater sampling and chemical characterisation of the HRL tunnel at Äspö, Sweden. SKB Progress Report PR 25-95-29, Stockholm, Sweden.

Laaksoharju M, Wallin B, 1997. Evolution of the groundwater chemistry at the Äspö Hard Rock Laboratory. Proceedings of the second Äspö International Geochemistry Workshop, June 6–7, 1995. SKB, International Cooperation Report 97-04.

Laaksoharju M, Skårman C, Skårman E, 1999b. Multivariate Mixing and Mass-balance (M3) calculations, a new tool for decoding hydrogeochemical information. Applied Geochemistry Vol. 14, #7, 1999, Elsevier Science Ltd., pp 861–871.

Laaksoharju M, 1999. Groundwater characterisation and modelling: problems, facts and possibilities. Department of Civil and Environmental Engineering. Royal Institute of Technology (KTH). Stockholm.

Laaksoharju M (ed), 2004a. Hydrogeochemical evaluation of the Simpevarp area, model version 1.2. Preliminary site description of the Simpevarp area. SKB R 04-74, Svensk Kärnbränslehantering AB, 463 p.

Laaksoharju M, Smellie J, Gimeno M, Auqué L, Gómez J, Tullborg E-L, Gurban I, 2004b. Hydrogeochemical evaluation of the Simpevarp area, model version 1.1. SKB R 04-16, Svensk Kärnbränslehantering AB.

Landström O, Tullborg E-L, 1995. Interactions of trace elements with fracture filling minerals from the Äspö Hard Rock Laboratory. SKB TR-95-13, Svensk Kärnbränslehantering AB.

Luukkonen A, 2001. Groundwater mixing and geochemical reactions. An inverse-modelling approach. In: Luukkonen, A. and Kattilakoski, E. (Eds.) Äspö Hard Rock Laboratory. Groundwater flow, mixing and geochemical reactions at Äspö HRL. Task 5. Äspö Task Force on groundwater flow and transport of solutes. SKB Progress Report SKB IPR-02-41), Svensk Kärnbränslehantering AB.

Milodowski A E, Tullborg E-L, Buil B, Gômez P, Turrero M-J, Haszeldine S, England G, Gillespie M R, Torres T, Ortiz J E, Zacharias J, Silar J, Chvátal M, Strnad L, Šebek O, Bouch J E, Chenery S R, Chenery C, Shepherd T J, McKervey J A, 2005. Application of mineralogical petrological and geochemical tools for evaluating the palaeohydrogeological evolution of the PADAMOT Study sites. PADAMOT PROJECT Technical Report WP2. EU FP5 Contract nr FIKW-CT2001-20129.

Nordstrom D K, Puigdomenech I, 1986. Redox chemistry of deep ground-waters in Sweden. SKB Technical Report 86-03, 30 p, Svensk Kärnbränslehantering AB.

Parkhurst D L, Appelo C A J, 1999. User's Guide to PHREEQC (Version 2), a computer program for speciation, batch-reaction, one-dimensional transport, and inverse geochemical calculations. U.S. Geological Survey Water-Resources Investigations Report 99-4259, 312 p.

Pedersen K, 1993. The deep subterranean biosphere. Earth-Science Reviews 34, 243–260.

Pedersen K, 2000. Microbial processes in radioactive waste disposal. SKB TR 00-04, 97 p, Svensk Kärnbränslehantering AB.

Pedersen K, 2001. Diversity and activity of microorganisms i deep igneous rock aquifers of the Baltic shield, pp 97–139 In J.K. Fredrickson and M. Fletcher (eds.), Subsurface microbiology and biogeochemistry. Wiley-Liss Inc., New York.

Pitkänen P, Luukkonen A, Ruotsalainen P, Leino-Forsman H, Vuorinen U, 1998. Geochemical modelling of groundwater evolution and residence time at the Kivetty site. POSIVA Report 98-07, Helsinki, Finland, 139 p.

Pitkänen P, Partamies S, Luukkonen A, 2004. hydrogeochemical interpretation of baseline groundwater conditions at the Olkiluoto site. Posiva Tech. Rep. (2003-07), Posiva, Helsinki, Sweden.

Påsse T, 2001. An empirical model of glacio-isostatic movments and shore-level displacement in Fennoscandia. SKB R-01-41, 59 pp, Svensk Kärnbränslehantering AB.

Samper J, Delgado J, Juncosa R, Montenegro L, 2000. CORE^{2D} v 2.0: A Code for non-isothermal water flow and reactive solute transport. User's manual. ENRESA Technical report 06/2000. Madrid.

SKB, 2002. Simpevarp – site descriptive model version 0. SKB R-02-35, Svensk Kärnbränslehantering AB.

SKB, 2004. Hydrogeochemical evaluation for Simpevarp model version 1.2. Preliminary site description of the Simpevarp area. SKB R-04-74, Svensk Kärnbränslehantering AB.

SKB, 2005. Preliminary site description. Simpevarp subarea version 1.2. SKB R-05-08, Svensk Kärnbränslehantering AB.

SKB, 2006. Preliminary site description Laxemar subarea – version 1.2. SKB R-06-10, Svensk Kärnbränslehantering AB.

Smellie J, Laaksoharju M, 1992. The Äspö Hard Rock Laboratory: Final evaluation of the hydrogeochemical pre-investigations in relation to existing geological and hydraulic conditions. SKB TR-92-31, Svensk Kärnbränslehantering AB.

Smellie J, Laaksoharju M, Tullborg E-L, 2002. Hydrogeochemical site descriptive model – a strategy for the model development during site investigations. SKB R-02-49, Svensk Kärnbränslehantering AB.

Svensson U, 1996. SKB Palaeohydrogeological programme. Regional groundwater flow due to advancing and retreating glacier-scoping calculations. In: SKB Project Report U 96-35, Svensk Kärnbränslehantering AB.

Waber H N, Smellie J A T, 2006b. Borehole KLX03: Characterisation of pore water. Part 2: Rock properties and diffusion experiments. Oskarshamn site investigation. SKB P-06-77, Svensk Kärnbränslehantering AB.

Westman P, Wastegård S, Schoning K, Gustafsson B, 1999. Salinity change in the Baltic Sea during the last 8,500 yearsw: evidence causes and models. SKB TR 99-38, Svensk Kärnbränslehantering AB.

Vilks P, Miller H, Doern D, 1991. Natural colloids and suspended praticles in Whiteshell Research area, Manitoba, Canada, and their potential effect on radiocolloid formation. Applied Geochemistry 8, 565–574.

Voss C I, Provost A M, 2003. SUTRA, A model for saturated-unsaturated variable-density ground-water flow with solute or energy transport. U.S. Geological Survey Water-Resources Investigations Report 02-4231, 250 p.

9 Appendix 1: Explorative analysis and expert judgement of major components and isotopes

Contribution to the model version 2.1

John Smellie, Conterra AB

Eva-Lena Tullborg, Terralogica AB

Niklaus Waber, University of Bern, Switzerland

August 2006

Contents

1 Geological and hydrogeological setting

1.1 Regional geology

1.1.1 Rock types and properties

The Simpevarp area is located at the Baltic Sea coast some 30 km north of Oskarshamn (Figure 1-1). The area forms part of the TransScandinavian Igneous Belt (TIB) of Precambrian basement rocks (dated to around 1.8 Ga) dominated by granitoids which, in the Simpevarp area, comprise porphyritic and even-grained rocks ranging from red/grey granites to quartz-monzodiorite. The porphyritic granitoids are referred to as the Ävrö granites and the grey, medium-grained monzodiorites which are dominantly quartz-monzodioritic in composition are simply referred to as quartz-monzodiorite. Along the southeastern part of the Laxemar subarea and the Simpevarp peninsula, a grey-coloured, fine-grained variety of quartz-monzodiorite occurs with a possible subvolcanic origin.

Because of its close relationship with the quartz-monzodiorite and similarity in composition, the term dioritoid has been suggested. A thin belt of this rock type is also identified in the central part of Ävrö island. Small amounts of aplitic (named fine-grained granite) and dioritic and gabbroic rock-types also occur sporadically in smaller bodies, and are much more common in an E-W belt in the southern part of the Simpevarp area.

Transecting all above-named rock-types are dykes characterised by fine- to medium-grained granite and pegmatites /SKB 2006/. In addition, a N-S trending dolerite dyke has been identified along the western margin of the Laxemar subarea.

A characteristic feature of the region is magma mingling and mixing relationships between the different rock types. Geochemically the various rocks display similar and overlapping compositional variations such that the most important criteria employed in distinguishing between the different rock types are texture and grain size. All rock types in the Laxemar and Simpevarp subareas display low contents of uranium (< 6 ppm), except for pegmatite in which the uranium content locally exceeds 16 ppm.

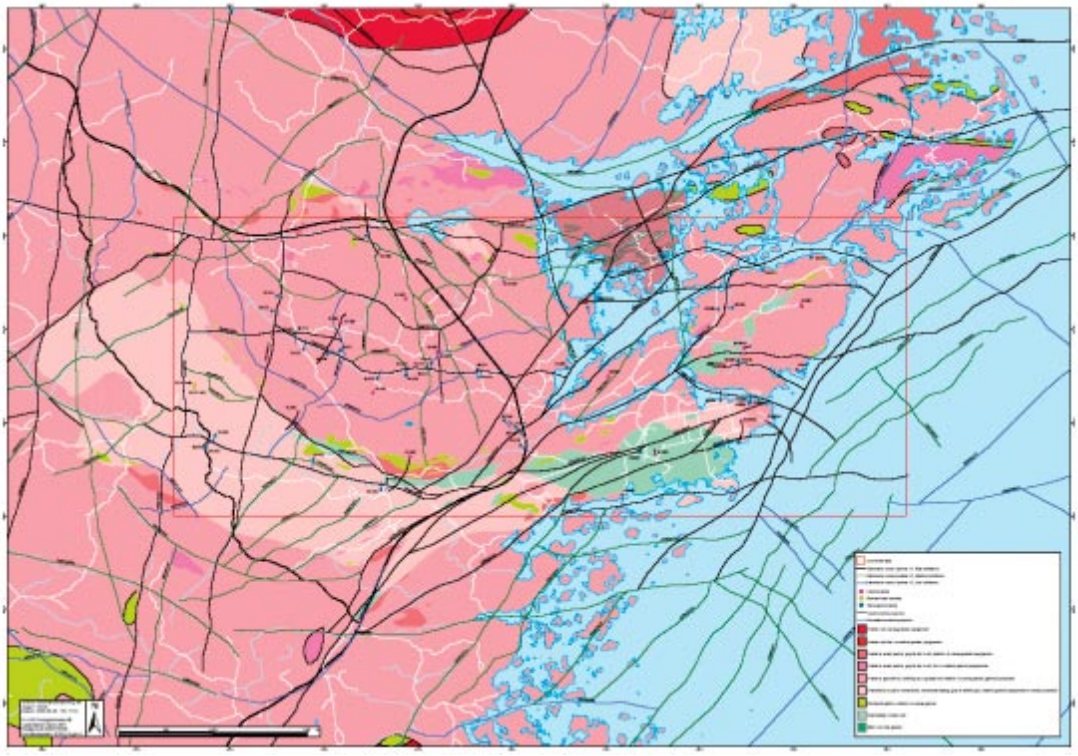

Figure 1-1. *Geological setting of the Simpevarp area /SKB 2006/.*

Generally the foliation in the Simpevarp area is weak but there are clear indications in the Laxemar subarea and immediate surroundings of an E-W to N-W strike and a variable dip, whereas the foliation in the Simpevarp subarea displays an E-W to N-E strike and steep dip. Furthermore, the foliation is more or less concordant to the contacts between the dominant rock types which suggests a genetic relationship between the formation of the foliation and the formation of the rocks /SKB 2006/.

All rock-types have also been subjected to alteration (red staining caused by disseminated micro-grains of haematite) largely due to post-crystallisation penetration of hydrothermal fluids along pre-existing zones of weakness (e.g. fractures).

Available porosity measurements from the Simpevarp area show low values, in general below 1%, which is normal for unaltered crystalline Swedish bedrock. Despite the few data and an overlap of porosity values of the diferent rock types, there is an indication that the fine-grained dioritoid and the diorite to gabbro have lower porosities than, for example, the Ävrö granite.

1.1.2 Structural features

The most spectacular and characteristic ductile, structural features in the Laxemar and Simpevarp subareas are the occurrences of protomylonitic to mylonitic, low-grade ductile to brittle-ductile shear zones (Figures 1-1, 1-2). Two areas or belts with a high concentration of low-grade ductile to brittle-ductile shear zones can be demarcated. The regional scale shear zones within this belt have a NE-SW strike and a vertical to subvertical dip, which, on a local scale, can be seen as two branches, denoting zone ZSMNE005A (Äspö shear zone) and zone ZSMNE004A, of a larger regional structure that divides the Laxemar subarea from the Simpevarp subarea.

The approx. E-W deformation zone ZSMEW007A, which is located centrally to the proposed repository area, is a complex structure which still has not been completely resolved. Its presence is based on a topographic and magnetic EW-lineament, seismics, ground geophysics and borehole

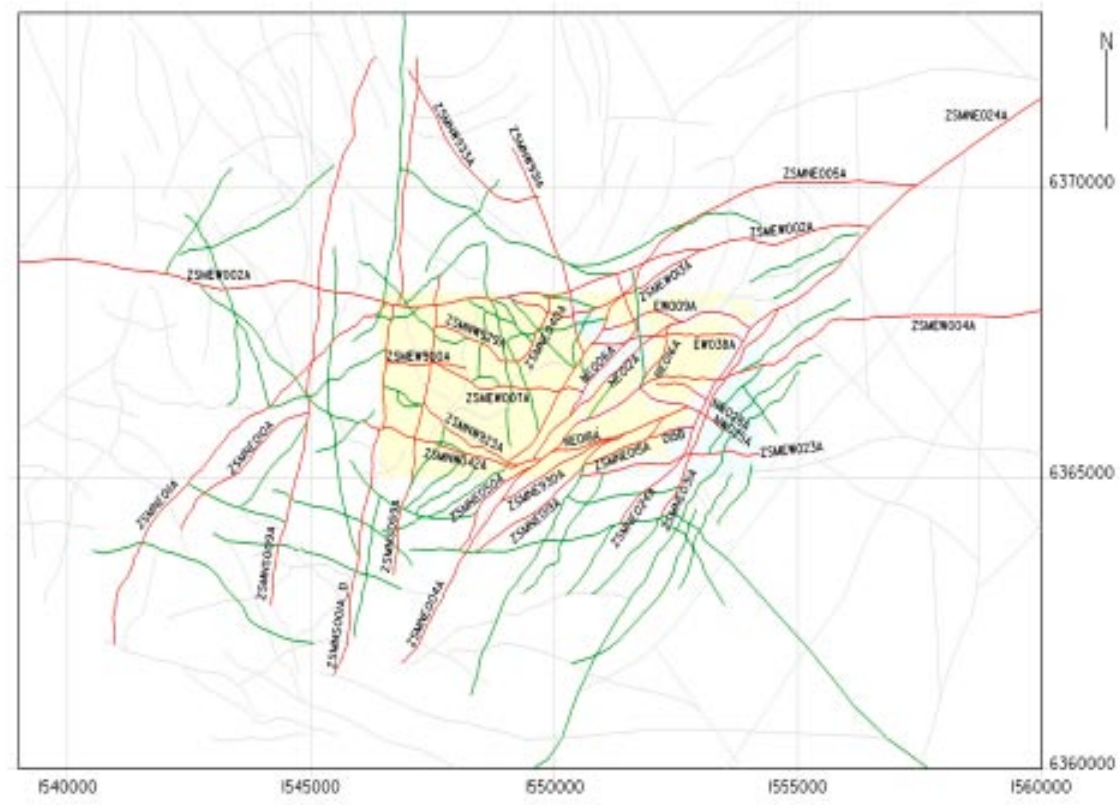

Figure 1-2. *Regional scale deformation zones that characterise the Simpevarp area (major zones in red). Refer to Figure 1 for geographical location and major rock types.*

intersections. The zone has been updated from the Simpevarp version 1.2 with new borehole intersections as well as new ground geophysics. However, alternative interpretations are available through borehole KLX04 which together with resistivity profiles indicate also a northerly dip of the central and eastern part of EW007. The magnetic anomaly also supports a division of EW007 into two separate structures (along its extent); one gently northerly dipping structure in the central/east and one steeply dipping towards the south (in the west). Refraction seismic profiling across EW007 shows a zone with a thickness of at least 10 m, and possibly several neighbouring splay structures /SKB 2006/.

As mentioned above, ZSMEW005A, the Äspö shear zone forms the boundary between the tectonically more deformed rock mass in the Simpevarp subarea and the comparatively less deformed Laxemar subarea. The deformation zone is a complex and dominantly ductile zone with smaller sections of brittle deformation. At Äspö, where it is best known, it is described as a primarily ductile shear zone with mylonites and epidotic anastomosing shear zones which are interpreted to control the orientation of later brittle deformation, evident in the form of increased fracturing and brecciation.

Hydrothermal alteration and formation of different fracture filling minerals probably had an important sealing effect on the main core of the zone. The most hydraulically conductive parts appears to coincide with some narrow highly fractured sections, or single open fractures, which are probably not connected along the entire extent of the zone. In the current model, an enveloping thickness of 250 m was attributed to the zone in order to contain all indicators from the geological field mapping.

A further important regional structure, the regional Mederhult deformation zone, ZSMEW002A, is considered to be mainly a ductile regional scale shear zone following a topographic and magnetic lineament running along the northern coastline of Äspö. The zone is dipping to the south (into the Laxemar subarea). This zone is penetrated by borehole KLX06 and is characterised by intense ductile deformation and subsequent hydrothermal reactivation and alteration. Large volumes of, for example, laumonitite, have been identified in this zone.

The regional N-S trending deformation zone ZSMNS001A-D constituting the western border of the Laxemar subarea coincides with a dolerite dyke.

Three dimensional representations of the structural fabric are shown in Figure 1-3 (regional scale) and Figure 1-4 (local site scale). These further clarify the approx. E-W and NE-SW trends of the major deformation zones and the structural complexity of the Simpevarp penninsula and Ävrö/Äspö island localities.

In conclusion, taking into consideration all available geophysical and geological (i.e. bedrock and borehole mapping) information, the indications are that the Simpevarp subarea is more strongly affected by low-grade ductile shear zones than the Laxemar subarea. This is also strongly indicated in the magnetic anomaly map where the Simpevarp subarea, i.e. east of the Äspö shear zone, is characterised by a much more banded, anomaly pattern than the Laxemar subarea west of the Äspö shear zone. This difference is interpreted to be a result of overprinting of the ductile shear zones. Thus, the Simpevarp and Laxemar subareas may be considered as two different structural domains, and indicates that the Simpevarp subarea is situated in a spaced ductile shear belt, while the Laxemar subarea more or less have escaped this ductile shearing and in respect to the latter constitutes a "tectonic lens" /SKB 2006/.

1.2 Regional hydrogeology

The Simpevarp area is characterised by small-scale topographical undulation (< 50 m.a.s.l.) and can be considered consisting of a large number of small catchments and mostly small water courses. The calculated annual run-off is 150–160 mm. Near-surface recharge/discharge is largely determined by the local topography and is sensitive to seasonal fluctuations in precipitation. Lakes are considered to be permanent discharge locations, streams sporadic discharge points during wet periods and wetlands/marshes/bogs can be either typical discharge areas in contact with groundwaters, or represent closed surface systems with no underlying hydraulic contact.

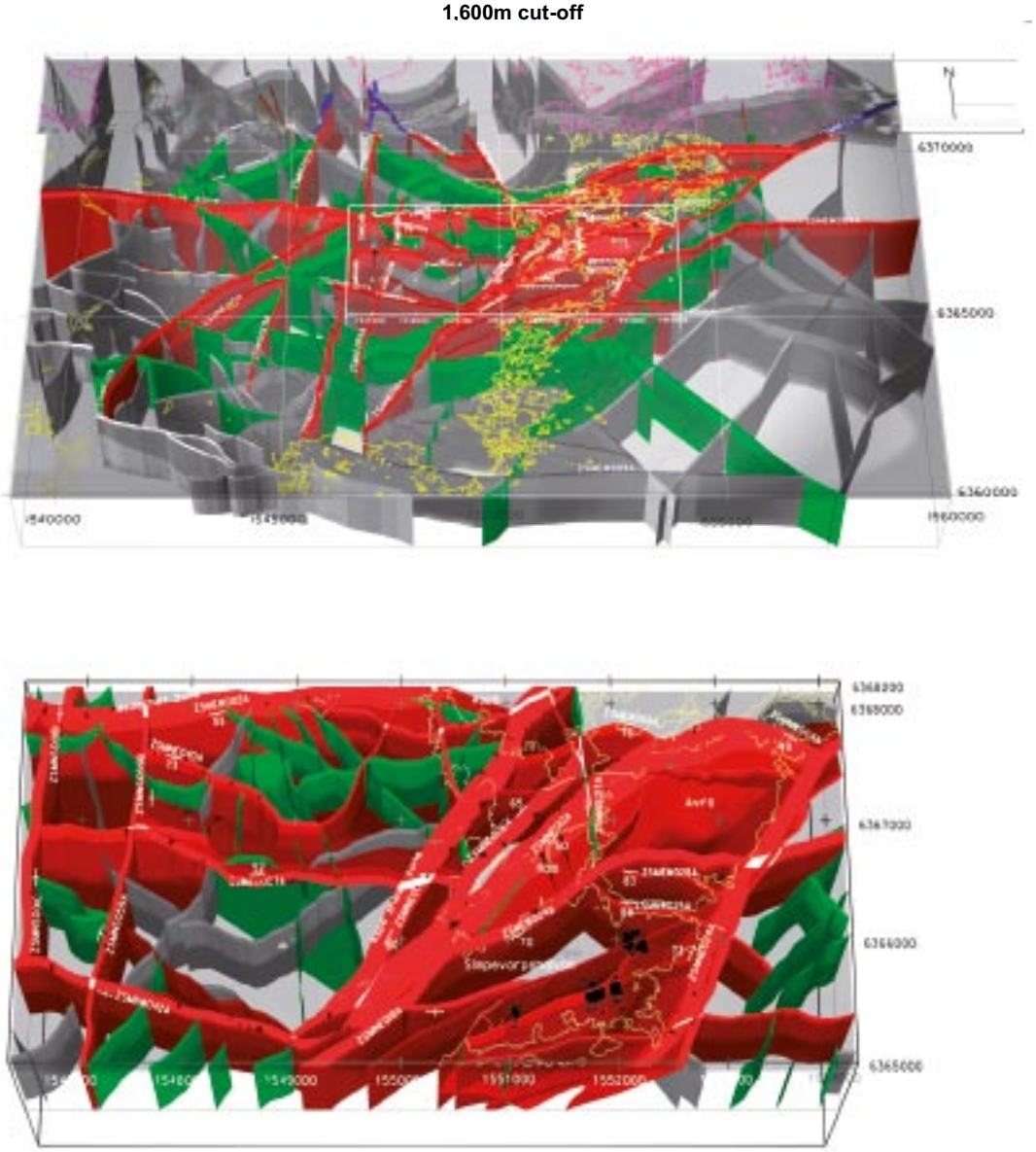

Figure 1-3. *3-D representation of the major deformation zones characterising the Simpevarp area on a regional scale (above figure) and on a local scale (lower figure). Red coloured zones represent high confidence interpreted zones; green colouration represents lower confidence interpreted zones.*

Since the last glaciation hydrological conditions have changed markedly due to shoreline displacement and changing salinity in the Baltic Sea region (fresh to brackish). This has resulted in the present spatial distribution of groundwater types /SKB 2005/.

In common with the surface environment, topography appears to control much of the groundwater flow pattern in the upper part of the rock mass, possibly down to 1,000 m depth; increasing salinity with depth will reduce the flow rates. Discharge areas are located to the extreme east of the Simpevarp area along the Baltic Sea coastline and also onshore in conjunction with fracture zones. Results from the Simpevarp 1.2 evaluation /SKB 2005/ and the Laxemar 1.2 evaluation /SKB 2006/ indicate that the Laxemar subarea is predominantly subjected to recharge conditions and that the Simpevarp subarea is an area of mainly groundwater discharge.

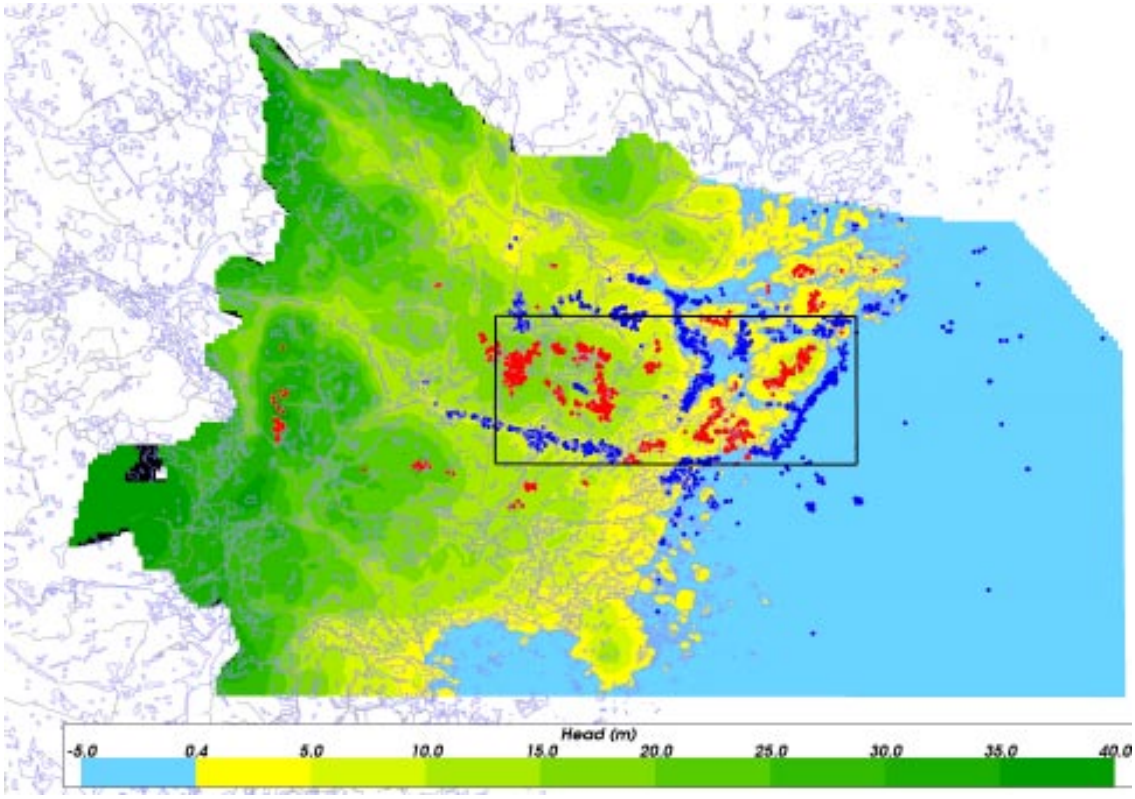

Figure 1-4. *Recharge (red) and discharge (blue) locations for particles released in the local scale area for the reference case. The local scale release area (black rectangle) is shown for geographical reference. The recharge points are the upstream start points on the model surface for flow paths through the release area. The discharge points are the equivalent downstream exit points /SKB 2006/.*

Hydraulic modelling using particle release to trace potential groundwater fow paths is illustrated in Figure 1-4; here the recharge (red) and discharge (blue) for particles released within the local scale area are shown for the reference case. All the major islands (Äspö, Ävrö and Hålö) together with the Simpevarp peninsula act as recharge areas, as does the central parts of the Laxemar subarea. A few recharge areas that influence the Laxemar subarea are located at hills several kilometres to the west and southwest. Generally the discharge areas are located mainly in valleys to the south and north of Laxemar and along the shoreline, especially south of Äspö; hydrochemically, the most convincing discharge point is situated in the central outflow area of Ävrö. There is also a minor discharge area associated with a small stream in the centre of the Laxemar subarea.

A comparison between the hydraulic conductor domains (HCD) and the hydraulic rock domains (HRD) shows that the evaluated geometric mean hydraulic conductivity (K) in the HCDs is about 10 times higher than the corresponding mean of the HRDs. Furthermore, there seems to be a significant depth trend in the hydraulic conductivity of HCDs, at least between 0–200 m depth and below 400 m depth. Anisotropic conditions, with the highest conductivity in an approx. NW direction, characterises the Laxemar subarea. The hydraulic conductivity (K) of the rock domains differs, i.e. rock domain A (i.e. Ävrö granite) at Ävrö and the southern part of Äspö appears more conductive than the corresponding domain A in the Laxemar subarea. The hydraulic rock domains with more basic rock types, B, C, D (and probably E – not data available), and M are less conductive than domain A (5–20 times lower). The fine-grained granites are probably an order of magnitude more conductive than the Ävrö granite (i.e. rock domain A).

1.3 Borehole locations and drilling

The Laxemar 2.1.hydrochemical evaluation involved four cored boreholes (KLX05, 07, 08 and 10) and 2 percussion boreholes (HLX28 and 34) from the Laxemar subarea, and two cored boreholes (KAV01 and KAV04A) and 10 percussion boreholes (HAV04–HAV07 and HAV09–HAV14) from Ävrö island. These are shown in Figure 1-5.

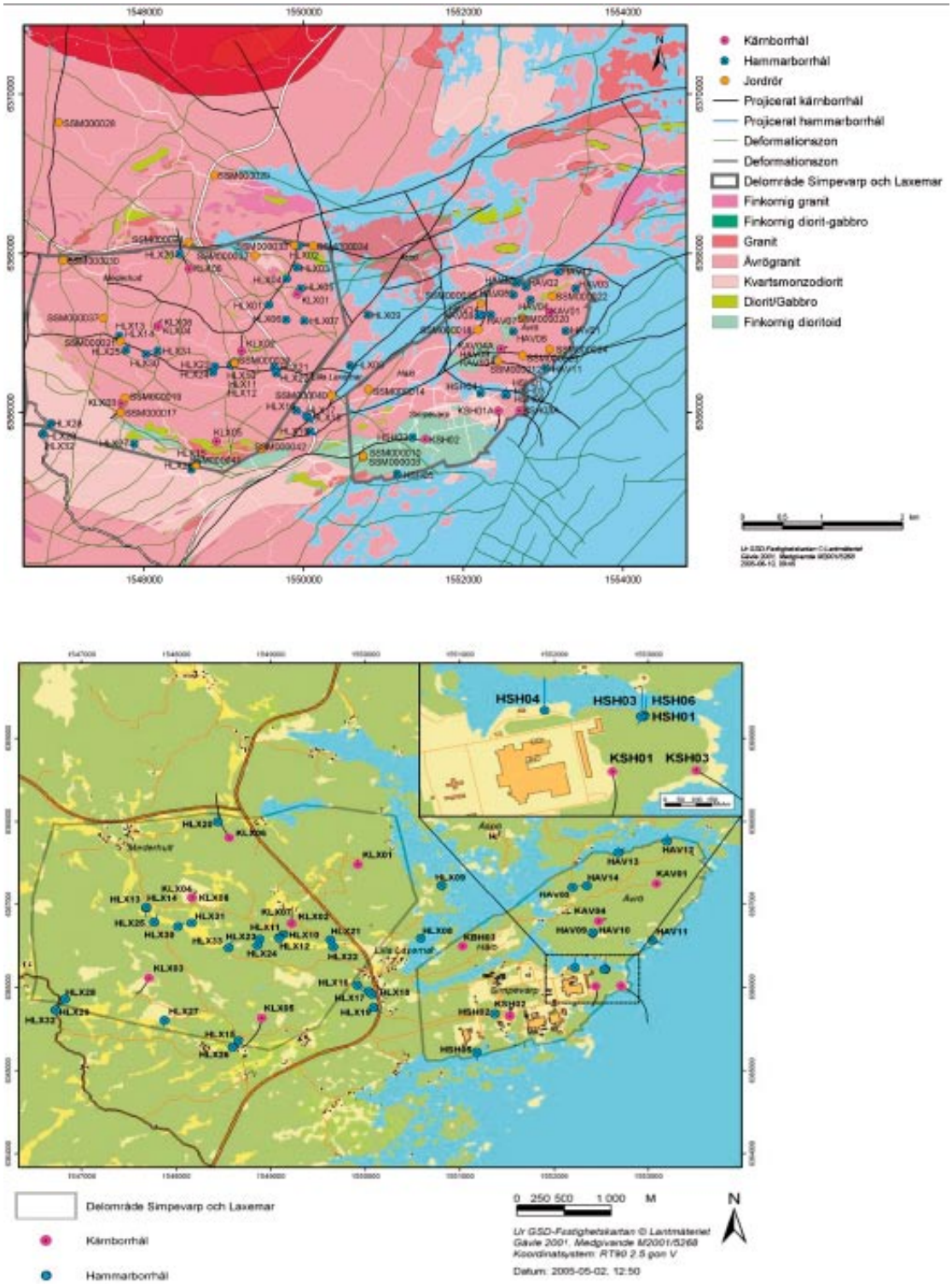

Figure 1-5. *Geology (above) and location (above and below) of the of hydrogeochemically prioritised boreholes KLX01, KLX02, KLX03, KLX04 and KLX06 (Laxemar subarea) and KAV01, KAV04A, KSH01A, KSH02 and KSH03 (Simpevarp subarea). Also indicated are the percussion boreholes, many of which are included in the Laxemar v. 2.1 evaluation.*

1.4 Studies of fracture fillings and wall rock alteration

1.4.1 General characteristics

Fracture minerals are determined macroscopically and are mapped within the Boremap system. However, since many of the minerals are difficult to identify and small crystals are easily overlooked, fracture mineral analyses have been carried out on additional samples for quantitative identification. Fracture samples have also been selected for sampling because they can provide information on the sequence of events that have resulted in fracturing and fracture mineralisation in the area. A number of samples have been taken from boreholes KLX02, KLX03, KLX04 and KLX06 for microscopy, in must cases including SEM/EDS, chemical analyses and stable isotope analyses of calcites. Results from these studies are reported in /Drake and Tullborg 2005/ and in manuscript.

A summary of available mineralogical information based on the Boremap data have been compiled for the SR-Can project. The abundance of different fracture minerals in open fractures are shown in Table 1 (from /Drake et al. 2006/). The reason for highlighting KLX02 is that this borehole was not drilled using the triple-drilling technique, thus larger disturbance has been caused to the drillcore.

Only a small number (in the order of 10 to 15%) of the fractures mapped as open are documented as water conducting by, for example, the Posiva Differential Flow Log. On the other hand all open fractures are possible water pathways even though the transport may de dominated by diffusion instead of advective flow. In this respect it may however be interesting to see if the mineralogy in the fractures with larger apertures deviates from the thinner ones. When comparing the result in the table with the plot in Figure 1-6 it is obvious that the differences are small.

The sequences of minerals identified in the Simpevarp and Laxemar drillcores are very similar to earlier observations made at the Äspö HRL /Landström and Tullborg 1995, Andersson et al. 2002/. However, the order of frequency and the amounts of certain minerals can vary considerably throughout the Simpevarp area, which is partly reflected by Table 1-1. Another reason for variation in the Boremap data between the Simpevarp and Laxemar subareas is the increased certainty in the core mapping, for example, it is suspected that clay minerals were underestimated in the earlier Simpevarp drillcore characterisation.

Table 1-1. Relative abundance of fracture minerals in open fractures. The percentage values represent the number of sealed fractures a specific mineral has been identified. Data from KSH01A+B, KSH02, KSH03A+B and KAV04A+B (Simpevarp subarea) and KLX03–KLX06, KLX07A+B, KLX08 and KLX02 (Laxemar subarea). All fractures = from all drillholes.

Mineral	Simpevarp %	Laxemar %	KLX02 %	All fractures %
Chlorite	68	74	69	70
Calcite	60	71	57	64
Haematite	25	13	4	18
Clay minerals	4	38	< 0.1	17
Epidote	20	5	15	14
Pyrite	5	18	5	10
Quartz	3	4	2	4
Adularia	< 0.1	7	0.1	3
No fill – broken	0.7	3	5	2
Laumontite	1	1	0.1	1
Prehnite	0.7	1	< 0.1	0.7
Goethite	0.7	< 0.1	< 0.1	0.4
Fluorite	0.2	0.6	< 0.1	0.4
Gypsum	< 0.1	0.9	< 0.1	0.4
Chalcopyrite	0.2	0.3	0.1	0.2
Muscovite	< 0.1	0.3	< 0.1	0.1

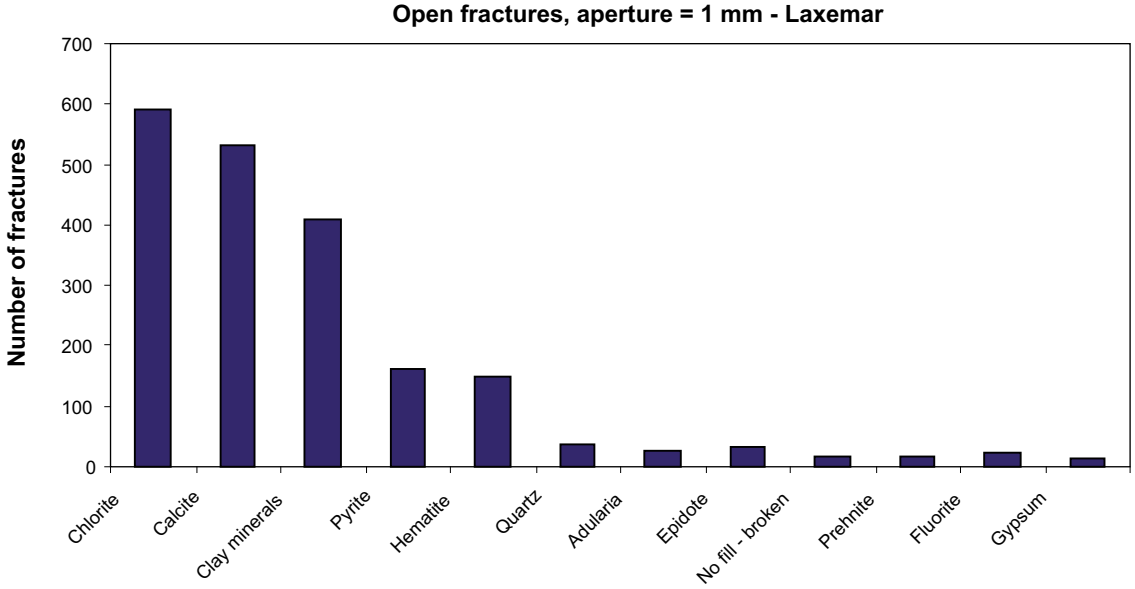

Figure 1-6. *Number of open fractures with an aperture ≥ 1 mm and their mineralogy. Data from KLX03–KLX08A and KLX07B, total number of fractures = 733. /Drake et al. 2006/.*

Valid for the entire region is the sequence of minerals which change from epidote facies, in combination with ductile deformation, over to brittle deformation and breccia sealing during prehnite facies, and subsequently zeolite facies with a further mineral formation series at decreasing temperature. This indicates that most of the fractures were initiated early in the geological history of the host rock and have been reactivated during several different periods of physiochemical conditions.

The locations of the hydraulically conductive fractures are mostly associated with the presence of gouge-filled faults produced by brittle reactivation of earlier ductile precursors or hydrothermally sealed fractures. The outermost coatings along the hydraulically conductive fractures consist mainly of clay minerals, usually illite and mixed layer clays (corrensite = chorite/smectite and illite/smectite) together with calcite and minor grains of pyrite.

1.4.2 Hydrochemical indicators

In the perspective of groundwater chemistry the presence of the four minerals, calcite ($CaCO_3$), gypsum ($CaSO_4$), barite ($BaSO_4$) and fluorite (CaF_2), are worth attention as their solutbility has an impact/controls the behaviour of some major ions.

Calcite is as mentioned above the most common of these minerals. It occurs frequently at all depths except in the upper tens of metres and below approx. 1,000 to 1,100 m were it is less common. A number of calcite generations have also been identified ranging from hydrothermal to possible recent /Bath et al. 2000, Drake and Tullborg 2004/. Stable isotope ratios represented as $\delta^{18}O$ and $\delta^{13}C$ are shown in Figures 1-7 and 1-8 plotted versus depth. $\delta^{18}O$ versus depth shows that the highest values representing possible Baltic Sea water precipitates are found in the upper 500 m in the Simpevarp subarea and Äspö. The Laxemar subarea in contrast has generally lower $\delta^{18}O$ values. Calcites with low $\delta^{18}O$ (< –15‰ PDB) are found at all depths except for the near surface 50 m. Such values are expected in calcite precipitated from a groundwater with large glacial component. Mineral paragenesis, trace element composition and Sr isotope studies reveal, however, that the low $\delta^{18}O$ calcites are older and have been precipitated during increased temperatures. The carbon isotopes show large variation and extremely low values ($\delta^{13}C$ < –25‰ PDB) have been observed down to 800 m depth. Such low values are produced by in situ microbial activity causing extreme local disequilibria. On average the $\delta^{13}C$-values are lower in the upper 500 m indicating a larger input of organic carbon. The few samples below 10,000 m are all higher than –10‰ supporting more stagnant conditions at depth with no sign of exchange with organic material contributed from the surface.

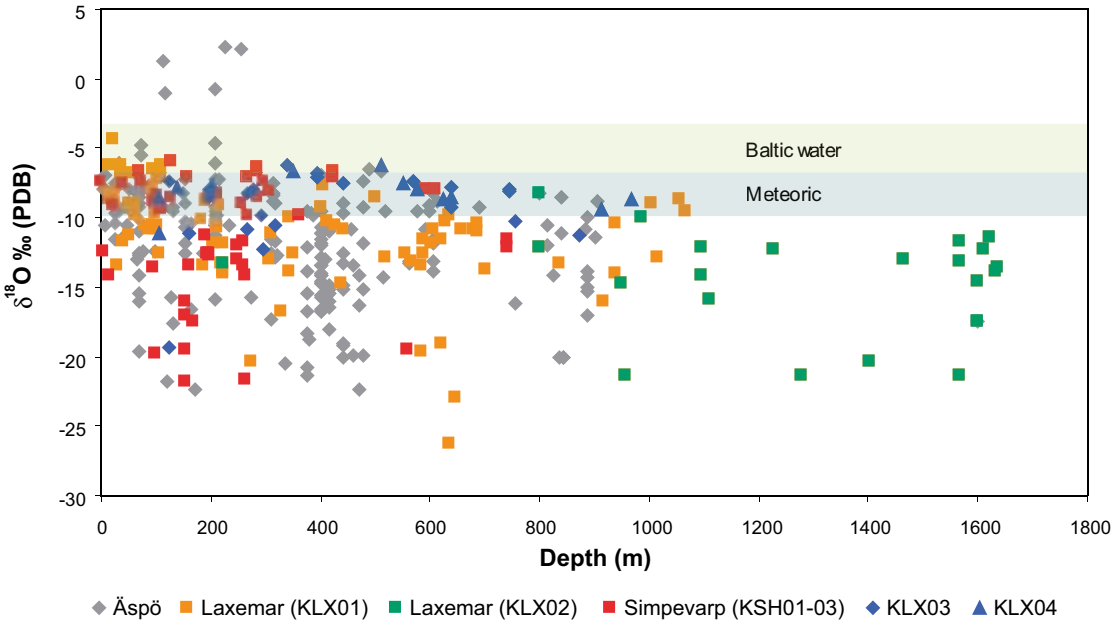

Figure 1-7. *Plot of $\delta^{18}O$ (PDB) vs depth (calcite) with samples from KLX03 and KLX04 along with calcite from Äspö, Simpevarp and Laxemar (KLX01 and KLX02). /Drake and Tullborg 2004, Milodowski 2005/. Range of calcite precipitates from Baltic Sea water and meteoric water at ambient temperatures is indicated.*

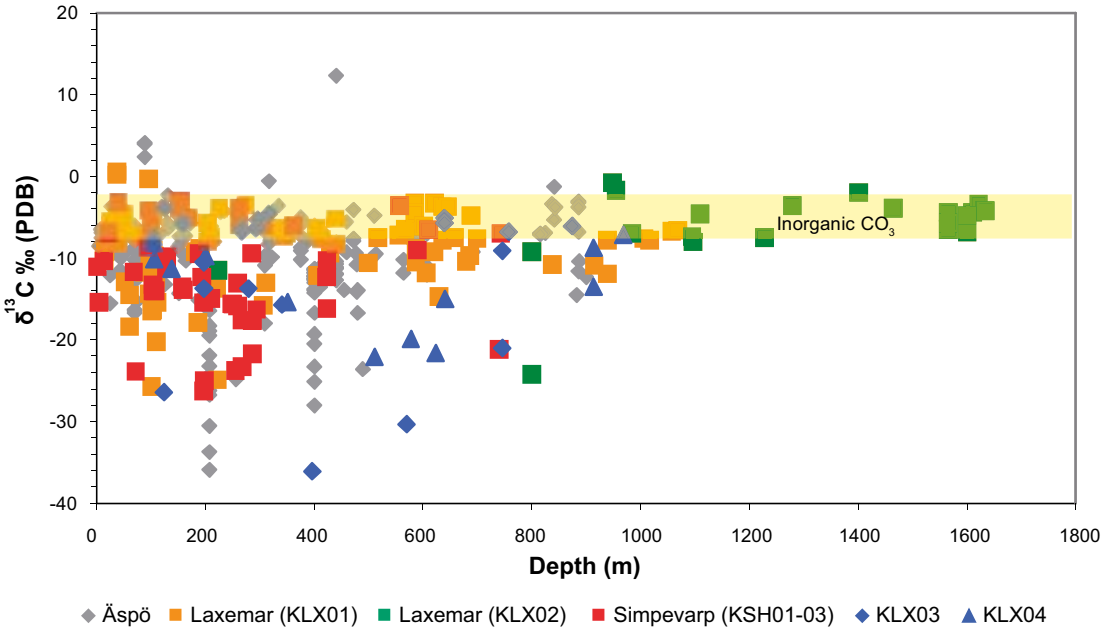

Figure 1-8. *Plot of $\delta^{13}C$ (PDB) vs depth (calcite) with samples from KLX03 and KLX04 along with calcite from Äspö, Simpevarp and Laxemar (KLX01 and KLX02). /Drake and Tullborg 2004, 2006a, Milodowski 2005/. Range of inorganic CO_3 is indicated.*

Barite occurs as very small grains but is relatively frequently observed (microscopically; not during the core logging) together with calcite, pyrite and the Ba-zeolite harmotome. In saline groundwater samples with very low SO_4 contents anomalously high Ba contents have been identified. For example, this was the case for the deepest saline groundwater from the KOV01 borehole at Oskarshamn, pointing towards a possible barite solubility control on the Ba and SO_4 content in the water. Solubility has an impact or controls the behaviour of some major ions.

Fluorite occurs in several hydrothermal mineral associations; together with epidote and the later prehnite but also together with the lower temperature (150°C) generation with calcite, barite and pyrite (Figure 1-9). Fluorite can be assumed to partly control the F content in the groundwaters.

Gypsum is relatively rare but has been identified in several boreholes in the Laxemar subarea (Figure 1-9). The gypsum-containing fractures are usually located in borehole sections showing a low degree of fracturing and low (or not measurable) transmissivity. Groundwater modelling /Laaksoharju 2004/ suggests dissolution of gypsum as an explanation for the relatively high SO_4 contents in the saline Laxemar groundwaters. Although gypsum has not been identified during the extensive work in the Äspö HRL, it can not be ruled out that it has been overlooked, but probably is only present in some of the low transmissive, relatively unfractured parts of the rock.

1.4.3 Wall rock alteration

The red staining of the wall rock around many fractures and mapped fractures zones has been the subject to a larger study focussing on the mineralogical and chemical changes in the altered wall rock compared with fresh host rock, with special attention to redox reactions /Drake and Tullborg 2005, 2006bc/ and synthesised by /Drake 2006/. The major conclusions from the study are presented below.

The red staining is caused by oxidation in association with hydrothermal alteration and the colour results mainly from minute inclusions of Fe(III)-rich minerals, in most cases haematite. These are present in secondary pores in albite and K-feldspar (adularia) that are replacing primary plagioclase. The Fe-inclusions are mainly hosted in adularia, making these crystals appear more intensively red coloured than the paler red albite. Accompanying this alteration is haematitisation of magnetite, chloritisation of biotite (and hornblende and augite) and formation of secondary sericite, prehnite, grothite (titanite) and epidote. An increase in micro-porosity and micro-fractures during alteration is also observed. Minerals such as quartz, primary K-feldspar (micro-perthite and groundmass microcline) and titanite remained rather fresh during alteration. Approximate alteration temperatures are 250–400°C, based on indications from temperatures of chloritisation, prehnite formation, epidote formation, feldspar composition (thermometry) and the low-temperature paragenesis in general. Intense local red staining caused by haematite, and possibly also Fe-oxyhydroxide in micro-fractures, is thought to have been formed subsequently to the major red-staining event. /Eliasson 1993/ proposed this red staining to occur at temperatures of about 150–250°C.

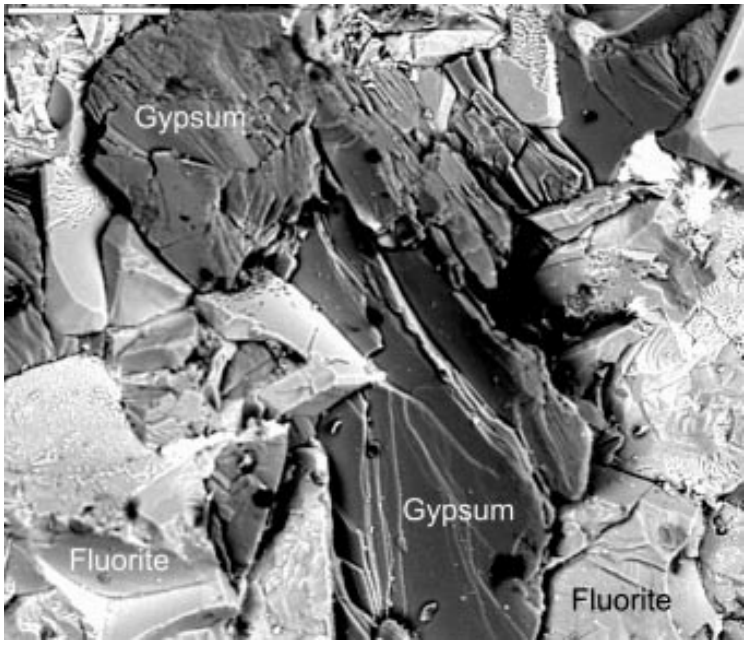

Figure 1-9. *Example of gypsum and fluorite in a fracture from KLX06:789 m /Drake and Tullborg 2006a/.*

The red-stained rock is highly enriched in K, Na, Rb as well as in H_2O; partial enrichment is evident in Ba, F and U. Significant depletion is recorded for Ca, Sr, Cs, Be, Ga and Cr whilst moderate depletion is evident for Al, Th, S and possibly Mn. The total Fe content, as well as related elements such as Ti, Mg, Sc, V and Co, remained fairly constant as well as Si, P, Y and the REEs. These elements are either redistributed and fixed in secondary minerals within a very limited rock volume, or completely fixed in resistant primary minerals during alteration.

Mössbauer analyses reveal that Fe^{3+} contents are elevated in the red-stained rock compared to the reference rock although the total Fe content remained fairly constant. This is caused by oxidation of magnetite to haematite and an increase in Fe(III)-bearing minerals such as epidote in the red-stained rock. The increase in Fe^{3+} is however not as high as the macroscopic features of the red-stained rock might suggest. The total increase in Fe^{3+}/Fe_{tot} is from about 3–10% in most of the samples. The mean Fe^{3+}/Fe_{tot} ratio in the Ävrö granite samples is 45% in the red-stained samples at around 48%. For the quartz-monzodiorite the mean Fe^{3+}/Fe_{tot} ratio is 36% and for the red stained samples around 39%. It can thus be concluded that despite the indicated oxidation (e.g. lower susceptibility) indicated around large fractures and deformation zones, there is still at least approx. 50% of the total Fe-content that remains as Fe(II). Drillcores from both the Simpevarp peninsula (KSH01 and KSH03) and from the Laxmear subarea (KLX04) have been studied and some differences are apparent between the two subareas which are shown in Figure 1-10.

Usually the ‘unaltered’ reference wall rock samples in this study were not completely unaltered and are characterised by chloritisation of biotite and partial alteration of plagioclase. These samples are however not extensively oxidised which shows that the hydrothermal alteration often reaches further into the wall rock than the oxidation does, which is in agreement with studies reported by /Landström et al. 2001/. Refer again to the schematic illustration of the characteristic features of the red staining in Figure 1-10.

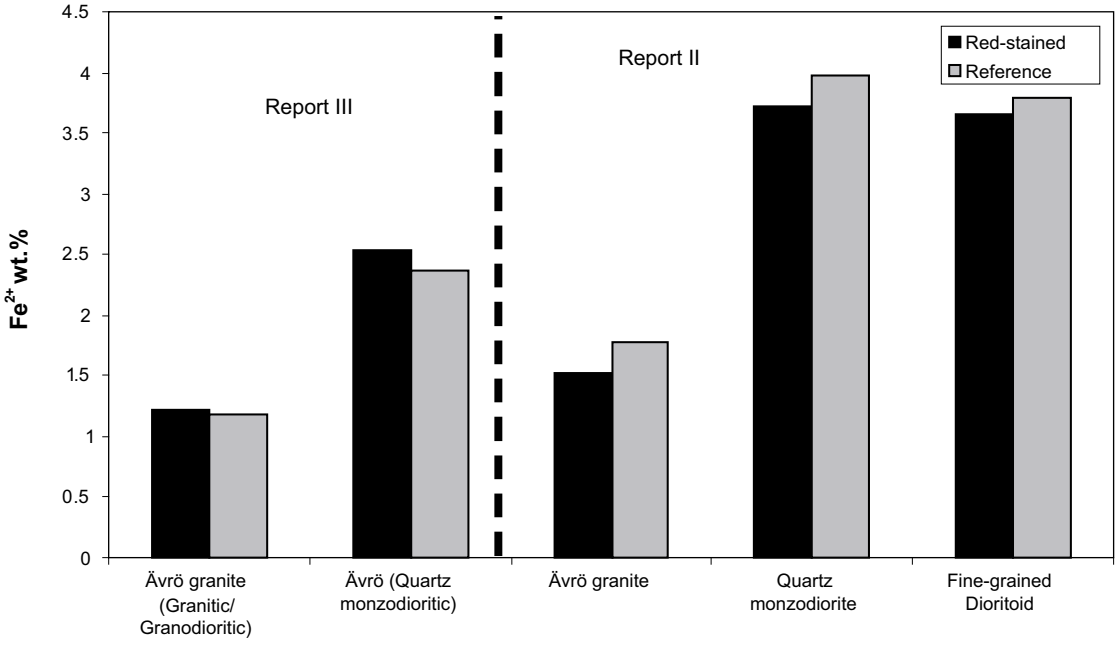

Figure 1-10. *Plot of Fe^{2+} contents in different rock types from the Simpevarp subarea /Drake and Tullborg 2005/ and Laxemar subarea /Drake and Tullborg 2006c/.*

2 Groundwater quality and representativeness

2.1 Background

The hydrogeochemical evaluation approach used in the Simpevarp area, the uncertainties involved and one of the objectives to identify representative or suitable hydrochemical data, are addressed in the methodology outlined in /Smellie et al. 2002/.

Prior to any hydrochemical evaluation is the necessity to judge the quality and the representativeness (or suitability) of the hydrochemical data derived from the site characterisation investigations. This should apply equally to borehole groundwaters (i.e. cored and percussion boreholes), to near-surface waters (shallow soil pipes and domestic wells) and to surface waters (i.e. Baltic Sea, streams, lakes and precipitation). However evaluating each location requires a different set of criteria and varying degrees of flexibility depending on the complexity of the sampled site. For example, surface waters may be subject to rapid seasonal fluctuations in chemistry and volume (and potentially microbial reactions) which contrasts to the deeper, more isolated bedrock groundwaters, although sampling at greater depth introduces additional problems. To evaluate representative or suitable data from all the sampled localities it is necessary therefore to consider a whole range of uncertainties of differing origin and importance.

The thoroughness of the data evaluation exercise will vary depending on the eventual use of the data and its origin, for example, high quality and complete borehole groundwater data are required to detect sensitive mixing or palaeoevolutionary trends (especially in the upper 300–500 m of the bedrock) and as input to geochemical equilibrium reaction modelling, whilst semi-quantitative (less complete) data may suffice to model large-scale lateral and vertical variations in groundwater chemistry or generally to distinguish time-series chemical trends during presampling monitoring and/or during the sampling interval. In contrast, for the reasons given above, hydrochemical data from surface and near-surface localities must be interpreted in more general terms because of the complex nature of the hydrochemical evolution through mixing and reaction.

It has been criticised by some of the field staff and reviewers that the evaluation approach employed for borehole groundwaters is too rigorous, revealing that less than 20% of the total number of water samples are considered to be representative or suitable for the Laxemar v. 1.2, inferring that there are large numbers of water samples that are not used and correspondingly much information lost. This is a common and understandable misconception. In reality all data provided by the SICADA database are available for use for all interested groups. However for each group to familiarise themselves with all the data is not practical given the time constraints. The selection of ‘representative’ or ‘suitable’ values is, therefore, severalfold, for example as an aid to help provide a degree of confidence or support (or otherwise) when using or interpreting other data which may be less reliable for different reasons (e.g. incomplete analyses; lack of chemical stability during sampling; contamination etc.). It is important also to point out that to arrive at ‘representative’ or ‘suitable’ values requires using all the available hydrochemical data, and that these data are evaluated as much as possible with reference to known hydraulic conditions in: a) the borehole, b) the fracture zone sections being sampled, and c) the surrounding host bedrock. The reliability of these data is therefore based as much as possible on prevailing hydraulic and geologic conditions during borehole drilling, monitoring and sampling. The fact that all the data are not used by all the groups is due more to a lack of time and resources and also the general need for a major input of hydrogeological expertise and modelling at the borehole scale to aid hydrochemical interpretation for which there is yet no adequate provision.

Without the integration of hydrochemistry, hydrogeology and borehole activities there is a great danger that data can be misrepresented. A major example of this is the open hole tube sampling carried out in KLX02 in 1993 and 1997 where the hydrochemical and isotopic data collected along the borehole has been accepted and modelled as representing the evolution of formation groundwater with depth in the surrounding host rock, despite reservations of open hole mixing noted by /Laaksoharju et al. 1995, Ekman 2001/, and more recently has been criticised during internal review. Other examples have included the use of tritium and radiocarbon data without considering closely enough: a) the possibility of induced mixing during borehole activities, b) natural dilution and radioactive decay of tritium with time when combining and comparing old and newly collected samples,

c) the potential surface input of tritium from the nearby nuclear power facilities, and d) lowering of detection levels throughout the years.

Of course there will be data which may be representative but will lack the full range of completed analyses or lack adequate background information to make a full evaluation possible. These data are also indicated in the database with the proviso that they should be used with caution.

2.1.1 Borehole data

The majority of representative or suitable hydrochemical data have been selected from borehole sampling where the borehole activity record is well documented and degrees of contamination and/or induced mixing can be evaluated at least semi-quantitatively. Contamination can be judged, for example, by plotting tritium against percentage drilling water, and using measured values with specifically defined limits, i.e. charge balance (± 5%) and drilling water component (< 1%), and supported qualitatively by expert judgement based on detailed studies of the distribution and behaviour of the major ions and isotopes.

The final selection of data which best represents the sampled borehole section is based on identifying as near as possible a complete set of major ion and isotope (particularly tritium, ^{18}O and deuterium) analytical data. This is not always the case, however, and a degree of flexibility is necessary in order to achieve an adequate dataset to work with. For example:

- A charge balance of ± 5% was considered acceptable. In some cases groundwaters were chosen when exceeding this range to provide a more representative selection of groundwaters. These groundwaters should be treated with some caution if used quantitatively.
- In many cases the drilling water content was either not recorded or not measured. Less or close to 1% drilling water was considered acceptable for suitable (representative) groundwaters. In some cases groundwaters were chosen when exceeding 1% (but < 5%) to provide a more representative selection of groundwaters (i.e. of limited suitability). Again these groundwaters should be treated with some caution if used quantitatively.
- Some of the older tritium data (before 2002) were analysed with a higher detection limit of 8TU; this detection limit was subsequently improved upon to around 0.8TU. For certain groundwaters an approximate tritium value is suggested where no recorded value is available. This value is selected normally from the same borehole section but representing an earlier or later sample from the same sampling campaign.
- In general it is recommended that for detailed modelling, only representative tritium data should be used that originate from the present site investigations, i.e. later than 2002.

Resulting from this assessment, two groundwater sample types are highlighted in the SICADA database; one type considered representative or suitable (in orange), the other type less representative or of limited suitability (in green) and should be used with caution.

Examples of data quality assurance

Figure 2-1, plotting all chloride data versus depth, provides an opportunity to compare quality assured representative (or suitable) data with unrepresentative (or unsuitable) data. For the Laxemar subarea the degree of groundwater representativeness is good down to a depth of approx. 400 m for the majority of samples; this is also the depth interval were there is most data. From approx. 400–700 m there is a greater variation in the salinity shown by the data as a whole, but less so when considering only the representative samples. From approx. 700–1,000 m there is an increased scatter in all data due to local hydraulic conditions affecting individual boreholes, but the representative data clearly indicate a distinct increase to greater salinity at around 800 m. From 1,000–1,700 m most of the data originate only from borehole KLX02, and there is a good overall correlation between the data types. Most of the unrepresentative data are from open hole tube sampling, deemed to be unsuitable with respect to some major ions other than chloride (see discussion below).

It should be noted that in the Laxemar subarea, the unrepresentative samples are in most cases less saline than the representative ones (when comparing samples from the same approximate depth)

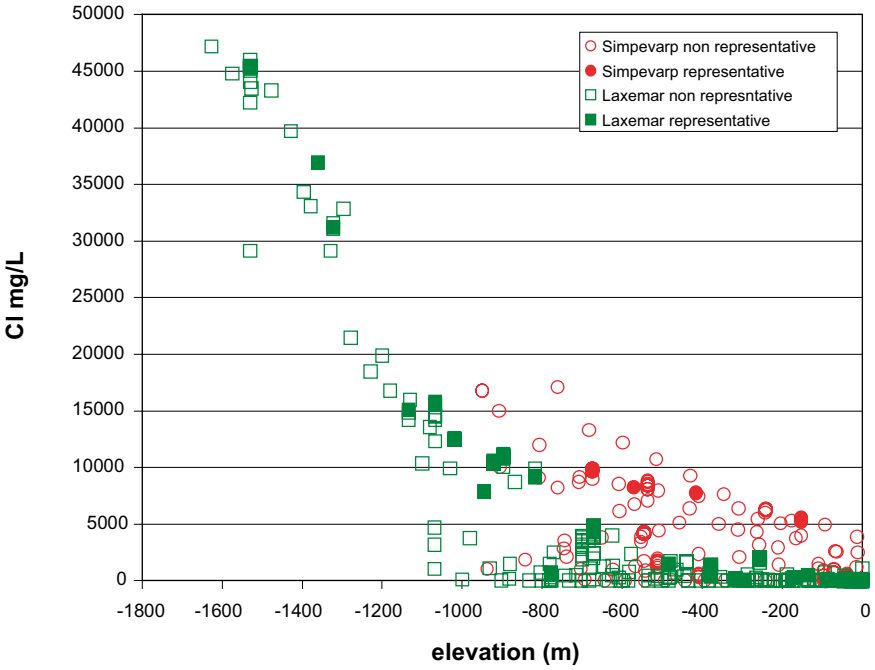

Figure 2-1. *All chloride data versus depth comparing representative with unrepresentative quality assured data.*

whereas in the Simpevarp subarea a number of unrepresentative samples are significantly more saline than the representative ones. This is in agreement with present understanding of the hydraulic conditions at the sites.

The value of data quality assurance is well illustrated by the Simpevarp subarea data. Figure 2-1 shows not only the overall increased salinity at shallower to intermediate depths (150–800 m), but also the wide scatter of values due to mixing/contamination. The representative samples, in contrast, show a regular increase in salinity with increasing depth; exceptions can be explained by borehole-specific hydraulic conditions.

Open hole tube sampling has been carried out in many of the cored boreholes listed in the Laxemar 2.1 data freeze. This approach can be very useful in evaluating borehole groundwater circulation pathways and groundwater budgets (e.g. water in and water out between the borehole and surrounding bedrock). Understanding these processes can help greatly in assessing water quality and representativeness. However, since these groundwaters are mixed to varying degrees due to borehole hydraulics, the borehole activities prior to sampling, and also perturbation during lowering and raising of the tube system in the borehole, their representativeness (or suitability) to describe the bedrock formation waters is questionable. Only at greatest depths where highly dense and saline groundwaters are typical, might they be considered more representative.

Consequently, all groundwater samples relating to the SICADA tube sampling data contained in the Laxemar 2.1 data freeze are considered unsuitable.

The bromide problem

Whilst checking the consistency range of various major ions, some anomalous features became evident in the bromide data, initially from the Baltic Sea samples but also evident in some of the borehole groundwater data. Under greater scrutiny it became apparent that these anomalously high bromide values were restricted to analyses carried out between September 2004 and March 2005 (see Figures 2-2 and 2-3). Consequently it is recommended that these discrepancies are checked with the laboratory and steps taken to reanalyse specifically the borehole samples.

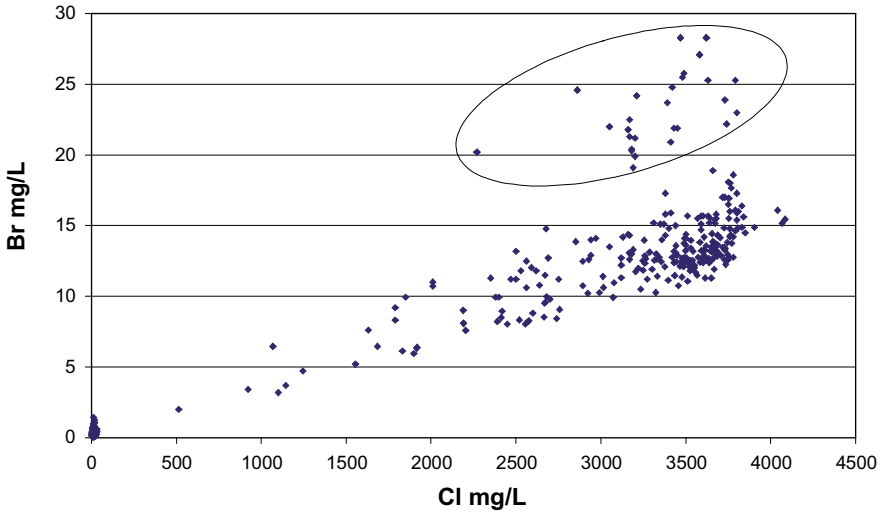

Figure 2-2. Baltic Sea samples: Bromide versus chloride showing the high bromide outlier (ringed) sampled and analysed during the period September, 2004 to March, 2005. Note: A similar pattern is obtained by plotting bromide versus magnesium.

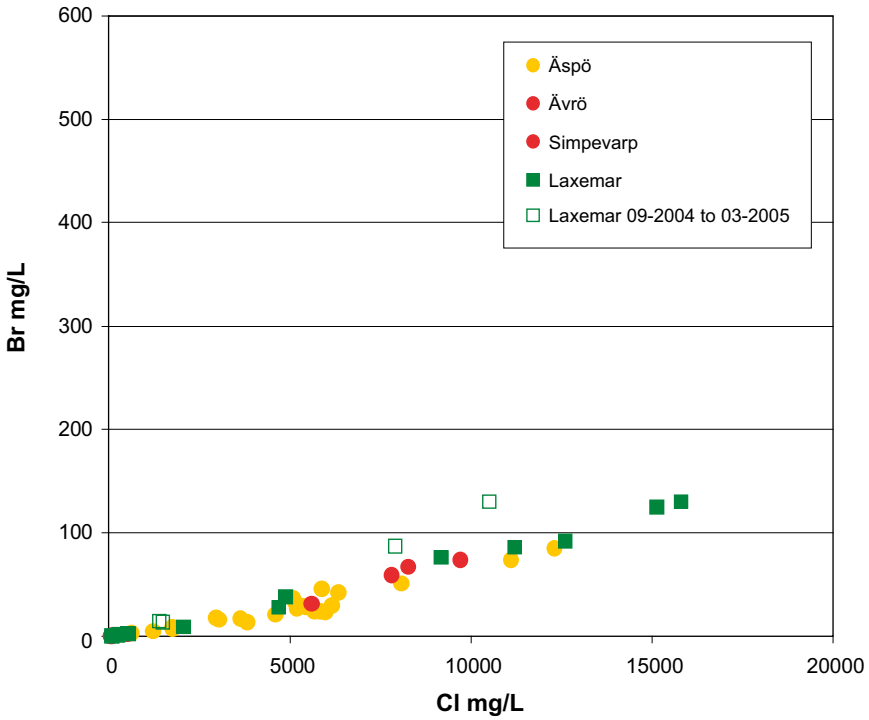

Figure 2-3. Borehole groundwater samples: Bromide versus chloride showing the two higher bromide values sampled and analysed during the period September, 2004 to March, 2005.

2.1.2 Shallow soil pipe data

Some of the soil pipes have been drilled in locations to monitor changes in the near-surface groundwater chemistry during percussion and core drilling of nearby deep boreholes. The remaining soil pipes have been located solely to monitor the natural undisturbed near-surface groundwater system.

An attempt was made to choose early or 'First-Strike' samples provided that there was no recorded major contamination with soil particles, that there were adequate analytical data and that the charge balance was within the ± 5% range. The analytical data considered most important are the major ions

and the environmental isotopes: tritium, ^{18}O and deuterium. Preferably ^{14}C (pmC) is also available, but this is not the case for all the selected soil pipe samples.

Of importance are data relating to seasonal changes over a period of months to years. Therefore, when a time-series of samples from the same campaign are available from a single location, all samples are considered for final evaluation if the analytical data listed above are complete. When only a single sample is available, it is recommended to be used with caution since the chemistry is inadequate to indicate whether there is any seasonal fluctuation or not. Suitable samples are highlighted in green in the Laxemar 2.1 data base.

2.1.3 Baltic Sea water samples

A large number of samples have been collected over a period of approx. 24 months ranging from the open Baltic Sea, to coastal areas comprising bays and coves, some of which border active freshwater drainage discharge areas of varying importance. From a hydrochemical viewpoint, the important selection criteria are:

- A representative Baltic Sea end member for the Simpevarp area latitude which has not been influenced by freshwater discharge.
- Representative compositions from coastal Baltic Sea localities which may be in hydraulic contact at depth with the mainland where deep boreholes are located.

Since presently there are inadequate data to assess the coastal locations, and more open Baltic Sea samples are being planned, it is not known which samples best represent the Baltic Sea end member. Consequently, the selection of waters at this juncture considered to be suitably close to a Baltic Sea end member for this latitude have been based on the charge balance (± 5%), chloride content within the range of 3,500–3,800 mg/L and complete environmental isotopes of tritium, ^{18}O, and deuterium (highlghted in green in the Laxemar 2.1 database). Samples restricted only to major ion analytical data also have been recommended for use (highlighted in pink).

2.1.4 Lake and stream water samples

Surface water samples have been evaluated based on charge balance (± 10%) and the presence of major ions and isotopic data. In common with some of the soil pipe groundwaters, these surface waters may have been subject to seasonal fluctuations, complex reaction processes in the biosphere and potential discharge influences. Consequently, in the absence of knowing what could be representative or not, all selected samples that conform to the above criteria are recommended at this juncture (highlghted in green in the Laxemar 2.1 database). Samples restricted only to major ion analytical data have also been recommended for use (highlighted in pink).

2.1.5 Precipitation

Fifty three samples are included, collected during an approx. two year nine month period. These waters have not undergone any representativity check *senso stricto*. On the other hand, the main intention has been to monitor $\delta^{18}O$, δD and tritium, since these parameters are used to identify modern meteoric groundwater components at depth. Disturbances, such as unpredictable annual and seasonal trends and possible evaporation, have not been evaluated in this present representativity check.

Because of the difficulty of assessing representativeness, suitable samples with isotopic values and adequate major ion data are highlighted in green in the Laxemar 2.1 data base.

2.1.6 Driling samples

In cases ’Drilling Samples’ are included in the data base (i.e.. KLX07, KLX07B, KLX08). Since these represent large components of drilling water mixed with formation groundwaters sampled during core drilling, they are not considered useful in the present hydrochemical evaluation.

2.1.7 Rock pore waters

Boreholes KLX03 and KLX08 have been sampled for rock pore water studies. Data from both boreholes are available in SICADA as separate folders and form part of the Laxemar 2.1 data freeze evaluation. The assessment of these data must be based on criteria which differ from those used for the formation groundwaters. Since the representativeness of the rock pore water can be influenced by several variables, for example rock stress/contamination and experimental artefacts, at this stage the data should be used with caution.

2.1.8 Nordic sites

Hydrogeochemical evaluation of the Laxemar subarea entails comparison with other geographically-located sites in its near-vicinity, i.e. Simpevarp, Äspö, Ävrö and Oskarshamn, and also other Fennoscandian sites such as Forsmark and Olkiluoto. Groundwater data from all these sites are compiled in the 'Nordic Table' and these data also have been evaluated with respect to their suitability. This was carried out in parallel to the evaluation of the Simpevarp v. 1.2 and Forsmark v. 1.2 data /Laaksoharju 2004, 2005/ and also involved earlier evaluations /e.g. Smellie and Laaksoharju 1992, Laaksoharju et al. 1995, Pitkänen et al. 1999, 2004/.

2.2 The Laxemar 2.1 evaluation

The Laxemar 2.1 database, extracted from SICADA, comprises data from: a) the Simpevarp 1.2 database (i.e. from the Simpevarp, Äspö, Ävrö and Laxemar sites), b) the Laxemar 1.2 database (i.e. from the Simpevarp, Ävrö and Laxemar sites, and c) recent data acquired since the Laxemar 1.2 data freeze (i.e. from the Laxemar, Ävrö and Simpevarp sites). In addition to recent data from new locations, additional data from existing Laxemar 1.2 locations are also included. These additional data mainly comprise the inclusion of isotopic and other analytical data which were not available at the Laxemar 1.2 data freeze stage. Also included are some new data originating from the resampling of old locations or resulting, for example, from hydraulic pump-tests conducted after the Laxemar 1.2 data freeze.

In common with the Simpevarp and Laxemar 1.2 databases, the tritium data for Laxemar 2.1 have been normalised to represent today's tritium levels (both measured and corrected are given in the database). Although the corrected values may in cases be more representative, it is impossible to derive true values because widespread mixing (natural and artificial) of the groundwaters has diluted and perturbed the original recharge tritium levels. As mentioned above the detection limits have changed over time so that the data from the pre-site investigation studies are less reliable. Special care is needed when using the tritium values (normalised or not normalised) for modelling purposes.

2.3 The Laxemar site

Site characterisation of the Laxemar subarea has included so far the drilling of up to 34 percussion drillholes (HLX01–34) to vertical depths varying from approx. 70–200 m, and eight cored boreholes (KLX01–08) of which KLX01 extends to 1,078 m, KLX02 to 1,705 m, KLX03, KLX04, KLX05 and KLX08 to around 1,000 m, KLX06 to 850 m, and KLX07 to 830 m. Boreholes KLX01 and KLX02 are subvertical whereas KLX03 is inclined at 75°, KLX05, KLX06, KLX07 at 65° and KLX08 at 60°. Of all these boreholes, percussion boreholes HLX01–08, 10, 14, 18, 20, 22, 24, 28 and 34, and cored boreholes KLX01, 02, 03, 04, 05, 06, 07 and 08, are included in the Laxemar 2.1 data freeze database. Figures 1.4 and 2.1 show the locations of the boreholes in the Simpevarp area.

Representativity checks have been carried out already in the Laxemar 1.2 data freeze database for the earlier drilled HLX01–08, 10, 14, 18, 20, 22 and 24 percussion boreholes and the KLX01, 02, 03, 04 and 06 cored boreholes /Laaksoharju 2006/. The remainder of the groundwaters sampled and analysed for the Laxemar 2.1 data freeze database are evaluated below (HLX28 and 34, and KLX05, 07, 08 and 10) and judged to be suitable, of limited suitability or unsuitable. It is important to note that some groundwaters considered suitable from the Laxemar 1.2 evaluation have been downgraded due to additional and more quantitative information contained in the Laxemar 2.1 data freeze (see Chapter 4).

2.3.1 Percussion boreholes

Borehole HLX28

Borehole HLX28 was drilled to a length 154.20 m at an inclination of ~ –60° to the horizontal, cased to 5.94 m length and was executed to characterise deformation zone ZSMNW042A (Figures 1-1 and 1-2). One groundwater sample (Class 3) was taken from the total borehole length; groundwater inflow to the borehole is greatest at 80–154.4 m.

Analytical data are restricted to HCO_3, Cl, SO_4, Br and F. The groundwater is very dilute (23 mg/L Cl) and probably Na-HCO_3 in type.

Representativity: Limited suitability because of inadequate analytical data.

Borehole HLX34

Borehole HLX34 was drilled to a depth of 151.80 m with the purpose of confirming deformation zone ZSMN001A. There are no available groundwater analytical data.

Representativity: Unsuitable.

Borehole KLX07B

Only drilling samples available showing drilling water concentrations. Not of direct use in the Laxemar 2.1 hydrogeochemical evaluation; recommended deletion from the Laxemar 2.1 database.

Figure 2-4. Location of hydrogeochemically prioritised boreholes KLX01, KLX02, KLX03, KLX04, KLX05, KLX06, KLX07 and KLX08 in the Laxemar subarea. Also indicated are the percussion boreholes (HLX01–33), many of which are included in the Laxemar v. 2.1 evaluation.

2.3.2 Cored boreholes

Boreholes KLX01 and KLX02

Since the Laxemar 1.2 data freeze additional data from boreholes KLX01 and KLX02 have been restricted to electrical conductivity and density measurements of water pumped from packed-off borehole sections during cleaning.

In KLX01 these have comprised borehole sections 171–190 m, 191–704 m and 705–1,078 m and the electrical conductivity values show a close range from 46.0–50.1 mSm^{-1} (i.e. < 30 mg/L Cl). In borehole KLX02 the sections measured were: 0–208 m, 209–347 m, 348–451 m, 452–494 m, 495–717 m and 718–1,144 m (electrical conductivity ranging from 43.6–49.5 mSm^{-1}, i.e. < 30 mg/L Cl), 1,145–1,164 m (155 mSm^{-1}, i.e. ~ 600 mg/L Cl) and 1,165–1,700 m (101 mSm^{-1}, i.e. ~ 500 mg/L Cl).

These measurements support the depths at which relatively recent, meteoric-derived groundwaters appear to have penetrated under natural recharge conditions.

Figure 2-5 represents a recent hydraulic correlation of pump tests and differential flow logging with observed open fractures. This correlation further underlines the fact that the upper ~ 350 m and from ~ 750–1,100 m the bedrock is markedly fractured and of moderate to high transmissivity. These two main fractured intervals or fracture zone intersections have controlled the groundwater circulation along the open borehole resulting in the mixing of different groundwater types. From the observed systematic increase in salinity (and other components) from samples selected along the borehole (i.e. Tube sampling method) thus gives an erroneous impression of the system and therefore their exclusion from the hydrogeochemical evaluation.

Borehole KLX03

Borehole KLX03 (Figure 2-4) was drilled to a vertical depth of 1,000.42 m; percussion drilling was initially carried out to 100.35 m followed by casing to this depth prior to the core drilling phase. The sequence of borehole activities since the Laxemar 1.2 data freeze is presented in Appendix 1, Table 1-1; the borehole activities prior to these are reported in /Laaksoharju 2006; Table 2.1/.

Details of borehole hydraulics and salinity profiles have been already presented, interpreted and discussed in /Laaksoharju 2006/. Groundwater samples from isolated packed-off borehole sections were taken on several occasions (Appendix 1, Table 1-1).

Figure 2-6 represents a recent hydraulic correlation of pump tests and differential flow logging with observed open fractures /Forssman et al. 2005/. This provides a convenient visualisation to help interpret the nature and quality of the sampled groundwaters.

Evaluation of new data

Borehole section 193.50–198.30 m

Sampling was carried out during a 11 day period. The data show consistent stability in the measured and analysed parameters during this period together with an acceptable charge balance (within ± 5%) and low drilling water content (< 0.3%). Although all groundwater samples can be considered suitable, the last sampled groundwater in the series was chosen to be most representative. The groundwaters at this level are shallow in origin and meteoric ($\delta^{18}O$ = –11.5‰ SMOW, δD = –84.8‰ SMOW), dilute (259 mg/L Cl), and Na-HCO_3 in type with a modern component (0.76 TU).

Representativity: Suitable and highlighted in orange in the database.

Borehole section 103.00–218.02 m (sampled during drilling)

In the Laxemar 1.2 evaluation, groundwater sampled during drilling from this level was considered suitable, mostly based on little drilling water contamination (1.02%), a charge balance which was only slightly high (–5.898) and a fairly complete set of data. In contrast with the 193.50–198.30 m level described above, this groundwater from a much longer borehole section is slightly more saline (507 mg/L Cl) and is also characterised by a cold recharge isotopic signature

($\delta^{18}O$ = –12.7‰ SMOW, δD = –89.7‰ SMOW). Based on the now available data, the higher salinity and cold climate signature may reflect an isolated pocket/lens initially intercepted by the borehole at an unknown depth. Alternatively, it could simply represent a mixed component of deeper groundwater(s) (see deeper levels described below) which tend to be brackish and contain a larger cold climate component. Because of this present doubt as to its origin, this sampled borehole section should now be considered of limited suitability.

Representativity: Limited suitability and highlighted in green in the database.

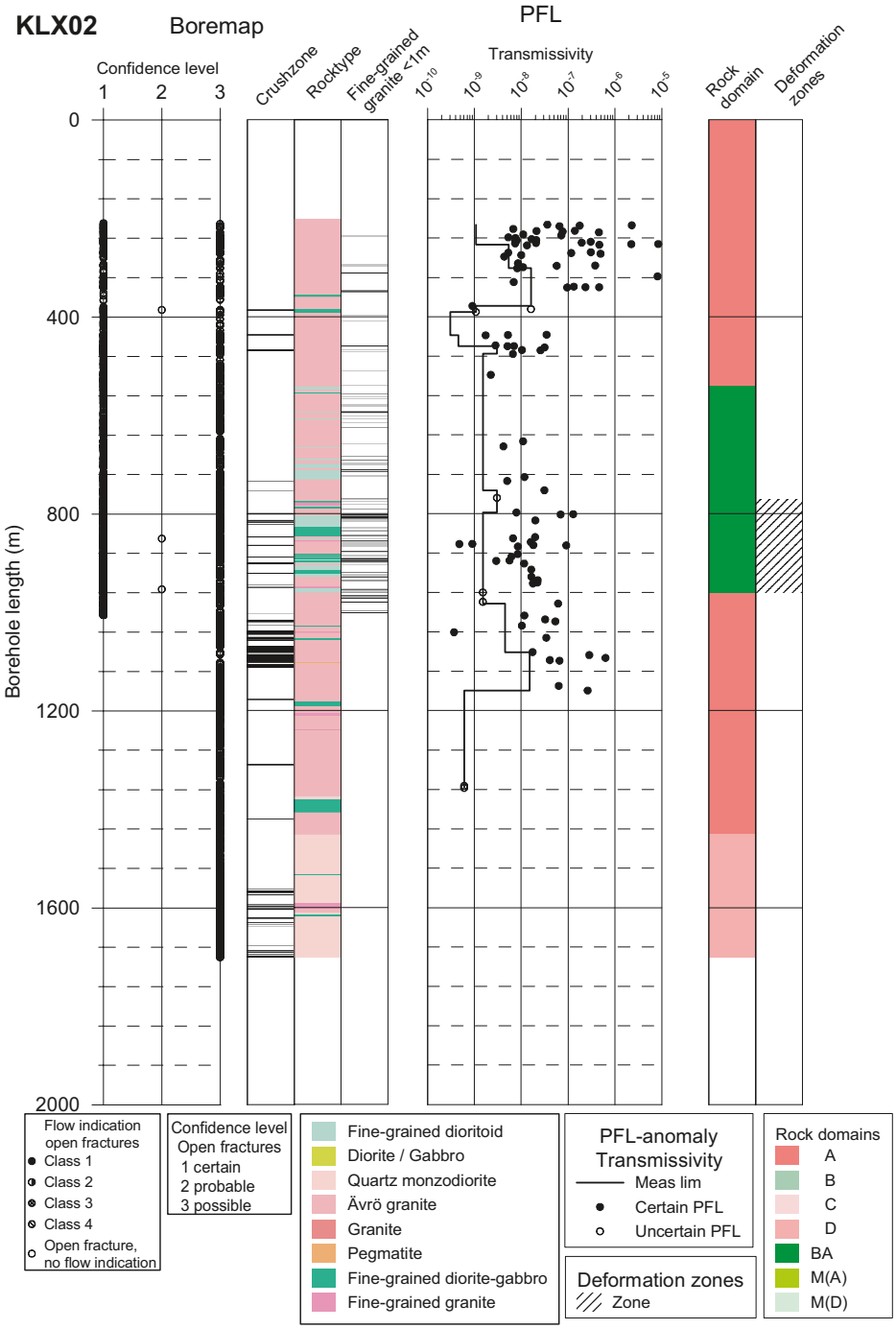

Figure 2-5. *Correlation of hydraulic features, based on PFL (i.e. pump and differential flow log data), overlapping measurements, to mapped open/partly open fractures (i.e. all plotted as open fractures above) or crush zones in KLX02. Interpreted deformation zones (i.e. mainly brittle or ductile) and Rock Domains are shown to the right. Fractures with PFL confidence > class 4 are not plotted. After /Forssman et al. 2005/.*

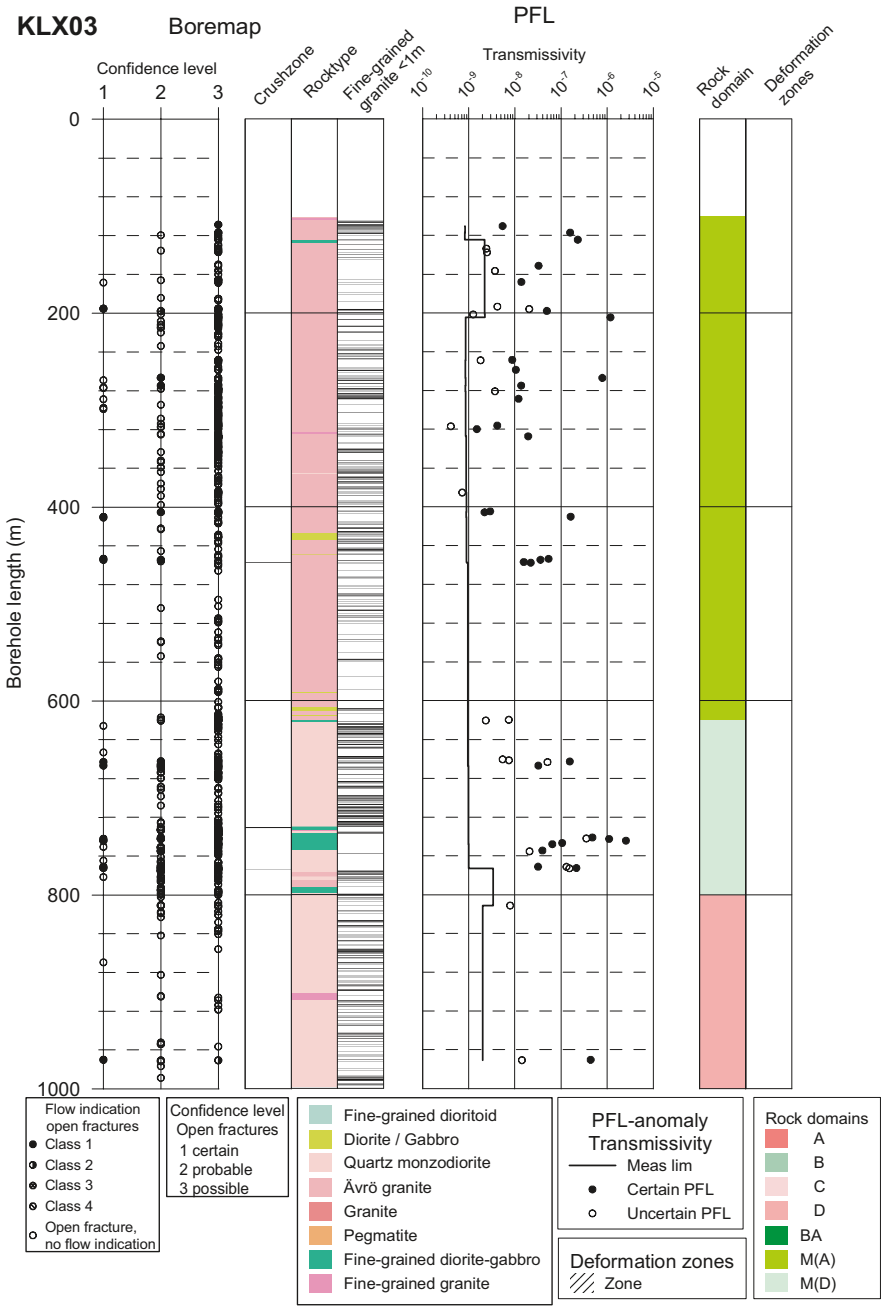

Figure 2-6. *Correlation of hydraulic features, based on PFL (i.e. pump and differential flow log data), overlapping measurements, to mapped open/partly open fractures (i.e. all plotted as open fractures above) or crush zones in KLX03. Interpreted deformation zones (i.e. mainly brittle or ductile) and Rock Domains are shown to the right. Fractures with PFL confidence > class 4 are not plotted. After /Forssman et al. 2005/.*

Borehole section 408.00–415.30 m

Sampling was carried out during a 29 day period. The data available show reasonable consistency in the measured and analysed parameters during this period together with an acceptable charge balance (within ± 5%). Although the drilling water content is low it is variable (0.72–3.3%) and mostly exceeds the 1% threshold. Unfortunately the analytical data are incomplete because of an absence of isotope information and therefore a quantitative assessment of representativeness is not possible. The last sampled groundwater in the series was chosen to be of limited suitability based only on major element data, and should be used therefore with caution. The groundwaters at this level are Na(Ca)-Cl(HCO_3) in type with a salinity of around 1,400 mg/L Cl and therefore probably intermediate in origin in relation to the shallower dilute types and the deeper brackish groundwaters.

Representativity: Limited suitability because of an incomplete data set (namely isotopes) and a slightly high drilling water component of 1.88%.

Borehole section 497.02–599.89 m

This groundwater, consisting of one sample and collected during drilling some 6 months earlier than section 408.00–415.30 m above, has now a fairly complete analysis of major ions and isotope data and an acceptable charge balance (< ± 5%). It is dilute (381 mg/L Cl) and Na-HCO_3 in type, meteoric in origin, not recent (0.8 TU; 47.52 pmC) and the isotopic data suggest a cold climate isotopic signature ($\delta^{18}O$ = –11.7‰ SMOW, δD = –85.2‰ SMOW). The drilling water content is significantly high (5.15%).

Representativity: Unsuitable because of significant drilling water contamination and mixing with shallower, more dilute formation groundwaters, characteristic of the borehole when initially sampled during drilling /Laaksoharju 2006/.

Borehole section 600.00–695.40 m

Sampled during drilling and considered unsuitable because of an excessively high drilling water content of 102.00% /Laaksoharju 2006/.

Representativity: Unsuitable; recommended deletion from the Laxemar 2.1 database.

Borehole section 660.00–671.00 m

Borehole section was sampled once every day for 3 days but only the final groundwater was analysed for the major ions Cl, HCO_3, SO_4, Br and F; drilling water registered 9.67%. The groundwater is brackish (4,010 mg/L Cl) and probably Na(Ca)-Cl(SO_4) in type.

Representativity: Unsuitable because of excessive drilling water contamination.

Borehole section 692.86–761.11 m

This sample was collected initially during drilling /Laaksoharju 2006/ and now there are additional isotope data available for this present Laxemar 2.1 evaluation. Major ion analyses are complete together with isotope data (tritium and stable isotopes); charge balance (within ± 5%) is acceptable. This groundwater is brackish (3,550 mg/L Cl) and Na(Ca)-Cl(SO_4) in type, contains a younger groundwater component (1.5TU) and has a significant cold climate signature ($\delta^{18}O$ = –13.1‰ SMOW, δD = –96.5‰ SMOW). The drilling water content is excessively high (30.30%).

Representativity: Unsuitable because of excessive drilling water contamination. Limited qualitative use in supporting the presence of brackish groundwaters with a significant cold climate recharge component at this depth.

Borehole section 735.50–748.03 m

Sampling was carried out during a 33 day period. The chloride data indicate a degree of stability after 15 days (1,840–3,480 mg/L) but a more consistent stability took a further 10 days finally recording values of around 3,950 mg/L Cl. The other ions showed similar increases with time consistent with an increase in salinity; HCO_3 showed a corresponding decrease from 163–33.5 mg/L. Although an acceptable charge balance is indicated (within ± 5%), the drilling water content is high, increasing during the sampling period from 2.79% to a maximum of 10.8% for the final collected sample in the series. Tritium content of the final sample is 1.2TU. This reduction of more dilute groundwaters of shallower origin and a corresponding increase in drilling water and salinity with time was predicted in /Laaksoharju 2006/.

The last sampled groundwater in the series has an almost complete set of data showing that groundwaters at this level are Na(Ca)-Cl(SO_4) in type and brackish in character. The isotope data indicate a strong cold climate signature ($\delta^{18}O$ = –13.6‰ SMOW, δD = –92.1‰ SMOW) which is probably representative for this level as the shallower groundwaters show typical recent to modern recharge signatures (see above). The tritium content of 1.2TU can be explained partly by a contaminating drilling water component (3.8TU) which originates from percussion borehole HLX14.

Representativity: Unsuitable because of incomplete analytical data (e.g. carbon isotopes) and a high content of 10.8% drilling water. Qualitative use in establishing the presence of brackish groundwaters with a significant cold climate signature at this depth.

Borehole section 964.00–975.00 m

Sampling was carried out during a 20 day period. With the exception of one sample collected midway through the series, the bulk of data show good consistency in the measured and analysed parameters during this period together with an acceptable charge balance (within ± 5%) and a correspondingly very low drilling water content (< 0.15%). Unfortunately the carbon isotope data are not available yet. The last sampled groundwater in the series was chosen to be representative.

The groundwaters at this level are typical of the saline (10,500 mg/L Cl) Ca-Na-Cl(SO_4) type, probably old (0.8TU; carbon data lacking) and non-marine in origin. The cold climate signature is somewhat less ($\delta^{18}O$ = –12.2‰ SMOW, δD = –94.8‰ SMOW) than the previously described shallower levels characterised by brackish groundwaters.

Representativity: Suitable and highlighted in orange in the database.

Borehole KLX04

Borehole KLX04 (Figure 1-1) was drilled to a depth of 993.49 m, at an angle of –84.68° to the horizontal, using flushing source HLX10; percussion drilling was initially carried out to 100.40 m followed by casing prior to the core drilling phase. The sequence of borehole activities since the Laxemar 1.2 data freeze is presented in Appendix 1, Table 1-2; the borehole activities prior to these are reported in /Laaksoharju 2006; Table 1.1/.

Details of borehole geology, hydraulics and salinity profiles have been presented already and interpreted and discussed in /Laaksoharju 2006/. Additional reporting of hydraulic tests at different measurement scales of 100 m and 20 m borehole sections have subsequently become available /Rahm and Enachescu 2005a/. Transient evaluation during the flow and recovery period provided additional information such as flow regimes, hydraulic boundaries and cross-over flows. From a hydrochemical viewpoint, these measurements basically confirm the differential flow measurements used in the Laxemar 1.2 evaluation.

Figure 2-7 represents a recent hydraulic correlation of pump tests and differential flow logging with observed open fractures /Forssman et al. 2005/. This provides a convenient visualisation to help interpret the nature and quality of the sampled groundwaters.

Evaluation of new data

Borehole section 0–162 m

No analytical data available; only measured electrical conductivity and density from water pumped from packed-off borehole sections during cleaning.

Representativity: Unsuitable; recommended deletion from the Laxemar 2.1 database.

Borehole section 0–976.21 m

No analytical data available; small amount of drilling water contamination (1.59%).

Representativity: Unsuitable; recommended deletion from the Laxemar 2.1 database.

Borehole section 0–993.49 m

No analytical data available; high drilling water contamination (1.19–43.3%) measured during a 1 day period.

Representativity: Unsuitable; recommended deletion from the Laxemar 2.1 database.

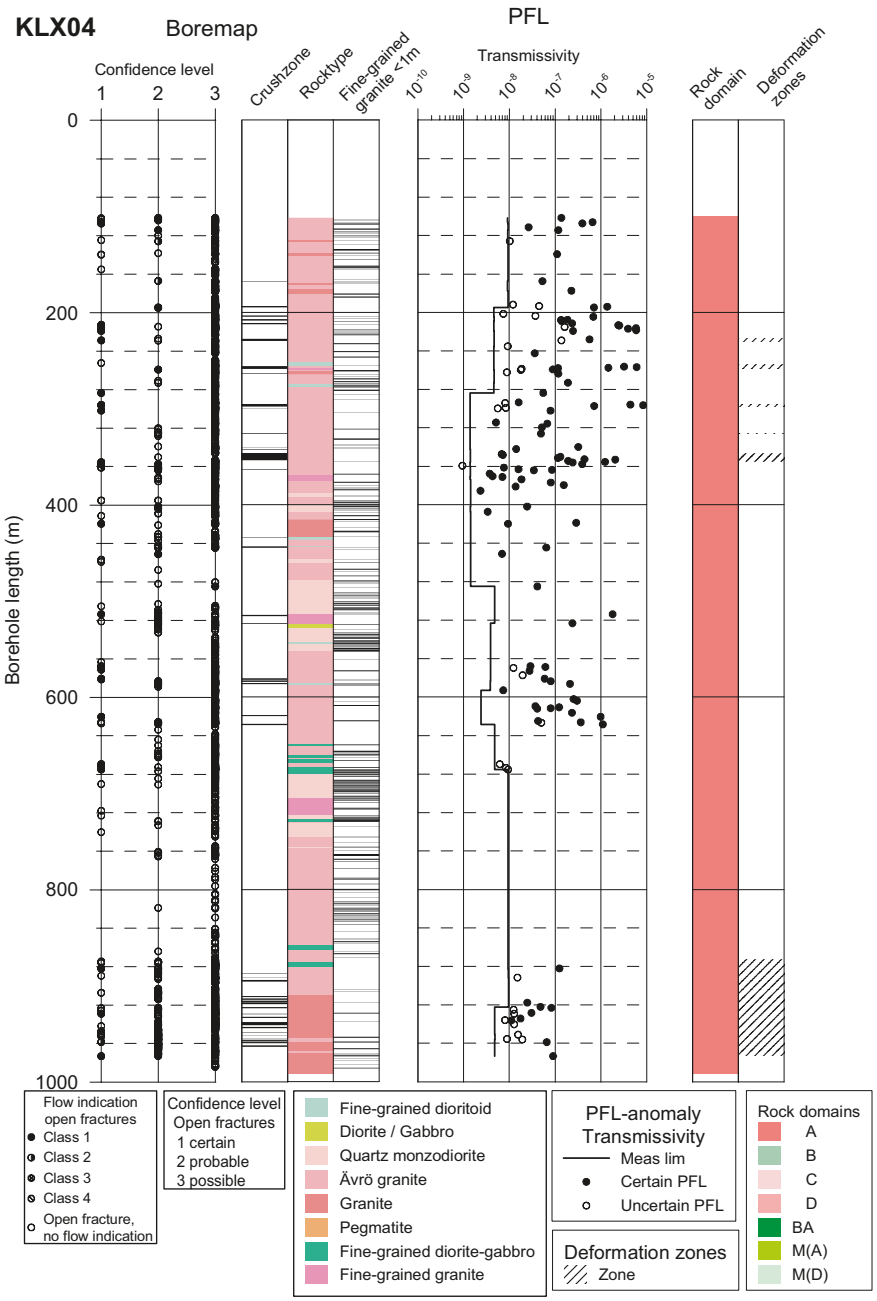

Figure 2-7. *Correlation of hydraulic features, based on PFL-overlapping measurements, to mapped open/partly open fractures (all plotted as open fractures above) or crush zones in KLX04. Interpreted deformation zones (mainly brittle or ductile) and Rock Domains shown to the right. Fractures with PFL confidence (flow indication class above) > 4 are not plotted. After /Forssman et al. 2005/.*

Borehole section 104.00–109.00 m

This groundwater series of three samples was collected over a period of 4 hours; there are sufficient data for only one sample, although the carbon isotope data are still not available. The groundwater has an acceptable charge balance (within ± 5%) and an insignificant drilling water content (0.09%).

The groundwater is dilute (23.5 mg/L Cl) and Na-HCO_3 in type, meteoric in origin, recent (5.4 TU) and has a present-day recharge isotopic signature ($\delta^{18}O$ = –10.3‰ SMOW, δD = –75.3‰ SMOW). The high tritium is typical for these depths, for example the flushing water from HLX10 (0–85 m) records 7.2TU.

Representativity: Suitable and highlighted in orange in the database.

Borehole section 103.00–213.14 m

This groundwater has a fairly complete analysis. It is dilute (28.6 mg/L Cl) and Na-HCO_3 in type, meteoric in origin, recent (4.1 TU; 61.3 pmC) and has a present-day recharge isotopic signature ($\delta^{18}O$ = –10.8‰ SMOW, δD = –76.8‰ SMOW). Furthermore the charge balance is acceptable (–1.026) but unfortunately the drilling water content is high (7.76%).

Representativity: Unsuitable; high drilling water contamination.

Borehole sections 163–230 m, 210–329 m, 329–403.82 m, 231–506, 401–515 m

Sections 210–329 m, 329–403.82 m and 401–515 m were sampled during drilling; sections 163–230 m and 231–506 m were sampled later following borehole pumping/cleaning and following tube sampling. No or little analytical data are available; excessive drilling water contamination when available (40.7–96.6%), i.e. for sections 210–329 m, 329–403.82 m and 401–515 m.

Representativity: Unsuitable; recommended deletion from the Laxemar 2.1 database.

Borehole section 510.00–515.00 m

Sampling was carried out during a 10 day period but full analysis was only carried out on the final sample of the series; an earlier sample was analysed for the major ions Cl, HCO_3, SO_4 and Br. Although only two chloride data are available for the series, these nevertheless indicated a degree of stability after 4 days (1,480 mg/L Cl) which continued to the final sample taken 6 days later (also 1,480 mg/L Cl). This was also reflected in the HCO_3, SO_4 and Br. Although an acceptable charge balance is indicated (within ± 5%), the drilling water content is high, increasing during the first 3 days from 1.79–7.25% and then decreasing slightly erratically to 4.41% for the final sample in the series. Tritium content of the final sample is 1.2TU.

The last sampled groundwater in the series has an almost complete set of data showing that groundwaters at this level are Na(Ca)-Cl(SO_4) in type, old (43.29 pmC) but still quite dilute (1,480 mg/L Cl). However some of this dilution may reflect the influence of the drilling water component (and also some shallower groundwaters) and thus the formation groundwater may be more brackish in type. The isotope data indicate a strong cold climate signature ($\delta^{18}O$ = –15.10‰ SMOW, δD = –112.9‰ SMOW) which is probably representative for this level as the shallower groundwaters show typical recent to modern recharge signatures (see above). The tritium content of 1.2TU most likely reflects: a) contaminating drilling water component which originates from percussion borehole HLX10 (7.2TU), and b) mixing of young meteoric groundwaters from shallower depths.

Representativity: Limited suitability because of the 4.41% drilling water. Good qualitative use in establishing the presence of dilute/brackish groundwaters with a significant cold climate signature at this depth. Highlighted in green in the database.

Borehole sections 507–530 m, 531–685 m, 614–701.16 m, 698–850.40 m, 686–869 m, 870–897 m, 849–993.49 m, 898–1,000 m

Sections 614–701.16 m, 698–850.40 m and 849–993.49 m were taken during drilling, the others taken some 7 months later. No or little analytical data available; excessive drilling water contamination when measured (91.10–105%%) apart from sections 507–530 m (0.07%) and 870–897 m (0.17%).

Representativity: Unsuitable; recommended deletion from the Laxemar 2.1 database. However sections 507–530 m and 870–897 m could be retained if further analysis is on-going.

Borehole section 971.21–976.21 m

Sampling was carried out during an 8 day period; an almost complete analysis (e.g. lacking carbon isotopes) was carried out on only one sample collected on the final day. A further sample was only analysed for the major ions Cl, HCO_3, SO_4 and Br. However the drilling water content was measured for all 13 samples.

Only two chloride data are available for the series and both of these were measured on the final day, so there is no time series to gauge whether stability had been achieved. The drilling water component however indicates a decrease from 77.80–8.89% during the first 5 days and from 6.62–3.94% during the following 3 days; there is a suggestion that during the final 2 days there was a levelling out of values thus prompting sampling for complete chemical analysis at this stage.

The sampled groundwater is Ca(Na)-Cl(SO_4) in type, not recent (0.76TU), brackish (7,910 mg/L Cl) and has a significant cold climate component ($\delta^{18}O$ = –13.8‰ SMOW, δD = –112.9‰ SMOW), although less so than the shallower level at 510–515 m.

Representativity: Limited suitability because of the 3.95% drilling water. Good qualitative use in establishing the presence of dilute/brackish groundwaters with a significant cold climate signature at this depth. Highlighted in green in the database.

Borehole section 971.26–976.21 m

No analytical data available; high to excessive drilling water contamination when measured (3.94–79.40%).

Representativity: Unsuitable; recommended deletion from the Laxemar 2.1 database.

Borehole section 971.26–976.21 m

Small packer adjustment and continued sampling on the same day. No analytical data available but drilling water contamination showed a small decrease from 4.11 to3.94% over a period of 4–5 hours.

Representativity: Unsuitable; recommended deletion from the Laxemar 2.1 database.

Borehole section ? – groundwater samples 7738,7739???

Sampling period is not registered in the activity logs. No analytical data available only drilling water contents ranging from 72.7–79.4%.

Representativity: Unsuitable; recommended deletion from the Laxemar 2.1 database.

Borehole KLX05

Borehole KLX05 (Figure 1-1) was drilled at an inclination of –65° from the horizontal to a length of 1,000.16 m (approx. 820 m vertical depth) using flushing source HLX10; percussion drilling was initially carried out to 108.35 m followed by casing prior to the core drilling phase. The sequence of borehole activities relating to the Laxemar 2.1 data freeze is presented in Appendix 1, Table 1-3.

Geological and hydrogeological character

Borehole KLX05 penetrates a rock mass were Ävrö granite and granite in the upper approx 400 m gives way to quartz-monzodiorite which dominates to the hole bottom (Figure 2-8). Apart from this very general subdivision, the geology is heterogeneous with the upper 100–212 m characterised by Ävrö granite and fine-grained granite with portions of fine-grained dioritoid. This changes to granite with subordinate Ävrö granite and fine-grained dioriroid from 212–290 m, and from 290–465 m inhomogeneous Ävrö granite occurs with layers of fine-grained granite, pegmatite, diorite/gabbro and fine-grained dioritoid. From 465–1,000 m quartz-monzodiorite diminates with layers of pegmatite and fine-grained diorite/gabbro. The general fracture frequency (Figure 2-8) is around 0–5 fractures/m with a small increase between 690–730 m. Crush zones occur at 101, 260, 510 and 655 m but alteration tends only to be localised to sporadic fractures.

The hydraulic character of borehole KLX05 is indicated in Figure 2-5 and in more detail in Figure 2-9; no differential flow measurements were available at this time. Figure 2-8 (hydraulic injection tests in 100 m sections) shows a systematic decrease in hydraulic conductivity from 10^{-7}–10^{-6} ms^{-1} in the 100–200 m section to 10^{-9}–10^{-8} ms^{-1} in the 400–500 m section; these values continue to 900 m were there is an increase to 10–8 ms^{-1} in the deepest 900–1,000 m section. A pump test and pressure measurement gave 1L/min water within this 902–1,000 m section.

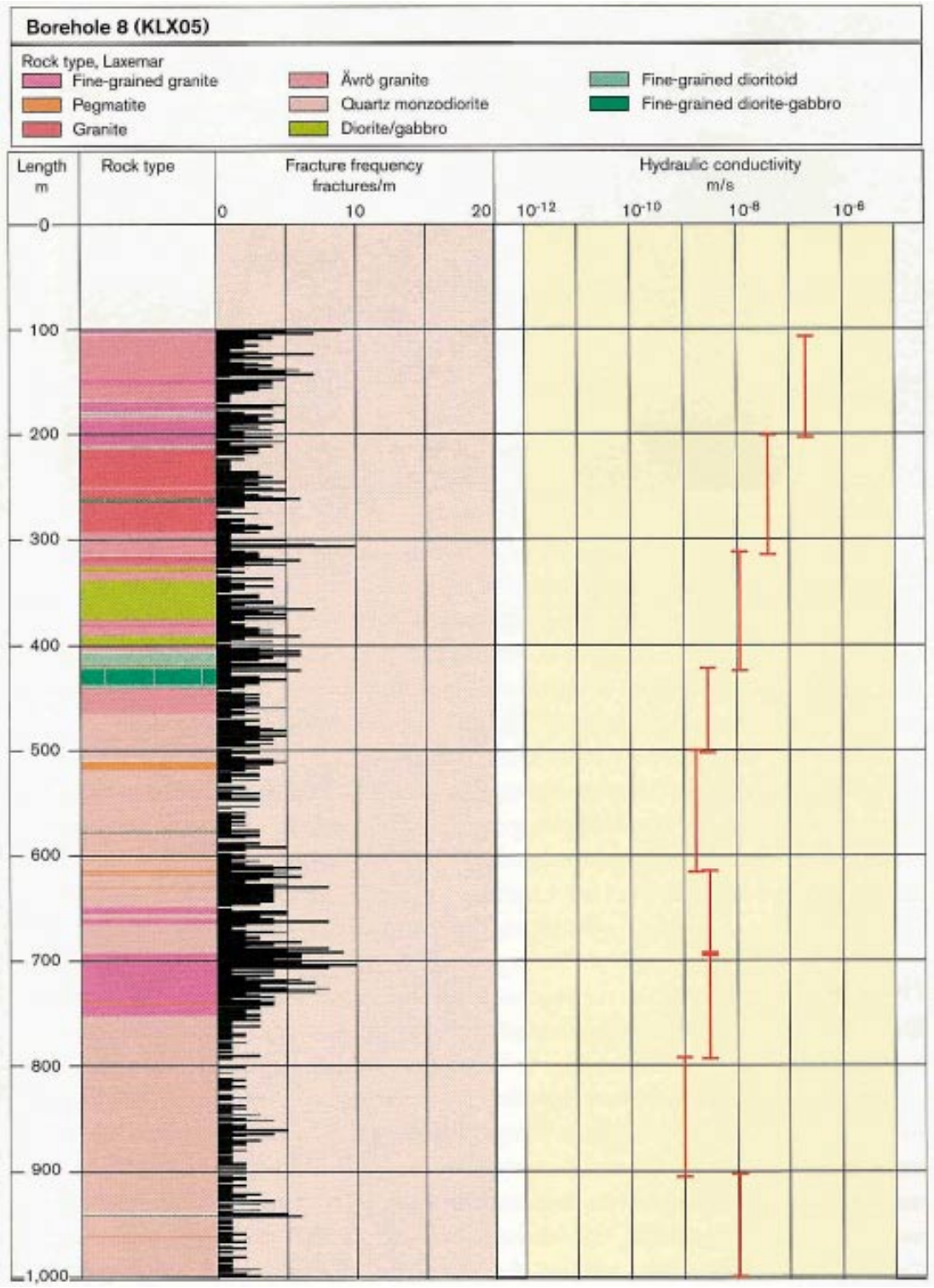

Figure 2-8. *Integrated geology, fracture frequency and hydraulic conductivity along borehole KLX05.*

Figure 2-9 shows added detail from hydraulic injection tests carried out in 20 m borehole sections. This indicates distinctive subdivisions not evident in Figure 2-8 which include: a) high transmissivities in the upper 260 m of the bedrock ($10^{-7.5}$–10^{-5} m^2s^{-1}), b) an area of low transmissivity from 320–380 m (10^{-11} m^2s^{-1}), c) a long borehole length from 380–900 m were transmissivity varies between around 10^{-11}–10^{-8} m^2s^{-1}, and d) an area of low transmissivity > 900 m ($10^{-11}m^2s^{-1}$). No measurements were made along the 500–600 m borehole length. This overall pattern in transmissivity generally reflects the fracture frequency pattern.

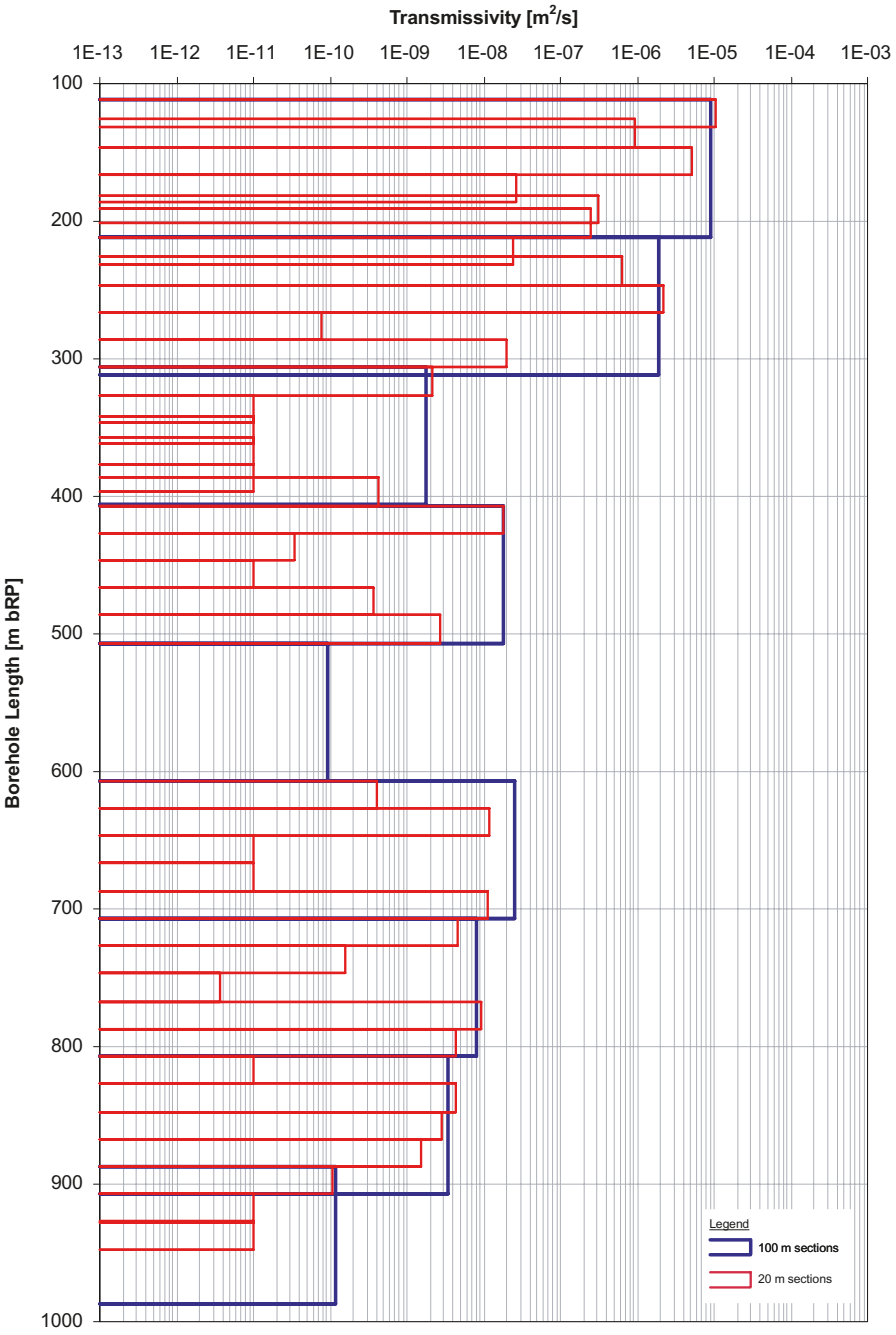

Figure 2-9. *Preliminary transmissivity data for KLX05 from hydraulic injection tests carried out in 100 m and 20 m borehole sections. From /Rahm and Enachescu 2005b/.*

From these data shallow, open-borehole conditions should be dominated by groundwater imput from the upper 300 m of bedrock; this, together with contamination from drilling water, will dominate the deeper parts of the borehole. The quality of the sampled groundwaters will therefore depend on the success of clearing the borehole and restricting the downward movement of the shallow meteoric groundwaters.

Evaluation of new data

Borehole section 0–100 m

Samples taken following the percussion drilling stage. No measured or analytical data available.

Representativity: Unsuitable; recommended deletion from database.

Borehole section 107.00–202.94 m

One sample taken during drilling; fairly complete analysis of major ions and partial isotope data and an acceptable charge balance (< ± 5%). It is dilute (45.7 mg/L Cl) and Na-HCO_3 in type, meteoric in origin, and may be recent (1.9 TU) although no tritium value is available for the drilling water. Isotopic data suggests present-day recharge ($\delta^{18}O$ = –10.6‰ SMOW, δD = –75.5‰ SMOW). The drilling water content is high (16.20%).

Representativity: Unsuitable because of high drilling water contamination.

Tube sampling (0–965 m)

Tube sampling was carried out on completion of the PLU pumping tests (Appendix 1, Table 1-4). The connected tube array was lowered into the hole on 2005-04-06, raised, emptied and the samples sent for analysis. A total of 20 tubes/samples were collected, each representing 50 m sections along the open borehole except for the uppermost borehole section which was 40 m.

The distribution of residual drilling water along borehole KLX05 consistently exceeds the 1% acceptance threshold, increasing from a minimum value of 2.17% in the shallowest borehole section to 66.50% in the deepest section (890–940 m). To around 400 m depth the drilling water content is consistently < 5%; below 500 m there is a rise in content to around 10% which continues to increase with increasing depth along the borehole.

Representativity: Unsuitable because of excessive contamination by drilling water and most likely partly by shallow dilute formation groundwaters from the upper part of the bedrock entering the borehole.

Borehole KLX06

Borehole KLX06 (Figure 1-1) is a 939.00 m long borehole inclined –60° to the horizontal and reaching a vertical depth of approx. 800 m; percussion drilling was initially carried out to 100.30 m followed by casing prior to the core drilling phase. The flushing water source was HLX20 and the subsequent sequence of borehole activities is presented in Appendix 1, Table 1-4. The aim of the borehole was to drill through the large Mederhult defomation zone (ZSMEW002A) which delineates the Simpevarp area to the north.

Details of borehole hydraulics and salinity profiles have been already presented, interpreted and discussed in /Laaksoharju 2006/.

Evaluation of new data

Borehole section 0–145 m

No analytical data available; only measured electrical conductivity and density from water pumped from packed-off borehole sections during cleaning. This followed the percussion drilling stage.

Representativity: Unsuitable; recommended deletion from the Laxemar 2.1 database.

Borehole section 103.00–202.26 m

Sampled during hydraulic air-lift pump testing. Major ion analyses are complete; environmental isotopic data are restricted to tritium and stable isotopes. The shallow groundwater (Na-HCO_3 in type) is dilute (25.4 mg/L Cl), meteoric in origin and showing a recent recharge character indicated from the tritium (2.8TU) and the stable isotope signature ($\delta^{18}O$ = –11.3‰ SMOW, δD = –78.0‰ SMOW), although the $\delta^{18}O$ value may suggest a weak cold climate signature. High drilling water contamination is present (17.4%).

Representativity: Unsuitable because of excessive drilling water contamination. Limited qualitative use in supporting the presence of dilute groundwaters at this depth with a possible cold climate signature.

Borehole section 146.00–255.00 m

No analytical data available; only measured electrical conductivity and density in one sample from water pumped from packed-off borehole sections during cleaning.

Representativity: Unsuitable; recommended deletion from the Laxemar 2.1 database.

Borehole section 200.50–310.20 m

Sampled during hydraulic air-lift pump testing. No analytical data available; excessive drilling water contamination (47.5%).

Representativity: Unsuitable; recommended deletion from the Laxemar 2.1 database.

Borehole section 265.50–268.50 m

This section was sampled once in 2004-09-10 and only analysed for the major ions Cl, HCO_3, SO_4 and Br; drilling water registered 19.3%.

Representativity: Unsuitable because of high drilling water contamination. Limited qualitative use in supporting the presence of dilute groundwaters at this depth

Borehole section 260.50–268.70 m

Following a lapse of one day during hydraulic air-lift pump testing the approx. same borehole section was sampled once; only incomplete data are available (e.g. lacking carbon isotopes) so it is not possible to follow any variation in major ion composition (e.g. salinity) during the sampling period. The charge balance is acceptable (< ± 5%) but there is a drilling water component of 4.03%.

The sampled groundwater is dilute (15.7 mg/L Cl) and Na-HCO_3 in type, has a modern component (1.5TU) and also a recharge isotopic signature ($\delta^{18}O$ = –11.20‰ SMOW, δD = –77.3‰ SMOW); a possible weak cold climate component is suggested from the $\delta^{18}O$.

Representativity: Unsuitable because of the 4.03% drilling water and an absence of a sample time series. However good qualitative use in establishing the presence of dilute groundwaters at this depth.

Borehole section 260.00–265.00 m

Sampling was carried out from almost the same borehole section during a 2 day period some 6 months later in 2005-03-09; an almost complete analysis (e.g. lacking carbon isotopes) was carried out on only one sample on the final day so it is not possible to follow any variation in major ion composition (e.g. salinity) during the sampling period. However the drilling water component indicates an initial increase from 2.59–9.53% during the first day followed by a decrease to 5.68% for the final and only sampled groundwater on the following day. This indicates a much longer pumping period is necessary to remove all the drilling water contamination as predicted in /Laaksoharju 2006/.

The sampled groundwater is Na-HCO_3 in type, recent but not modern (0.8TU), dilute (36.8 mg/L Cl) and has a recharge isotopic signature ($\delta^{18}O$ = –11.10‰ SMOW, δD = –80.4‰ SMOW), possibly indicating also a weak cold climate component.

Comparing this section with the earlier sampled section described above (i.e. 260.50–268.70 m after a lapse of approx. 6 months and open hole conditions) shows that the tritium (from recent recharge contamination) has been flushed out and also some of the flushing water (i.e. 2.59% at initial pumping stage).

Representativity: Limited suitability because of the 5.68% drilling water. Good qualitative use in establishing the presence of dilute groundwaters at this depth. Highlighted in green in the database.

Borehole section 256.00–275.00 m

After a further three months (2005-06-15) the same approx. borehole section (this time somewhat 14 m longer) was resampled and showed that the drilling water component had decreased to 2.96% as expected. Only electrical conductivity and density were measured. No activity log information.

Representativity: Unsuitable; recommended deletion from the Laxemar 2.1 database.

Borehole section 276.00–412.00 m

No analytical data available; only measured electrical conductivity and density from water pumped from packed-off borehole sections during cleaning. No activity log information.

Representativity: Unsuitable; recommended deletion from the Laxemar 2.1 database.

Borehole section 331.02–364.23 m

During hydraulic pump testing borehole section was measured for electrical conductivity and density. It was sampled once and analysed for the major ions Cl, HCO_3, SO_4, Br and F; drilling water registered 36.5%.

Representativity: Unsuitable because of excessive drilling water contamination. Limited qualitative use in supporting the presence of dilute groundwaters at this depth

Borehole section 307.50–415.49 m

Sampled during hydraulic pump testing; no analytical data.

Representativity: Unsuitable; recommended deletion from database.

Borehole section 411.00–553.00 m

No analytical data available; only measured electrical conductivity and density from water pumped from packed-off borehole sections during cleaning. No activity log information.

Representativity: Unsuitable; recommended deletion from database.

Borehole section 558.20–563.20 m

No major ion or isotopic analytical data; only drilling water monitoring during a 6 day period which recorded an increase from 5.41–21.20%. This was predicted from the evaluation in /Laaksoharju 2006/.

Representativity: Unsuitable; recommended deletion from database.

Borehole section 558.20–583.20 m

After a lapse of approx. 5.5 months and along approx. the two borehole lengths described above (558.20–563.20 m and 554.00–570.00 m), a further monitoring was carried out during hydraulic injection testing. This still indicates a drilling water content of 21.40%; the groundwater is dilute (348 mg/L Cl) with a small modern component (1.0TU) and generally indicates small increases in salinity, SO_4, Ca and a decrease in HCO_3 which might be expected at these depths. A component of cold climate recharge is also indicated ($\delta^{18}O$ = –11.8‰ SMOW, δD = –84.8‰ SMOW). However, in addition to drilling water contamination, similarly dilute groundwaters from shallower depths are also present as suggested from the measurable tritium which does not derive from the drilling water from HLX20 (0.8TU).

Representativity: Unsuitable because of excessive drilling water and also contamination from shallower formation groundwaters. Limited qualitative use in supporting the presence of dilute groundwaters at this depth.

Borehole section 554.00–570.00 m

From approx. the same sections as above (558.20–563.20 m and 558.20–583.20 m), one sample was collected for drilling water analysis after a lapse of 3 months. This recorded 2.49% which is a substantial improvement. No major ion or isotopic analytical data are available; electrical conductivity and density measured. No activity log information.

Representativity: Unsuitable; recommended deletion from database.

Borehole section 514.60–613.94 m

Sampled during hydraulic pump testing but no analytical data available; excessive drilling water contamination (74.70%).

Representativity: Unsuitable; recommended deletion from database.

Borehole section 571.00–760.00 m

No measured or analytical data.

Representativity: Unsuitable; recommended deletion from database.

Borehole section 715.14–784.94 m

Sampled during hydraulic pump testing but no time series information to indicate variations in salinity. Major ion analyses are complete; no isotopic data are available. The groundwater (Na-Ca-Cl-SO_4 type) is almost brackish (1,330 mg/L Cl) with a high drilling water contamination (48.70%).

Representativity: Unsuitable because of excessive drilling water contamination.

Borehole section 776.20–781.94 m

Monitoring of the drilling water content for a 6 day period during hydraulic injection testing. An almost complete analysis (e.g. lacking carbon isotopes) was carried out on only one sample on the final day so it is not possible to follow any variation in major ion composition (e.g. salinity) during the sampling period. However the drilling water component indicates an initial increase from 9.04% during the first day to a maximum of 25.2% on the fourth day. This was followed by a small decrease to 23.20% for the final and only sampled groundwater two days later. This indicates a much longer pumping period is necessary to remove all the drilling water contamination as predicted in /Laaksoharju 2006/.

The sampled groundwater has an acceptable charge balance (< ± 5%) is Na(Ca)–Cl(SO_4, HCO_3) in type, recent with a small modern component (1.2TU), almost brackish (1,240 mg/L Cl) and has a significant cold climate isotopic signature ($\delta^{18}O$ = –12.60‰ SMOW, δD = –91.4‰ SMOW).

Comparing this section with the earlier sampled section described above (i.e. 776.20–784.94 m after a lapse of approx. 5 months and open hole conditions) shows that the drilling water component has been reduced by about 50% and the salinity has remained the same.

Representativity: Unsuitable because of the excessive drilling water contamination. Some qualitative use in establishing the presence of dilute/brackish groundwaters at this depth.

Borehole section 761.00–994.94 m

No analytical data available; only measured electrical conductivity and density in one sample from water pumped from packed-off borehole sections during cleaning. The conductivity indicated a very dilute groundwater (~ 80 mg/L Cl).

Representativity: Unsuitable; recommended deletion from database.

Tube sampling (0–965 m)

Tube sampling was carried out on completion of a series of air-lift pumpings to clear the borehole of accumulated formation and drilling water and drilling debris, and following the PLU pumping tests (Appendix 1, Table 1-4). The connected tube array was lowered into the hole on 2004-12-21, raised, emptied and the samples sent for analysis. A total of 20 tubes/samples were collected, each representing 50 m sections along the open borehole except for the uppermost borehole section which was 40 m.

The distribution of residual drilling water along borehole KLX06 consistently exceeds the 1% acceptance threshold, increasing from a minimum value of 8.057% in the shallowest borehole section to a high of 50.40% at around 600 m, followed by a decrease to 37.9% at approx. 800 m and, finally, an increase to a maximum of 64.00% at around 950 m.

The complete borehole shows a very dilute Na-HCO_3 type groundwater (30–156 mg/L Cl) with a small increase in salinity (to 430 mg/L Cl) at the deepest section.

Representativity: Unsuitable because of excessive contamination by drilling water and mixing with shallow dilute formation groundwaters from the upper part of the bedrock entering the borehole.

Borehole KLX07

Borehole KLX07 (Figure 2-1) is approx. 845 m long borehole inclined –60° to the horizontal and reaching a vertical depth of approx. 755 m; percussion drilling was initially carried out to 200 m followed by casing prior to the core drilling phase. The flushing water source was HLX10 and the aim of the borehole was to confirm the orientation of deformation zones by combining data from nearby KLX02. No borehole activity log was available.

Details of borehole geology, hydraulics and salinity profiles have been already presented, interpreted and discussed in /Laaksoharju 2006/.

Evaluation of new data

Tube sampling (0–805 m)

The connected tube array was lowered into the hole on 2005-06-08, raised, emptied and the samples sent for analysis. A total of 17 tubes/samples were collected, each representing 50 m sections along the open borehole except for the uppermost borehole section which was 30 m.

The distribution of residual drilling water along borehole KLX07 consistently exceeds the 1% acceptance threshold, with the first approx. 400 m showing consistent values from 2.21–2.83%, thereafter increasing steadily to a maximum of 8.99% at the deepest level around 800 m. Apart from electrical conductivity and density only HCO_3 has been recorded; this shows even values for the total borehole length (195–214 mg/L HCO_3).

Representativity: Unsuitable because of excessive contamination by drilling water, mixing of groundwaters from different origins and a lack of analytical data.

Drilling samples

Taken at regular depth intervals during drilling of the borehole and provides an important indication as to the potential degree of drilling water concentrations in the borehole accessible for contamination. Not of direct use in the Laxemar 2.1 hydrogeochemical evaluation; recommended deletion from the Laxemar 2.1 database.

Borehole KLX08

Borehole KLX08 (Figure 1-1) is a 1,000.41 m long borehole inclined –60° to the horizontal and reaching a vertical depth of approx. 870 m; percussion drilling was initially carried out to approx. 100 m followed by casing prior to the core drilling phase. The flushing water source was HLX10 and the aim of the borehole was to validate the orientation of deformation zone ZSMEW007 and to collect information of the rock volume south of this zone. No borehole activity log was available.

Drilling samples

Taken at regular depth intervals during drilling of the borehole and provides an important indication as to the potential degree of drilling water concentrations in the borehole accessible for contamination. Not of direct use in the Laxemar 2.1 hydrogeochemical evaluation; recommended deletion from the Laxemar 2.1 database.

Pore water samples

Rock core samples were collected to extract, analyse and interpret the pore water in the rock matrix. From a total of 25 samples 10 will be selected for full analysis. The samples are presently being investigated and no data are yet available.

Borehole KLX10

Borehole KLX10 (Figure 1-1) is a 1,001 m long borehole inclined -85° to the horizontal and reaching a vertical depth of approx. 995 m; percussion drilling was initially carried out to 100.60 m followed by casing prior to the core drilling phase. The flushing water source was HLX10 and the aim of the borehole was to provide information from the rock block south of deformation zone EW007. No borehole activity log was available.

Few published data are available on borehole geology and hydraulics; some preliminary salinity profiles (electrical conductivity) can be obtained from Lägesrapport (50–51), but these fall outside the Laxemar 2.1 data freeze, as do some hydrochemical data from groundwater samples collected during drilling (also shown in Lägesrapport, 50–51).

Evaluation of new data

Borehole section 0–100.60 m

Represents the percussion drilled part of the borehole. Two samples were taken 4 days apart, measured for pH, electrical conductivity and density and analysed for HCO_3. The groundwater is as expected, shallow in origin, dilute (~ 60 mg/L Cl) and with a high HCO_3 content (~ 305 mg/L); lab. pH is ~ 8.3.

Representativity: Unsuitable; recommended deletion from database.

2.4 The Simpevarp site

The Laxemar 2.1 database also contains new data from the Simpevarp subarea collected since the Laxemar 1.2 data freeze. These have involved systematically sampling packed-off borehole sections of varying lengths during cleaning of the borehole section.

2.4.1 Cored boreholes

Evaluation of new data

Borehole KSH01A

Borehole sections 0–180 m, 181–237 m, 238–277 m, 278–330 m, 331–531 m, 532–572 m, 573–670 m, 671–799 m and 800–1,000 m

Groundwaters collected in 2004-10-29. No analytical data available; only measured electrical conductivity and density from water pumped from packed-off borehole sections during cleaning.

Representativity: Unsuitable; recommended deletion from database.

Borehole KSH02

Borehole sections 91–110 m, 111–410 m, 411–439 m, 440–648 m, 649–954 m, 955–963 m and 964–1,000 m.

Groundwaters collected in 2004-12-15. No analytical data available; only measured density from water pumped from packed-off borehole sections during cleaning.

Representativity: Unsuitable; recommended deletion from database.

2.5 All sites: Adjustment of existing evaluated data

No new data but some reajustment with respect to representativeness.

2.5.1 Cored boreholes

Borehole KAV01

Borehole section 226.00–235.00 m

Sample 1374; downgrading from orange to blank due to excessive drilling water (~ 15%).

Representativity: Unsuitable.

Borehole KAV04A

Borehole section 245.85–293.05 m

Sample 7106; downgrading from green to blank due to excessive drilling water (~ 12.3%) and restricted time-series data.

Representativity: Unsuitable.

Borehole KLX01

Borehole section 830.00–841.00 m

Sample 1761; downgrading from orange to green due to restricted time-series data.

Representativity: To be used with caution.

Borehole KLX02

Tube samples

Samples collected during 1999-08-03 (all highlighted in green) and 1999-09-25 (2,406, 2,421, 2,424, 2,427) to be downgraded from green to blank due to open hole mixing effects prior to, and during, sampling.

Representativity: Unsuitable.

Borehole KLX03

Borehole section 103.00–218.02 m

Sample 7441; downgrading from orange to green due to restricted time-series data. See discussion in p.30.

Representativity: To be used with caution.

Borehole KLX04

Borehole section 103.00–213.14 m

Sample 7253; downgrading from green to blank due to restricted time series data and high drilling water content (7.76%).

Representativity: Unsuitable.

Borehole KSH01A

Borehole section 245.00–261.50 m

Sample 5268; downgrading from green to blank due to high drilling water content (8.02%).

Representativity: Unsuitable.

Borehole KSH01A

Borehole section 548.00–565.00 m

Sample 5288; downgrading from green to blank due to high drilling water content (10.74%).

Representativity: Unsuitable.

2.5.2 Percussion boreholes

Borehole HLX14

Borehole section 11.90–115.90 m

Sample 7345; downgrading from orange to green due to restricted time-series data.

Representativity: To be used with caution.

Borehole HSH03

Borehole section 0–201 m

Sample 3759; downgrading from orange to green due to erratic salinity profile with time and earliest sample selected.

Representativity: To be used with caution.

3 Hydrogeochemical evaluation

In common with the Laxemar 1.2 evaluation, the additional percussion and cored borehole data available for the Laxemar 2.1 evaluation has been used in this chapter (section 3.1) mostly to update selected plots which serve to best illustrate the evolutionary trends of the groundwaters, together with specific advances in interpretation of some of the specific isotope systematics. In addition, Chapter 3, section 3.2 provides new input to the geosphere/biosphere interface and Chapter 4 updates the status of the pore water studies.

The data used in the plots, unless otherwise stated, represent the quality assured data highlighted in orange and green colour in the database.

3.1 Updated major ion and isotope plots for the Simpevarp area

3.1.1 Chloride depth trends

The Simpevarp area data (Figure 3-1) continue to emphasise: a) the dilute nature of recharge meteoric waters (< 500 mg/L Cl) to average depths of around 500 m in the Laxemar subarea (to greater depths in borehole KLX02), followed by a marked and steady rise in salinity which, in KLX02 achieves 47g/L Cl at the maximum depth sampled (1,700 m), b) in comparison the dilute recharge meteoric waters for the Ävrö and Simpevarp sites (Simpevarp subarea) are restricted to around 100 m depth, c) at Ävrö there is an increase to a brackish composition at around 100 m depth which appears to level off at about 4,000–5,000 mg/L Cl at 600 m depth; there are no deeper groundwater data, d) at the Simpevarp site there is a similar but more marked increase in salinity to around 8,000–9,000 mg/L Cl at 600 m; again there are no deeper groundwater data, e) the greater salinity between 100–600 m at the more coastal Ävrö and Simpevarp sites is explained by discharge hydraulic conditions (cf. section 1.2).

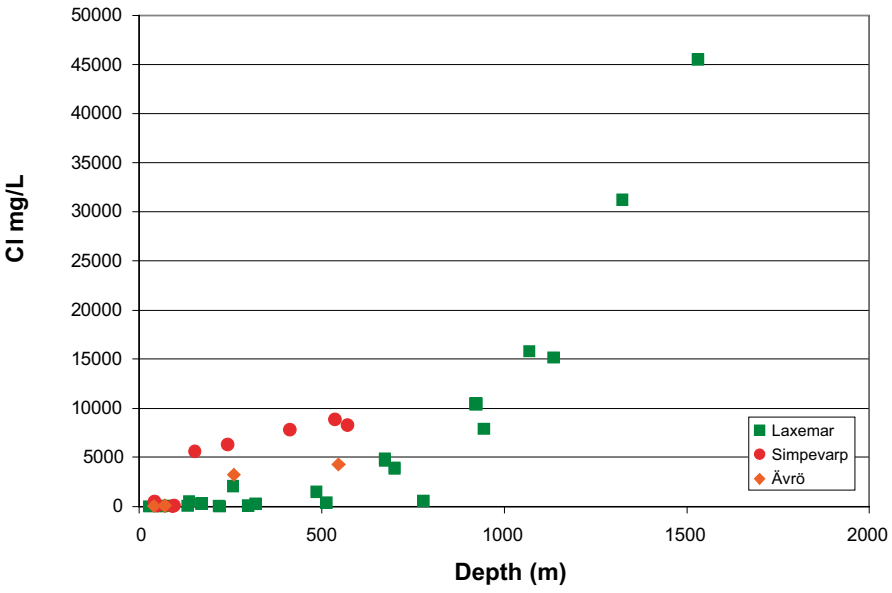

Figure 3-1. *Depth variation of chloride in the Simpevarp and Laxemar subareas.*

3.1.2 Sodium versus chloride and calcium

As expected, sodium versus depth shows similarities to that of Figure 3-1. However, when comparing sodium versus chloride (Figure 3-2) the subdivision of the Simpevarp area groundwaters into lower sodium (Laxemar subarea) and higher sodium (Simpevarp subarea) becomes more apparent. The Ävrö site groundwaters plot close to those of Laxemar, but there is a tendency to a slightly intermediate composition although more data are required to substantiate this. Figure 3-3, plotting calcium versus sodium, cleaarly shows that the Simpevarp groundwaters, in addition to being more saline from approx. 100–600 m depth, show a greater Na:Ca ratio than at Laxemar and Ävrö.

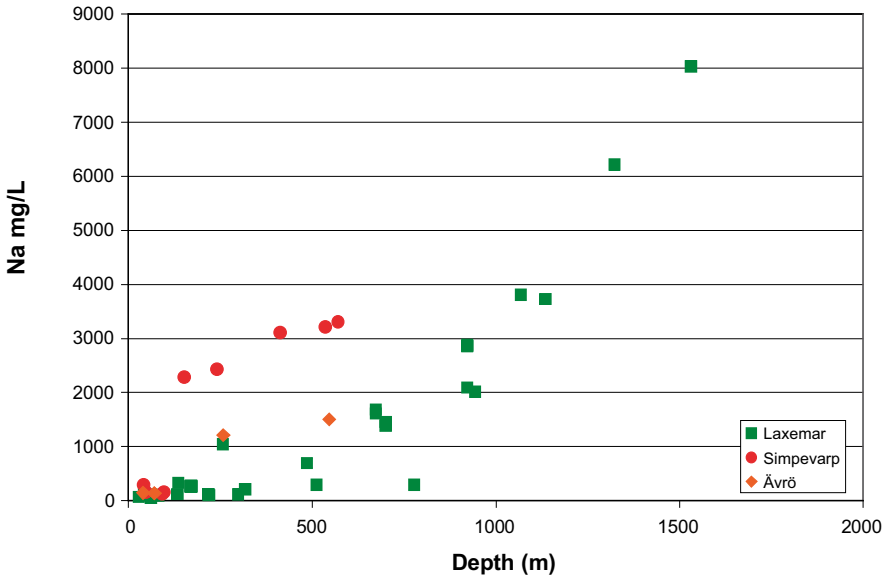

Figure 3-2. Plot of Na vs Cl for the Simpevarp and Laxemar subareas.

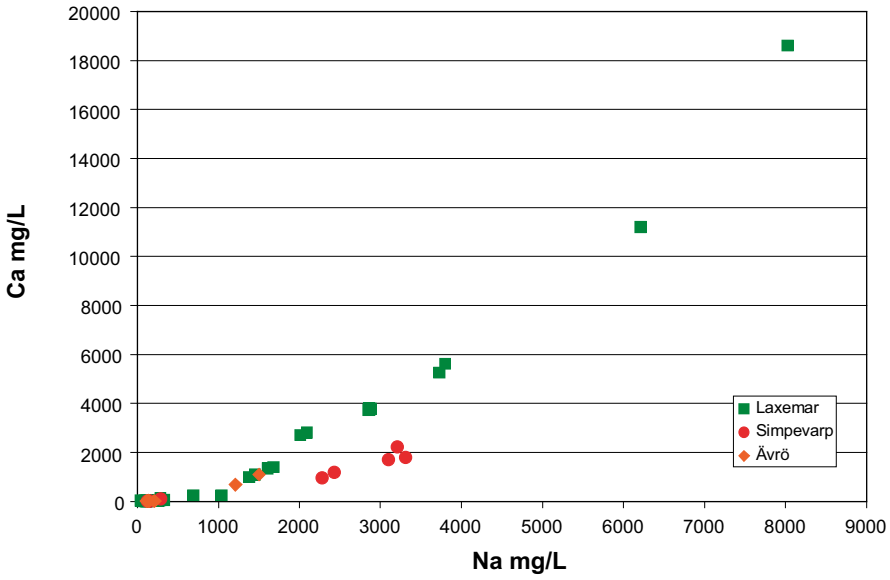

Figure 3-3. Plot of Ca vs Na for the Simpevarp and Laxemar subareas.

3.1.3 Magnesium versus depth and chloride

With the exception borehole KLX01, all of the Laxemar groundwaters plot close to or less than 10 mg/L Cl irrespective of depth (Figure 3-4). There is, however, a tendency for magnesium to decrease with increasing depth from around 500–600 m if the shallow groundwaters (0–250 m) are excluded. In contrast, the Ävrö and Simpevarp site groundwaters show a wide variation with high magnesium values (40–70 mg/L) occurring between approx. 150–600 m depth. The anomalous KLX01 groundwaters have been atttributed to Baltic Sea effects since it is located close to a sea inlet.

The plot of magnesium versus chloride (Figure 3-5) shows that the higher magnesium groundwaters coincide with a narrow range of brackish compositions (~ 3,000–7,000 mg/L Cl). These brackish groundwaters, restricted to maximum depths of around 500–600 m, are considered to represent a significant component of Littorina Sea mixing, although this is less prevalent than at Forsmark.

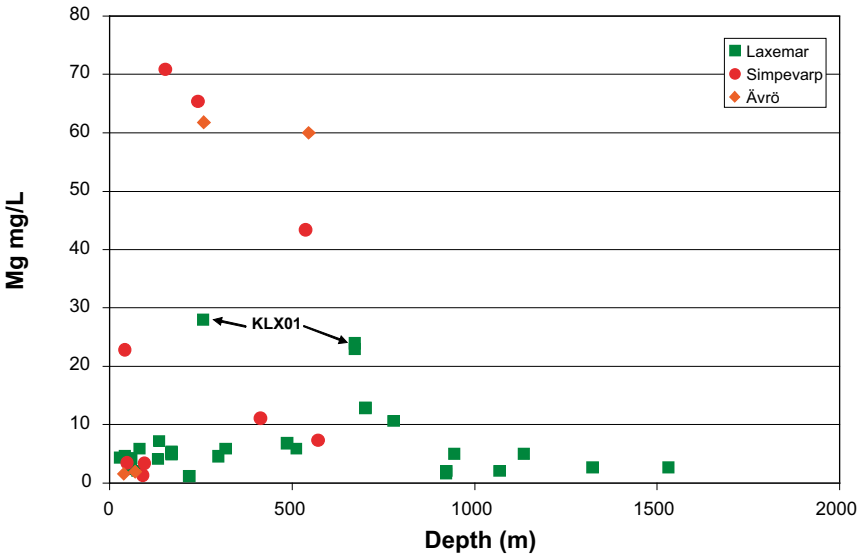

Figure 3-4. Plot of Mg vs depth for the Simpevarp and Laxemar subareas.

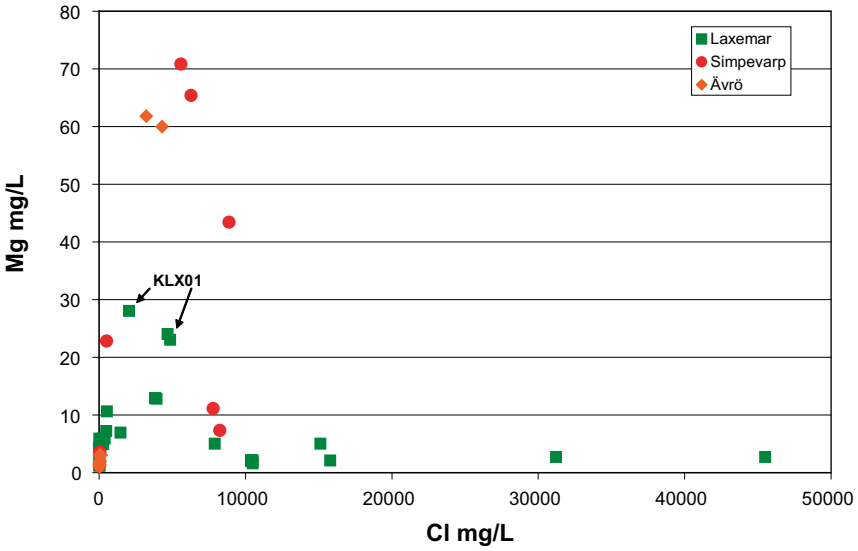

Figure 3-5. Plot of Mg vs Cl for the Simpevarp and Laxemar subareas.

3.1.4 Bicarbonate versus depth and chloride

Figures 3-6 and 3-7 plot bicarbonate against depth and chloride respectively. Both plots show the expected rapid decrease in bicarbonate with increasing depth and correspondingly with increasing chloride. The small deviations or scatter in the depth trends caused by some of the Laxemar subarea cored boreholes (Figure 3-6) reflect on one hand the differing hydrology at the borehole locations sampled and on the other hand possibly some open-hole mixing effects.

3.1.5 Sulphate versus depth and chloride

Sulphate versus depth (Figure 3-8) shows low concentrations characterising the shallow 0–400 m groundwaters; because of the increased recharge depth measured in KLX02, these low sulphate values at Laxemar continue to around 800 m depth. Deeper than 400 m the sulphate contents at the Simevarp and Ävrö sites begin to increase rapidly and this trend is continued by the deeper Laxemar site groundwaters. A levelling out of sulphate at around 800–1,000 mg/L SO4 occurs at approx. 1,000 m depth.

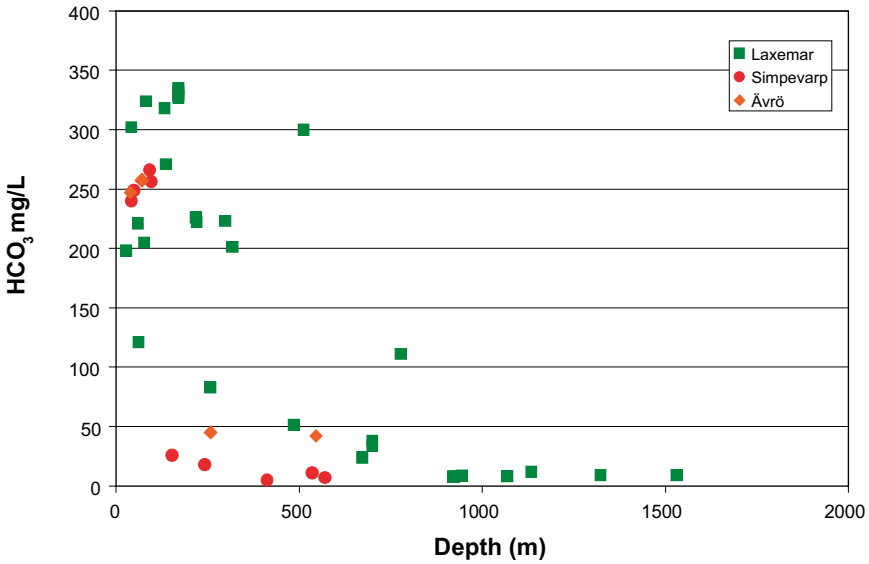

Figure 3-6. Plot of HCO_3 vs depth for the Simpevarp and Laxemar subareas.

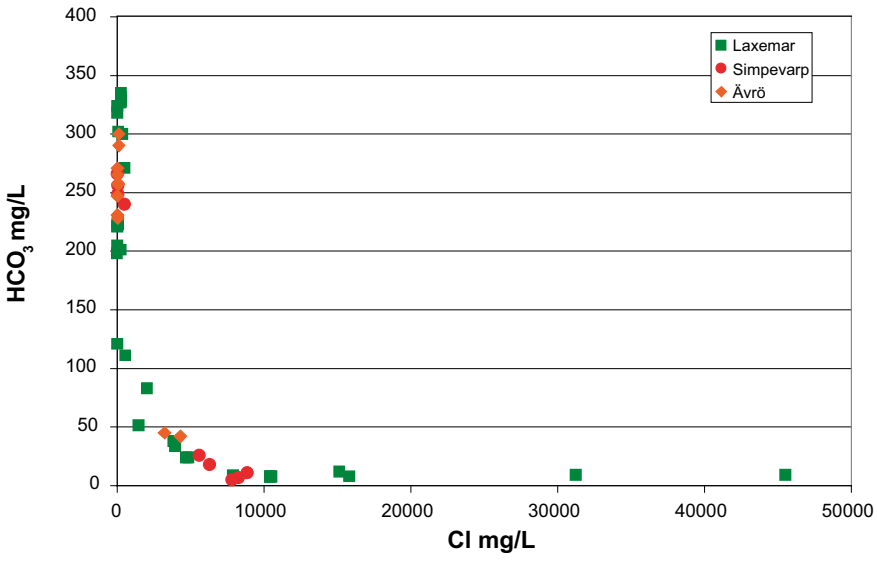

Figure 3-7. Plot of HCO_3 vs Cl for the Simpevarp and Laxemar subareas.

In Figure 3-9 sulphate is plotted against chloride and shows that the Laxemar subarea groundwaters indicate a levelling of sulphate at around 900–1,000 mg/L despite a significant increase in salinity from 15,000–50,000 mg/L Cl. This limitation of sulphate content in saline groundwaters was also noted by /Gascoyne 2004/ at the URL site in Canada; in this case it was attributed it to the solubility control exerted by gypsum which was close to saturation in the groundwaters. This is in accordance with geochemical modelling of the Simpevarp subarea groundwaters which identified the dissolution of gypsum as a possible source for sulphate in these groundwaters /Gimeno et al. in Laaksoharju 2004/, and also the observation of gypsum in sealed fractures in the Laxemar subarea (cf. section 1.4).

In the Simpevarp subarea groundwaters Figure 3-9 also reveals the generally higher chloride contents associated with the increase in sulphate, although there doesn't appear to be any difference in the actual sulphate content to the depth so far sampled and analysed.

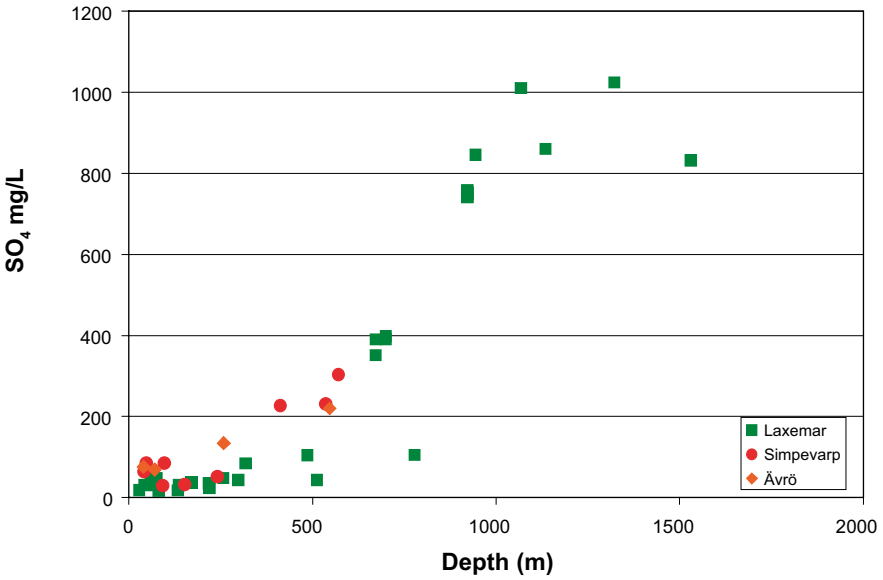

Figure 3-8. *Plot of SO_4 vs depth for the Simpevarp and Laxemar subareas.*

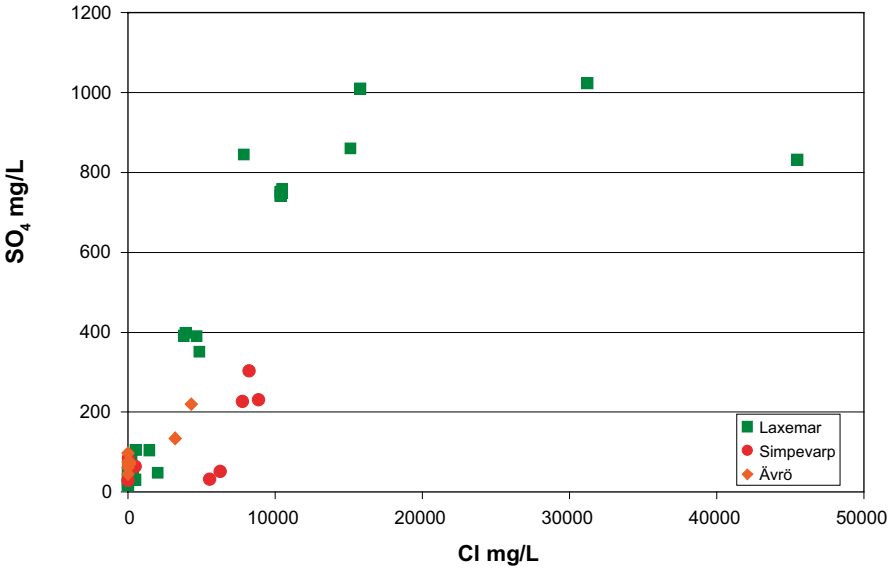

Figure 3-9. *Plot of SO_4 vs Cl for the Simpevarp and Laxemar subareas.*

3.1.6 Oxggen-18 versus depth, deuterium and chloride

Figure 3-10 shows the variation of $\delta^{18}O$ with depth associating the shallow (~ 0–150 m) meteoric groundwaters (all sites) with an input recharge of around –11.5 to –10‰ SMOW. Intermediate depth groundwaters from all sites (150–700 m) indicate a mixture of waters characterised by both a modern recharge $\delta^{18}O$ component and a light isotope cold climate $\delta^{18}O$ recharge component (–15 to –12.5‰ SMOW). Finally, there is a gradual enrichment in $\delta^{18}O$ (–10 to –9‰ SMOW) with increasing depth indicated by the deep Laxemar subarea groundwaters. Such enrichments have also been reported from the deep brines of the Canadian Shield /e.g. Frape and Fritz 1987/.

Figure 3-11 plots $\delta^{18}O$ against deuterium showing the isotopic composition of the Simpevarp area waters with respect to the Global Meteoric Water Line (MWL). The positions of the various water groups have been approximately delineated with each group showing distinct isotopic compositions,

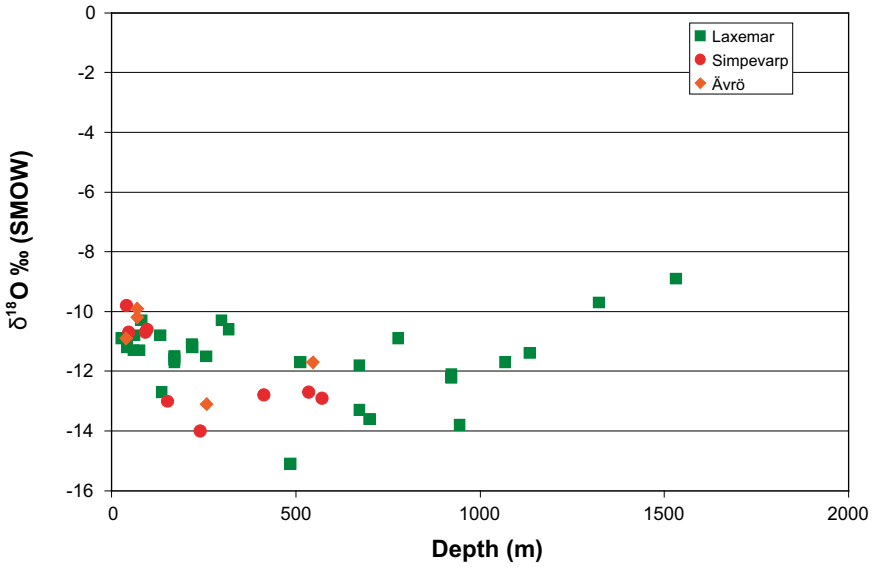

Figure 3-10. Plot of $\delta^{18}O$ vs depth for the Simpevarp and Laxemar subareas.

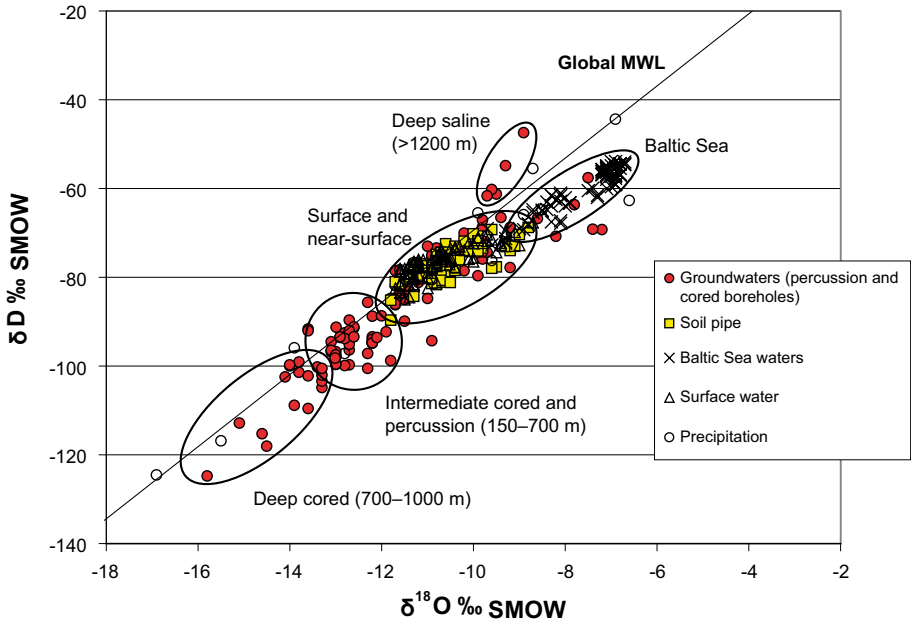

Figure 3-11. Plot of $\delta^{18}O$ vs deuterium for the Simpevarp and Laxemar subareas showing the main groundwater groups (ringed). (Global MWL = Global Meteoric Water Line).

further emphasising the groupings illustrated in Figure 3-10. The deviation of Baltic Sea waters from the MWL is typical of evaporation effects which to a lesser extent have influenced the surface lake and stream waters, and also some of the soil pipe near-surface waters more dominated by rapid recharge from the surface. Most of the soil pipes, intermediate-depth percussion and deeper cored boreholes plot on or close to the MWL which is quite normal for the Fennoscandian groundwater environment. As noted from Figure 3-10, the enrichment in $\delta^{18}O$ seen in the deep saline groundwaters is clearly seen as a deviation above the MWL in Figure 3-11 and usually explained by very intensive water/rock interactions under long residence times and near-stagnant conditions /Frape and Fritz 1987/.

The above general trends are further illustrated in Figure 3-12 by plotting $\delta^{18}O$ against chloride. In addition, the plot more specifically links the restriction of the light isotope cold climate signatures to groundwaters (mostly the Simpevarp and Ävrö sites) of brackish composition (~ 3,000–8,000 mg/L Cl), which includes the groundwaters associated with a Littorina Sea component and also a mixed component of non-marine saline groundwaters from the Laxemar subarea.

3.1.7 Redox-sensitive species

Manganese and uranium are sensitive to redox conditions and have been used here to detect possible groundwater redox trends.

Manganese versus depth and chloride

Manganese has been plotted against depth (Figure 3-13) and chloride (Figure 3-14). No systematic depth trends are apparent (Figure 3-13) and the majority of manganese values plot under 0.5 mg/L irrespective of depth. Interestingly, however, values greater than 0.5 are restricted to the Simpevarp and Ävrö site groundwaters, and with one exception, to those of brackish, Littorina-type composition amd partly associated with a cold climate recharge component (Figure 3-14).

Figures 3-15 and 3-16 include surface and shallow overburden waters; these will not be discussed here. Significant depth trends in the bedrock groundwaters are absent with uranium contents all plotting close to or less than 1 µg/L (Figure 3-15). In addition no trends are observed when uranium is plotted against bicarbonate (Figure 3-16).

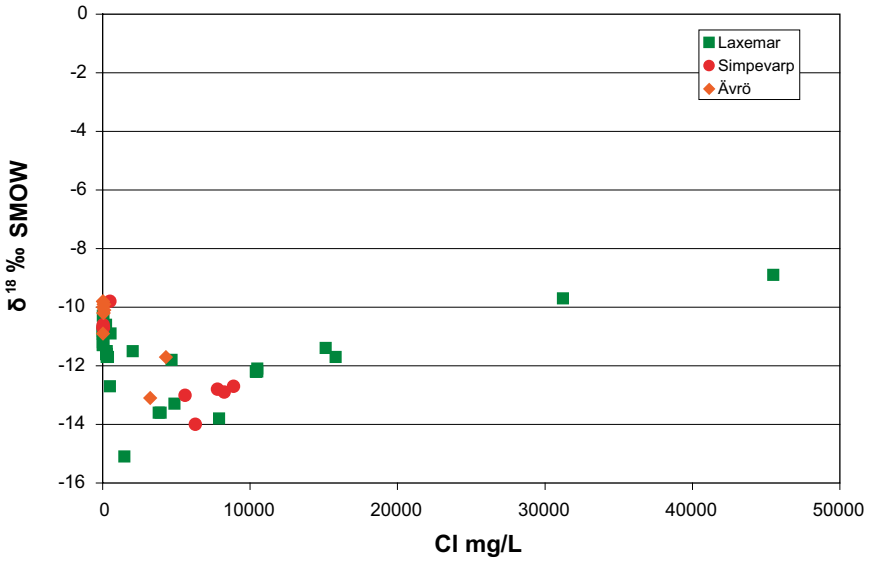

Figure 3-12. *Plot of $\delta^{18}O$ vs Cl for the Simpevarp and Laxemar subareas.*

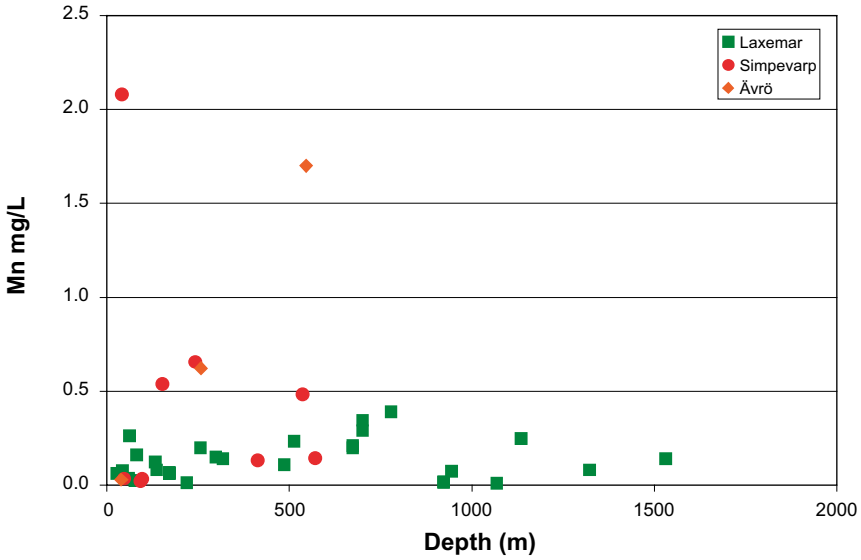

Figure 3-13. Plot of Mn vs depth for the Simpevarp and Laxemar subareas.

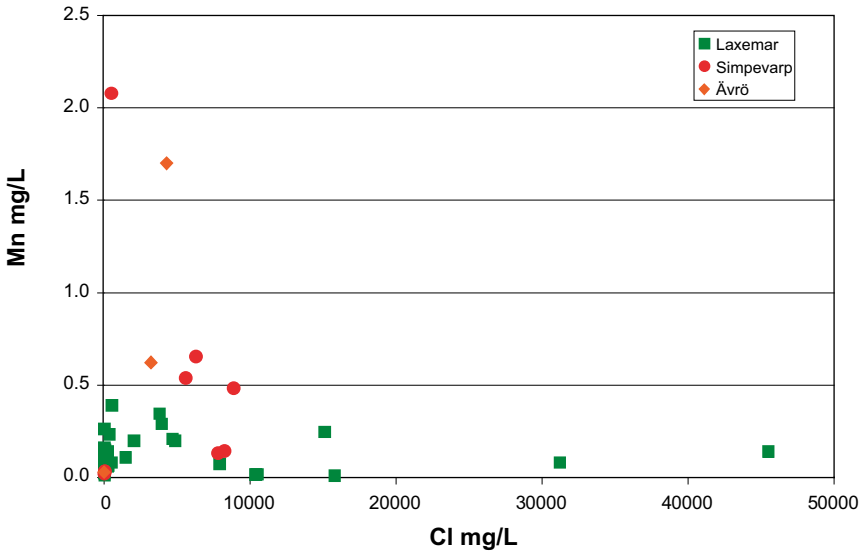

Figure 3-14. Plot of Mn vs Cl for the Simpevarp and Laxemar subareas.

3.2 Updating of specific isotope plots and their relevance to the bedrock/overburden interface

This section presents updated groundwater isotope data relating specifically to the interpretation and consequences of tritium, stable carbon and radiocarbon, stable sulphur ($\delta^{34}S$), and stable and radiogenic strontium ($^{87/86}Sr$). Since the Laxemar 1.2 evaluation many new data from surface (lakes, streams and sea) and near-surface (soil pipe) localities have become available. In the following plots these data have been incorporated with the percussion and cored borehole groundwater data with the specific objective of achieving a better understanding of the processes which are occurring at and adjacent to the geosphere/biosphere interface.

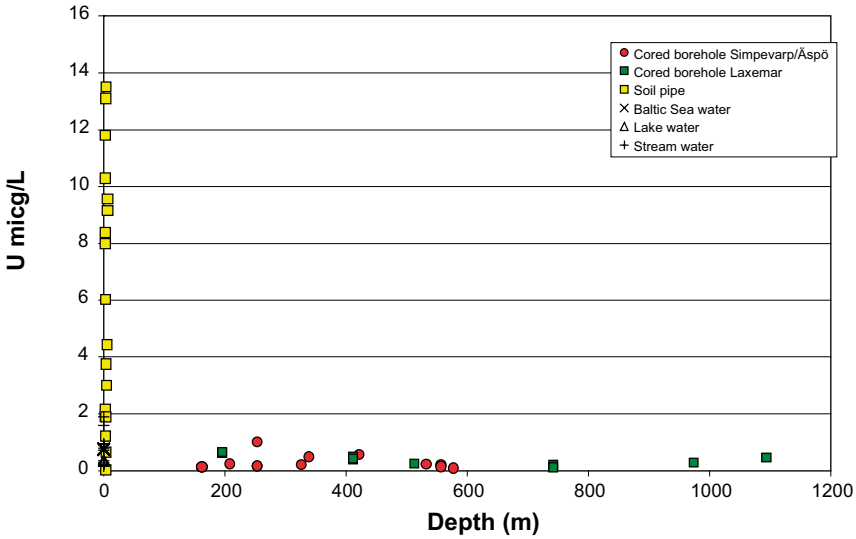

Figure 3-15. *Plot of U vs depth for the Simpevarp and Laxemar subareas.*

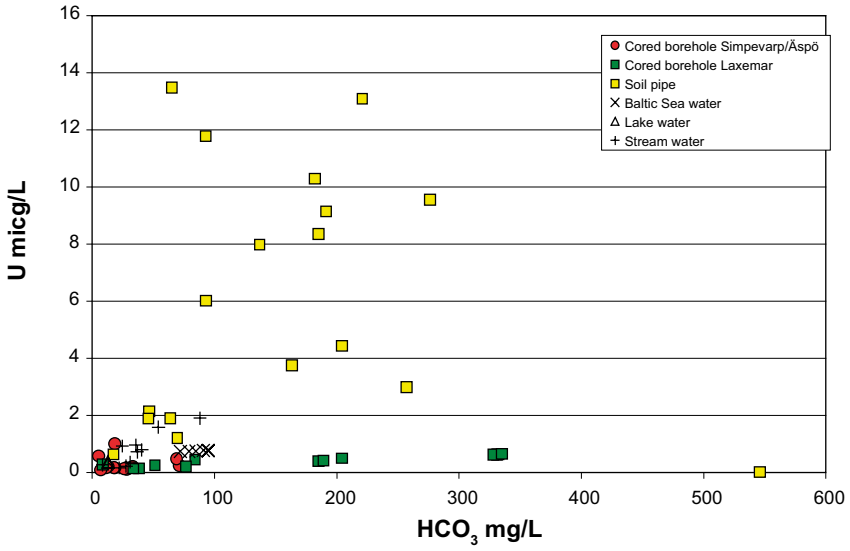

Figure 3-16. *Plot of U vs HCO_3 for the Simpevarp and Laxemar subareas.*

3.2.1 Tritium

Tritium versus depth

Tritium versus $\delta^{18}O$ in precipitation and the different surface waters and near-surface groundwaters in the Simpevarp area is illustrated in Figure 3-17; no correlation is observed.

In precipitation, tritium is variable in the range of 9–19 TU which also covers the range for the near-surface and Baltic Sea waters. The $\delta^{18}O$ shows a wide variability (season-specific) in precipitation (–17 to –7‰ SMOW) and to a lesser extent in the surface waters. Some near-surface groundwaters showed lower tritium contents. These originate from soil pipes in overburden sediments related to deformation zones that may act as discharge points, at least during specific periods of the year depending on local climate conditions. Despite the large variations in tritium contents in the surface waters there is a tendency towards higher values in the eastern part of the Simpevarp area which,

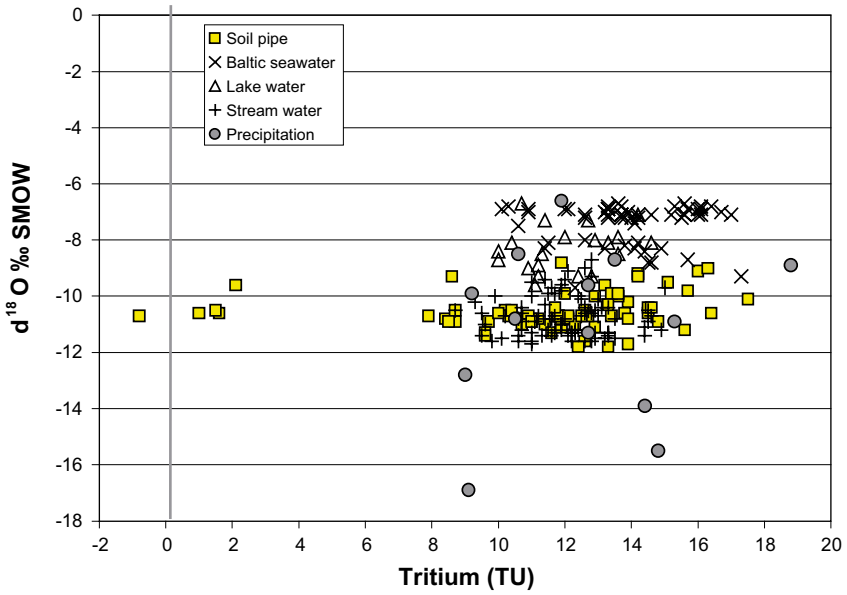

Figure 3-17. *Tritium vs $\delta^{18}O$ for precipitation, surface waters and near-surface groundwaters in the Simpevarp and Laxemar subareas.*

in part, may have emanated from the nuclear power plant. Nevertheless, based on the present data set the initial tritium input to the surface waters can be assumed to be in the range of 10–18 TU in the Simpevarp and Laxemar subareas and that of $\delta^{18}O$ from –17 to –7‰ SMOW with mean values around –10 ± 0.5‰ SMOW, possibly with a tendency towards higher values in the Simpevarp subarea and lower values in the inland part of the Laxemar subarea. From this surface environment these isotopes gradually percolate to the shallow overburden groundwaters, to the upper bedrock, and eventually deeper into the bedrock depending on local hydraulic conditions.

Figure 3-18 illustrates well this hydrochemical sequence from the overburden to deep bedrock environments. A rapid decrease of tritium can be observed in the groundwaters from recharge values close to the surface (10–18 TU) to values levelling out close to zero (less than ± 2 TU) around 200 m depth and remaining constant down to around 1,000 m. Since ± 2 TU is greater than the analytical detection limit of ± 0.8 TU, the question to ask is whether the measurable tritium content at depths greater than 200 m is due to contamination from drilling water or the downward penetration of recent, shallow meteoric waters.

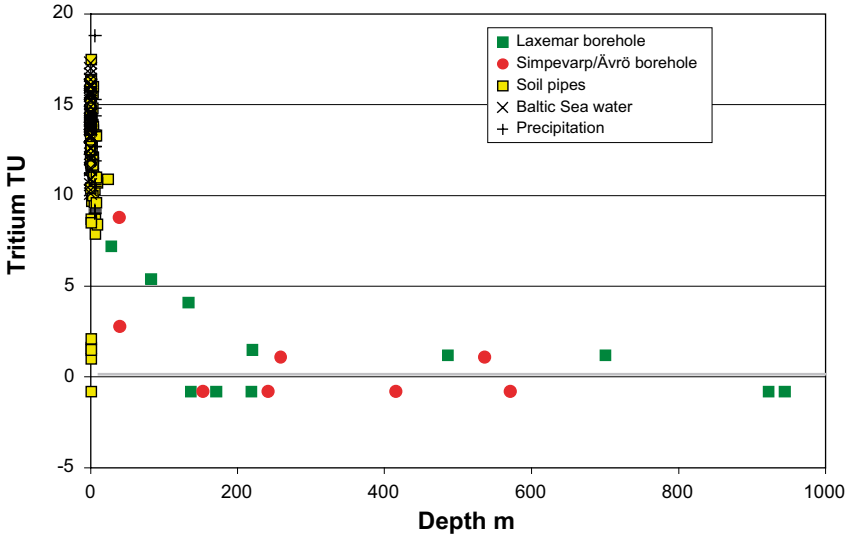

Figure 3-18. *Tritium vs depth in the Simpevarp and Laxemar subareas.*

The plot of drilling water versus tritium (Figure 3-19) indicates the presence of tritium in groundwater samples containing different percentages of drilling water, but also indicates the presence of tritium in some groundwater samples containing no drilling water. Since the drilling water is taken from the upper 150–200 m of the bedrock, i.e. the high transmissive horizon which may or may not contain tritium from naturally recharging recent meteoric waters (or residual older meteoric waters originating from the 1950s), contamination from drilling water and/or recent meteoric waters during open-hole conditions, might be expected at greater depths along the boreholes if they are not removed completely prior to sampling. Because complete removal of these contaminating waters have not been successful during the drilling and sampling campaign, the low tritium values at depth shown in Figure 3-18 therefore may be due to contamination.

3.2.2 Carbon

Radiocarbon (^{14}C), in common with tritium, is produced in the atmosphere and enters the groundwater through recharge. In addition, both isotopes (^{14}C and ^{3}H) were increased heavily during the nuclear bomb tests in the 1950's and 1960's. Furthermore, small but significant contributions have also entered the hydrological cycle in traceable amounts during the last 15–20 years from the nuclear power plants in both the Oskarshamn and Forsmark areas. However the presence of ^{14}C content, in contrast to tritium, is not only affected by the above input sources, but is also influenced by water reactions since carbon cycling in the recharge waters is complex and involves both inorganic and organic processes.

Available $^{14}C_{(HCO3)}$ data from percussion and cored boreholes from the Laxemar subarea are still limited. Results have been obtained for percussion boreholes HLX10, HLX 14 and HLX20 and from cored boreholes KLX03 103–218 m, KLX03: 497–599 m, KLX04 103–213 m and KLX04 510–515 m. However only data from borehole section KLX04 510–515 m has been sampled so far for complete hydrochemical characterisation. In addition a ^{14}C analysis from the saline water at KLX02: 1,345–1,355 m is included. This was measured during the pre-investigation phase and, as expected, showed not only very low radiocarbon content but also very low bicarbonate content.

Figure 3-20, showing ^{14}C (pmC) versus depth, indicates values in the range 40–80 pmC down to 150 m depth (ignoring the near-surface groundwaters (i.e. soil pipes) and surface waters) which drop to 30–40 pmC at greater depth for the Simpevarp/Ävrö sites. For the Laxemar site this drop is less marked, to 40–50 pmC. Overall there is an older ^{14}C signature at increasing depth, compared to the upper approx. 150 m. The surface waters showing ^{14}C values exceeding 100% are either produced by emission from the Oskarshamn Power Plant or contain remnants of nuclear bomb-test radiocarbon.

The plot of tritium versus ^{14}C (Figure 3-21) shows that all of the surface waters and most of soil pipes have high tritium contents but variable ^{14}C; the percussion boreholes from Simpevarp also reflect this pattern. The tritium free waters mainly from cored boreholes at both Laxemar and

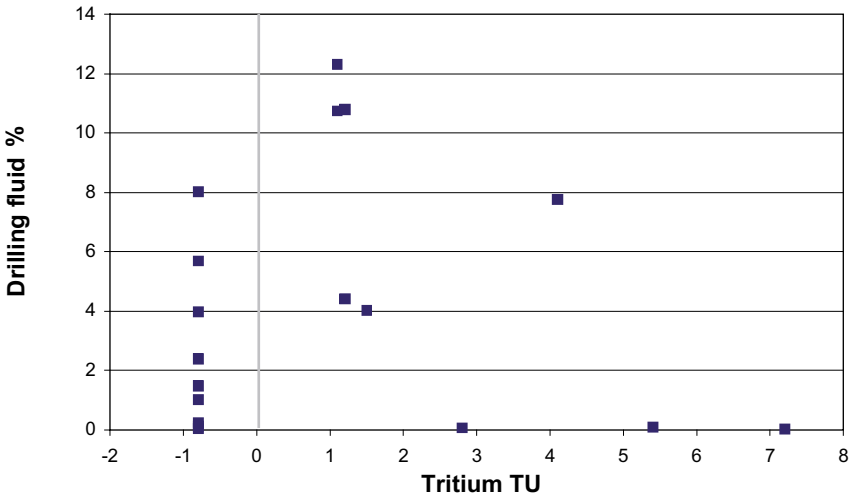

Figure 3-19. *Drilling fluid vs tritium in the Simpevarp and Laxemar subareas.*

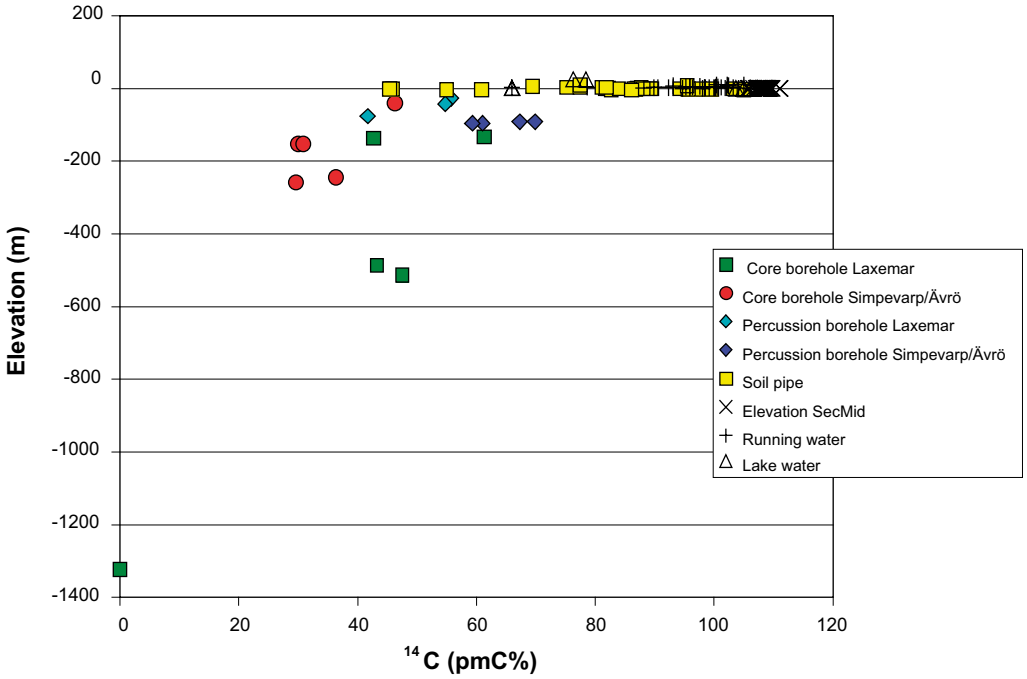

Figure 3-20. *^{14}C (pmC) vs depth in the Simpevarp and Laxemar subareas.*

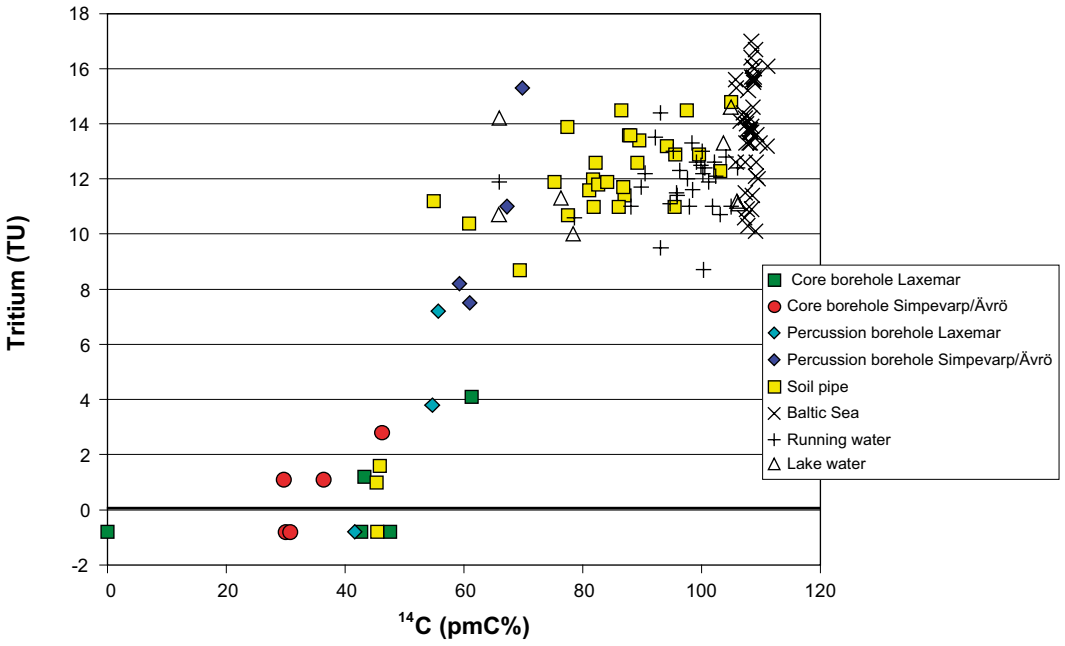

Figure 3-21. *Tritium vs ^{14}C (pmC%) in the Simpevarp and Laxemar subareas.*

Simpevarp but also including HLX20 and soil pipe SM00022 at Ävrö, show ^{14}C values in the range 30 to 47.5 pmC except for the deep water in KLX02 with no measurable radiocarbon.

From the plot of HCO_3 versus ^{14}C (Figure 3-22) it is obvious that the increase in bicarbonate characterising the near-surface groundwaters dilutes the ^{14}C signal. All soil pipes (with one exception), all the percussion boreholes samples and the shallow sample (0–100 m) from cored borehole KAV04, together with cored boreholes KLX03 103–218 m, KLX03: 497–599 m and KLX04 103-213 m, follow the same negative correlation between HCO_3 and ^{14}C contents. One way to explain this is the dissolution of old ^{14}C free calcite. It is, however, not realistic to assume that such high bicarbonate contents are produced by calcite dissolution alone. Additional and significant microbial activity can be assumed to take place producing CO_2 and in turn dissolved bicarbonate. The age of the oxidised

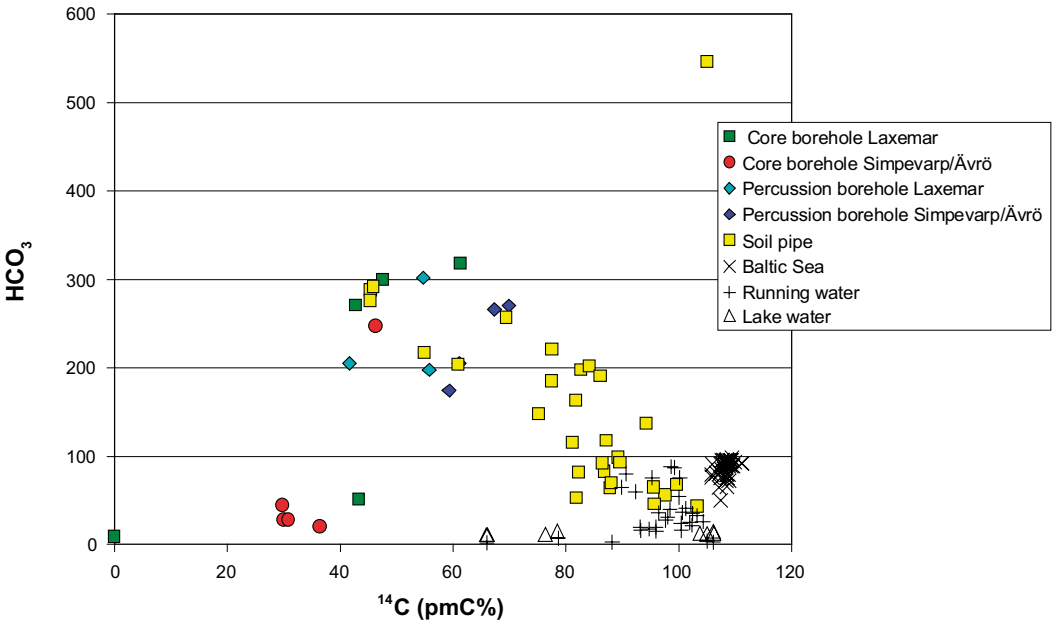

Figure 3-22. *HCO_3 vs ^{14}C (pmC%) in the Simpevarp and Laxemar subareas.*

organic material is unknown but a decrease in ^{14}C content can at least partly explain the lowering of $^{14}C_{HCO3}$ in combination with the strong increase in HCO_3 content. Another possibility is that these waters are old and very little ^{14}C has been contributed during a long period of time. A combination of some or several of these processes are possible to explain the groundwater samples, but for the soil pipe samples with high tritium contents a combination of calcite dissolution and breakdown of organic material, probably of various ages, is most probable.

Figure 3-23 shows no clear trend between $\delta^{13}C$ and ^{14}C content but a biogenic origin for the added carbon (bicarbonate) seems to be more compatible with the $\delta^{13}C$ signatures of the groundwaters (–16 to –22‰ PDB) than dissolution of fracture calcite which on average has higher $\delta^{13}C$ values (around –13‰ PDB for the 0–250 m interval; cf section 1.4). On the other hand, $\delta^{13}C$ values in the calcites are quite variable and it is possible that different flow paths may contribute distinctly lower $\delta^{13}C$ than the average calcite. Unfortunately no $\delta^{13}C$ value was obtained for the KLX04:510–515 m samples showing the lowest ^{14}C contents.

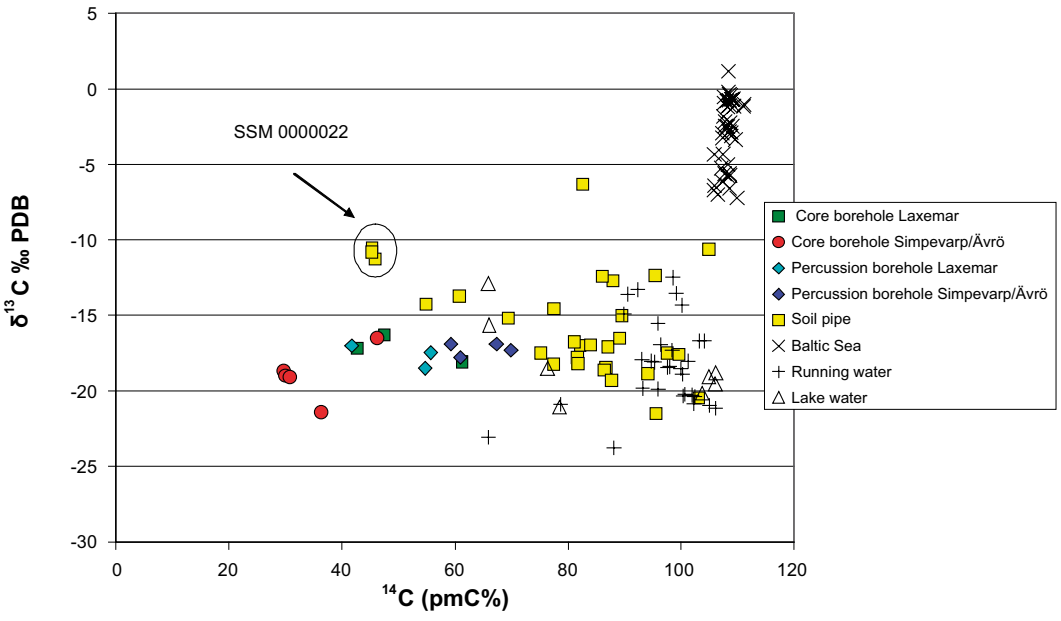

Figure 3-23. *$\delta^{13}C$ (‰ PDB) vs ^{14}C (pmC) in the Simpevarp and Laxemar subareas.*

Sampling and analyses of microbes has been carried out in borehole KLX03; these show the activities of the Fe- and Mn-reducing bacteria as well as the sulphate-reducing bacteria /Hallbeck 2006/. Activities of sulphate-reducing bacteria are also indicated by high $\delta^{34}S$ values in some of the groundwater samples. Moreover, Figure 3-24 plotting $\delta^{34}S$ versus ^{14}C shows a correlation between high $\delta^{34}S$ and decreased ^{14}C values. One explanation is that organic material with low ^{14}C enters the groundwater bicarbonate through in situ microbial activity. Three analyses of ^{14}C in dissolved organic carbon compounds have been performed on groundwaters from borehole KLX03 showing values of 65.2 pmC (193–198 m), 68.7 pmC (408–415 m) and 85 pmC (964–969.5 m); unfortunately no corresponding $^{14}C_{(HCO3)\ values}$ are available yet.

Notably, the upper section KLX03:193–198 m showed a high DOC content (approx. 20 mg/L), a high HCO_3 content (327 mg/L) and low drilling fluid content (0.24%), in contrast to the deepest section showing the higher $^{14}C_{(org)}$ (81.4 pmC) but lower DOC and HCO_3 contents, 1.4 and 7.7 mg/L respectively, making the latter ^{14}C results less certain. The drilling content was, however, low (0.04%). Although more data are necessary to validate more thoroughly the results, the indication is that organic material with significantly decreased ^{14}C is present in the groundwater to depths of around 200 m. The $\delta^{13}C$ signature in the organic material is in the range of –23.4 to –27.10‰ for all three samples.

Figure 3-25 showing ^{14}C (pmC) versus $\delta^{18}O$ (‰ SMOW) indicates lowest $\delta^{18}O$ in waters with the lowest ^{14}C content. This is expected since low $\delta^{18}O$ groundwater is interpreted as being of partly glacial origin (old in ^{14}C perspective; half time of 5,730 years). However, the ^{14}C content in these waters still lies in the interval 25–40 pmC, indicating mixing with post- glacial carbon sources. For example, the Laxemar groundwaters with the most distinct glacial component (KLX04:510 and 515 m) shows a ^{14}C (pmC) content of 43% and a tritium content of 1.2 TU. However, mixed in with this groundwater is also a 4% component of drilling water which prior to dilution contained 7.2 TU. Nevertheless, the groundwater from KLX04:510 and 515 m with a Cl content of approx. 1,500 mg/L therefore can be assumed to be a mixture of glacial and old saline waters with a (small?) meteoric water component which may be partly or completely a result of borehole activities. It is likely, however, that this meteoric water component has affected the ^{14}C content significantly.

In conclusion, only a small number of carbon isotope analyses are available from the groundwaters at depths greater than 200 m. A distinct lowering of the ^{14}C carbon content can be identified in the near-surface groundwaters (0–200 m), clearly visible already at very shallow depths (0–10 m) and in tritium-containing waters. This may be partly caused by dissolution of old radiocarbon-free carbonates present in the soil cover and upper bedrock fractures, but involves probably to larger extent the breakdown of organic material of various ages, some significantly older than the present.

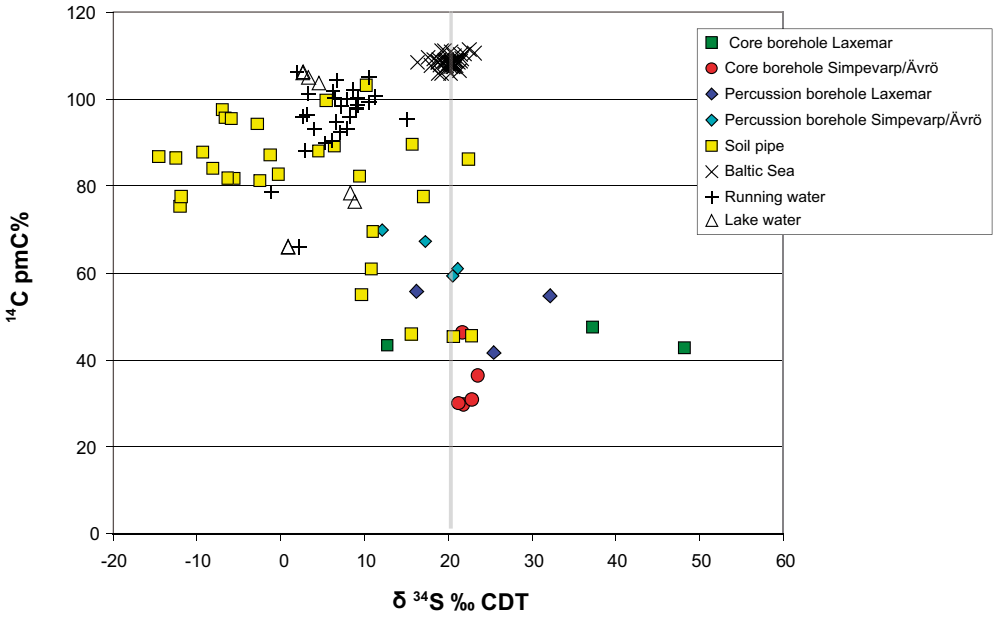

Figure 3-24. *$\delta^{34}S$ (‰ CDT) vs ^{14}C (pmC%) in the Simpevarp and Laxemar subareas.*

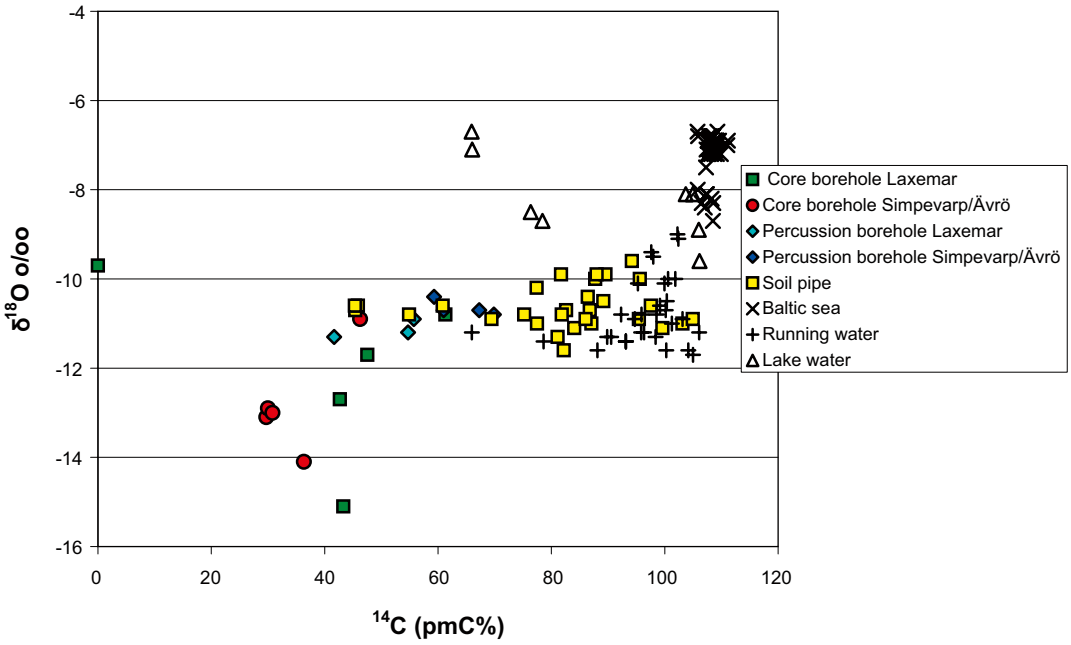

Figure 3-25. *^{14}C (pmC) versus $\delta^{18}O$ (‰ SMOW) in the Simpevarp and Laxemar subareas.*

Despite these uncertainties to the origin of ^{14}C, it is interesting from a hydraulic viewpoint to compare the tritium and ^{14}C plots versus depth (Figures 3-18 and 3-20). Here the ^{14}C plot reveals an added sensitivity to each of the sites at depths below approx. 150 m. At Simpevarp/Ävrö, which is generally a discharge area, lower ^{14}C values (i.e. older groundwaters) would be expected at higher, shallower levels, which is the case. In comparison, Laxemar, a recharge area, would be expected to show higher values at equivalent depths, which also is the case. Also, for the same reason, Simpevarp/Ävrö would be expected to have higher ^{14}C values within the 0–150 m interval since these younger groundwaters are not dispersed downwards to the same extent as for the Laxemar shallow groundwaters. This is the case for the Simpevarp/Ävrö persussion boreholes. For Laxemar within this 0–150 m level, dispersion downwards would result in a 'dilution' to lower ^{14}C values than the Simpevarp/Ävrö groundwaters, which is the case with the Laxemar percussion boreholes.

3.2.3 Strontium

^{87}Sr is a radiogenic isotope produced by the decay of ^{87}Rb (half-life $5 \cdot 10^{10}$a). Strontium isotope ratios ($^{87}Sr/^{86}Sr$) in surface waters, Baltic Sea water and shallow and deep groundwaters from the Simpevarp area are plotted against strontium content in Figure 3-26.

Marine waters show a distinct Sr isotope signature (0.7092) which is very close to the measured values in the Baltic Sea waters. The surface waters vary between 0.719 and 0.728 and but show very low Sr contents (< 0.1 mg/L), whilst the near-surface groundwaters sampled in the soil pipes generally also show low, but slightly higher Sr contents (< 0.3 mg/L) and a much larger variation in strontium isotope ratios from 0.712 to 0.733. This variation indicates interaction (leaching) of minerals with different Rb/Sr ratios present in the overburden. Possible addition of marine strontium, for example leaching of sediments, also may have contributed (Figure 3-26).

The deeper groundwater samples from the Laxemar subarea analysed for Sr isotope ratios relate to both percussion and cored boreholes, respectively HLX10, HKX14, HLX20, HLX22 and HLX24, and KLX02: 1,155–1,165 and 1,345–1,355 m, KLX03: 193–198 m, 497–599 m and 964–975 m, KLX04: 510–515 m and 971–976 m and, finally, KLX06:250–264. The Cl contents of the waters sampled spans from very dilute to more than 31,230 mg/L. Compared with the surface waters and near-surface soil pipe samples, the groundwaters show a relatively small variation in Sr isotope ratios indicating that water/rock reactions (especially ion exchange) tend to homogenise the isotope

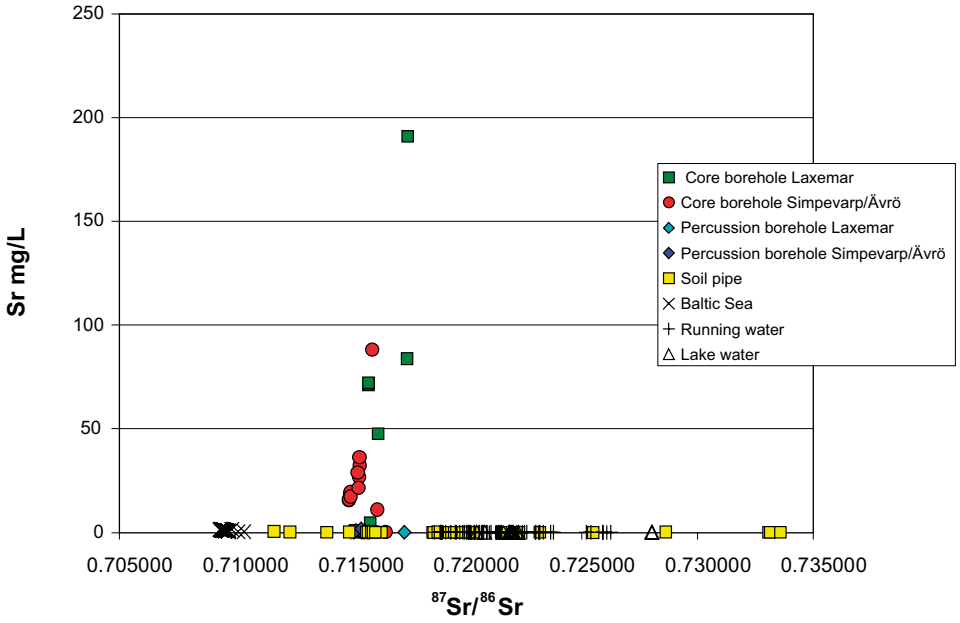

Figure 3-26. *Plot of $^{87}Sr/^{86}Sr$ ratios versus Sr content in the Simpevarp and Laxemar subareas.*

ratios in the bedrock fractures. In Figure 3-27 the strontium isotopes are plotted against the 1/Sr ratio for the percussion and cored borehole samples from the Simpevarp and Laxemar subareas, together with values for Baltic Sea water. There appears a tendency towards higher Sr isotope ratios (more radiogenic Sr) in the bedrock samples with Sr contents > 10 mg/L. These correspond to groundwaters of composition > 5,000 mg/L Cl. One explanation for the correlation of higher Sr isotope ratios with higher Sr contents is more extensive water rock reactions and lower water/rock ratios at depth. The spread is, however, large and more samples are needed to validate this statement.

The present findings are supported by /Peterman and Wallin 1999/ who, based on a larger set of samples, identified a similar trend of increasing Sr isotope ratios with increasing salinity for samples with salinities greater than 4,000 mg/L Cl.

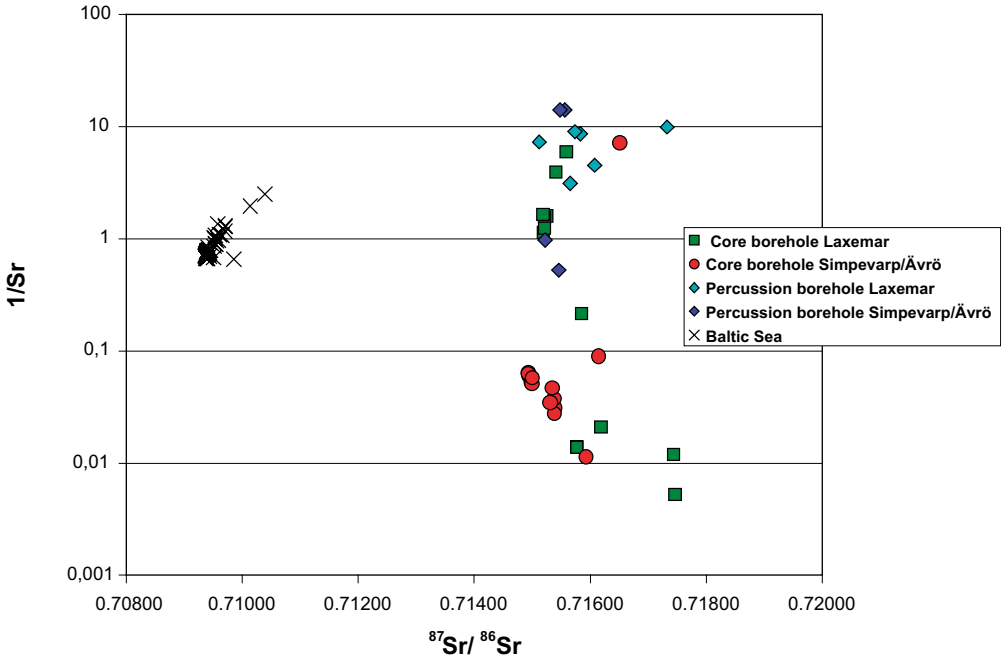

Figure 3-27. *Plot of $^{87}Sr/^{86}Sr$ ratios versus 1/Sr in the Simpevarp and Laxemar subareas.*

No marine Sr isotope signatures have been preserved, for example the Littorina Sea component identified in the Simpevarp subarea samples is not reflected by any marine Sr isotope imprint. Instead, modification of the Sr isotope values is probably attributable to ion exchange processes. To emphasise this, three samples have been analysed from borehole KLX03 section 193–198 m and four from section 964–975 m; six of these samples show a charge balance below ± 1.3% and a drilling water content below 1%. Both the Sr isotope ratio and Sr content are stable in these six water samples.

In conclusion, the available Sr isotope information from surface waters, Baltic Sea waters, near-surface groundwaters and deeper groundwaters, show two or possibly three distinct correlations between Sr isotopes, 1/Sr and salinity:

- Large variation in Sr isotope ratios but relatively small variation in Sr content for the near-surface groundwaters indicating interaction (leaching) from overburden with different mineralogical compositions.
- Large variation in Sr content but small variation in Sr isotope ratios for the fresh groundwaters indicating homogenisation of the Sr isotope ratios due to mineral/water interactions along the flow paths (mainly ion exchange).
- Tendency towards higher Sr isotope ratios with increasing Sr content for the saline samples possibly as a result of increasing more stagnant conditions.

3.2.4 Sulphur

Sulphur isotope ratios, expressed as $\delta^{34}S$ ‰ CDT, have been measured in dissolved sulphate in Baltic Sea waters, surface waters and groundwaters from the Simpevarp and Laxemar subareas. New for the present model version is the large number of soil pipe waters analysed. Specifically from the Laxemar subarea, three percussion borehole samples and twelve cored borehole samples are included in the data set. The isotope results are plotted versus SO_4^{2-} (Figure 3-28), Cl (Figure 3-29) and HCO_3 (Figure 3-29). The chloride contents of the analysed groundwaters range from approx. 10 to 17,000 mg/L.

The recorded sulphur isotope values vary within a wide range (–15 to +48‰ CDT) indicating different sulphur sources for the dissolved SO_4^{2-}. The surface waters (lake and streams) and parts of the near-surface groundwaters (soil pipes) show SO_4^{2-} contents below 50 mg/L and low but variable

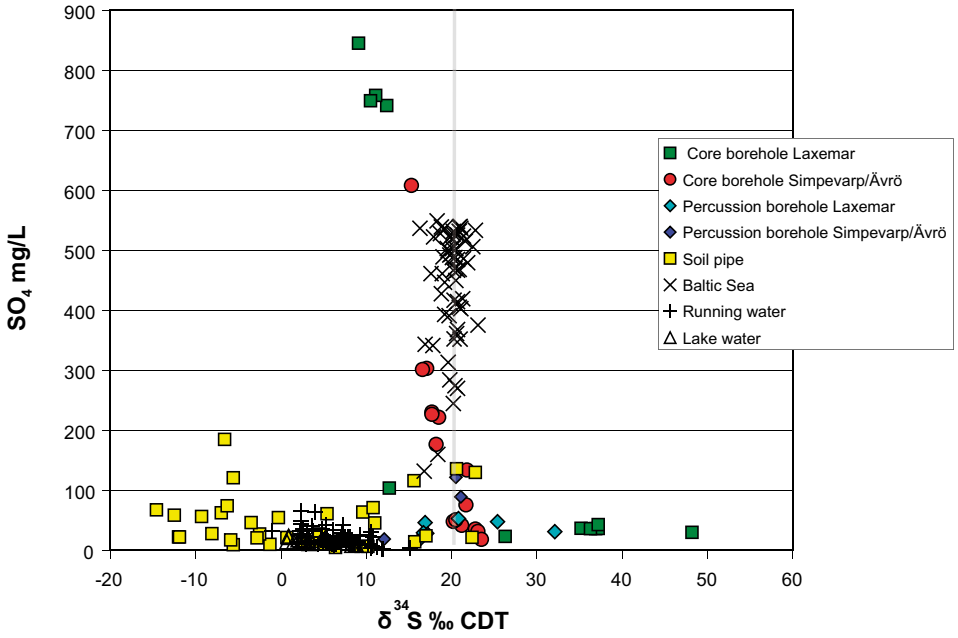

Figure 3-28. *Plot of $\delta^{34}S$ versus SO_4^{2-} in the Simpevarp and Laxemar subareas. The marine value is approx. +20‰ CDT.*

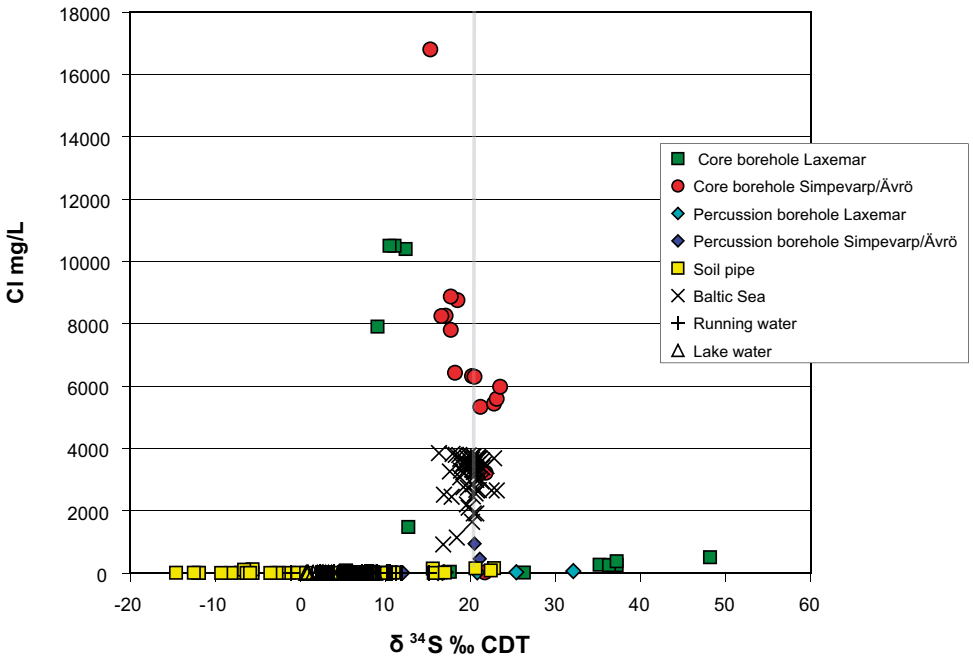

Figure 3-29. *Plot of $\delta^{34}S$ versus Cl in the Simpevarp and Laxemar subareas. The marine value lies at around +20‰ CDT.*

$\delta^{34}S$ (0 to +15‰ CDT). The relatively low sulphur isotope ratios probably reflect that of atmospheric deposition at the studied sites, possibly with some contribution from the oxidation of sulphides in the overburden.

The soil pipe waters show large variations in sulphur isotope composition (–15 to + 22‰ CDT). Two samples show close to marine values (soil pipes SM00022 and SM00029) which contrasts to most of the soil pipe samples with SO_4 contents above 50 mg/L where very low $\delta^{34}S$ values (–15 to –5‰ CDT) are typical. This is a possible indication of oxidation of sulphides. There is a tendency also towards lower $\delta^{34}S$ values with higher SO_4^{2-} contents in these waters, but the spread is large. The Baltic Sea waters cluster around the +20‰ CDT marine line but show a relatively large spread (+16 to +23‰ CDT). The reason for this is not fully understood but suggestions include: a) contribution from land discharge sources (e.g. streams) to various degrees (low values), and b) potential bacterial modification creating high values in the remaining SO_4^{2-}.

The borehole groundwaters (Figure 3-28) show $\delta^{34}S$ values between +9.1 to +48.2‰ CDT. Most of the Simpevarp subarea samples show values in the range +15 to +25‰ CDT, whereas the Laxemar samples show both very high and low values. Values higher than marine (< 20‰ CDT) are found in samples with chloride contents < 6,500 mg/L (Figure 3-30). These $\delta^{34}S$ values are interpreted as being produced in situ by sulphate-reducing bacteria. The highest values (+32 and +48‰ CDT) are detected in Laxemar waters with Cl contents less than approx. 500 mg/L (HLX 14 and KLX03: 103–218 m and KLX03:193–198 m). The SO_4^{2-} contents in these waters are low (around 30 mg/L). Such an extreme $\delta^{34}S$ value as +48‰ CDT is a strong indicator of biological activity in closed conditions. It is therefore interesting to note that the water showing this value is from an early sampling campaign in borehole KLX03 (KLX03:103–218 m) which showed also a component of glacial meltwater and thus has probably has been hydraulically isolated for a long time.

Groundwaters with SO_4 contents higher than 200 mg/L show decreasing $\delta^{34}S$ with increasing sulphate content. Deep saline SO_4^{2-} sources may have resulted from the leaching of sediments and/or dissolution of gypsum previously present in fractures. Lowering of the $\delta^{34}S$ signature by oxidation of sulphides seems to be less probable for the groundwater samples and is not supported by fracture mineral investigations /Drake and Tullborg 2004/. Gypsum has been identified in a number of fractures from boreholes KLX03, KLX06 and KLX08 (cf section 1.4). Recent sulphur isotope analyses of two fracture gypsum samples from borehole KLX03:533 and 590 show values in the interval +6.3

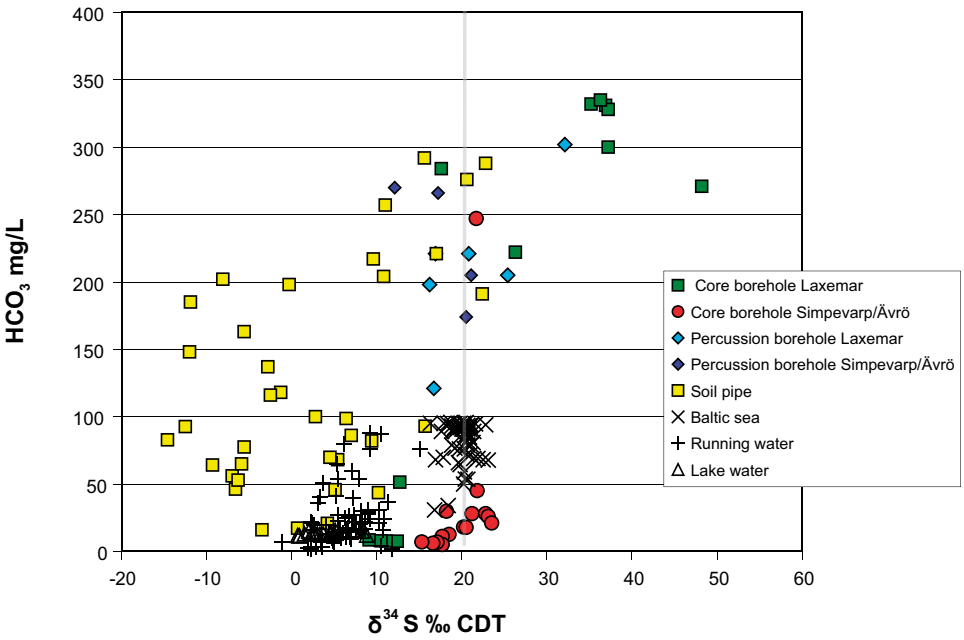

Figure 3-30. *Plot of $\delta^{34}S$ versus HCO_3 in surface waters and groundwaters from the Smpevarp and Laxemar subareas. The marine value lies at around +20‰ CDT.*

and +6.8‰ CDT, supporting a lowering of the $\delta^{34}S$ signature by dissolution of gypsum. Geochemical modelling /Gimeno et al. in Laaksoharju 2004/ also supports dissolution of gypsum as a possible source for SO_4 in the groundwaters.

Within the present data set three samples from section 964–975 m in KLX03 are included. These show relatively large variations in $\delta^{34}S$ (+10.5 to 12.4‰ CDT) taking into account that the Cl and SO_4 values were quite stable for the three samples. The four samples analysed from KLX03:193–198 in contrast, show very stable $\delta^{34}S$ values together with Cl and SO_4. The reason for the larger variation in $\delta^{34}S$ in the deep saline water compared with the more shallow fresh water is not at presently understood. One possibility is that it reflects the variation in isotopic composition of the fractures minerals dissolved, but additional groundwater/fracture mineral sample pairs are needed for further understanding the processes.

The possible indication of a Littorina component present in the Simpevarp subarea groundwaters, but (almost?) absent in groundwaters from the Laxemar subarea, is once again indicated in Figure 3-29 were the Simpvarp groundwaters with Cl contents below 6,500 mg/L generally show $\delta^{34}S$ values close to marine.

The variation in $\delta^{34}S$ versus bicarbonate (Figure 3-30) shows as expected the highest HCO_3 in the waters associated with very high $\delta^{34}S$, supporting that sulphate-reducing bacteria have modified the chemical composition of these waters. It is also evident that the soil pipe waters showing the lowest $\delta^{34}S$ also show relatively high bicarbonate content. It can be assumed, therefore, that microbial activity is high in these shallow groundwater samples but more detailed microbe information is lacking for the soil pipe waters.

Stable isotopes

Stable chlorine isotopes may be used as an indicator of marine versus non-marine derived groundwaters and therefore provides further support for detecting a transition from marine towards non-marine, deeper saline groundwaters. According to /Frape et al. 1996/ modern Baltic Sea and possibly palaeo-Baltic waters may be recognised by negative $\delta^{37}Cl$ signatures related to salt leachates from Palaeozoic salt deposits south of the Baltic Sea. Influence by water-rock interaction (i.e. characteristic of deep, highly saline groundwaters and brines) tends to result in positive $\delta^{37}Cl$ signatures. /Clark and Fritz 1997/ also show a clear distinction between groundwaters from the Fennoscandian and Canadian Shield crystalline rock and groundwaters from sedimentary aquifers.

Figure 3-31 shows that non-marine derived groundwaters (i.e. from the Laxemar subarea) show the highest $\delta^{37}Cl$, but when taking the analytical uncertainty of around ± 0.2‰ SMOC into consideration the difference between the Baltic Sea waters and the deep saline groundwaters is not very large. However, when comparing the Laxemar and Simpevarp groundwaters with the Forsmark site, were a clear marine Littorina signature has been detected, two different patterns can be observed (Figure 3-32). The Forsmark waters show an even greater spread in $\delta^{37}Cl$ but tend to be centred around the marine 0‰ SMOC line. Notably the Baltic Sea waters show larger variation in $\delta^{37}Cl$ than the marine groundwaters at Forsmark. The few samples representing deep saline (non-marine?) groundwaters from Forsmark still show low $\delta^{37}Cl$ values (–0.5 to +0.2‰ SMOC).

Common for both sites (Forsmark and Simpevarp) is that the surface waters and non-saline shallow groundwaters (soil pipes) show the largest variation in $\delta^{37}Cl$ values.

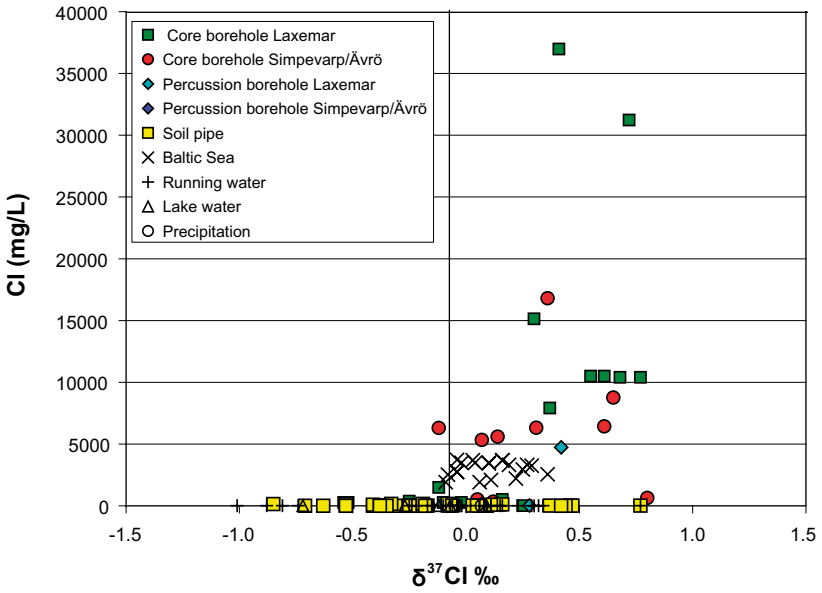

Figure 3-31. *Plot of $\delta^{37}Cl$ versus Cl in surface and Baltic Sea waters and groundwaters from the Simpevarp area.*

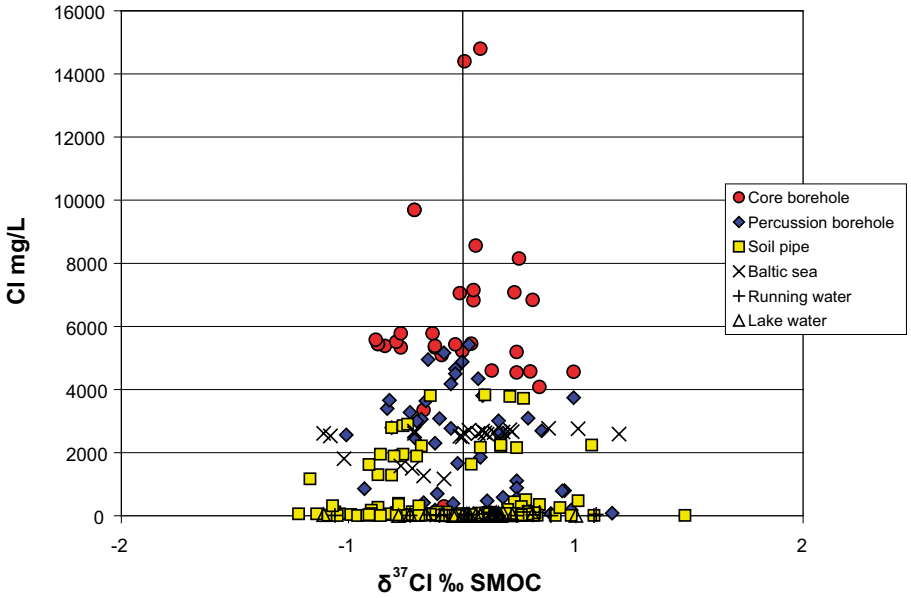

Figure 3-32. *Plot of $\delta^{37}Cl$ versus Cl in surface and Baltic Sea waters and groundwaters from the Forsmark area.*

4 Pore water studies on borehole KLX08

4.1 Introduction

Since the Laxemar 1.2 hydrogeochemical evaluation, the pore water studies on borehole KLX03, partly described in /SKB 2006/, now have been completed and published as two P-Reports /Waber and Smellie 2006ab/. The present data freeze for the Laxemar 2.1 evaluation includes pore water data for borehole KLX08, the second hydrogeochemically prioritised borehole of the Simpevarp area site characterisation programme. Presentation of these data and some provisional interpretation are given below. At the time of the data freeze there were no groundwater chemical data available from KLX08.

The term *'pore water'* as used here refers to the water in the connected pore space of the rock matrix that is accessible for diffusion-dominated interaction with groundwater circulating in nearby (micro-) fractures. Accessible, interconnected pore water has been extracted successfully by laboratory out-diffusion methods using drillcore samples from borehole KLX03, and now from borehole KLX08, as part of the Simpevarp area hydrogeochemical site investigation programme. The objective is to characterise these waters chemically and isotopically and relate these data to the present and past groundwater evolution of the site. In addition, the method of extraction, together with interfaced measurements of interconnected porosity, provides the opportunity to derive diffusion coefficient values of potential use in predicting future rates of solute transport. All analytical data are tabulated in Appendix 2.

Borehole KLX08, of length 1,000.41 m, was drilled at an inclination of 60 degrees. To facilitate close comparison with borehole logging data the length along the borehole is used rather than vertical depth.

The samples from borehole KLX08 investigated for their pore water composition are listed in Table 4-1, and the types of experiments and measurements performed are listed in Table 4-2. Besides the sample depth the table also gives the major geological features such as rock type, and qualitative descriptions of the rock alteration and fracture frequency in the near-vicinity of the samples. Such information is required for the interpretation of the acquired data with respect to chemical reactions that occur during the experiments and the extent of in situ interaction between pore water and fracture groundwater. The complete analytical protocol was performed on 10 out of the 19 pore water samples listed, based on their occurrence with respect to lithology, rock alteration and fracture intensity. An additional 8 pore water samples were analysed for $\delta^{18}O$, $\delta^{2}H$ and Cl; these were selected based on promising results from the first batch of samples.

4.2 Water content and water-content (connected) porosity

The water content of crystalline rock samples from drillcore material depends on sample depth and rock type. Two largely independent methods were used to determine the water content: a) the isotope diffusive-exchange method, and b) by drying at 105°C until stable weight conditions were achieved. For the three major rock types in KLX08 the water contents are generally below 0.4%, and there is good agreement in the water contents derived by the two methods (Figure 4-1; Appendix 2, Table 1).

The water contents for the Avrö granite agree well with those obtained from borehole KLX03 /Waber and Smellie 2006b/. The KLX08 borehole shows that there is a general trend towards decreasing water contents with increasing depth with no marked change between the Avrö granite, diorite and quartz-monzodiorite. This change contrasts somewhat with borehole KLX03, although the difference may reflect an absence of measured deep quartz-monzodiorite samples in KLX08 (i.e. samples taken from 819 m and 850 m vertical depth). The few samples that deviate from the general decrease in water content with depth (i.e. increased values) can be explained by more tectonised and hydrothermally altered zones in the different host rocks.

Table 4-1. Borehole KLX08: List of samples used for pore-water studies

Sample No	SKB Sample No	Average depth along borehole (m)	Lithology	Alteration / tectonisation[1)]	Fracture intensity (per metre)
KLX08-1	SKB 09700	150.22	Avrö granite	± 1.6 m	8-9
KLX08-2	SKB 09701	199.45	Fine-grained granite	± 1.0 m	7-8
KLX08-3	SKB 09702	200.26	Avrö granite	± 1.5 m	7-8
KLX08-4	SKB 09703	250.19	Avrö granite	± 13 m	4-5
KLX08-5	SKB 09704	302.34	Avrö granite	± 1.2 m	9-10
KLX08-6	SKB 09705	347.10	Avrö granite	± 37 m	2-3
KLX08-7	SKB 09706	395.65	Avrö granite	± 3.0 m	7-8
KLX08-8	SKB 09707	451.62	Avrö granite	± 2.0 m	6-7
KLX08-9	SKB 09708	499.78	Avrö granite	± 16 m	6-7
KLX08-10	SKB 09709	550.23	Avrö granite	± 64 m	2-3
KLX08-11	SKB 09710	601.68	Diorite	± 2.3 m	3-4
KLX08-12	SKB 09711	660.03	Diorite	± 4.0 m	5-6
KLX08-13	SKB 09712	702.05	Diorite	± 23 m	7-8
KLX08-14	SKB 09713	750.80	Avrö granite	± 72 m	1-2
KLX08-15	SKB 09714	802.22	Avrö granite	± 52 m	1-2
KLX08-16	SKB 09715	857.98	Avrö granite	± 4.0 m	2-3
KLX08-17	SKB 09716	903.28	Avrö granite	± 47 m	2-3
KLX08-18	SKB 09717	945.75	Qtz-monzodiorite	± 92 m	5-6
KLX08-19	SKB 09718	983.18	Qtz-monzodiorite	± ? m	2-3

[1)] Approximate distance to next major alteration zone above and below sample

Table 4-2. Borehole KLX08: Experiments and measurements performed on drillcore samples.

Sample	Water-content porosity	Density	Isotope diffusive exchange	Out-diffusion experiment		
				chemistry, pH, alkalinity	Sr- & Cl isotopes	chloride time-series
KLX03-1	X	X	O	X		X
KLX03-2	X	X	O	X		X
KLX03-3	X	X	X	X		X
KLX03-4	X	X	X	X	X	X
KLX03-5	X	X	X	X		X
KLX03-6	X	X	X	X	X	X
KLX03-7	X	X	X	X		X
KLX03-8	-	X	-	X		X
KLX03-9	X	X	-	X	X	X
KLX03-10	X	X	X	X	X	X
KLX03-11	X	X	X	X	X	X
KLX03-12	X	X	X	X		X
KLX03-13	X	X	X	X	X	X
KLX03-14	X	X	X	X	X	X
KLX03-15	X	X	X	X	X	X
KLX03-16	X	X	X	X		X
KLX03-17	X	X	X	X	X	X
KLX03-18	X	X	X	X		X
KLX03-19	X	X	X	X	X	X

X = experiment performed, analyses available
- = inadequate material to perform the experiment
O = experiment performed, analytical data not produced based on final sample collection

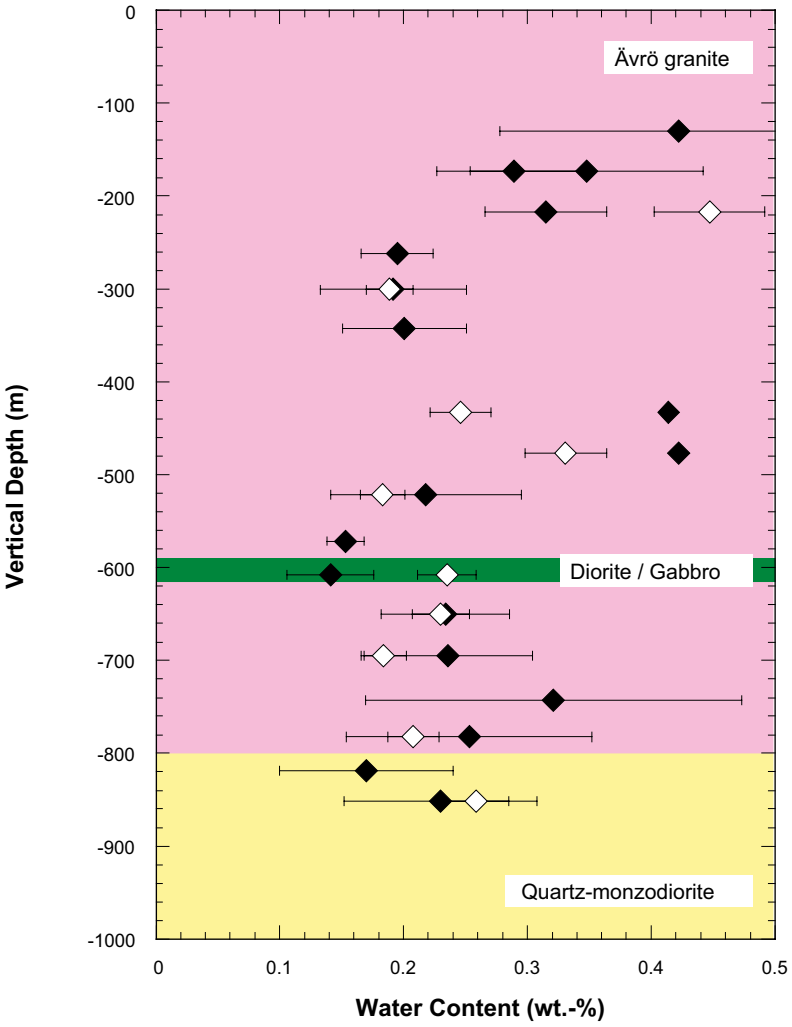

Figure 4-1. *Borehole KLX08: Water content in rock core samples derived by the isotope diffusive-exchange method (open symbols) and by drying at 105°C (closed symbols). Both methods show essentially the same trends independent of lithology and sample depth. Note the overall trend towards a decrease of the water content with increasing depth.*

4.3 Extraction and chemical composition of 'pore water'

Extraction of the pore water is carried out by out-diffusion experiments. Strictly speaking, these experiments only deliver direct information about chemically conservative elements of the pore water due to the inevitable interactions between rock and test water during the experiment. The more mineralised a pore water is, however, the more the observed elemental concentrations in the final experiment solution will be dominated by those prevailing in the pore water compared to the contributions of mineral dissolution reactions. Thus, the chemical composition of the experiment solution can also reveal certain indications about general chemical trends in the pore water before applying sophisticated geochemical modelling.

4.3.1 Extraction

Steady-state conditions of the out-diffusion experiments were controlled by taking small-sized samples (0.5 mL) of the experiment solution at regular intervals. The experiments were terminated and the supernatant solution removed for chemical and isotope analyses when the chloride concentrations had reached a plateau as a function of time, i.e. when steady-state conditions were reached (Figure 4-2). The experiments were run at 45°C and terminated after about 90 days.

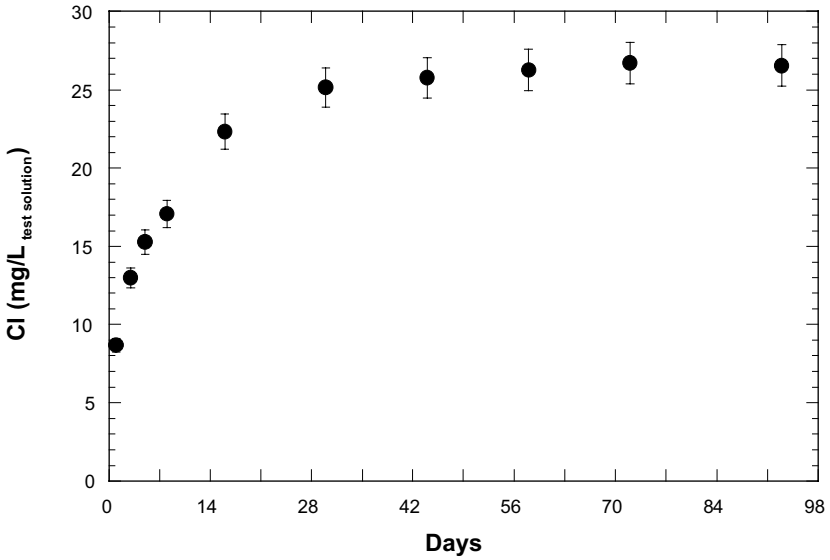

Figure 4-2. *Chloride concentration of the experiment solutions as a function of diffusion time (chloride time-series). The achieved plateau indicates steady-state conditions for chloride diffusion at 45°C after about 70 days (sample KLX08–10, Ävro Granite at 550.23 m borehole length and 476.5 m vertical depth respectively)*

4.3.2 Chemistry of the experiment solutions

Following termination of the out-diffusion experiment the supernatant experiment solutions initially were analysed for their chemical and Cl- and Sr-isotopic composition (Appendix 2, Tables 2 and 3). Figure 4-3 shows the major ion composition of the experiment solutions derived from the out-diffusion experiments at different vertical depths. The different water types can be summarised as follows:

- 0–400 m : Na-Ca-HCO_3
- 400–500 m : Na-Ca- HCO_3-Cl
- 500–650 m : Na-Ca-HCO_3
- 650–800 m : Ca-Na-SO_4
- 800–900 m : Na-Ca-Cl-HCO_3

For such experiment solutions HCO_3 might not be representative for the in situ pore water composition due to its high reactivity. However, in the low mineralised solutions extracted from the shallow drillcore samples the other anion concentrations are low and HCO_3 might also be a dominant anion in the pore water. In contrast, the deep samples yielding strongly mineralised experiment solutions and HCO_3, stems mainly from reactions during the experiment. In common with borehole KLX03 /Waber and Smellie 2006b/, the experiment solutions suggest the occurrence of weakly to moderately mineralised Na-Ca-HCO_3-(Cl) type pore water in the shallow zones, and strongly mineralised pore water of Ca-Na-SO_4 type with up to about 6 g/kgH_2O Cl (see below) occurring just above the Avrö granite/quartz-monzodiorite boundary. The overall chemical stratification with depth compares well to that obtained for the KLX03 borehole, which suggests highly mineralised (about 8 g/kgH_2O Cl) pore water of a general Na-Ca-Cl type at greatest depth.

4.3.3 Chloride concentrations of the pore water

The non-reactive behaviour of chloride and the non-destructive nature of the out-diffusion experiments make the pore water the only source for dissolved chloride in the experiment solutions. Therefore, the chloride concentration of the experiment solution can be converted to pore water concentrations using mass balance calculations given that steady-state conditions in the out-diffusion

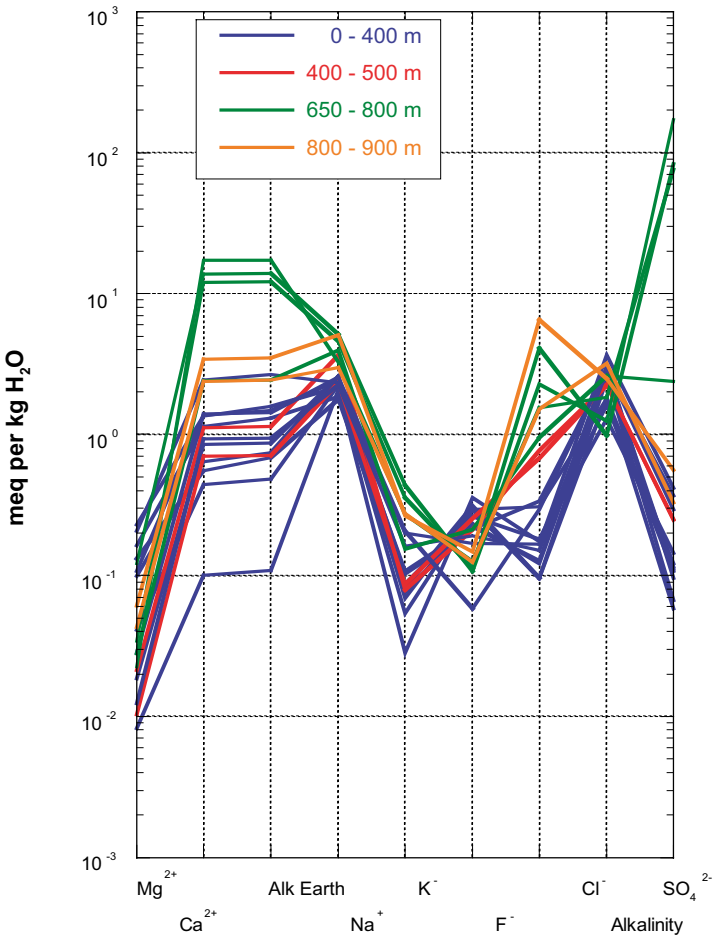

Figure 4-3. *Borehole KLX08: Schoeller diagram of experiment solutions from the KLX08-drillcore samples showing the change in chemical type and degree of mineralisation as a function of depth below surface. Note the distinct changes in solution composition with the Avrö granite/quartz-monzodiorite boundary being at about 800 m depth below surface.*

experiment are achieved. At steady-state conditions the chloride concentration in the connected porosity of the rock sample will be equal to that of the experiment solution. With knowledge of the mass of pore water in the rock sample, the chloride concentration of the pore water can be calculated (Appendix 2, Table 3).

In borehole KLX08 (Figure 4-4), chloride concentrations of less than 1 g/kgH_2O pore water are obtained for the shallower depths down to about 500–600 m were there is a high frequency of hydraulically conductive fractures and a corresponding increase in transmissivity (up to 10^{-5} m^2s^{-1}). Furthermore, the pore water chloride increases significantly towards the transition between the Ävrö granite and quartz-monzodiorite coinciding with decreased transmissivities down to $10^{-8.5}$ m^2s^{-1} and less. From here there is a steady chloride increase to values of 8.2 g/kgH_2O at 983 m borehole length (851 m below surface).

In comparison with borehole KLX03 /Waber and Smellie 2006b/ the pore water chloride profile in KLX08 shows exactly the same general pattern, i.e. dilute water in the Avrö granite until the boundary with quartz-monzodiorite, followed by a strong increase to the top of the quartz-monzodiorite and then a decrease, and finally a strong increase at maximum depth. In contrast, the chloride pore water concentrations below about 750 m are significantly higher than the highest chloride concentrations observed in borehole KLX03.

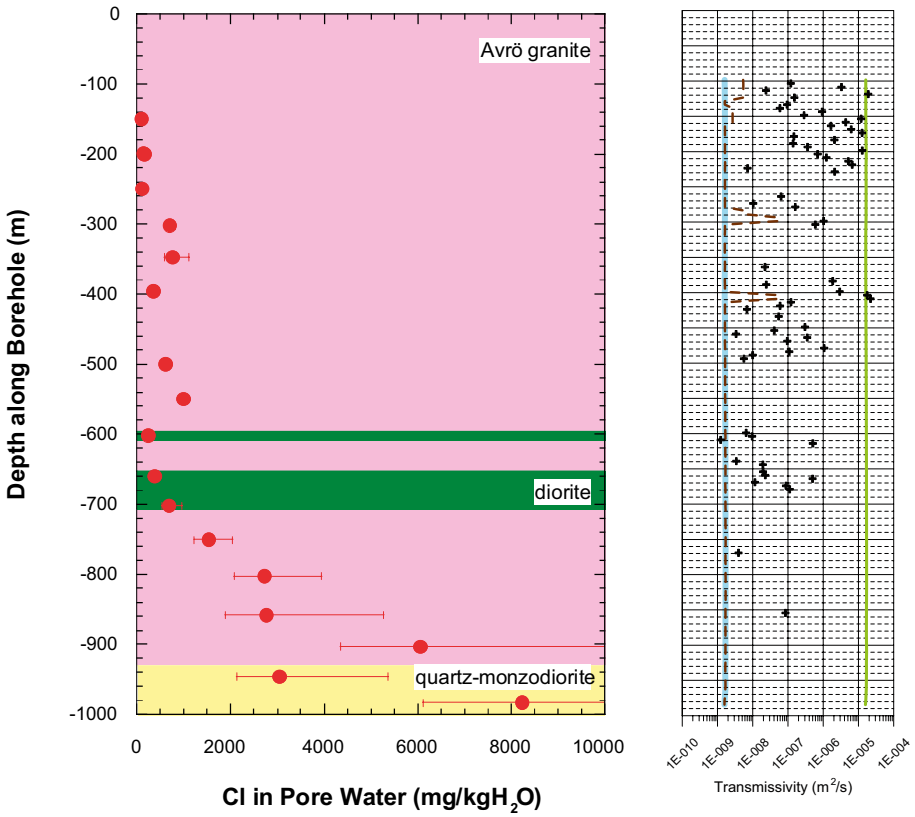

Figure 4-4. *Borehole KLX08: Chloride concentration in pore water as a function of borehole length compared to fracture transmissivity.*

4.3.4 Uncertainties

The uncertainty of the above chloride concentrations, especially when considering potential disturbances from drilling and stress release effects, can be estimated as follows. The breakthrough curves for Cl in the out-diffusion experiments (Figure 4-2) show that the transport of Cl in these experiments is controlled by diffusion. Pore diffusion coefficients become $2–5 \cdot 10^{-11}$ $m^2 s^{-1}$ (25°C) for the quartz-monzodiorite at Laxemar for the measured water-content (connected) porosity /Waber and Smellie 2006b/. Thus, since the calculation of the pore water concentration is inversely proportional to the water content, the error attached to this concentration is essentially determined by that of the water content and thus the uncertainty range is given by that of the standard deviation of the water content measurements (cf. section 4.2). Because the water contents have been determined by two independent methods which have resulted in the same values, any potential effects induced by drilling activites and/or stress release would appear to be minimal. A detailed discussion of the effects of drilling activites and/or stress release on the pore-water Cl concentration is given in /Waber and Smellie 2006c/ (submitted to Appl. Geochem.).

4.4 Influence of fracture hydraulics on pore water chemistry

As part of the KLX03 study which is included in Waber and Smellie (op. cit.), the influence of hydraulically-active fractures on pore water chemistry was addressed. On a 1-D scale (the only possibility from single borehole data) the distance of the analysed rock sample for pore water to the nearest hydraulically-conductive zone(s) was determined from the differential flow log.

Figure 4-5 attempts to combine: a) distance to the nearest water-conducting fracture(s), b) transmissivity of the fracture zone(s), and c) the pore-water chloride contents. The plot shows no definitive trends since the pore water chemistry will be influenced both by the location of the

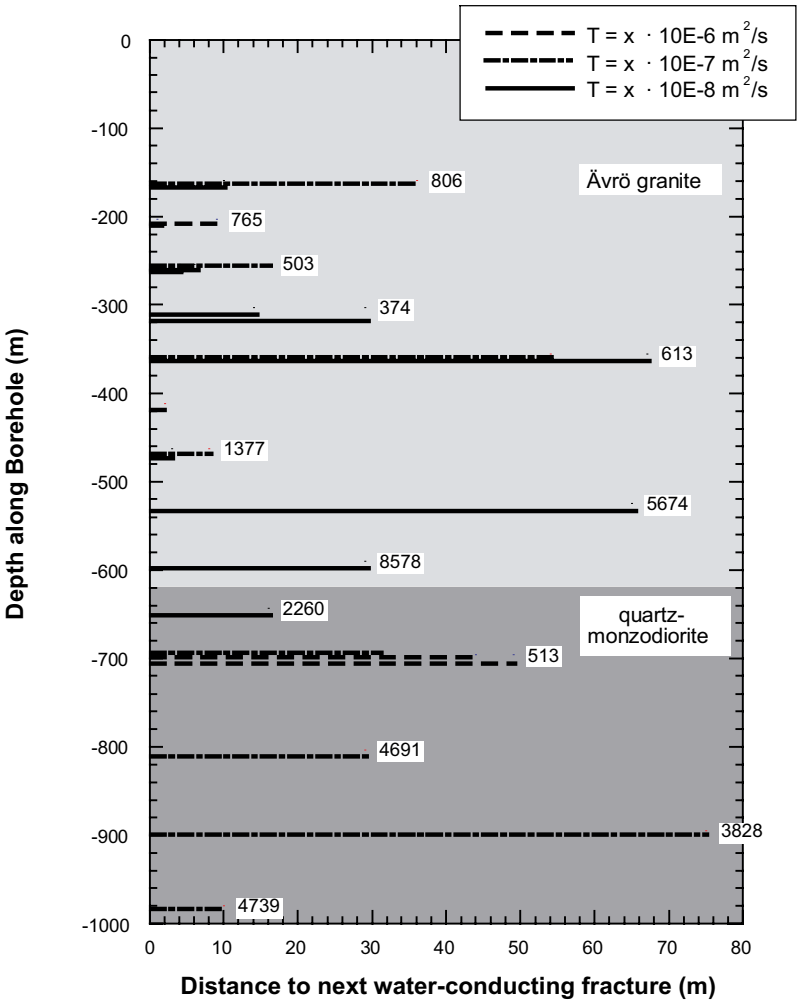

Figure 4-5. *Distance between the rock samples used for pore-water characterisation and the next water-conducting fracture in the Laxemar site borehole KLX03. Numbers indicate pore-water Cl concentration and the line styles give the measured fracture transmissivites (data from /Rouhiainen et al. 2005/).*

nearest water-conducting fracture and also its transmissivity, e.g. a closer, low transmissive fracture may influence the pore water chemistry less than a high transmissive fracture further away, and this appears to be the case at certain locations in borehole KLX03. In particular, the high chloride values (5.6 and 8.5 g/kgH_2O) in the Ävrö granite at around 530 m and 590 m depth respectively, are anomalously high when compared to those samples immediately above and below. This can be explained by the fact that these two cores have been sampled from within a very low transmissive rock mass (< 10–9 m^2s^{-1}) of low fracture frequency, extending from approx. 500–600 m depth, such that steady state conditions with the nearest fracture groundwaters are still far from being achieved.

4.5 General pore water trends at the Oskarshamn and Forsmark sites

Within the SKB site characterisation programme at Oskarshamn /Waber and Smellie 2006ab/ and Forsmark /Waber and Smellie 2005/, out-diffusion experiments on more than 40 rock samples of homogeneous rock samples of different lithologies suggest that the transport of chloride in the undisturbed rock mass occurs mainly by diffusion. Under such conditions the chemical gradient established between pore water and fracture groundwater depends on the time of interaction and the distance of the pore water sample to the closest water-conducting zone. An observed concentration gradient between pore water and fracture water therefore depends on the distance between the rock

sample and water-conducting fractures and the time period during which a groundwater with a different, but constant Cl content, flows in these fractures. Compared to boreholes KLX03 and KLX08 at Laxemar, the bedrock down to about 400 m depth in borehole KFM06A at Forsmark is characterised by a higher fracture frequency, higher transmissivities and shorter distances between pore water samples and the closest water-conducting fracture(s). The contrary is observed at greater depth.

It should be noted here that a borehole only yields a 1-D representation of the entire fracture network present in crystalline rocks and the actual fracture frequency might be underestimated. Nevertheless, the coherent picture obtained for the Laxemar subarea site allows some statements on the life-span of the presently active fracture-groundwater system. This becomes evident when the differences between the Cl contents in pore water and fracture groundwater as a function of depth, together with the distances to the closest water-conducting fracture, are compared. Such a comparison shows that the differences in Cl correlate with fracture frequency (and thus distances to the closest water-conducting fractures) and hydraulic transmissivity of the rocks (Figure 4-5). However, in the more transmissive, shallower levels, equivalent Cl contents indicate steady-state conditions existing between pore water and fracture groundwater in the Laxemar subarea site (at Forsmark the lower pore-water Cl contents indicate a transient state). At both sites the fracture frequency and hydraulic transmissivity decreases with increasing depth, and this coincides with an increase in the pore water chloride content. In contrast to the shallow levels, a transient state is now established at depth at Laxemar (while at Forsmark the Cl contents in pore water and fracture groundwater become similar indicating steady-state conditions at greater depth).

The complexity of the palaeohydrogeological evolution as recorded in the pore water is also shown by its isotopic composition (Appendix 2, Table 5). At Laxemar (and Forsmark) the water isotopic signature ($\delta^{18}O$ and $\delta^{2}H$) suggests a steady-state situation in the more transmissive shallow levels and a transient state with less negative values in the pore water at greater depth. This seems to contradict the distribution patterns established for Cl, but can be explained by the composition of possible end-member compositions that have contributed to the situation observed today. For example, the brine end-member would have a ten times higher Cl concentration than Baltic and Littorina seawater, but only a small difference in the isotope composition. In addition, steady-state conditions are faster attained for $\delta^{18}O$ and $\delta^{2}H$ compared to Cl due to the different diffusion coefficients in low permeability rocks /e.g. Gimmi and Waber 2004/.

4.6 Conclusions

Pore waters characterised by direct and indirect methods from low-permeable crystalline rocks from the Laxemar (and Forsmark) sites have a distinct chemical and isotopic composition. Pore-water compositions differ from those of fracture groundwaters depending on the distance between the location of the pore-water sample in the rock matrix and the nearest water-conducting fracture, and the time period of constant composition of the fracture groundwater. Combined with measured and experimentally derived hydraulic properties, these compositional differences support diffusion-dominated solute transport in the low-permeable rock masses. From the present investigations it can be concluded that in such a rock mass the diffusion-accessible porosity extends over significant distances (at least metres to tens of metres).

Pore water compositions derived by indirect methods from drillcore samples from the Laxemar subarea (and Forsmark) site can be interpreted within a larger palaeohydrogeological framework. The methods applied minimise experimental disturbances and effects induced by drilling activities and/or stress release effects, and the obtained pore water compositions have well definable uncertainties. Further methodological improvements are, however, required to reduce these uncertainties. The pore-water chemical and isotope compositions show distinct trends correlating with rock types and with depth, becoming more saline with increasing depth at both sites. Concentration gradients established between pore water and fracture groundwaters coincide with higher fracture frequency and transmissivity in the host rocks, were the location of the pore water sample is closer to water-conducting fractures. Differences developed in the attainment of steady-state conditions between pore water and fracture water between the Laxemar and Forsmark sites support a different hydrogeological, and therefore hydrogeochemical evolution, at least during Holocene times.

5 Visualisation of the Simpevarp area data

Details of the construction of an integrated 2-D model of the Simpevarp area to help explain the lateral and and vertical spatial variation in the hydrochemical data have been documented in the Laxemar 1.2 evaluation /SKB 2006/. Since then new data of varying quality have been obtained from additional percussion boreholes HLX28 and 34, and cored boreholes KLX05, 07, 08 and 10 (cf. section 2.3). Some outstanding analytical data (and also some new borehole data) for the Laxemar 1.2 evaluation boreholes, received after the Laxemar 1.2 data freeze, are also included.

Figure 5-1 shows the locations of the two transects used for the 2-D integrated Laxemar 1.2 model evaluation. Of the new data, boreholes KLX07 and KLX10 fall along or close to the WNW-ESE transect and KLX08 is common to both both transects, being located at the intersection of the WNW-ESE and the SSW-NNE transects. Borehole KLX05 lies well away from the two transects close to the southern boundary of the Laxemar subarea. For the Laxemar 2.1 hydrogeochemical visualisation, and to integrate closely with the hydrogeological modelling (I. Rhén, per. comm.), an additional WNW-ESE transect has been selected further to the south to link boreholes KLX11, KLX03 and KLX05/12 (Figure 5-2). These three transects therefore have been designated to model and illustrate both the hydrogeology and hydrochemistry for the Laxemar 2.1 evaluation. At the moment, however, there are insufficient hydrochemical data to satisfactorily address the newly proposed WNW-ESE transect, and the discussion below will be confined to the earlier Laxemar 1.2 version (Figure 5-1).

Figure 5-1. *Location of new Laxemar 2.1 boreholes (ringed) in relation to the two transects designated for the 2-D integrated Laxemar 1.2 model evaluation.*

Figure 5-2. *Location of the newly proposed Laxemar 2.1 evaluation WNW-ESE transect (compare Figure 5-1).*

Of the new Laxemar 2.1 hydrochemical data only borehole KLX08 is prioritised for complete chemical characterisation. Borehole KLX07 was drilled to confirm the deformation zones in the vicinity of KLX02, borehole KLX08 to assess the orientation of deformation zone ZSMEW007, borehole KLX10 to gain more knowledge of the rock block south of deformation zone ZSMEW007, and borehole KLX05 to confirm the deformation zone demarcating the southern boundary of the Laxemar subarea.

Basically, the additional Laxemar 2.1 quality assured hydrochemical data serve to support further the 2-D conceptualisation already presented in the Laxemar 1.2 evaluation /Laaksoharju 2006, SKB 2006/, and reproduced below in Figure 5-3. In particular, there is no convincing evidence of a Littorina Sea component in the hydraulic rock domains of the Laxemar subarea. The presence of such old marine waters, and additional waters with a glacial melt water component, may be preserved as lenses/pockets along dead-end fractures and/or within rock masses of low transmissivity, but as yet the drilling campaign has not revealed such sources. Since the onus has been to quantify the structural understanding of the site, most of the boreholes, and subsequently the groundwater samples, are associated with major water-conducting zones where preservation of palaeowaters would be least expected.

Borehole KLX08 has also confirmed the strong recharge environment generally represented by the Laxemar subarea, with deep penetration of meteoric waters. At depth mixing with a cold climate component is sometimes observed.

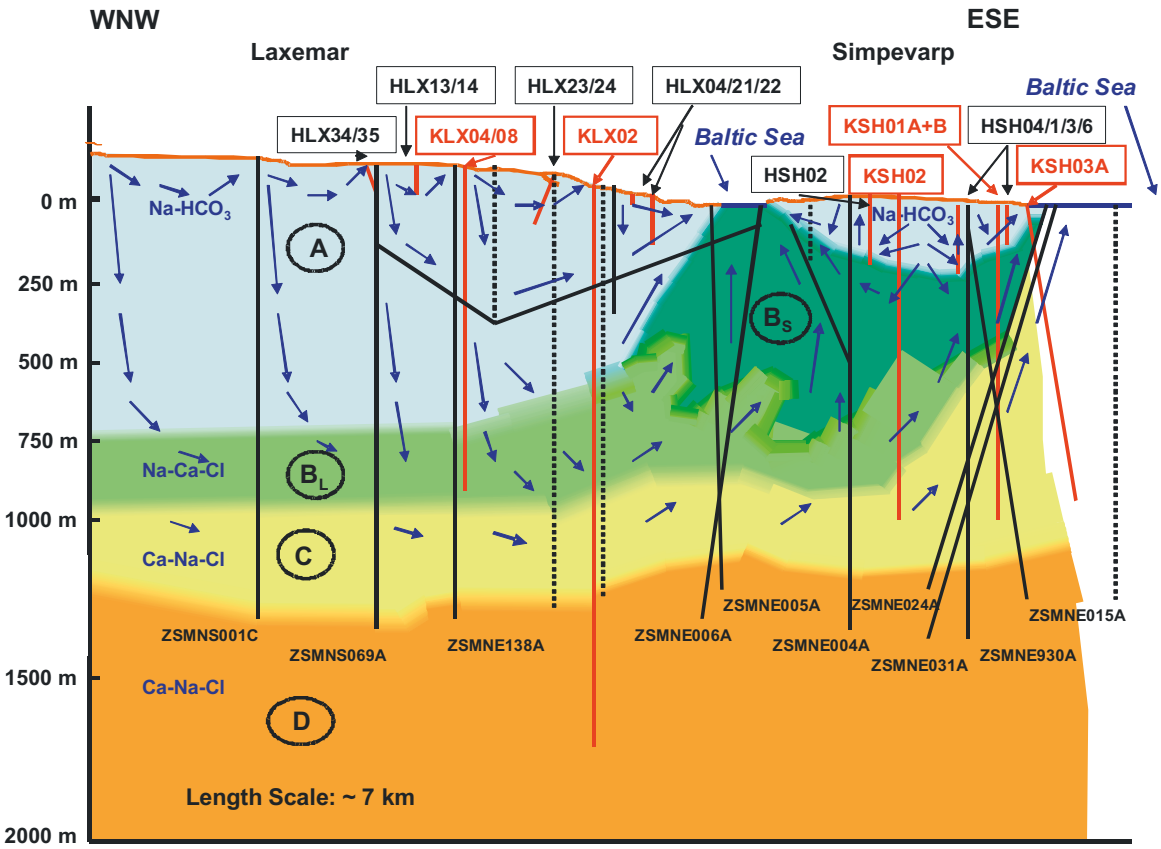

Figure 5-3. *Laxemar 1.2 evaluation: Schematic 2-D visualisation along the WNW-ESE transect (cf. Figure 5-1) integrating the major structures, the major groundwater flow directions and the variation in groundwater chemistry from the sampled boreholes. Sampled borehole sections are indicated in red, major structures are indicated in black (full lines = confident; dashed lines = less confident), and the major groundwater types A–D are also indicated. The blue arrows are estimated groundwater flow directions; short arrows low flow rates, long arrows greater flow rates. Note that the position of the Laxemar 2.1 borehole KLX08 coincides with KLX04 along the transect.*

6 Conclusions

The new Laxemar 2.1 data freeze information has served to further support the Laxemar 1.2 evaluation /Laaksoharju 2006, SKB 2006/. Major ion trends and their interpretation based on quality assured data have been strengthened and similarly for the major environmental isotopes of tritium, oxygen-18, deuterium and carbon-13/14. There is now a good understanding of the origin and evolution (e.g. mixing processes) of the different groundwater groups characterising the Simpevarp area. Additional isotope data of sulphur and strontium isotopes have added further knowledge of water/rock interactions and, specifically from sulphur, the local influence of microbial activity on groundwater redox conditions and chemistry.

The main conclusions are:

1. In the Simpevarp subarea and in borehole KLX01 (from the Laxemar subarea and located close to a Baltic Sea inlet), a marine component can be distinguished based on slightly higher Mg values, lower Br/Cl ratios and marine $\delta^{34}S$ values in groundwaters with Cl values < 6,500 mg/L. In all of the remaining boreholes drilled in the Laxemar subarea no marine signatures have yet been identified. The marine component in the Simpevarp subarea is, however, not as prominent as in Forsmark.
2. The Cl versus depth trend for the Laxemar subarea indicated in model version L 1.2 is further supported and underlines that the sharp transition between fresh and very saline waters in borehole KLX02 is probably structurally controlled on a local scale and not representative for the Laxemar subarea as a whole. However, in common with the other boreholes, fresh to brackish groundwaters (Cl < 5,000 mg/L) seem to dominate down to 600–700 m depth. A detectable glacial component (i.e. $\delta^{18}O$ < –12‰ SMOW) is found often at greater depths.
3. Significant bicarbonate production is recorded in the near-surface groundwaters (upper 200 m) in the Laxemar subarea and both carbon and sulphur isotope ratios support microbial activity, although some contribution from calcite dissolution has probably also taken place at shallow depths.
4. However one area of caution concerns the interpretation of the tritium (and carbon-14) values. Detailed examination of data at and close to the overburden/geosphere interface shows that some emissions from the nearby nuclear power plant have contributed to the amounts of tritium and carbon-14 analysed in the surface waters and near-surface groundwaters.
5. Pore waters characterised by direct and indirect methods from low-permeable crystalline rocks from the Laxemar subarea have a distinct chemical and isotopic composition. Pore water compositions differ from those of fracture groundwaters depending on the distance between the location of the pore water sample in the rock matrix and the nearest water-conducting fracture, and the time period of constant composition of the fracture groundwater.
6. In the Laxemar subarea investigated pore water compositions show: a) at shallower levels (i.e. to around 600 m in KLX08), were there is a generally high fracture frequency and a correspondingly high transmissivity, equivalent Cl contents indicate steady-state conditions existing between pore water and fracture groundwater, and b) a decrease in fracture frequency and hydraulic transmissivity with increasing depth to around 900 m coincides with an increase in the pore water chloride content and a transient state is now established.
7. The new hydrochemical data support the 2-D integrated Laxemar 1.2 conceptual model of the Simpevarp area, and no significant change of the various groundwater types are considered necessary. Because of a lack of hydrochemical data from some of the new Laxemar 2.1 boreholes, it was not possible at this stage to address satisfactorily the additional WNW-ESE transect proposed for the site area.

8. The interaction between surface waters, shallow groundwaters and the deeper groundwater aquifers can be studied by using the chemistry in combination with isotope systematics:
   - The very dilute surface waters show inhomogeneous environmental isotopic signatures ($\delta^{18}O$ and $\delta^{2}H$) indicating seasonal variations in precipitation. In addition, evaporation contributes to the overall inhomogeneity, for example some of the lake samples show a high $\delta^{18}O$‰ deviation from the Global Meteoric Water Line signifying open-surface evaporation conditions. This surface inhomogeneity, however, becomes successively diminished at increasing depth due to longer term mixing (i.e. homogenising) processes. This results in groundwaters in the percussion boreholes and some of the soil pipes being characterised by $\delta^{18}O$ and $\delta^{2}H$ signatures representing present-day annual mean values (in some percussion borehole samples also with a possible small glacial contribution) and tritium contents of around 10 TU or lower.
   - Interaction of surface waters and near-surface groundwaters with the overburden affects the carbon system resulting in increased HCO_3 and diluted ^{14}C signals being observed in some of the surface waters and, more significantly, in groundwaters in the near-surface soil pipes and deeper in the percussion boreholes.
   - $^{87}Sr/^{86}Sr$ and $\delta^{34}S$ show large variations in the surface waters even though the contents of strontium and sulphur are generally very low. In the near-surface soil pipe groundwaters large isotopic variations still persist although their contents are increasing. Obviously, different mineral/water interactions contribute to this behaviour.

Combining this information shows that the transition between the surface water and deeper groundwater is most evident in the soil pipe samples, i.e. the near-surface groundwaters. Here the seasonal variations level out and the biogenic activity and the water/mineral reactions are extensive. Most of the soil pipe groundwaters show tritium values around 9–15 TU which is very close to the surface waters and today's precipitation values. This may indicate that the waters are very young, but since the interplay between fall-out from the nearby power plants and decreasing global values since the 1960's are very difficult to evaluate, it can only be concluded that the major portion of these waters are younger than 50 years. The transition from open to semi-closed/closed conditions in respect of, for example, some biogenic reactions, seems to occur between soil pipe depths (5–10 m) and greater depths along the percussion boreholes. However not all boreholes show this behaviour.

7 References

Andersson P, Byegård J, Dershowitz B, Doe T, Hermanson J, Meier P, Tullborg E L, Winberg A, 2002. Final report of the TRUE Block Scale. 1. Characterisation and model development. SKB TR-02-13, Svensk Kärnbränslehantering AB.

Bath A, Milodowski A, Ruotsalainen P, Tullborg E-L, Cortés Ruiz A, Aranyossy J-F, 2000. Evidences from mineralogy and geochemistry for the evolution of groundwater systems during the quaternary for use in radioactive waste repository safety assessment (EQUIP project). EUR 19613 EN, Luxembourg.

Clark I, Fritz P, 1997. Environmental isotopes in hydrogeology. Lewis Publishers, New York.

Drake H, Tullborg E-L, 2004. Fracture mineralogy – results from XRD, microscopy, SEM/EDS and stable isotopes analyses. SKB P-04-250, Svensk Kärnbränslehantering AB.

Drake H, Tullborg E-L, 2005. Fracture mineralogy and wall rock alteration, results from drill cores KAS04, KA1755A and KLX02. SKB P-05-174, Svensk Kärnbränslehantering AB.

Drake H, 2006. Fracture fillings and red stained wall-rock in the Simpevarp area, SE Sweden. Licentiate Thesis, Göteborg University, Sweden (A102 2006).

Drake H, Tullborg E-L, 2006a. Mineralogy in water conducting zones. Results from boreholes KLX03, KLX04 and KLX06. SKB P-Report (In manuscript). Svensk Kärnbränslehantering AB.

Drake H, Tullborg E-L, 2006b. Mineralogical, chemical and redox features of red-staining adjacent to fractures, Results from drill cores KSH01A+B and KSH03A+B. SKB P-Rep. (In manuscript). Svensk Kärnbränslehantering AB.

Drake H, Tullborg E-L, 2006c. Mineralogical, chemical and redox features of red-staining adjacent to fractures, Results from drill core KLX04. SKB P-Rep. (In manuscript). Svensk Kärnbränslehantering AB.

Drake H, Sandström B, Tullborg E-L, 2006. Mineralogy and geochemistry of the rocks and fracture fillings from Forsmark and Oskarshamn: Compilation of data for SR-Can. SKB R-Rep. (In press). Svensk Kärnbränslehantering AB.

Ekman L, 2001. Project Deep Drilling KLX02. Phase 2. Methods, scope, summary and results. Summary Report. SKB TR-01-11, Svensk Kärnbränslehantering AB.

Eliasson T, 1993. Mineralogy, geochemistry and petrophysics of red-coloured granite adjacent to fractures SKB TR-93-06, Svensk Kärnbränslehantering AB.

Frape S K, Fritz P, 1987. Geochemical trends from groundwaters from the Canadian Shield. In: (Eds.) P. Fritz and S.K. Frape. Saline waters and gases in crystalline rocks. Geol. Assoc. Canada Spec. Paper 33, 19–38.

Frape S K, Byrant G, Blomqvist R, Ruskeeniemi T, 1996. Evidence from stable chlorine isotopes for multiple sources of chloride in groundwaters from crystalline shield environments. In: *Isotopes in Water Resources Management, 1966.* IAEA-SM-336/24, Vol. 1, 19–30.

Forssman I, Zetterlund M, Forsmark T, Rhén I, 2005. Correlation of Posiva Flow Log anomalies to core mapped features in KLX02, KLX03, KLX04, KLX04A and KAV04B. SKB P-05-241, Svensk Kärnbränslehantering AB.

Gascoyne M, 2004. Hydrogeochemistry, groundwater ages and sources of salts in a granitic batholith on the Canadian Shield, southeastern Manitoba. Appl. Geochem., 19, 4, 519–560.

Gimmi T, Waber H N, 2004. Modelling of tracer profiles in pore water of argillaceous rocks in the Benken borehole: Stable water isotopes, chloride and chlorine isotopes. Nagra Technical Report (NTB 04-05), Nagra, Wettingen, Switzerland.

Hallbeck L, 2006. Explorative interpretation of microbe, colloid, and gas data combined with modelling of microbial processes. Laxemar Hydrogeochemical Evaluation, version 2.1.

Laaksoharju M, Smellie J, Nilsson A-C, Skårman C, 1995. Groundwater sampling and chemical characterisation of the Laxemar deep borehole KLX02. SKB TR-95-05, Svensk Kärnbränslehantering AB..

Laaksoharju M (Ed.), 2004. Hydrogeochemical evaluation of the Simpevarp area, version 1.2. SKB R-04-74, Svensk Kärnbränslehantering AB.

Laaksoharju M (Ed.), 2005. Hydrogeochemical evaluation of the Forsmark area, version 1.2. SKB R-05-17, Svensk Kärnbränslehantering AB.

Laaksoharju M (Ed.), 2006. Hydrogeochemical evaluation of the Laxemar subarea, version 1.2. SKB R-06-12, Svensk Kärnbränslehantering AB.

Landström O, Tullborg E-L, 1995. Interactions of trace elements with fracture filling minerals from the Äspö Hard Rock Laboratory. SKB TR-95-13, Svensk Kärnbränslehantering AB.

Landström O, Tullborg E-L, Eriksson G, Sandell Y, 2001. Effects of glacial/post-glacial weatheringf compared with hydrothermal alteration - implications for matrix diffusion. SKB R-01-37, Svensk Kärnbränslehantering AB.

Peterman Z E, Wallin B, 1999. Synopsis of strontium isotope variations in groundwater at Äspö, southern Sweden. Appl. Geochem., 14, 939–951.

Pitkänen P, Luukkonen A, Ruotsalainen P, Leino-Forsman H, Vuorinen U, 1999. Geochemical modelling of groundwater evolution and residence time at the Olkiluoto site. Posiva Tech Rep. (98-10), Posiva, Helsinki, Finland.

Pitkänen P, Partamies S, Luukkonen A, 2004. hydrogeochemical interpretation of baseline groundwater conditions at the Olkiluoto site. Posiva Tech. Rep. (2003-07), Posiva, Helsinki, Sweden.

Rouhiainen P, Pöllänen J, Sokolnicki M, 2005. Oskarshamn site investigations. Difference flow logging of borehole KLX03. SKB P-05-67, Svensk Kärnbränslehantering AB.

SKB, 2005. Preliminary site description. Simpevarp subarea – version 1.2. SKB R-05-08, Svensk Kärnbränslehantering AB.

SKB, 2006. Preliminary site description Laxemar subarea – version 1.2. SKB R-06-10, Svensk Kärnbränslehantering AB.

Smellie J, Laaksoharju M, 1992. The Äspö Hard Rock Laboratory: Final evaluation of the hydrogeochemical pre-investigations in relation to existing geological and hydraulic conditions. SKB TR-92-31, Svensk Kärnbränslehantering AB.

Smellie J, Laaksoharju M, Tullborg E-L, 2002. Hydrogeochemical site descriptive model – a strategy for the model development during site investigations. SKB R-02-49, Svensk Kärnbränslehantering AB.

Waber H N, Smellie J A T, 2005. SKB Site Investigations Forsmark Borehole KFM06: Characterisation of pore water. Part I: Diffusion experiments. SKB P-05-196, Svensk Kärnbränslehantering AB.

Waber H N, Smellie J A T, 2006a. Borehole KLX03: Characterisation of pore water. Part 1: Methodology and analytical data. Oskarshamn site investigation. SKB P-06-12, Svensk Kärnbränslehantering AB.

Waber H N, Smellie J A T, 2006b. Borehole KLX03: Characterisation of pore water. Part 2: Rock properties and diffusion experiments. Oskarshamn site investigation. SKB P-06-77, Svensk Kärnbränslehantering AB.

Waber H N, Smellie J A T, 2006c. Characterisation of pore water in crystalline rocks (submitted to Appl. Geochem.).

Appendix 1

Borehole activities prior to, during, and subsequent to groundwater sampling

Samples collected for groundwater analysis are highlighted in light blue.

Table 1.1. KLX03.

ACTIVITY_ID	ACTIVITY TYPE CODE	SITE	ACTIVITY	START_DATE	STOP_DATE	IDCODE	SECUP	SECLOW
13019167	WC106	LAXEMAR	Pore water sampling and analysis	2004/06/01 00:00:00	2004/06/07 00:00:00	KLX03	159.04	159.40
13035048	GE044	LAXEMAR	Core logging, preliminary – BOREMAP	2004/06/08 15:41:00	2004/09/30 13:48:00	KLX03	100.35	1,000.42
13020246	WC106	LAXEMAR	Pore water sampling and analysis	2004/06/10 00:00:00	2004/09/06 00:00:00	KLX03	355.50	355.82
13059629	GE041	LAXEMAR	Core logging – BOREMAP/BIPS	2004/10/27 08:45:00	2004/12/10 13:19:00	KLX03	101.48	998.21
13056734	EG058	LAXEMAR	Cleaning of drilling/borehole equipment	2004/11/04 00:00:00	2004/11/04 00:00:00	KLX03	0.00	1,000.00
13056707	HY681	LAXEMAR	PLU DIFF SPR and Caliper logging	2004/11/04 11:33:00	2004/11/05 12:52:00	KLX03	98.99	996.86
13056708	HY683	LAXEMAR	PLU DIFF-EC Temp and Pressure measurements	2004/11/05 15:39:00	2004/11/06 02:38:00	KLX03	16.11	997.18
13056709	HY680	LAXEMAR	PLU Flowlogging-PFL-DIFF_sequential	2004/11/06 11:19:00	2004/11/10 15:47:00	KLX03	101.30	992.42
13056715	HY685	LAXEMAR	PLU Flowlogging-PFL-DIFF_overlapping	2004/11/06 11:19:00	2004/11/08 03:51:00	KLX03	100.30	996.38
13056710	EG017	LAXEMAR	Pumping, start	2004/11/08 08:28:00	2004/11/08 08:28:00	KLX03		
13056712	HY687	LAXEMAR	PLU PFL DIFF Pressure measurement	2004/11/08 08:28:00	2004/11/09 07:23:00	KLX03		
13059943	HY610	LAXEMAR	PLU Pumping test-submersible pump	2004/11/08 08:28:00	2004/11/09 07:25:00	KLX03		
13056725	HY685	LAXEMAR	PLU Flowlogging-PFL-DIFF_overlapping	2004/11/09 09:46:00	2004/11/10 15:46:00	KLX03	91.27	996.48
13059950	HY610	LAXEMAR	PLU Pumping test-submersible pump	2004/11/09 12:20:00	2004/11/10 16:32:00	KLX03		
13056716	HY685	LAXEMAR	PLU Flowlogging-PFL-DIFF_overlapping	2004/11/10 17:43:00	2004/11/14 07:51:00	KLX03	91.29	978.57
13059956	HY610	LAXEMAR	PLU Pumping test-submersible pump	2004/11/11 07:30:00	2004/11/17 12:05:00	KLX03		
13056663	RM100	LAXEMAR	Ultra sonic wave velocities	2004/11/23 00:00:00	2004/11/23 00:00:00	KLX03	478.85	478.85
13072456	WC040	LAXEMAR	Chemmac measurement	2004/11/25 00:00:00	2004/12/17 00:00:00	KLX03	193.50	198.37
13060035	WC120	LAXEMAR	Water sampling series	2004/11/26 09:06:00	2004/12/15 11:45:00	KLX03	193.50	198.30
13056683	RM118	LAXEMAR	Tilt test	2004/12/01 12:58:00	2004/12/01 12:58:00	KLX03	244.60	244.60
13061434	WC170	LAXEMAR	Enrichment, org C-isotopes	2004/12/01 14:00:00	2004/12/16 07:13:00	KLX03	193.50	198.37

ACTIVITY_ID	ACTIVITY TYPE CODE	SITE	ACTIVITY	START_DATE	STOP_DATE	IDCODE	SECUP	SECLOW
13076389	GE002	LAXEMAR	Rock type sampling and chemical analysis	2004/12/02 00:00:00	2004/12/02 00:00:00	KLX03	817.53	817.75
13076413	GE200	LAXEMAR	Thin section	2004/12/02 00:00:00	2004/12/02 00:00:00	KLX03	817.53	817.75
13076388	GE002	LAXEMAR	Rock type sampling and chemical analysis	2004/12/02 00:00:00	2004/12/02 00:00:00	KLX03	650.08	650.31
13076412	GE200	LAXEMAR	Thin section	2004/12/02 00:00:00	2004/12/02 00:00:00	KLX03	650.08	650.31
13060179	GE300	LAXEMAR	Geological single hole interpretation	2004/12/14 00:00:00	2004/12/14 00:00:00	KLX03	227.00	973.00
13061433	WC165	LAXEMAR	Fractionation of colloidal metals	2004/12/14 10:09:00	2004/12/15 09:49:00	KLX03	193.50	198.37
13061432	WC160	LAXEMAR	Analys and fractionation of humic and fulvic	2004/12/14 10:09:00	2004/12/15 09:49:00	KLX03	193.50	198.37
13072609	RM113	LAXEMAR	Uniaxial test	2004/12/15 00:00:00	2005/03/30 00:00:00	KLX03	690.77	690.91
13072595	RM117	LAXEMAR	Shear test	2004/12/15 00:00:00	2005/04/30 00:00:00	KLX03	708.89	709.01
13078852	RM110	LAXEMAR	Indirect tensile test (Brazil test)	2004/12/15 00:00:00	2005/03/30 00:00:00	KLX03	711.08	711.11
13072583	RM115	LAXEMAR	Triaxial test	2004/12/15 00:00:00	2005/04/30 00:00:00	KLX03	693.86	694.00
13072573	RM110	LAXEMAR	Indirect tensile test (Brazil test)	2004/12/15 00:00:00	2005/03/30 00:00:00	KLX03	711.91	711.94
13072596	RM113	LAXEMAR	Uniaxial test	2004/12/15 00:00:00	2005/03/30 00:00:00	KLX03	291.62	291.76
13074154	WC001	LAXEMAR	Sampling,dissolved gas	2004/12/15 15:04:00	2004/12/16 08:07:00	KLX03	193.50	198.37
13074155	WC177	LAXEMAR	Microbe investigation	2004/12/15 15:04:00	2004/12/16 08:07:00	KLX03	193.00	198.00
13074156	WC175	LAXEMAR	Colloid filtration	2004/12/16 15:04:00	2004/12/16 15:04:00	KLX03	193.50	198.37
13061376	EG019	LAXEMAR	Flushing borehole	2004/12/18 07:00:00	2004/12/19 19:00:00	KLX03	0.00	994.94
13068899	RM090	LAXEMAR	Sampling for thermal properties and expansion	2004/12/28 00:00:00	2005/02/02 00:00:00	KLX03	519.17	519.42
13065198	EG042	LAXEMAR	Packer expansion	2005/01/18 10:38:00	2005/01/18 10:47:00	KLX03	660.00	671.00
13061971	EG017	LAXEMAR	Pumping, start	2005/01/18 10:59:00	2005/01/18 10:59:00	KLX03	660.00	671.00
13061972	WC040	LAXEMAR	Chemmac measurement	2005/01/18 10:59:00	2005/01/21 11:00:00	KLX03	660.00	671.00
13061391	WC120	LAXEMAR	Water sampling series	2005/01/19 08:15:00	2005/01/21 08:30:00	KLX03	660.00	671.00
13065199	EG043	LAXEMAR	Packer release	2005/01/21 11:00:00	2005/01/21 11:07:00	KLX03		
13061970	EG016	LAXEMAR	Pumping, stop	2005/01/21 11:00:00	2005/01/21 11:00:00	KLX03	660.00	671.00
13061973	WC040	LAXEMAR	Chemmac measurement	2005/01/21 13:20:00	2005/02/15 08:07:00	KLX03	964.50	975.15
13065070	EG017	LAXEMAR	Pumping, start	2005/01/21 13:20:00	2005/01/21 13:20:00	KLX03	964.10	975.40
13065071	EG042	LAXEMAR	Packer expansion	2005/01/21 13:25:00	2005/01/21 13:30:00	KLX03		
13068893	RM090	LAXEMAR	Sampling for thermal properties and expansion	2005/01/24 00:00:00	2005/03/31 00:00:00	KLX03	695.45	695.51
13061939	WC120	LAXEMAR	Water sampling series	2005/01/25 09:00:00	2005/01/25 09:42:00	KLX03	964.00	975.00

ACTIVITY_ID	ACTIVITY TYPE CODE	SITE	ACTIVITY	START_DATE	STOP_DATE	IDCODE	SECUP	SECLOW
13064748	WC170	LAXEMAR	Enrichment, org C-isotopes	2005/01/25 10:00:00	2005/02/14 09:07:00	KLX03	964.50	975.15
13067628	RM080	LAXEMAR	Density and porosity measurement	2005/01/31 00:00:00	2005/03/08 00:00:00	KLX03	695.51	695.57
13064749	WC160	LAXEMAR	Analys and fractionation of humic and fulvic	2005/02/10 08:38:00	2005/02/10 12:36:00	KLX03	964.50	975.15
13064887	WC175	LAXEMAR	Colloid filtration	2005/02/15 07:00:00	2005/02/15 08:23:00	KLX03	964.50	975.15
13064888	WC001	LAXEMAR	Sampling,dissolved gas	2005/02/15 07:00:00	2005/02/15 08:23:00	KLX03	964.00	975.00
13064886	WC177	LAXEMAR	Microbe investigation	2005/02/15 07:00:00	2005/02/15 08:03:00	KLX03	964.50	975.20
13065068	EG042	LAXEMAR	Packer expansion	2005/02/17 14:50:00	2005/02/17 15:05:00	KLX03	408.00	415.30
13066423	WC040	LAXEMAR	Chemmac measurement	2005/02/17 15:06:00	2005/03/22 08:01:00	KLX03	408.00	415.30
13065065	EG017	LAXEMAR	Pumping, start	2005/02/17 15:06:00	2005/02/17 15:06:00	KLX03	408.00	415.30
13065067	EG016	LAXEMAR	Pumping, stop	2005/02/17 15:18:00	2005/02/17 15:18:00	KLX03	408.00	415.30
13065069	EG043	LAXEMAR	Packer release	2005/02/17 15:18:00	2005/02/17 15:18:00	KLX03	408.00	415.30
13077314	HY112	LAXEMAR	Manual flow measurements surface boreholes	2005/02/19 13:12:00	2005/02/19 13:12:00	KLX03		
13064889	WC120	LAXEMAR	Water sampling series	2005/02/21 11:00:00	2005/02/28 12:30:00	KLX03	408.00	415.30
13069079	WC170	LAXEMAR	Enrichment, org C-isotopes	2005/02/23 16:30:00	2005/03/22 06:05:00	KLX03	408.00	415.30
13075238	HY244	LAXEMAR	In situ formation factor determination	2005/03/01 00:00:00	2005/05/15 00:00:00	KLX03	412.06	998.13
13065843	EG043	LAXEMAR	Packer release	2005/03/07 10:30:00	2005/03/07 17:00:00	KLX03	408.00	415.30
13065844	EG042	LAXEMAR	Packer expansion	2005/03/09 09:14:00	2005/03/18 14:19:00	KLX03	408.00	415.30
13065845	EG017	LAXEMAR	Pumping, start	2005/03/09 14:20:00	2005/03/09 14:20:00	KLX03	408.00	415.30
13066370	WC165	LAXEMAR	Fractionation of colloidal metals	2005/03/17 08:52:00	2005/03/18 09:54:00	KLX03	408.00	415.30
13066369	WC160	LAXEMAR	Analys and fractionation of humic and fulvic	2005/03/17 08:52:00	2005/03/18 09:54:00	KLX03	408.00	415.30
13070900	WC175	LAXEMAR	Colloid filtration	2005/03/22 05:57:00	2005/03/22 06:45:00	KLX03	408.00	415.30
13070898	WC001	LAXEMAR	Sampling,dissolved gas	2005/03/22 05:57:00	2005/03/22 06:45:00	KLX03	408.00	415.30
13070899	WC177	LAXEMAR	Microbe investigation	2005/03/22 05:57:00	2005/03/22 06:45:00	KLX03	408.00	415.30
13066426	EG042	LAXEMAR	Packer expansion	2005/03/22 14:35:00	2005/03/22 14:48:00	KLX03	735.50	748.00
13066427	EG017	LAXEMAR	Pumping, start	2005/03/22 14:51:00	2005/03/22 14:51:00	KLX03	735.50	748.00
13070901	WC040	LAXEMAR	Chemmac measurement	2005/03/22 14:51:00	2005/04/26 06:44:00	KLX03	735.50	748.04
13066424	EG043	LAXEMAR	Packer release	2005/03/23 06:45:00	2005/03/23 06:46:00	KLX03	408.00	415.30
13066425	EG016	LAXEMAR	Pumping, stop	2005/03/23 08:01:00	2005/03/23 08:01:00	KLX03	408.00	415.30
13066432	WC120	LAXEMAR	Water sampling series	2005/03/23 08:10:00	2005/04/25 09:37:00	KLX03	735.50	748.03

ACTIVITY_ID	ACTIVITY TYPE CODE	SITE	ACTIVITY	START_DATE	STOP_DATE	IDCODE	SECUP	SECLOW
13066428	EG016	LAXEMAR	Pumping, stop	2005/03/23 08:15:00	2005/03/23 08:15:00	KLX03	735.50	748.00
13066429	EG043	LAXEMAR	Packer release	2005/03/23 08:15:00	2005/03/23 08:15:00	KLX03	735.50	748.00
13066430	EG042	LAXEMAR	Packer expansion	2005/03/23 11:15:00	2005/03/23 11:15:00	KLX03	735.50	748.00
13066431	EG017	LAXEMAR	Pumping, start	2005/03/23 11:51:00	2005/03/23 11:51:00	KLX03	735.50	748.00
13067111	EG016	LAXEMAR	Pumping, stop	2005/03/31 13:12:00	2005/03/31 13:12:00	KLX03	735.50	748.00
13067112	EG043	LAXEMAR	Packer release	2005/03/31 13:12:00	2005/03/31 13:12:00	KLX03	735.50	748.00
13067113	EG042	LAXEMAR	Packer expansion	2005/03/31 13:30:00	2005/03/31 14:00:00	KLX03	735.50	748.00
13067114	EG017	LAXEMAR	Pumping, start	2005/03/31 14:00:00	2005/03/31 14:00:00	KLX03	735.50	748.00
13070903	EG043	LAXEMAR	Packer release	2005/04/11 17:46:00	2005/04/11 17:58:00	KLX03	735.50	748.03
13070904	EG017	LAXEMAR	Pumping, start	2005/04/11 17:58:00	2005/04/11 17:58:00	KLX03	735.50	748.03
13070905	EG016	LAXEMAR	Pumping, stop	2005/04/11 18:33:00	2005/04/11 18:33:00	KLX03	735.50	748.03
13070906	EG042	LAXEMAR	Packer expansion	2005/04/13 10:22:00	2005/05/13 10:32:00	KLX03	735.50	748.03
13070728	WC001	LAXEMAR	Sampling,dissolved gas	2005/04/26 05:46:00	2005/04/26 06:43:00	KLX03	735.50	748.04
13070779	WC177	LAXEMAR	Microbe investigation	2005/04/26 05:46:00	2005/04/26 06:43:00	KLX03	735.50	748.00
13070729	WC175	LAXEMAR	Colloid filtration	2005/04/26 05:46:00	2005/04/26 06:43:00	KLX03	735.50	748.04
13070727	EG016	LAXEMAR	Pumping, stop	2005/04/26 06:44:00	2005/04/26 06:44:00	KLX03		
13077352	EG058	LAXEMAR	Cleaning of drilling/borehole equipment	2005/05/03 00:00:00	2005/05/03 00:00:00	KLX03		
13075579	HY660	LAXEMAR	PLU Injection test	2005/05/05 11:05:00	2005/05/19 15:28:00	KLX03	106.31	206.31

Table 1-2. KLX04.

ACTIVITY_ID	ACTIVITY TYPE CODE	SITE	ACTIVITY	START_DATE	STOP_DATE	PROJECT	IDCODE	SECUP	SECLOW
13024615	WC080	LAXEMAR	Water sampling, class 3	2004/07/08 19:25:00	2004/07/08 19:27:00	PLU	KLX04	0.00	35.00
13049194	GE041	LAXEMAR	Core logging – BOREMAP/BIPS	2004/07/22 00:00:00	2004/12/03 13:23:00	PLU	KLX04	101.50	991.22
13027319	EG058	LAXEMAR	Cleaning of drilling/borehole equipment	2004/07/28 00:00:00	2004/07/28 00:00:00	PLU	KLX04		
13030439	HY681	LAXEMAR	PLU DIFF SPR and Caliper logging	2004/07/28 10:20:00	2004/07/29 06:29:00	PLU	KLX04	95.86	988.81
13030440	HY687	LAXEMAR	PLU PFL DIFF Pressure measurement	2004/07/29 09:57:00	2004/07/30 09:00:00	PLU	KLX04		
13059789	HY610	LAXEMAR	PLU Pumping test-submersible pump	2004/07/29 09:57:00	2004/07/30 11:21:00	PLU	KLX04	12.03	201.00
13030441	HY685	LAXEMAR	PLU Flow logging-PFL-DIFF_overlapping	2004/07/30 11:24:00	2004/07/31 11:36:00	PLU	KLX04	95.20	988.23
13056700	HY680	LAXEMAR	PLU Flow logging-PFL-DIFF_sequential	2004/07/30 11:24:00	2004/11/03 19:34:00	PLU	KLX04	100.20	986.22
13059795	HY610	LAXEMAR	PLU Pumping test-submersible pump	2004/07/30 11:45:00	2004/08/01 09:53:00	PLU	KLX04	12.03	201.00
13030442	HY685	LAXEMAR	PLU Flow logging-PFL-DIFF_overlapping	2004/08/01 11:25:00	2004/08/04 06:32:00	PLU	KLX04	94.68	986.76
13059806	HY610	LAXEMAR	PLU Pumping test-submersible pump	2004/08/01 16:00:00	2004/08/04 07:55:00	PLU	KLX04	12.03	201.00
13030443	HY684	LAXEMAR	PLU PFL DIFF Fracture EC Measurements	2004/08/04 07:59:00	2004/08/05 07:16:00	PLU	KLX04	138.84	973.69
13059814	HY610	LAXEMAR	PLU Pumping test-submersible pump	2004/08/04 12:30:00	2004/08/05 07:30:00	PLU	KLX04	12.03	201.00
13030529	HY050	LAXEMAR	Recovery test	2004/08/05 07:36:00	2004/08/06 07:19:00	PLU	KLX04		
13059817	HY610	LAXEMAR	PLU Pumping test-submersible pump	2004/08/05 07:36:00	2004/08/06 12:10:00	PLU	KLX04	12.03	201.00
13026258	GE041	LAXEMAR	Core logging – BOREMAP/BIPS	2004/08/09 16:17:00	2004/08/09 16:18:00	PLU	KLX04	552.50	1,005.27
13056047	EG058	LAXEMAR	Cleaning of drilling/borehole equipment	2004/11/02 00:00:00	2004/11/02 00:00:00	PLU	KLX04		
13030494	HY685	LAXEMAR	PLU Flow logging-PFL-DIFF_overlapping	2004/11/02 10:55:00	2004/11/03 19:34:00	PLU	KLX04	95.22	988.34
13060684	EG004	LAXEMAR	Instrumentation, section installation	2004/11/17 15:10:00	2004/11/17 15:10:00	PLU	KLX04		
13055699	EG502	LAXEMAR	Instrumentation, transducer installation	2004/11/17 15:10:00	2004/11/17 15:10:00	PLU	KLX04		
13063005	EG012	LAXEMAR	Section activate	2004/11/17 15:12:00	2004/11/17 15:12:00	PLU	KLX04		
13069646	EG506	LAXEMAR	Instrumentation, packer removal	2005/01/13 13:00:00	2005/01/13 13:00:00	PLU	KLX04		
13069645	EG501	LAXEMAR	Instrumentation, section removal	2005/01/13 13:00:00	2005/01/13 13:00:00	PLU	KLX04		
13069644	EG011	LAXEMAR	Section deactivate	2005/01/13 13:00:00	2005/01/13 13:00:00	PLU	KLX04		
13061890	WC060	LAXEMAR	Water sampling, class 1	2005/01/28 14:00:00	2005/01/28 14:00:00	PLU	KLX04	686.00	869.00
13069647	EG505	LAXEMAR	Instrumentation, packer installation	2005/01/29 00:00:00	2005/01/29 00:00:00	PLU	KLX04		
13069648	EG004	LAXEMAR	Instrumentation, section installation	2005/01/29 00:00:00	2005/01/29 00:00:00	PLU	KLX04		
13069649	EG012	LAXEMAR	Section activate	2005/01/29 00:01:00	2005/01/29 00:01:00	PLU	KLX04		
13075244	HY244	LAXEMAR	In situ formation factor determination	2005/03/01 00:00:00	2005/05/15 00:00:00	PLU	KLX04	413.37	988.07

Table 1-3. KLX05.

ACTIVITY ID	ACTIVITY TYPE CODE	SITE	ACTIVITY	START_DATE	STOP_DATE	PROJECT	IDCODE	SECUP	SECLOW
13032627	EG077	LAXEMAR	Drill cuttings field observation	2004/08/11 00:00:00	2004/08/12 00:00:00	PLU	KLX05	0.30	100.30
13031059	EG058	LAXEMAR	Cleaning of drilling/borehole equipment	2004/08/11 00:00:00	2004/08/11 00:00:00	PLU	KLX05		
13031052	EG051	LAXEMAR	Percussion drilling	2004/08/11 07:00:00	2004/08/25 11:30:00	PLU	KLX05	0.00	100.30
13030519	EG149	LAXEMAR	Drill rigg setting out & inclination	2004/08/11 09:00:00	2004/08/11 09:00:00	PLU	KLX05		
13031058	EG058	LAXEMAR	Cleaning of drilling/borehole equipment	2004/08/12 00:00:00	2004/08/12 00:00:00	PLU	KLX05		
13061373	WC080	LAXEMAR	Water sampling, class 3	2004/08/16 17:00:00	2004/08/16 17:00:00	PLU	KLX05	0.00	100.00
13061374	WC100	LAXEMAR	Water sampling, class 5	2004/08/16 23:55:00	2004/08/16 23:55:00	PLU	KLX05	0.00	100.00
13031057	EG058	LAXEMAR	Cleaning of drilling/borehole equipment	2004/08/17 00:00:00	2004/08/17 00:00:00	PLU	KLX05		
13031350	EG070	LAXEMAR	Percussion drilling penetration	2004/08/18 00:00:00	2004/08/18 00:00:00	PLU	KLX05	7.60	100.30
13031054	EG075	LAXEMAR	Grouting in borehole	2004/08/18 09:30:00	2004/08/18 11:15:00	PLU	KLX05	0.00	100.30
13031053	EG075	LAXEMAR	Grouting in borehole	2004/08/18 11:15:00	2004/08/18 12:00:00	PLU	KLX05	0.00	15.00
13031055	EG058	LAXEMAR	Cleaning of drilling/borehole equipment	2004/08/23 00:00:00	2004/08/23 00:00:00	PLU	KLX05		
13031056	EG058	LAXEMAR	Cleaning of drilling/borehole equipment	2004/08/24 00:00:00	2004/08/24 00:00:00	PLU	KLX05		
13060128	EG050	LAXEMAR	Core drilling	2004/08/25 17:00:00	2004/11/25 11:30:00	PLU	KLX06	0.00	994.94
13030751	EG150	LAXEMAR	Borehole coordinate surveying	2004/08/27 11:15:00	2004/08/27 11:15:00	PLU	KLX05		
13030752	EG151	LAXEMAR	Borehole direction surveying	2004/08/27 11:15:00	2004/08/27 11:15:00	PLU	KLX05		
13066979	EG058	LAXEMAR	Cleaning of drilling/borehole equipment	2004/09/20 00:00:00	2004/09/20 00:00:00	PLU	KLX05		
13066201	EG050	LAXEMAR	Core drilling	2004/10/01 14:00:00	2005/01/22 13:45:00	PLU	KLX05	100.30	1,000.16
13055522	EG061	LAXEMAR	Core drilling record	2004/10/01 14:20:00	2005/01/22 13:45:00	PLU	KLX05	76.48	1,000.16
13066981	EG058	LAXEMAR	Cleaning of drilling/borehole equipment	2004/10/02 00:00:00	2004/10/02 00:00:00	PLU	KLX05		
13055404	HY630	LAXEMAR	PLU Pumping test – air lift pumping	2004/10/03 15:38:00	2004/10/04 14:20:00	PLU	KLX05		
13055594	WC140	LAXEMAR	Sampling of drilling water	2004/10/04 13:24:00	2005/01/12 07:23:00	PLU	KLX05	0.00	874.27
13055587	EG082	LAXEMAR	Flush water out	2004/10/04 13:24:00	2005/01/12 07:23:00	PLU	KLX05	95.03	874.27
13055596	WC141	LAXEMAR	Sampling of returned water	2004/10/04 13:24:00	2005/01/12 07:23:00	PLU	KLX05	0.00	874.27
13055408	HY050	LAXEMAR	Recovery test	2004/10/04 13:45:00	2004/10/05 14:47:00	PLU	KLX05	0.00	97.00
13055407	HY630	LAXEMAR	PLU Pumping test – air lift pumping	2004/10/04 14:56:00	2004/10/04 17:43:00	PLU	KLX05		
13055409	HY050	LAXEMAR	Recovery test	2004/10/04 17:14:00	2004/10/05 06:00:00	PLU	KLX05	15.00	102.26
13055531	HY630	LAXEMAR	PLU Pumping test – air lift pumping	2004/10/05 06:11:00	2004/10/06 07:13:00	PLU	KLX06		
13067010	EG075	LAXEMAR	Grouting in borehole	2004/10/08 15:00:00	2004/10/08 16:00:00	PLU	KLX05	99.75	104.05
13067023	EG075	LAXEMAR	Grouting in borehole	2004/10/09 07:10:00	2004/10/09 09:00:00	PLU	KLX05	93.75	99.72

ACTIVITY ID	ACTIVITY TYPE CODE	SITE	ACTIVITY	START_DATE	STOP_DATE	PROJECT	IDCODE	SECUP	SECLOW
13055414	HY630	LAXEMAR	PLU Pumping test – air lift pumping	2004/10/10 08:47:00	2004/10/13 19:47:00	PLU	KLX05		
13046229	EG148	LAXEMAR	Borehole direction surveying for Maxibor	2004/10/13 10:25:00	2004/10/13 10:25:00	PLU	KLX05		
13066982	EG058	LAXEMAR	Cleaning of drilling/borehole equipment	2004/10/14 00:00:00	2004/10/14 00:00:00	PLU	KLX05		
13055424	HY630	LAXEMAR	PLU Pumping test – air lift pumping	2004/10/14 06:20:00	2004/10/14 19:35:00	PLU	KLX05		
13055504	EG058	LAXEMAR	Cleaning of drilling/borehole equipment	2004/10/15 00:00:00	2004/10/15 00:00:00	PLU	KLX05		
13055425	HY630	LAXEMAR	PLU Pumping test – air lift pumping	2004/10/15 06:10:00	2004/10/15 13:05:00	PLU	KLX05		
13055428	HY600	LAXEMAR	PLU Pumping test_wire line eq.	2004/10/15 12:30:00	2004/10/16 08:25:00	PLU	KLX05	107.80	202.94
13055427	HY630	LAXEMAR	PLU Pumping test – air lift pumping	2004/10/15 14:02:00	2004/10/15 14:08:00	PLU	KLX05		
13055505	EG058	LAXEMAR	Cleaning of drilling/borehole equipment	2004/10/16 00:00:00	2004/10/16 00:00:00	PLU	KLX05		
13055648	WC080	LAXEMAR	Water sampling, class 3	2004/10/16 07:15:00	2004/10/16 07:15:00	PLU	KLX05	107.80	202.94
13055556	HY630	LAXEMAR	PLU Pumping test – air lift pumping	2004/10/16 07:24:00	2005/01/11 19:53:00	PLU	KLX06		
13061975	GE044	LAXEMAR	Core logging, preliminary – BOREMAP	2005/01/11 12:55:00	2005/02/02 13:28:00	PLU	KLX05	0.00	1,000.16
13061196	HY630	LAXEMAR	PLU Pumping test – air lift pumping	2005/01/12 06:25:00	2005/03/10 15:05:00	PLU	KLX05		
13073086	EG157	LAXEMAR	Magnetic – accelerometer measurement	2005/03/13 00:00:00	2005/03/13 00:00:00	PLU	KLX05	0.00	984.00
13073322	GE041	LAXEMAR	Core logging – BOREMAP/BIPS	2005/03/14 16:38:00	2005/06/07 15:01:00	PLU	KLX05	108.33	995.22
13069348	GE041	LAXEMAR	Core logging – BOREMAP/BIPS	2005/03/14 16:38:00	2005/04/27 17:54:00	PLU	KLX05	108.33	995.22
13066300	HY630	LAXEMAR	PLU Pumping test – air lift pumping	2005/03/15 06:25:00	2005/03/18 06:56:00	PLU	KLX05		
13067188	EG019	LAXEMAR	Flushing borehole	2005/03/22 10:35:00	2005/04/11 11:15:00	PLU	KLX05	0.00	994.00
13067220	EG019	LAXEMAR	Flushing borehole	2005/03/22 12:30:00	2005/04/11 13:00:00	PLU	KLX05	0.00	994.00
13067222	EG019	LAXEMAR	Flushing borehole	2005/03/22 13:10:00	2005/04/11 13:40:00	PLU	KLX05	0.00	994.00
13066915	EG058	LAXEMAR	Cleaning of drilling/borehole equipment	2005/03/23 00:00:00	2005/03/31 00:00:00	PLU	KLX05		
13066917	GE046	LAXEMAR	BIPS-logging in borehole	2005/03/23 09:00:00	2005/03/23 23:00:00	PLU	KLX05	108.00	991.50
13070686	GP142	LAXEMAR	Radar logging – Dipol several freq interpret	2005/03/30 10:00:00	2005/03/31 12:00:00	PLU	KLX05	100.00	990.00
13066921	GP141	LAXEMAR	Radar logging – Dipol Antenna, one freq	2005/03/30 10:00:00	2005/03/31 12:00:00	PLU	KLX05	100.00	993.30
13067044	EG073	LAXEMAR	Drill cuttings balance	2005/04/01 00:00:00	2005/04/01 00:00:00	PLU	KLX05	0.00	1,000.16
13068344	WC080	LAXEMAR	Tube groundwater samples; Class 3	2005/04/06 12:39:00	2005/04/06 13:55:00	PLU	KLX05	0.00	40.00
13067405	GP160	LAXEMAR	Geophysical Logging	2005/04/06 17:14:00	2005/04/07 18:00:00	PLU	KLX05	8.55	996.45
13067466	GP140	LAXEMAR	Radar logging – Directional Antenna	2005/04/07 17:00:00	2005/04/07 18:00:00	PLU	KLX05		
13077099	RM080	LAXEMAR	Density and porosity measurement	2005/04/11 00:00:00	2005/06/14 00:00:00	PLU	KLX05	361.25	361.31
13069287	EG058	LAXEMAR	Cleaning of drilling/borehole equipment	2005/04/13 08:00:00	2005/04/13 08:00:00	PLU	KLX05		
13069166	HY681	LAXEMAR	PLU DIFF SPR and Caliper logging	2005/04/13 12:56:00	2005/04/14 10:40:00	PLU	KLX05	105.75	991.44

ACTIVITY ID	ACTIVITY TYPE CODE	SITE	ACTIVITY	START_DATE	STOP_DATE	PROJECT	IDCODE	SECUP	SECLOW
13069167	HY682	LAXEMAR	PLU DIFF – EC and Temp measurements	2005/04/14 14:54:00	2005/04/14 16:43:00	PLU	KLX05	12.58	991.18
13069168	HY685	LAXEMAR	PLU Flowlogging-PFL-DIFF_overlapping	2005/04/15 10:45:00	2005/04/16 16:30:00	PLU	KLX05	0.00	988.00
13069266	EG017	LAXEMAR	Pumping, start	2005/04/17 14:09:00	2005/04/17 14:09:00	PLU	KLX05		
13069267	HY685	LAXEMAR	PLU Flowlogging-PFL-DIFF_overlapping	2005/04/18 14:52:00	2005/04/19 19:09:00	PLU	KLX05	95.89	990.42
13069268	EG016	LAXEMAR	Pumping, stop	2005/04/20 07:35:00	2005/04/20 07:35:00	PLU	KLX05		
13069269	EG017	LAXEMAR	Pumping, start	2005/04/20 08:20:00	2005/04/20 08:20:00	PLU	KLX05		
13069278	HY685	LAXEMAR	PLU Flowlogging-PFL-DIFF_overlapping	2005/04/20 11:20:00	2005/04/22 06:01:00	PLU	KLX05	95.88	966.37
13069280	EG016	LAXEMAR	Pumping, stop	2005/04/22 07:31:00	2005/04/22 07:31:00	PLU	KLX05		
13069281	EG017	LAXEMAR	Pumping, start	2005/04/22 08:05:00	2005/04/22 08:05:00	PLU	KLX05		
13069282	HY685	LAXEMAR	PLU Flowlogging-PFL-DIFF_overlapping	2005/04/22 08:20:00	2005/04/25 07:15:00	PLU	KLX05	0.00	796.00
13072441	HY684	LAXEMAR	PLU PFL DIFF Fracture EC Measurements	2005/04/22 08:34:00	2005/04/25 07:06:00	PLU	KLX05	123.76	791.51
13069283	EG016	LAXEMAR	Pumping, stop	2005/04/25 08:14:00	2005/04/25 08:14:00	PLU	KLX05		
13069284	EG017	LAXEMAR	Pumping, start	2005/04/25 08:47:00	2005/04/25 08:47:00	PLU	KLX05		
13069285	HY682	LAXEMAR	PLU DIFF – EC and Temp measurements	2005/04/25 09:04:00	2005/04/25 10:59:00	PLU	KLX05	25.59	990.67
13069286	EG016	LAXEMAR	Pumping, stop	2005/04/25 11:21:00	2005/04/25 11:21:00	PLU	KLX05		
13069350	HY050	LAXEMAR	Recovery test	2005/04/25 11:21:00	2005/04/26 05:56:00	PLU	KLX05	980.00	995.00
13077116	RM090	LAXEMAR	Sampling for thermal properties and expansion	2005/05/01 00:00:00	2005/06/02 00:00:00	PLU	KLX05	223.22	223.28
13070677	GP161	LAXEMAR	Resistivity, focused 140 cm	2005/05/02 17:18:00	2005/05/02 18:53:00	PLU	KLX05	15.60	992.30
13070679	GP120	LAXEMAR	Natural gamma logging	2005/05/02 17:18:00	2005/05/02 18:53:00	PLU	KLX05	12.70	992.00
13070678	GP040	LAXEMAR	Caliper logging	2005/05/02 17:18:00	2005/05/02 18:53:00	PLU	KLX05	13.10	900.00
13070676	GP090	LAXEMAR	Density logging	2005/05/02 17:18:00	2005/05/02 18:53:00	PLU	KLX05	12.70	994.40
13077118	RM090	LAXEMAR	Sampling for thermal properties and expansion	2005/05/03 00:00:00	2005/06/15 00:00:00	PLU	KLX05	243.00	243.06
13077251	GE301	LAXEMAR	Geophysical borehole interpretation	2005/05/16 00:00:00	2005/06/22 00:00:00	PLU	KLX05	0.00	999.90
13077312	GP070	LAXEMAR	Salinity calculation	2005/05/16 00:00:00	2005/06/22 00:00:00	PLU	KLX05	18.00	994.00
13077313	GP080	LAXEMAR	Temperature gradient calculation	2005/05/16 00:00:00	2005/06/22 00:00:00	PLU	KLX05	113.00	990.00
13077131	RM090	LAXEMAR	Sampling for thermal properties and expansion	2005/05/16 00:00:00	2005/06/18 00:00:00	PLU	KLX05	495.50	495.56
13072270	EG058	LAXEMAR	Cleaning of drilling/borehole equipment	2005/05/18 00:00:00	2005/05/18 00:00:00	PLU	KLX05		
13072269	GP140	LAXEMAR	Radar logging – Directional Antenna	2005/05/18 15:15:00	2005/05/19 19:00:00	PLU	KLX05	108.00	988.00
13077134	RM090	LAXEMAR	Sampling for thermal properties and expansion	2005/05/19 00:00:00	2005/06/19 00:00:00	PLU	KLX05	530.73	530.79
13076130	EG157	LAXEMAR	Magnetic – accelerometer measurement	2005/05/19 00:00:00	2005/05/20 00:00:00	PLU	KLX05	0.00	990.00
13077135	RM090	LAXEMAR	Sampling for thermal properties and expansion	2005/05/20 00:00:00	2005/06/24 00:00:00	PLU	KLX05	543.18	543.24

Table 1-4. KLX06.

ACTIVITY_ID	ACTIVITY TYPE CODE	SITE	ACTIVITY	START_DATE	STOP_DATE	PROJECT	IDCODE	SECUP	SECLOW
13032628	EG077	LAXEMAR	Drill cuttings field observation	2004/08/03 00:00:00	2004/08/05 00:00:00	PLU	KLX06	0.20	100.30
13031255	EG058	LAXEMAR	Cleaning of drilling/borehole equipment	2004/08/03 00:00:00	2004/08/03 00:00:00	PLU	KLX06	0.00	9.10
13031071	EG070	LAXEMAR	Percussion drilling penetration	2004/08/03 00:00:00	2004/08/05 00:00:00	PLU	KLX06	0.20	100.30
13031261	EG051	LAXEMAR	Percussion drilling	2004/08/03 10:30:00	2004/08/10 11:30:00	PLU	KLX06	0.00	100.30
13025106	EG149	LAXEMAR	Drill rigg setting out & inclination	2004/08/03 11:45:00	2004/08/03 11:45:00	PLU	KLX06		
13032357	EG058	LAXEMAR	Cleaning of drilling/borehole equipment	2004/08/04 00:00:00	2004/08/05 00:00:00	PLU	KLX06	0.00	202.26
13031259	EG075	LAXEMAR	Grouting in borehole	2004/08/05 11:30:00	2004/08/05 13:00:00	PLU	KLX06	0.00	11.88
13031881	EG058	LAXEMAR	Cleaning of drilling/borehole equipment	2004/08/09 00:00:00	2004/08/09 00:00:00	PLU	KLX06		
13030518	EG151	LAXEMAR	Borehole direction surveying	2004/08/13 10:00:00	2004/08/13 10:00:00	PLU	KLX06		
13030517	EG150	LAXEMAR	Borehole coordinate surveying	2004/08/13 10:00:00	2004/08/13 10:00:00	PLU	KLX06		
13060941	EG061	LAXEMAR	Core drilling record	2004/08/28 10:37:00	2004/11/25 10:38:00	PLU	KLX06	103.94	997.98
13032373	WC141	LAXEMAR	Sampling of returned water	2004/08/28 14:10:00	2004/11/02 11:10:00	PLU	KLX06	103.09	841.27
13032381	EG082	LAXEMAR	Flush water out	2004/08/28 14:10:00	2004/08/28 14:10:00	PLU	KLX06	103.09	992.73
13032385	WC140	LAXEMAR	Sampling of drilling water	2004/08/28 14:10:00	2004/11/02 11:10:00	PLU	KLX06	103.09	841.27
13032288	HY630	LAXEMAR	PLU Pumping test – air lift pumping	2004/08/31 08:05:00	2004/08/31 11:24:00	PLU	KLX06		
13030829	EG148	LAXEMAR	Borehole direction surveying for Maxibor	2004/08/31 11:30:00	2004/08/31 11:30:00	PLU	KLX06		
13032296	HY630	LAXEMAR	PLU Pumping test – air lift pumping	2004/09/01 09:56:00	2004/09/02 08:52:00	PLU	KLX06		
13060965	GE044	LAXEMAR	Core logging, preliminary – BOREMAP	2004/09/02 09:21:00	2005/01/18 18:24:00	PLU	KLX06	100.29	1,000.00
13032308	HY630	LAXEMAR	PLU Pumping test – air lift pumping	2004/09/02 09:49:00	2004/09/05 08:00:00	PLU	KLX06		
13031878	WC080	LAXEMAR	Water sampling, class 3	2004/09/05 06:17:00	2004/09/05 06:17:00	PLU	KLX06	103.00	202.26
13032339	HY630	LAXEMAR	PLU Pumping test – air lift pumping	2004/09/05 07:52:00	2004/09/05 11:37:00	PLU	KLX06		
13032341	HY630	LAXEMAR	PLU Pumping test – air lift pumping	2004/09/05 12:40:00	2004/09/05 15:26:00	PLU	KLX06		
13032338	HY590	LAXEMAR	PLU pressure measurement- wire line eq.	2004/09/05 15:30:00	2004/09/06 07:20:00	PLU	KLX06	103.00	214.26
13032423	EG156	LAXEMAR	Maxibor measurement	2004/09/06 00:00:00	2004/09/06 00:00:00	PLU	KLX06	0.00	222.00
13032342	HY630	LAXEMAR	PLU Pumping test – air lift pumping	2004/09/06 07:33:00	2004/09/09 11:00:00	PLU	KLX06		
13032631	EG058	LAXEMAR	Cleaning of drilling/borehole equipment	2004/09/10 00:00:00	2004/09/10 00:00:00	PLU	KLX06		268.70
13032635	HY600	LAXEMAR	PLU Pumping test_wire line eq.	2004/09/10 10:00:00	2004/09/11 11:00:00	PLU	KLX06	260.50	268.70
13032387	WC080	LAXEMAR	Water sampling, class 3	2004/09/10 10:22:00	2004/09/10 10:22:00	PLU	KLX06	265.50	268.50

ACTIVITY_ID	ACTIVITY TYPE CODE	SITE	ACTIVITY	START_DATE	STOP_DATE	PROJECT	IDCODE	SECUP	SECLOW
13032632	EG058	LAXEMAR	Cleaning of drilling/borehole equipment	2004/09/11 00:00:00	2004/09/11 00:00:00	PLU	KLX06		289.50
13032388	WC080	LAXEMAR	Water sampling, class 3	2004/09/11 09:09:00	2004/09/11 09:09:00	PLU	KLX06	260.50	268.70
13032647	HY630	LAXEMAR	PLU Pumping test – air lift pumping	2004/09/11 10:09:00	2004/09/11 17:42:00	PLU	KLX06		
13032637	HY590	LAXEMAR	PLU pressure measurement- wire line eq.	2004/09/11 17:30:00	2004/09/12 08:30:00	PLU	KLX06	260.50	289.50
13032633	EG058	LAXEMAR	Cleaning of drilling/borehole equipment	2004/09/12 00:00:00	2004/09/12 00:00:00	PLU	KLX06		310.20
13032648	HY630	LAXEMAR	PLU Pumping test – air lift pumping	2004/09/12 08:29:00	2004/09/12 15:32:00	PLU	KLX06		
13032636	HY600	LAXEMAR	PLU Pumping test_wire line eq.	2004/09/12 15:30:00	2004/09/13 09:35:00	PLU	KLX06	200.50	310.20
13034800	EG156	LAXEMAR	Maxibor measurement	2004/09/13 00:00:00	2004/09/13 00:00:00	PLU	KLX06	0.00	390.00
13032390	WC080	LAXEMAR	Water sampling, class 3	2004/09/13 08:41:00	2004/09/13 08:41:00	PLU	KLX06	200.50	310.20
13032649	HY630	LAXEMAR	PLU Pumping test – air lift pumping	2004/09/13 09:56:00	2004/09/13 17:05:00	PLU	KLX06		
13032641	HY590	LAXEMAR	PLU pressure measurement- wire line eq.	2004/09/13 16:30:00	2004/09/14 08:30:00	PLU	KLX06	200.50	317.84
13032634	EG058	LAXEMAR	Cleaning of drilling/borehole equipment	2004/09/14 00:00:00	2004/09/14 00:00:00	PLU	KLX06		317.84
13034787	HY630	LAXEMAR	PLU Pumping test – air lift pumping	2004/09/14 07:55:00	2004/09/17 14:00:00	PLU	KLX06		
13034785	EG058	LAXEMAR	Cleaning of drilling/borehole equipment	2004/09/18 00:00:00	2004/09/18 00:00:00	PLU	KLX06		
13034792	HY630	LAXEMAR	PLU Pumping test – air lift pumping	2004/09/18 06:59:00	2004/09/18 13:38:00	PLU	KLX06		
13034786	HY600	LAXEMAR	PLU Pumping test_wire line eq.	2004/09/18 13:00:00	2004/09/19 10:44:00	PLU	KLX06	331.02	364.23
13034741	WC080	LAXEMAR	Water sampling, class 3	2004/09/19 09:56:00	2004/09/19 09:56:00	PLU	KLX06	331.02	364.23
13034793	HY630	LAXEMAR	PLU Pumping test – air lift pumping	2004/09/19 11:23:00	2004/09/21 17:35:00	PLU	KLX06		
13055579	EG058	LAXEMAR	Cleaning of drilling/borehole equipment	2004/09/22 00:00:00	2004/09/22 00:00:00	PLU	KLX06		
13055516	HY630	LAXEMAR	PLU Pumping test – air lift pumping	2004/09/22 06:08:00	2004/09/22 14:03:00	PLU	KLX06		
13055568	HY600	LAXEMAR	PLU Pumping test_wire line eq.	2004/09/22 14:03:00	2004/09/23 10:30:00	PLU	KLX06	307.50	415.49
13055581	EG058	LAXEMAR	Cleaning of drilling/borehole equipment	2004/09/23 00:00:00	2004/09/23 00:00:00	PLU	KLX06		
13043459	WC080	LAXEMAR	Water sampling, class 3	2004/09/23 09:26:00	2004/09/23 09:26:00	PLU	KLX06	307.50	415.49
13055517	HY630	LAXEMAR	PLU Pumping test – air lift pumping	2004/09/24 09:16:00	2004/10/09 08:00:00	PLU	KLX06		
13043460	WC080	LAXEMAR	Water sampling, class 3	2004/10/09 06:32:00	2004/10/09 06:32:00	PLU	KLX06	514.60	613.94
13055537	HY630	LAXEMAR	PLU Pumping test – air lift pumping	2004/10/10 06:28:00	2004/10/29 09:30:00	PLU	KLX06		
13055586	EG058	LAXEMAR	Cleaning of drilling/borehole equipment	2004/10/29 00:00:00	2004/10/29 00:00:00	PLU	KLX06		
13055649	WC080	LAXEMAR	Water sampling, class 3	2004/10/29 06:40:00	2004/10/29 06:40:00	PLU	KLX06	715.14	784.94
13055552	HY630	LAXEMAR	PLU Pumping test – air lift pumping	2004/10/29 09:17:00	2004/11/30 17:38:00	PLU	KLX06		

ACTIVITY_ID	ACTIVITY TYPE CODE	SITE	ACTIVITY	START_DATE	STOP_DATE	PROJECT	IDCODE	SECUP	SECLOW
13076391	GE002	LAXEMAR	Rock type sampling and chemical analysis	2004/12/02 00:00:00	2004/12/02 00:00:00	PLU	KLX06	208.23	208.43
13062810	EG156	LAXEMAR	Maxibor measurement	2004/12/06 00:00:00	2004/12/06 00:00:00	PLU	KLX06	0.00	987.00
13060129	EG073	LAXEMAR	Drill cuttings balance	2004/12/15 00:00:00	2004/12/15 00:00:00	PLU	KLX06	0.00	994.94
13060630	WC080	LAXEMAR	Water sampling, class 3	2004/12/21 12:03:00	2004/12/21 13:29:00	PLU	KLX06	0.00	40.00
13060251	EG058	LAXEMAR	Cleaning of drilling/borehole equipment	2004/12/27 00:00:00	2004/12/29 00:00:00	PLU	KLX06		
13060244	GE046	LAXEMAR	BIPS-logging in borehole	2004/12/27 15:00:00	2004/12/27 16:30:00	PLU	KLX06	11.00	97.00
13060245	GE046	LAXEMAR	BIPS-logging in borehole	2004/12/28 07:00:00	2004/12/28 21:30:00	PLU	KLX06	101.00	961.00
13060246	GP141	LAXEMAR	Radar logging – Dipol Antenna, one freq	2004/12/28 21:30:00	2004/12/28 23:59:00	PLU	KLX06	0.00	991.00
13060249	GP140	LAXEMAR	Radar logging – Directional Antenna	2004/12/28 21:30:00	2004/12/30 11:00:00	PLU	KLX06	0.00	991.00
13060247	GP141	LAXEMAR	Radar logging – Dipol Antenna, one freq	2004/12/29 07:00:00	2004/12/29 11:00:00	PLU	KLX06	0.00	989.00
13060248	GP141	LAXEMAR	Radar logging – Dipol Antenna, one freq	2004/12/29 11:00:00	2004/12/29 15:00:00	PLU	KLX06	0.00	981.00
13061437	GP164	LAXEMAR	Geophysical Logging	2005/01/04 11:55:00	2005/01/05 12:48:00	PLU	KLX06	103.10	990.00
13064754	GE041	LAXEMAR	Core logging – BOREMAP/BIPS	2005/01/11 11:53:00	2005/02/28 07:58:00	PLU	KLX06	101.43	965.28
13063200	GE301	LAXEMAR	Geophysical borehole interpretation	2005/01/31 00:00:00	2005/02/15 00:00:00	PLU	KLX06	0.10	989.90
13063856	GP080	LAXEMAR	Temperature gradient calculation	2005/01/31 00:00:00	2005/02/15 00:00:00		KLX06	101.90	989.90
13063857	GP070	LAXEMAR	Salinity calculation	2005/01/31 00:00:00	2005/02/15 00:00:00		KLX06	101.90	989.90
13077283	RM100	LAXEMAR	Ultra sonic wave velocities	2005/02/08 00:00:00	2005/02/11 00:00:00	PLU	KLX06	220.40	220.40
13065010	HY681	LAXEMAR	PLU DIFF SPR and Caliper logging	2005/02/14 15:13:00	2005/02/15 13:43:00	PLU	KLX06	96.20	990.56
13073838	RM115	LAXEMAR	Triaxial test	2005/02/15 00:00:00	2005/05/30 00:00:00	PLU	KLX06	261.85	261.99
13065007	HY683	LAXEMAR	PLU DIFF-EC Temp and Pressure measurements	2005/02/16 07:47:00	2005/02/16 09:27:00	PLU	KLX06	11.10	987.25
13065008	HY680	LAXEMAR	PLU Flowlogging-PFL-DIFF_sequential	2005/02/16 11:00:00	2005/02/22 07:43:00	PLU	KLX06	0.00	986.00
13070812	HY610	LAXEMAR	PLU Pumping test-submersible pump	2005/02/18 16:52:00	2005/02/28 13:47:00	PLU	KLX06		
13065017	EG017	LAXEMAR	Pumping, start	2005/02/18 16:52:00	2005/02/18 16:52:00	PLU	KLX06		
13065023	EG016	LAXEMAR	Pumping, stop	2005/02/19 09:15:00	2005/02/19 09:15:00	PLU	KLX06		
13065018	EG017	LAXEMAR	Pumping, start	2005/02/19 11:45:00	2005/02/19 11:45:00	PLU	KLX06		
13075255	HY640	LAXEMAR	PLU Interference test – CRwr	2005/02/19 11:45:00	2005/03/09 20:00:00	PLU	KLX06	11.88	994.94
13065011	HY685	LAXEMAR	PLU Flowlogging-PFL-DIFF_overlapping	2005/02/20 10:44:00	2005/02/21 22:27:00	PLU	KLX06	91.33	988.54
13065024	EG016	LAXEMAR	Pumping, stop	2005/02/22 07:43:00	2005/02/22 07:43:00	PLU	KLX06		
13065019	EG017	LAXEMAR	Pumping, start	2005/02/22 08:36:00	2005/02/22 08:36:00	PLU	KLX06		

ACTIVITY_ID	ACTIVITY TYPE CODE	SITE	ACTIVITY	START_DATE	STOP_DATE	PROJECT	IDCODE	SECUP	SECLOW
13065012	HY685	LAXEMAR	PLU Flowlogging-PFL-DIFF_overlapping	2005/02/22 11:58:00	2005/02/25 07:48:00	PLU	KLX06	96.34	944.43
13065025	EG016	LAXEMAR	Pumping, stop	2005/02/25 08:28:00	2005/02/25 08:28:00	PLU	KLX06		
13065020	EG017	LAXEMAR	Pumping, start	2005/02/25 09:09:00	2005/02/25 09:09:00	PLU	KLX06		
13065013	HY684	LAXEMAR	PLU PFL DIFF Fracture EC Measurements	2005/02/25 11:37:00	2005/02/26 13:55:00	PLU	KLX06	195.81	927.96
13065026	EG016	LAXEMAR	Pumping, stop	2005/02/26 13:55:00	2005/02/26 13:55:00	PLU	KLX06		
13065021	EG017	LAXEMAR	Pumping, start	2005/02/26 14:35:00	2005/02/26 14:35:00	PLU	KLX06		
13065014	HY682	LAXEMAR	PLU DIFF – EC and Temp measurements	2005/02/26 14:49:00	2005/02/26 16:38:00	PLU	KLX06	20.00	990.00
13065015	HY105	LAXEMAR	Grw pressure monitoring surface boreholes	2005/02/26 16:52:00	2005/02/28 09:17:00	PLU	KLX06	0.00	990.00
13065027	EG016	LAXEMAR	Pumping, stop	2005/02/26 16:53:00	2005/02/26 16:53:00	PLU	KLX06		
13065016	HY685	LAXEMAR	PLU Flowlogging-PFL-DIFF_overlapping	2005/02/28 09:17:00	2005/02/28 15:30:00	PLU	KLX06	0.00	270.00
13065022	EG017	LAXEMAR	Pumping, start	2005/02/28 10:17:00	2005/02/28 10:17:00	PLU	KLX06		
13065028	EG016	LAXEMAR	Pumping, stop	2005/02/28 13:47:00	2005/02/28 13:47:00	PLU	KLX06		
13073497	RM090	LAXEMAR	Sampling for thermal properties and expansion	2005/03/01 00:00:00	2005/04/30 00:00:00	PLU	KLX06	243.18	243.24
13070778	HY660	LAXEMAR	PLU Injection test	2005/03/07 08:59:00	2005/03/10 08:15:00	PLU	KLX06	260.00	265.00
13066572	WC060	LAXEMAR	Water sampling, class 1	2005/03/07 10:20:00	2005/03/09 09:45:00	PLU	KLX06	260.00	265.00
13065191	WC090	LAXEMAR	Water sampling, class 4	2005/03/09 11:00:00	2005/03/09 11:00:00	PLU	KLX06	260.00	265.00
13070782	HY660	LAXEMAR	PLU Injection test	2005/03/10 18:56:00	2005/03/17 08:19:00	PLU	KLX06	558.20	563.20
13066577	WC060	LAXEMAR	Water sampling, class 1	2005/03/10 19:32:00	2005/03/15 17:00:00	PLU	KLX06	558.20	563.20
13066570	WC080	LAXEMAR	Water sampling, class 3	2005/03/16 08:30:00	2005/03/16 08:30:00	PLU	KLX06	558.20	583.20
13066583	WC060	LAXEMAR	Water sampling, class 1	2005/03/16 08:40:00	2005/03/16 08:40:00	PLU	KLX06	558.20	563.20
13070785	HY660	LAXEMAR	PLU Injection test	2005/03/17 16:07:00	2005/03/23 07:08:00	PLU	KLX06	776.20	781.20
13066584	WC060	LAXEMAR	Water sampling, class 1	2005/03/17 16:41:00	2005/03/23 09:05:00	PLU	KLX06	776.20	781.20
13066571	WC080	LAXEMAR	Water sampling, class 3	2005/03/23 09:10:00	2005/03/23 09:15:00	PLU	KLX06	776.20	781.20
13073490	RM080	LAXEMAR	Density and porosity measurement	2005/03/30 00:00:00	2005/05/20 00:00:00	PLU	KLX06	263.54	263.60
13070788	HY660	LAXEMAR	PLU Injection test	2005/04/01 14:25:00	2005/04/19 19:33:00	PLU	KLX06	106.38	206.38
13073342	EG157	LAXEMAR	Magnetic – accelerometer measurement	2005/04/29 07:26:00	2005/04/29 07:26:00	PLU	KLX06	0.00	990.00
13076659	GE300	LAXEMAR	Geological single hole interpretation	2005/06/29 00:00:00	2005/06/29 00:00:00	PLU	KLX06	100.00	994.90

Appendix 2

Rock water contents and analytical data from out-diffusion solutions

Table 1. Water content by drying at 105°C, bulk density, and watercontent porosity of rock samples from borehole KLX08.

Laboratory sample no	Lithology	Number of samples	Bulk density wet [1)] (g/cm^3)	Water content average (wt.%)	Water content 1 σ (wt.%)	Water-content porosity average (Vol.%)	Water-content porosity 1 σ (Vol.%)
KLX08-1	Avrö granite	3	2.67	0.422	0.144	1.12	0.38
KLX08-2	Fine-grained graite	3	2.67	0.349	0.095	0.92	0.25
KLX08-3	Avrö granite	3	2.68	0.289	0.062	0.77	0.16
KLX08-4	Avrö granite	3	2.68	0.315	0.049	0.84	0.13
KLX08-5	Avrö granite	3	2.66	0.195	0.029	0.52	0.08
KLX08-6	Avrö granite	3	2.68	0.192	0.060	0.51	0.16
KLX08-7	Avrö granite	3	2.68	0.201	0.050	0.54	0.13
KLX08-8	Avrö granite	0 [2)]	2.65	-	-	-	-
KLX08-9	Avrö granite	2	2.69	0.414	0.044	1.10	0.12
KLX08-10	Avrö granite	1	2.65	0.292	-	0.77	-
KLX08-11	Diorite	3	2.92	0.218	0.078	0.63	0.22
KLX08-12	Diorite	3	2.84	0.175	0.013	0.49	0.04
KLX08-13	Diorite	3	2.85	0.151	0.043	0.43	0.12
KLX08-14	Avrö granite	3	2.67	0.246	0.062	0.65	0.16
KLX08-15	Avrö granite	3	2.66	0.248	0.078	0.66	0.21
KLX08-16	Avrö granite	3	2.74	0.331	0.160	0.90	0.43
KLX08-17	Avrö granite	3	2.69	0.263	0.107	0.70	0.29
KLX08-18	Qtz-monzodiorite	3	2.81	0.183	0.080	0.51	0.22
KLX08-19	Qtz-monzodiorite	3	2.80	0.238	0.085	0.66	0.24

[1)] Determined from mass and volume of saturated (wet) drillcore sample used for out-diffusion experiment.
[2)] Not enough sample material and/or fractured material received to perform analyses.

Table 2. Chemical composition of solutions from out-diffusion experiments at steady state conditions.

Out-Diffusion Experiment Solution	Units	KLX08-1	KLX08-2	KLX08-3	KLX08-4	KLX08-5	KLX08-6	KLX08-7	KLX08-8
SAMPLE DESCRIPTION									
Depth along Borehole	m	150.22	199.45	200.26	250.19	302.34	347.10	395.65	451.62
Rock Type		Avrö granite	Fine-grained granite	Avrö granite	Avrö granite	Avrö granite	Avrö granite	Avrö granite	Avrö granite
Water-Rock Ratio		0.119	0.105	0.109	0.107	0.109	0.109	0.109	0.106
Experiment Temperature	ºC	45	45	45	45	45	45	45	45
Experiment Time	days	91	91	91	91	91	91	91	93
MISC. PROPERTIES									
Chemical Type		Na-Ca-HCO3	Na-Ca-HCO3	Na-Ca-HCO3	Na-Ca-HCO3	Na-Ca-HCO3-Cl	Na-Ca-HCO3	Na-HCO3-Cl	Na-Ca-HCO3
pH (lab)	-log(H+)	7.64	7.74	7.51	7.42	7.5	7.18	7.21	7.47
Electrical Conductivity	µS/cm								
Sample Temperature	ºC	20	20	20	20	20	20	20	20
CATIONS									
Sodium (Na^+)	mg/L	40.6	49.9	42.8	59.7	52.1	56.4	47.8	59.1
Potassium (K^+)	mg/L	3.2	4.2	3.0	2.7	2.1	4.0	1.1	3.4
Magnesium (Mg^{+2})	mg/L	1.6	2.8	2.0	1.2	0.5	1.3	0.1	0.2
Calcium (Ca^{+2})	mg/L	11.1	27.2	22.8	12.9	8.9	27.5	2	17.1
Strontium (Sr^{+2})	mg/L	<0.5	<0.5	<0.5	<0.5	<0.5	<0.5	<0.5	<0.5
ANIONS									
Fluoride (F^-)	mg/L	5.9	4.2	4.4	5.6	5.6	4.1	6.8	5.0
Chloride (Cl^-)	mg/L	3.4	4.5	4.3	3.4	12.5	13.5	6.7	6.4
Bromide (Br^-)	mg/L	<0.1	<0.1	<0.1	<0.1	<0.1	<0.1	<0.1	0.5
Sulphate (SO_4^{-2})	mg/L	2.8	4.6	3.2	5.5	5.8	5.3	6.9	5.1
Nitrate (NO_3^-)	mg/L	<0.5	<0.5	<0.5	4.2	1.5	<0.5	1.9	<0.5
Total Alkalinity as HCO_3^-	mg/L	111.1	187.9	160.5	150.7	108.6	173.9	78.7	166.6
CALC. PARAMETERS									
Total dissolved solids	mg/L	178	283	241	241	196	285	150	263
Charge Balance	%	5.16	4.63	3.04	5.66	4.33	6.29	4.83	3.59

Table 2. (continued).

Out-Diffusion Experiment Solution	Units	KLX08-9	KLX08-10	KLX08-11	KLX08-12	KLX08-13	KLX08-14	KLX08-15	KLX08-16
SAMPLE DESCRIPTION									
Vertical Depth	m	499.78	550.23	601.68	660.03	702.05	750.80	802.22	857.98
Rock Type		Avrö granite	Avrö granite	Diorite	Diorite	Diorite	Avrö granite	Avrö granite	Avrö granite
Water-Rock Ratio		0.101	0.106	0.096	0.113	0.099	0.110	0.108	0.106
Experiment Temperature	ºC	45	45	45	45	45	45	45	45
Experiment Time	days	93	93	93	93	93	93	93	93
MISC. PROPERTIES									
Chemical Type		Na-Ca-HCO3-Cl	Na-Ca-HCO3-Cl	Na-Ca-HCO3	Na-Ca-HCO3	Na-Ca-HCO3	Na-Ca-HCO3-SO4	Ca-Na-SO4	Ca-Na-SO4
pH (lab)	-log(H+)	7.24	7.47	7.32	7.13	7.37	7.14	7.01	7.01
Electrical Conductivity	µS/cm								
Sample Temperature	ºC	20	20	20	20	20	20	20	20
CATIONS									
Sodium (Na^{+})	mg/L	53.6	84.8	51.7	53.4	58.8	91.2	75.5	118.6
Potassium (K^{+})	mg/L	3.4	3.1	6.4	7.8	8.1	6.0	10.7	17.2
Magnesium (Mg^{+2})	mg/L	0.1	0.3	0.2	2.5	0.3	0.3	0.3	1.5
Calcium (Ca^{+2})	mg/L	14.0	22.3	18.7	49.2	27.9	48.5	245.9	274.6
Strontium (Sr^{+2})	mg/L	<0.5	<0.5	<0.5	<0.5	<0.5	<0.5	1.5	1.6
ANIONS									
Fluoride (F^{-})	mg/L	4.8	4.0	3.6	3.2	1.1	4.0	2.4	2.0
Chloride (Cl^{-})	mg/L	24.2	27.1	5.4	6.0	10.5	33.8	61.8	84.4
Bromide (Br^{-})	mg/L	0.3	0.8	0.3	0.6	0.4	0.6	0.3	0.6
Sulphate (SO_4^{-2})	mg/L	12.0	12.0	17.7	20.0	14.2	114.0	571.7	714.1
Nitrate (NO_3^{-})	mg/L	<0.5	<0.5	<0.5	<0.5	<0.5	<0.5	<0.5	<0.5
Total Alkalinity as HCO_3^{-}	mg/L	106.8	206.8	146.4	223.9	181.2	160.5	112.9	76.3
CALC. PARAMETERS									
Total dissolved solids	mg/L	219	360	250	366	302	458	1081	1289
Charge Balance	%	3.08	2.92	3.73	7.83	7.23	3.12	0.74	2.21

Table 2. (continued).

Out-Diffusion Experiment Solution	Units	KLX08-17	KLX08-18	KLX08-19	Blank Solution
SAMPLE DESCRIPTION					
Vertical Depth	m	903.28	945.75	983.18	
Rock Type		Avrö granite	Quartz-monzodiorite	Quartz-monzodiorite	
Water-Rock Ratio		0.108	0.104	0.105	
Experiment Temperature	ºC	45	45	45	
ExperimentTime	days	93	93	93	
MISC. PROPERTIES					
Chemical Type		Ca-Na-SO4	Na-Ca-HCO3-Cl	Na-Ca-Cl-HCO3	
pH (lab)	-log(H+)	6.98	7.27	7.47	
Electrical Conductivity	µS/cm				14
Sample Temperature	ºC	20	20	20	20
CATIONS					
Sodium (Na^{+})	mg/L	105.1	68.5	116.4	0.2
Potassium (K^{+})	mg/L	14.0	10.7	10.4	<0.1
Magnesium (Mg^{+2})	mg/L	0.4	0.5	0.7	0.3
Calcium (Ca^{+2})	mg/L	241.9	48.1	68.8	0.1
Strontium (Sr^{+2})	mg/L	0.9	<0.5	<0.5	
ANIONS					
Fluoride (F^{-})	mg/L	2.1	2.4	3.1	<0.1
Chloride (Cl^{-})	mg/L	145.4	53.4	183.1	1.1
Bromide (Br^{-})	mg/L	1.2	1.0	1.8	<0.1
Sulphate (SO_4^{-2})	mg/L	570.5	15.9	24.9	<0.1
Nitrate (NO_3^{-})	mg/L	<0.5	0.0	1.1	
Total Alkalinity as HCO_3^{-}	mg/L	60.4	195.3	153.2	<0.1
CALC. PARAMETERS					
Total dissolved solids	mg/L	1140	394	560	<2
Charge Balance	%	-0.12	4.82	2.49	2.57

Table 3. Isotopic composition of solutions from out-diffusion experiments at steady state conditions.

Laboratory sample No	Depth along borehole (m)	$\delta^{37}Cl$ ‰ V-SMOC	Sr ppm[2)]	$^{87}Sr / ^{86}Sr$	$^{87}Sr / ^{86}Sr$ 1 σ
KLX08-1	150.22				
KLX08-2	199.45				
KLX08-3	200.26				
KLX08-4	250.19	b.d.[1)]	0.185	0.715976	0.000013
KLX08-5	302.34				
KLX08-6	347.10	b.d.	0.278	0.716791	0.000010
KLX08-7	395.65				
KLX08-8	451.62				
KLX08-9	499.78	0.4	0.190	0.717947	0.000032
KLX08-10	550.23	0.44	0.185	0.717305	0.000013
KLX08-11	601.68	b.d.	0.144	0.722642	0.000013
KLX08-12	660.03				
KLX08-13	702.05		0.184	0.720575	0.000015
KLX08-14	750.80	3.43	0.492	0.715582	0.000011
KLX08-15	802.22	1.22	1.320	0.714670	0.000010
KLX08-16	857.98				
KLX08-17	903.28	1.26	2.042	0.713231	0.000019
KLX08-18	945.75				
KLX08-19	983.18	0.66	0.856	0.715639	0.000016

[1)] b.d. = below detection due to low Cl content, [2)] mass-spectrometric measurement

Table 4. Chloride concentration of pore water calculated from out-diffusion solutions and the water content of the samples.

Laboratory sample No	Depth along borehole (m)	Lithology	Pore water Cl (mg/kg H_2O)	Pore water Cl + error [1)] (mg/kg H_2O)	Pore water Cl - error [1)] (mg/kg H_2O)
KLX08-1	150.22	Avrö granite	99	24	49
KLX08-2	199.45	Fine-grained granite	139	29	50
KLX08-3	200.26	Avrö granite	164	28	44
KLX08-4	250.19	Avrö granite	117	15	21
KLX08-5	302.34	Avrö granite	705	90	122
KLX08-6	347.10	Avrö granite	773	180	341
KLX08-7	395.65	Avrö granite	365	71	118
KLX08-8	451.62	Avrö granite	-	-	-
KLX08-9	499.78	Avrö granite	614	56	69
KLX08-10	550.23	Avrö granite	998	100	100
KLX08-11	601.68	Diorite	240	61	129
KLX08-12	660.03	Diorite	388	27	31
KLX08-13	702.05	Diorite	687	150	270
KLX08-14	750.80	Avrö granite	1534	302	506
KLX08-15	802.22	Avrö granite	2722	637	1221
KLX08-16	857.98	Avrö granite	2764	873	2504
KLX08-17	903.28	Avrö granite	6059	1709	4048
KLX08-18	945.75	Qtz-monzodiorite	3041	909	2319
KLX08-19	983.18	Qtz-monzodiorite	8228	2112	4448

[1)] Error based on the standard deviation of multiple water-content measurements.

Table 5. $\delta^{18}O$ and $\delta^{2}H$ of pore water and water content derived from isotope diffusive exchange method.

Laboratory sample No	Average depth along borehole (m)	$\delta^{18}O$ [1)] pore water (‰ V-SMOW)	$\delta^{2}H$ [1)] pore water (‰ V-SMOW)	Water content from isotope exchange (wt.%)	Water content error [1), 2)] 1 σ (wt.%)
KLX08-1	150.22	-	-	-	-
KLX08-2	199.45	-	-	-	-
KLX08-3	200.26	-9.56	-83.5	*0.377*	*0.003*
KLX08-4	250.19	-8.58	-81.3	0.378	0.010
KLX08-5	302.34	-7.47	-76.7	0.183	0.003
KLX08-6	347.10	-8.58	-95.1	0.149	0.006
KLX08-7	395.65	-12.59	-105.6	0.258	0.003
KLX08-8	451.62	-	-	-	-
KLX08-9	499.78	-	-	-	-
KLX08-10	550.23	-13.99	-101.6	0.274	0.011
KLX08-11	601.68	-12.53	-100.8	0.137	0.009
KLX08-12	660.03	-8.50	-89.4	*0.452*	*0.007*
KLX08-13	702.05	-7.59	-83.9	0.187	0.007
KLX08-14	750.80	-5.15	-71.3	0.194	0.003
KLX08-15	802.22	-2.00	-54.4	0.159	0.007
KLX08-16	857.98	-9.72	-72.1	*0.725*	*0.004*
KLX08-17	903.28	-3.51	-53.1	0.189	0.007
KLX08-18	945.75	-6.89	-59.5	*0.366*	*0.003*
KLX08-19	983.18	-3.11	-43.0	0.233	0.007

[1)] Average error (calculated with Gauss' law of error propagation): $\delta^{18}O$ = ±1.7‰, $\delta^{2}H$ = ± 9.7‰, and given for each sample for the water content

[2)] Shaded areas with data in italics: too high water content due erroneous analysis of traced test water (memory effect during ^{2}H mass spectrometric measurement); pore-water $\delta^{2}H$ value remains unaffected within the error

10 Appendix 2: Explorative analyses of microbes, colloids and gases

Contribution to the model version 2.1

Lotta Hallbeck, Vita vegrandis

August 2006

Contents

1 Microbiology and microbial model

1.1 Introduction

Micro-organisms are abundant in Fennoscandian Shield groundwater, from the surface down to a depth of at least 1,500 m /Pedersen 1993, Haveman et al. 1999/. To understand the current undisturbed hydro–biogeochemical conditions at a given site, the following parameters are of interest: pH, E_h, S^{2-}, S^0, SO_4^{2-}, HCO_3^-, HPO_4^{2-}, Fe^{2+}, nitrogen species, and TDS, (total dissolved solids), together with colloids, fulvic and humic acids, dissolved organic compounds, and micro-organisms. In addition, knowing the concentrations of dissolved gases is crucial in seeking a complete model, since many micro-organisms consume and/or produce different gases. Furthermore, for a full understanding it is necessary to be able to predict how changing conditions, during the construction and following phases of a repository, will influence microbes in the groundwater and vice versa.

In their energy-harvesting reactions, microbes use available energy-rich compounds as electron donors and various electron acceptors from groundwater and fracture minerals. In this way, they are intimately coupled to the redox conditions in the groundwater system.

The microbial parameters of interest are the total number of cells and the presence of different metabolic groups of micro-organisms /Pedersen 2001/. These data will indicate the activity of specific microbial populations at a certain site and how they interact with the geochemistry. The groups cultured in the microbial part of the site investigation were iron-reducing bacteria (IRB), manganese-reducing bacteria (MRB), sulphate-reducing bacteria (SRB), auto- and heterotrophic methanogens (AM and HM), and auto- and heterotrophic acetogens (AA and HA).

The most probable number (MPN) of micro-organisms is a statistical cultural method for calculating the most probable number of different cultivable metabolic groups of micro-organisms /Anonymous 1992/.

This part of the report will deal with the microbial data available so far from the site investigation in the Laxemar sub area, but also in the regional Simpevarp area as well.

1.2 The subsurface microbial model

Investigations of micro-organisms in groundwater in the Fennoscandian Shield have been ongoing since the mid 1980s /Pedersen 2002/. Comparisons of data compiled from the different investigated sites have made it possible to create a conceptual model of the biogeochemical system consisting of surface and subsurface groundwater in the Fennoscandian Shield (Figure 1-1).

The model includes five different biospheres or zones and one abiotic chemosphere in a layered structure. The depths at which the described biospheres can be found may differ between sites. All groups of micro-organisms will not be present at all sites, because the particular geochemical environment may be such that one or several groups cannot be active at certain sites. The presence of iron-reducing bacteria can be used as an example. This group depends on the presence of bioavailable ferric iron compounds. If no such compounds are present at a given site, the iron-reducers will be absent. Despite this, the *relative* positions of the different zones and microbial groups will always be the same. The microbes and chemical characterisations of the different zones were described in detail in the geochemical report for Laxemar 1.2 /SKB 2006/ and will not be repeated in detail here. A brief description of the different organism groups is found in section 1.11.2.

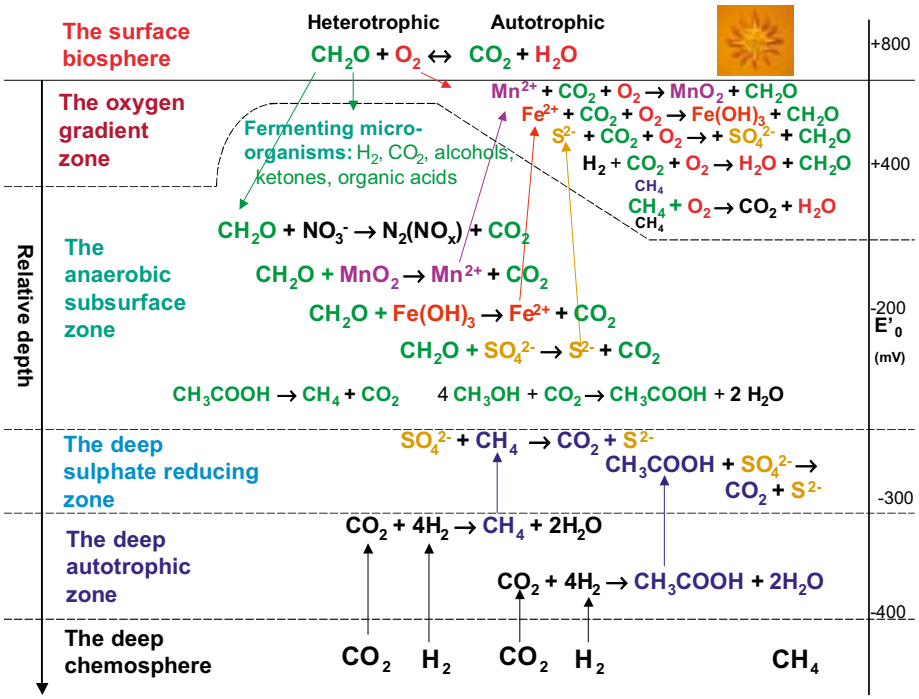

Figure 1-1. *Conceptual model of microbial processes in Fennoscandian Shield groundwater. The reactions should be considered as descriptive and are not balanced.*

1.3 Data available

At the time of the data freeze for the Laxemar model, version 2.1 (30 June 2005), microbial data from four depths in borehole KLX03 were available. These data are the first to originate from the ongoing site investigation in the Laxemar subarea and are presented in Figure 1-2. Data were also available from borehole KSH01A in the Simpevarp subarea. The data pertaining to the different groups will be discussed in detail in the following sections.

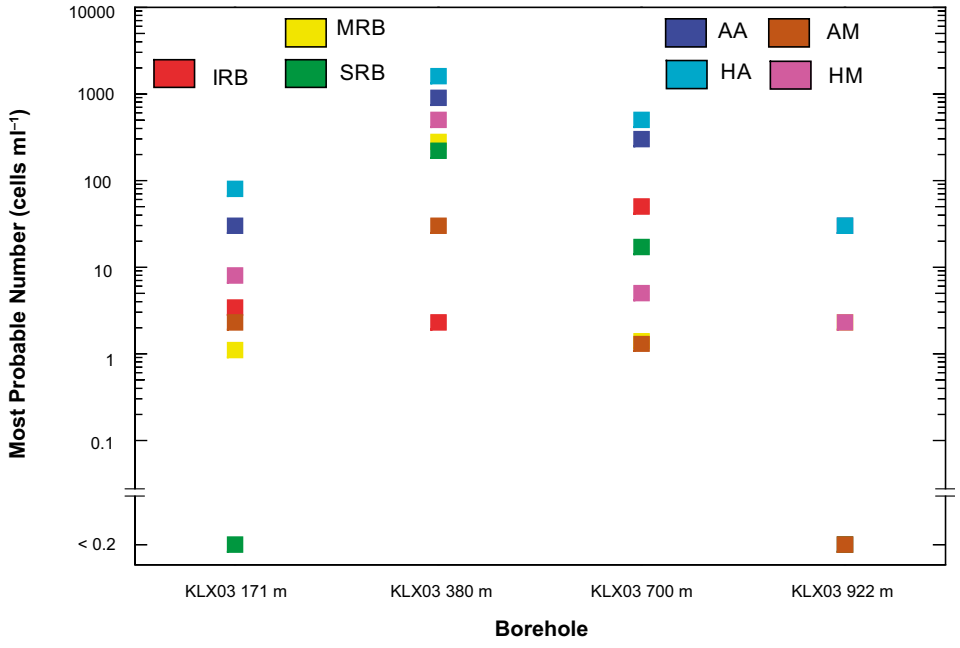

Figure 1-2. *The most probable numbers (MPN) of different physiological groups of micro-organisms in borehole KLX03 in the Laxemar subarea. Data from the Laxemar version 2.1 data freeze.*

1.4 Evaluation of the microbial and chemical data

1.4.1 Total number of micro-organisms and organic carbon (OC)

There is a positive correlation between total numbers of micro-organisms and the amount of carbon in the subsurface system. Figure 1-3 shows the total number of micro-organisms in boreholes in the Laxemar subarea. The total number of cells was approximately $1 \cdot 10^5$ ml^{-1} down to a depth of approximately 700 to 800 m. The numbers increased with increasing depth, to $2 \cdot 10^6$ ml^{-1} at 1,350 m. The amount of OC followed the same trend, as can be seen in Figure 1-4, which shows the total number of cells and amount of organic carbon in Simpevarp area boreholes. The amount of organic carbon in borehole KLX02 at a depth of 1,160 m was very high, at 98 mg l^{-1}. We need more data from these depths to be able to evaluate the accuracy of these measurements. One plausible explanation of the increased numbers of cells is the higher temperature at such depths, as higher temperatures enhance the activity of micro-organisms by increasing their growth rate. There is also a suggestion that shallow groundwater containing organic material has been drawn to deeper depths, resulting in higher numbers of micro-organisms and amounts of organic carbon /Ekman 2001/.

1.4.2 Fractionation filtration for humic and fulvic acids

To understand the size distribution of the organic material in groundwater, groundwater from the 161.8 m and 556.5 m depth sections of borehole KSH01A and from the 171, 380, and 922 m sections of borehole KLX03 were subject to fractionation filtration. Defined cut-off filters of 1,000 and 5,000 Dalton (D) were used (see also section 2.3). The filtration showed that most of the organic material was smaller than 1,000 D and that some was in the > 5,000 D fraction. The results are compiled in Table 1-2, which presents the DOC values from the standard analyses. Measurable amounts of organic material in the > 1,000 D but < 5,000 D fraction were found in the 380 m depth section in borehole KLX03. The MPN results from this section of the borehole indicated the highest concentrations of AA, HA, and SRB (see Figure 1-2).

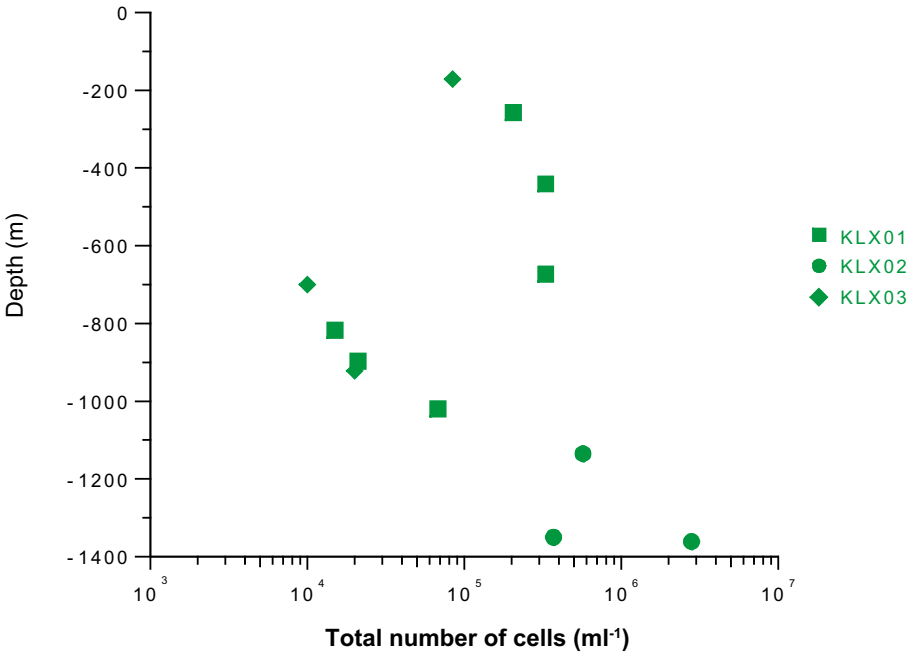

Figure 1-3. Total number of cells versus depth in the Laxemar boreholes, KLX1–KLX3.

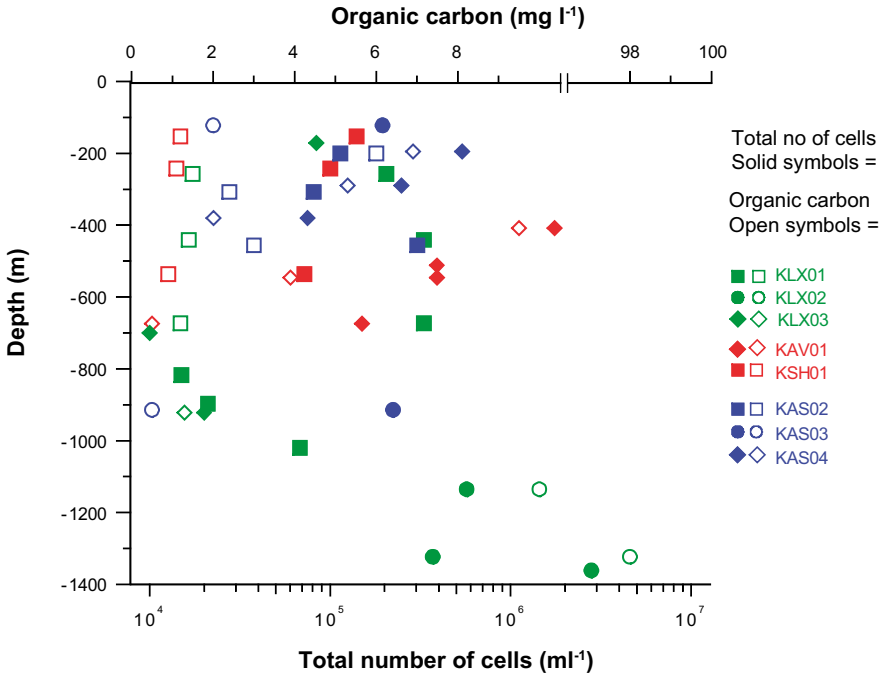

Figure 1-4. *Total number of micro-organisms and amount of organic carbon versus depth in the regional Simpevarp area.*

Table 1-1. Organic material (mg l^{-1}) in groundwater in boreholes KSH01A and KLX03, in the Simpevarp area, measured for three fractions using fractionation filtration and common DOC measurements.

Borehole section	< 1,000 D	> 1,000 D < 5000 D	> 5,000 D	DOC (in SICADA)
KSH01A, 161.8 m	1.0 ± 0.1	n.d.1	0.06 ± 0.04	0.9–1.5
KSH01A, 556.5 m	1.0 ± 0.1	n.d.	0.04 ± 0.03	< 1–1.1
KLX03, 171 m	8.30 ± 0.9	n.d.	12.8 ± 1.5	20
KLX03, 380 m	5.90 ± 0.8	1.40 ± 0.1	n.d.	d.m.2
KLX03, 922 m	1.40 ± 0.2	n.d.	1.40 ± 0.2	1.4

[1] n.d. = not detected

[2] d.m. = data missing

1.5 Manganese-reducing bacteria and manganese

Manganese in solution is in the manganese(II) state. MnO_2, the form of manganese(IV) found in groundwater, is insoluble in natural water in the pH 5–8 range. Figure 1-5 shows the amount of manganese(II) in groundwater in the regional Simpevarp area. The data indicate that the highest amount was found in borehole KAV01, at Ävrö, between 400 and 600 m in depth, where the concentration exceeded 2.5 mg l^{-1}. Amounts of approximately 1 mg l^{-1} were found between 100 and 600 m in depth, the highest amounts being found in the Äspö subarea.

High manganese(II) concentrations in groundwater can be a result of manganese-reducing bacteria oxidizing organic matter in an anaerobic environment. The highest MPN value for manganese-reducing bacteria was 280 ml^{-1}, found at a depth of 380 m in borehole KLX03. In the other sections in boreholes KLX03 and KSH01 only a few cells were found, or the numbers were below the detection limit of 0.2 cells ml^{-1}. The relatively high manganese levels in borehole KAS02 could be a result of manganese reduction; unfortunately, no microbial data were available from this borehole.

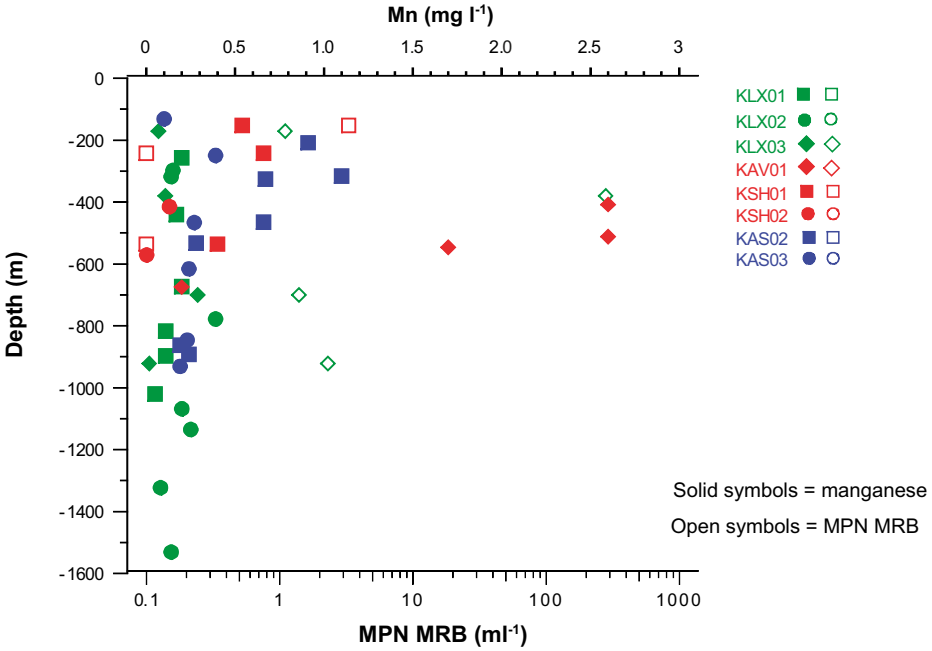

Figure 1-5. *Concentrations of manganese and manganese-reducing bacteria (MRB) versus depth in groundwater in the regional Simpevarp area. The Laxemar subarea is represented by boreholes KLX01, KLX02, and KLX03.*

1.6 Ferrous iron and iron-reducing bacteria

Figure 1-6 shows ferrous iron and the MPN of iron-reducing bacteria (IRB) versus depth in the Laxemar subarea. The highest number of IRB was 50 ml^{-1}, found at a depth of 700 m in borehole KLX03. The amounts of ferrous iron corresponded quite well with the numbers of IRB found. Figure 1-7 shows that the highest amounts of ferrous iron in the Simpevarp area were found in borehole KAV01, at depths of 422.5, 526.5, and 560.5 m. These three depths coincide with those at which the highest manganese values were found as well (see section 1.5). This is in agreement with a common observation of concomitant high amounts of iron and manganese. In borehole KLX02, the ferrous iron amounts were high at relatively greater depths (1 to 1.5 mg l^{-1}). From this section, 330 IRB ml^{-1} could be cultured.

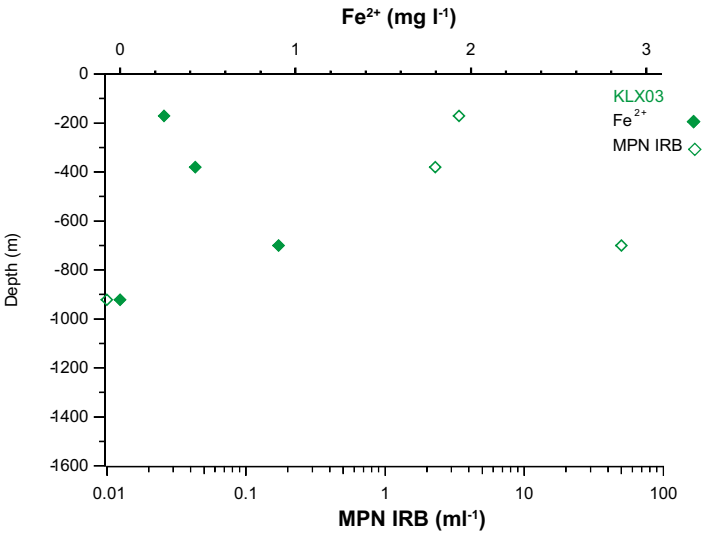

Figure 1-6. *Ferrous iron and MPN of iron-reducing bacteria (IRB) in borehole KLX03 in the Laxemar subarea.*

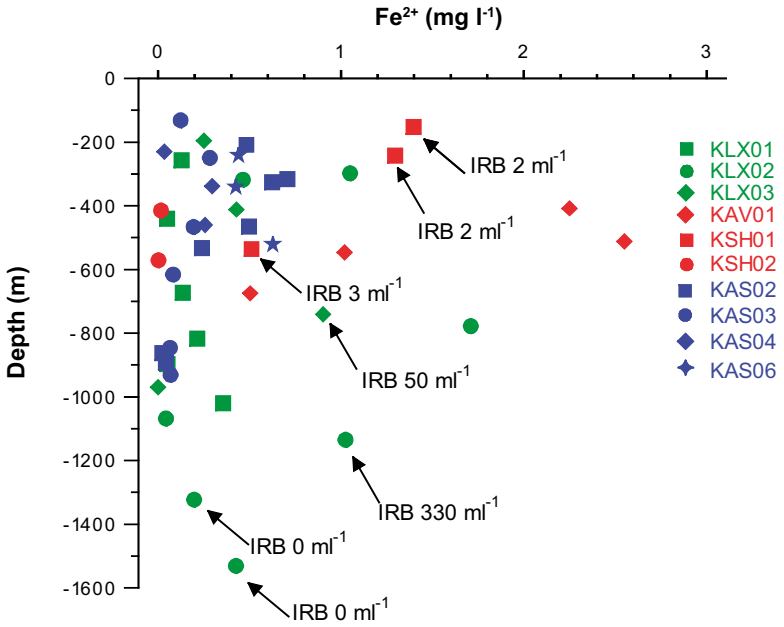

Figure 1-7. *Concentration of ferrous iron versus depth in the Simpevarp area. The local subarea of Laxemar is represented by boreholes KLX01, KLX02, and KLX03.*

1.7 Sulphate-reducing bacteria, sulphate, and sulphide

Sulphate concentrations increase with depth, as shown in Figure 1-8, to a maximum of 1,000 mg l^{-1} in the deepest groundwater sampled in borehole KLX02. The increase found in KLX02 was exponential at deeper depths. The explanation of this phenomenon is probably the same as for the organic matter content and total cell number, namely, a draw-down of shallower water to deeper depths (see section 1.4.1). In a more or less closed system with high sulphate-reducing activity, a decrease in sulphate should be seen. In groundwater systems with high amounts of sulphate plus a continuous supply of sulphate from the inflow of groundwater, such a decrease will be less pronounced.

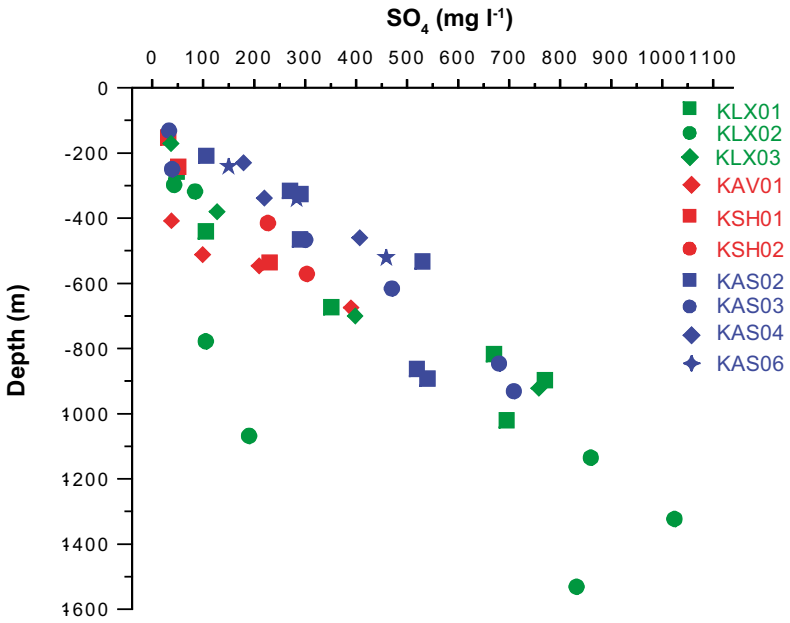

Figure 1-8. *The concentration of sulphate versus depth in the regional Simpevarp area. The Laxemar subarea is represented by boreholes KLX01, KLX02, and KLX03.*

In Figure 1-9 the sulphide values can be coupled to the MPN for SRB. The highest MPN, $5.6 \cdot 10^4$ ml^{-1}, was found in borehole KLX01 at a depth of 680 m together with the highest amount of sulphide, 2.5 mg l^{-1}. The second highest sulphide content, 1.5 mg l^{-1} in borehole KAS04 at a depth of 195 m, has a corresponding MPN of 1,600 SRB ml^{-1}. At 380 m in borehole KAS04 the sulphide content was below 0.5 mg l^{-1} and the MPN of under 100 SRB ml^{-1}. The MPN values for SRB in borehole KLX03 tend to decrease with depth, along with lower sulphide values. It is worth noting that the sulphide values from the site investigation were generally low. Samples taken before the site investigation sometimes displayed values of at least one to several mg l^{-1} groundwater. No high values have been reported from the site investigations, either in Laxemar or in Forsmark.

1.8 Methanogens

Figure 1-10 presents the MPN values for auto- and heterotrophic methanogens in the Simpevarp subarea. The highest MPNs found were for heterotrophic methanogens (HM) at 300–400 m in depth. Autotrophic methanogens (AM) were found in borehole KLX03, but were below the detection limit of 0.2 ml^{-1} in KSH01A. Methanogens have been found in high numbers in boreholes along the Äspö tunnel /Kotelnikova and Pedersen 1998/ and in boreholes at the MICROBE site in the tunnel /Pedersen 2005/.

Figure 1-11 shows the concentration of methane gas in groundwater at different depths in boreholes in the Simpevarp area. A trend toward decreasing methane content with depth is evident in borehole KLX03, with a content of 39 µM at 171 m declining to nearly zero at a depth of 922 m. The other measurements revealed low methane concentrations (see also section 3.2.3, concerning carbon dioxide and methane gas).

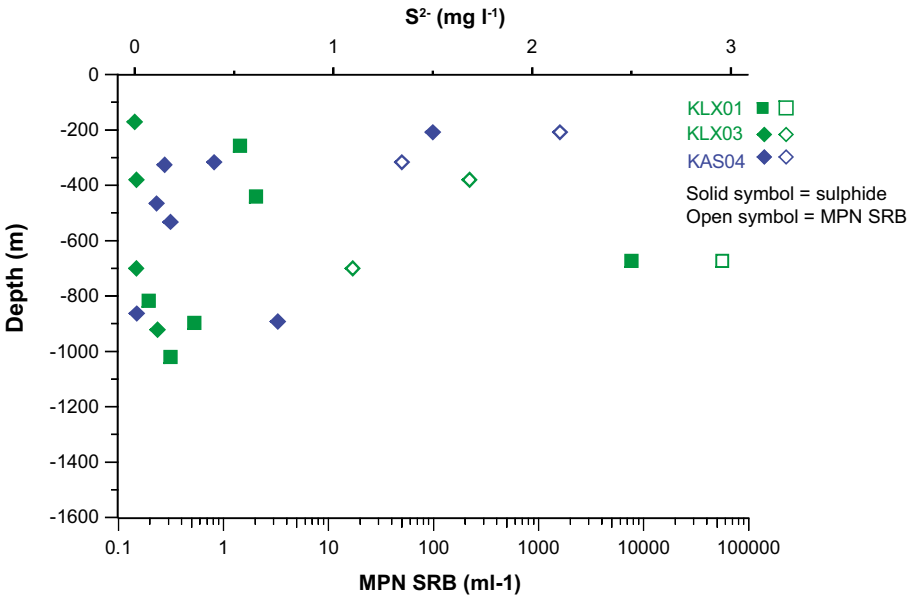

Figure 1-9. *The concentration of sulphide and the MPN of sulphate-reducing bacteria (SRB) versus depth in the regional Simpevarp area. The Laxemar subarea is represented by boreholes KLX01, KLX02, and KLX03.*

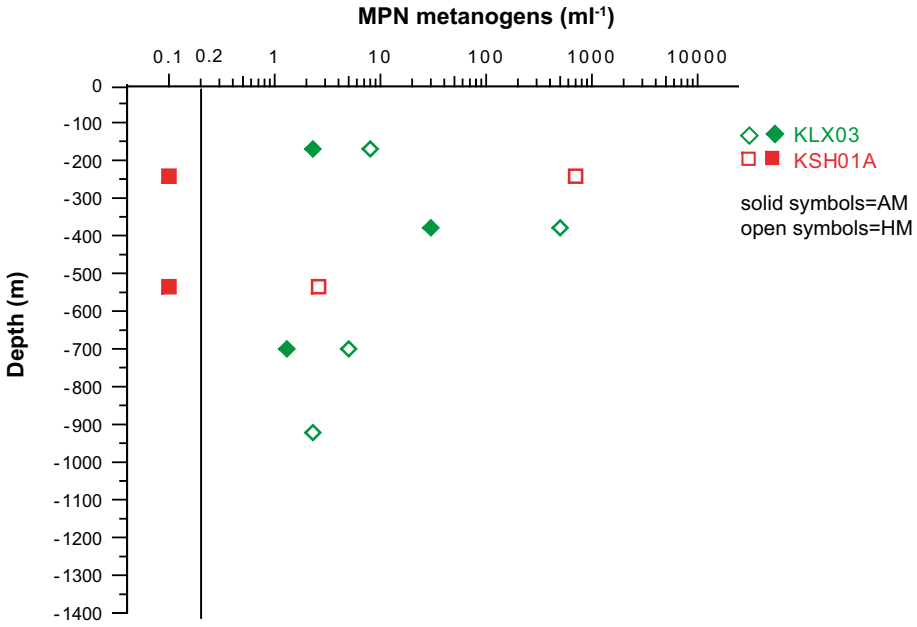

Figure 1-10. *MPN of methanogens in the Simpevarp subarea in boreholes KLX03 and KSH01A. AM = autotrophic methanogens, HM = heterotrophic methanogens.*

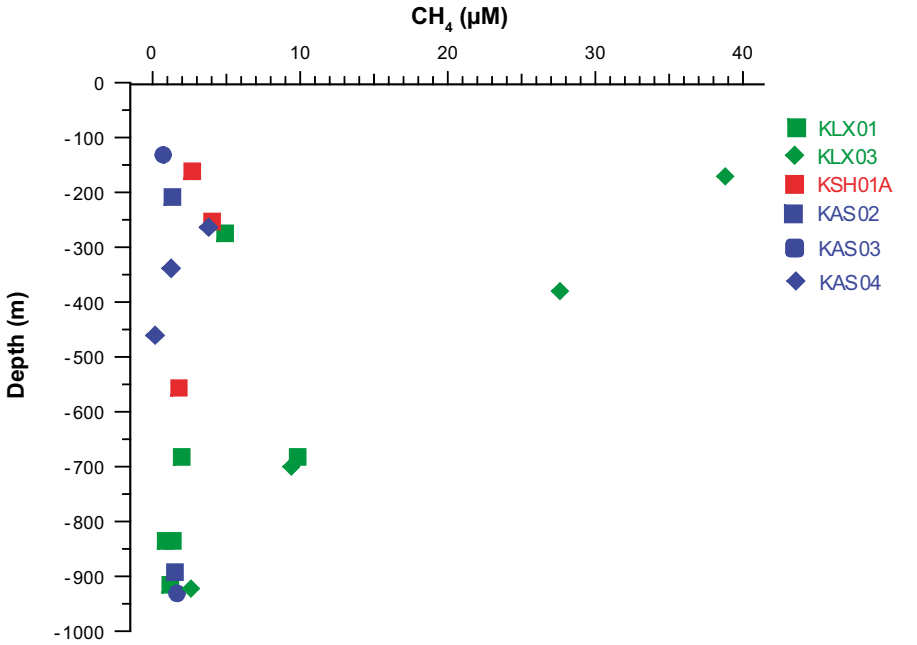

Figure 1-11. *The concentration of methane gas in groundwater from the regional Simpevarp area.*

1.9 Acetogens

There are two types of acetogens, autotrophs (AA) and heterotrophs (HA). The first group uses carbon dioxide as its carbon source and hydrogen as its energy source. Heterotrophs use organic C_1 compounds in their metabolism. The highest MPNs of acetogens found in the Simpevarp area were 1,600 and 900 ml^{-1} for HA and AA, respectively, in borehole KLX03 at a depth of 380 m. At a depth of 1,160 m in borehole KLX02, 100–200 acetogens ml^{-1} were found. Heterotrophic acetogens have been found at lesser depths than autotrophic acetogens have. The acetogens is a group of organisms that seems to be present at most depths, but in different amounts depending on the depth. Their ability to fix carbon dioxide as organic material, comprising both cell constituents and acetate,

makes them indigenous primary producers that can supply, for example, sulphate-reducing bacteria with energy and organic carbon. So far, there are no acetate concentration data available; however, acetate would be an important parameter to measure in the future.

1.10 Redox potential in groundwater

Measurement of the redox potential of groundwater gives an understanding of whether the groundwater chemistry system has a reducing or oxidising capacity. All metabolic reactions catalysed by micro-organisms are oxidation−reduction reactions, and influence the redox potential of the system of which they are part (see discussion of the microbial model, section 1.11).

The available redox data pertaining to groundwater in the Laxemar subarea are plotted versus depth in Figure 1-13. In this figure all data available in the data file extracted from SICADA are used.

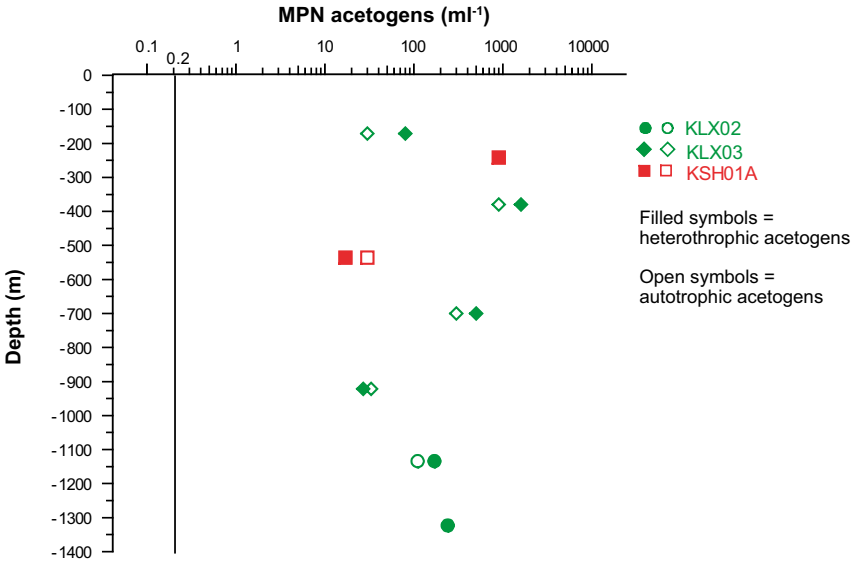

Figure 1-12. *MPN of auto- and heterotrophic acetogens versus depth in two boreholes in the Simpevarp area.*

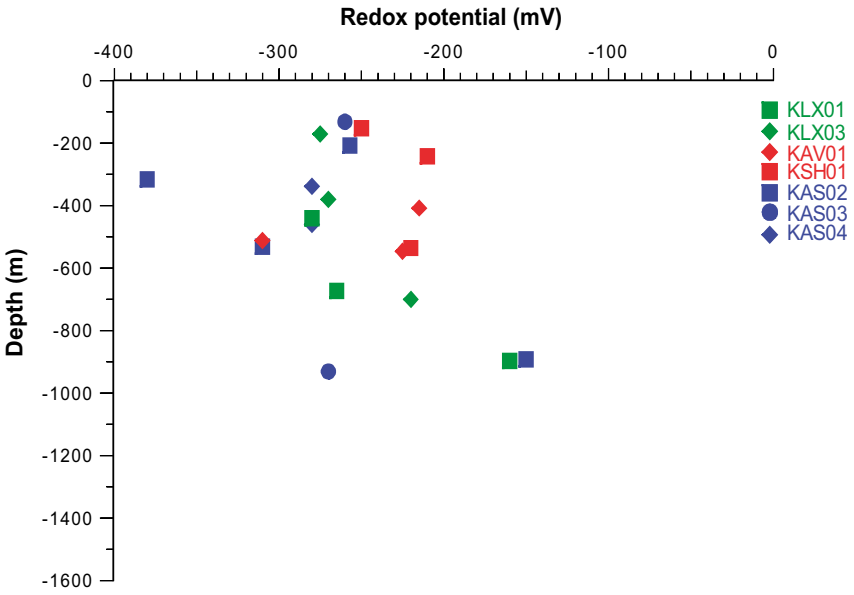

Figure 1-13. *The measured redox potential in the Simpevarp area versus depth.*

There is no obvious trend in redox values versus depth. At most depths, the redox is between –200 and –300 mV. The highest values, of approximately –150 mV, were found at a depth of 900 m in boreholes KLX01 and KAS02.

In Figure 1-14, redox values from boreholes KLX03 and KSH01A are plotted against depth, together with MPN values for the different physiological groups of micro-organisms. Low redox values correlate with the presence of sulphate-reducing bacteria. In sections with high amounts of iron-reducing bacteria the redox is higher. At a depth of 922 m in borehole KLX03, no redox measurement was possible. Presumably because the concentrations of electro-active chemical species were low in the water, Very few micro-organisms could be cultured from this sample.

During the site investigation, no redox values below –275 mV were measured. Earlier investigations have several times reported values as low as –400 mV. If the sulphide/sulphate system is what determines the redox, the new higher redox values correspond to the relatively low sulphide concentrations measured during the site investigation.

Borehole KLX03 in the Laxemar area is the only borehole with four sampled sections in this version and for which there are MPN data for all of the different physiological groups of micro-organisms cultured. Figure 1-15 presents the results versus depth. It can be seen that the most active section was at a depth of 380 m. At this depth the acetogens dominated, as they did in all sections, but at this particular depth (380 m) they were found in very high numbers. In addition, there were high numbers of manganese and sulphate reducers. At a depth of 700 m the numbers of acetogens were high. Low numbers of iron- and sulphate reducers were found here. The low redox value of –275 mV found at 176 m could depend on the SO_4^{2-}/S^{2-} system, but no SRB were found in samples from this section. The contents of both SO_4^{2-} and S^{2-} were very low, at 12.6 mg l^{-1} and < 0.002 mg l^{-1}, respectively.

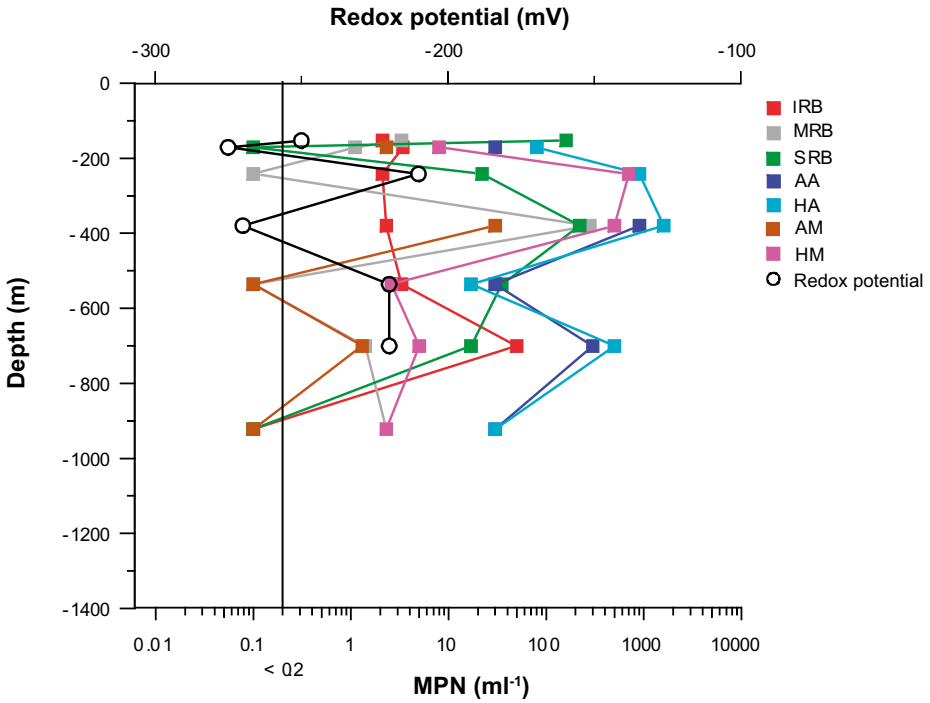

Figure 1-14. *MPN values for seven different physiological groups of micro-organisms as well as redox values measured in groundwater from boreholes KLX03 and KSH01A in the Simpevarp area. All data available in SICADA were included. The MPN values to the left of the vertical bar are below the detection limit of 0.2 ml^{-1}.*

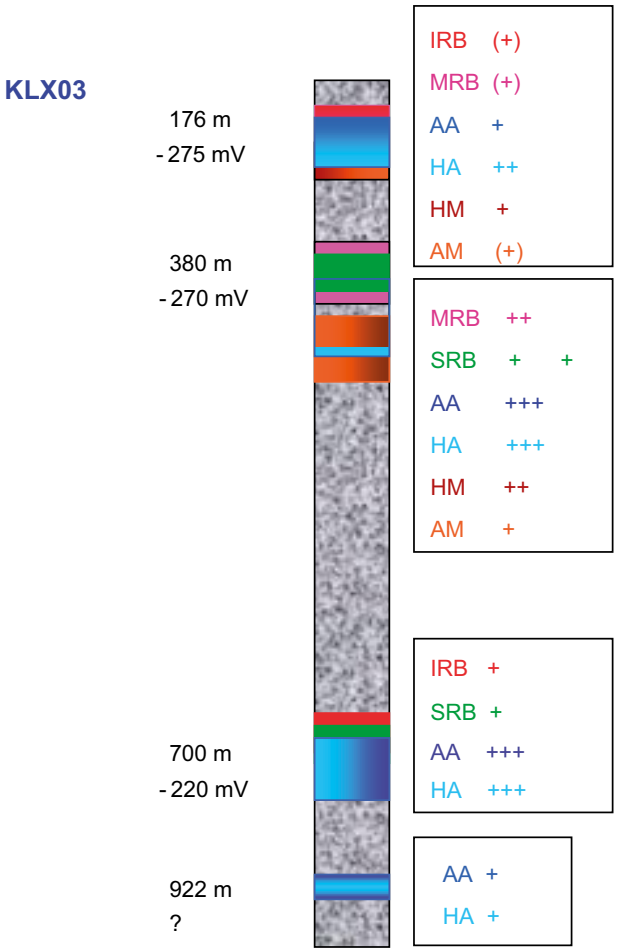

Figure 1-15. *A schematic presentation of MPN results versus depth in borehole KLX03 in the Laxemar area.*

1.11 The microbial model

In this section the available microbiology and chemistry data are merged in the microbial model for the regional Simpevarp area.

1.11.1 Classification of most probable number (MPN) values into *-symbols to be used in the Microbial Subsurface Model

A classification system has been developed for ranking the measured MPN values in relation to their relative influence on the geochemical conditions in the analysed groundwater (Table 1-2).

Table 1-2. Classification and interpretation of measured MPN values in groundwater.

Measured MPN value	Classification	Interpretation
Below detection limit	–	Not present
1–10	(*)	Present without influence[1]
11–50	*	Present with putative influence[1] if growth-promoting changes occur
51–500	**	Present with influence[1]
> 500	***	Dominant with high influence[1]

[1] Influence here means that the organism group has an effect on the geochemistry of the groundwater.

Recall that the groundwater samples from one section isolated with packers includes groundwater from fractures connected to the section, which is extracted from the aquifers by pumping. Because of this, two or more micro-organism groups may appear to be abundant in a single section, but their habitats could well be separate under natural circumstances due to their occurrence in different fractures.

The MPN measurements used in this report have been obtained over the past 14 years. Over this time, the analytical sensitivity has increased, especially in the last three years. Because of this, some of the older data may be inaccurate and misleading. Finite results indicate that the physiological group was present, but that the actual number could have been higher.

1.11.2 Characterisation of the influence of different metabolic groups of micro-organisms

Different microbial groups will influence the surrounding environment in different ways, depending on the metabolic group that is dominant. In Table 1-3, the activities and possible effects of these groups on their surroundings are listed.

Table 1-4. Activities and effects of the different physiological groups of micro-organisms found in deep groundwater.

Activity	Effect	
Aerobic respiration	• Oxidation of organic material by oxygen reduction	• Depletion of oxygen and organic material • Increase in alkalinity • Lowering of redox potential
Anaerobic respiration:	• Oxidation of organic material with reduction of compounds other than oxygen	• See below for each specific group of bacteria
Iron-reducing bacteria	• Oxidation of organic material with ferric iron reduction	• Depletion of organic material and ferric iron • Increase in ferrous iron and alkalinity • Lowering of redox potential
Manganese-reducing bacteria	• Oxidation of organic material with manganese(IV) ion reduction	• Depletion of organic matter and manganese(IV). • Increase of manganese(II) and alkalinity • Lowering of redox potential
Sulphate-reducing bacteria	• Oxidation of organic material with sulphate reduction	• Depletion of organic matter and sulphate • Increase of sulphide and in alkalinity • Lowering of redox potential
Methanogens		
Heterotrophic methanogens	• Convert organic material to methane and carbon dioxide	• Decrease of organic material • Increase of methane gas and carbon dioxide (alkalinity) • Redox not influenced
Autotrophic methanogens	• Oxidation of hydrogen gas and reduction of carbon dioxide to methane gas	• Depletion of hydrogen gas and alkalinity • Increase of methane • Redox lowered
Acetogens		
Heterotrophic acetogens	• Convert organic material to acetate	• Decrease of organic material other than acetate • Increase in the concentration of acetate Redox not influenced
Autotrophic acetogens	• Oxidation of hydrogen gas with reduction of carbon dioxide to acetate	• Depletion of hydrogen gas and alkalinity • Increase of acetate • Redox lowered

1.11.3 The microbial model in the Simpevarp regional area

Since the microbe data set is limited to microbes from the Laxemar subarea, the microbial model will be presented at the regional scale only.

The colours in the model are used as listed below:

- ■, light grey: A process not yet studied
- ■, dark grey: A process present but without influence
- ■, green: Carbon compounds originating from the surface biosphere
- ■, blue: Carbon compounds originating from the deep autotrophic zone
- ■, black: Compounds from the deep chemosphere
- ■, turquoise: Processes found but not anticipated and not yet confirmed
- ■, yellow: Sulphur compounds

The model shows, so far, that the dominant microbial process in the *anaerobic subsurface zone* is heterotrophic sulphate reduction (Figure 1-16). This zone is found at depths of 100−500 m. The *deep sulphate-reducing zone* is found at depths of approximately 600−900 m, while the *deep autotrophic zone* is in the 1,000−1,400 m depth region. Here we also found iron- and manganese reduction, though it is unclear whether this is because of shallow water being drawn down to deeper depths. We also found heterotrophic acetogenesis relatively deep in the bedrock. The *deep chemosphere* origin of the carbon dioxide and hydrogen gas in this zone also needs to be verified by stable isotope studies of the gas in the groundwater.

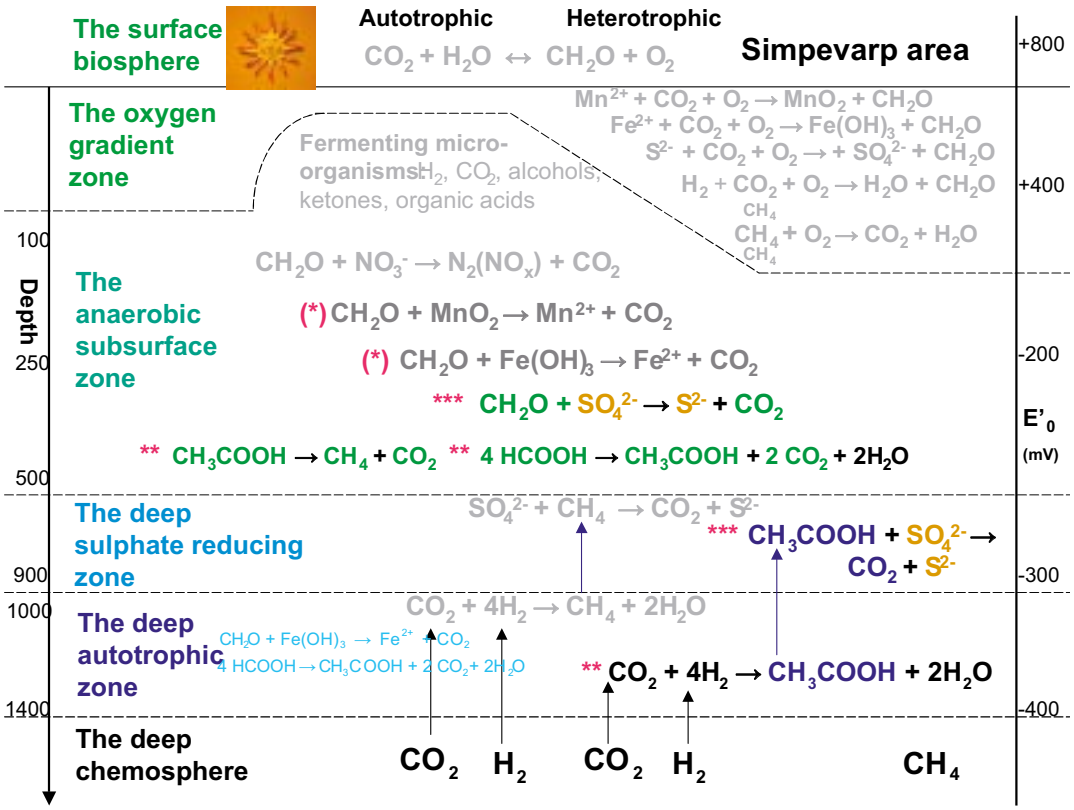

Figure 1-16. *The microbial model of the regional Simpevarp area based on data available at the time of the Laxemar version 2.1 data freeze. Asterisks before the reactions indicate the significance of the reaction according to the classification system presented in Table 1-3 (see section 1.11.1). No reactions are balanced.*

1.12 Conclusions

From the data used in this report the following conclusions can be drawn:

- Acetogens, both autotrophic and heterotrophic, were present at all sampled depths in borehole KLX03. Their autotrophic ability to produce acetate by oxidising hydrogen gas makes them a source of organic carbon that can be used, for example, by sulphate-reducing bacteria (SRB). This ecosystem is independent of organic material from the ground surface.
- The highest numbers of anaerobic micro-organisms in borehole KLX03 were found in the section at a depth of 380 m. We hypothesise that a fracture or fractures cross this zone, and that groundwater containing organic material is transported, probably from near the surface, to this depth. Comparison with hydrological data will be done when such data are available.
- The redox potential correlates well with the occurrence of SRB, suggesting that the SO_4^{2-}/S^{2-} couple controls the system. One exception is the section at a depth of 176 m in borehole KLX03, which has a low redox potential of –275 mV, but no SRB and low concentrations of sulphate and sulphide.

2 Colloids

2.1 Introduction

Particles in the 10^{-3} to 10^{-6} mm size range are regarded as colloids. Their small size prohibits them from settling and gives them the potential to transport radionuclides in groundwater. The aim of the colloid study in the Laxemar site investigation is to quantify and determine the composition of colloids in groundwater from boreholes. The results will be included when modelling the hydrochemistry at the site.

The last hydrogeochemical model report from the Simpevarp area, Laxemar version 1.2 /SKB 2006/, analysed colloid data from several sources, as follows: from 1987−1989, from one borehole in the Simpevarp subarea, KAV01 at Ävrö, and one in the Laxemar subarea, KLX01, together with data from the site investigation; from April−September 2003, from borehole KSH01A in the Simpevarp subarea, at depths of 161.75, 253.3, and 556.5 m. The present report includes a new set of data from borehole KLX03; four depths were sampled, 171, 380, 700, and 922 m.

2.2 Methods

The method used to obtain colloid samples was to filter the groundwater through a series of connected filters under pressurised argon The filters had pore sizes of 0.2 and 0.05 μm; before these filters, a pre-filter with a pore size of 0.4 μm was placed. The mineral composition of the colloids collected on the filters was determined using inductively coupled plasma spectroscopy (ICP), and the quantities of the analysed elements were recalculated in μg l^{-1} (ppb) using the water flow rate (ml h^{-1}) measured through the filters. The elements determined in the colloids were calcium (Ca), iron (Fe), sulphur (S), manganese (Mn), aluminium (Al), and silicon (Si). The residue on the pre-filter was also analysed.

The composition of inorganic colloids was determined, together with fractions of humic and fulvic acids, from two sections in borehole KSH01A, at depths of 161.8 and 556.5 m, and three sections in borehole KLX03, at depths of 171, 380, and 922 m. The equipment for this testing consisted of membrane filters with defined size cut-offs (pore sizes), a peristaltic pump, flexible tubing, and vessels. The equipment and method is described in SKB MD 431.043 (SKB internal control document). Samples were analysed using ICP-AES (Inductively Coupled Plasma – Atomic Emission Spectrometry). The determined elements were Ca, Fe, K Na S, Si, Al, Ba, Cd, Co, Cr, Cu, Hg, Li, Mn, Mo, Ni, P, Pb, Sr, V, and Zn. Of these elements, data for Fe, Si, Al, and Mn have already been reported /Wacker et al. 2004/.

2.2.1 Databases

The data used were extracted from the file *p_colloid_filtration_gw.xls* prepared by Maria Gimeno, and stored on the Project Place site and included in the SKB P report, P-04-12 /Wacker et al. 2004/. The data from the colloid filtration used here are compiled in Table 2-1.

Table 2-1. Element analyses of the 0.05 and 0.2 µm colloid fractions and the 0.4 µm precipitation fraction from borehole KSH01A, Simpevarp subarea.

Borehole	KSH01A, 161.75 m depth			KSH01A, 253.3 m depth			KSH01A, 556.5 m depth		
Pore Size (µm)	0.05	0.2	0.4	0.05	0.2	0.4	0.05	0.2	0.4
Chloride (mg l^{-1})	5,590	5,590	5,590	6,298	6,298	6,298	8,876	8,876	8,876
Iron (mg l^{-1})	1.413	1.413	1.413	1.318	1.318	1.318	0.523	0.523	0.523
Colloid phase (µg l^{-1})									
Ca as Calcite $CaCO_3$	267.2	199.2	244.75	385.2	d.m.[2]	262.6	448.5	436.2	703
Fe as $Fe(OH)_3$	3.82	8.02	389.5	0.764	d.m.	150.2	3.44	5.73	10.7
S as sulphur	b.d.[1]	b.d.	1.4	16.4	d.m.	5.2	7.8	7.7	15.6
Mn as $Mn(OH)_2$	0.168	0.162	1.70	0.162	d.m.	1.05	0	0	0.162
Al as K-Mg-illite clay: $K_{0.6}Mg_{0.25}Al_{2.3}Si_{3.5}O_{10}(OH)_2$	3.09	3.71	92.7	2.47	d.m.	82.2	1.236	2.47	4.9
Si as SiO_2	b.d.	b.d.	b.d.	b.d.	d.m.	26.6	b.d.	b.d.	18.08
Sum (ppb, µg l^{-1})	274.3	211.1	730.0	405.0	–	527.8	461.0	452.1	752.4
Sum, omitting calcite	7.08	11.9	485.3	19.8	–	265.25	12.5	15.9	49.4
Sum, omitting calcite and sulphur	7.08	11.9	483.9	3.4	–	260.0	4.7	8.2	33.8

[1] b.d. = below detection limit.

[2] d.m. = data missing due to broken filter.

Table 2-2. Element analyses of the 0.05 and 0.2 µm colloid fractions and the 0.4 µm precipitation fraction from borehole KLX03, Laxemar subarea.

Borehole	KLX03 171 m			KLX03 380 m			KLX03 700 m			KLX03 922 m*		
Pore Size (µm)	0.05	0.2	0.4	0.05	0.2	0.4	0.05	0.2	0.4	0.05	0.2	0.4
Chloride (mg l^{-1})	270	270	270	1,300	1,300	1,300	3,900	3,900	3,900	10,400	10,400	10,400
Iron (mg l^{-1})	0.25	0.25	0.25	0.7	0.7	0.7	1.5	1.5	1.5	0.01	0.01	0.01
Colloid phase (µg l^{-1})												
Ca as Calcite $CaCO_3$	b.d.[1]	b.d.	b.d	b.d.	b.d.	b.d.	b.d.	b.d.	b.d.	1,529	147.3	926.1
Fe as $Fe(OH)_3$	10.7	16.8	9.45	0.9	1.0	11.95	1.05	3.3	3.1	1.2	2.7	4.4
S as sulphur	b.d.	b.d.	b.d.	b.d.	b.d.	b.d.	b.d.	b.d.	b.d.	35.8	b.d.	16.2
Mn as $Mn(OH)_2$	b.d.	b.d.	b.d.	b.d.	b.d.	0.2	b.d.	b.d.	b.d.	b.d.	b.d.	b.d.
Al as K-Mg-illite clay: $K_{0.6}Mg_{0.25}Al_{2.3}Si_{3.5}O_{10}(OH)_2$	0.5	1.3	2.2	0.3	0.4	13.3	0.3	0.4	0.7	0.95	1.9	2.7
Si as SiO_2	b.d.	b.d.	b.d.	b.d.	b.d.	b.d.	37.4	b.d.	b.d.	35.6	b.d.	b.d.
Sum (ppb, µg l^{-1})	11.2	18.1	11.6	1.2	1.4	25.2	1.35	3.7	10.1	1,567	152	981.2
Sum, omitting calcite	11.2	18.1	11.6	1.2	1.4	25.2	1.35	3.7	10.1	38	4.7	52.1
Sum, omitting calcite and sulphur												

* Pressure was increased during filtration.

[1] b.d. below detection limit.

2.3 Evaluation of the colloid data

In a report by /Laaksoharju et al. 1995/, calcium values, calculated as calcite, and sulphur values, calculated as pyrite, were both withdrawn from the total amount of colloids, since they were regarded as sampling artefacts. In the present report the same approach is used, except that the sulphur values are not recalculated as pyrite but are shown as sulphur. The data from borehole KSH01A were evaluated in the report, Laxemar, version 1.2 /SKB 2006/, which also includes data from borehole KLX03. Several of the reported amounts of the elements under study were below the detection limit (Table 2-1).

2.3.1 Colloids versus depth

In evaluating the background levels of colloids in groundwater, the amount of colloids versus depth was examined. Figure 2-1 shows that the amount of colloids was highest at 92.03 µg l^{-1} in borehole KLX01 at a depth of 458.5 m. This stemmed from the great amount of aluminium colloids in this sample (see section 2.3.4), likely due to contamination from drilling. The other data indicate levels below 50 µg l^{-1}. The more recent data from borehole KSH01A and from the depths of 380 and 700 m in borehole KLX03 indicate the lowest levels. One explanation of the very low colloid values at these two depths in borehole KLX03 could be the presence of high numbers of micro-organisms at these depths (see section 1.3); colloids can adsorb to the surfaces of the micro-organisms, thus being taken out of solution.

The colloid values obtained from the Simpevarp area agree well – except for the value from borehole KLX01 – with data from colloid studies in Switzerland, i.e. 30 ± 10 and 10 ± 5 µg l^{-1} /Degueldre 1994/, but are approximately ten times lower than those reported from Canada, i.e. 300 ± 300 µg l^{-1} /Vilks et al. 1991, Laaksoharju et al. 1995/.

2.3.2 Colloids versus chloride

Figure 2-2 shows the variation of colloid versus chloride concentrations. In groundwater with a high chloride concentration, the amount of colloids usually decreases because higher ionic strength increases the precipitation of various solid particles. The chloride concentrations in this data set range from 500 to 10,400 mg l^{-1}. The only sample with a greater amount of colloids is from borehole KLX01 at a depth of 458.5 m, where it reaches 92.03 µg l^{-1}, a level probably due to contamination from drilling, as mentioned above (see section 2.3.4). The lowest colloid levels were found at the two mid-depths in borehole KLX03. These low values were not a consequence of high chloride concentrations, since at these depths they were 1,300 and 3,900 mg l^{-1}, respectively. Higher chloride concentrations were found in several other samples that contained more colloids (Figure 2-2). All other data indicated low colloid concentrations, which varied little despite large variations in chloride concentration.

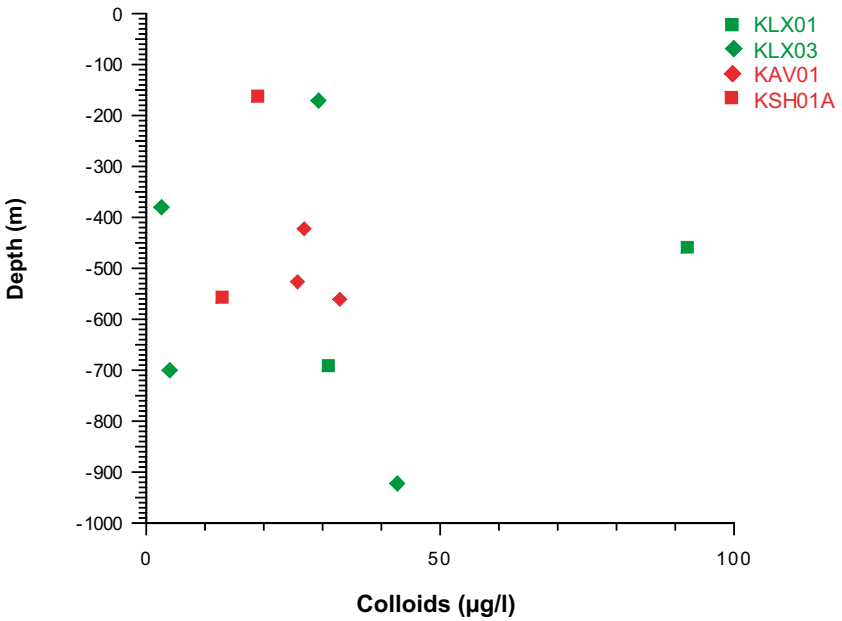

Figure 2-1. *Colloid concentration (µg l^{-1}) versus depth in samples from boreholes KLX01, KLX03, KAV01, and KSH01A in the regional Simpevarp area.*

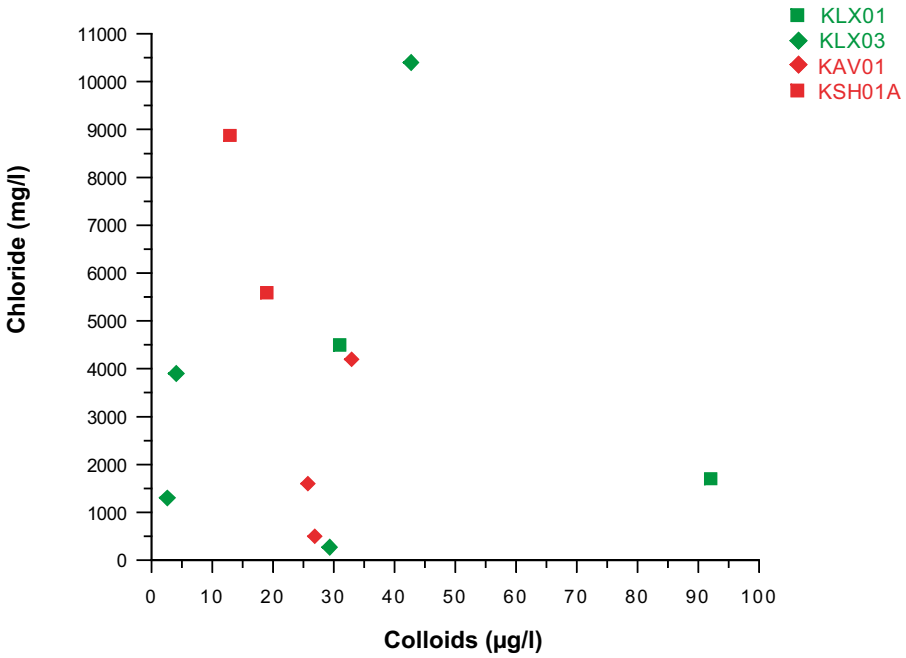

Figure 2-2. *Colloid versus chloride concentrations in groundwater samples from boreholes KLX01, KLX03, KAV01, and KSH01A in the regional Simpevarp area.*

2.3.3 Colloids versus iron

High concentrations of iron in groundwater force the precipitation of other compounds, due to the ability of iron to co-precipitate and produce large particles. Thus, the amount of colloids will decrease with increasing iron concentration. Figure 2-3 shows the colloids versus the iron content in groundwater from the regional Simpevarp area. The data display no clear trend. The only sample with a much higher concentration than that of the others is from a depth of 458.5 m at borehole KLX01, were it reaches 92.03 µg 1^{-1}, as discussed above. It is not clear whether this high colloid concentration depends on the iron level or whether it represents contamination from drilling.

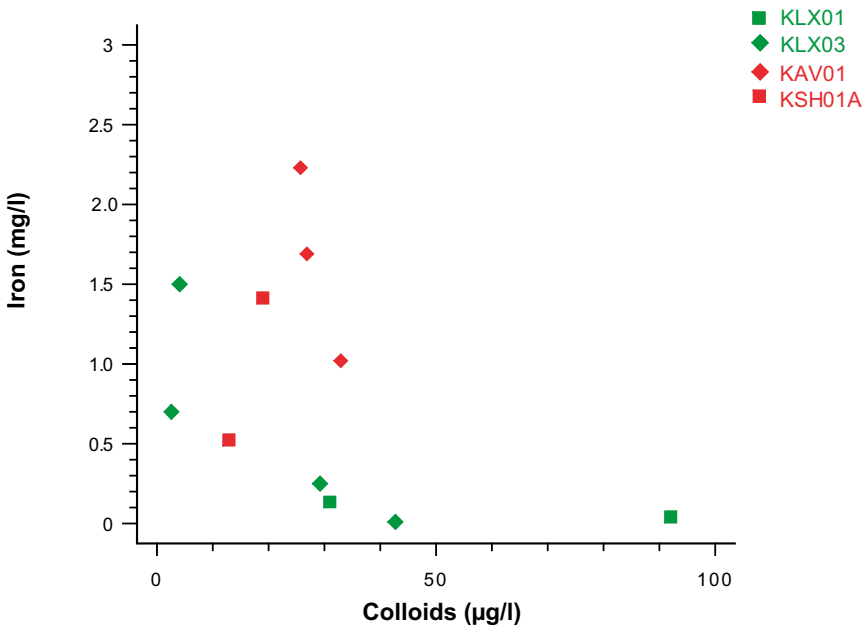

Figure 2-3. *Colloid versus iron concentrations in groundwater in samples from boreholes KLX01, KLX03, KAV01, and KSH01A in thel Simpevarp area.*

2.3.4 Composition of the colloids

The composition of the colloids has also been studied. Table 2-1 shows the concentrations for the elements analysed (Ca, Fe, S, Mn, Al, and Si), recalculated as the colloid phases calcite, iron hydroxide, manganese dioxide, K-Mg-illite clay, and silica. Sulphur was not recalculated as any other colloid phase.

Figure 2-4 shows the composition of colloids sampled from different depths in three of the boreholes. Figure 2-5 shows the composition of the colloids in borehole KLX03. Calcite is omitted in both figures, since it could be an artefact caused by pressure changes during sampling. The calcite values are listed in Table 2-1 for comparison with other elements.

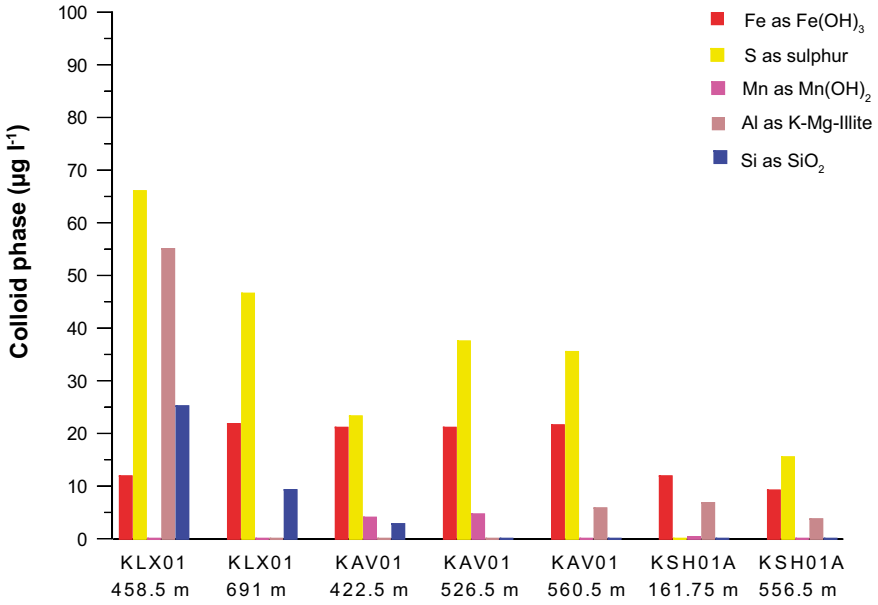

Figure 2-4. The composition of colloids sampled from boreholes KLX01, KAV01, and KSH01A in the regional Simpevarp area.

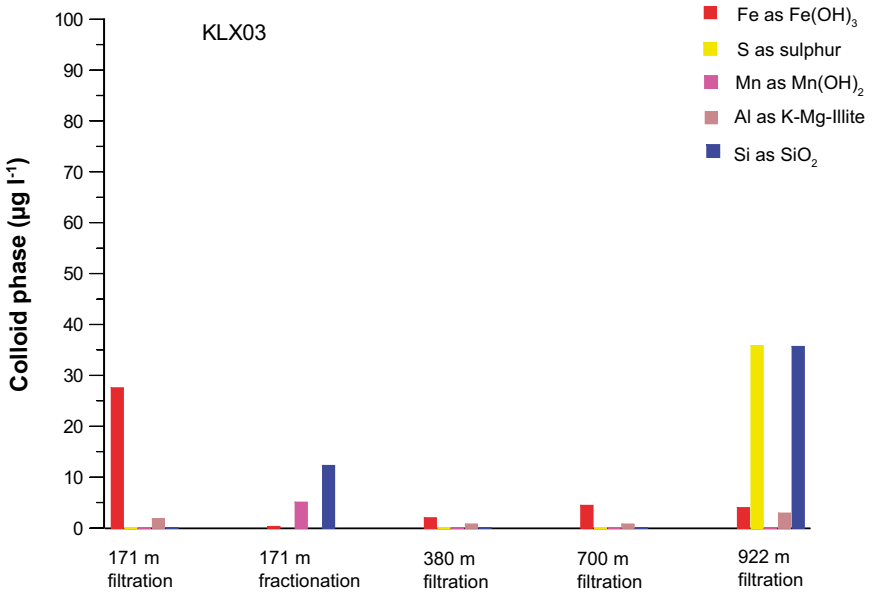

Figure 2-5. The composition of colloids sampled from four depths in borehole KLX03 in the Laxemar subarea.

In Figure 2-4 it can be seen that manganese oxides were found in borehole KAV01 at the depths of 422.5 and 526.5 m; this in agreement with the relatively high manganese levels found in this borehole (see section 1.5). As well, one of the highest iron levels was found in this borehole. The 691 m section in KLX01, while containing similar levels of Fe, contains no Mn, however.

Figure 2-4 also shows the high aluminium level at a depth of 458.5 m in borehole KLX01. Some aluminium, represented here as K-Mg-illite, was also found in borehole KAV01 at 560.5 m and in borehole KSH01A, but in low amounts. There were high amounts of sulphur in boreholes KLX01 and KAV01, but whether or not this is an artefact still has to be evaluated. If sulphate reduction is occurring, and thus sulphide is being produced, the colloid sulphur might be iron sulphide. Some of the iron would then also occur as iron sulphide and not as iron hydroxide, as assumed in previous figures in this report.

Filtration data from borehole KLX03 indicate that there were high amounts of iron colloids at a depth of 171 m and high sulphur levels at 922 m. The iron content does not correlate with the iron concentration in the groundwater. The sulphur levels, on the other hand, coincide with high sulphide values at a depth of 922 m,

In the colloid fraction obtained via filtration, > 1,000 D but < 5,000 D, amounts of iron, silicon, and manganese were found only in the 171 m depth section in borehole KLX03 (see Figure 2-5). The dominant colloids were Si and Mn oxides. Interestingly, filtering data indicated iron compounds to be dominant. More fractionation data are needed before any comparative evaluation of the two methods can be done.

2.4 Conclusions

The amount of colloids reported here seems to be comparable to the amount reported previously from Switzerland, and from the Äspö and Bangombe areas /Laaksoharju et al. 1995, Pedersen et al. 1996/. The possibility that some of the iron and sulphur colloids might occur as iron sulphides has to be further investigated.

Data regarding particle numbers could increase the value of colloid analyses, by making it possible to calculate the number of radionuclide binding sites in the different colloid fractions.

3 Gases

3.1 Introduction

Earlier studies of groundwater in the Fennoscandian Shield have found high amounts of dissolved gases. If the total amount of gas exceeds saturation, gas bubbles may form /Pedersen 2002/. The surface tension of the bubbles can capture different compounds, such as radionuclides, from the groundwater. The bubbles will move rapidly in groundwater and can cause the dispersion of radionuclides over large areas, in particular, to the ground surface. In a site investigation it is therefore crucial to evaluate gas data, and to include it in hydrogeochemical models.

Some gases are involved in microbiological reactions. The most important of these gases are oxygen, methane, carbon dioxide, and hydrogen. Methane is produced by methanogens in reduced anaerobic environments and can be used as a substrate by methanotrophic bacteria. Carbon dioxide is used as a carbon source by autotrophic organisms and is the end product of microbial degradation. Hydrogen is the energy and electron source for methanogens, acetogens, and some other autotrophic micro-organisms, i.e. various sulphate reducers. It is also one of the end products of microbiological fermentation.

In this study up to 12 gases were analyzed: helium, argon, nitrogen, carbon dioxide, methane, carbon monoxide, oxygen, hydrogen, ethyne, ethene, ethane, and propane. Gas contents were analysed in groundwater from seven depths in two boreholes, KLX03 and KSH01A.

Table 3-1 shows the boreholes and depths from which data have been available for this report.

3.2 The dissolved gases

3.2.1 Total volume of gas

Figure 3-1 shows the total volume of gas for all groundwater samples. It shows an increasing amount of gas with depth in borehole KLX03, with the highest volume, 76.2 ml l^{-1} groundwater, being found at the lowest level, 922 m, and 40.3 ml l^{-1} at the shallowest sampled depth. In contrast, in borehole KSH01A the highest amount, 106.7 ml l^{-1} groundwater, was found at a depth of 234 m. In the Fennoscandian Shield, the volume of gas commonly increases with depth, as, for example, in Olkiluoto in Finland /Pitkänen et al. 2004/ and in the Forsmark area in Sweden /SKB 2005/.

Table 3-1. Boreholes, depths, sampling dates, and gas volumes available in SICADA for analysis in the Laxemar model, version 2.1.

Borehole	Depth centre (m)	Gas volume (ml L^{-1} of groundwater)
KSH01A	153	76.4
	242	106.7
	536	75.6
KLX03	176	40.3
	380	51.2
	700	64.5
	922	76.2

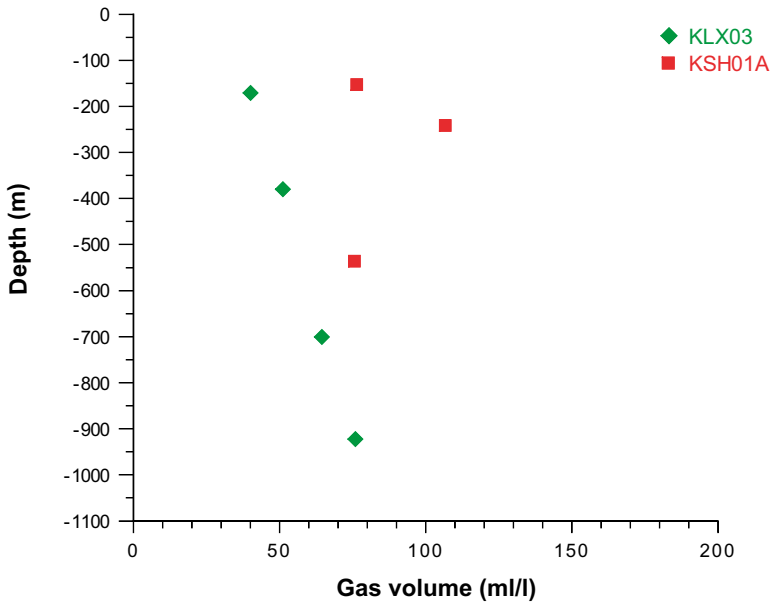

Figure 3-1. *Total volume of gas in groundwater samples from the Laxemar subarea.*

3.2.2 Nitrogen and helium

The compositions of the gas in the various samples are shown in Figure 3-2, a–g. The dominant gas at all depths in both boreholes is nitrogen. This corresponds with the gas content in some groundwater in Olkiluoto, Finland, for example, although some samples from there contain more methane than nitrogen /Pitkänen et al. 2004/. The content of nitrogen calculated in p.p.m. decreases slightly with depth, mainly because the content of helium increases with depth. The source of nitrogen and helium in deep groundwater is considered to be crustal degassing of the bedrock. Another source of helium may be radioactive decay, also occurring in the bedrock.

a)

KLX03, –170.8 m, 40.3 ml/L

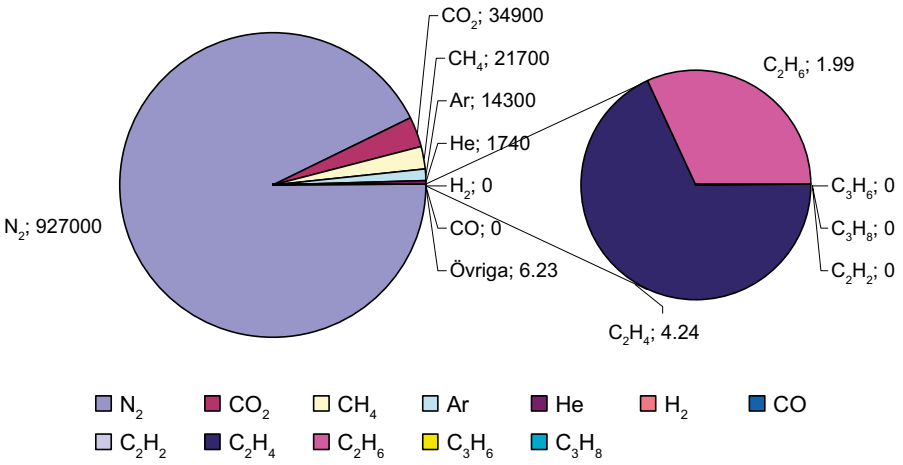

b)

KLX03, –379.6 m, 51.2 ml/L

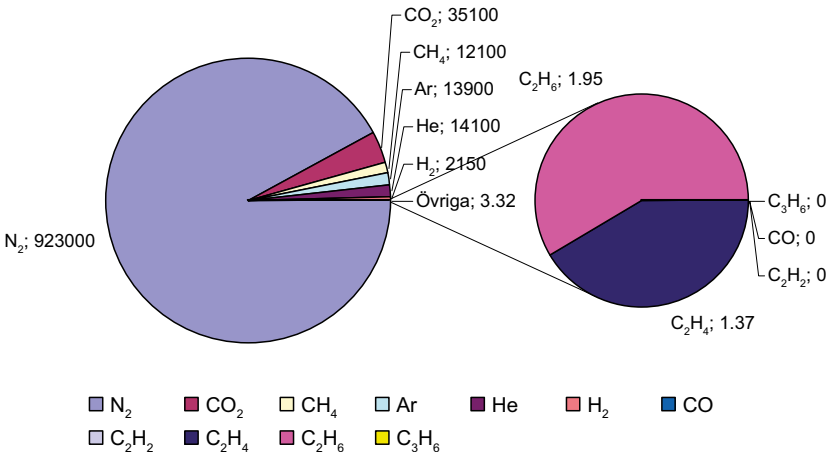

c)

KLX03 –700.2 m, 64.5 ml/L

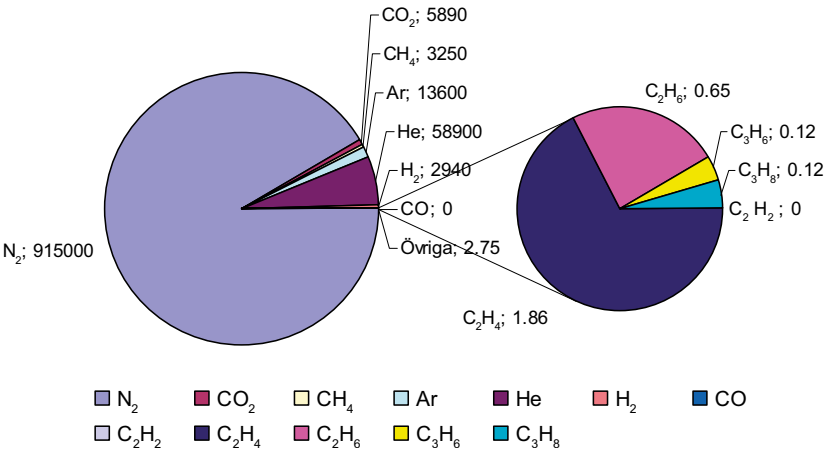

d)

KLX03, –922 m, 76.2 ml/L

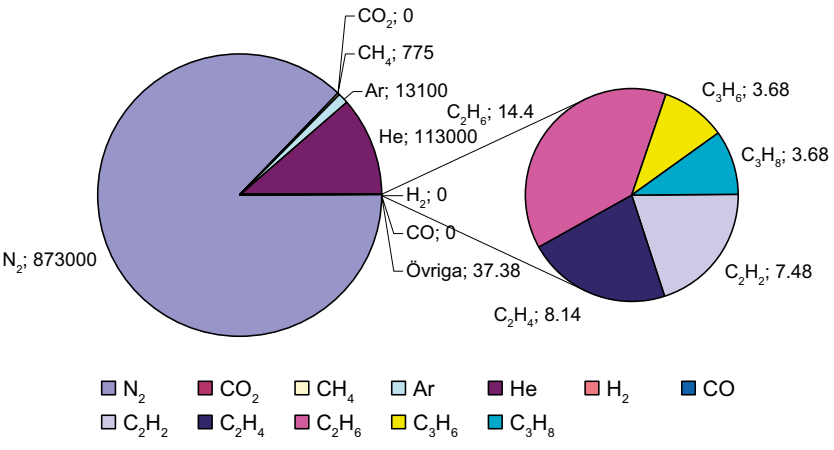

e)

KSH01A, –152.7 m, 76.4 ml/L

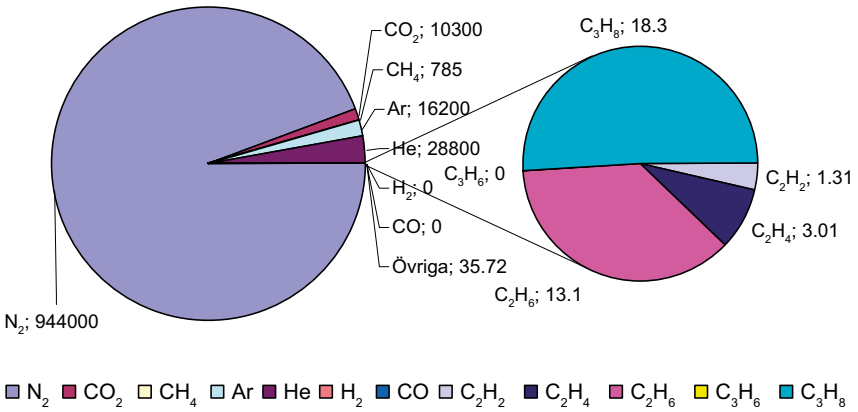

f)

KSH01A, –241,7 m, 106.7 ml/L

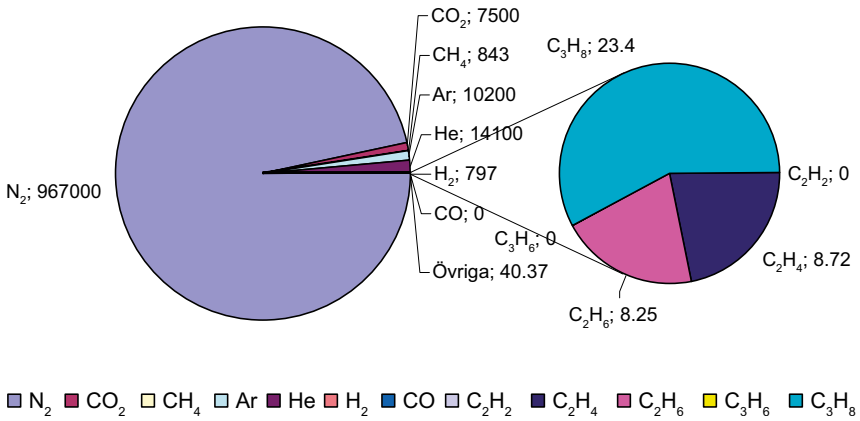

g)

KSH01A, –535.8 m, 75.6 ml/L

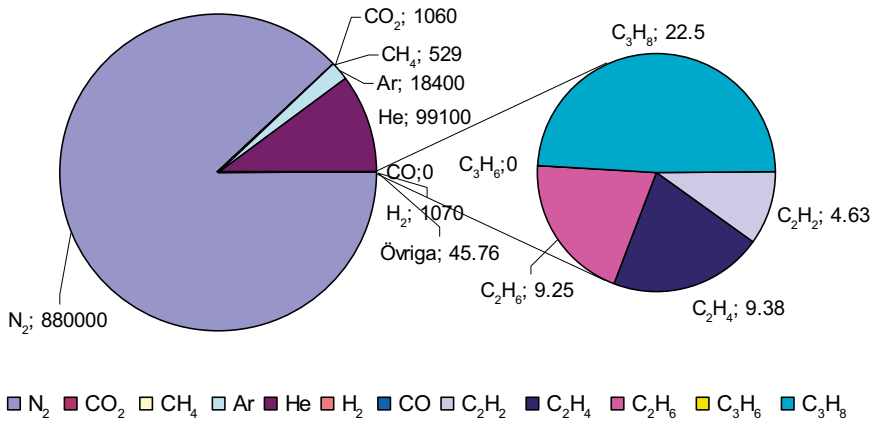

Figure 3-2, a–g. *Volumes and distribution of the measured gases in samples from boreholes KLX03 and KSH01A in the Simpevarp area.*

3.2.3 Carbon dioxide and methane

Carbon dioxide in groundwater is a dissociation product of dissolved carbonates from fractures in the bedrock, but can also be a degradation product of organic carbon. The carbon dioxide concentrations in samples from both boreholes KLX03 and KSH01A display a decreasing trend with depth. This is probably because the degradation of organic material is greater at shallower depths and because autotrophic metabolism with the fixation of carbon dioxide as organic carbon is more common at greater depths. This pattern has also been observed for carbon dioxide concentrations in groundwater from the Olkiluoto site in Finland /Pitkänen et al. 2004/.

The origin of methane in groundwater can be either biotic or abiotic. Biotic methane is produced by methanogenic archaea, a group of prokaryotic organisms that can utilise either organic C_1 compounds or acetate; the case of acetate is presented in Equation 1. Methanogens can also assimilate carbon dioxide, using hydrogen gas as the energy and electron source (see Equation 2). The origin of their substrate can be biodegraded organic matter, as in sea and lake sediments or composts, or carbon dioxide and hydrogen originating in the mantle /Apps and van de Kamp 1993/.

$$CH_3COOH \rightarrow CH_4 + CO_2 \qquad \text{(Equation 1)}$$

$$CO_2 + 4H_2 \rightarrow CH_4 + 2H_2O \qquad \text{(Equation 2)}$$

Abiogenic methane is produced in, for example, hydrothermal systems during water–rock interactions involving the Fischer−Tropsch synthesis reaction, which is the same as Equation 2 above. This methane can act as precursor for polymerisation to higher hydrocarbons, such as short-chain alkanes (see section 3.2.4).

The amount of methane in borehole KLX03 is the highest at the shallower depths and very low at a depth of 922 m. This is likely because there is biological methanogenesis, especially at depths of 171 and 380 m. This is verified by the occurrence of methanogens, and by the fact that the ratio of methane to C_2 and C_3 hydrocarbons at these depths is greater than 10^3 (see section 3.2.4). In borehole KSH01A the methane content is low at all depths.

3.2.4 Hydrocarbons

In Figure 3-2, the hydrocarbon content is indicated by the small segment in the circle graphs labelled “övriga”. The amount of hydrocarbons increases with depth. At the two shallowest depths in borehole KLX03, ethane (C_2H_3) and ethene (C_2H_4) dominate, while in deeper groundwater ethyne (C_2H_2), propane (C_3H_8), and propene (C_3H_6) are more prevalent. In borehole KSH01A, on the other hand, propane dominates at all three depths.

The hydrocarbons come from a deep abiogenic source and move slowly by diffusion towards the surface. Calculating the C1/(C2+C3) ratio can elucidate the source of the methane found. If this ratio is high, greater than 1,000, it is considered to indicate biogenic methane. In contrast, thermogenic and abiogenic methane will give a ratio of approximately 10 /Sherwood-Lollar et al. 1993, 2002, 2005, Clark and Fritz 1997, Whiticar 1999/. The ratios for the gas samples are presented in Table 2-2. From this ratio it can be concluded that the methane present in borehole KLX03 at depths of 176, 380, and 700 m, is mainly biogenic, but that the methane in the deepest groundwater at a depth of 922 m and in all sampled sections of borehole KSH01A is mainly abiotic in origin. To be able to state this conclusively, more hydrocarbon data need to be generated together with stable isotope values for methane.

Table 3-2. The ratio of methane to C_2 and C3 hydrocarbons in boreholes in the Simpevarp area.

Borehole	Depth centre (m)	$C_1/(C_2 + C_3)$
KSH01A	153	24
	242	21
	536	12
KLX03	176	3,486
	380	3,644
	700	1,181
	922	21

3.2.5 Hydrogen

Hydrogen is an important gas in several anaerobic microbial metabolisms, such as methanogenesis and acetogenesis. Autotrophic iron- and sulphate-reducing bacteria can also use hydrogen as an energy and electron source concomitant with iron or sulphate reduction.

There are at least six possible processes in which crustal hydrogen is generated: (1) reaction between dissolved gases in the C-H-O-S system in magmas, especially in those with basaltic affinities; (2) decomposition of methane to carbon (graphite) and hydrogen at temperatures above 600°C; (3) reaction between CO_2, H_2O, and CH_4 at elevated temperatures in vapours; (4) radiolysis of water by radioactive isotopes of uranium, thorium, and their decay daughters, and potassium; (5) cataclasis of silicates under stress in the presence of water; and (6) hydrolysis by ferrous minerals in mafic and ultramafic rocks /Apps and van de Kamp 1993/. It is important to explore the scale of these processes and the rates at which the produced hydrogen becomes available to deep microbial ecosystems.

In borehole KLX03, hydrogen was found at depths of 380 and 700 m. At these depths, we have the highest numbers of hydrogen-utilising micro-organisms, i.e. acetogens and methanogens (see Chapter 1). Access to hydrogen could be one explanation of this observation. Relatively small amounts of hydrogen were found in borehole KSH01A. A comparison with hydrogen data from this report with hydrogen data from other sites in Sweden and Finland indicates that they they are all in the same range /Pedersen 2000/.

3.3 Conclusions

- The volume of gas in groundwater increase with depth.
- The available gas data for the Laxemar area indicate that the gas content is of the same order of magnitude as in most Nordic sites studied.
- Nitrogen is the dominant gas at all depths.
- The volume of helium increases with depth.
- The greatest amounts of methane were found at depths above 400 m in borehole KLX03; The C1/(C2+C3) ratio was over 3,000 here, suggesting that the methane is biologically produced.
- The amount of hydrocarbons increases with depth.
- The gases found are probably mostly mantle-generated.
- Gases are oversaturated in relation to atmospheric pressure but not to the pressures at the sampled depths.

4 References

Anonymous, 1992. Estimation of bacterial density, pp 977–980 Standard methods for the examination of water and wastewater, 18th ed. American Public Health Association, Washington, D.C.

Apps J A, van de Kamp P C, 1993. Energy gases of abiogenic origin in the Earth's crust. The future of Energy gases. U.S. Geological Survey Professional Papers. United States Government Printing Office, Washington., pp 81–132.

Clark I, Fritz P, 1997. Environmental isotopes in hydrogeology. Lewis Publishers, Boca Raton, 328 p.

Degueldre C, 1994. Colloid properties in groundwater from crystalline formation. Paul Scherrer Institute, Villigen, Switzerland.

Ekman L, 2001. Project Deep Drilling KLX02, Phase 2.Methods, scope, summary and results. Summary Report. SKB TR-01-11, Svensk Kärnbränslehantering AB.

Haveman S A, Pedersen K, Ruotsalainen P, 1999. Distribution and Metabolic Diversity of Microorganisms in Deep Igneous Rock Auifers of Finland. Geomicrobiology Journal 16, 277–294.

Kotelnikova S, Pedersen K, 1998. Distribution and activity of methanogens and homoacetogens in deep granitic aquifers at Äspö Hard Rock Laboratory, Sweden. FEMS Microbiology Ecology 26, 121–134.

Pedersen K, 1993. The deep subterranean biosphere. Earth-Science Reviews 34, 243–260.

Pedersen K, Arlinger J, Hallbeck L, Pettersson C, 1996. Diversity and distribution of subterranean bacteria in groundwater at Oklo in Gabon, Africa, as determined by 16S rRNA gene sequencing. Molecular Ecology 5, 427–436.

Pedersen K, 2000. The hydrogen driven biosphere and its influence on hydrochemical conditions in crystalline bedrock aquifers. In: Hydrogeology of crystalline rocks. Eds: Stober, I. and Bucher, K. pp 249–259. Kluwer Academic Publisher, The Netherlands.

Pedersen K, 2001. Diversity and activity of microorganisms i deep igneous rock aquifers of the Baltic shield, pp 97–139 In J.K. Fredrickson and M. Fletcher (eds.), Subsurface microbiology and biogeochemistry. Wiley-Liss Inc., New York.

Pedersen K, 2002. Microbial processes in the disposal of high level radioactive waste 500 m underground in Fennoscandian shield rocks, pp 279–311 In M.J. Keith-Roach and F.R. Livens (eds.), Interactions of microorganisms with radionuclides. Elsevier, Amsterdam.

Pedersen K, 2005. Äspö Hard Rock Laboratory. The MICROBE framework. Site descriptions, instrumentation, and characterisation. SKB IPR 05-05, Svensk Kärnbränslehantering AB.

Pitkänen P, Partamies S, Luukonen A, 2004. Hydrochemical interpretation of baseline groundwater conditions at the Olkiluoto site. POSIVA 2003-07, Posiva, Olkiluoto, Finland.

Sherwood Lollar B, Frape S K, Fritz P, Macko S A, Welhan J A, Blomqvist R, Lahemo P W, 1993. Evidence for bacterially generated hydrocarbon gas in Canadian Shield and Fennoscandian Shield rocks. Geochimica et Cosmochimica Acta 57, 5087–5097.

Sherwood Lollar B, Westgate T D, Ward J A, Slater G F, Lacrampe-Couloume G, 2002. Abiogenic formation of gaseous alkanes in the Earth's crust as a minor source of global hydrocarbon reservoirs.Nature 416, 522–524.

Sherwood Lollar B, Lacrampe-Couloume G, Slater G F, Ward J, Moser D P, Gihring T M, Lin L-H, Onstott T C, 2005. Unravelling abiogenic and biogenic sources of methane in the Earth's deep subsurface. Chemical Geology 226. 328–339.

SKB, 2005. Preliminary site description. Forsmark area – version 1.2. Updated 2005-11-09. SKB R-05-18, Svensk Kärnbränslehantering AB.

SKB, 2006. Hydrogeochemical evaluation. Preliminary site description. Laxemar subarea – version 1.2. SKB R-06-12, Svensk Kärnbränslehantering AB.

Vilks P, Miller H, Doern D, 1991. Natural colloids and suspended praticles in Whiteshell Research area, Manitoba, Canada, and their potential effect on radiocolloid formation. Applied Geochemistry 8, 565–574.

Wacker P, Berg C, Bergelin A, 2004. Complete hydrochemical characterisation in KSH01A. Results from four investigated sections, 156.5–167.0, 245.0–261.6, 586.0–596.7 and 548.0–565.4 metres. Oskarshamn site investigation. SKB P-04-12, Svensk Kärnbränslehantering AB.

Whiticar M J, 1990. A geochemical perspective of natural gas and atmospheric methane. Organic Geochemistry 16, 531–547.

11 Appendix 3: PHREEQC modelling

Contribution to the model version 2.1

María J. Gimeno, Luis F. Auqué, Javier B. Gómez

Department of Earth Sciences, University of Zaragoza

August 2006

Introduction

For this new Site Descriptive Modelling phase in Laxemar (Laxemar 2.1), the chosen formalism has been to include all relevant data in the Simpevarp and Laxemar subareas together with the available information from Äspö (before the tunnel construction) and Ävrö.

Most groundwater samples have been already used in the Simpevarp 1.2 phase /Laaksoharju et al. 2004a/, and the Laxemar 1.2 phase /SKB 2006/. Therefore, this work has been oriented towards the verification of previous hypothesis using the new information supplied with the latest data freeze.

The contribution of the authors is now focussed on the following main points:

- Tabular compilations of the chemical, physicochemical and isotopic data from SICADA to create the final tables for modellers.
- Evaluation of the quality and representativity of the new hydrogeochemical data.
- Reevaluation of previous models in the light of new available geological and hydrogeological information.

This report is organized into five chapters:

- Chapter 1: presentation of the data, where the newly delivered dataset is included together with the previously compiled data.
- Chapter 2: preliminary explorative analysis.
- Chapter 3: speciation solubility and reaction path calculations for the carbonate, sulphate, silica and aluminosilicates systems.
- Chapter 4: redox system modelling.
- Chapter 5: discussion and conclusions.

Contents

1 Evaluation of primary data

The dataset for this new Site Descriptive Modelling phase in Laxemar Area (Laxemar 2.1), was supplied by SICADA as Laxemar 2.1 Data Freeze, and includes old (Laxemar 1.2 Data Freeze) and new (post-Laxemar 1.2 Data Freeze) samples. Therefore, it includes all relevant data in the Simpevarp and Laxemar subareas together with the available information from Äspö (before the tunnel construction) and Ävrö.

Next we present the list of samples included in the dataset for this site. The number of samples corresponding to the new Data Freeze (samples and data taken after December the 1st, 2004) are indicated in order to make clear for the reader the additional information compiled up to now.

- 152 groundwater samples (GW) from the Äspö subarea:
  - 25 representative samples (13 orange and 12 green).
- 123 groundwater samples (GW) from the Ävrö subarea:
  - 6 representative samples (1 orange and 5 green).
  - Four new samples were delivered in the Laxemar 2.1 datafreeze.
- 592 GW from Laxemar (37 representative; 5 orange and 32 green), and 51 Near Surface Groundwaters (NSGW; 45 representative, green).
  - 53 samples from percussion boreholes.
  - 285 samples including tube samples, samples taken during drilling, and samples for the matrix fluid experiments. 118 of them were delivered in the Laxemar 2.1 datafreeze.
  - 254 samples from cored boreholes and taken between packers. 68 of them were delivered in the Laxemar 2.1 datafreeze.
  - 51 shallow groundwater samples from soil pipes.
- 282 GW and NSWG, 1,271 surface waters and 56 precipitation samples from Simpevarp.
  - 171 groundwater samples (5 representative, green) and 111 NSGW (32 representative, green):
    - 22 samples from percussion boreholes.
    - 99 samples including tube samples, samples taken during drilling, and samples for the matrix fluid experiments.
    - 51 samples from cored boreholes and taken between packers.
    - 111 shallow groundwater samples from soil pipes. 53 of them were delivered in Laxemar 2.1 datafreeze.
  - 1,271 surface water samples:
    - 363 sea water samples (161 representative, 29 green, 132 pink). 46 of them were delivered in Laxemar 2.1 datafreeze.
    - 249 lake water samples (167 selected as representative samples; 9 green, 158 pink). 24 of them were delivered in Laxemar 2.1 datafreeze.
    - 659 running water samples (297 selected as representative samples; 46 green, 251 pink). 75 of them were delivered in Laxemar 2.1 datafreeze.
  - 56 samples of precipitation (13 selected as representative samples). 17 of them were delivered in Laxemar 2.1 datafreeze.

Altogether, there are 1,200 groundwater samples (deep and near surface groundwaters), 243 of them delivered in the Laxemar 2.1 datafreeze, and 1,271 surface water samples, 145 of them were delivered in this datafreeze[1]. Some of them have been considered representative for modelling purposes.

Analysed data include the same parameters chosen in the previous stage. pH, Eh, temperature and conductivity values used in this report are the ones determined in the field when available (Chemmac logs). In the rest of the cases, laboratory determinations have been used. The new data freeze has added some new data for these physicochemical parameters.

[1] However, not all the new samples had a complete chemical analysis at the time of the data freeze.

The available physycochemical data from the Laxemar area, compiled and supplied by the SKB geodatabase SICADA, have a variable number of functioning Eh electrodes (from one to six) and logging times are also rather variable. This fact clearly demonstrates the technical difficulties associated with the application of the methodology. We decided to re-analyse all the available continuous logs for the Laxemar area (it has also been done for Forsmark and some other Swedish sites, /Auqué et al. 2006, submitted/) in order to select a high-quality Eh and pH datasets based on a common and well defined set of criteria to create an Eh database as complete as possible which can be used for geochemical modelling. For a more detailed description of the SKB methodology and the problems associated to the potentiometrically measured Eh, see /Auqué et al. 2006, submitted/).

The selection of an Eh value for a borehole section must be based on a very careful analysis of the results obtained with the different electrodes at depth and at the surface, the logging time, the pH, the conductivity, and the dissolved oxygen values. The basic requirement is that the measured potential corresponds to the equilibrium potential and this fact can only be demonstrated when the different electrodes give coincident results. Ideally, the Eh values selected as representative should only be those obtained simultaneously and within a small Eh range (± 50 mV) by the six electrodes over a long period of time. However this criterion seems excessively restrictive. There can be undesirable effects selectively affecting one electrode or the other, or technical problems affecting one of the two measurement cells (downhole or at the surface; /Auqué et al. 2006, submitted/).

Taking into account all these issues, we decided to apply the following selection criteria:

- logs longer than 3 days (usually longer than a week),
- logs with stable and coincident readings (in a range smaller than 50 mV) by several electrodes in the long term, and
- logs with simultaneous and stabilised pH logging (in order to minimize the uncertainty associated with the pH).

The sets of Eh logs that fulfilled these criteria were then checked for the quality of the redox values. We defined two groups of representative Eh values depending on the number of electrodes giving coincident readings:

- Group 1 Eh values: stable and coincident readings in, at least, three electrodes, two of them at depth.
- Group 2 Eh values: stable and coincident readings in two electrodes, at depth or at the surface.

This grouping reflects the difference in the quantity and quality of the information used to define the representative Eh value. Group 1 includes the Eh values with more complete information and based on the readings at depth, i.e. more trustworthy values. Group 2 includes good quality values but limited by frequently interrupted logs, different recording times for the different electrodes, or other technical difficulties. In other words, less reliable values.

There are 36 sets of logs in the Laxemar area (Äspö, Ävro, Laxemar and Simpevarp) corresponding to 36 packered sections in 8 different boreholes (KAS02, 03, 04; KAV01; KLX01, 02, 03; KSH01), from 130 to 1,780 m depth. Only 18 of them passed the acceptation criteria (see Table 1-1) and the evaluation of their quality gave the result of 5 Group 1 Eh values, and 13 Eh belonging to Group 2.

The final set of samples with representative Eh values is shown in Table 1-1. The comparison of these values with the ones selected and reported by previous authors for the same set of logs can be seen in /Auqué et al. 2006, submitted/. The results from this comparative analysis indicate that the criteria used in this work to select a representative Eh value are more restrictive (even in the Group 2 category) than the ones previously used. Moreover, the definition of a very high quality set of values (Group 1) gives added value to this selection, more so when we acknowledge that the Laxemar area have more than one Group 1 Eh value.

This set of selected Eh data have been used to analyse the redox state of the groundwater system plotting their distribution against depth and pH and using them in the geochemical modelling together with the complementary information from the redox pairs, the solubility calculations and the microbiological data (see Chapter 4).

Table 1-1. Eh values selected in this work and in previous works in Laxemar area where SKB methodology has been used. Highlighted figures in bold are Group 1 values; the rest are Group 2 values. The pH values correspond to the values selected from chemmac loggs, down-hole or surface, following the same criteria as for the Eh selection.

Area	Subarea	Borehole	Depth (m)	Eh value (mV)	pH
Laxemar	Äspö	KAS02	212–214	–260	7.5
			314–319	–380	8.2
			530–535	–310	8.0
		KAS03	129–134	**–260**	8.0
			860–1,002	–270	7.2
		KAS04	226–235	**–300**	7.8
			334–343	**–280**	7.9
	Ävrö	KAV01	420–425	**–215**	7.35
			522–531	–310	7.0
			558–563	–225	7.2
	Laxemar	KLX01	456–462	–280	8.6
			680–702	–265	7.8
		KLX03	193–198	–275	8.17
			408–415	–270	8.0
			735–748	**–220**	7.5
	Simpevarp	KSH01	156–167	–250	8.1
			245–261	–210	8.05
			548–565	–220	8.1

2 Explorative analysis

Following the same approach used in previous stages for geochemical groundwater modelling (Simpevarp 1.1 and 1.2; /Laaksoharju et al. 2004ab/ and Laxemar 2.1, /SKB 2006/), the evaluation of this new set of data started with the explorative analysis of different groundwater variables.

The analysis was performed following the same methodology (ion-ion plots) developed in Simpevarp 1.1 and 1.2 and Laxemar 1.2 reports. All new samples are included in the range covered by the previous samples and follows exactly the same trends. Therefore, we will only state the main conclusions without including all the plots with the new samples[2].

Hydrochemical data were graphically presented in previous reports using X-Y plots to derive trends that may facilitate interpretation. Since chloride is generally conservative in normal groundwaters, its use is appropriate to study hydrochemical evolution trends when coupled to ions, ranging from conservative to non-conservative, to provide information on mixing, dilution, sources and sinks. Moreover, here chloride acts as a tracer of the main irreversible process operating in the system -mixing-, which has been demonstrated in previous works /Laaksoharju et al. 2004a, SKB 2006/. What follows is a summary of the diverse geochemical trends apparent in Laxemar area groundwaters, including the new samples from the Laxemar 2.1 data freeze. Plotted samples include the representative groundwater samples (green and orange) and the more complete surface samples (the green ones). Four groups of samples will be indicated in the following plots: groundwaters (below 100 m depth; red circles), near surface groundwaters (shallow groundwaters down to 100 m depth; yellow circles), sea waters (green circles) and fresh surface waters (lakes and running waters; blue circles).

The updated dataset nicely follows the trends described in previous reports /Laaksoharju et al. 2004ab, SKB 2006/. As a general rule chloride increases with depth (Figure 2-1, *panel a*): as we already pointed out, the Laxemar data show dilute groundwaters extending to about 600 m and for KLX02 to around 1,000 m before a rapid increase in salinity to maximum values of around 47 g/L (1.4 mol/kg) Cl at 1,700 m. There are still not enough data from Simpevarp (nor from Äspö or Ävrö) to check whether in these sites groundwaters will follow the same rapid increase in salinity with depth as in Laxemar.

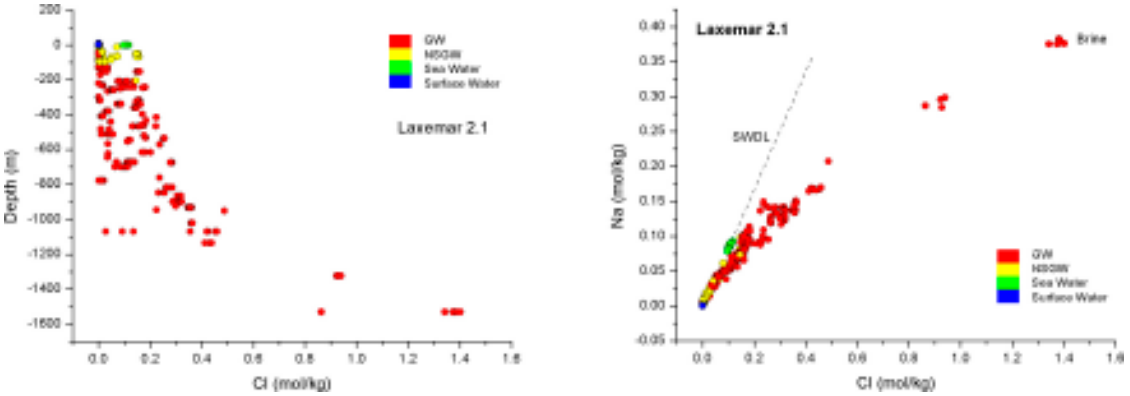

Figure 2-1. *(a) Evolution of chloride with depth in the Laxemar area using the whole set of samples from Laxemar 2.1. (b) Evolution of sodium with chloride. Samples with the symbol of Surface waters (red horizontal bar) include: seawater, lakes, streams and precipitation; all other samples in plot (b) are groundwaters.*

[2] They have been presented in the HAG meetings and are included in the presentations from the UZ.

Except for some shallow groundwater samples, which can be the result of mixing with a marine component, the potassium content in groundwaters (Figure 2-2, *panel a*) increases very slowly with depth (and with chloride), with values always below the sea water dilution line. This behaviour is common to the four subareas showing a global dilution trend towards the saline end member (Brine). This may reflect the influence of mixing with a saline (non marine) component in saline groundwaters from Laxemar. Additional water-rock interactions seem to be controlling this element (reaction with K feldspars and clay minerals, or cation-exchange) as suggested by the scattering of brackish waters with less than 10,000 mg/L Cl.

Magnesium (also below the SWDL, Figure 2-2, *panel b*) shows a steeper increase with depth in the shallower groundwaters, probably related to a marine component /Laaksoharju and Wallin 1997/. Deeper groundwaters, however, show a decrease in magnesium, following a trend towards the saline end member. This trend suggests the influence of a magnesium-depleted saline component. The broad scatter in the 1,000–10,000 mg/L Cl range suggests that reactions involving chlorite and montmorillonite could have been active. Initial K and Mg enrichment in fresh waters (obscured by the graph scale) is probably caused by mineral weathering (micas, K-feldspars, etc.) in surface conditions.

As for the other chemical variables, their behaviour in the new samples with respect to chloride falls on the same trends as before (Simpevarp 1.2 phase; /Laaksoharju et al. 2004a/; Laxemar 1.2; /SKB 2006/) and, therefore, the description and conclusion presented in previous reports, are still valid for Laxemar 1.2.

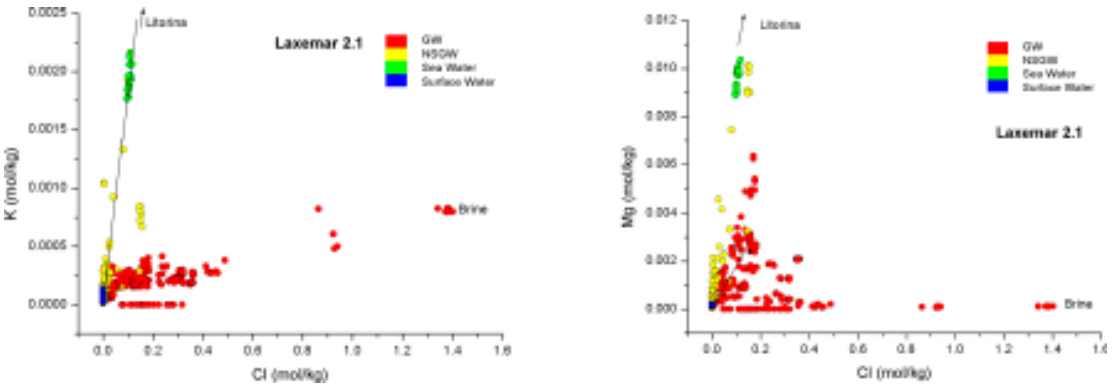

Figure 2-2. *Potassium and magnesium vs chloride in water samples from POM area.*

3 Speciation-solubility calculations

Hydrogeochemical modelling has been carried out with PHREEQC /Parkhurst and Appelo 1999/ using the WATEQ4F thermodynamic database. The modelling has focussed on speciation-solubility calculations (carbonate, silica and sulphate systems), and reaction path simulations (for the aluminosilicate system). The redox system modelling will be presented in the following chapter. These calculations were used to investigate the processes that control water composition. Only the modelling results for representative groundwaters (shallow, up to 100 m depth, and deep groundwaters) are shown in this section.

3.1 Carbonate system modelling

Evaluation of the main parameters controlling the carbonate system (pH, alkalinity, log pCO_2 and calcium) in Laxemar is presented here. Shallow groundwaters show a wide range of pH values as a consequence of their multiple origin (Figure 3-1, *panel a*). The lowest values are associated with waters from soil pipes with a marked influence of atmospheric and biogenic CO_2; the highest values (up to 8.5 pH units) are associated with the most diluted groundwater (up to 100 m depth) affected by dissolution of carbonates and aluminosilicates. In general, for the deeper groundwaters the pH values range between 7 and 8.5 (considering the values determined in the field; Figure 3-1, *panel b*) reflecting a control mainly by calcite equilibrium.

Alkalinity (HCO_3^-) is, together with chloride and sulphate, the third major anion in the systems, and is the most abundant in the non-saline waters. Its concentration increases in the shallower groundwaters (Figure 3-2, *panels a, b and c*) as a result of atmospheric and biogenic CO_2 influence and/or calcite and aluminosilicate dissolution (Figure 3-2, *panel c*). The alkalinity content reaches equilibrium (or oversaturation) with calcite in the shallow groundwaters (Figure 3-2, *panel c*) and then decreases dramatically with depth as it is consumed by calcite precipitation, whereas calcium keeps increasing as a result of mixing with more saline waters (Figure 3-2, *panel d*).

As can be seen in Figure 3-2 *panel d*, calcium shows a good positive correlation with increasing chloride concentration in saline groundwaters, suggesting that mixing is the main process controlling this element. In spite of the extent of reequilibrium with calcite affecting Ca, the high Ca content of the mixed waters (coming from the brine end member) obliterates the effects of mass transfer with respect to this mineral. This fact justifies the quasi-conservative behaviour of calcium, at least in waters with chloride contents higher than 10,000 mg/L (0.35 mol/kg). Simple theoretical simulations of mixing between a brine end member and a dilute water, with and without calcite equilibrium, have shown the negligible influence of reequilibrium on the final dissolved calcium contents.

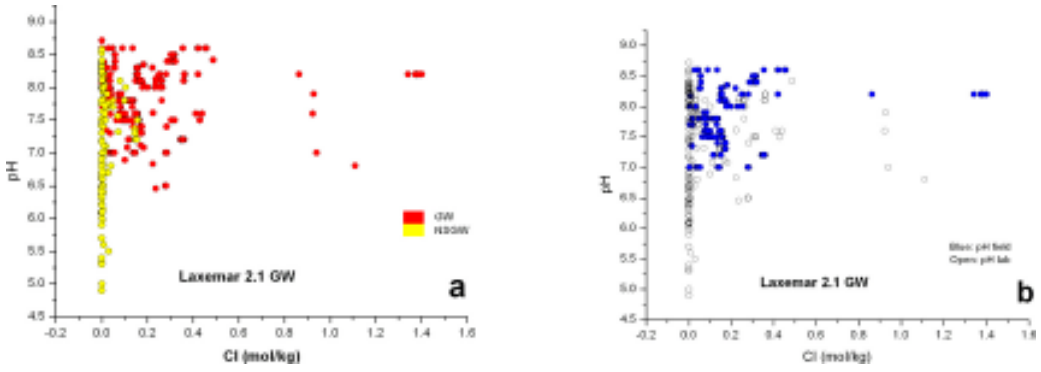

Figure 3-1. *pH values for Laxemar area groundwaters as a function of chloride content. (a) Distribution of pH in the different groundwater types. (b) pH values for shallow groundwaters were determined in the laboratory but most of the deep groundwaters have field pH measurements as it is indicated in the plot.*

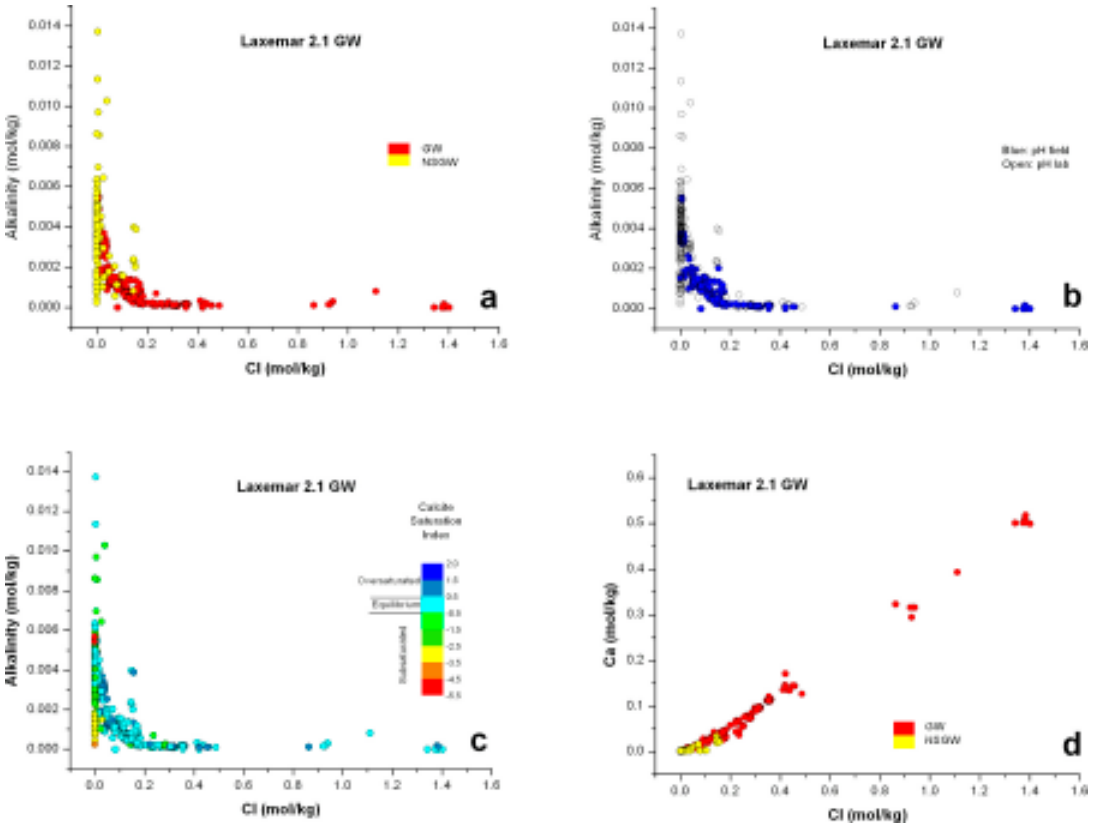

Figure 3-2. *Carbonate system plots. Alkalinity (a, b, c) and calcium (d) contents with respect to chloride in Laxemar groundwaters.*

Figure 3-3, *panel a* shows the trend of decreasing partial pressure as depth increases, reaching values well below the atmospheric in the more saline groundwaters. As for calcite saturation index in the groundwaters, Figure 3-2, *panels f, g and h,* shows the evolution towards the equilibrium or even a slight oversaturation in the more saline groundwaters. The model proposed for the carbonate system evolution is in a good agreement with the already classical work from /Nordstrom et al. 1989/ in the Stripa groundwaters, also verified in other sites such as Olkiluoto /Pitkänen et al. 1999/. In fact, even the possible oversaturation state of calcite in these groundwaters was already suggested by /Nordstrom et al. 1989/.

3.2 Sulphate system modelling

Figure 3-4a,b, showing SO_4 vs Cl, suggests three possible sulphate evolution trends for the Laxemar area: (1) an obvious modern Baltic Sea water dilution line, including some shallow groundwaters (soil pipes and percussion boreholes); (2) a brackish groundwater dilution trend moving away from trend (1) towards very high sulphate values, suggesting some Littorina influence /Laaksoharju et al. 2004a, Appendix 2; 2004b, Appendix 2; 2004c, Appendix 4; 2005, Appendix 3/; some shallow groundwaters (soil pipe samples) are also included in this trend; (3) a continuous increase in sulphate with chloride.

Analysing the saturation state of waters with respect to gypsum (Figure 3-4 *panels c,d*) some conclusions can be drawn. For the Laxemar area groundwaters, the gypsum SI trend indicates a clear evolution towards equilibrium which is reached at chloride values of 10,000 mg/L and maintained even in the most saline waters. This equilibrium, defined mainly in the most saline and deepest groundwaters from Laxemar, introduces a new controlling phase in the groundwater system. In fact, /Laaksoharju et al. 1995/ reported the presence of gypsum as a fracture filling mineral in this subarea. In addition, the influence of gypsum as sulphate limiting phase has been already reported in the Canadian Shield /Gascoyne 2004/.

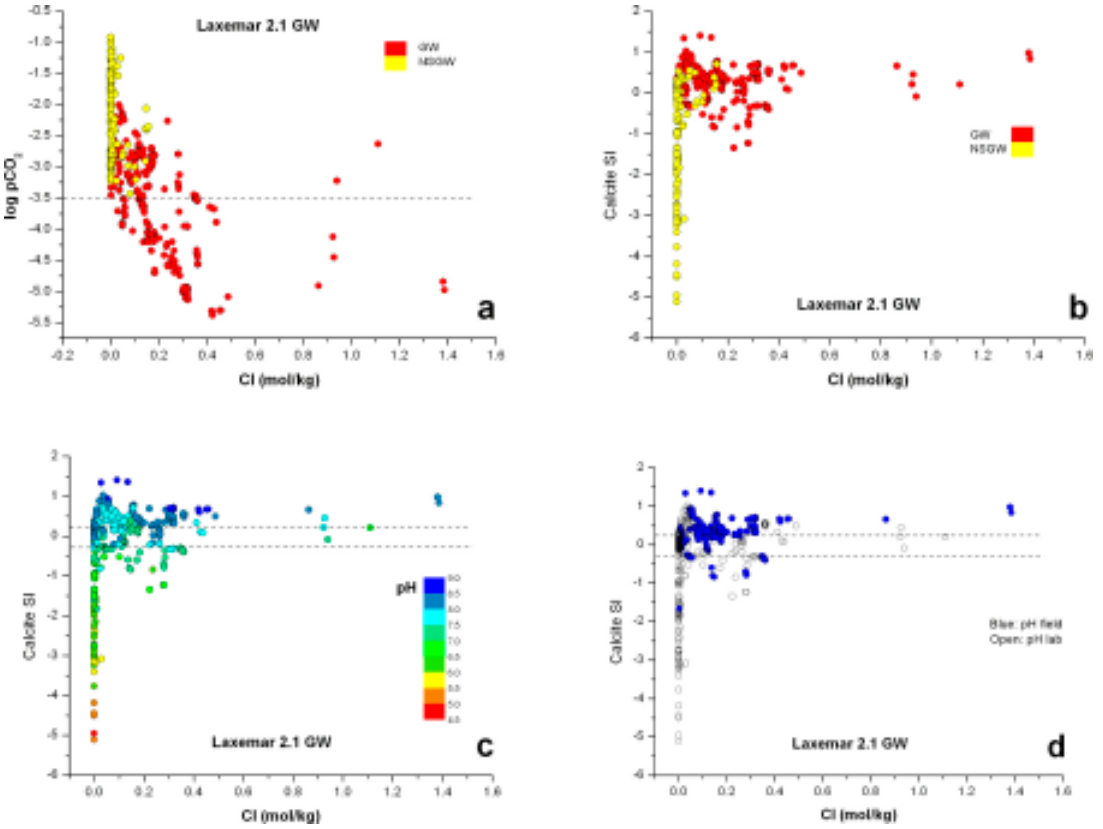

Figure 3-3. *Carbonate system plots. Calculated pCO_2 (a) and calcite saturation indexes (b, c, d) with respect to chloride. The dashed lines represent the atmospheric log pCO_2 value in panel e and the uncertainty associated with SI calculations in panels g and h.*

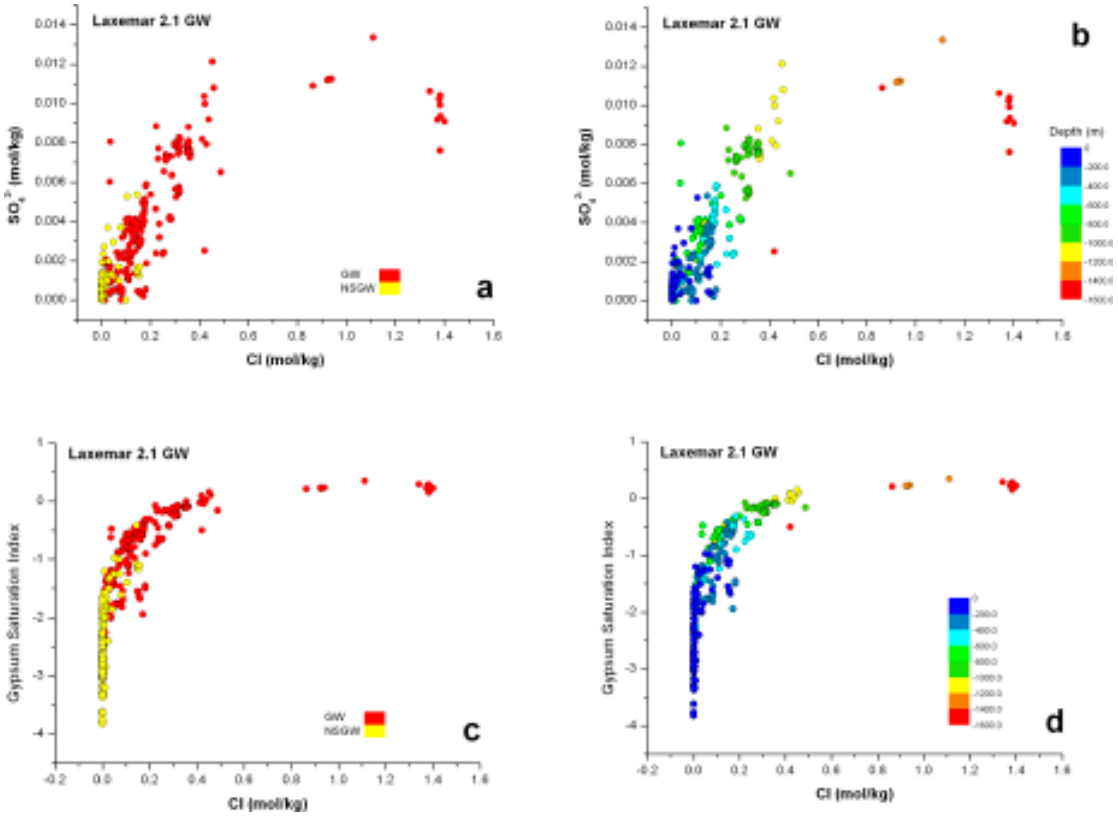

Figure 3-4. *Sulphate contents (a,b) and calculated gypsum saturated indexes (c,d) in the Laxemar groundwaters as a function of chloride concentration.*

3.3 The silica and aluminosilicates systems

The content of dissolved SiO_2 in shallow groundwaters indicates a typical trend of weathering, while in deep groundwaters it has a narrow range of variation indicative of partial reequilibrium (Figure 3-5 *panels a,b*). The general process evolves from an increase in dissolved SiO_2 by dissolution of silicates in shallow groundwaters to a progressive decrease related to the participation of silica polymorphs and aluminosilicates which control dissolved silica as the residence time of the waters increases. This can be clearly seen in Figure 3-5 *panels a, b*.

The weathering of rock-forming minerals is the main source of dissolved silica. Shallow groundwaters have a variable degree of saturation with respect to silica phases (quartz and chalcedony; Figure 3-5 *panels c,d*), compatible with the weathering hypothesis, and a rather unclear control by secondary phases. This is a rough generalization, useful for this general description but it should be specified with more detailed studies considering kinetics (see Reactive transport modelling, Molinero et al. in this report).

Deep groundwaters are close to equilibrium with chalcedony (Figure 3-5 *panels c,d*). Saturation indices are relatively constant and independent of chloride content; this suggests that the groundwater has already reached, at least, an apparent equilibrium state associated with the formation of aluminosilicates or secondary siliceous phases like chalcedony, which seems to be controlling dissolved silica.

As it has been commented on in previous reports, the mineralogical studies of boreholes in Laxemar area have demonstrated the presence of a complex sequence of fracture filling minerals (besides chlorite and calcite, epidote, prenhite, laumontite, Ba-zeolite, adularia, albite, hematites and pyrite have also been reported; small amounts of outermost coatings with smectite, interstratified clay minerals and illite, with high surface area, have also been identified). In addition to granite rock-forming minerals, most fracture filling phases are aluminosilicate minerals with which waters have been in contact during their geochemical evolution. Therefore, they are important water-rock interaction phases.

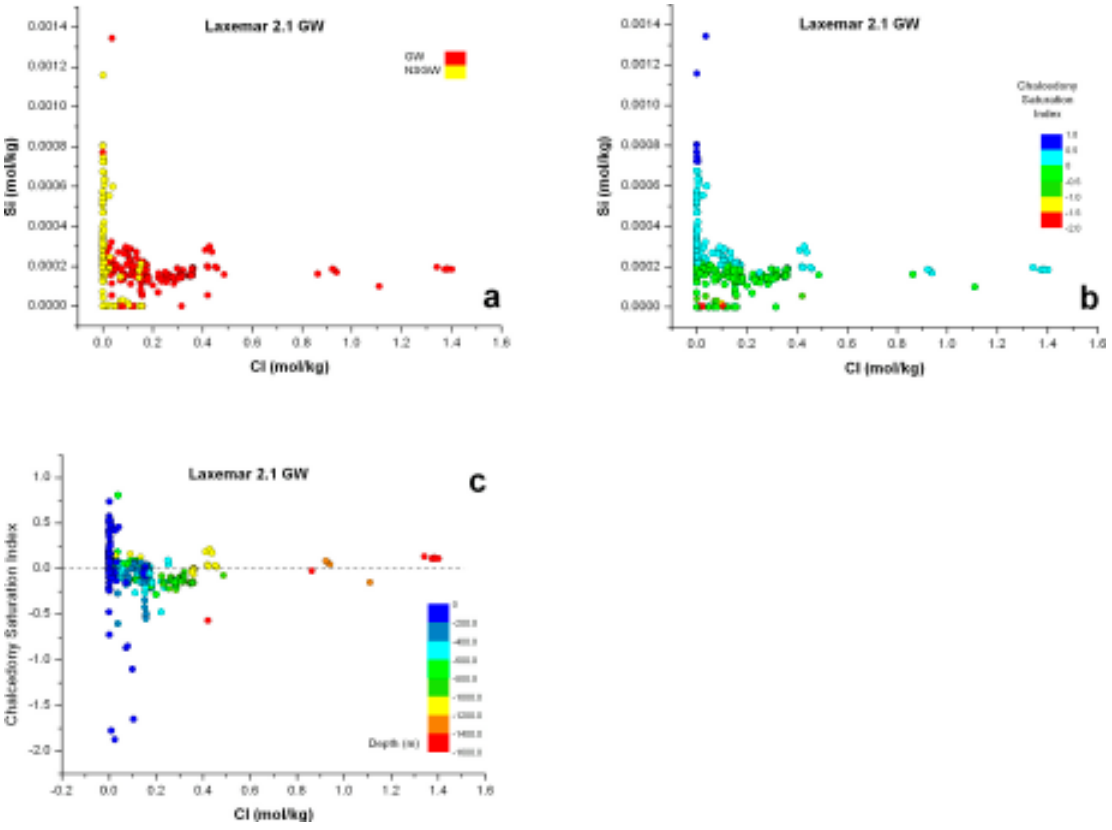

Figure 3-5. *(a) and (b) Plots of SiO_2 vs Cl for Laxemar groundwaters. (c) Saturation indexes of chalcedony as a function of Cl.*

The lack of QA aluminium data for Laxemar groundwaters precludes a speciation-solubility analysis of aluminosilicates. Therefore, activity diagrams were used to study the relationship between silicate minerals and their stability. This study has already been presented in previous reports /Laaksoharju et al. 2004a, Appendix 2; 2004b, Appendix 2; 2004c, Appendix 4; 2005, Appendix 3/ and here we will only show the results obtained using the whole set of data from Laxemar 2.1. A more comprehensive explanation of the reaction path calculations performed for this systems can be found in the already mentioned reports. The following includes a general evaluation of Laxemar groundwaters from their position in one of the stability diagrams[3] and a discussion on the effects of mixing and reaction on the groundwaters' chemistry.

Figure 3-6, *panels a and b*, shows the diagram kaolinite-albite-adularia for the Laxemar waters (including surface and groundwaters). Two main trends can be distinguished. *The first trend* crosses the kaolinite stability field and goes towards the limit with adularia. This trend is defined by surface and shallow groundwaters. They are modern waters with low chloride contents and whose geochemical evolution is the result of water-rock interaction.

The evolution of these waters in the kaolinite field follows the typical weathering-alteration path in granitic materials, representing the effects of a progressive dissolution of the rock forming minerals (calcite, chlorite, plagioclase, K-feldspars, etc). Along this process, partial reequilibria with phyllosilicates (e.g. kaolinite) can be reached. Ionic exchange and, finally, calcite precipitation can also take place. Waters close to or on the kaolinite-adularia boundary would correspond to the more evolved samples in this water-rock interaction process.

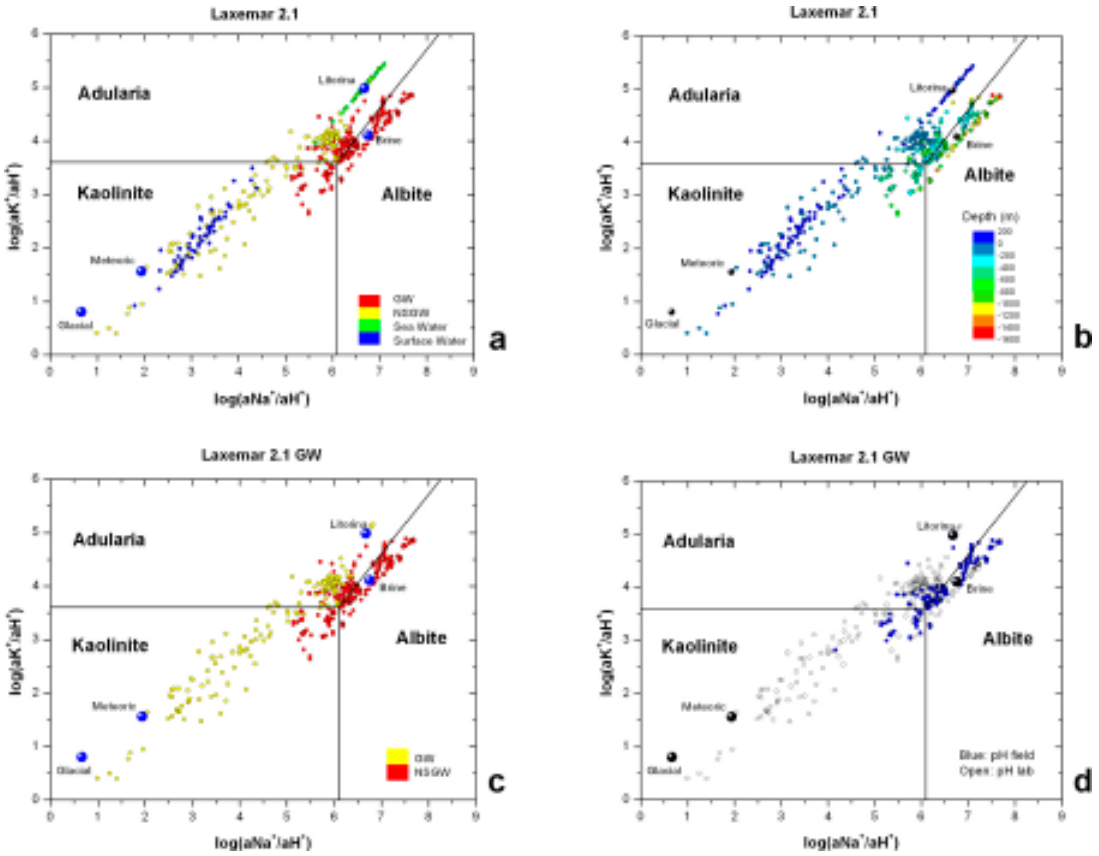

Figure 3-6. *Position of the water samples (surface and groundwaters in a and b; and only groundwaters in c and d) from Laxemar area in the Adularia-Albite-Kaolinite stability diagram.*

[3] The study of aluminosilicate phases presented here has been restricted to those with low uncertainties, using thermodynamic data already tested and verified in comparable systems. The selected thermodynamic data are taken from /Grimaud et al. 1990/ at 15°C in their study of Stripa groundwaters.

Some shallow groundwaters (soil pipes and percussion boreholes) plot inside the adularia stability field. Some of these samples show clear evidences of mixing with modern Baltic Sea waters, and even with another older marine (Littorina) and saline (non marine) end members. Therefore, they could correspond to waters whose chemistry is not only controlled by water-rock interaction and plot together with groundwaters characterised by mixing.

The second trend, followed by all Laxemar brackish and saline groundwaters, runs parallel to the adularia-albite border, indicating an "apparent" equilibrium (or near equilibrium) situation. Even considering only waters that have a field pH value, the position of the groundwaters is well represented in this trend (Figure 3-6, *panel d*). This result is similar to what is found in Stripa /Grimaud et al. 1990/, but with an important difference: maximum chloride content in Stripa reaches only 700 mg/L, whereas Laxemar groundwaters, plotted in the same position, have Cl contents up to 45,000 mg/L. The residence time of Stripa groundwaters has been estimated at roughly 20,000 years /Fritz et al. 1989/, meaning that water-rock interaction processes can only provide up to 700 mg/L of chloride in such a long time span. It is clear, therefore, that an additional source of salinity is needed to justify the existence of younger waters with much higher chloride concentrations in the Laxemar area. This source of chlorine comes from mixing with a saline component of marine and/or non marine origin. And therefore, this points again to mixing as the key process controlling the chemistry of these waters, as it has been repeatedly reported in previous works /Laaksoharju and Wallin 1997, Laaksoharju et al. 1999, Laaksoharju et al. 2004a, Appendix 2; 2004b, Appendix 2; 2004c, Appendix 4; 2005, Appendix 3/.

Another interesting finding is the broad salinity range of the samples that run parallel to the adularia-albite limit. These waters include not only the most saline ones (close to the brine end member composition), but also waters with around 5,000 mg/L Cl. This points again to the central effect of mixing, as it has been reported before /Laaksoharju and Wallin 1997, Laaksoharju et al. 1999/.

The position of the end-members waters is also shown in Figure 3-6 (Brine, Litorina, Glacial and Meteoric). It is fairly clear that the evolution path of these waters is the result of (a) reaction between the rock and dilute waters (shallow groundwaters), (b) mixing at depth with more saline groundwaters in different proportions, depending on location and residence time, and (c) the simultaneous interaction of these deep waters with the rock.

The study of the stability diagrams has been completed with several reaction-path simulations which have tried to reproduce the chemistry of the groundwaters as a result of a complex sequence of mixing steps and reactions with the phases included in the diagrams. A very detailed description of these simulations can be found in Appendix 4 of /Laaksoharju et al. 2004c/ and Appendix 3 of /Laaksoharju et al. 2005/. The key conclusion is that most of the synthetic waters (generated by mixing the end member waters in the proportions obtained with M3 and PHREEQC mass balance calculations) plot exactly in the same positions as the real waters. In the rest of the cases, the position of the synthetic and real waters can be made coincide just by imposing equilibrium with calcite. The inclusion of equilibrium with aluminosilicates (adularia-albita, for example) do not change neither the position (chemical composition) nor the pH of the waters, and predict very low mass transfers for those phases. Therefore, pure mixing and the simple calcite equilibrium are enough to justify the composition of most of the samples on the adularia-albite border. Additional stability reactions, including montmorillonite, smectite, etc., are being now considered in order to asses their effect on ionic exchange, which should be kinetically favoured with respect to dissolution-precipitation.

Ionic exchange involving illite, smectites or zeolites could be an alternative way to express constraints on cations like K^+, Na^+ or Ca^{2+} in low temperature systems. The ionic exchange control on groundwater composition can be particularly significant in waters affected by the most recent mixing event, where the interaction time with minerals is short. Therefore, this uncertainty means that aluminosilicate dissolution-precipitation and ionic exchange in clay minerals can result in the same water chemistry. This typical ambiguity is present in the studied sites /Laaksoharju et al. 2004c, Appendix 4; 2005, Appendix 3/.

4 Redox system modelling

The understanding of the redox state is one of the most fundamental safety requirements since reducing conditions will guarantee that radionuclides are not transported to the biosphere in case of canister failure. Therefore, redox modelling is a key step during site investigation. The two possibilities suggested in previous studies about the main compositional systems influencing the redox state of the groundwaters, namely the iron system /Grenthe et al. 1992/ and the sulphur system /e.g. Nordstrom and Puigdomenech 1986/, have been revisited.

Here we present a detailed description and discussion of the redox system. The chapter starts with the presentation and evaluation of the data and continues with a comprehensive modelling exercise including a redox pairs analysis, some redox minerals solubility calculations, and the integration of these results with the available microbiological and mineralogical data.

4.1 Evaluation of redox data

For this modelling exercise samples with enough redox data were selected. This includes Eh and pH data from continuous loggings (selected with the criteria described in section 1), analytical data for Fe^{2+}, S^{2-} and CH_4, and microbiological information. These criteria, used together, have drastically reduced the number of suitable samples for the redox characterization of the system. In spite of this, the selected samples cover a wide range of depths (from 130 to 1,000 m; Table 1-1).

Eh values in Laxemar area are between –200 and –380 mV (Figure 4-1, *panel a*). The lack of very reducing values (only one value of –380 mV in KAS02 at 316 m depth has been reported) has nothing to do with the Eh selection criteria. It may be a sampling bias that could disappear as more samples are analysed.

Eh distribution with depth (Figure 4-1, *panel b*) does not show any evident trend. This conclusion does not change when individual subareas are considered, or when specific sections in each borehole are analysed, or when only Group 1 Eh values are taken into account. This behaviour was already noticed by /Nordstrom and Puigdomenech 1986/ in their work on different Swedish groundwaters up to 600 m depth. Therefore, the Swedish groundwater systems can not be compared with most aquifers elsewhere, where a marked decrease of redox potential is observed as the residence time and depth of the waters increase /Drever 1997/.

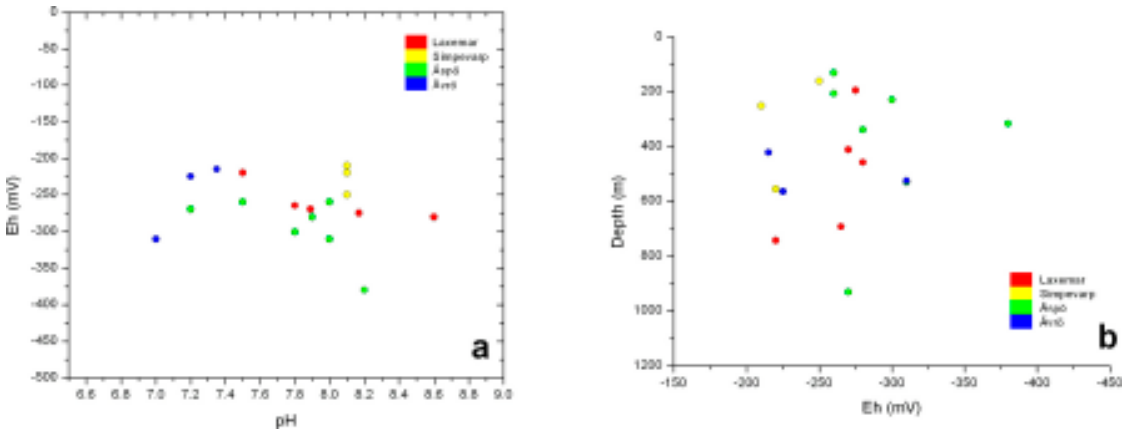

Figure 4-1. *(a) pH-Eh plot for the Laxemar area groundwaters. (b) Eh distribution with depth in the Laxemar area groundwaters.*

The Eh-pH diagram (Figure 4-1, *panel a*) indicates that all the samples plot in the reducing zone, close to the lower limit of water stability and roughly parallel to it between pH 7 and 8.6. This situation limits the redox pairs that can be participating in the control of the potentiometrically measured Eh to those related to the iron and sulphur systems. Previous studies of Swedish groundwaters suggest the active participation of two electroactive pairs on the measured Eh control: the $S_{(c)}/HS^-$ pair /Nordstrom and Puigdomenech 1986/ and the $Fe^{2+}/Fe(OH)_{3(s)}$ pair /Grenthe et al. 1992/.

For the waters studied here, none of them provide completely suitable results. The $S_{(c)}/HS^-$ pair gives much less reducing values than the ones determined in all the studied groundwaters. Therefore, it can not be the responsible for the control of the measured Eh. As we will present later, values provided by the pair $Fe^{2+}/Fe(OH)_{3(s)}$ (using the Grenthe et al.'s calibration) agree well with some of the measurements in the Laxemar area /Laaksoharju et al. 2004ab, SKB 2006/. This result was expected, as some of these samples were already used by /Grenthe et al. 1992/ in the calibration of the $Fe^{2+}/Fe(OH)_{3(c)}$ pair. However, the discrepancies could indicate the presence of either several Fe-oxyhydroxides with equilibrium constants different to those considered by /Grenthe et al. 1992/, or only one type of oxyhydroxide (e.g. hematite, frequently found as a fracture filling) with a variable specific surface area (or a variable particle size).

The position of most of the selected values in the Eh-pH diagram corresponds to the range defined by /Drever 1997/ for groundwaters buffered by sulphate-reduction (only the most reducing values, below –300 mV, are well below this range). The occurrence of sulphate reducing bacteria (SRB) has been confirmed in a wide range of depths and even the MPN (most probable number) seems to be correlated with the measured Eh (Hallbeck, in this report, Appendix 2). The evaluation of the saturation state of sulphide minerals will be analysed in the following sections.

All these observations can be related to the noticeable and surprisingly good agreement between the potentiometrically measured Eh and the values calculated using the *non-electroactive* pair SO_4/HS^-. This agreement was already pointed out by /Glynn and Voss 1999/ for some Laxemar groundwaters and has repeatedly been mentioned in later studies /Laaksoharju et al. 2004ab, SKB 2006/. The suggestion that the electrodes could respond to sulphur species generated during sulphate-reduction is presently being considered.

In order to understand more in depth all these observations, an integrated study and modelling of the redox pairs, including speciation-solubility calculations, and the mineralogy and the microbiological analysis, is being addressed. Next we present some of the main results obtained up to now.

4.2 Redox pair modelling

The modelling is based on redox pair calculations using PHREEQC and the WATEQ4F database. The following pairs have been analysed: the dissolved SO_4^{2-}/S^{2-} and CH_4/CO_2 redox pairs, and the heterogeneous $Fe(OH)_3/Fe^{2+}$, pyrrhotite (or FeS_{am})/SO_4^{2-} and pyrite/ SO_4^{2-} couples. The use of other redox pairs (Fe^{3+}/Fe^{2+} and Fe^{3+}-clay/Fe^{2+}-clay; /Banwart 1999/), and a detailed description of the modelling methodology can be found in /Laaksoharju et al. 2004a, Appendix 2; Laaksoharju et al. 2004b, Appendix 2; Laaksoharju et al. 2004c, Appendix 4; and Laaksoharju et al. 2005, Appendix 3/. The main results are summarised in Table 4-1 a and b.

As we mentioned above, the potentiometrically measured Eh varies from –210 to –380 mV. Sulphur redox pairs and, in less degree, the iron pair calibrated by /Grenthe et al. 1992/ show, in general, good agreement with the measured Eh (Figure 4-2).

4.3 Sulphides solubility calculations

The position of the selected values in the Eh-pH diagram (Figure 4-2) in the zone defined by /Drever 1997/ for groundwaters buffered by sulphate-reduction, together with the occurrence of sulphate reducing bacteria (SRB) in a wide range of depths very well correlated with the measured Eh (Hallbeck, in this report, Appendix 2), suggest the possibility of an active precipitation of sulphide mineral phases.

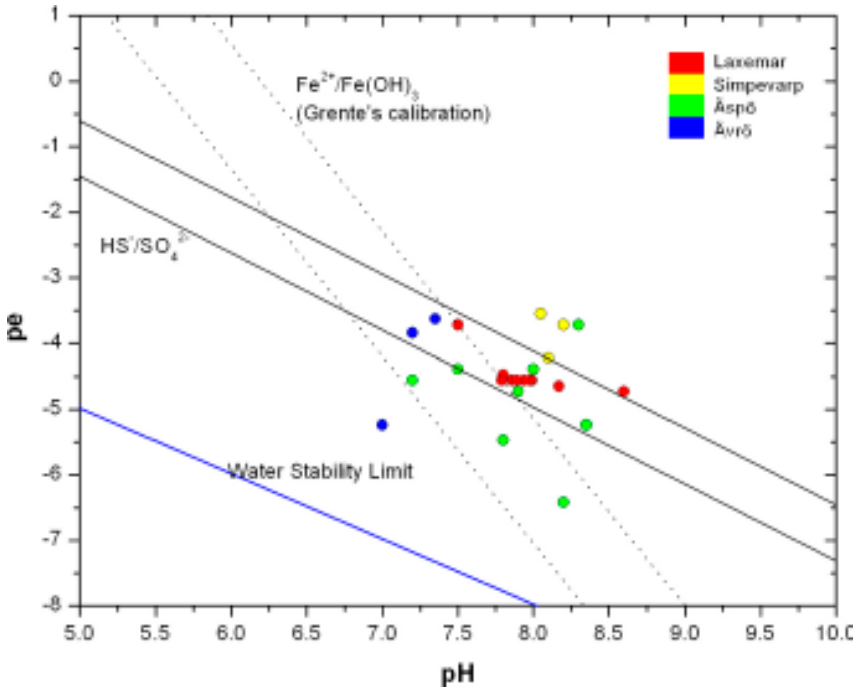

Figure 4-2. *Eh-pH diagram showing the measured Eh and pH of the selected samples in Laxemar area. Boundaries for $Fe^{2+}/Fe(OH)_3$ and SO_4^{2-}/HS^- (dotted and solid black lines, respectively) are also shown for the range of pH, Fe^{2+} and S^{2-} concentration in the Laxemar groundwaters. Data for the $Fe^{2+}/Fe(OH)_3$ are from /Grenthe et al. 1992/ and data for the SO_4^{2-}/HS^- are from the WATEQ4F database included in PHREEQC /Parkhurst and Appelo 1999/.*

In order to check the occurrence of this precipitation in the natural system, the analysis of the saturation state of the groundwaters with respect to ferrous sulphides, and/or the identification of these monosulphides in areas where pyrite is forming, is necessary /Wilkin and Barnes 1997ab/. Up to now, monosulphides have not been found as fracture fillings in the Laxemar are, and groundwaters are clearly oversaturated with respect to pyrite; however, the saturation state of amorphous monosulphides has not been evaluated yet. This is the main aim of this section.

Ferrous sulphide formation in low temperature environments is tightly related to the activity of sulphate-reducers bacteria (SRB) as the principal source of H_2S. Pyrite formation in these medium can be produced by two mechanisms: (a) by the direct precipitation from pyrite-oversaturated and monosulphide-undersaturated groundwaters /Howard 1979, Giblin and Howard 1984, Perry and Pedersen 1993/ or (b) by the transformation of precursor monosulphides precipitated from pyrite- and monosulphide-oversaturated groundwaters. The first mechanism is unlikely as pyrite precipitation seems to be kinetically inhibited in low temperature conditions. The second one is the most frequently observed mechanism in laboratory and natural systems /Berner 1967, 1970, 1984, Rickard 1969, 1975, 1997, Sweeney and Kaplan 1973, Schoonen and Barnes 1991, Wilkin and Barnes 1997ab, Benning et al. 2000 and references therein/.

Under the term "iron monosulphides" the following phases are included: the amorphous monosulphide ($FeS_{am,}$ also named disordered mackinawite; /Wolthers et al. 2003, 2005/), the ordered or crystalline mackinawite (tetragonal FeS) and greigite (Fe_3S_4). All of them can be involved in the transformation to pyrite (FeS_2). Although there are different "reaction pathways" to explain this transformation /Wilkin and Barne, 1997b, Benning et al. 2000/, all of them start with the precipitation of an initially amorphous iron monosulphide and its successive transformation through ordered mackinawite, greigite and, finally, pyrite.

Table 4-1a. Eh values for the selected samples in the Forsmark area. The potentiometrically measured values (column Chem) are shown for comparison with the values calculated with the different redox pairs. Additional information for each sample is also included.

Site	Borehole	Section sampled	Sample_No	pH	Fe^{2+}	S^{2-}	CH_4	Eh					
								Chem.	SO_4/HS^-	SO_4/Pyrite	SO_4/FeS_{am}	CO_2/CH_4	$Fe^{2+}/Fe(OH)_3$ Grenthe et al. (1992)
ÄSPÖ	KAS02	212 - 214	1548	7.5	0.483	0.5	0.03	-260	-211	-190	-231	-224	-273
		308 - 344	1474	7.6	0.624	0.15	---	---	-215	-193	-233	---	-296
		314 - 319	1419	8.2	0.788	0.01	---	-380	-246	-233	-268	---	-403
		463 - 468	1428	8.4	0.941	0.13	---	---	-272	-246	-279	---	-441
		530 - 535	1433	8.0	0.24	0.18	---	-310	-245	-219	-258	---	-340
		860 - 924	1560	8.5	0.049	0.72	0.034	---	-293	-256	-293	-319	-386
	KAS03	129 - 134	1569	8.0	0.123	0.71	0.016	-260	-244	-231	-269	-252	-324
		860 - 1002	1582	8.0	0.077	1.28	0.037	-270	-264	-221	-260	-287	-313
	KAS04	226 - 235	1596	7.8	0.04	1.1	---	-300	-230	-213	-255	---	-330
		334 - 343	1603	7.9	0.324	0.41	0.028	-280	-237	-216	-254	-253	-331
		440 - 480	1588	8.1	0.256	0.6	0.004	---	-254	-227	-258	-268	-359
	KAS06	238 - 243	1606	7.6	0.44	0.17	---	---	-213	-196	-237	---	-287
		338 - 243	1610	7.5	0.425	0.02	---	---	-217	-187	-229	---	-270
		518 - 523	1618	7.3	0.627	0.02	---	---	-184	-171	-214	---	-246
ÄVRÖ	KAV01	420 - 425	1391	7.35	1.6	0.59	---	-215	-207	-172	-214	---	-201
		522 - 531	1383	7.0	2.23	1.2	---	-310	-188	-153	-197	---	-226
		558 - 563	1374	7.2	1.02	0.81	---	-225	-201	-166	-202	---	-241
SIMPE VARP	KSH01A	156 - 167	5263	8.1	1.4	0.01	0.06	-257	-235	-233	-267	-262	-400
		245 - 261	5268	8.05	1.3	0.01	---	-210	-188	-228	-263	---	-390
		548 - 565	5288	8.1	0.51	---	---	-230	---	-228	-267	---	-392

Table 4-Ib. Continuation with the Laxemar samples.

SITE	Borehole	Section sampled	Sample _No	pH	Fe^{2+}	S^{2-}	CH_4	Eh					
								Chem.	SO_4/HS^-	SO_4/Pyrite	SO_4/ FeS_{am}	CO_2/CH_4	$Fe^{2+}/Fe(OH)_3$ Grente et al. (1992)
LAXEMAR	KLX01	272 - 277	1537	8.5	0.129	0.53	0.11	----	- 275	- 263	- 297	- 291	- 409
		456 - 461	1528	8.6	0.04	0.46	----	- 280	- 289	- 269	- 303	----	- 414
		680 - 702	1633	7.8	0.135	0.65	0.044	----	- 242	- 208	- 249	- 263	- 292
		680 - 702	1516	7.8	0.03	2.5	0.22	- 265	- 242	- 211	- 254	- 263	- 254
		910 - 921	1773	8.4	0.06	0.29	0.27	----	- 285	- 241	- 279	- 314	- 354
	KLX02	315 - 321	2738	7.5	1.04	0.04	----	----	- 208	- 226	- 261	----	- 393
		335 - 340	2705	8.0	0.464	bdl	----	-----	----	- 225	- 255	----	- 373
		798 - 803	2712	7.7	1.71	bdl	----	----	----	- 202	- 240	---	- 346
		1090 - 1096	3035	8.6	2.81	0.05	----	----	- 279	- 261	- 290	----	- 501
		1420 - 1706	2731	8.2	0.426	bdl	----	----	----	- 230	- 266	----	- 356
	KLX03	193 - 198	7952	8.4	0.254	bdl	0.87	- 275	----	- 241	- 276	- 268	- 370
		408 - 415.3	10091	7.9	0.429	bdl	0.62	- 270	-----	- 216	- 254	- 261	- 336
		735 - 748	10242	7.5	0.903	bdl	0.21	- 220	- 280	- 184	- 225	- 251	- 288
		964 - 975	10076	8.4	bdl	0.115	0.059	----	- 281	----	----	- 316	----

The amorphous iron monosulphide is the first phase to precipitate in most natural aqueous environments, as it is the most soluble of the solids mentioned above (log K=–3 for amorphous monosulphides; log K=–3.6 for mackinawite; log K=–12.85 for greigite; and log K=–16.40 for pyrite; /Berner 1967, Morse et al. 1987, Davison et al. 1999/. Moreover, its precipitation rate is very fast (seconds; /Rickard 1989, 1995/) compared with the other sulphides (days to hundreds of days; /Chen and Liu 2005 and references cited there/). When waters reach the amorphous iron monosulphide saturation, although they are already oversaturated with respect to the other monosulphides, this amorphous phase precipitates first.

4.3.1 Methodology

The samples selected were those with a continuous logging of temperature, dissolved oxygen, pH and sometimes Eh for the sampled sections. Several additional samples were also selected because they had analytical data of dissolved S^{2-} and Fe^{2+} and in situ pH values. Moreover, all the selected samples have a charge balance lower than 5%.

From this set of samples, we selected for modelling purposes those with a sulphidic signature, indicated by a total dissolved sulphide concentration ($S^{2-}_{(tot)}$=S^{2-}+H_2S+HS^-+polisulphides, hereinafter S^{2-}) above the detection limit. This point has been carefully managed. Special attention has been paid to the detection limits and analytical uncertainties associated to dissolved Fe^{2+} and S^{2-}, as they are fundamental in the evaluation of the saturation state of waters with respect to iron monosulphides (sampling and analytical methodology is reported in /Smellie and Laaksoharju 1992, Laaksoharju et al. 1995, Wacker et al. 2004/).

The detection limits vary from 0.01 to 0.02 mg/l for iron and from 0.01 to 0.03 mg/l for S^{2-}. In the more recent SKB's P-reports the reported detection limit for S^{2-} is 0.03 mg/l and 0.02 mg/l for Fe^{2+}, with an uncertainty of 20% and 22%, respectively. In the whole set of sulphidic samples there are several whose S^{2-} concentration is in the 0.01–0.03 mg/l range or close to it; several more have Fe^{2+} values in the 0.01–0.02 range.

In order to check the influence of the analytical uncertainty in the calculations, the selected sulphidic samples were separated into two sets: (a) clearly sulphidic samples with dissolved sulphide higher than 0.1 mg/l, and dissolved Fe^{2+} higher than 0.05 mg/l; and (b) samples with a less sulphidic signature with concentrations close to the uncertainty range, or sulphidic samples with very low dissolved Fe^{2+} concentrations or close to the detection limit. In the Laxemar area there are groundwaters samples from the two subsets, 17 from the clearly sulphidic group (dissolved sulphide between 0.13 and 2.5 mg/l, and dissolved Fe^{2+} between 0.05 and 2.23 mg/l) and 6 from the other, less sulphidic group.

The ionic activity product (IAP) of the monosulphides has been calculated for the following reaction:

$$FeS_{sol} + H^+ \leftrightarrow Fe^{2+} + HS^- \qquad \text{(Equation 1)}$$

such as:

$$IAP = (aFe^{2+} \cdot aHS^-) / aH^+ \qquad \text{(Equation 2)}$$

These IAP values have been obtained with PHREEQC /Parkurst and Appelo 1999/ and the WATEQ4F database using the classical speciation-solubility options /Plummer 1992, Drever 1997, Zhou and Anderson 2002/. The code uses the WATEQ-type Debye-Hückel equation /Truesdell and Jones 1974/ for the activity coefficients of the charged species Ca^{2+}, Mg^{2+}, Na^+, K^+, Cl^-, SO_4^{2-}, HCO_3^-, CO_3^{2-} and Sr^{2+} (this equation is valid for solutions with ionic strengths up to 1 molal, /Langmuir 1997/). For the rest of the charged species, the code uses the extended Debye-Hückel or the Davies equations /Davies 1962/. The Davies equation is the one used for the species involved in the IAP defined by Equation (2) and its range of validity extends up to the ionic strength of sea water (0.7 molal; /Langmuir 1997/). The maximum ionic strength of the clearly suphidic waters is 0.64 molal, and 82% of them have values lower than 0.13 molal, thus supporting the use of the Davies equation /Davies 1962/ in this system.

4.3.2 Ionic Activity Product calculations

The selected groundwaters span a depth range from 130 to 1,560 m although the clearly sulphidic samples only reach 1,000 m (972 m in KLX03 borehole of Laxemar). Their salinity is very variable, with chloride concentrations ranging from 70 up to 15,000 mg/l.

Figure 4-3 shows the IAP (expressed as –log IAP) with respect to depth and chloride contents. These data define a constant range between 2.5 and 3.5 independently of chloride concentration or of depth. This is specially significant in the case of chloride as it is the main tracer of the irreversible process (mixing) undergone by the groundwaters in their evolution. A constant IAP value independent of the chloride content suggests a generalised equilibrium with respect to iron monosulphides in the clearly sulphidic waters.

The mean and standard deviation (1σ) of the –log IAP values obtained for the 17 clearly sulphidic samples is 2.98 ± 0.36. This value, considered as the solubility product of the amorphous FeS, agrees very well with the values obtained for this phase in laboratory experiments and in other natural systems[4].

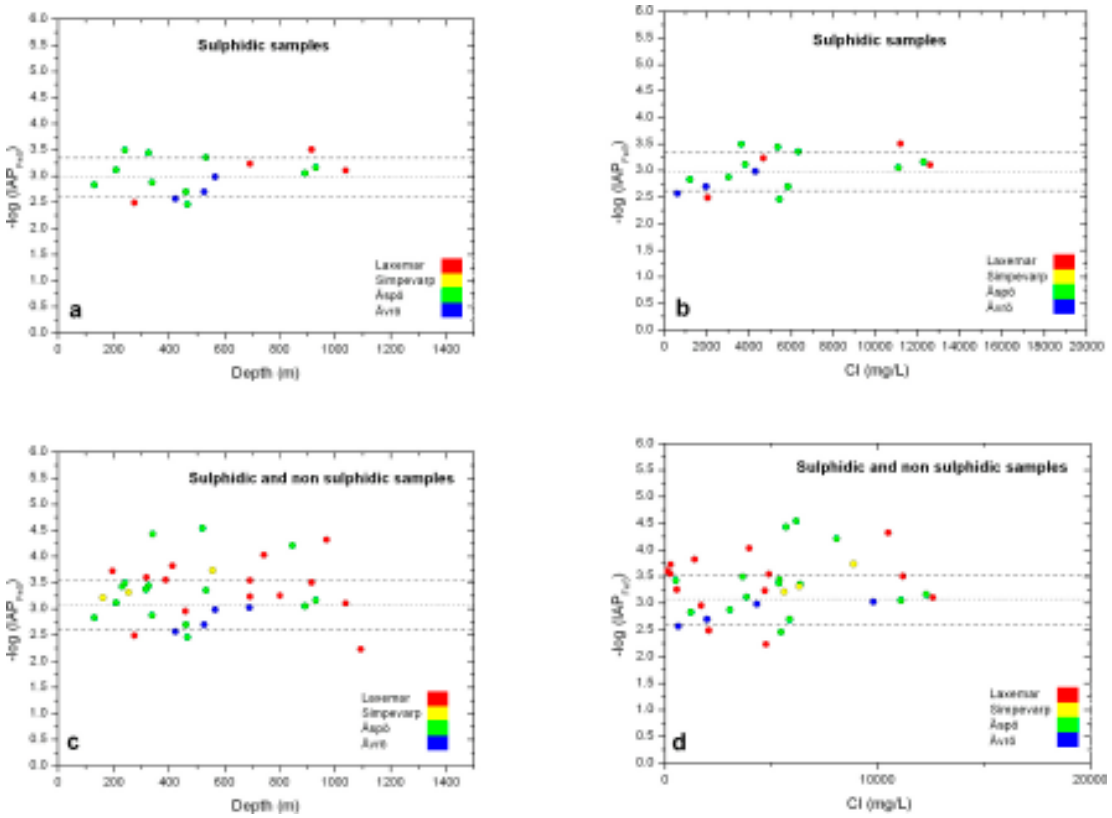

Figure 4-3. *IAP values for the monosulphides in the suphidic groundwaters from Laxemar area, as a function of depth (left) and chloride content (right). (a) and (b) panels include only the 17 clearly sulphidic samples. (c) and (d) include all the analysed samples (23). The dotted and dashed lines represent the mean value and the standard deviation, respectively, for the two different sets of samples (2.984 ± 0.36 in the sulphidic set, a and b; 3.07 ± 0.36 in the whole set, c and d).*

[4] /Berner 1967/ reported a value of 2.95 ± 0.1 at 25 ºC, pH_2S = 1 atm and pH = 3.6–4.0. /Davison et al. 1999/ obtained a value of 3.00 ± 0.12 at 20°C, with pH between 3 and 7.9 and under different H_2S partial pressures (10^{-1} to 10^{-5} MPa). /Bagander and Carman 1994/ obtained a pK = 3.15 for the amorphous FeS in an in situ study of sediments from the Baltic Sea. /Chen and Liu 2005/ reported a value of 3.07 ± 0.34 in a study of the groundwaters from the Chosui Delta (Taiwan) with a similar methodology to the one applied here. /Chen and Liu 2005/ also obtained an average value of 2.98 studying the sulphidic waters from different aquifers in different bedrocks (limestones, coastal plain sediments, wetlands, fractured limestones, etc).

The variability (standard deviation) in the solubility product in the Laxemar area groundwaters can be attributed to analytical uncertainties, to sampling or to sample preservation problems /Chen and Liu 2005/. This is clearly seen when we include the rest of the selected samples (the 6 less sulphidic samples from group b). The -log IAP value for the whole set of samples (23 samples) is 3.07, almost identical to the one obtained only with group 1 samples, although the standard deviation increases (from 0.36 to 0.46).

The equilibrium situation with respect to the monosulphides in the Laxemar groundwaters has been compared to the rest of the Swedish and Finish sites and it seems to apply also to all of them (except in Forsmark). Moreover, the equilibrium is independent of the type of water and the paleohydrogeological history of the systems.

This implies that the equilibrium must be imposed by common factors to all sites but independent of the evolution history and the type of system. The most obvious factor is the activity of sulphate-reducing bacteria. The second one is the existence of an iron source in the system with enough intensity to keep the waters saturated with respect to these metastable phases.

The activity of SRB is necessary to supply H_2S to the waters. The occurrence of these microorganisms depends on the presence of anoxic conditions, the nutrient supply, the competition with other biological groups, etc. All these factors can interact with each other in order to enhance their activity in very different hydrogeochemical systems.

The importance of these two factors (SRB and an iron source) has been demonstrated in many low temperature natural systems with active precipitation of sulphides. The predominance of one or the other is the responsible of the development of waters with high dissolved sulphide or of waters with low sulphide contents in spite of the SRB activity /Wilkin and Barnes 1997ab, Hurtgen et al. 1999, etc./. We will go into more detail in the following section.

The good agreement between the field and laboratory amorphous iron monosulphide equilibrium constants (–log K=3) highlights its suitability for thermodynamic calculations in natural systems. The standard deviation associated to the calculated IAP can be used as a reasonable approximation to the uncertainty of the calculated saturation indices (± 0.4).

It is important to notice that the amorphous FeS (FeS_{ppt}) equilibrium constant included in the WATEQ4F and PHREEQC databases of the code PHREEQC /Parkhurst and Appelo 1999/ and in the code WATEQ4F /Ball and Nordstrom 1999/, is –log K=3.91, that is, almost an order of magnitude lower than the values obtained here. /Ball and Nordstrom 1999/ indicate that this value comes from the work of /Berner 1967/. However, /Chen and Liu 2005/ have demonstrated that the value included in these databases is the consequence of a mistake in the calculations performed to convert the reactions and thermodynamic data from /Berner's 1967/ formalism to the format accepted by the databases. Considering the wide diffusion and use of these databases, they should be corrected as it has already been done in the other thermodynamic database supplied with PHREEQC, the MINTEQ (version 4) database.

4.3.3 Bacterial activity and the source of iron

The equilibrium with respect to the amorphous iron monosulphides found in most Laxemar groundwaters has important implications. The metastability of the amorphous iron monsulphides has been demonstrated in the field and in the laboratory, becoming mackinawite or pyrite in a "short time" [5]. Therefore, the occurrence of this equilibrium indicates a continuous and present supply of H_2S by the activity of SRB. When dissolved Fe^{2+} (or a source for this component) is also present, waters become oversaturated with respect to the amorphous monosulphides and they can precipitate maintaining the equilibrium in the system (the precipitation rate of this phase is very fast in general, even instantaneous in neutral-alkaline conditions once its solubility product is attained; /Rickard 1989, 1995/). Therefore, the equilibrium observed in Laxemar waters corresponds to a monosulphide precipitation process active at present.

[5] Recrystallization of amorphous monosulphide to mackinawite starts in a matter of days and can last up to two years /Rickard 1995, Wilkin and Barnes 1997ab/. More recent works /Benning et al. 2000/ suggest a shorter time (several months). Transformation to pyrite can be accomplished in a time span from hours to decades /e.g. Hurtgen et al. 1999/. Even the longest time span is short compared to the residence time of the studied groundwaters (10^2–10^4 years).

This active precipitation process is not equally distributed in all the subareas. Most of the Äspö and Ävrö groundwaters are clearly sulphidic and in equilibrium with monosulphides; in Laxemar, only KLX01 borehole is in the same situation. In the rest of the Laxemar boreholes and in the Simpevarp subarea, many sampled waters are not sulphidic and, *a priori*, can not be in equilibrium with these phases. Therefore, as the precipitation of monosulphides is conditioned by the activity of SRB and the concentration of Fe^{2+}, we will now discuss these two topics in each of the studied subareas.

Äspö and Ävrö subareas

Most of these waters have a sulphidic signature (Table 4-2) and are in equilibrium with iron monosulphides. Microbiological studies in Äspö (there are no data for Ävrö) indicate, in many of the studied sections, the occurrence of SRB with significant values of MPN (*most probable number*). They have been identified at 230.5 m and 338.5 m depth in borehole KAS04 (MPN between 100 and 1,600 cells/ml), at 450 m coexisting with other bacterial groups /Haveman and Pedersen 2002/ and up to 626 m in KAS03 (1,390 cells/ml; /Pedersen 1997/). That is, SRB activity seems to be widely distributed in depth. Therefore, it can be considered enough to supply the necessary dissolved sulphide to surpass the iron monosulphides IAP.

The Fe^{2+} content of these groundwaters is significant (Table 4-2), which suggests the existence of an Fe^{2+} source if we accept that SRB have been active for a long time. This source can be the hematite found in fracture fillings in all the studied sections /e.g. Smellie and Laaksoharju 1992/.

Therefore, in the Äspö subarea all the system characteristics point to an active precipitation of amorphous iron monosulphides. Moreover, the presence at 930 m depth of waters in equilibrium with this phase indicates that at present the biological activity of SRB extends down to that depth. It is expected that in Ävrö groundwaters (as they are similar to Äspö) exists also a noticeable activity of SRB and an iron source.

Laxemar subarea

Groundwaters in this subarea are both sulphidic and non-sulphidic. All the waters in KLX01 borehole are sulphidic and in equilibrium with amorphous monosulphides at almost all studied depths. Microbiological data are restricted to 691 m depth (sample 1515 taken in 1988, with 2.5 mg/l of HS^-, the most sulphidic water in all the subareas) and the MPN for the SRB is the highest at 56,000 cells/ml. Obviously, the effects of this bacteria population on the water chemistry must be very important, and the H_2S supply together with the precipitation of iron monosulphides must be able to keep the dissolved Fe^{2+} contents at the low levels found in these waters (sample 1516, 0.029 mg/l Fe^{2+}). Nevertheless, the presence of Fe^{2+}, although in low concentrations, suggests the existence of a source of iron that compensates the biological effects of the SRB and decreases the high H_2S content associated to their activity. Fracture filling studies at that depth have detected hematite /Laaksoharju et al. 1995/[6] as the most probable source of iron.

Most waters from KLX02 and KLX03 boreholes are less sulphidic and dissolved S^{2-} is below detection limit. Taking into account the analytical uncertainty range, IAP calculations for these samples were repeated using a S^{2-} concentration of 0.03 mg/l.

Non sulphidic samples from KLX03 are undersaturated with respect to amorphous monosulphides from 195.9 to 741.8 m depth (Figure 4-2). Microbiological information available for 411.5 and 741.8 m indicates MPN values between 20 and 100 cells/ml for SRB. The influence of the bacterial activity (represented by these numbers) if any, is not enough to allow waters to reach monosulphides oversaturation, more considering that dissolved Fe^{2+} is not low. The only sulphidic sample in this borehole is the deepest one (sample 10076 at 969.5 m depth) but its Fe^{2+} content is below detection limit. Considering a hypothetic Fe^{2+} concentration of 0.02 mg/l (detection limit) the –log IAP obtained is 4.32, that is, a clear undersaturation with respect to iron monosulphides. There are no

[6] This section was resampled one year later (sample 1633 from 1989) and the chemical composition was very similar (even in pH and Eh) showing the same equilibrium with respect to iron monosulphides. The main difference was the lower dissolved S^{2-} and the higher Fe^{2+} contents. There are no microbiological analysis from this sampling but it seems that the SRB activity had decreased being unable to keep the Fe^{2+} levels as low as the ones found in 1988.

microbiological information at that depth but dissolved S^{2-} concentration (0.115 mg/l) suggests the occurrence of SRB. On the other hand, the very low dissolved Fe^{2+} and the clear undersaturation of these waters with respect to monosulphides would indicate the absence of an iron source and, therefore, it would be the limiting factor in this case. Unfortunately, there are no specific studies on the fracture filling minerals at this depth to verify the hypothesis.

In KLX02 slightly sulphidic and non sulphidic waters show equilibrium or quasi-equilibrium with respect to iron monosulphides. The only clearly undersaturated sample is the deepest one at 1,562 m. The available microbiological data correspond to 1,160, 1,350 and 1,390 m /Haveman and Pedersen 2002/. Reported MPN for the SRB at 1,160 m depth is 330 cells/ml, which could explain the low dissolved S^{2-} (sample 3035 at 1,093 m). A source of iron should favour the keeping of the low dissolved S^{2-} levels, compensating the effects of the bacterial activity. At 1,350 and 1,390 m depth no SRB was detected, in agreement with these waters being the most saline in the Scandinavian Shield. If, as /Haveman and Pedersen 2002/ suggest, salinity is one of the possible limiting factors in SRB activity, it is perfectly understandable the pronounced undersaturation with respect to monosulphides in sample 2731 (at 1,592 m depth). In general, using the equilibrium state of monosulphides as a proxy for SRB activity, these bacteria could be present at depths down to 1,038.5 m (sample 1785), close to the maximum depth (1,093 m) at which this type of bacteria have been found.

Simpevarp subarea

There are still few analytical data for this subarea (only three sections in one borehole, KAS01A, at 161.7, 253.2 and 556.5 m). The first two sections have dissolved S^{2-} contents below detection limit and there are no data for the deepest. Using the value of 0.03 mg/l for dissolved S^{2-} in the three cases, the first two sections are in equilibrium with respect to the amorphous iron monosulphide and the deepest sample is slightly undersaturated.

Microbiological analysis at these depths indicate SRB occurrence but with low MPN (160, 20 and 35 cells/ml, respectively). This low activity and the high iron content (dissolved and in the fracture filling minerals; hematite has been reported at 253.2 and 556.5 m) could justify the low S^{2-} concentrations during monosulphide precipitation, at least in waters at 161.7 and 253.2 m.

The undersaturation of waters at 556.5 m depth is not significant as dissolved S^{2-} has not been analysed. IAP calculated with 0.03 mg/l of S^{2-} could be bias as we do not know the real concentration and it could have been higher allowing the equilibrium with these phases.

4.3.4 Monosulphide precipitation and pyrite formation in low temperature conditions

The equilibrium of the groundwaters with respect to amorphous monosulphides and its hypothetical precipitation in the Laxemar area contrast with the absence of a clear mineralogical evidence of their occurrence as fracture fillings.

However, if the process is active at present the detection of the phase can be very difficult because: (1) these precipitates form as scattered and very small aggregates or as thin films over previous solids /Morse and Cornwell 1987, Herbert et al. 1988/, and they are easily destroyed during sampling; (2) although some remains of these precipitates could be still present, their proportion would be below the detection limit of the frequently used X-ray diffraction method /e.g. Tullborg 1989, Tullborg et al. 1991, Drake and Tullbrog 2004, 2005/; the analysis by SEM-EDAX, able to identify the monosulphides' stoichiometry, is oflimited utility due to its local character and the small amount of sample used.

Fortunately, the presence of monosulphides could have left other kind of signatures in the system, mainly (1) their occurrence as colloidal phases, and (2) the occurrence of pyrite formed in the hydrogeochemical system at present.

Pyrite formation by monosulphides recrystallization is the most frequent and best documented process in low temperature media. Some details are still open with respect to the specific mechanisms of the transformation /e.g. Benning et al. 2000/ and, therefore, on its kinetics

too: Transformation from monosulphide to pyrite can proceed in time spans from hours to decades /e.g. Hurtgen et al. 1999/. In any case, it is a fast process compared with the residence time of many of the studied waters and therefore the occurrence of pyrite as a modern phase is perfectly feasible.

Isotopic values of $\delta^{34}S$ in pyrite from the fracture fillings in the Äspö subarea /Tullborg et al. 1999 and references there/ range from 0 to –26‰ (Table 4-2). The more negative values (mainly found between 400 and 500 m depth) would indicate a biogenic origin, in agreement with the recrystallisation mechanism being active in the past or at present. Moreover, they support the hypothesis suggested by some authors /Drake and Tullborg 2004/ that pyrite crystals identified in the most external and latest filling stage in conductive fractures are the result of a low temperature and recent formation event.

4.3.5 Discussion

The active precipitation of iron monosulphides in the deeper reaches of granitic groundwater systems has been described for the first time here. Its identification improves the understanding of the geochemical properties of these systems and can be specially relevant in explaining the redox behaviour, always complex and difficult to characterize.

This precipitation is directly related to microbiological activity. Sulphate-reducing bacteria, as H_2S producers, are essential for the initiation and development of the process, and a source of iron must also be available in order to surpass the IAP of the amorphous monosulphides, allowing their precipitation. Microcrystalline hematite coatings in fractures, very common in the studied areas, are the prime candidates as the source of Fe^{2+}. The dissolution of hematite can be mediated by *iron reducing bacteria* present in other parts of the groundwater system (and the posterior transport of dissolved Fe^{2+} towards the sulphate-reduction areas); or can be accomplished in the same zone where the sulphate-reduction process is active by the reductive dissolution of hematite promoted by H_2S or by the effect of the cellular hydrogenase associated to the sulphate-reducer metabolic activity /Neal et al. 2001/.

SRB activity has an additional consequence: the formation of recent pyrite as a result of the transformation (ripening) of amorphous monosulphides.

The identification of an equilibrium situation with respect to the amorphous monosulphides in the groundwaters can be used as an indicator of the activity of SRB. However, the absence of equilibrium does not preclude their existence, as they can be present but the absence or low reactivity of iron oxides prevent the monosulphides equilibrium; or SRB activity can be very low, giving off not enough H_2S to reach the monosulphides solubility product.

The SRB-mediated precipitation of amorphous monosulphides and its coupling with other organic and inorganic geochemical processes should be taken into account in safety assessment studies. Its potential influence on the genesis of colloidal phases is only one of the many important consequences because, independently of the iron monosulphides occurring as mineral or colloidal phases, their capacity to retain pollutants is very high. However, as the stability of the iron monosulphides under any hydrogeochemical perturbation is low, their behaviour should be carefully assessed.

One of the classical issues addressed in safety assessment studies in the Swedish program is the corrosion of the copper canister by dissolved sulphides, that is, the influence of the sulphate-reducer activity /e.g. Pedersen and Karlsson 1995, Pedersen 1997, 2000/. Therefore, monosulphide precipitation could be an additional factor to include in the conceptual and geochemical models developed up to now.

Finally, it has been shown that the equilibrium constant of the amorphous monosulphides obtained in this work for the Laxemar groundwaters, log K = –3, is consistent with previous estimations in other natural systems and laboratory experiments. As /Chen and Liu 2005/ suggest, this value must be corrected in the thermodynamic databases WATEQ4F and PHREEQE distributed with the code PHREEQC /Parkhurst and Appelo 1999/. This is especially important for safety assessment issues, as these databases are a basic references in the field.

6 Conclusions

Groundwaters in the Laxemar area can be divided into three groups based on their salinity: (1) non saline and shallow groundwaters; (2) brackish groundwaters; and (3) saline groundwaters. In general terms, their distribution depends on depth as the salinity increases with it. However, in the Laxemar subarea dilute groundwaters extend to approx. 600–1,000 m before they rapidly increase in salinity to maximum values of around 47 g/L (1.4 mol/kg) Cl at 1,700 m. Apart from their salinity, the main difference among these waters is the dominant geochemical processes affecting their chemical contents and physicochemical characters.

Shallow groundwaters are mainly controlled by "pure" water-rock interaction (infiltration water) with minor influence of mixing with older waters. They lack a clear thermodynamic control; if there is any, it is by fast chemical reactions (ionic exchange, surface complexation reactions, calcite dissolution-precipitation, etc.) coupled to several irreversible processes (RFM dissolution, decomposition of organic matter, etc.). Major ions show a constant increase as reactions proceed. The dissolution of calcite and silicates controls alkalinity and pH until equilibrium is attained, as they evolve towards the more saline and deeper groundwaters.

Chemical contents in deep groundwaters (specially for Cl concentrations higher than 10,000 mg/L) are mainly controlled by mixing with a brine end member. Most of the major ions are controlled by mixing with minor influence from reactions (even Ca and sulphate in spite of calcite and gypsum equilibrium). Alkalinity is low because it has been consumed by calcite precipitation. Calcite reaches equilibrium or keeps slightly oversaturated. pH is mainly controlled by calcite equilibrium and, possibly, by aluminosilicate reactions which keep pH values higher than calcite equilibrium would impose.

The potentiometrically measured Eh ranges from –210 to –380 mV. Sulphur redox pairs and the iron pair calibrated by /Grenthe et al. 1992/, show, in general, good agreement with the measured Eh.

Apart from this analysis and comparison, the speciation-solubility calculations have shown a clear equilibrium with amorphous iron monosulphides in most of the groundwaters from this area. This fact implies an important SRB activity at present (in agreement with the microbiological information, see Halbeck, in this report and reference therein) and an iron source (in agreement with the mineralogical information, see Tullborg et al. in this report). An additional conclusion can be drawn from this, and it is the pyrite formation at present from monosulphide precursors (isotopic values from pyrite seem to support this).

As a summary, the redox state of groundwaters in the Laxemar area appears to be well described by sulphur redox pairs in agreement with some previous studies in this area /Glynn and Voss 1999, Laaksoharju et al. 2004a/ and in other sites from the Fennoscandian Shield /Nordstrom and Puigdomenech 1986, Laaksoharju et al. 2004b, Pitkänen et al. 2004/. The presence of sulphate reducing bacteria widely distributed in the Äspö and Simpevarp subareas can be related to this successful description and supports the idea that sulphur redox pairs could be controlling the microbiologically-mediated redox state.

However, in agreement with /Grenthe et al. 1992/, the work presented here also supports the conclusion that the iron system contributes to the redox control in some of the groundwaters through different oxide-oxihydroxides. The problem here is to clearly identify its real contribution in the different geochemical environments, due to the variable crystallinity of the phases involved. This fact indicates that more than one iron phase could be controlling the Eh in different groundwaters.

The coupling between the iron and sulphur systems is materialized via sulphate reducing bacteria and sulphide mineral precipitation. Several lines of reasoning indicate that this process is effective at different levels in the Laxemar area. For instance, pyrite coatings have been identified in fracture fillings, which is an additional evidence of the active participation of sulphur redox pairs.

The good results obtained with the monosulphides saturation index analysis in the Scandinavian groundwaters as tracers of SRB activity indicates that the methodology is useful in this kind of systems. It can solve the common problem related to the absence of correlation between SRB occurrence and its effects (dissolved S^{2-}) in the geochemistry of waters /Pedersen 2000/.

Finally, in the framework of the safety assessment, the precipitation of monosulphides can have important consequences: (1) it is a processes not considered (up to now) in the geochemical evolution of this kind of systems; (2) it can affect the canister integrity and the stability of colloids; and (3) a more reliable thermodynamic value for their equilibrium constant has been deduced and it must be included in the databases in common use in safety evaluations.

7 References

Auqué L, Gimeno M J, Gómez J, Nilsson A-C, 2006. Potentiometrically measured Eh in groundwaters from the Scandinavian Shield. Journal of Applied Geochemistry, submitted.

Bagander L E, Carman R, 1994. In situ determination of the apparent solubility product of amorphous iron sulphide. Applied Geochemistry, 4, 379–386.

Ball J W, Nordstrom D K, 2001. User's manual for WATEQ4F, with revised thermodynamic data base and test cases for calculating speciation of major, trace, and redox elements in natural waters. US geological Survey, Open File Report 91-183, USA.

Banwart S A, 1999. Reduction of iron (III) minerals by natural organic matter in groundwater. Geochim. Cosmochim. Acta, 63(19/20), 2919–2928.

Benning L G, Wilkin R T, Barnes H L, 2000. Reaction pathways in the Fe-S system below 100°C. Chem. Geol., 167, 25–51.

Berner R A, 1967. Thermodynamic stability of sedimentary iron sulfides. Am. J. Sci., 265, 773–785.

Berner R A, 1970. Sedimentary pyrite formation. Am. J. Sci., 268, 1–23.

Berner R A, 1984. Sedimentary pyrite formation.: an update. Geochim. Cosmochim. Acta, 48, 605–615.

Chen W-F, Liu T-K, 2005. Ion activity products of iron sulfides in groundwaters: implications from the Choshui fan-delta, Western Taiwan. Geochim. Cosmochim. Acta., 69, 3535–3544.

Davies C W, 1962. Ion association. Butterworth, Washington D.C.

Davison W, Phillips N, Tabner B J, 1999. Soluble iron sulfide species in natural waters: reappraisal of their stoichiometry and stability constants. Aqua. Sci., 61, 23–43.

Drake H, Tullborg E-L, 2004. Oskarshamn site investigation. Fracture mineralogy and wall rock alteration. Results from drill core KSH01A+B. SKP P-04-250, 120 p, Svensk Kärnbränslehantering AB.

Drake H, Tullborg E-L, 2005. Oskarshamn site investigation. Fracture mineralogy and wall rock alteration. Results from drill cores KAS04, KA1755A and KLX02. SKB P-05-174, 69 p, Svensk Kärnbränslehantering AB.

Drever J I, 1997. The Geochemistry of Natural Waters: Surface and Groundwater Environments. 3rd ed., Prentice Hall, New York, USA, 436 p.

Fritz P, Fontes J-Ch, Frape S K, Louvat D, Michelot J-L, Baldered W, 1989. The isotope geochemistry of carbon in groundwater at Stripa. Geochim. Cosmochim. Acta, 53, 1765–1775.

Gascoyne M, 2004. Hydrogeochemistry, groundwater ages and sources of salts in a granitic batholith on the Canadian Shield southeastern Manitoba. Appl. Geochem., 19, 519–560.

Giblin A E, Howard R W, 1984. Porewater evidence for a dynamic sedimentary iron cycle in salt marshes. Limnology and Oceanography, 29, 47–33.

Glynn P D, Voss C I, 1999. SITE-94. Geochemical characterization of Simpevarp ground waters near the Äspö Hard Rock laboratory. SKI Report 96-29, SKI, Stockholm, Sweden, 210 p.

Grenthe I, Stumm W, Laaksoharju M, Nilsson A C, Wikberg P, 1992. Redox potentials and redox reactions in deep groundwater systems. Chem. Geol., 98, 131–150.

Grimaud D, Beaucaire C, Michard G, 1990. Modelling of the evolution of ground waters in a granite system at low temperature: the Stripa ground waters, Sweden. Appl. Geochem., 5, 515–525.

Haveman S A, Pedersen K, 2002. Distribution of culturable microosganisms in Fennoscandian Shield groundwater. FEMS Microbiology Ecology, 39, 129–137.

Herbert R B, Benner S G, Pratt A R, Blowes D W, 1998. Surface chemistry and morphology of poorly crystalline iron sulfides precipitated in media containing sulfate-reducing bacteria. Chemical Geology, 144, 87–97.

Howard R W, 1979. Pyrite: its rapid formation in a salt marsh and its importance in ecosystem metabolism. Science, 203, 49–51.

Hurtgen M, Lyons T, Ingall E D, Cruse A, 1999. Anomalous enrichments of iron monosulphide in euxinic marine sediments and the role of H_2S in iron sulphide transformations: examples from Effingham inlet, Orca Basin, and the Black Sea. Am. J. Sci., 299, 556–588.

Laaksoharju M, Smellie J A T, Nilsson A-C, Skarman C, 1995. Groundwater sampling and chemical characterisation of the Laxemar deep borehole KLX02. SKB Technical Report 95-05, Svensk Kärnbränslehantering AB.

Laaksoharju M, Wallin B (Ed.), 1997. Evolution of the groundwater chemistry at the Äspö Hard Rock Laboratory. Proceedings of the second Äspö International Geochemistry Workshop, Äspö, Sweden, June 6–7, 1995. Svensk Kärnbränslehantering AB.

Laaksoharju M, Tullborg E L, Wikberg P, Wallin B, Smellie J, 1999. Hydrogeochemical conditions and evolution at the Äspö HRL, Sweden. Appl. Geochem., 14, 835–860.

Laaksoharju M (Ed.), 2004a. Hydrogeochemical evaluation of the Simpevarp area, model version 1.2. Preliminary site description of the Simpevarp area. SKB R 04-74, 463 p, Svensk Kärnbränslehantering AB.

Laaksoharju M, Smellie J, Gimeno M, Auqué L, Gómez J, Tullborg E-L, Gurban I, 2004b. Hydrogeochemical evaluation of the Simpevarp area, model version 1.1. SKB R 04-16, 398 p, Svensk Kärnbränslehantering AB.

Laaksoharju M, Gimeno M, Auqué L, Gómez J, Smellie J, Tullborg E-L, Gurban I, 2004c. Hydrogeochemical evaluation of the Forsmark site, model version 1.1. SKB R 04-05, 342 p, Svensk Kärnbränslehantering AB.

Laaksoharju M (Ed.), 2005. Hydrogeochemical evaluation of the Forsmark site, model version 1.2. Preliminary site description of the Forsmark area. SKB R 05-17, Svensk Kärnbränslehantering AB.

Langmuir D, 1997. Aqueous Environmental Geochemistry. Prentice Hall, New York, USA, 600 p.

Morse J W, Cornwell J C, 1987. Analysis and distribution of iron sulfide minerals in recent anoxic marine sediments. Mar. Chem., 22, 55–69.

Morse J W, Millero F J, Cornwell J C, Rickard D, 1987. The chemistry of the hydrogen sulfide and iron sulfide systems in natural waters. Earth Sci. Rev., 24, 1–42.

Neal A L, Techkarnjanaruk S, Dohnalkova A, McCready D, Peyton B M, Geesey G G, 2001. Iron sulphides and sulfur species produced at hematite surfaces in the presence of sulfate-reducing bacteria. Geochim. Cosmochim. Acta, 65, 223–235.

Nordstrom D K, Puigdomenech I, 1986. Redox chemistry of deep ground-waters in Sweden. SKB Technical Report 86-03, 30 p, Svensk Kärnbränslehantering AB.

Nordstrom D K, Ball J W, Donahoe R J, Whittemore D, 1989. Groundwater chemistry and water-rock interactions at Stripa. Geochim. Cosmochim. Acta, 53, 1727–1740.

Parkhurst D L, Appelo C A J, 1999. User's guide to PHREEQC (Version 2), a computer program for speciation, batch reaction, one dimensional transport, and inverse geochemical calculations. (Science Report WRRIR 99-4259), USGS, 312 p.

Pedersen K, Karlsson F, 1995. Investigations of subterranean microorganisms. Their importance for perfomance assessment of radioactive waste disposal. SKB TR 95-10, 222 p, Svensk Kärnbränslehantering AB.

Pedersen K, 1997. Investigations of subterranean microorganisms and their importance for performance assessment of radioactive waste disposal. Results and conclusions achieved during the period 1995 to 1997. SKB TR 97-22, 274 p, Svensk Kärnbränslehantering AB.

Pedersen K, 2000. Microbial processes in radioactive waste disposal. SKB TR 00-04, 97 p, Svensk Kärnbränslehantering AB.

Perry K A, Pedersen T F, 1993. Sulfur speciation and pyrite formation in meromictic ex-fjords. Geochim. Cosmochim. Acta., 57, 4405–4418.

Pitkänen P, Luukkonen A, Ruotsalainen P, Leino-Forsman H, Vuorinen U, 1999. Geochemical modelling of groundwater evolution and residence time at the Olkiluoto site. Posiva report 98-10, 184 p.

Pitkänen P, Partamies S, Luukkonen A, 2004. Hydrogeochemical interpretation of baseline groundwater conditions at the Olkiluoto Site. (Technical Report POSIVA 2003-07), POSIVA, Helsinki, Finland, 159 p.

Plummer L N, 1992. Geochemical modeling of water-rock interaction. Past, present, future. In: Kharaka, Y.K. and Maest, J. (Eds.) Proceedings of the 6th International Symposium on Water-Rock Interaction. Balkema, Rotterdam, Nederlands, pp 23–33.

Rickard D T, 1969. The chemistry of iron sulphide formation at low temperatures. Stockholm Contributions in Geology, 20, 67–95.

Rickard D T, 1975. Kinetics and mechanism of pyrite formation at low temperatures. Am. J. Sci., 275, 636–652.

Rickard D T, 1989. Experimental concentration-time curves for the iron (II) sulphide precipitation precess in aqueous solutions and their interpretation. Chem. Geol., 78, 315–324.

Rickard D T, 1995. Kinetics of FeS precipitation. Part 1, competing reaction mechanisms. Geochim. Cosmochim. Acta, 59, 4367–4379.

Rickard D T, 1997. Kinetics of pyrite formation by the H_2S oxidation of iron (II) monosulfide in aqueous solutions between 25 and 125°C: the rate equation. Geochim. Cosmochim. Acta, 61, 115–134.

Schoonen M A A, Barnes H L, 1991. Reactions forming pyrite and marcasite from solution. II: via FeS precursors below 100°C. Geochim. Cosmochim. Acta.,55, 1495–1504.

SKB, 2006. Preliminary site description. SKB R-06-10, 656 p, Svensk Kärnbränslehantering AB.

Smellie J, Laaksoharju M, 1992. The Äspö Hard Rock Laboratory: Final evaluation of the hydrogeochemical pre-investigations in relation to existing geologic and hydraulic conditions. SKB TR 92-31, 239 p, Svensk Kärnbränslehantering AB.

Sweeney R E, Kaplan I R, 1973. Pyrite framboid formation. Laboratory synthesis and marine sediments. Econ. Geol., 68, 618–634.

Truesdell A H, Jones B F, 1974. WATEQ, a computer program for calculating chemical equilibria of natural waters. Journal of Research, U.S. Geological Survey, v.2, pp 233–274.

Tullborg E L, 1989. Fracture fillings in the drillcores KAS05–KAS08 from Äspö, southern Sweden. SKB Progress Report 25-89-16, Svensk Kärnbränslehantering AB.

Tullborg E L, Wallin B, Landström O, 1991. Hydrogeochemical studies of fracture minerals from water conducting fractures and deep groundwaters at Äspö. SKB Progress Report 25-90-01, Svensk Kärnbränslehantering AB.

Tullborg E L, Landström O, Wallin B, 1999. Low-temperature trace element mobility influenced by microbial activity. Indications freom fracture calcite and pyrite in crystalline basement. Chemical Geology, 157, 199–218.

Wacker P, Berg C, Bergelin A, 2004. Oskarshamn site investigation. Complete hydrochemical characterisation in KSH01A. Results from four investigated sections, 156.5.167.0, 245.0–261.6, 586.0–596.7 and 548.0–565.4 m. SKB P-04-12, 35 pp, Svensk Kärnbränslehantering AB.

Wilkin R T, Barnes H L, 1997a. Pyrite formation by reactions of iron monosulfides with dissolved inorganic and organic sulfur species. Geochim. Cosmochim. Acta, 60, 4167–4179.

Wilkin R T, Barnes H L, 1997b. Pyrite formation in an anoxic estuarine basin. Am. J. Sci., 297, 620–650.

Wolthers M, van der Gaast S J, Rickard D, 2003. The structure of disordered mackinawite. Am. Mineralogist, 88, 2007–20015.

Wolthers M, Charlet L, van der Linde P R, Rickard D, van der Weidjen C H, 2005. Surface chemistry of disordered mackinawite (FeS). Geochim. Cosmochim. Acta, 69, 3469–3481.

Zhu C, Anderson G, 2002. Environmental Applications of Geochemical Modelling. Cambridge Univ. Press, Cambridge, UK, 284 p.

12 Appendix 4: M3 calculations

Contribution to the model version 2.1

Ioana Gurban, 3D-Terra, Montreal

Marcus Laaksoharju, Geopoint AB, Stockholm

August 2006

Contents

1 Introduction

This paper presents the results of the water classification, mixing modeling and 2D visualization of Laxemar 2.1 groundwater data. The focus is on updating the hydrochemical model, to make uncertainty tests and to present models that can be better integrated with the hydrodynamic models. The need for additional uncertainty tests was identified during the Laxemar 1.2 modelling phase. Issues like the use of tritium as variable in the PCA and the use of different end members are addressed. The code M3 was updated to a new version including hyperspace option calculations. The new M3 code was tested and compared with the old version, in 2D and in hyperspace. A DIS (Drilling Impact Study) evaluation was done for the section 408–415 m in KLX03. An attempt to use the electrical conductivity values, gathered during the DIFF (Differential flow measurements) measurements, as a hydrochemical variability indicator was made for the borehole KLX03.

2 Descriptive and quantitative modelling by using M3 code

2.1 M3 modelling

A challenge in groundwater modelling is to reveal the origin, mixing and reactions altering the groundwater samples. The groundwater modelling concept M3 (Multivariate Mixing and Mass-balance calculations) /Laaksoharju and Skårman 1995b, Laaksoharju et al. 1999b/, can be used for making judgment on this.

In M3 modelling the assumption is that the groundwater is always a result of mixing and reactions. M3 modelling uses a statistical method to analyse variations in groundwater compositions so that the mixing components, their proportions, and chemical reactions are revealed. The method quantifies the contribution to hydrochemical variations by mixing of groundwater masses in a flow system by comparing groundwater compositions to identified reference waters. Subsequently, contributions to variations in non-conservative solutes from reactions are calculated.

The M3 method has been tested, evaluated, compared with standard methods and modified over several years within domestic and international research programmes supported by SKB. The main test and application site for the model has been the Äspö HRL /Laaksoharju and Wallin 1997, Laaksoharju et al. 1999c/. Mixing seems to play an important role at many crystalline and sedimentary rock sites where M3 calculations have been applied such as in different Swedish sites /Laaksoharju et al. 1998/, Canada /Smellie and Karlsson 1996/, Oklo in Gabon /Gurban et al. 1998/ and Palmottu in Finland /Laaksoharju et al. 1999a/.

The features of the M3 method are:

- It is a mathematical tool which can be used to evaluate groundwater field data, to help construct a conceptual model for the site and to support expert judgement for site characterisation.
- It uses the entire hydrochemical data set to construct a model of geochemical evolution, in contrast to a thermodynamic model that simulates reactions or predicts the reaction potential for a single water composition.
- The results of mixing calculations can be integrated with hydrodynamic models, either as a calibration tool or to define boundary conditions.
- Experience has shown that to construct a mixing model based on physical understanding can be complicated especially at site scale. M3 results can provide additional information of the major flow paths, flow directions and residence times of the different groundwater types which can be valuable in transport modelling.
- The numerical results of the modelling can be visualised and presented for non-expert use.

The M3 method consists of 4 steps where the first step is a standard principal component analysis (PCA), selection of reference waters, followed by calculations of mixing proportions, and finally mass balance calculations (for more details see /Laaksoharju et al. 1999b, Laaksoharju 1999d/).

The M3 2D version is being updated and hyperspace calculations are now possible. The new M3 hyperspace version, called here for simplification M3 n-PC (n principal components, where n is the number of end members of the model) was tested. The M3 calculations were compared with the new M3 2D results and with the M3 n-PC calculations. This helped to verify that the new M3 2D works exactly like the old M3 code, and then to compare and judge the benefits or limitations by using 2D or n-PC calculations.

For the Simpevarp 1.1 phase /Laaksoharju et al. 2004/, 2 models were built: at regional scale and at local scale. 113 samples from Simpevarp met the M3 criteria (data for major elements and isotopes) and were used in the M3 modelling. These samples were from boreholes (core and percussion), soil

pipes, lake water, stream water and precipitation. In the Simpevarp 1.2 phase (applied on data from Simpevarp area) the version 1.1 was up-dated with the new available data. For Simpevarp 1.2 phase, 2 models were built: at regional scale and at local scale. 326 samples from Simpevarp met the M3 criteria (data for major elements and isotopes) and were used in the M3 modelling. These samples were from boreholes (core and percussion), soil pipes, lake water, stream water and precipitation. From the 326 samples available, 180 were considered representative from hydrochemical point of view and 146 non representative. The Laxemar 1.2 exercise employed the data from Simpevarp 1.2 model and the data available at Laxemar site. From the 355 samples available, 175 were considered representative from hydrochemical point of view.

The present Laxemar 2.1 modeling employs only groundwater data, from percussion and core boreholes, meaning 205 groundwater samples. From the 205 samples, 59 are considered representative from hydrochemical point of view and 146 non representative. The representative samples are labelled in green and orange in the table in the Appendix 1.

2.2 Test of models

Several M3 modeling concerns were identified during the stage Laxemar 2.1 of the site modeling project. In this exercise the following concerns were adressed:

- *Based on the previous modeling results, only bedrock samples were analyzed in the PCA*
- *Variables useful in the PCA:* As many meaningful variables as possible are used in the M3 modelling. A fixed set of variables will e.g. allow comparisons between the groundwater features of the Laxemar and Forsmark sites. The variables used are the major components (Na, K, Ca, Mg, Cl, HCO_3 and SO_4) and the isotopes H^2, O^{18} and H^3. Several test runs were made with different variables (conservative and non conservative) and with several data sets corresponding to the data available. For example, old data don't have the Br analyzed; therefore these samples could not be included in the modeling, when Br was used as a variable. For exemplification, 6 models based on 2 data sets are presented bellow.

1. **Data set 1**: from the whole table, were selected only samples with major elements, D, O18 and Tr; then the models 1, 2 3, 5 and 6 were considered-
2. **Data set 2**: from the whole table, were selected only samples with D, O18, Cl and Br and then the model 4 was considered.

- *End members used in the modeling: which one should be the "surface" end member capable to describe the data?* The end members used are the brine, glacial, Littorina and a "surface/ recharge" end member. In the Laxemar 1.2 modeling for the recharge was used a "dilute groundwater" end member, but this could not describe all the data. In addition, it was shown that the data can not be explained without the Tr values. Several tests were made by using the "shallow groundwater" or the meteoric (called "rain60") as end members in the calculations.

Six representative tests runs are presented on the Laxemar data with the following model features:

- **model1**: all bedrock samples (dataset1); the variables are: all major components, D and O18 (no Tr); end members: glacial, Littorina, brine and dilute groundwater,
- **model2**: all bedrock samples (dataset1); the variables are: only conservative elements: D, O18 and Cl; end members: glacial, Littorina, brine and dilute groundwater,
- **model3**: all bedrock samples (dataset1); the variables are: only conservative elements: D, O18, Cl and Br; end members: glacial, Littorina, brine and dilute groundwater,
- **model4**: all bedrock samples (dataset 2); the variables are: only conservative elements: D, O18, Cl and Br; end members: glacial, Littorina, brine and dilute groundwater,

- **model5**: all bedrock samples (dataset1); the variables are: all major components, D and O18 and Tr non corrected; end members: glacial, Littorina, brine and Rain 60 (168TU),
- **model6**: all bedrock samples (dataset1); the variables are: only conservative elements D, O18 and Cl; end members: glacial, Littorina, brine and Rain 60 (168TU).

The 6 models from above are presented in Figures 1 to 6. The reference waters and end members used are listed in Table 2-1. To illustrate the impact of the changes on each model, the mixing proportions along the borehole KLX02 calculated for the models are presented in Figures 7 to 10.

Model 1: The PCA applied on Laxemar 2.1 data is illustrated in Figure 1. A total of 205 groundwater samples were used for this plot. The PCA in Figure 2 shows surface water affected by seasonal variation (winter – summer precipitation), a marine trend showing Baltic Sea water influence and for some Äspö samples a possible Littorina sea water influence. A glacial and finally a deep groundwater trend are also shown. This model was the model suggested by the Laxemar 1.2 exercise (model 5 from Laxemar 1.2).However, there are samples that can not be modelled (being outside the PCA) with the chosen dilute groundwater end member. Therefore, the following modelling attempts to improve the previous model by including new knowledge and understanding from the site.

Model 2: The PCA is applied on Laxemar 2.1 dataset1. Only the conservative elements, Cl, O^{18} and D, are used as variables.

Model 3: The PCA applied on Laxemar 2.1 dataset1 is illustrated in Figure 3. Only the conservative elements, Cl, O^{18},D and Br are used as variables.

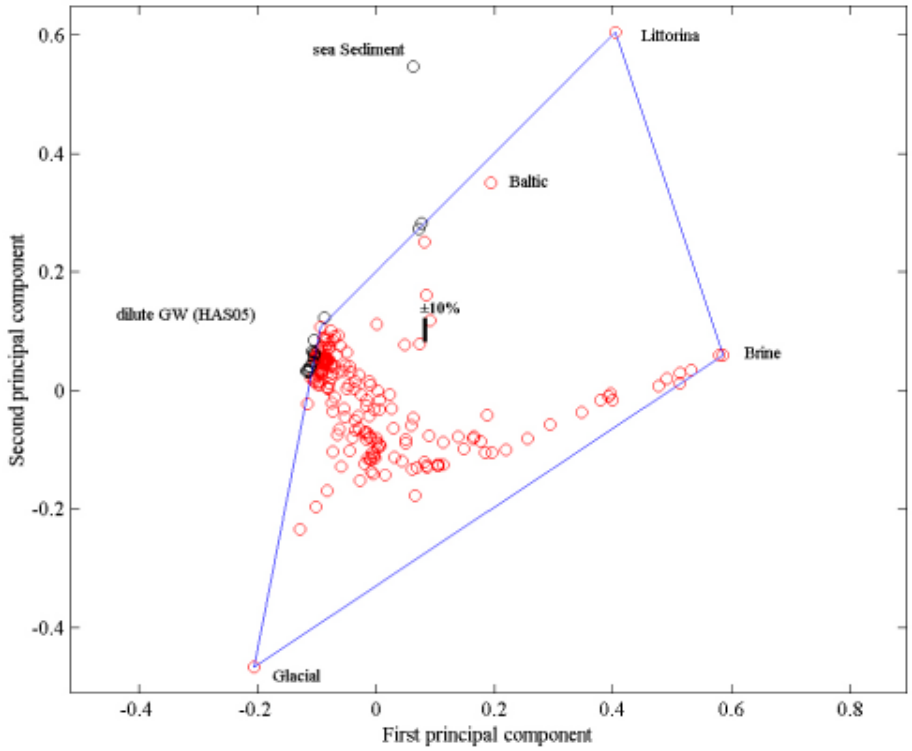

Figure 1. *The picture shows the principal component analysis and the identification of the reference waters. (Variance: First principal component: 0.49191, First and second principal components: 0.75759, First, second and third principal components: 0.90738). The figure shows the groundwater dataset1 for Laxemar 2.1. All the major elements, O^{18} and D are used as variables. The Sea sediment, Littorina, Brine, Glacial and Dilute Groundwater reference waters are used as end members for the modelling. The model uncertainty of ± 10% is shown as an error bar; the analytical uncertainty is ± 5% and represents therefore half of the error bar.*

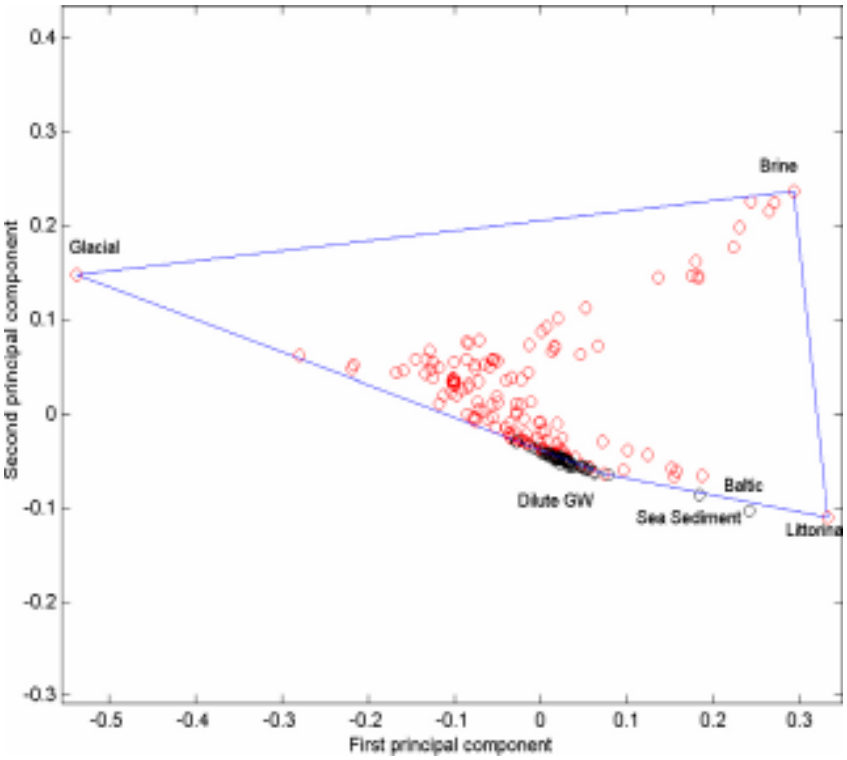

Figure 2. *The picture shows the principal components analysis and the identification of the reference waters. (Variance: First principal component: 0.67993, First and second principal components: 0.981512, First, second and third principal components: 1). The Littorina, Brine, Glacial and Dilute Groundwater reference waters are used as end members for the modelling. Only the conservative elements are used as variables: Cl, O^{18} and D.*

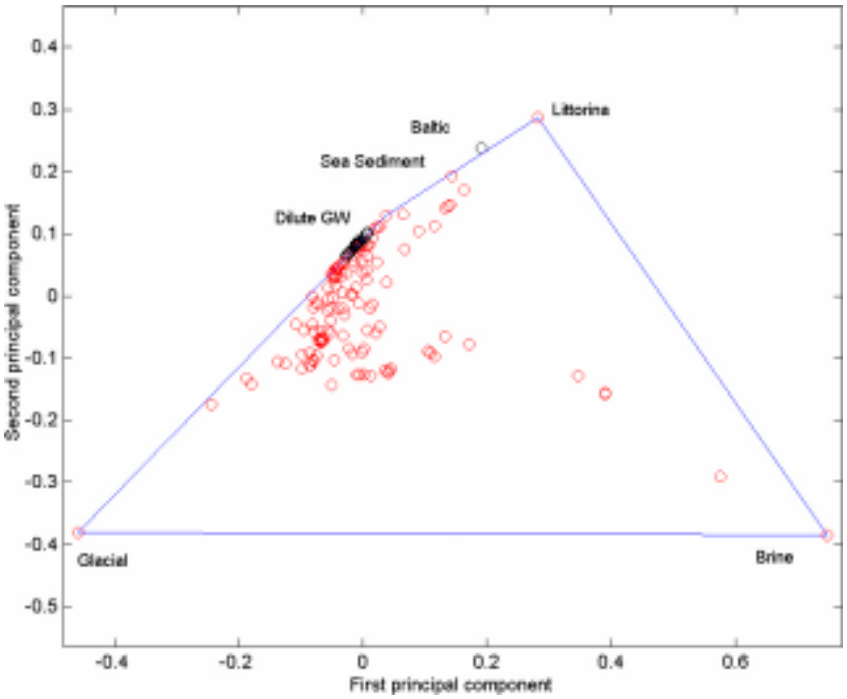

Figure 3. *The picture shows the principal components analysis and the identification of the reference waters. (Variance: First principal component: 0.56588, First and second principal components: 0.97182, First, second and third principal components: 0.98955). The figure shows the Laxemar 2.1 dataset1. The Littorina, Brine, Glacial and Dilute Groundwater reference waters are used as end members for the modelling. The conservative elements Cl, O^{18}, D and Br are used as variables.*

Model 4: The PCA applied on Laxemar 2.1 dataset2 (data selected only based on the Cl, O^{18}, D and Br).

Model 5: The PCA applied on Laxemar 2.1 dataset 1 is illustrated in Figure 5. The variables used in the modelling are the major elements and the O^{18}, D and Tritium. The measured tritium values are used in the modelling. The Rain60 with the normalised tritium value was used as surface end member, instead of the local dilute groundwater. The rain60, which had a tritium value equal to 2000TU in 1960, was selected as an end-member for this model and the tritium value was recalculated with the radioactive decay to a today value of 168TU. The numerical values of the rain60 are listed in Table 2-1.

Model 6: The PCA applied on Laxemar 2.1 dataset 1 is illustrated in Figure 6. The variables used in the modelling are the Cl, O^{18} and D. The Rain60 with the normalised tritium value was used for as surface end member, instead of the local dilute groundwater, like in the model 5. The model 6 employs the same data set as model2, but the surface end member is the rain60 instead of Dilute Groundwater.

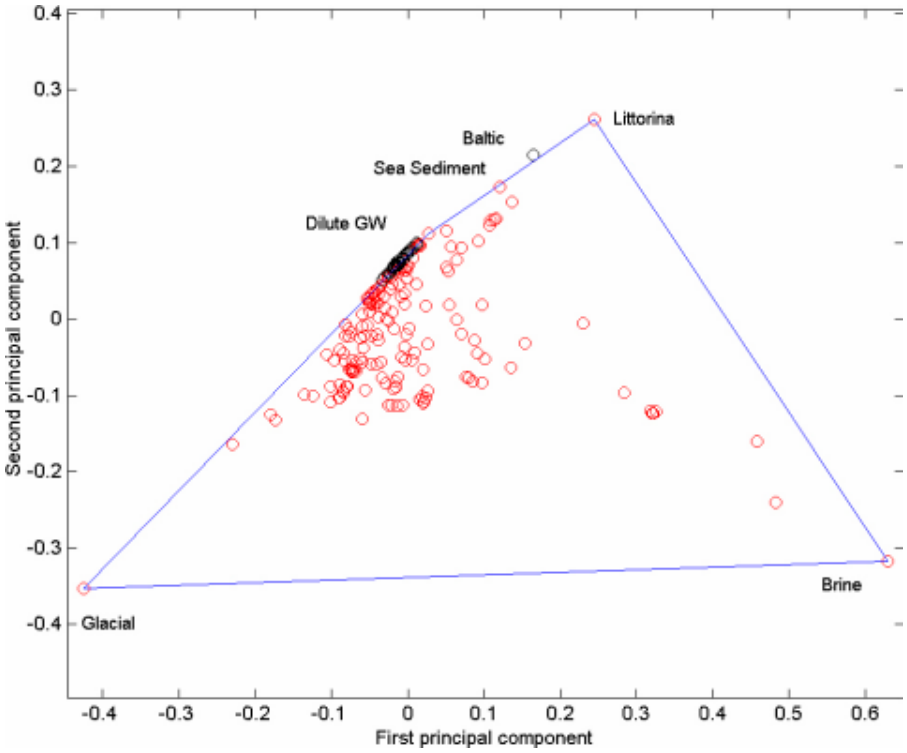

Figure 4. *The picture shows the principal components analysis and the identification of the reference waters. (Variance: First principal component: 0.58604, First and second principal components: 0.96974, First, second and third principal components: 0.98672). The figure shows the Laxemar 2.1 bedrock data. The Littorina, Brine, Glacial and Dilute Groundwater waters are used as end members for the modeling. The conservative elements Cl, O^{18}, D and Br are used as variables.*

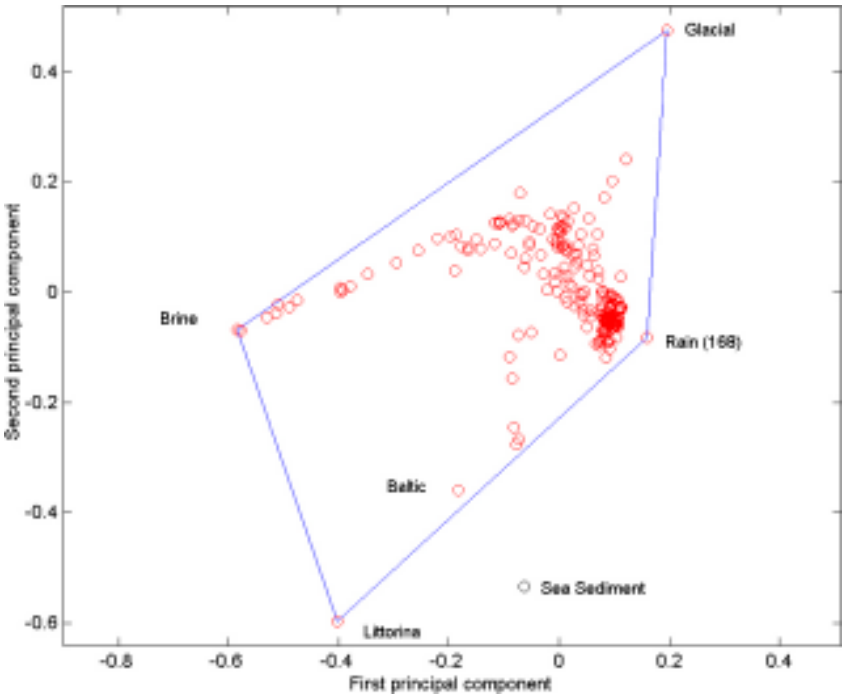

Figure 5. *The picture shows the principal components analysis and the identification of the reference waters. (Variance: First principal component: 0.44655, First and second principal components: 0.68745, First, second and third principal components: 0.82627). The figure shows the Laxemar 2.1 data. The Littorina, Brine, Glacial and rain60 reference waters are used as end members for the modeling. The model employed the dataset1, using as variables the major elements, D, O^{18} and Tritium (measured values).*

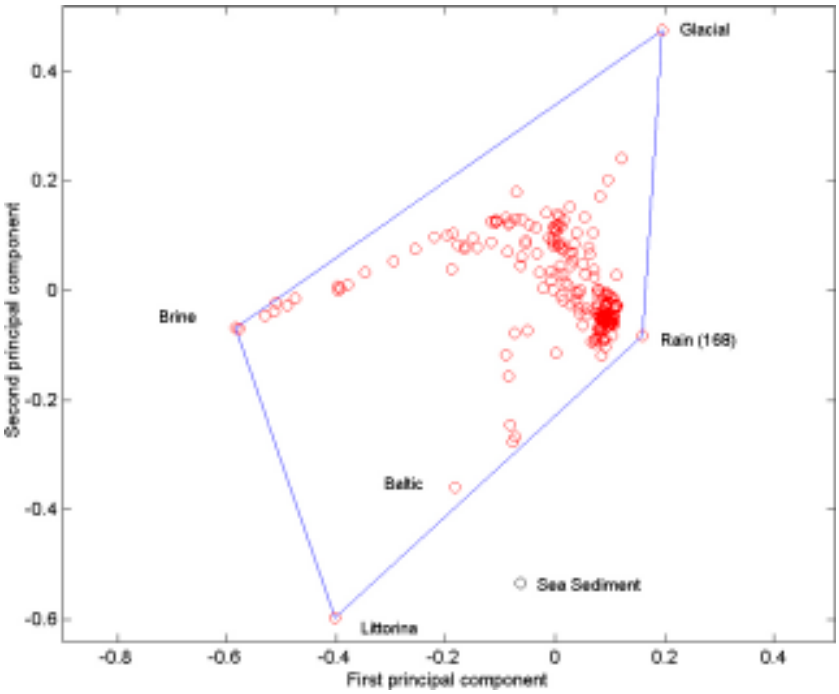

Figure 6. *The picture shows the principal components analysis and the identification of the reference waters. (Variance: First principal component: 0.67993, First and second principal components: 0.98151, First, second and third principal components: 1). The figure shows the Laxemar 2.1 data. The Littorina, Brine, Glacial and rain60 reference waters are used as end members for the modeling. The model employed the dataset1, using as variables the Cl, D and O^{18}.*

2.2.1 The reference waters used

The following reference waters were used in the M3 modelling (for analytical data see Table 2-1):

- **Brine type of reference water:** Represents the sampled deep brine type (Cl = 47,000 mg/L) of water found in KLX02: 1,631–1,681 m /Laaksoharju et al. 1995a/. An old age for the Brine is suggested by the measured ^{36}Cl values indicating a minimum residence time of 1.5 Ma for the Cl component /Laaksoharju and Wallin 1997/.
- **Glacial reference water:** Represents a possible melt-water composition from the last glaciation > 13,000 BP. Modern sampled glacial melt water from Norway was used for the major elements and the $\delta^{18}O$ isotope value (−21‰ SMOW) was based on measured values of $\delta^{18}O$ in calcite surface deposits /Tullborg and Larson 1984/. The $\delta^{2}H$ value (−158‰ SMOW) is a modelled value based on the equation ($\delta H = 8 \cdot \delta^{18}O + 10$) for the meteoric water line.
- **Littorina Water:** Represents modelled Littorina water (see Table 2-1).
- **Modified Sea water (Sea sediment):** Represents Baltic Sea affected by microbial sulphate reduction.
- **Baltic:** Corresponds to modern Baltic sea water.
- **Age corrected Rain 1960:** Corresponds to infiltration of meteoric water (the origin can be rain or snow) from 1960. Sampled modern meteoric water with a modelled high tritium content was used to represent precipitation from that period. The age corrected value for the tritium was 168TU.
- **Modern Rain:** Corresponds to modern precipitation.
- **Dilute Groundwater:** corresponds to a shallow groundwater (–56.35 m depth) representing the shallow end member for the local model in Laxemar and Simpervarp area.

2.2.2 Mixing proportions along KLX02 calculated with five different models

The M3 mixing modeling results for KLX02 are shown in Figures 7–10. They are based on the six models presented in section 2.2.

The models 1 and 5 give very similar and feasible mixing proportions along KLX02. The results did not change from the original model (Laxemar 1.2) where all available data major elements, O18 and D were used (Model 5, used for Laxemar 1.2 modeling). The use of a dilute groundwater for the local bedrock model or of a meteoric/rain60 end member gives similar values as well.

Table 2-1. Groundwater analytical or modelled data* used as reference waters in the M3 modelling for Laxemar 2.1.

	Cl (mg/L)	Na (mg/L)	K (mg/L)	Ca (mg/L)	Mg (mg/L)	HCO_3 (mg/L)	SO_4 (mg/L)	^{3}H (TU)	$\delta^{2}H$ ‰	$\delta^{18}O$ ‰
Brine	47,200	8,500	45.5	19,300	2.12	14.1	906	0	–44.9	–8.9
Glacial	0.5	0.17	0.4	0.18	0.1	0.12	0.5	0	–158*	–21*
Littorina sea*	6,500	3,674	134	151	448	93	890	0	–38	–4.7
Sea Sediment	3,383	2,144	91.8	103	258	793	53.1	0	–61	–7
Baltic	3,760	1,960	95	234	93.7	90	325	20	–53.3	–5.9
Rain 1960	0.23	0.4	0.29	0.24	0.1	12.2	1.4	2,000	–80	–10.5
Age corrected Rain 1960	0.23	0.4	0.29	0.24	0.1	12.2	1.4	168	–80	–10.5
Modern Rain	0.23	0.4	0.29	0.24	0.1	12.2	1.4	20	–80	–10.5
Dilute GW	119	237	4	25	6	370	118		–73.8	–9.9

The models 3 and 4 where the Br was used as a variable seem to give unrealistic mixing proportions. The datasets including the Br are very limited, since the Br was not analysed in the older samples. Therefore the datasets are uncompleted for the analyse and the calculations may be erroneous.
The models 2 and 6, where the variables used where only the conservative elements O18, D and Cl are very similar; the use of the dilute groundwater (model2) or of the rain60 (model6) don't change the overall calculations. The Figure 11 shows the comparison between the models 5 and 6. The use of only conservative variables doesn't give unique solution, therefore the benefit of using also non conservative elements. Therefore the bedrock model 5 with all the major components and isotopes as variables and the Littorina, brine, glacial and Meteoric/rain60 (168TU) end-member seems to be the most suitable. The use of rain60 end member allows including more data in the modelling. In addition, when comparing Laxemar and Forsmark sites a common Meteoric end member can help to describe both sites.

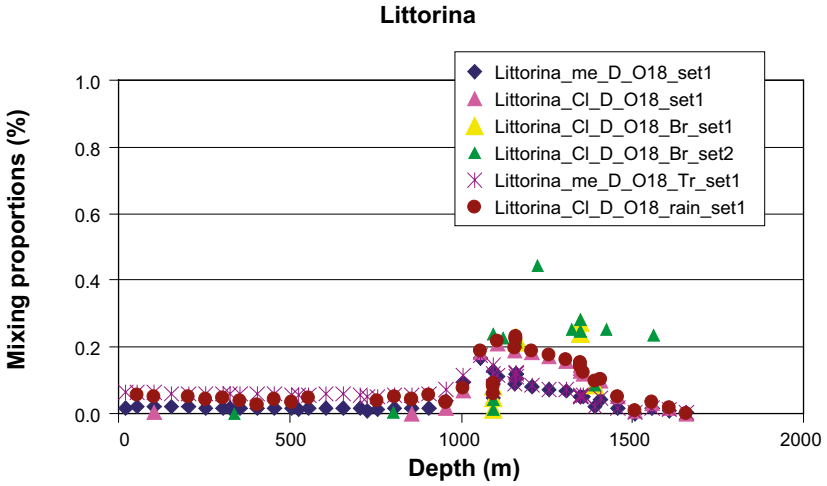

Figure 7. *Littorina mixing proportions along KLX02 calculated for the 6 models, as presented in the paragraph 2.2.*

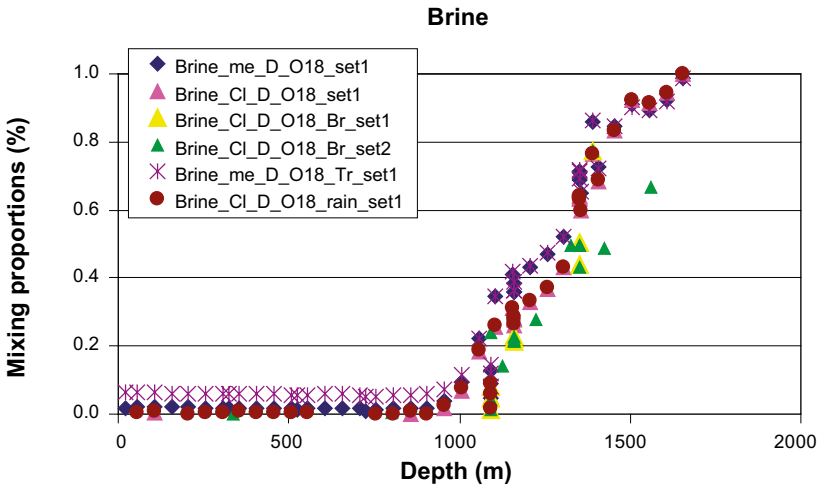

Figure 8. *Brine mixing proportions along KLX02 calculated for the 6 models, as presented in the paragraph 2.2.*

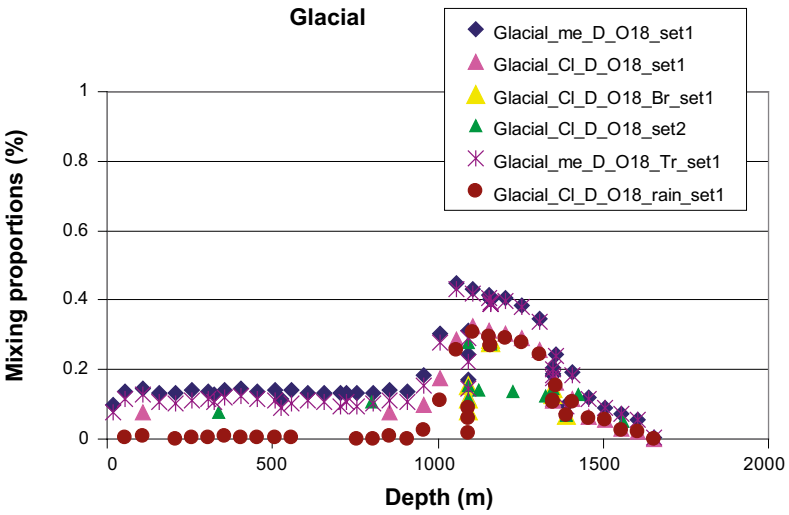

Figure 9. *Glacial mixing proportions along KLX02 calculated for the 6 models, as presented in the paragraph 2.2.*

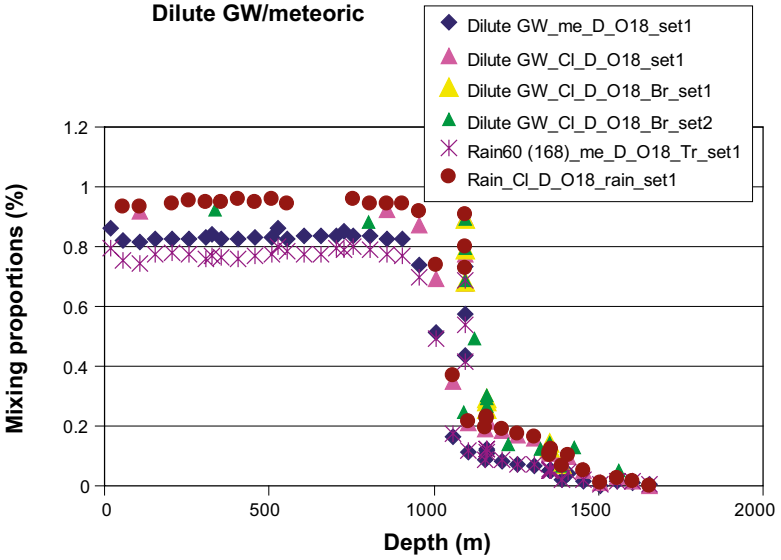

Figure 10. *Surface end member (Dilute Groundwater or Meteoric/Rain60) mixing proportions along KLX02 calculated for the 6 models, as presented in the paragraph 2.2.*

2.3 Conclusions for alternative M3 modelling of the bedrock in Laxemar 2.1

The PCA analysis employing all samples with major elements (Na, K, Ca, Mg, SO4, HCO3, Cl) and isotopes the D, O18 and Tr (non corrected) and with the End members: Littorina, Brine, Glacial, Meteoric (rain60 age corrected) give the most suitable characterization of the Laxemar 2.1 dataset, as following:

- a) more robust calculations and almost all the samples included in the PCA,
- b) the borehole data are not affected by the problems with the Tritium at the surface,
- c) the use of only conservative variables don't give unique solution, therefore the benefit of using also non conservative elements,
- d) returns mixing proportions including the same end members used by the hydrogeologists,
- e) the Br could be a good variable, but not enough data, especially in the old boreholes.

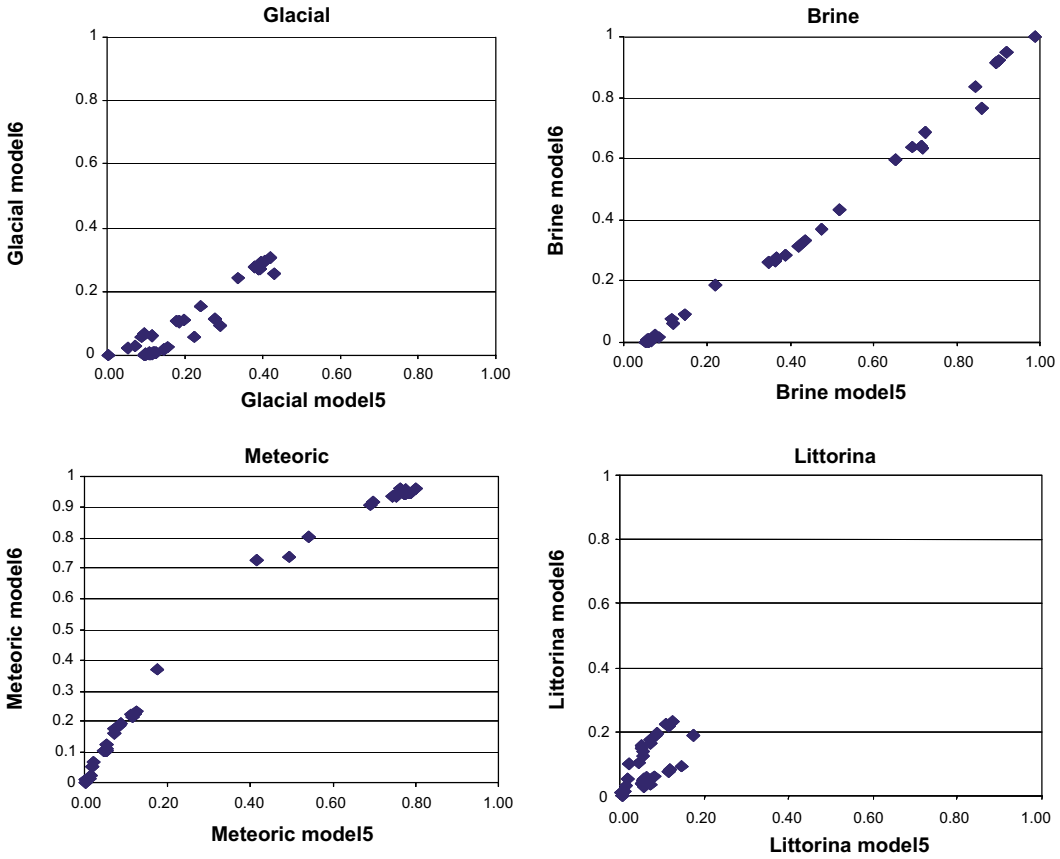

Figure 11. *Comparison of the Mixing proportions along KLX02 for Model 5 and 6.*

Taking into account all these considerations, the model 5 is suggested, based on bedrock data from the K and H boreholes, using as variables major elements, D, O^{18} and Tr, and employing the end members: Littorina, Brine, Glacial and Meteoric (Rain 60 age corrected, with 168TU), as shown in Figure 12. The numerical values are listed in Appendix 1.

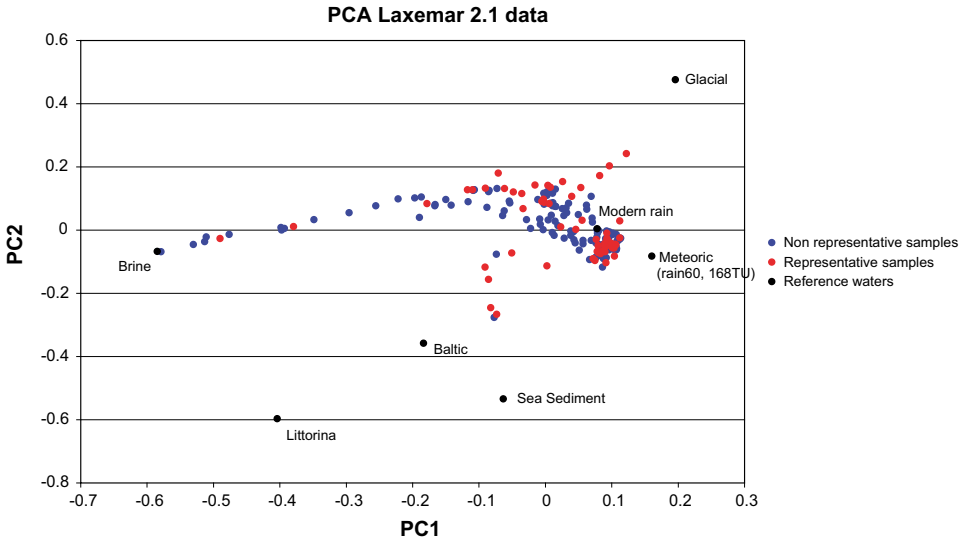

Figure 12. *The picture shows the principal components analysis and the identification of the reference waters for the chosen model number 5 (similar to Figure 6), based on the Laxemar 2.1 bedrock data, and having as variables the major elements, D, O^{18} and Tritium. The Littorina, Brine, Glacial and Meteoric (rain60 with 168 TU) reference waters are used as end members for the modeling and represented in black filled circles. The representative samples are represented in red and the non-representative in blue.*

2.4 Comparison between M3 2D and M3 n-PC codes

The Figures 13 shows the comparison between the different mixing proportions calculated with the old M3 code and the new version M3 2D and M3 hyperspace n-PC. The M3 code is described at the Chapter 2 of this report. The M3 hyperspace code is a new version of the M3 code where to the 2D option is added the possibility to calculate in n dimensions. The new M3 code is on the verification now. The old M3 and the new M3 2D are identical and give the same mixing proportions as shown in the Figure 13. The trend of the M3 2D and M3 n-PC mixing proportions is similar. M3 2D and M3 n-PC calculate similar amount of Brine mixing proportions. M3 n-PC calculates slightly higher values for the Glacial and Littorina mixing proportions. M3 calculates higher Meteoric mixing proportions.

2.5 Discussion regarding the use of the M3 2D and/or M3 n-PC codes

The model used should describe as well as possible the measured data. In order to check the accuracy of the model, the conservative variables Cl and O18 were used. Being considered conservative, the Cl and O^{18} should not be affected by reactions; therefore the values predicted by the models should be as close as possible to the measured data. The Figure 14 shows the calculated values of the Cl and O^{18} versus the measured values.

In order to quantify the accuracy of the model, the RMSE (root mean square error) was calculated for the 2 models, M3 2D and M3 n-PC. The best model is the one with the smallest error, as per the following calculations:

1. Calculate the difference between data and model = the "error" on the model with respect to the data: y_data – y_model.
2. Compute the signed variance of the errors: sigma (error) and the mean error to get rid of biases.
3. Get the RMSE (Root-mean-square error) = SQRT (sigma (error) + (mean_error)^2).
4. The model with the smallest RMSE-ul gives the best predictions.

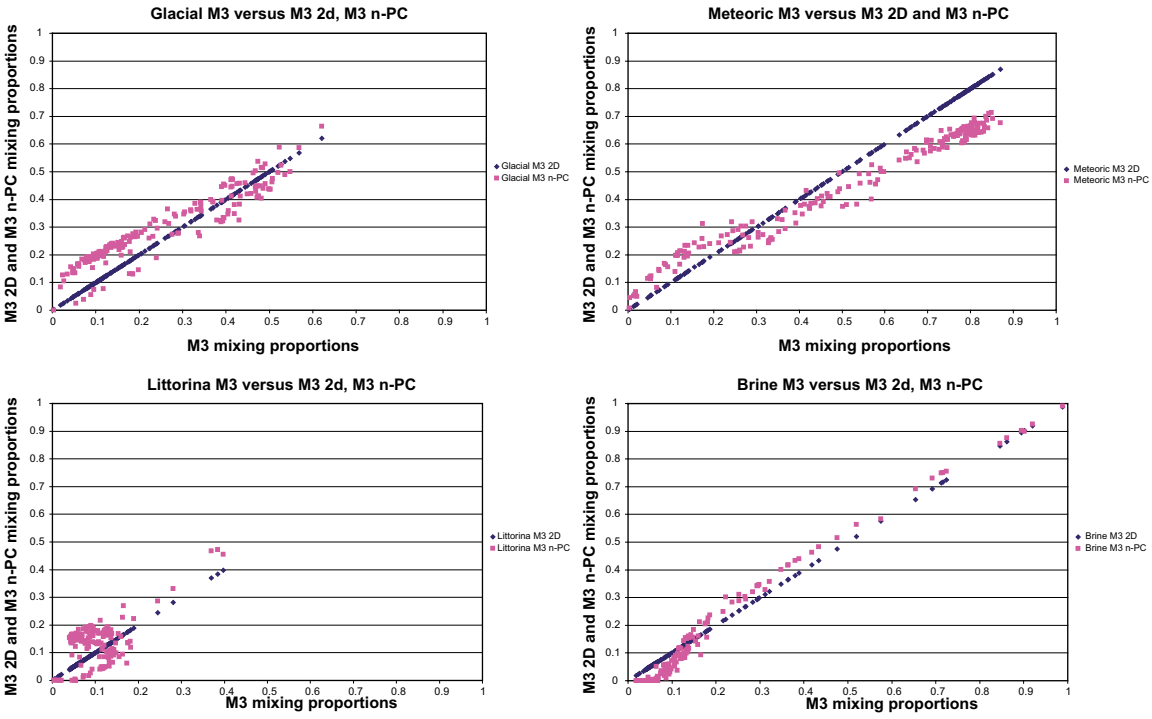

Figure 13. *M3 2D and M3 n-PC glacial, meteoric, Littorina and Brine mixing proportions versus the old M3 code mixing proportions.*

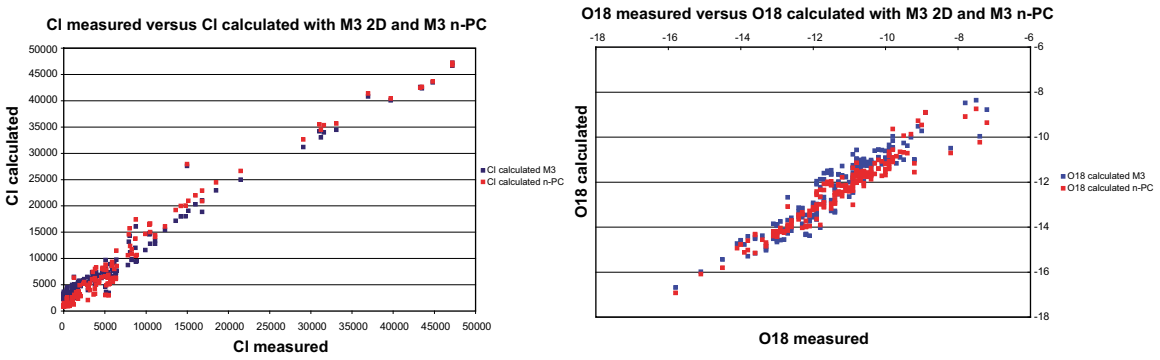

Figure 14. *The Cl and O^{18} values predicted by the M3 2D and M3 n-PC models versus the measured data.*

For example, for the Cl, the RMSE M3 2d is 2,980.4 and RMSE M3 n-PC is 2,625.3.

The Figure 15 shows the measured Cl values and the calculated Cl values with the 2 models.

Both models predict well the Cl. However, for small Cl values, the M3 n-PC model seems to be more adequate.

2.6 Mixing proportions along the core boreholes

The Figure 16 shows the mixing proportions calculated with the models M3 2D and M3 n-PC along the core (K) boreholes.

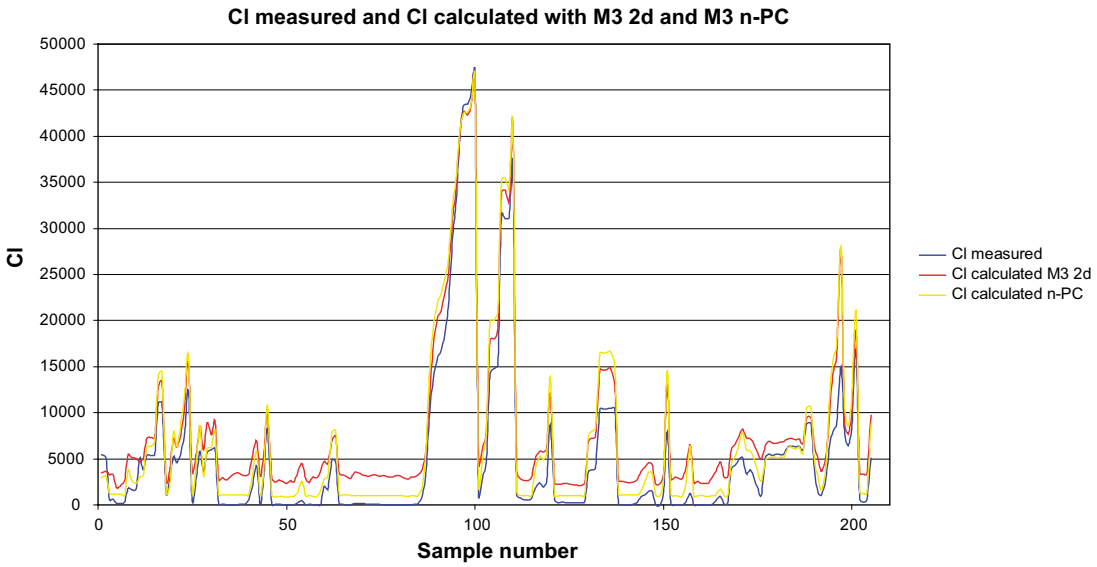

Figure 15. *The measured Cl values and the calculated Cl values with the M3 2D and M3 n-PC models.*

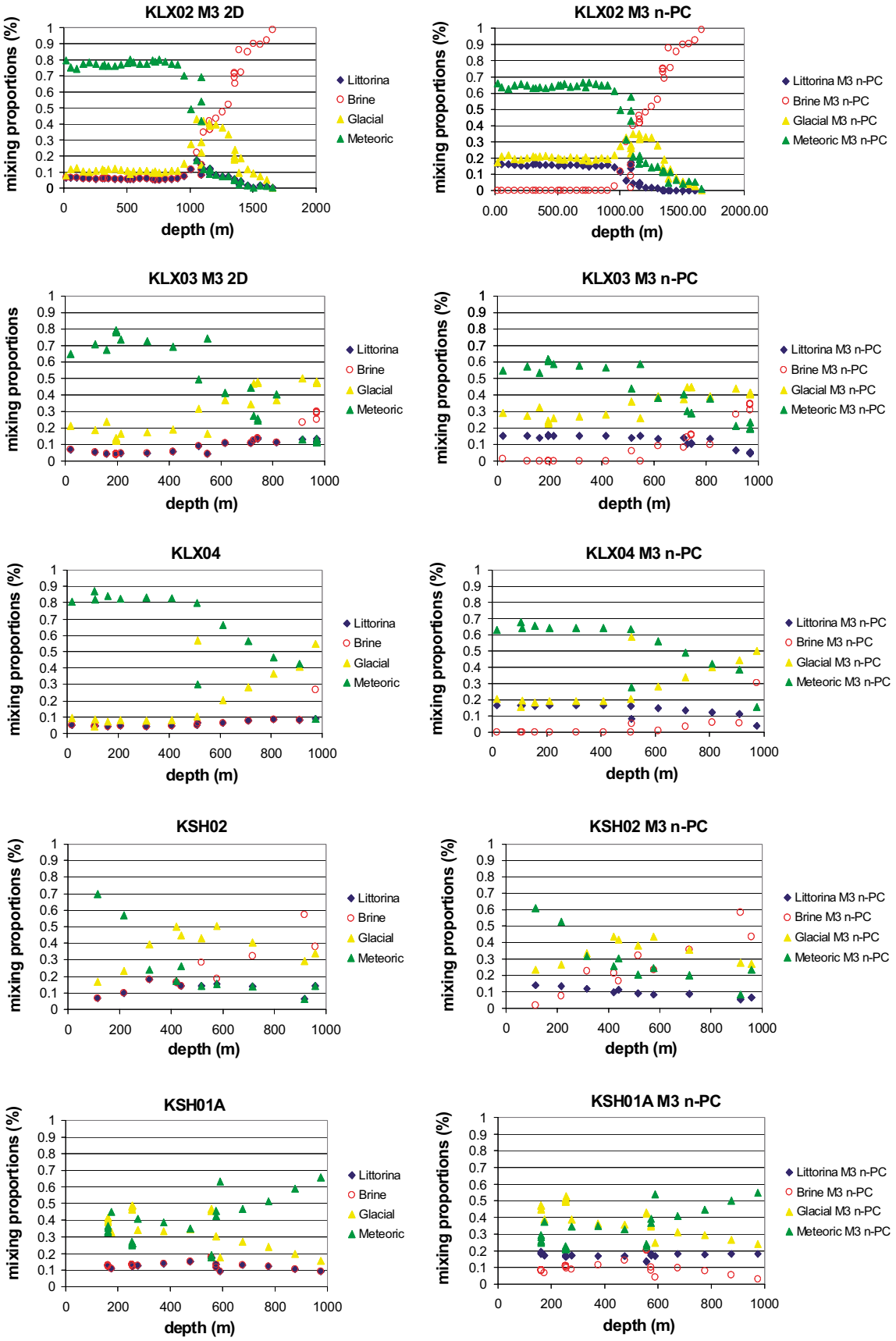

Figure 16. *Mixing proportions calculated with the M3 2D (left) and M3 n-PC (right) along the boreholes KLX02, KLX03, KLX04, KSH02A and KSH01A. In general, M3 n-PC predicts less meteoric and more Littorina and less brine mixing proportions at smallest depths than M3 2D. This can help perhaps to better differentiate, at smallest depths (under 500 m depth), the source of Cl (from brine or sea water).*

3 Site specific hydrogeochemical uncertainties

At every phase of the hydrogeochemical investigation programme – drilling, sampling, analysis, evaluation, modelling – uncertainties are introduced which have to be accounted for, addressed fully and clearly documented to provide confidence in the end result, whether it will be the site descriptive model or repository safety analysis and design /Smellie et al. 2002/. Handling the uncertainties involved in constructing a site descriptive model has been documented in detail by /Andersson et al. 2001/. The uncertainties can be conceptual uncertainties, data uncertainty, spatial variability of data, chosen scale, degree of confidence in the selected model, and error, precision, accuracy and bias in the predictions. Some of the identified uncertainties recognized during the Laxemar modelling exercise and during the DIS exercise are discussed below.

The following data uncertainties have been estimated, calculated or modelled:

- Drilling; may be ± 10–70%.
- Effects from drilling during sampling; is < 5%.
- Sampling; may be ± 10%.
- Influence associated with the uplifting of water; may be ± 10%.
- Sample handling and preparation; may be ± 5%.
- Analytical error associated with laboratory measurements; is ± 5%.
- Mean groundwater variability at Laxemar during groundwater sampling (first/last sample); is about 25%.
- The M3 model uncertainty; is ± 0.1units within 90% confidence interval.

Conceptual errors can occur from e.g. the paleohydrogeological conceptual model. The influences and occurrences of old water end-members in the bedrock can only be indicated by using certain element or isotopic signatures. The uncertainty is therefore generally increasing with the age of the end-member. The relevance of an end-member participating in the groundwater formation can be tested by introducing alternative end-member compositions or by using hydrodynamic modelling to test if old water types can resign in the bedrock during prevailing hydrogeological conditions.

3.1 Model uncertainties

The following factors can cause uncertainties in M3 calculations:

Input hydrochemical data errors originating from sampling errors caused by the effects from drilling, borehole activities, extensive pumping, hydraulic short-circuiting of the borehole and uplifting of water which changes the in situ pH and Eh conditions of the sample, or as analytical errors.

Conceptual errors such as wrong general assumptions, selecting wrong type/number of end-members and mixing samples that are not mixed. Methodological errors such as oversimplification or bias or non-linearity in the model could occur. The systematic uncertainty, which was attributable to use of the centre point to create a solution for the mixing model in the old M3 model, was solved by the new M3 hyperspace model.

Another example of a conceptual error is assuming that the groundwater composition is a good tracer for the flow system. The water composition is not necessarily a tracer of mixing directly related to flow since there is not a point source as there is when labelled water is used in a tracer test.

In M3 2D, another source of uncertainty in the mixing model is the loss of information in using only the first two principal components. The third principal component gathers generally around 10% of the groundwater information compared with the first and second principal components, which contain around 70% of the information. A sample could appear to be closer to a reference water in the 2D surface than in a 3D volume involving the third principal component. In the new version of M3 hyperspace (M3 n-PC) the calculations can also be performed in n dimensions. The results of the modelling show that in M3 2D more data is gathered. In M3 n-PC less data is gathered inside the polyhedron, therefore fewer samples can be modelled but the accuracy of the model/results is higher.

In the old M3 code, the uncertainty in mixing calculations was smaller near the boundary of the PCA polygon and larger near the center. The uncertainties have been handled in the old M3 by calculating an uncertainty of 0.1 mixing units (with a confidence interval of 90%) and stating that a mixing portion < 10% is under the detection limit of the method /Laaksoharju et al. 1999b/.

4 Drilling Impact Study in KLX03

A drilling impact study for the section 408–415 m in KLX03 was intended to be done. The following data were compiled.

- Drilling water in and out from the borehole during drilling.
- Uranine concentration in drilling water in and out from the borehole, Figure 17.
- Water pressure and drawdown during drilling.
- Sampling after drilling: pumping time and uranine concentration.

The uranine concentration in the drilling water should be stable at around 0.200 mg/l. Low concentrations of uranine may reflect some problems with the uranine supply to the drilling water or an analysis problem. Sometimes, how is the case in the fracture that is investigated here, the uranine concentration in the drilling water is even 0.039 mg/l. Unfortunately the quality of the uranine data didn't allow the DIS calculations.

The drilling water pumped out is higher than the volume in and this makes the calculations more difficult. More return water is due the air-lift pumping. This creates a complex situation with mixing of formation water and ingoing flushing water (in general tendency to have more return water in poor rock conditions and more of a balance between in and out in tight rock, H. Ask, personal communication). However, if the uranine is correctly monitored, the return water can be calculated based on the percentage of uranine, and a water balance and DIS calculations can be done.

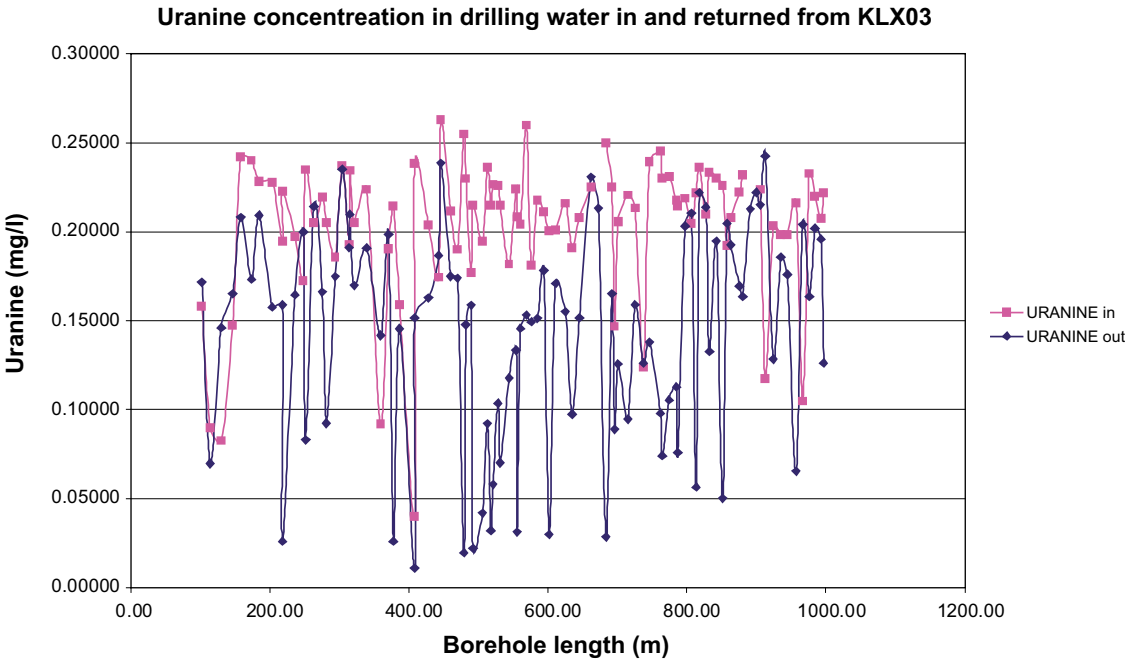

Figure 17. *Uranine concentration in the drilling water pumped in and out from the KLX03 borehole during drilling.*

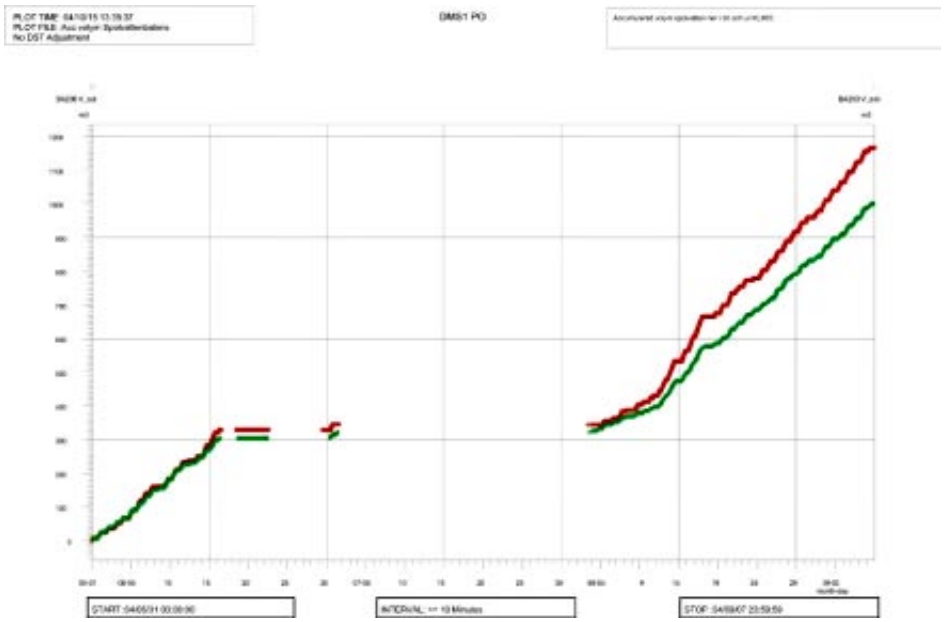

Figure 18. *Drilling water pumped in and out from the borehole KLX03 during drilling.*

5 The use of DIFF measurements

The electrical conductivity (EC) measurements performed during the DIFF (differential flow measurements) measurements could give valuable information about not only the inflow/outflow from the borehole but also disturbances of and changes in chemistry. These measurements are the first measurements conducted after drilling and it is therefore of special interest to follow these changes in comparison with chemistry such as Cl obtained from the borehole at sampling campaigns. The variability can indicate e.g. disturbances and can hence be used for confidence building.

The EC was measured along KLX02 without and during pumping. The EC and the measured Cl during sampling along the borehole are compared in Figure 19. The measured Cl sampled in open borehole seems to resemble the EC measured without pumping. The EC measured during pumping show a much higher salinity than samples taken in open borehole conditions. This indicates again that samples in open borehole reflect mixing processes in the open borehole rather than undisturbed bedrock conditions. For modeling and model calibrations with hydrogeology only sample from sealed off bedrock sections should be used. The EC distribution and the comparison with measured Cl should be investigated in all boreholes.

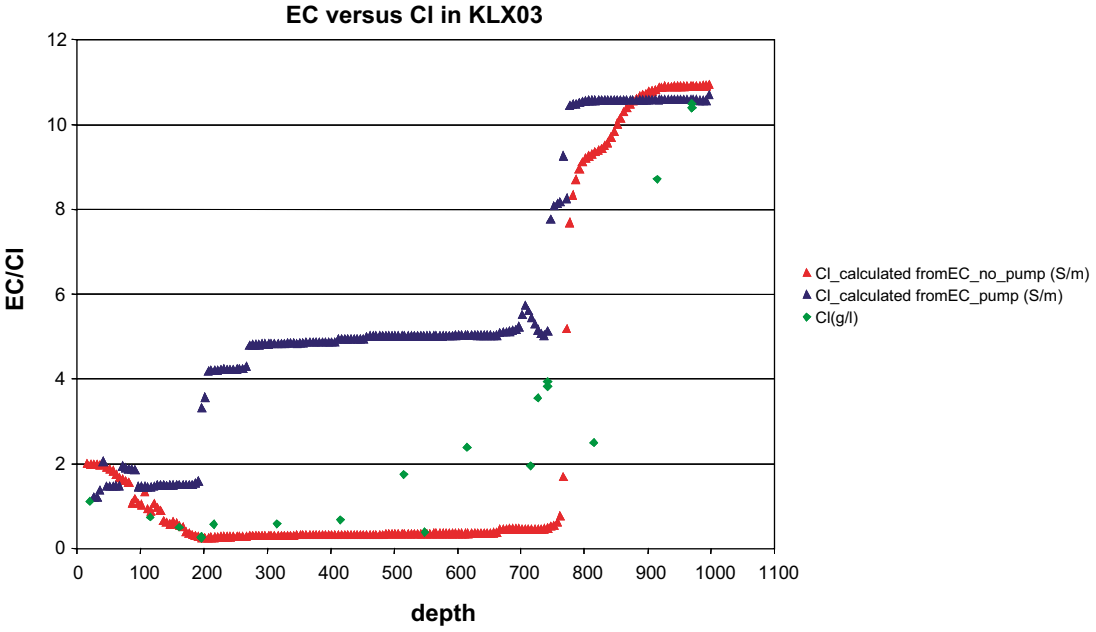

Figure 19. *Electrical conductivity and Cl measured along KLX03.*

6 Concluding remarks

This work represents the phase 2.1 of the hydrochemical evaluation and modelling of the Laxemar data. This comprises M3 modelling, alternative models, explorative data tests and 2D visualisation of the data along the boreholes. The following conclusions are drawn:

- M3 modelling helped to summarize and understand the data. The new M3 code has 2 options: 2D and n-PC (hyperspace), which were used, discussed and the results compared. The new M3 2D code was tested versus the old M3, and the results are identical. The 2D version gathers more data. The n-PC version models fewer samples (the ones included in the polyhedron) but return more accurate mixing proportions.
- The alternative models helped to address different previously unsolved issues such as: the use of tritium as a variable, tests with different end members, the use of the whole data set in order to build a bedrock model, the use of a model built only on conservative variables and the use of other variables as Br.
- The visualisation of the mixing proportions along the boreholes help to understand the distribution of the data in the domain and to check and compare the results of different models; and therefore to chose the model which describes the best the measured data.
- The DIFF and Cl measurements along a borehole can be used to validate the variance in mixing proportions along the borehole. This information can be used for confidence building.
- The different M3 modelling tests resulted in the following conclusions: a) When calculating mixing proportions only samples from the boreholes will be used, b) the meteoric end member which describes the best the more shallow groundwater compositions is defined by the rain60 water composition, with the tritium value age corrected (168TU); the other end-members such as Littorina and Glacial employed the existing modeled compositions. The use of the Littorina, Glacial, Brine and Meteoric end members makes possible the comparison of different sites such as Laxemar and Forsmark.

7 References

Andersson J, Christiansson R, Munier R, 2001. Djupförvarsteknik: Hantering av osäkerheter vid platsbeskrivande modeller. SKB TD-01-40, Svensk Kärnbränslehantering AB.

Gurban I, Laaksoharju M, Ledoux E, Made B, Salignac AL, 1998. Indications of uranium transport around the reactor zone at Bagombé (Oklo). SKB TR-98-06, Svensk Kärnbränslehantering AB.

Laaksoharju M, Smellie J, Nilsson A-C, Skårman C, 1995a. Groundwater sampling and chemical characterisation of the Laxemar deep borehole KLX02. SKB TR 95-05, Svensk Kärnbränslehantering AB.

Laaksoharju M, Skårman C, 1995b. Groundwater sampling and chemical characterisation of the HRL tunnel at Äspö, Sweden. SKB Progress Report PR 25-95-29, Svensk Kärnbränslehantering AB.

Laaksoharju M, Wallin B (eds.), 1997. Evolution of the groundwater chemistry at the Äspö Hard Rock Laboratory. Proceedings of the second Äspö International Geochemistry Workshop, June 6–7, 1995. SKB International Co-operation Report ISRN SKB-ICR-91/04-SE. ISSN 1104-3210, Svensk Kärnbränslehantering AB.

Laaksoharju M, Gurban I, Skårman C, 1998. Summary of the hydrochemical conditions at Aberg, Beberg and Ceberg. SKB TR 98-03, Svensk Kärnbränslehantering AB.

Laaksoharju M, Gurban I, Andersson C, 1999a. Indications of the origin and evolution of the groundwater at Palmottu. The Palmottu NaturalAnalogue Project. SKB TR 99-03, Svensk Kärnbränslehantering AB.

Laaksoharju M, Skårman C, Skårman E, 1999b. Multivariate Mixing and Mass-balance (M3) calculations, a new tool for decoding hydrogeochemical information. Applied Geochemistry Vol. 14, #7, 1999, Elsevier Science Ltd., pp 861–871.

Laaksoharju M, Tullborg E-L, Wikberg P, Wallin B, Smellie J, 1999c. Hydrogeochemical conditions and evolution at Äspö HRL, Sweden. Applied Geochemistry Vol. 14, #7, 1999, Elsevier Science Ltd., pp 835–859.

Laaksoharju M, 1999d. Groundwater Characterisation and Modelling: Problems, Facts and Possibilities. Dissertation TRITA-AMI-PHD 1031; ISSN 1400-1284; ISRN KTH/AMI/PHD 1031-SE; ISBN 91-7170-. Royal Institute of Technology, Stockholm, Sweden. Also as SKB TR-99-42, Svensk Kärnbränslehantering AB.

Laaksoharju M (editor), Smellie J, Gimeno M, Auqué L, Gomez, Tullborg E-L, Gurban I, 2004. Hydrochemical evaluation of the Simpevarp area, model version 1.1. SKB R 04-16, Svensk Kärnbränslehantering AB.

Smellie J, Karlsson F, 1996. A reappraisal of some Cigar-Lake issues of importance to performance assessment. SKB TR-96-08, Svensk Kärnbränslehantering AB.

Smellie J, Laaksoharju M, Tullborg E-L, 2002. Hydrochemical site descriptive model – a stategy for the model development during site investigation. SKB R-02-49, Svensk Kärnbränslehantering AB.

Tullborg E-L, Larson S Å, 1984. δ18O and δ13C for limestones, calcite fissure infillings and calcite precipitates from Sweden. Geologiska föreningens i Stockholm förhandlingar 106(2).

Appendix 1

Measured data and M3 mixing calculations for Laxemar 2.1, bedrock data, model 5

This file is stored in the SKB database SIMON.

13 Appendix 5: Coupled hydrogeological and solute transport modelling

Contribution to the model version 2.1

Jorge Molinero and Juan Ramón Raposo

Área de Ingeniería del Terreno

Universidade de Santiago de Compostela.

Escola Politécnica Superior. Lugo

August 2006

Contents

1 Introduction

The work presented here constitutes an attempt to combine hydrogeological and hydrochemical analysis of the Laxemar subarea, within the framework of the study performed by the ChemNet Group supported by SKB.

It was determined in previous modelling phases that one of the weakest points of the hydrochemical analysis and, especially, for integration with hydrogeology, was related to the lack of spatial representation and visualization of available data. During the last year, the USC team has been working on the development of a tool for visual modelling of available hydrochemical and isotopic information, both in the near-surface and in the bedrock environments, combined with geographical information (topography, coast lines, etc.), geometrical objects (such as boreholes and tunnel) and geo-hydrological information (deformation zones – hydraulic conductor domains). There are a number of commercial tools able to represent hydrochemical information in space, but usually they are intended to visualize either computed model results or geo-statistically interpolated trends, which are not appropriate when few data and/or highly heterogeneous and fractured media are analysed.

Chapter 2 summarized the main findings achieved by using advanced 3D visualization techniques with the available Laxemar 2.1 hydrochemical database. It includes the spatial analysis measured field data as well as the visualization of the externally computed results such as mixing and geo-chemical models. As a novelty, in this report a combined visualization of the hydrogeological model results and hydrochemical information is shown for the first time.

Chapter 3 presents a summary of the main results of flow and reactive transport numerical modelling. A two-step methodology was developed and tested in previous modelling phases which allows fluid density-driven groundwater flow and reactive solute transport numerical modelling. The methodology has been applied to a 2D large scale cross section model which accounts for an accurate topographic representation of the site. The model has been calibrated against available hydraulic parameters and hydrochemical information. The reactive transport model has been improved accounting for a number of coupled hydrochemical processes, including mineral dissolution/precipitation under both local equilibrium and kinetic approaches. It is woth noting that the present model is restricted to current hydrogeological settings, neglecting recent paleo events such as glacial melt water infiltration or coastline displacement. In this way, computed results can not be calibrated/compared with some available information such as environmental isotopes. These paleo events are being studied by means of other model approaches such as pure hydrochemical mixing models or pure hydrogeological models in the framework of HydroNet activities.

Finally, the main conclusions and possible future developments are summarized in Chapter 4.

2 Visualization and spatial analysis of the hydrochemical database

2.1 Visualization of bedrock hydrochemical database

Figure 2-1 shows a view for the location of the main cored boreholes (from the point of view of the number of representative samples) available in Laxemar and Simpevarp subareas, as they are named in the datafreeze of Laxemar 2.1.

Figure 2-2 shows all the available representative chloride data in the bedrock samples.

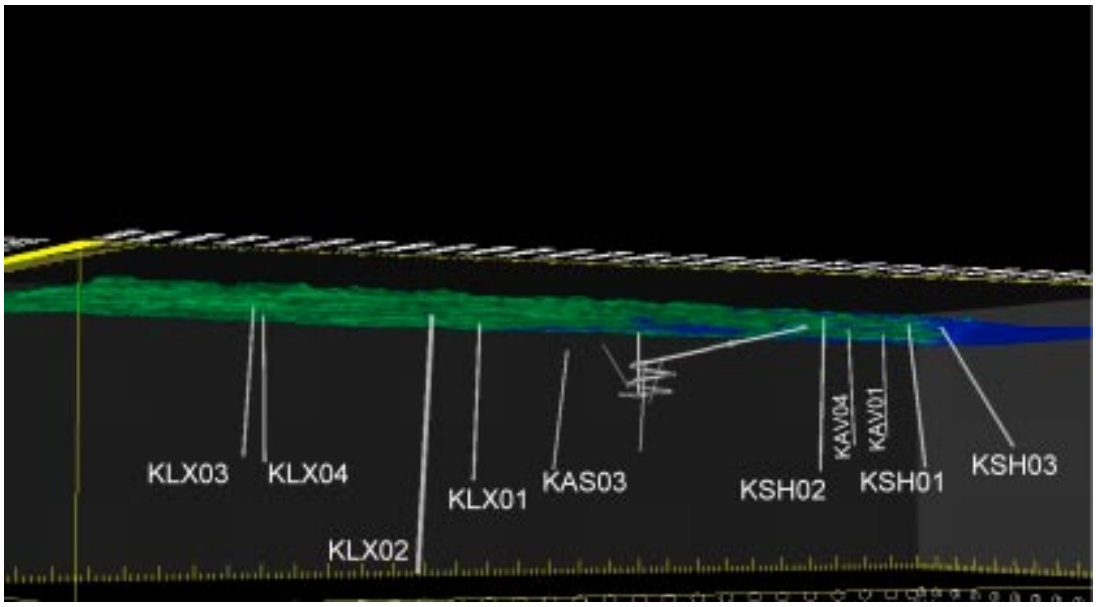

Figure 2-1. *3D-view (from the southwest) of Laxemar and Simpevarp subareas. Main cored boreholes, as well as the Äspö tunnel, have been included as geographical references in the visualization.*

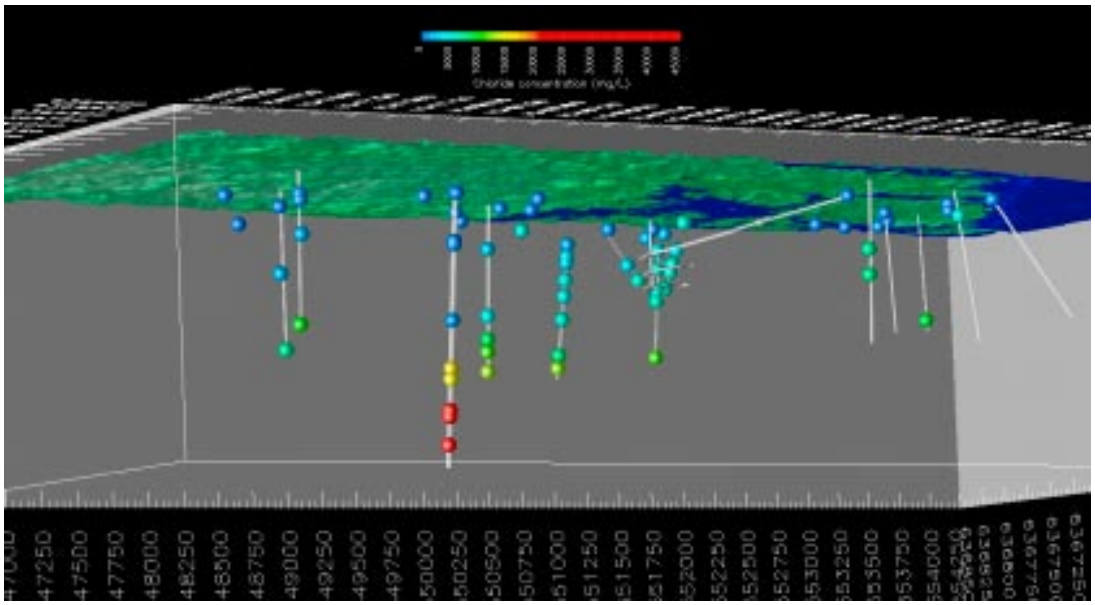

Figure 2-2. *Distribution of chloride concentrations at the bedrock under the Laxemar and Simpevarp subareas. Symbol size is proportional to the chloride concentration value.*

Figure 2-2 shows the occurrence of brine water at depth in Laxemar subarea. The brine has been detected in water samples of borehole KLX02 at a depth greater than 1,100 m. It is worth noting the difference of salinity between the groundwater of Laxemar and Simpevarp subareas. Laxemar subarea represents a continental (inland) hydrogeological framework, with a thick fresh water body reaching depths of nearly 1,000 m. However, the Simpevarp subarea represents a coastal hydrogeological framework where fresh water bodies are confined to the first 100–200 m of the bedrock.

According to the water classification used by /Laaksoharju et al. 2004/, four main hydrochemical water types have been identified in the Simpevarp area, named from type A to type D /Laaksoharju et al. 2004/.

Water Type A. This type comprises dilute groundwaters (< 1,000 mg/L Cl; 0.5–2.0 g/L TDS) mainly of Na-HCO_3 type present at shallow (< 200 m) depths at Simpevarp subarea, but at greater depths (0–900 m) at Laxemar subaraea. At both subareas the groundwaters are marginally oxidising close to the surface, but otherwise reducing. Figure 2-3 shows a visualization of the spatial distribution of water type A (diluted). This type of water is interpreted as related to a meteoric origin, and shows higher bicarbonate contents. Figure 2-4 shows the spatial distribution of bicarbonate concentrations. It can be seen that the higher values of bicarbonate concentrations coincides almost exactly with diluted groundwater (type A). The high bicarbonate concentration can be mainly attributed to the occurrence of organic matter oxidation coming from the soil layers at emerged lands.

Water Type B. This type comprises brackish groundwaters (1,000–6,000 mg/L Cl; 5–10 g/L TDS) present at shallow to intermediate (150–300 m) depths at Simpevarp subarea, but at greater depths (approx. 900–1,100 m) at Laxemar subarea. The origin of this water type could be different from one place to another. At Simpevarp subarea there is potentially some residual Littorina Sea (old marine) influence. In contrast, at the Laxemar subarea this water type could mainly be attributed to the influence (dispersion/diffusion) of deep brine water. Figure 2-5 shows a visualization of the spatial distribution of water type B (brackish).

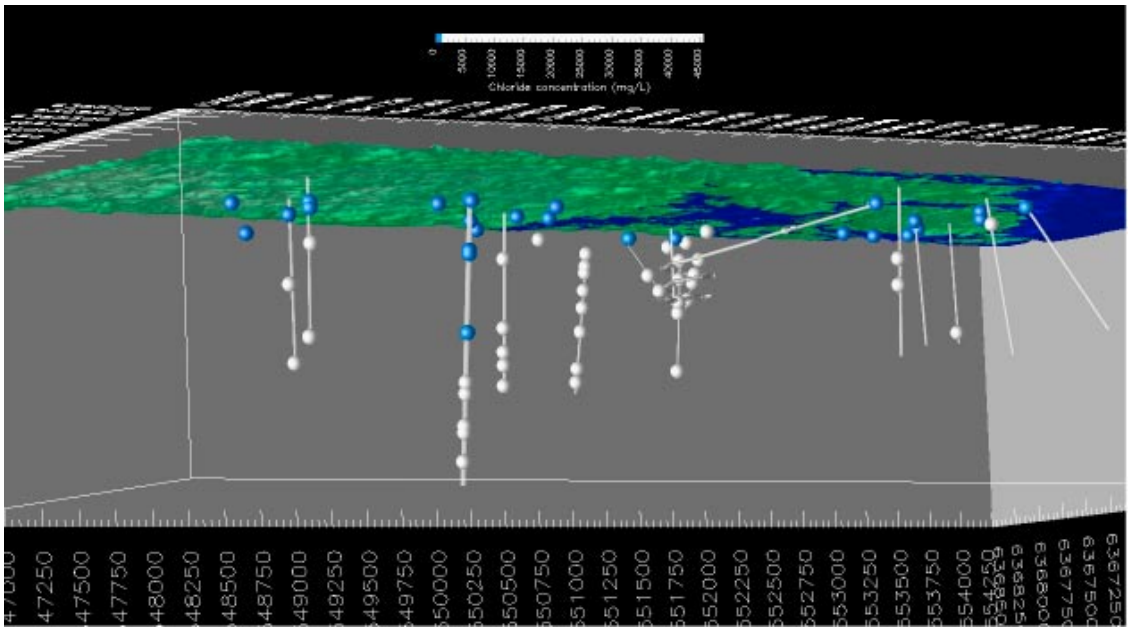

Figure 2-3. *Spatial distribution of water type A (diluted), which can be related to a meteoric origin. It can be noticed that this type of water reaches much higher depths at Laxemar subarea than at Simpevarp subarea.*

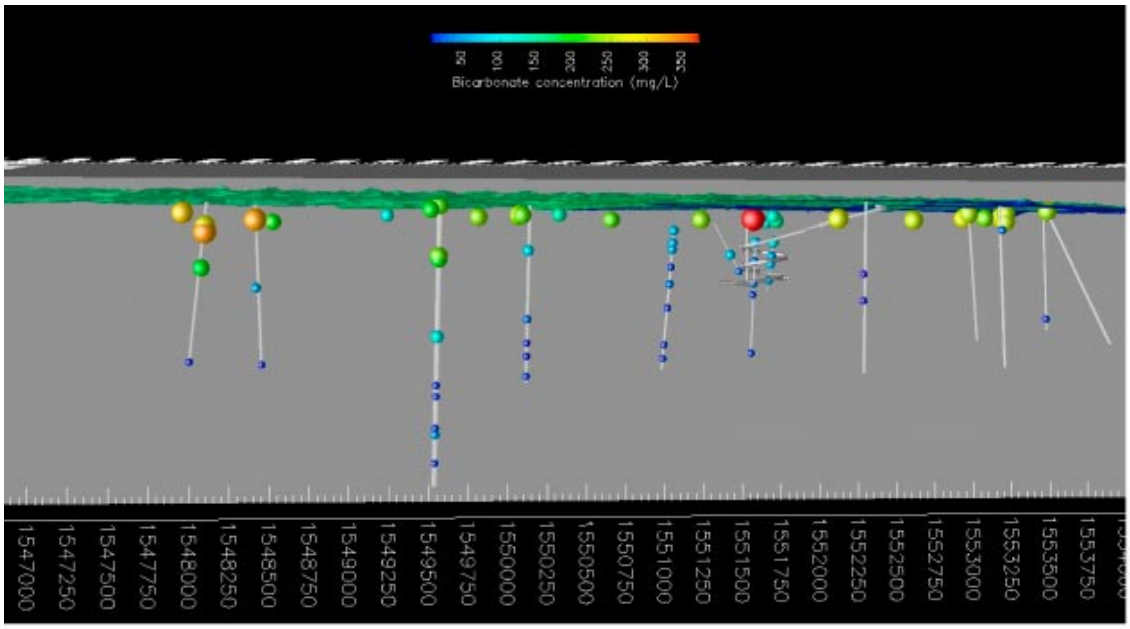

Figure 2-4. *Spatial distribution of bicarbonate concentrations. By comparing this figure with Figure 2-3 it can be noticed that diluted water (type A) show the highest bicarbonate concentrations, probably related with oxidation of organic matter from the surface soil layers.*

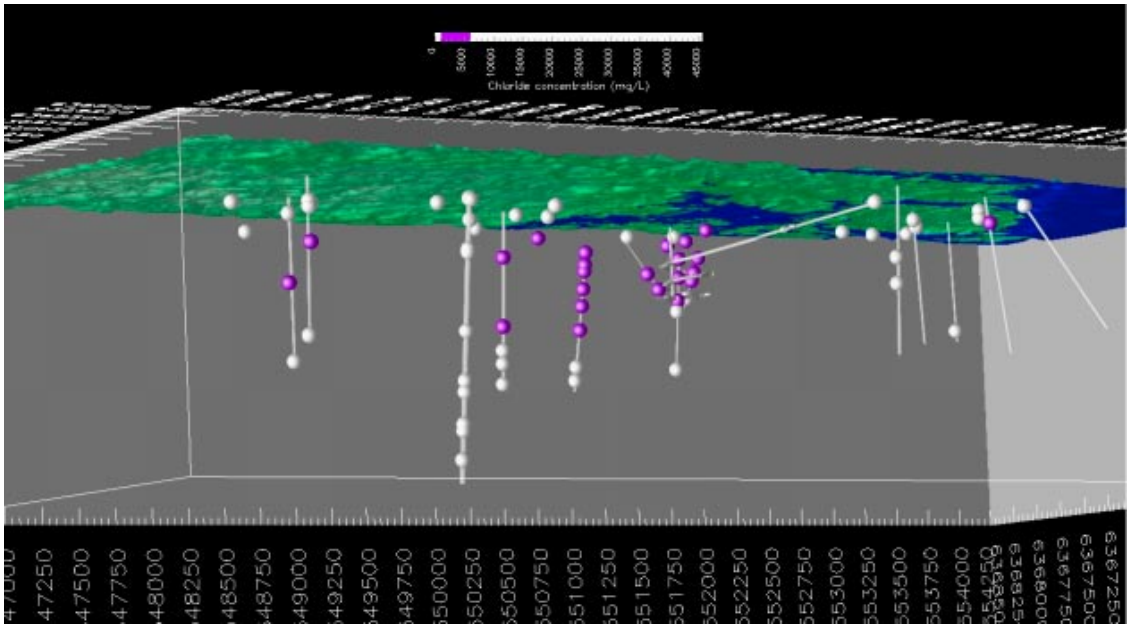

Figure 2-5. *Spatial distribution of water type B (brackish). This type of water is found at relatively shallow depths in Simpevarp subarea (mainly under Äspö), but also in Laxemar close to the coast (KLX01). Inland (KLX02-03-04) this type of water is found deeper, from 600 to 1,100 meters.*

The complex origin of this water type B can be better understood by analysing other hydrochemical information. Figure 2-6 shows the spatial distribution of magnesium in groundwater. It can be noticed that high magnesium concentrations are found in the Simpevarp subarea, exactly for the same water samples corresponding to water type B (brackish). However, water type B at the Laxemar subarea shows low magnesium contents compared to the Simpevarp subarea. Magnesium is not a conservative element. On the contrary, it is well known that Mg can be involved in cation

exchange processes, mainly in fractures and fracture zones containing clay minerals. However, according to /Laaksoharju 1999/ the average magnesium concentration in Baltic water is 234 mg/L, while deep brine waters at KLX02 shows very low concentrations of magnesium (about 2 mg/l). This high contrast could be qualitatively useful to establish a difference between the salinity of the brackish waters at Laxemar and Simpevarp subareas. By comparing Figures 2-5 and 2-6 it can be seen that brackish waters at Laxemar are most likely related to the occurrence of a dispersion zone between deep saline waters and shallow diluted water of meteoric origin, while brackish waters of the Simpevarp subarea show an influence of marine waters. These marine waters could be older than the current Baltic Sea corresponding to the Littorina sea stage.

Water Type C. This type comprises saline groundwaters (6,000–20,000 mg/L Cl; 25–30 g/L TDS) present at intermediate depths (> 200–300 m) at the Simpevarp subarea, and at greater depths (> 1,000 m) at Laxemar subarea. Similarly to water type B, this type C shows different hydrochemical signatures from one place to another. At the Simpevarp subarea (but also at coastal Laxemar locations; i.e.KLX01) signatures of old marine influence can be recognized (see magnesium in Figure 2-6), together with glacial signatures (as will be shown latter on). On the contrary, at the Laxemar subarea this water type could mainly be attributed to the influence (dispersion/diffusion) of deep brine which is found adjacent in depth. Figure 2-7 shows a visualization of the spatial distribution of water type C (saline).

Glacial isotopic signatures have been postulated to be present in groundwater at different places of Scandinavian bedrock locations. According to /Laaksoharju 1999/, when the continental ice melted and retreated (about 13,000 years ago), glacial meltwater was hydraulically injected under considerable head pressure into the bedrock. The exact penetration depth of glacial water is uncertain but, according to /Jaquet and Siegel 2003/, a depth of several hundreds meters can be expected according to hydrogeological models.

The best tracers for glacial water signatures are assumed to be the stable isotopes 18-O and 2-H. According to /Laaksoharju 1999/, the isotopic composition for a Glacial end-member water is –21‰ SMOW for $\delta^{18}O$, and –158‰ SMOW for $\delta^{2}H$. The clearest glacial signature at the Simpevarp area was found under the Äspö island (KAS03) during the site characterization process before the construction of the tunnel. Figures 2-8 and 2-9 show the spatial distribution of water samples with ^{18}O lower than –13‰ and ^{2}H lower than –90‰, respectively. Those "cutting values" are arbitrarily assumed, but has been postulated in previous modelling phases as useful values to detect possible glacial signatures in brackish and saline groundwaters.

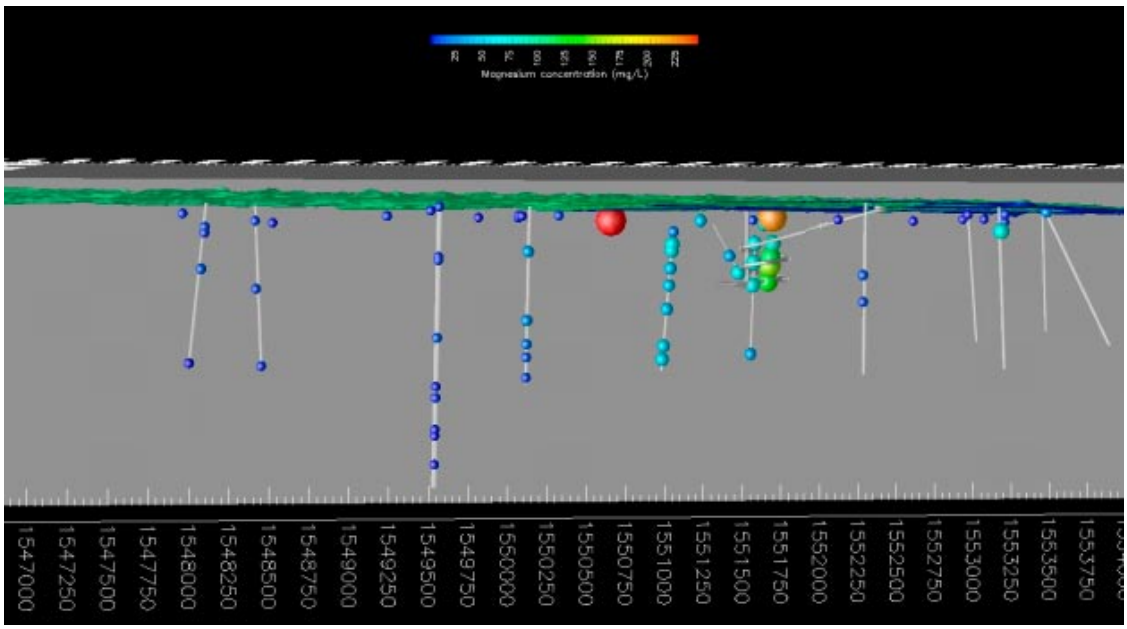

Figure 2-6. *Spatial distribution of dissolved magnesium in groundwater. It can be seen that maximum magnesium concentrations are found in the Simpevarp subarea, indicating a possible influence of older marine waters.*

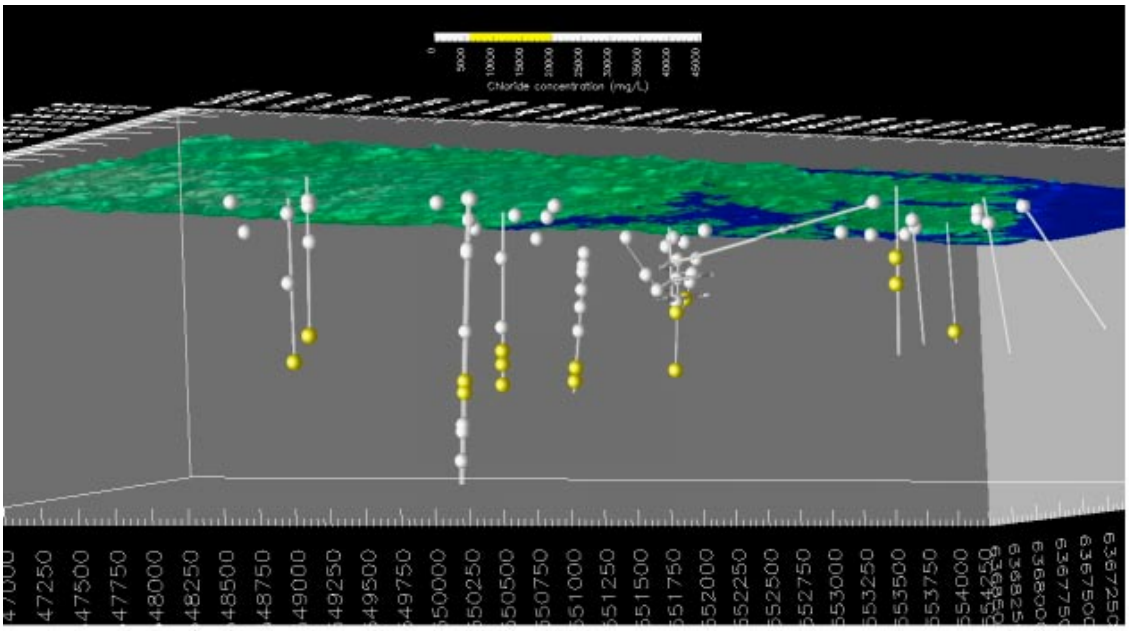

Figure 2-7. *Spatial distribution of water type C (saline). This type of water is found at shallow to intermediate depths in Simpevarp subarea, and deeper at Laxemar (800–1,200 meters).*

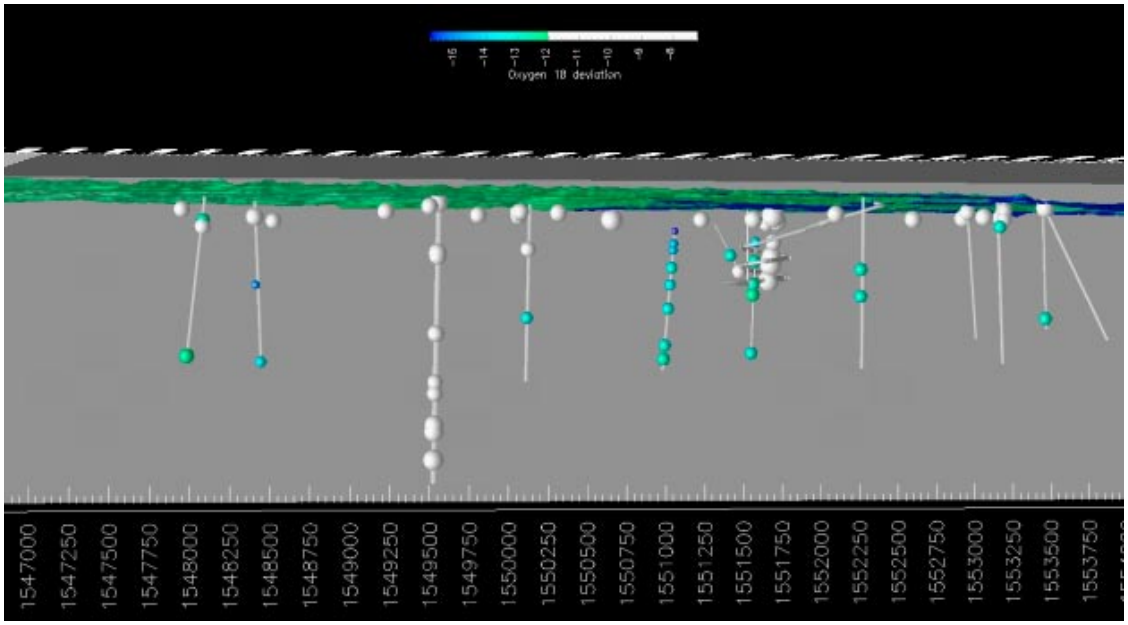

Figure 2-8. *Spatial distribution of ^{18}O deviations at Laxemar and Simpevarp subareas. A clear minimum value at KAS03 (under Äspö) can be seen which correspond to the Glacial Reference Water /Laaksoharju 1999/.*

According to Figures 2-8 and 2-9, glacial isotopic signatures can be recognized at the Simpevarp subarea, specially under the Äspö island and the Simpevarp peninsula. The clearest signature corresponds to borehole KAS03 at a shallow depth (about –120 m.a.s.l.). At the Laxemar subarea, week glacial signatures appear to be present deeper than in Simpevarp subarea. It is worth noting that all glacial signatures are found at groundwater type samples B and C (brackish or saline).

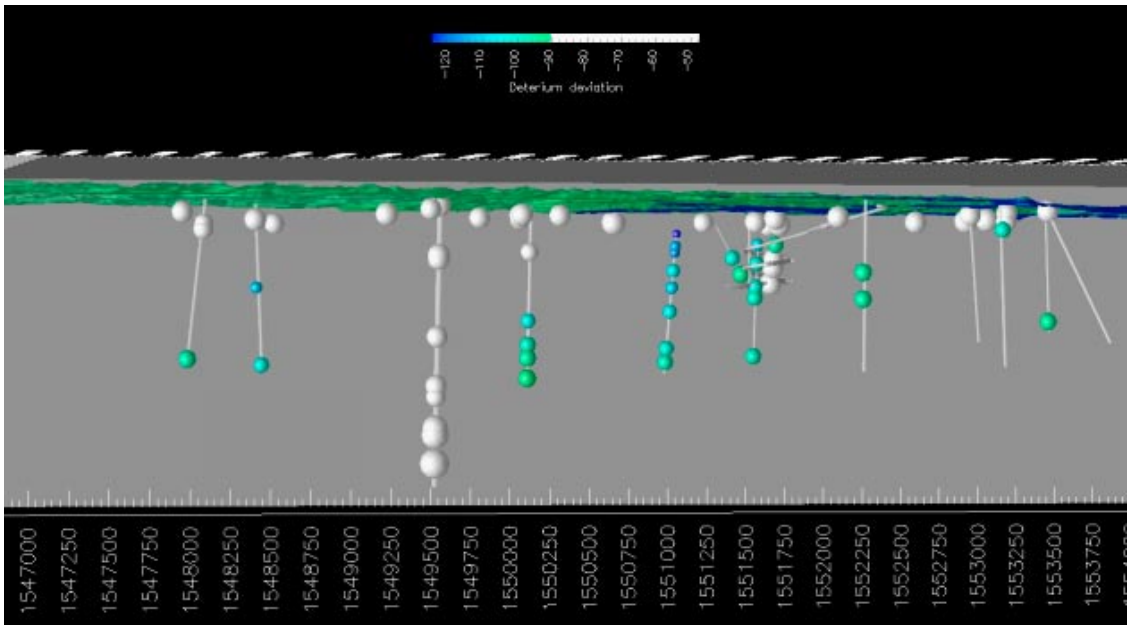

Figure 2-9. *Spatial distribution of ^{2}H deviations at Laxemar and Simpevarp subareas. A clear minimum value at KAS03 (under Äspö) can be seen which correspond to the Glacial Reference Water /Laaksoharju 1999/.*

Water Type D. This type comprises highly saline groundwaters (> 20,000 mg/L Cl; to a maximum of ~ 70 g/L TDS) and have only been identified in one borehole at Laxemar (KLX02) at depths exceeding 1,200 m. Figure 2-10 shows a visualization of the spatial distribution of water type D (highly saline, also named "brine").

Water samples of type D (highly saline) show also the highest concentrations of sulphates in bedrock groundwater (Figure 2-11).

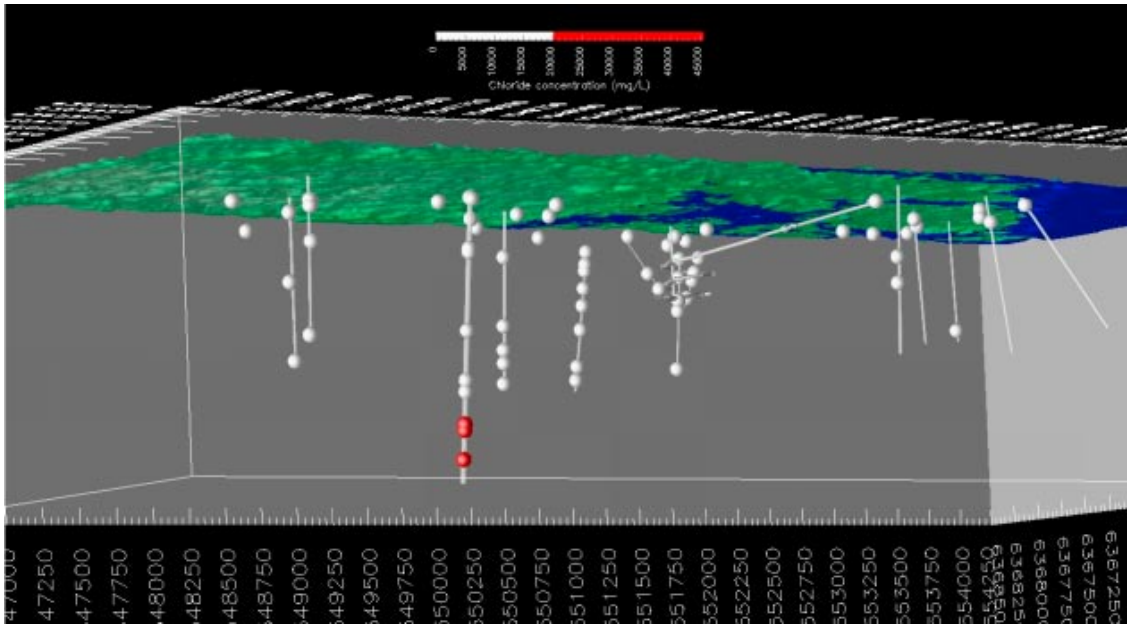

Figure 2-10. *Spatial distribution of water type D (highly saline). This type of water has been only found at borehole KLX02 (Laxemar), at depths from –1,200 to –1,600 m.a.s.l.*

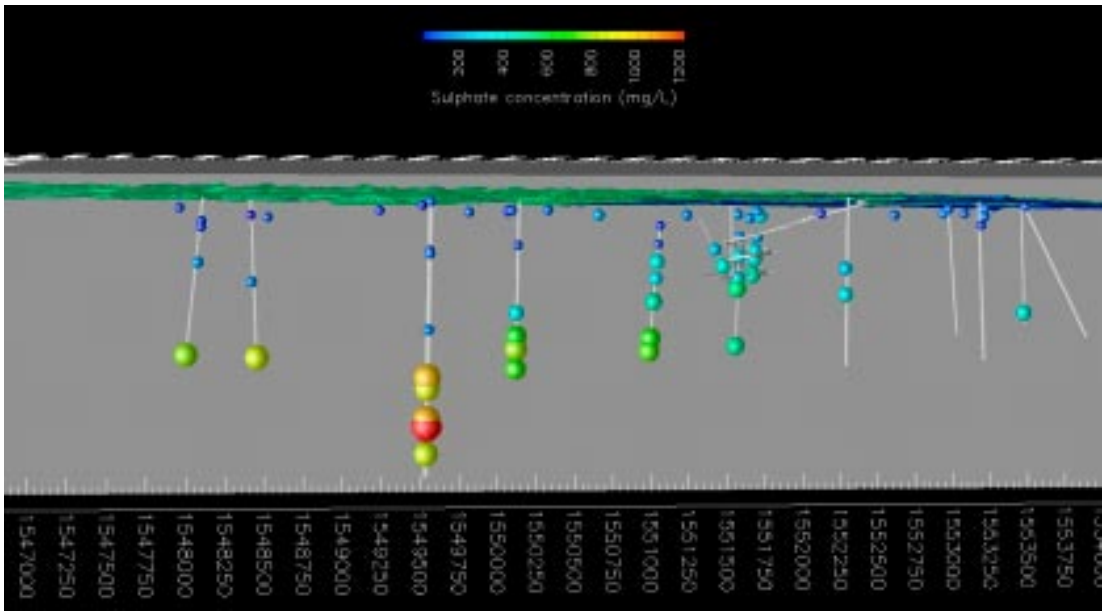

Figure 2-11. *Spatial distribution of dissolved sulphates at Laxemar and Simpevarp subareas.*

Figure 2-12, shows a visualizations of the spatial distribution of the four water types in Laxemar and Simpevarp subareas. It can be seen that diluted water (type A) extends deeper at inland Laxemar positions compared to Laxemar coastal positions and the Simpevarp subarea, where diluted waters are only found at very shallow depths in the bedrock. On the contrary, brackish and saline waters (types B and C) are predominant at Laxemar coastal areas (KLX01) and at the Simpevarp subarea. Within the Simpevarp subarea, saline waters (type C) are found at much shallower depths under the Simpevarp Peninsula than under Äspö and Ävrö islands.

Even it is not shown in this report, most dissolved species show qualitative trends very similar to chlorides. This could be taken as an indication of the important role of physical transport processes (dispersion-diffusion; i.e mixing) in the hydrochemical nature of bedrock groundwater in Laxemar and Simpevarp subareas.

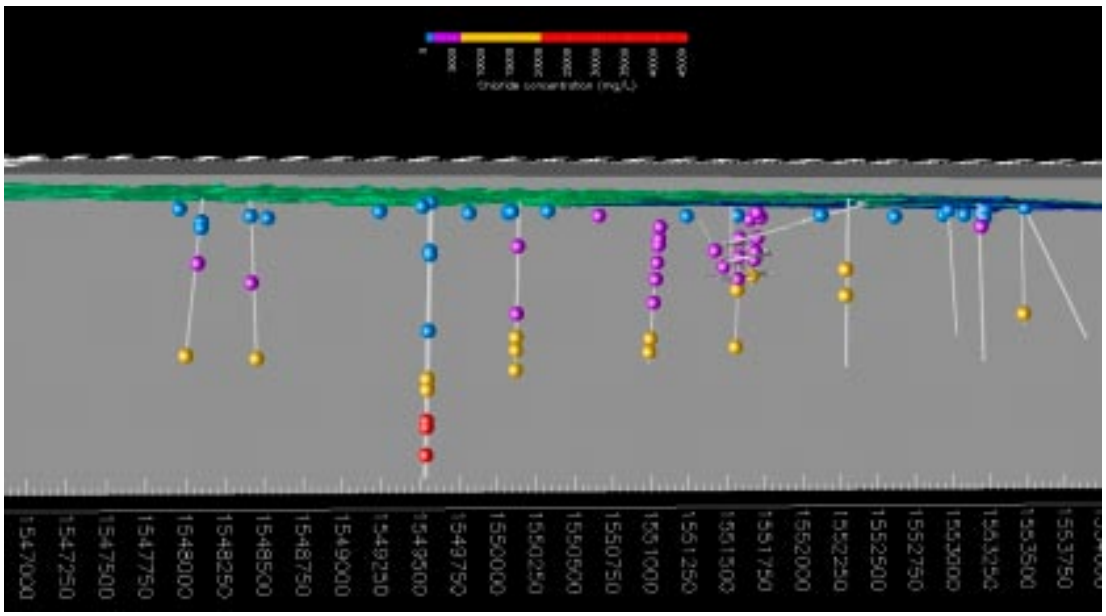

Figure 2-12. *Bottom view from the Southwest of the spatial distribution of water types in Laxemar and Simpevarp subareas. Water type A (blue), B (purple), C (yellow) and D (red).*

2.2 Combined visualization of bedrock hydrochemical database and hydrogeological model results

Combined visualization of measured hydrochemical concentrations and computed results obtained with hydrogeological models constitute a useful tool for qualitative assessment of model performance. On the other hand, the visualization of hydrogeological model results performed within the framework of HydroNet Team /Hartley et al. 2004, 2005, 2006/ provide also a useful tool in order to understand the spatial variability of the site hydrochemistry, since the hydrogeological models account for the discrete nature of the fractured bedrock. In this respect, to analyse hydrogeological model results combined with discrete hydrochemical data could provide a better approach than pure data interpolation in order to understand the hydrochemisty of the site. For that purpose, three reference cross sections have been selected to extract computed results from hydrogeological models /Hartley et al. 2005/, coinciding with the maximum number of available deep hydrochemical observations. 2 NW-SE sections and 1 SW-NE section were selected. Figure 2-13 shows the location of the 3 selected cross sections.

Figures 2-14, 2-15 and 2-16 show two different views of computed chloride concentrations together with the main boreholes and the Äspö tunnel for easiest location.

Figure 2-16 illustrates the hydrogeological effect on the chloride distribution. The fresh water body is much thicker under Laxemar subarea (inland) than under Simpevarp subarea (near the coast). The groundwater discharge zone under the Baltic estuary between the Laxemar subarea and the Simpevarp peninsula can be seen clearly in Figures 2-15 and 2-16. The heterogeneity of fractured bedrock is reflected in the computed chloride concentrations (Figure 2-16).

Figures 2-17, 2-18 and 2-19 show three examples of combination between hydrogeologic computed results and chloride measurements. It can be seen than there is a very good qualitative agreement between model results and measurements in terms of a conservative tracer such as chloride.

Figure 2-13. *Plan view of the traces of the 3 selected cross sections to extract computed results from the hydrogeological models.*

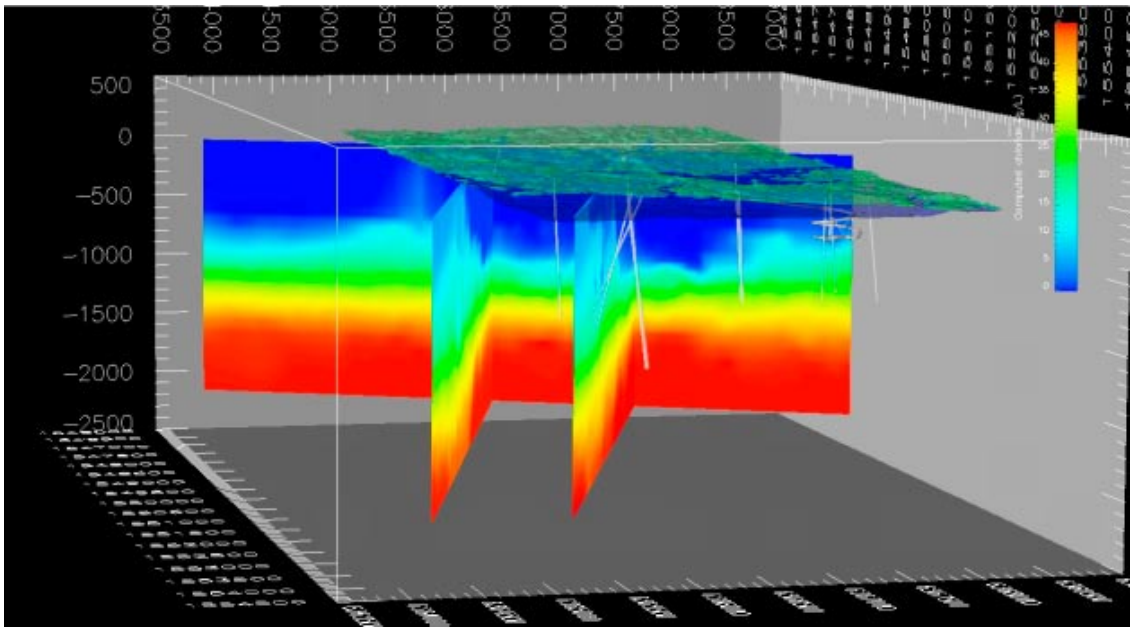

Figure 2-14. *3D view from the South-West of computed chloride distribution in the 3 selected cross sections. Computed results from /Hartley et al. 2005/.*

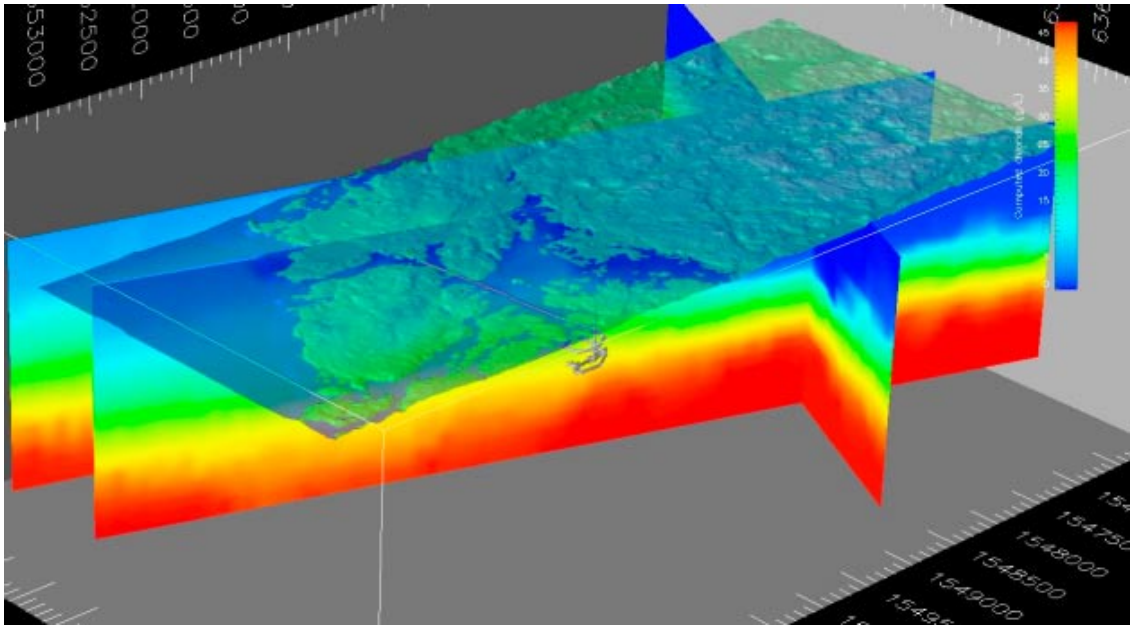

Figure 2-15. *3D-top view from the North-West of computed chloride distribution in the 3 selected cross sections. Computed results from /Hartley et al. 2005/.*

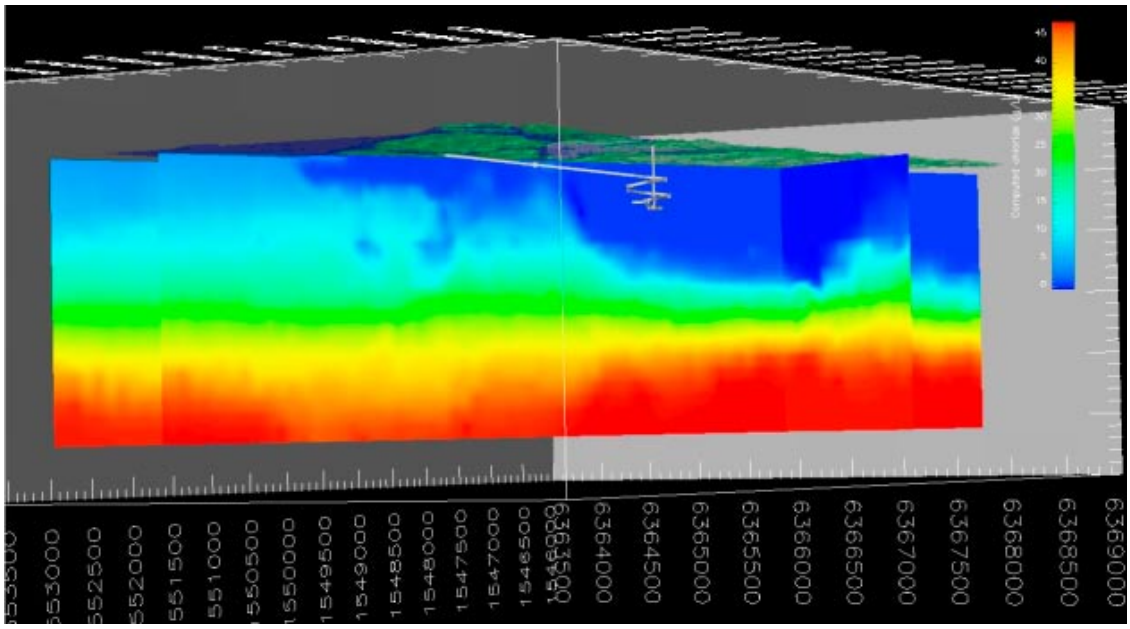

Figure 2-16. *3D view from the North-West of computed chloride distribution in the 3 selected cross sections. Computed results from /Hartley et al. 2005/.*

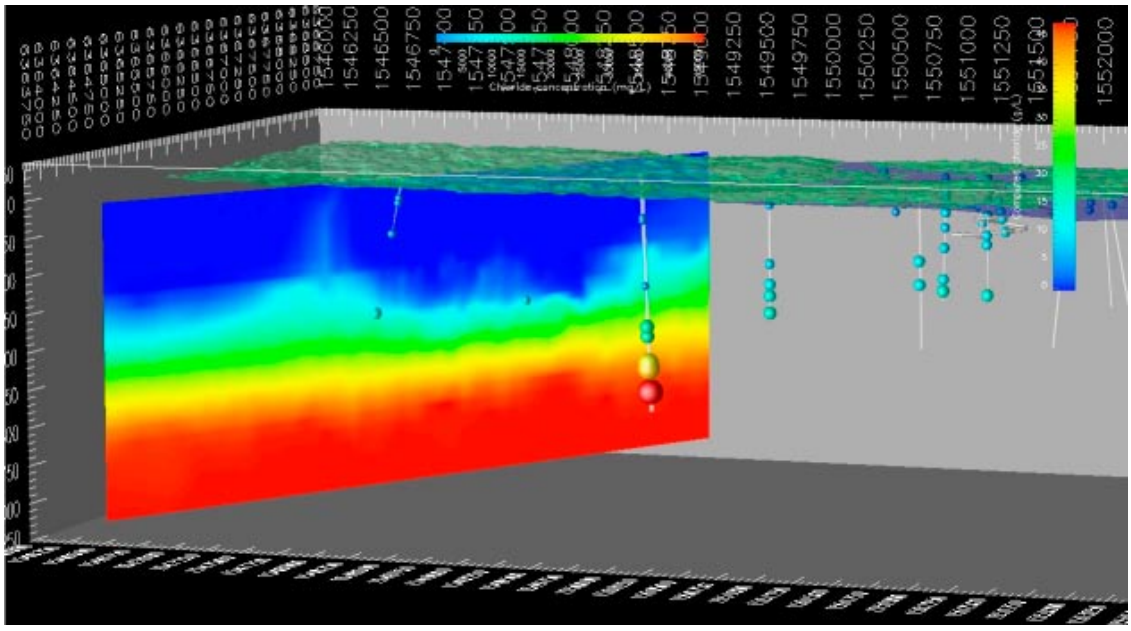

Figure 2-17. *3D view of computed and measured chloride distribution. Computed results correspond to the second NW-SE cross-section. Colour scale is the same for both computed and measured chlorides. Computed results from /Hartley et al. 2005/.*

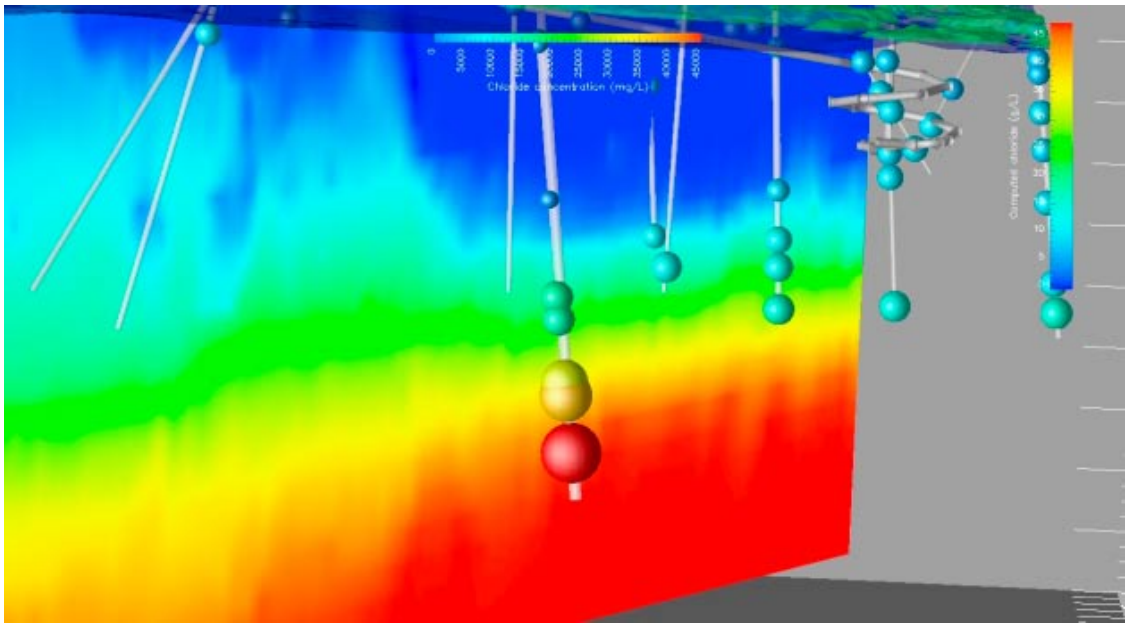

Figure 2-18. *Close-up view of computed and measured chloride distribution. Computed results correspond to the first NW-SE cross-section. Colour scale is the same for both computed and measured chlorides. Computed results from /Hartley et al. 2005/.*

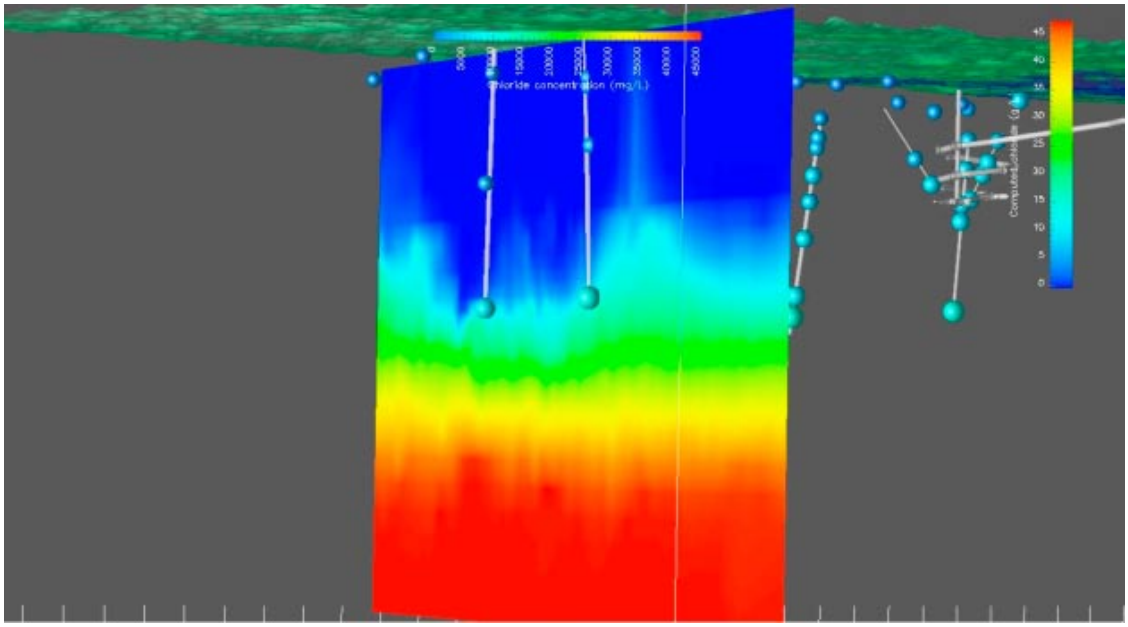

Figure 2-19. *3D view of computed and measured chloride distribution. Computed results correspond to the second SW-NE cross-section. Colour scale is the same for both computed and measured chlorides. Deep boreholes in the front are KLX03 and KLX04. Computed results from /Hartley et al. 2005/.*

2.3 Visualization of M3 model results

Figures 2-20 to 2-23 show the spatial distribution of computed M3 mixing fraction for meteoric, Littorina, glacial and brine reference waters, respectively.

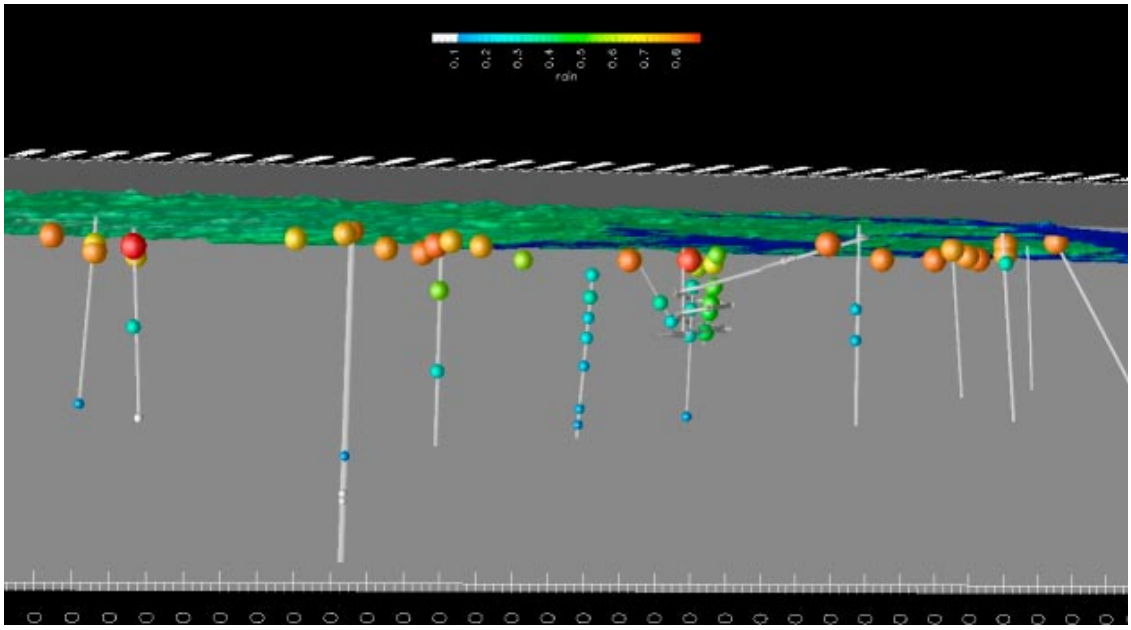

Figure 2-20. *3D view of meteoric water proportions computed with M3 model. White colour represents mixing proportions lower than 10% which corresponds to the estimated M3 uncertainty.*

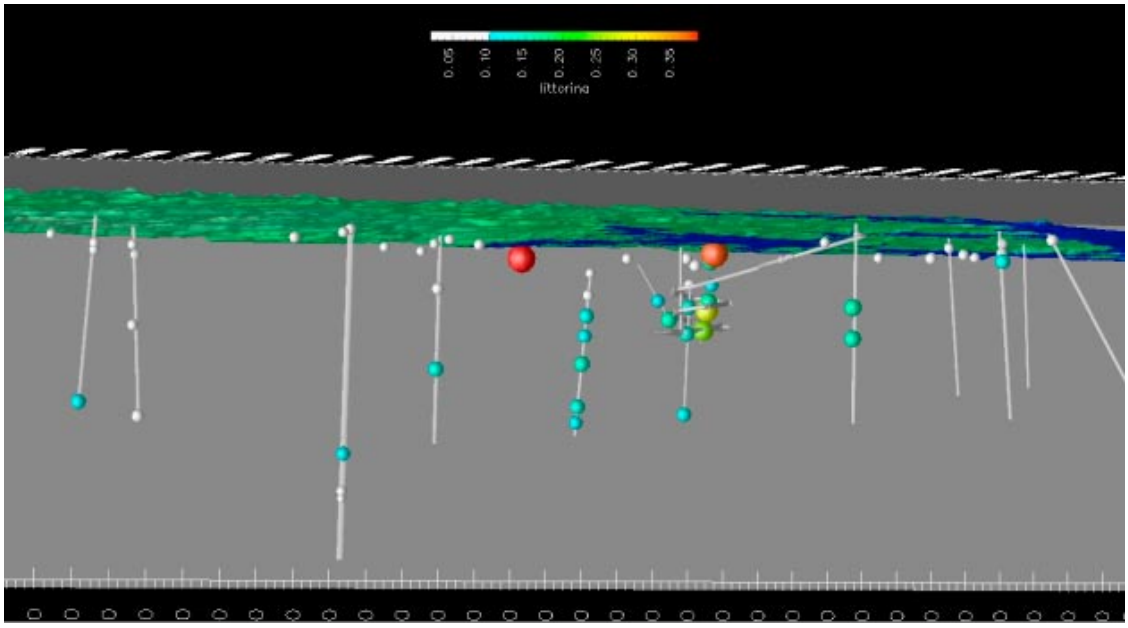

Figure 2-21. *3D view of Littorina water proportions computed with M3 model (Appendix 4, in this report). White colour represents mixing proportions lower than 10% which corresponds to the estimated M3 uncertainty.*

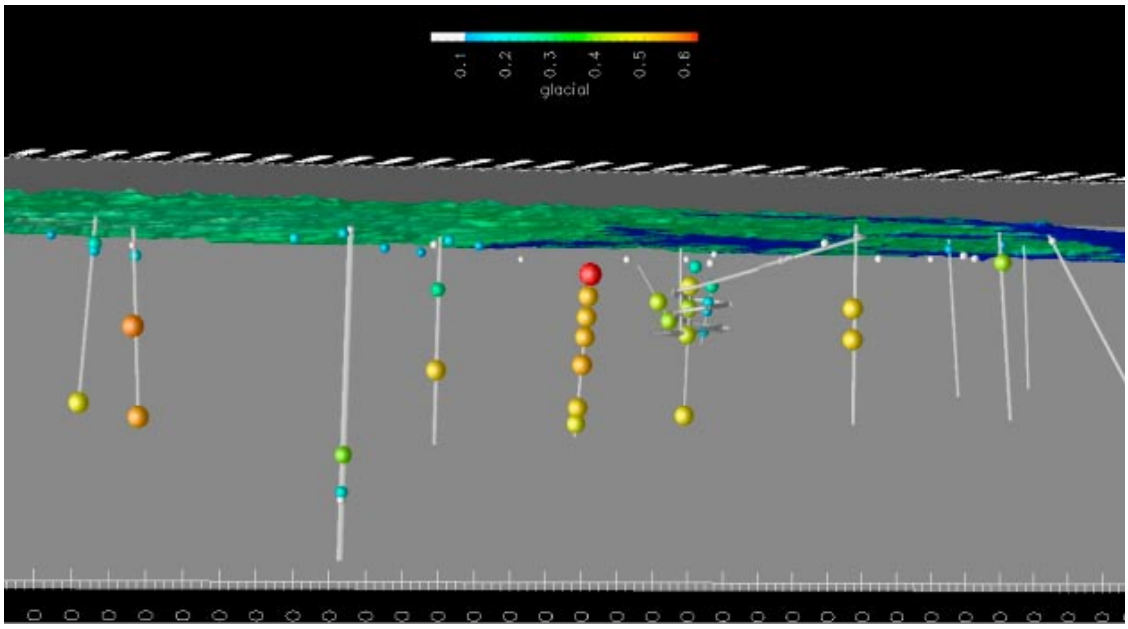

Figure 2-22. *3D view of glacial water proportions computed with M3 model (Appendix 4, in this report). White colour represents mixing proportions lower than 10% which corresponds to the estimated M3 uncertainty.*

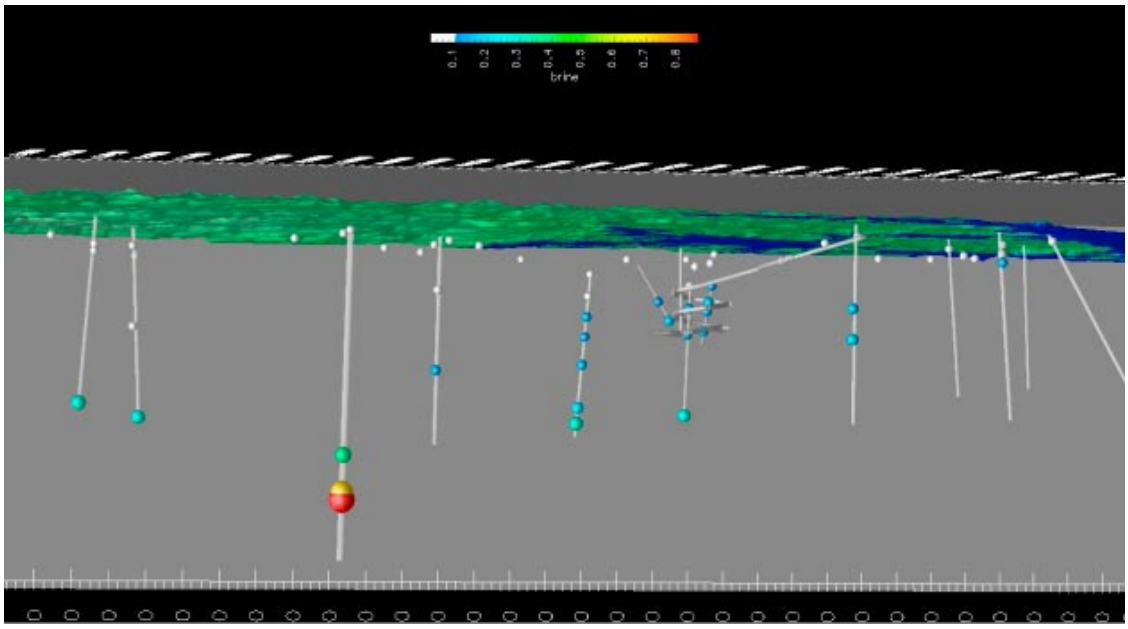

Figure 2-23. *3D view of brine water proportions computed with M3 model (Appendix 4, in this report). White colour represents mixing proportions lower than 10% which corresponds to the estimated M3 uncertainty.*

3 Numerical modelling of groundwater flow, salinity and tritium transport

3.1 MODEL FORMULATION

3.1.1 Density-dependent groundwater flow

When modelling groundwater flow and solute transport, situations may arise where solute concentration is high enough that its influence on fluid density can not be neglected. Since fluid density, affects flow itself, this variation should be taken into account in order to properly describe the actual subsurface phenomena. Where groundwater density varies spatially, flow may be driven by difference either in fluid pressure or by unstable variations in fluid density. Density-driven flows are directed from dense regions of fluid toward less dense regions.

Pressure and density-driven forces for groundwater flow can be accounted for combining Darcy's Law and the mass balance equation, as expressed by /Voss and Provost 2003/:

$$\left(\theta\rho S_{op} + \frac{\rho}{\phi}\frac{\partial\theta}{\partial p}\right)\frac{\partial p}{\partial t} + \left(\frac{\theta}{\phi}\frac{\partial p}{\partial c}\right)\frac{\partial c}{\partial t} - \nabla\cdot\left[\left(\frac{k\rho}{\mu}\right)\cdot\left(\nabla p - \rho g\right)\right] = Q_p \qquad \text{(Equation 1)}$$

where ρ is density, θ is the volumetric water content, S_{op} is specific pressure storativity, φ is porosity, p is pressure, g is gravity acceleration, k is intrinsic permeability tensor, μ is dynamic viscosity and Q_p is a fluid mass source.

Total fluid density is the sum of pure water density and solute volumetric concentration. Approximate density-models can be employed using first order Taylor expansions in C (solute mass fraction) about a base density, as suggested by /Voss and Provost 2003/:

$$\rho(C) \cong \rho_0 + \frac{\partial\rho}{\partial C}\left(C - C_0\right) \qquad \text{(Equation 2)}$$

where ρ_0 is the base fluid density at base concentration, C_0 (usually, C_0=0, and the base density is that of pure water). The factor $\frac{\partial\rho}{\partial C}$ is a constant value of density change with concentration.

3.1.2 Hydrochemistry

Geochemical evolution in subsurface environments is mainly constrained by aqueous chemical speciation reactions and dissolution-precipitation reactions involving solid phases. For chemical speciation and mineral equilibrium calculations a set of nonlinear mole-balance and mass-action equations that define an ion-association model have to be solved. However, the water-mineral interactions sometimes can not be approached through thermodynamic equilibrium. Thus, the dissolution of primary silicates from the granitic rocks (i.e. feldspars) in fractured environments is usually incongruent, leading to the precipitation of relatively amorphous metastable products that may be transformed to clay minerals with time. Therefore, the overall transformation process is dependent on the dissolution of granite-forming minerals, which follow a very slow kinetic rate in the near-neutral pH range (below 10^{-16} moles/cm^2•s for most feldspars, /Blum and Stillings 1995/. For mineral dissolution precipitation, /Lasaga 1981/ proposed the following expression:

$$r_m = \varsigma_m A_m e^{-\frac{Ea_m}{RT}} \sum_{k=1}^{N_K} K_{mk} \prod_{i=1}^{N_C+N_X} a_i^{p_{mki}} \left(\Omega_m^{\theta_{mk}} - 1\right)^{\eta_{mk}} \qquad \text{(Equation 3)}$$

where r_m is dissolution-precipitation rate (mol/m^2/ s); ς_m: is equal to 1 (dissolution) or –1 (precipitation) depending on whether Ω_m is larger or smaller than 1, respectively; Ω_m is the ratio between the ion activity product and the equilibrium constant; $e^{-\frac{Ea_m}{RT}}$ is a thermodynamic factor, Ea_m is the apparent activation energy of the overall reaction process (KJ/mol); R is the gas constant

(KJ/mol·K); T is absolute temperature (° K); N_k is the number kinetic reactions for mineral m, (it is usually equal to 1); K_{mk} is the kinetic rate constant of m^{th} mineral in k^{th} kinetic reaction ($mol/m^2/s$); $\prod_{i=1}^{N_C+N_X} a_i^{p_{mki}}$ accounts for the catalytic effect of some species such as H^+. For relatively deep groundwaters the interaction of water with rock-forming minerals from the surface to their present-day location results in the approach to the feldspar equilibrium, decreasing the kinetic dissolution rate for these minerals /Blum and Stillings 1995/.

Moreover sheet silicates can play a significant role in the system by means of their cation exchange capacity, as this process can be considered instantaneous instead of kinetically driven, and may exert a control on the concentration of both major cations and some trace elements. Cation exchange reactions can be described according to the Gaines-Thomas convention /Gaines and Thomas 1953/:

$$n\,X^- + A^{n+} = AX_n \qquad \text{(Equation 4)}$$

where X^- refers to the exchangeable site, A is the cation to be sorbed and n refers to the positive charge of the cation.

3.1.3 Reactive solute transport

Dissolved species in hydrogeologic systems are subject to transport processes. Main transport processes include advection, molecular diffusion and hydrodynamic dispersion. Considering these three mass transfer processes there are several methods to derive the solute transport equations. The classical procedure leads to the well-known general advection-dispersion equation /Bear 1972, Samper 1994/ which in 2 dimensions can be written as; /Samper et al. 2000, Yeh 2000/

$$\nabla\cdot\left(\theta bD\nabla c\right)-bq\nabla c+r\left(c^*-c\right)+b\theta R=b\theta\frac{\partial c}{\partial t} \qquad \text{(Equation 5)}$$

where *b* is the transverse thickness of the cross-section, *D* is the dispersion tensor that lump the effects of molecular diffusion and hydrodynamic dispersion, *c* is solute concentration expressed as solute mass per unit fluid volume, *q* is the Darcy velocity, *r* is the fluid source term per unit surface area, *c** is solute concentration in fluid sinks/sources and *R* is a chemical sink/source term.

The total dissolved concentration of a given component, *C* (in Equation 5) can be written in an explicit form as a function of the concentration of the N_C primary species:

$$C_k = c_k + \sum_{j=1}^{N_x} \nu_{jk} x_j = c_k + \sum_{j=1}^{N_x} \nu_{jk} K_j^{-1} \gamma_j^{-1} \prod_{i=1}^{N_c} c_{ji}^{\nu_{ji}} \gamma_i^{\nu_{ji}} \qquad \text{(Equation 6)}$$

where K_j is the equilibrium constant which depends on the pressure and temperature of the system; x_j and c_i are molar concentrations of secondary and primary species, respectively, and γ are activity coefficient and N_x is the number of secondary species, ν_{ij} is stoichiometric coefficient of the *i*-th primary species in aqueous complexation of the *j*-th secondary species. Mathematical expressions of other types of chemical reactions are given by /Xu et al. 1999/ and /Samper et al. 2000/.

A sequential iterative approach /Xu et al. 1999, Samper et al. 2000/ is used in the current model to solve the reactive transport problem. In such an approach, mass transport is solved first in terms of total dissolved concentrations of components accounting for respective geochemical source/sink terms. After solving transport equations, total concentrations of components and immobile species, minerals, gases (transport of gaseous phase is not taken account), adsorbed and exchanged species, are calculated for each node. Transport-updated total nodal concentrations are then evaluated by geochemical equilibrium or kinetic procedures, leading to updated values of aqueous and immobile species which in turn are incorporated into transport equations in the next iteration.

3.2 Numerical model

3.2.1 Methodological approach

The numerical strategy starts by using the latest version of SUTRA code /Voss and Provost 2003/, a finite-element-based code able to simulate fluid movement and transport of dissolved substances under saturated and unsaturated conditions, accounting for the variation of fluid density due to the amount of solids dissolved. However, although a powerful and well established modelling tool, the SUTRA code is unable to simulate reactive transport phenomena.

In order to set up 2D reactive transport models under this approach, a program interface has been developed which allows the user to link computed outputs of SUTRA as inputs of CORE^{2D} /Samper et al. 2000/. In this way, the flow field with variation of fluid density is calculated with the SUTRA code. When the model arise a pseudo-steady state the velocity field can be considered as permanent. Then, this pseudo-steady state water velocity field is exported to the reactive transport codes in order to simulate the coupled groundwater flow and hydrogeochemical problem. This two-step methodological approach allows performing reactive transport modelling considering a density-driven flow field, as illustrated in Figure 3-1.

3.2.2 Model description

Two-dimensional groundwater flow has been modelled along a profile from the highest regional peaks to the Baltic Sea (Figure 3-2). Its total length is 35 km, 28 km of which correspond to land surface and the remaining 7 km are under the sea.

According to the SKB site characterization strategy, the Simpevarp area has been divided into the Simpevarp subarea (coastal) and the Laxemar subarea (inland). The simulated profile goes through the middle of the Simpevarp area, across both subareas, as shown in Figure 3-3.

The simulated profile has a depth of 2,000 m under sea level. The lateral and bottom boundaries are assumed to be impervious. A mixed Neumann-Dirichlet condition has been used at the top boundary as follows: Neumann condition was applied over most of the domain with a given recharge value, and a Dirichlet condition was applied at presumed discharge zones (valleys) by imposing piezometric head equal to topographic level. The recharge rate adopted in this model was 10 mm/year, based upon computed results obtained by hydrogeological modelling of the site. The adopted recharge rate value for Simpevarp is consistent with previous results obtained by groundwater flow modelling in the framework of the Äspö HRL /Molinero 2000, Molinero and Samper 2004/.

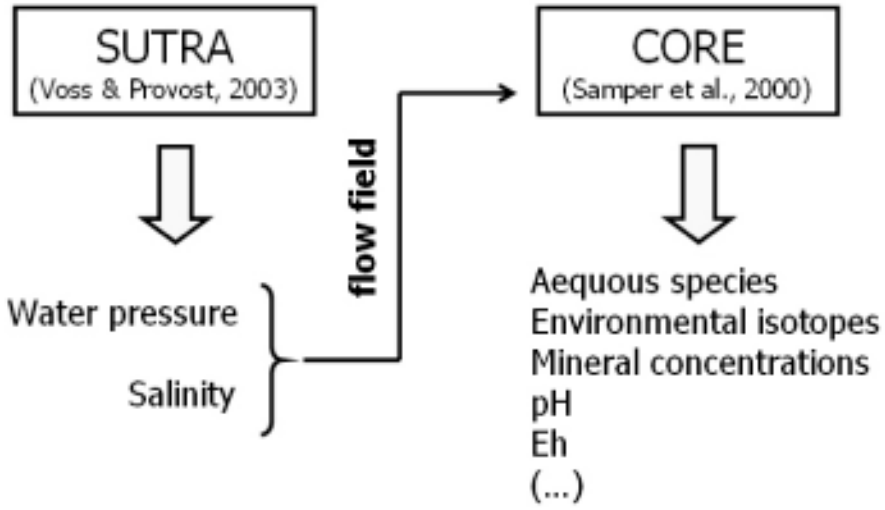

Figure 3-1. *Two-step methodological approach for reactive transport modelling considering density-driven flow.*

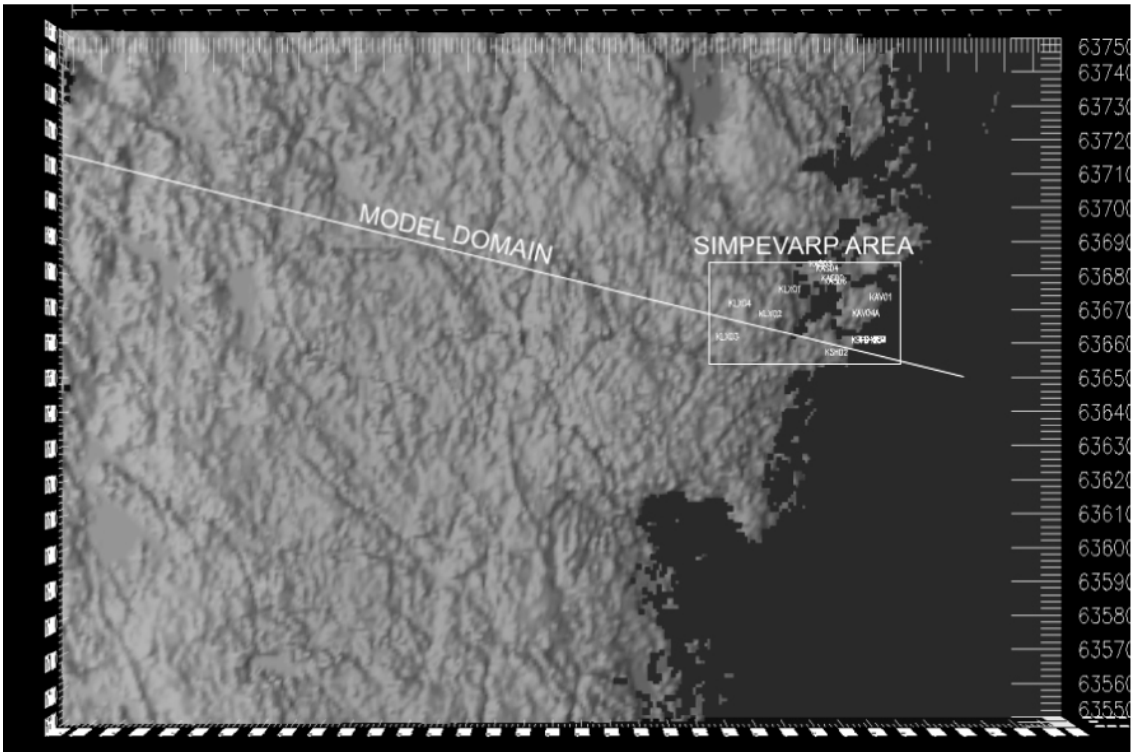

Figure 3-2. *Location of Simpevarp area and plan view of the 2-dimensional large-scale model profile.*

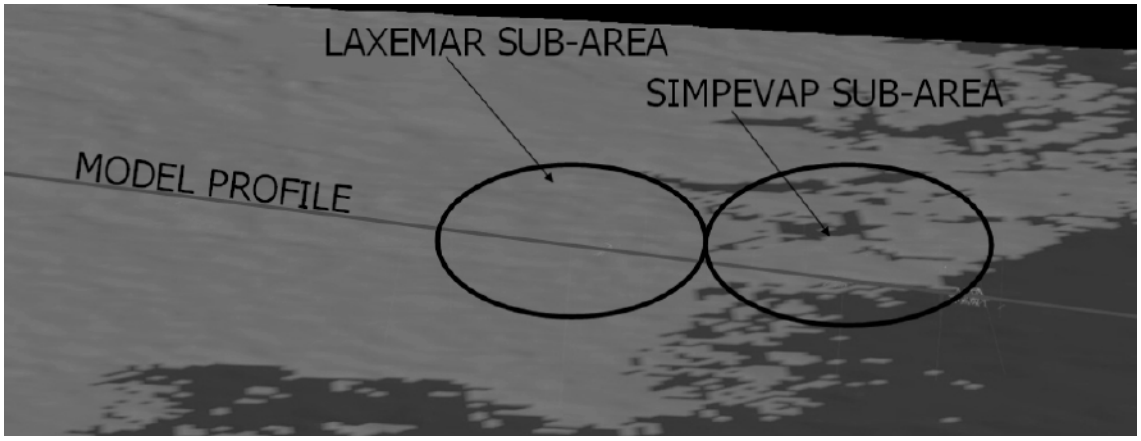

Figure 3-3. *Close-up view of the location of the modelled profile, along Laxemar subarea (inland) and Simpevarp subarea (coastal).*

Prescribed salinity at boundaries include: 0.1 g/g at the bottom boundary, 0.034 g/g at the Baltic Sea, and $2 \cdot 10^{-5}$ g/g at the recharge fresh water, which correspond to available information of the site. Initial conditions of salinity were generated by assuming a linear gradient between the top and the bottom boundaries in the model. Figure 3-4 shows a sketch of the boundary conditions used in the model.

The domain under study was discretized into quadrilateral elements, as required by the latest version of SUTRA code /Voss and Provost 2003/. The characteristic dimensions of the elements were approximately 200 m each side, except close to the surface, where the mesh was refined. The final mesh consists of 2,145 elements and 2,371 nodes.

According to recent results of the hydrogeologic site characterization it seems to be a depth dependency of hydraulic conductivity in both Laxemar and Simpevarp subareas /SKB 2006, Hartley et al. 2006/. A zonation scheme was used in order to account for the spatial heterogeneity of hydraulic conductivity. The model domain has been divided into 6 material zones in Simpevarp subarea and 6 material zones in Laxemar subareas. Each material zone is composed by a set of elements which share the same hydrodynamic and transport parameters.

3.2.3 Hydrochemical processes and boundary conditions

A preliminary analysis was carried out of the subsurface and deep waters in the Laxemar area. The main goal was to determine the chemical composition of boundary waters in the model. As a result, three different boundary waters were defined (Table 1), namely the Fresh recharge water, the Bottom saline water and the Baltic estuary water.

The chemical composition of fresh recharge water in granite derives from the interaction between rainfall water and the near-surface quaternary deposits, which results in calcite dissolution and organic matter degradation producing an increase of the dissolved bicarbonates. The bottom boundary water was derived taking into account the chemical composition sampled at the maximum depth available (borehole KLX-02 at 1,600 m aprox.). The chemical composition of Baltic Sea water was defined consistently with the available sea water compositions.

Table 2 shows the complete set of hydrogeochemical processes that have been considered in the reactive transport model. A total of 58 homogeneous aqueous processes, 4 mineral dissolution/precipitation processes and 1 cation exchange reaction have been considered. The dissolution/precipitation of calcite was assumed to be under equilibrium whereas processes involving feldspars, silica and phyllosilicates obey kinetic laws. Cation exchange processes have also been taken into account using a local equilibrium approach and assuming the Gaines–Thomas convention.

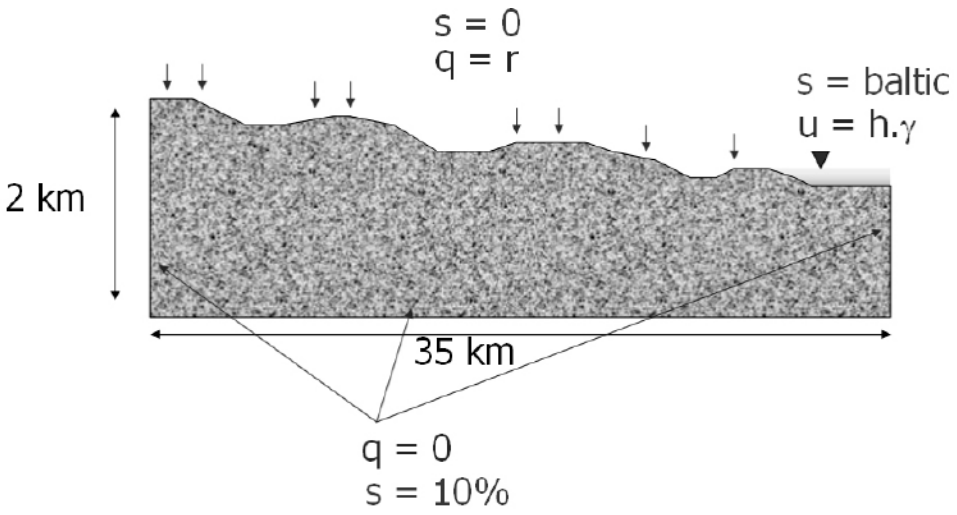

Figure 3-4. *Sketch of boundary conditions used in the numerical model.*

Table 1. Chemical compositions of the boundary waters used in the numerical model of the Laxemar Area.

Chemical component	Recharge fresh water (Mol/L)	Baltic estuary water (Mol/L)	Bottom saline water (Mol/L)
HCO_3^-	$2.53 \cdot 10^{-3}$	$1.52 \cdot 10^{-3}$	$1.47 \cdot 10^{-4}$
Li^+	$1.44 \cdot 10^{-6}$	$4.50 \cdot 10^{-6}$	$6.64 \cdot 10^{-4}$
Na^+	$6.52 \cdot 10^{-4}$	$8.56 \cdot 10^{-2}$	$4.78 \cdot 10^{-1}$
K^+	$6.52 \cdot 10^{-5}$	$1.90 \cdot 10^{-3}$	$1.02 \cdot 10^{-3}$
Sr^{2+}	$1.71 \cdot 10^{-6}$	$1.65 \cdot 10^{-5}$	$4.57 \cdot 10^{-3}$
Cl^-	$3.04 \cdot 10^{-4}$	$1.03 \cdot 10^{-1}$	1.69
Mn^{2+}	$1.00 \cdot 10^{-5}$	$1.89 \cdot 10^{-7}$	$2.55 \cdot 10^{-6}$
Ca^{2+}	$1.10 \cdot 10^{-3}$	$2.38 \cdot 10^{-3}$	$6.24 \cdot 10^{-1}$
SiO_2	$1.88 \cdot 10^{-4}$	$1.66 \cdot 10^{-5}$	$1.71 \cdot 10^{-4}$
Mg^{2+}	$2.48 \cdot 10^{-4}$	$9.68 \cdot 10^{-3}$	$1.11 \cdot 10^{-4}$
SO_4^{2-}	$2.39 \cdot 10^{-4}$	$5.31 \cdot 10^{-3}$	$9.99 \cdot 10^{-3}$
$Al(OH)_4^-$	$1.00 \cdot 10^{-7}$	$1.00 \cdot 10^{-7}$	$1.00 \cdot 10^{-7}$

Table 2. Hydrogeochemical processes considered in the reactive transport model.

Homogeneous Hydrochemical Processes	Log K
$Ca(H_3SiO_4)_{2(aq)} + 2H^+ \leftrightarrow 2SiO_{2(aq)} + Ca^{2+} + 4H_2O$	15.0530
$CaCl^+ \leftrightarrow Ca^{2+} + Cl^-$	0.6956
$CaCl_{2(aq)} \leftrightarrow Ca^{2+} + 2Cl^-$	0.6436
$CaCO_{3(aq)} + H^+ \leftrightarrow Ca^{2+} + HCO_3^-$	7.0017
$CaH_2SiO_{4\,(aq)} + 2H^+ \leftrightarrow SiO_{2(aq)} + Ca^{2+} + 2H_2O$	18.5620
$CaH_3SiO_4^+ + H^+ \leftrightarrow SiO_{2(aq)} + Ca^{2+} + 2H_2O$	8.7916
$CaHCO_3^+ \leftrightarrow Ca^{2+} + HCO_3^-$	–1.0467
$CaOH^+ + H^+ \leftrightarrow Ca^{2+} + H_2O$	12.8500
$CaSO_{4(aq)} \leftrightarrow Ca^{2+} + SO_4^{2-}$	–2.1111
$CO_{2(aq)} + H_2O \leftrightarrow HCO_3^- + H^+$	–6.3447
$CO_3^{2-} + H^+ \leftrightarrow HCO_3^-$	10.3290
$H_{2(aq)} + 1/2\ O_{2(aq)} \leftrightarrow H_2O$	46.1070
$H_2SiO_4^{2-} + 2H^+ \leftrightarrow SiO_{2(aq)} + H_2O$	22.9120
$H_4(H_2SiO_4)_4^- + 4H^+ \leftrightarrow 4SiO_{2(aq)} + 8H_2O$	35.7460
$H_6(H_2SiO_4)_4^- + 2H^+ \leftrightarrow 4SiO_{2(aq)} + 8H_2O$	13.4460
$HCl_{(aq)} \leftrightarrow H^+ + Cl^-$	0.6700
$HS^- + 2O_{2(aq)} \leftrightarrow H^+ + SO_4^{2-}$	138.3200
$HSiO_3^- + H^+ \leftrightarrow SiO_{2(aq)} + H_2O$	9.9525
$HSO_4^- \leftrightarrow H^+ + SO_4^{2-}$	–1.9791
$KCl_{(aq)} \leftrightarrow K^+ + Cl^-$	1.4946
$KHSO_{4(aq)} \leftrightarrow K^+ + SO_4^{2-} + H^+$	–0.8136
$K(OH)_{(aq)} + H^+ \leftrightarrow K^+ + H_2O$	14.4600
$KSO_4^- \leftrightarrow K^+ + SO_4^{2-}$	–0.8796
$LiCl_{(aq)} \leftrightarrow Li^+ + Cl^-$	1.5115
$Li(OH)_{(aq)} + H^+ \leftrightarrow Li^+ + H_2O$	13.6400
$LiSO_4^- \leftrightarrow Li^+ + SO_4^{2-}$	–0.7700
$Mg(H_3SiO_4)_{2(aq)} + 2H^+ \leftrightarrow 2SiO_{2(aq)} + Mg^{2+} + 4H_2O$	13.7230
$MgCl^+ \leftrightarrow Mg^{2+} + Cl^-$	0.1349

Homogeneous Hydrochemical Processes	Log K	
$MgCO_{3(aq)} + H^+ \leftrightarrow Mg^{2+} + HCO_3^-$	7.3499	
$MgH_2SiO_{4\,(aq)} + 2H^+ \leftrightarrow SiO_{2(aq)} + Mg^{2+} + 2H_2O$	17.4820	
$MgH_3SiO_4^+ + H^+ \leftrightarrow SiO_{2(aq)} + Mg^{2+} + 2H_2O$	8.5416	
$MgHCO_3^+ \leftrightarrow Mg^{2+} + HCO_3^-$	–1.0357	
$MgSO_{4(aq)} \leftrightarrow Mg^{2+} + SO_4^{2-}$	–2.4117	
$Mn(OH)_{2(aq)} + 2H^+ \leftrightarrow Mn^{2+} + 2H_2O$	22.2000	
$Mn_2(OH)_3^+ + 3H^+ \leftrightarrow 2Mn^{2+} + 3H_2O$	23.9000	
$Mn_2OH^{3+} + H^+ \leftrightarrow 2Mn^{2+} + H_2O$	10.5600	
$MnCl^+ \leftrightarrow Mn^{2+} + Cl^-$	–0.3013	
$MnCl_3^- \leftrightarrow Mn^{2+} + 3Cl^-$	0.3324	
$MnCO_{3(aq)} + H^+ \leftrightarrow Mn^{2+} + HCO_3^-$	5.8088	
$MnHCO_3^+ \leftrightarrow Mn^{2+} + HCO_3^-$	–0.8816	
$MnO_4^- + 3H^+ \leftrightarrow Mn^{2+} + 3/2\ H_2O + 5/4\ O_{2(aq)}$	20.2960	
$MnOH^+ + H^+ \leftrightarrow Mn^{2+} + H_2O$	10.5900	
$MnSO_{4(aq)} \leftrightarrow Mn^{2+} + SO_4^{2-}$	–2.3529	
$NaCl_{(aq)} \leftrightarrow Na^+ + Cl^-$	0.7770	
$NaCO_3^- + H^+ \leftrightarrow Na^+ + HCO_3^-$	9.8144	
$NaHCO_{3(aq)} \leftrightarrow Na^+ + HCO_3^-$	–0.1544	
$NaHSiO_{3\,(aq)} + H^+ \leftrightarrow SiO_{2(aq)} + Na^+ + H_2O$	8.3040	
$Na(OH)_{(aq)} + H^+ \leftrightarrow Na^+ + H_2O$	14.1800	
$NaSO_4^- \leftrightarrow Na^+ + SO_4^{2-}$	–0.8200	
$SrCl^+ \leftrightarrow Sr^{2+} + Cl^-$	0.2485	
$SrCO_{3(aq)} + H^+ \leftrightarrow Sr^{2+} + HCO_3^-$	7.4635	
$SrOH^+ + H^+ \leftrightarrow Sr^{2+} + H_2O$	13.2900	
$SrSO_{4(aq)} \leftrightarrow Sr^{2+} + SO_4^{2-}$	–2.3000	
$Al^{3+} + 4H_2O \leftrightarrow 4H^+ + Al(OH)_4^-$	–22.148	
$Al(OH)_2^+ + 2H_2O \leftrightarrow Al(OH)_4^- + 2H^+$	–12.049	
$Al(OH)_{3(aq)} + H_2O \leftrightarrow Al(OH)_4^- + H^+$	–5.9900	
$Al(OH)^{2+} + 3H_2O \leftrightarrow Al(OH)_4^- + 3H^+$	–17.136	
$OH^- + H^+ \leftrightarrow H_2O$	13.995	
Mineral Processes under equilibrium approach	Log K	
$CaCO_{3(s)} + H^+ \leftrightarrow Ca^{2+} + HCO_3^-$	1.8487	
Mineral Processes under kinetic approach		
$Na_{0.45}Ca_{0.55}Al_{1.5}Si_{2.5}O_8 + 3H_2O \leftrightarrow 0.55Ca^{2+} + 0.45Na^+ + 2.5SiO_{2(aq)} + 1.5Al(OH)_4^-$	$7.5e^{-3}*a_H^{0.5} + 2.5e^{-17}*a_H^{0.3}$	(1)
$Al_2O_3 \cdot 2SiO_2 \cdot 2H_2O + 3H_2O \leftrightarrow 2H^+ + 2SiO_{2(aq)} + 2Al(OH)_4^-$	$-1.7e^{-11}*a_H^{0.5} + 1.2e^{-14}*a_H^{0.3}$	(2)
$SiO_{2(s)} \leftrightarrow SiO_{2(aq)}$	$4.1e^{-14}$	(3)
Cation Exchange Processes	$K_{Na/Ca}$	
$Na^+ + 0.5Ca–X \leftrightarrow 0.5Ca^{2+} + Na\text{-}X$	0.5	

(1) /Chow and Wollast 1985, Casey et al. 1991/.

(2) /Wieland and Stumm 1992, Ganor et al. 1995/.

(3) /Rimstidt and Barnes 1980/.

3.2.4 Model calibration

Hydraulic conductivity is one of the key parameters conditioning groundwater flow and solute transport processes. In fracture crystalline bedrocks hydraulic conductivity values displays high variability and its determination is uncertain to a large extent. Calibration is thus required in order to best fit the actual chemical composition as measured at observation points. In this mode, the process of calibration was aimed at reproducing the total dissolved solute profiles described by the values measured at several boreholes in the Laxemar and Simpevarp subareas. First guess of hydraulic conductivity values (Figures 3-5 and 3-6) were estimated on the basis of available field test data /SKB 2006/.

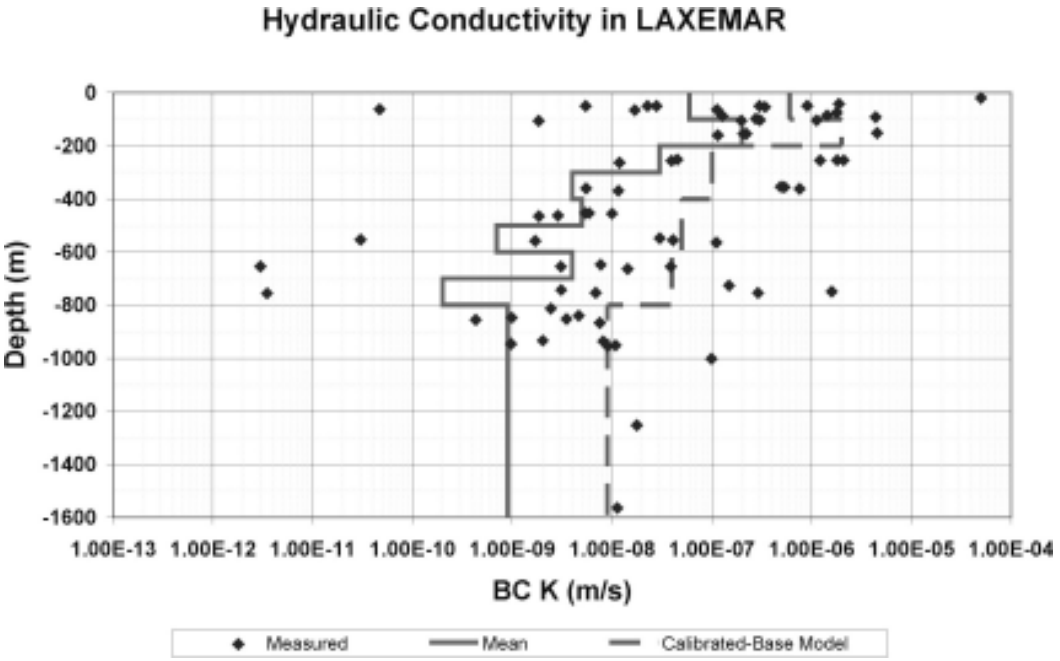

Figure 3-5. *Comparison of hydraulic conductivity values derived from field test (test scale = 100 m, /SKB 2006/) and model-calibrated values at Laxemar subarea.*

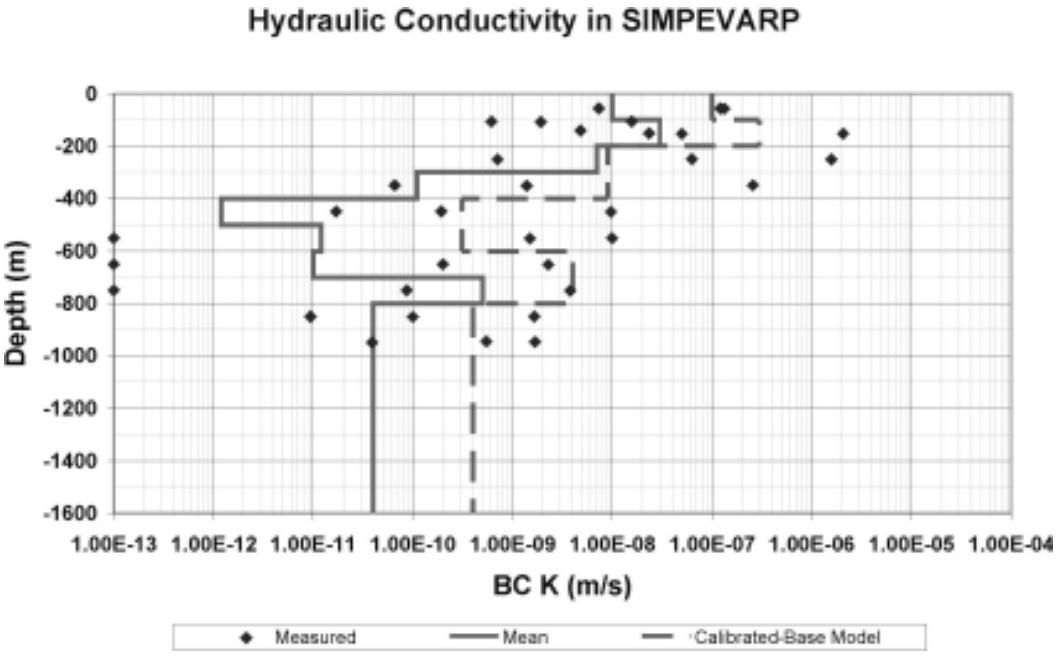

Figure 3-6. *Comparison of hydraulic conductivity values derived from field test (test scale = 100 m /SKB 2006/) and model-calibrated values Simpevarp subarea.*

The presence of highly saline waters at great depth makes it necessary to take into account the influence of the variation of water density on groundwater flow. Indeed, at an initial stage, the velocity field over the domain considered was determined by calculating the variably-density dependent flow by means of SUTRA code /Voss and Provost 2003/ (Figure 3-7).

CORE^{2D} /Samper et al. 2000/ was then employed to couple reactive transport processes accompanying the flow field as determined by SUTRA. The amount of total dissolved solids was considered as a conservative species in the calculation process. Figures 3-8 and 3-9 show the fit obtained in the final calibrated model in Laxemar and Simpevarp subareas respectively. As expected, saline water reaches lower depth in Simpevarp (coastline) than Laxemar subarea (inland).

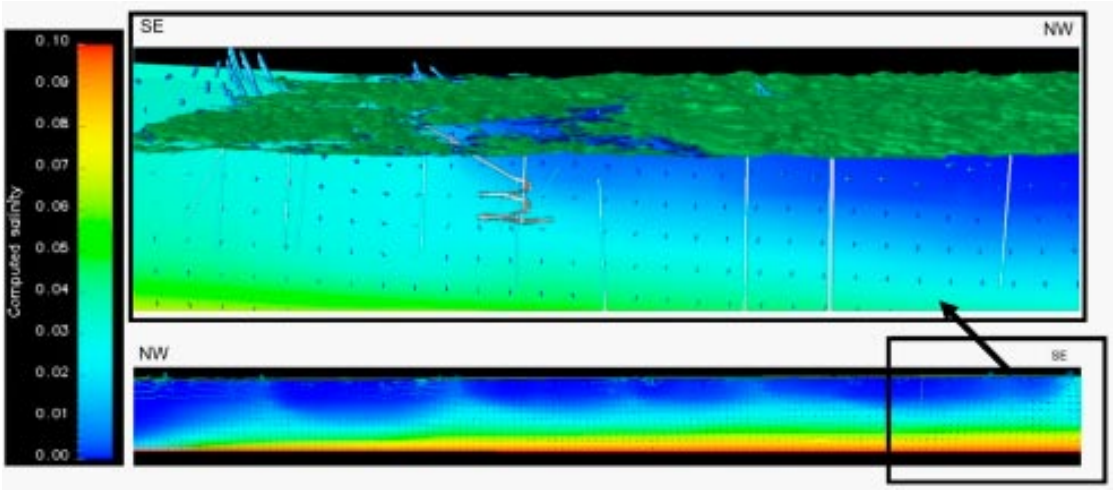

Figure 3-7. *Calibrated water velocity and salinity fields. General view of the model domain (lower) and close up view of the Simpevarp area (upper).*

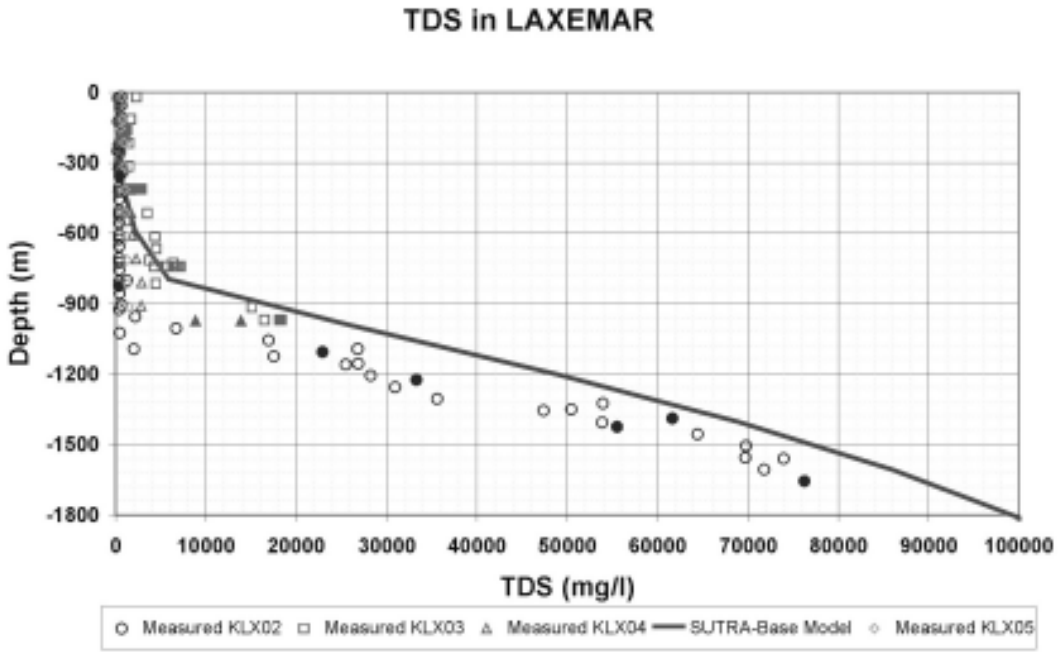

Figure 3-8. *Computed values of Total Dissolved Solids (solid line) and measurements (symbols) at Laxemar subarea. Computed results correspond to the final calibrated model. Filled symbols correspond to representative samples.*

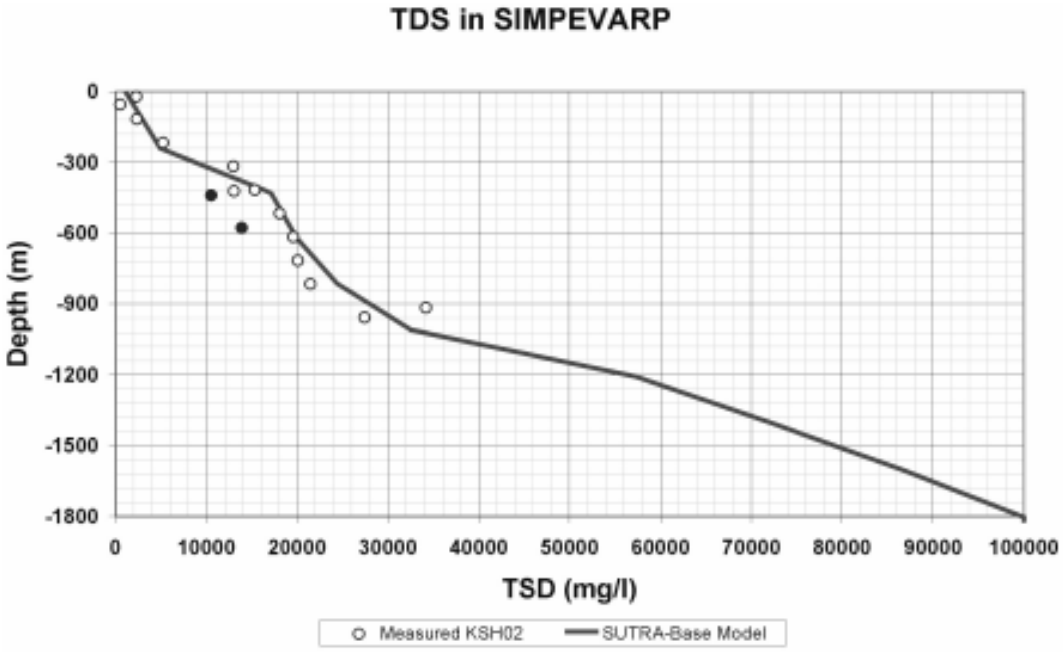

Figure 3-9. *Computed values of Total Dissolved Solids (solid line) and measurements (symbols) at Simpevarp subarea. Computed results correspond to the final calibrated model. Filled symbols correspond to representative samples.*

3.2.5 Model results

Conservative transport

The assumption of conservative transport has proved to provide acceptable fit to the distribution of concentration of most species, as shown in Figures 3-10 and 3-11, where it can be seen that concentration of chloride, sodium, calcium, strontium, potassium, and lithium mimic the concentration profile of TDS. The concentration of these species increases gradually from the upper fresh water towards the lower saline water. Even depth trends of sulpahte and magnesium concentrations (Figure 3-11) can be reasonably reproduced by a conservative transport model.

On the contrary, the conservative transport model is unable to reproduce the trend of bicarbonate concentration, of dissolved bicarbonates, iron, manganese and silica, as can be seen in Figure 3-12, indicating that it becomes necessary to consider hydrochemical processes in order to explain the field measured values of this dissolved species.

Reactive transport

As pointed out in the previous section, computed results obtained by assuming pure conservative solute transport can explain the distribution of some of the major dissolved components, but clearly diverge from the measured data in some others. Figure 3-13 shows the comparison between measured data and computed results obtained by using both conservative and reactive transport models. It is worth noting that calcite dissolution/precipitation processes were included into the reactive transport model (Table 2) and, then, an impact on the computed bicarbonate concentrations was expected. It can be seen in Figure 3-13 that computed bicarbonate concentration rises slightly at shallow depths due to the dissolution of calcite, and decreases below 300 m due to slight precipitation. However, computed results were not greatly improved compared with the conservative base model. In general, it can be said that measured bicarbonate values are much larger than computed results with both conservative and reactive transport models.

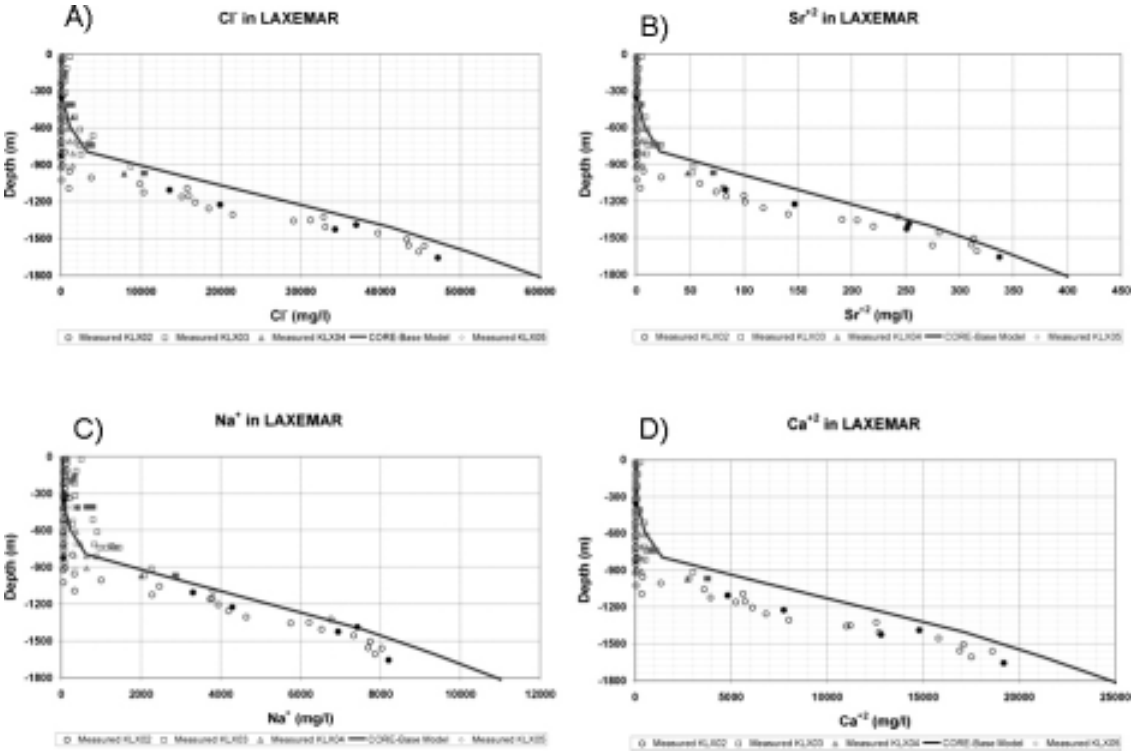

Figure 3-10. *Comparison of measured values (symbols) and computed results (solid line) of: A) Chloride, B) Strontium, C) Sodium, and D) Calcium, at Laxemar subarea. Filled symbols correspond to representative samples.*

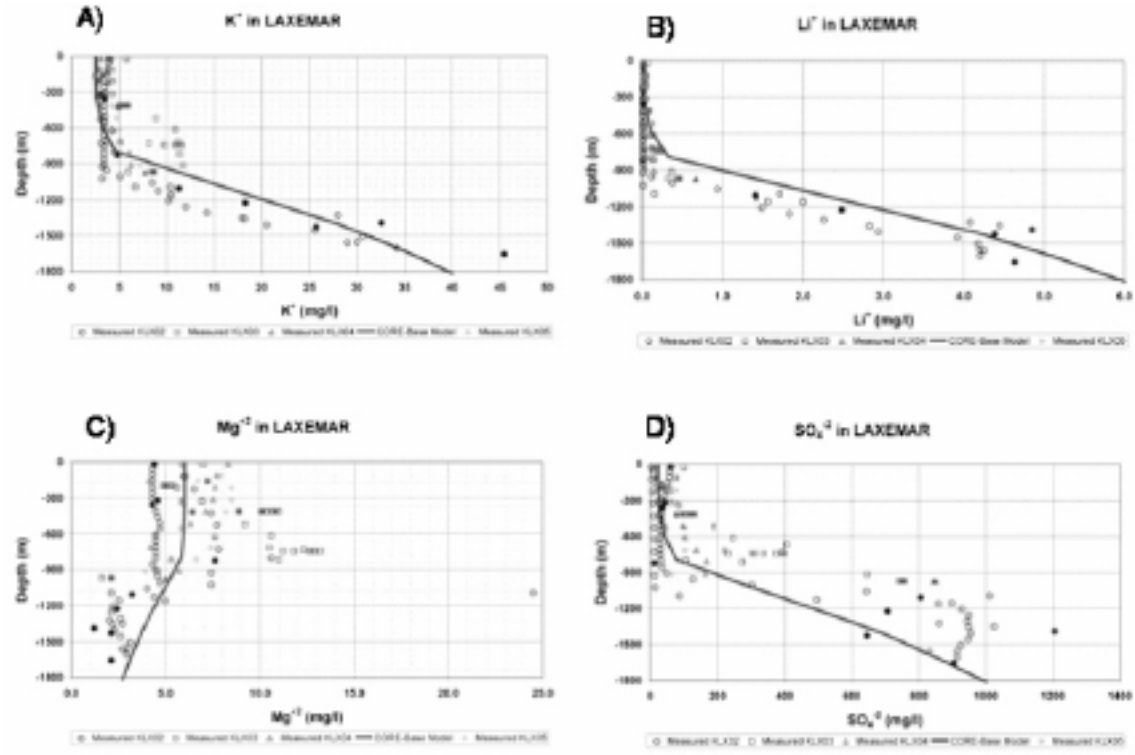

Figure 3-11. *Comparison of measured values (symbols) and computed results (solid line) of: A) Potassium, B) Lithium, C) Magnesium, and D) Sulphate, at Laxemar subarea. Filled symbols correspond to representative samples.*

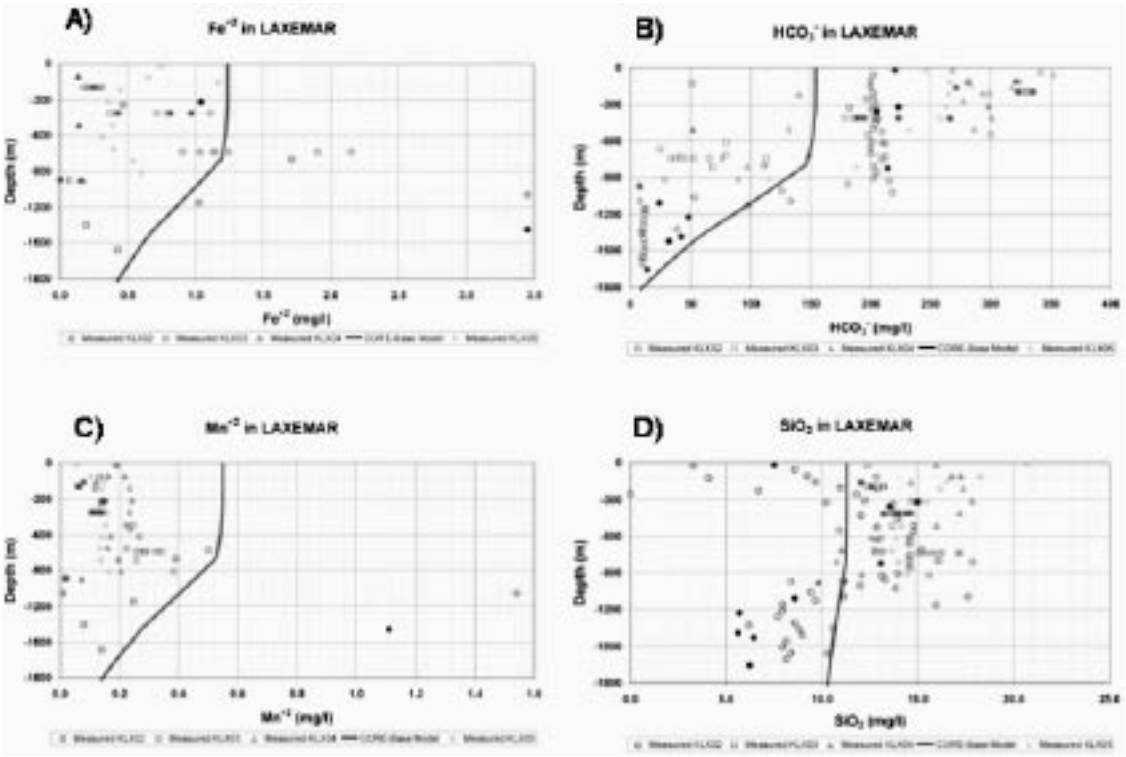

Figure 3-12. *Comparison of measured values (symbols) and computed results (solid line) of: A) Iron, B) Bicarbonate, C) Manganese, and D) Silica, at Laxemar subarea. Filled symbols correspond to representative samples.*

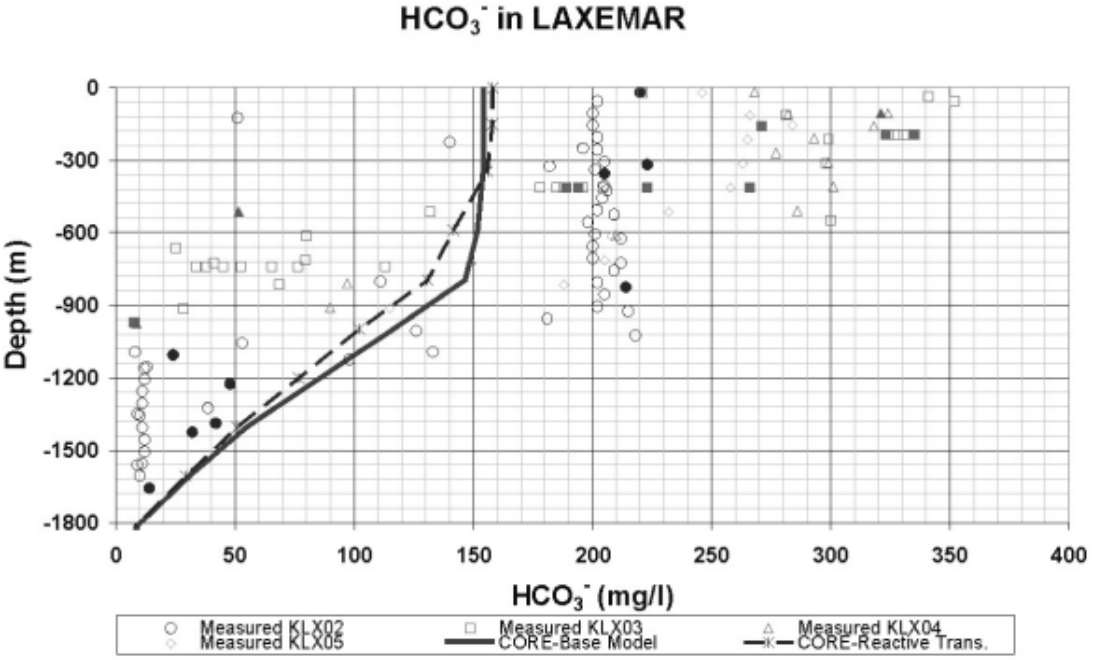

Figure 3-13. *Behaviour of dissolved bicarbonates with respect to the calcite geochemical system. Solid line corresponds to computed results of the calibrated conservative model. Dashed line corresponds to computed results of reactive transport model considering calcite dissolution-precipitation. Filled symbols correspond to representative samples.*

Figure 3-14 shows the comparison between measured values and computed results of dissolved silica. It can be seen that the computed profile of silica concentrations improves noticeably in the reactive transport model, which accounts for the silicates weathering processes, including dissolution of quartz and feldspars, as well as the precipitation of clay minerals under kinetic approach. The concentration of silica on the upper boundary is the same as the concentration of recharge water. The agreement between measured and computed results of dissolved silica is particularly good at depth, down to 900 m, where the system is dominated by saline waters with high residence time.

A similar behaviour can be observed in the comparison between measured and computed pH values (Figure 3-15). Reactive transport model results are able to reproduce the measured trends, especially well at depth were old saline waters dominate the system.

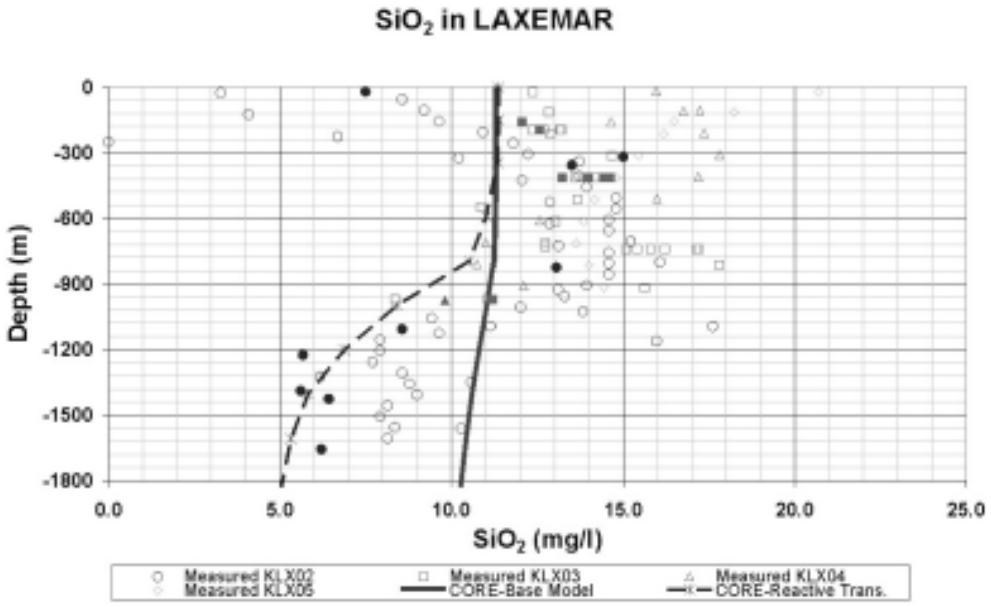

Figure 3-14. *Behavior of dissolved silica with respect to the silicates geochemical system. Solid line corresponds to computed results of the calibrated conservative model. Dashed line corresponds to computed results of reactive transport model considering silicates weathering processes. Filled symbols correspond to considered representative samples.*

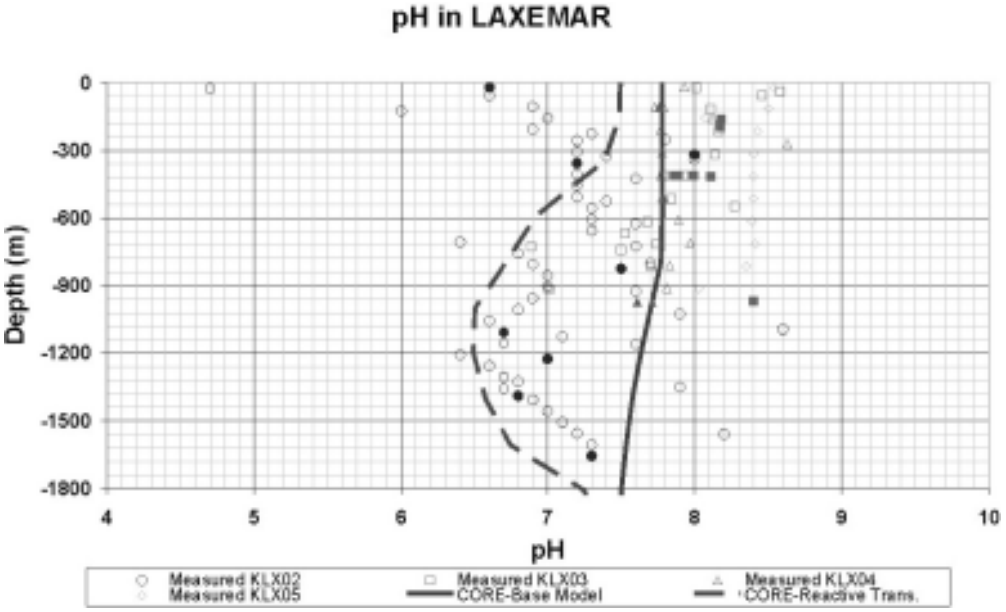

Figure 3-15. *Behavior of computed pH under conservative transport approach (solid line) with respect to the reactive transport approach (dashed line). Filled symbols correspond to representative samples.*

3.2.6 Sensitivity analyses

Available data of hydraulic conductivity values were observed to vary over a wide range (of several orders of magnitude; see Figures 3-5 and 3-6). In order to evaluate the uncertainties associated to the hydraulic conductivity values used in the calibrated model, a sensitivity analysis was carried out. The sensitivity exercise has been designed in order to track the influence of hydraulic conductivity changes on the distribution of groundwater salinity. The results of the sensitivity analysis are summarized in Table 3 which shows the sensitivity of computed salinity

Table 3. Quantitative results of sensitivity analysis of hydrochemical composition with respect to hydrogeologic variations. It can be seen that computed salinity at Laxemar is highly sensitive to changes in hydraulic conductivity at layers 4 and 5 (600–1,000 m). Computed salinity at Simpevarp is most sensitive to changes in hydraulic conductivity at Layer 8 (200–300 m) *

	PARAMETER			OUTPUT (Salinity)			
				LAXEMAR		SIMPEVARP	
	Name	Relative Change (%)		Rel. Change (%)	Rel. Sensitivity (%)	Rel. Change (%)	Rel. Sensitivity (%)
LAXEMAR	K1	90	Max.	31.17	0.3463	2.08	0.0232
			Min.	0.00	0.0000	0.00	0.0000
			Mean	8.59	0.0954	0.63	0.0070
			Est. dev.	13.79	0.1533	0.76	0.0084
	K2	90	Max.	60.10	0.6678	2.12	0.0236
			Min.	0.00	0.0000	0.00	0.0000
			Mean	11.97	0.1330	0.75	0.0084
			Est. dev.	17.88	0.1987	0.84	0.0093
	K3	90	Max.	79.66	0.8851	27.27	0.3030
			Min.	0.00	0.0000	0.00	0.0000
			Mean	15.67	0.1741	4.94	0.0549
			Est. dev.	25.67	0.2852	7.78	0.0864
	K4	90	Max.	306.18	3.4020	47.26	0.5251
			Min.	0.00	0.0000	0.00	0.0000
			Mean	44.79	0.4977	6.05	0.0672
			Est. dev.	93.65	1.0405	13.80	0.1534
	K5	90	Max.	315.63	3.5092	62.57	0.6952
			Min.	0.00	0.0000	0.00	0.0000
			Mean	38.86	0.4318	11.37	0.1263
			Est. dev.	93.16	1.0352	18.25	0.2027
	K6	90	Max.	88.47	0.9830	39.39	0.4376
			Min.	0.00	0.0000	0.00	0.0000
			Mean	29.01	0.3223	9.29	0.1032
			Est. dev.	30.18	0.3353	12.73	0.1414
SIMPEVARP	K7	90	Max.	0.03	0.0003	46.00	0.5111
			Min.	0.00	0.0000	0.00	0.0000
			Mean	0.01	0.0001	9.45	0.1050
			Est. dev.	0.01	0.0001	13.83	0.1537
	K8	90	Max.	0.70	0.0078	362.25	4.0250
			Min.	0.00	0.0000	0.00	0.0000
			Mean	0.27	0.0030	43.37	0.4819
			Est. dev.	0.24	0.0027	107.02	1.1891
	K9	90	Max.	0.15	0.0017	39.81	0.4423
			Min.	0.00	0.0000	0.00	0.0000
			Mean	0.06	0.0007	9.65	0.1072
			Est. dev.	0.05	0.0006	12.35	0.1372
	K10	90	Max.	0.29	0.0032	24.52	0.2724
			Min.	0.00	0.0000	0.00	0.0000
			Mean	0.11	0.0013	6.05	0.0672
			Est. dev.	0.10	0.0011	9.19	0.1021
	K11	90	Max.	0.63	0.0070	18.34	0.2038
			Min.	0.00	0.0000	0.00	0.0000
			Mean	0.24	0.0027	4.92	0.0547
			Est. dev.	0.22	0.0024	6.79	0.0755
	K12	90	Max.	0.86	0.0096	4.72	0.0524
			Min.	0.00	0.0000	0.00	0.0000
			Mean	0.35	0.0039	1.56	0.0173
			Est. dev.	0.30	0.0034	1.69	0.0188

* Relative changes in parameter CP are defined as $|P_s - P_b|/P_b*100$, and relative changes in output concentrations AS are defined as $|C_s - C_b|/C_b*100$, where P_s and P_b are parameters (hydraulic conductivity) used for sensitivity and base runs, respectively, and C_s and C_b are concentrations of salinity computed in sensitivity and calibrated base runs, respectively. Relative sensitivities are defined as AS/CP.

concentrations at Laxemar and Simpevarp subareas, with respect to changes in hydraulic conductivity. Relative changes in parameters and computed salinity are defined for comparison. The relative sensitivity of concentration with respect to a parameter is defined as the relative change in concentration divided by the relative change of the parameter. It can be seen that the results of the hydrogeochemical model are most sensitive to changes in hydraulic conductivity at layers where there are an interface between saline and fresh water systems. So, Layers 4 and 5 (600–1,000 m) are the most sensitive to changes in Laxemar, whereas Layer 8 (200–300 m) is the most sensitive at Simpevarp subarea (Table 3). Computed salinity at Simpevarp subarea is sensitive to changes in hydraulic conductivity at Laxemar. As expected, computed salinity at Laxemar (up stream) lacks sensitivity with respect to changes in hydraulic conductivity at Simpevarp subarea (down stream).

Table 4. Quantitative results of sensitivity analysis with respect to reactive transport processes. *

PARAMETER		OUTPUT LAXEMAR	PARAMETER		OUTPUT LAXEMAR
Name		Rel. Change (%)	Name		Rel. Change (%)
TDS	Max.	0.00	Ca^{+2}	Max.	4.48
	Min.	0.00		Min.	0.05
	Mean	0.00		Mean	1.48
	Est. dev.	0.00		Est. dev.	1.73
Cl^-	Max.	0.00	HCO_3^-	Max.	12.64
	Min.	0.00		Min.	0.51
	Mean	0.00		Mean	7.12
	Est. dev.	0.00		Est. dev.	4.19
Na^+	Max.	0.32	SiO_2	Max.	50.71
	Min.	0.00		Min.	0.32
	Mean	0.09		Mean	25.28
	Est. dev.	0.12		Est. dev.	22.71

* Relative changes in output concentrations are defined as $|C_s - C_b|/C_b*100$, where C_s and C_b are concentrations of species computed in sensitivity (with reactive transport) and calibrated base (conservative transport) runs, respectively.

4 Conclusions

Spatial analysis and advanced visualization of Laxemar 2.1 hydrochemical database has been done, including the combined analyses of hydrochemical data and computed results obtained with hydrogeological models.

Spatial analysis of the bedrock hydrochemical database indicates that dilute groundwaters of Na-HCO_3 type dominates at the Laxemar subarea reaching considerable depths, whilst this kind of water is confined to shallow depths at Simpevarp subarea. This is consistent with the hydrogeological framework of the site, where the dynamic fresh water body is thicker inland and much thinner at the coastal areas. Brackish and saline groundwater is present at shallow to intermediate depth at the Simpevarp subarea, but at greater depths (down to 800–900 m) at the Laxemar subarea. The origin of these waters could be different from one place to another. At the Simpevarp subarea, brackish and saline waters show some residual marine signatures (Littorina) together with clear glacial isotopic signatures. In contrast, brackish and saline waters at Laxemar can be attributed to a relatively narrow dispersion zone between old and highly saline deep waters and diluted waters with recent (modern) meteoric origin. These highly saline waters are confined to depths higher than 1,200 m, and have been also detected at KLX02 borehole.

A coupled groundwater flow and reactive solute transport model of the Simpevarp area has been presented which integrate current hydrogeological and hydrochemical data and knowledge of the site. After calibration, it has been possible to reproduce the salinity fields corresponding to the current hydrogeological pseudo steady-state flow field. The numerical model has been calibrated under the assumption of heterogeneous equivalent porous media approach, and calibrated values of hydraulic conductivity are consistent with measurements, on the range of field-derived values.

Contrary to what it was expected, the distribution of most major dissolved species could be predicted by using the calibrated model, showing a conservative behaviour similarly to TDS distribution. The reason for such an apparent conservative behaviour is due to the large concentration contrast existing between fresh meteoric and deep saline waters. Thus, small amounts of mixing (by effect of hydrodynamic dispersion) induce mass transfers much larger than those produced by active geochemical process, which are eventually masked. It is woth noting that the present model is restricted to current hydrogeological settings, neglecting recent paleo events such as glacial melt water infiltration or coastline displacement. In this way, computed results can not be calibrated/compared with some available information such as environmental isotopes. These paleo events are being studied by means of other model approaches such as pure hydrochemical mixing models or pure hydrogeological models in the framework of HydroNet activities.

The reactive transport model accounts for mineral dissolution/precipitation processes under both local equilibrium and kinetic approach. Taking into account silicates weathering processes under kinetic approach leads to a better agreement between model results and field observations in terms of dissolved silica and pH. The reactive transport model fails at reproducing measured bicarbonate concentrations, most probably because the occurrence of microbially-mediated respiration of dissolved organic matter present in the fresh groundwater of meteoric origin. These kinds of processes should be further studied in the near future by incorporating the simulation of microbially-catalysed processes.

5 References

Bear J, 1972. Dynamics of fluid in porous media. Elsevier, new York, 764 pp.

Blum AE, Stillings LL, 1995. Chemical weathering of feldspars. In White AF and Brantley SL, eds, Chemical Weathering Rates of Silicate Minerals, Min Soc Am Rev Min v 31, pp 291–351.

Casey W H, Westrich H R, Holdren G R, 1991. Dissolution rates of plagioclase at pH = 2 y 3. Am. Mineral. 76, 211–217.

Chou L, Wollast R, 1985. Steady state kinetics and dissolution mechanism of albite. Am. J. Sci. 285, 963– 993.

Gaines G L, Thomas H C, 1953. J.Chem. Phys. 21, 7114–718.

Ganor J, Mogollón J L, Lasaga A C, 1995. The effect of pH on kaolinite dissolution rates and on activation energy. Geochim. Cosmochim. Acta 59, 1037– 1052.

Hartley L, Gylling B, Marsic N, Holmén J, Worth D, 2004. Preliminary Site Description: Groundwater flow simulations Oskarshamn area (version 1.1) modelled with ConnectFlow, SKB R-04-63, Svensk Kärnbränslehantering AB.

Hartley L, Hoch A, Hunter F, N Marsic, 2005. Regional hydrogeological simulations – Nu-merical modelling using ConnectFlow. Preliminary site description Simpevarp subarea – version 1.2. SKB R-05-12, Svensk Kärnbränslehantering AB.

Hartley L, Hunter F, Jackson P, McCarthy R, Gylling B, Marsic N, 2006 (in prep). Regional hydrogeological simulations – Numerical modelling using ConnectFlow. Preliminary site description, Laxemar subarea – version 1.2. SKB R-06-23, Svensk Kärnbränslehantering AB.

Jaquet O, Siegel P, 2003. Groundwater flow and transport modelling during a glaciation period. SKB R-03-04, Svensk Kärnbränslehantering AB.

Laaksoharju M, 1999. Groundwater characterisation and modelling: problems, facts and possibilities. Ph.D. dissertation. Department of Civil and Environmental Engineering. Royal Institute of Technology (KTH). Stockholm.

Laaksoharju (ed.) et al. 2004. SKB R-04-74. Svensk Kärnbränslehantering AB.

Lasaga A C, 1981. Rate laws of chemical reactions. In: Kinetics of geochemical processes (Lasaga, A.C. & Kirkpatrick, R.J. Eds.). Reviews in Mineralogy, 8, 1–68. Mineralogical Society of America.

Molinero J, 2000. Testing and Validation of Numerical Models of Groundwater Flow, Solute Transport and Chemical Reactions in Fractured Granites. PhD Thesis, Civil Engineering School, University of A Coruña, Spain. (Latter published as ENRESA Publicación Técnica 06/01).

Molinero J, Samper J, 2004. Modeling Groundwater Flow and Solute Transport in Fracture Zones: Conceptual and Numerical Models of the Redox Zone Experiment at Äspö (Sweden). Journal of Hydraulic Research, 42, 157–172.

Rimstidt J D, Barnes H L, 1980. The kinetics of silica– water reactions. Geochim. Cosmochim. Acta 44, 1683–1699.

Samper F J, 1994. Modelos de acuíferos. In: Temas actuales de hidrología subterránea: 79–101. Universidad Nacional de Mar del Plata. Argentina.

Samper J, Delgado J, Juncosa R, Montenegro L, 2000. CORE^{2D} v 2.0: A Code for non-isothermal water flow and reactive solute transport. User's manual. ENRESA Technical report 06/2000.

SKB, 2006. Preliminary site description. Laxemar subarea - version 1.2. SKB R-06-10, Svensk Kärnbränslehantering AB.

Svensson U, 1997. A regional analysis of groundwater flow and salinity distribution in the Äspö area. SKB TR 97-09, Svensk Kärnbränslehantering AB.

Voss C I, Provost A M, 2003. SUTRA, A model for saturated-unsaturated variable-density groundwater flow with solute or energy transport. U.S. Geological Survey Water-Resources Investigations Report 02-4231, 250 p.

Wieland E, Stumm W, 1992. Dissolution kinetics of kaolinite in acidic aqueous at 25°C. Geochim. Cosmochim. Acta 56, 3339– 3355.

Xu T, Samper J, Ayora C, Manzano M, Custodio E, 1999. Modeling of non-isothermal multi-component reactive transport infield scale porous media flow systems. Journal of Hydrology, 214: 144–164.

Yeh G T, 2000. Computational subsurface hydrology, reactions, transport and fate. Kluwer Acdemic Publishers, The Netherland, 318P.

14 Appendix 6: Modelling of the dilute groundwater system

Contribution to the model version 2.1

David Arcos, Jordi Guimerà

ENVIROS, Barcelona, Spain

August 2006

Contents

1 Background and objectives

The chemical composition of groundwater in the Simpevarp area is a result of geochemical reactions and mixtures between several water end-members of different origin such as glacial, marine, meteoric and brine, which relative contribution depends on the location in the bedrock /see Laaksoharju et al. 2004, SKB 2004/.

Groundwater mixing, especially when high salinity waters are involved, could mask the effect of water-rock interaction processes. Therefore, a careful analysis of the chemical data is essential to identify these processes, moreover, considering the relatively long residence times of these groundwaters in the Simpevarp area that can enhance some kinetically slow geochemical processes. The understanding of these processes is crucial for a proper interpretation of the geochemical evolution of the system and for the assessment of the geochemical stability of the deep repository.

Therefore, the understanding of which are the main water-rock interaction processes accounting for the modification of the composition of groundwater at different residence times are essential for the site assessment exercise.

The upper part of the system is, specifically, of special relevance, given that the repository will be presumably located at depths around 500 m, much above the dominance of the brine in Simpevarp.

The integration of the mixing groundwater processes with water-rock interactions and the hydrogeological characteristics of the area need of the development and implementation of coupled hydrogeochemical models able to cope with all the variables of interest in the system.

Molinero and cols. /see SKB 2004/ have used a continuum finite element model to reproduce hydrogeological trends and simplified water composition. The success of this model prompted the authors to include the geochemical processes which were more likely responsible for the major ion concentration at the upper part of the system, were groundwater is not heavily influenced by mixing with saline water /SKB 2004/.

The aim of the model was to demonstrate that despite implicit simplifications, mixing was an important process. It was indeed successful at reproducing the main observed trends, but as agreed by authors, lacked of sufficient detail in the description of some processes able to control the observed high alkalinities or the redox potential analysed in Simpevarp.

The work presented here aims at contributing to the understanding of the hydrogeochemistry of Laxemar through the assessment of the main water-rock interaction processes likely to contribute to the analysed groundwater compositions in the upper part of the Simpevarp area.

The geochemical modelling presented in the following sections consider speciation-solubility calculations, reaction path modelling and redox system analysis. The numerical calculations have been conducted with the PHREEQC code (Laxemar SDM 1.2, ch.9) and the Multivariate Mixing and Mass-balance calculations (M3), which provide a quantitative description of the groundwater composition through a mixture proportion of waters of different origins- and compositions- /SKB 2004/.

The methodology used in this analyses, though simple, aims at setting the basis for achieving a proper understanding of some of the main water-rock interaction processes acting in the upper part of the system, where the mixing process with saline water is though to be of minor importance or it has no substantial effects on the chemical composition of groundwaters (i.e. only diluted groundwaters are considered, despite of their origin). Therefore, the obtained methodology could be further implemented in more sophisticated models able to describe the spatial and temporal evolution of the system.

2 Methodology

The development of the conceptual and numerical model of the area requires of a prior selection of the geochemical data to use. Data available so far corresponds to the second "data freeze" of the site. Those samples clearly affected by the mixing with deep brine have been excluded, in order to focus the analyses on those geochemical processes, other than mixing, that may affect the groundwater compositions. The remaining chemical data have been carefully treated to identify any compositional trend as a function of depth or any correlation between chemical components.

The identified chemical trends and correlations will give important hints on which can be the main geochemical processes responsible for the geochemistry of the system. The different processes identified will be included in a conceptual model for the geochemical evolution of the system and then implemented in a numerical geochemical model.

3 Evaluation of chemical data and conceptual model

As reported in /Laaksoharju et al. 2004/, the main geochemical process in the Simpevarp area result from the mixing of different types of groundwater. This mixing process is so important that can mask the effect of the water-rock interaction processes if the whole set of data is considered. Therefore, in order to discriminate these other processes we have selected for this analyses the samples where the mixing fingerprint is not so important, that is, those presenting chloride concentrations below 15 mmoles/L. These samples are located above 1,000 m-depth and far from the coast, as shown in Figure 1 /Molinero and Raposo 2004/.

The resulting set of data include samples from the subareas of Laxemar and Simpevarp, excluding those sampled near the coast line (Äspö and Ävrö), at depths below 1,000 m, and from the lower part of deep boreholes when chloride concentration exceeds a value of 14 mmoles/L (half the chloride concentration in seawater[7]) avoiding samples that have been largely modified by a mixing process with highly saline waters.

The analysis of the selected data set indicates that there are two relatively independent sub-systems, one corresponding to near surface groundwaters (PLX- and SSM-boreholes) and the other represented by the rest of the samples (KLX- and HLX-bedrock boreholes).

For near surface groundwaters there is a clear evolution increasing both the concentration of calcium and aqueous carbonate (see PLX+SSM samples in Figure 2).

This type of evolution is typical of diluted waters in contact with calcite-bearing rocks, leading to the dissolution of calcite according to the following reaction:

$CaCO_3 + H^+ \rightarrow Ca^{2+} + HCO_3^-$

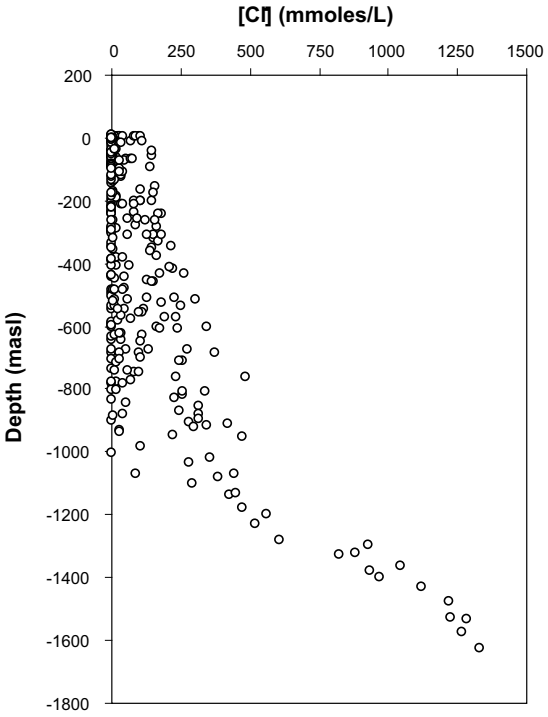

Figure 1. *Chloride concentration versus depth for the Simpevarp area.*

[7] We considered the chloride concentration in seawater as 28 mmoles/L, although in the Baltic Sea the mean concentration is around 100 mmoles/L.

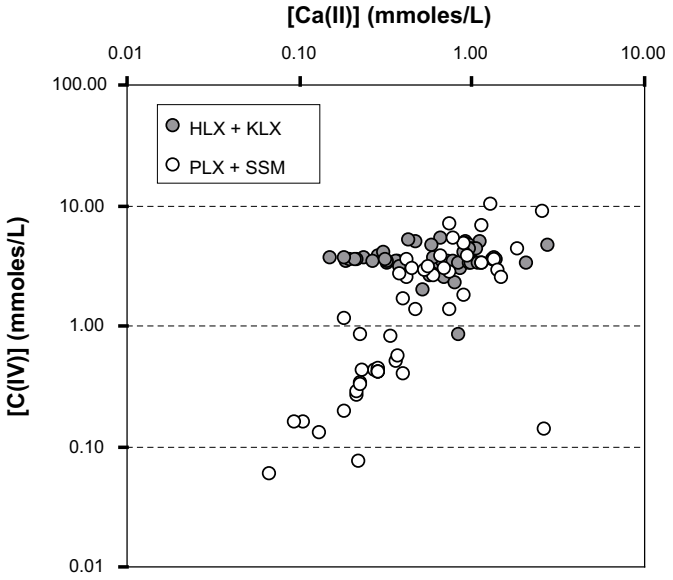

Figure 2. *Graphic showing the correlation between the concentrations of aqueous carbonate and calcium for the selected samples.*

Other carbonates can be also present in the system, leading to a similar evolution of groundwater composition. For this reason we compared the calcium concentration of near surface groundwaters with other major cations. Not surprisingly, there was a positive correlation of calcium with magnesium, as well as of calcium with strontium (Figure 3). The Ca/Mg ratio close to one indicates that the carbonate being dissolved is not calcite but dolomite, according to the following reaction:

$$CaMg(CO_3)_2 + 2\ H^+ \rightarrow Ca^{2+} + Mg^{2+} + 2\ HCO_3^-$$

Whereas, the high Ca/Sr ratio indicates that strontium is only present in trace amounts in dolomite.

Independently of the mineral dissolving in this part of the system, calcite or dolomite, both reactions imply the consumption of protons and therefore an increase in pH is expected to occur simultaneously with the increase in calcium, magnesium and total carbonate (see Figure 4).

The saturation index of the groundwaters with respect to dolomite (see Figure 5) confirms the dolomite dissolution as the main process controlling the geochemical evolution of near surface groundwaters, as it increases in near surface groundwaters until reaching saturation with this mineral (SI = 0 ± 1).

The rest of major cations (K and Na) and anions (chloride and sulphate) do not show any clear trend or correlation, probably indicating that their concentrations are not controlled by any major water-rock interaction process.

The trends or correlations for the deep groundwater samples (HLX and KLX boreholes) are very different than those for near surface waters. As can be seen in Figure 2 and Figure 4, neither calcium-carbonate, nor pH-carbonate correlations exist in deep groundwaters. In these samples, there is a clear inverse correlation between pH and Ca, (in contrast with the positive correlation that exists for near surface waters), showing a pH increase with the decrease of the calcium concentration (Figure 6).

Although deep groundwaters seem to be in equilibrium with calcite, the increase in pH can not be attributed to the dissolution of calcite, given that the carbonate concentration is maintained nearly constant and calcium concentration slightly decreases (Figure 2).

A possible explanation for the variation of calcium concentration in these samples could be a mixing process with seawater (samples suggesting mixing with deep seated brines have been skipped). From Figure 7, it is clear that deep groundwaters reflect the effect of minor mixing with seawater

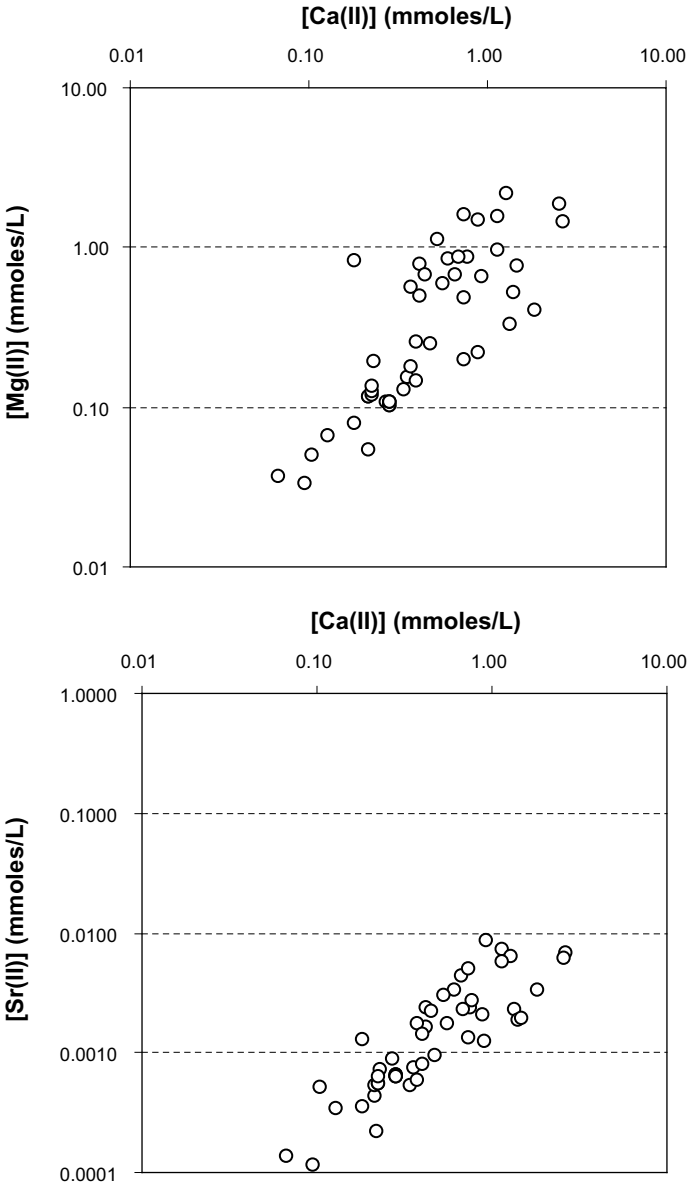

Figure 3. *Graphics showing the positive correlation between calcium and magnesium and calcium and strontium for the near surface groundwaters.*

(< 10% of seawater in the resulting groundwater), according to the increase of sodium and chloride concentrations and a Na/Cl ratio equivalent to that of Baltic seawater. The effect of this mixing with seawater is clearer when samples with a higher salinity from Simpevarp, but still below that of seawater, are included (Figure 7). Nevertheless, the increase in calcium concentration does not match the mixing trend; actually, samples departs from this line, indicating that other process is additionally affecting the calcium system.

The lack of correlation between aqueous sulphate and calcium also indicates that gypsum (or anhydrite) is not dissolving.

Assuming that near surface waters infiltrate downwards, the expected evolution is of increasing pH as the concentration of calcium, previously increased due to calcite dissolution in the upper part of the system, decreases (Figure 6). The only likely reaction or type of reactions that can lead to such variation of calcium concentration and pH is the weathering of primary silicates. Weathering

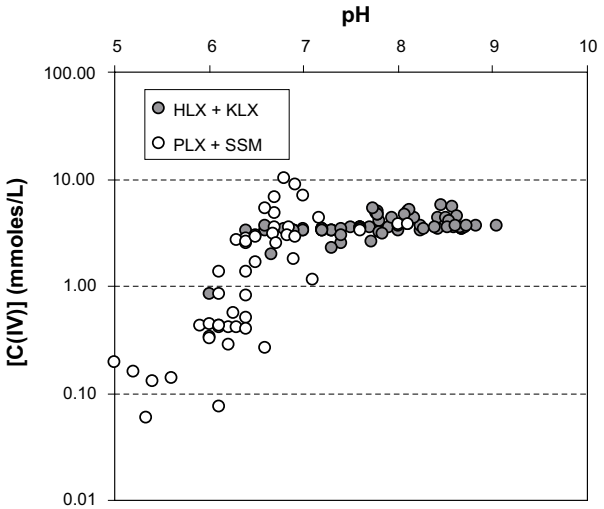

Figure 4. *Graphic showing the correlation between pH and the concentration of aqueous carbonate for the selected samples.*

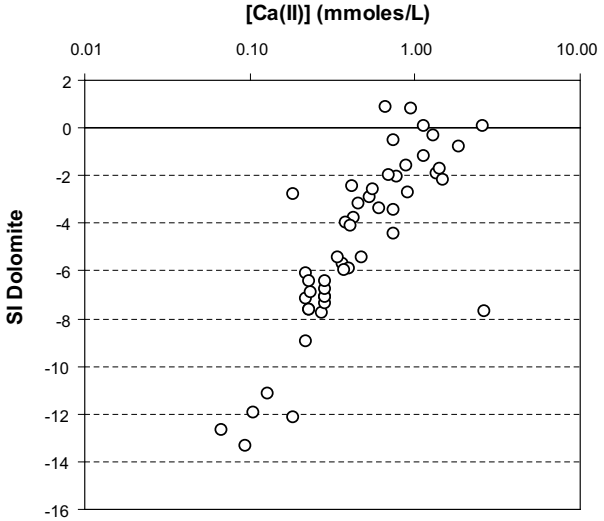

Figure 5. *Graphic showing the saturation index of dolomite as a function of the calcium concentration for the selected samples.*

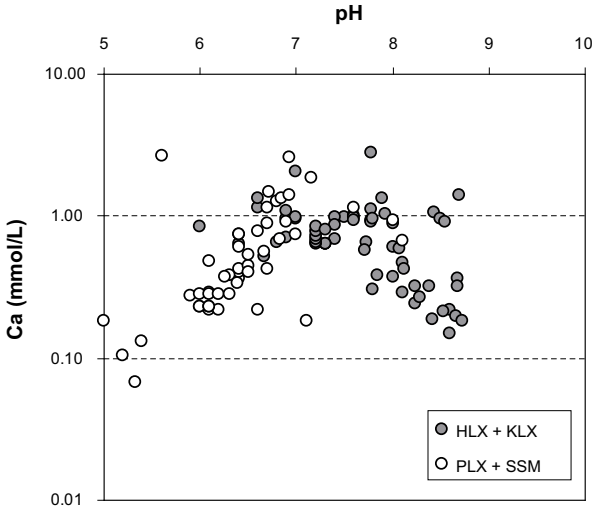

Figure 6. *Graphic showing the correlation between pH and the calcium concentration for the selected samples.*

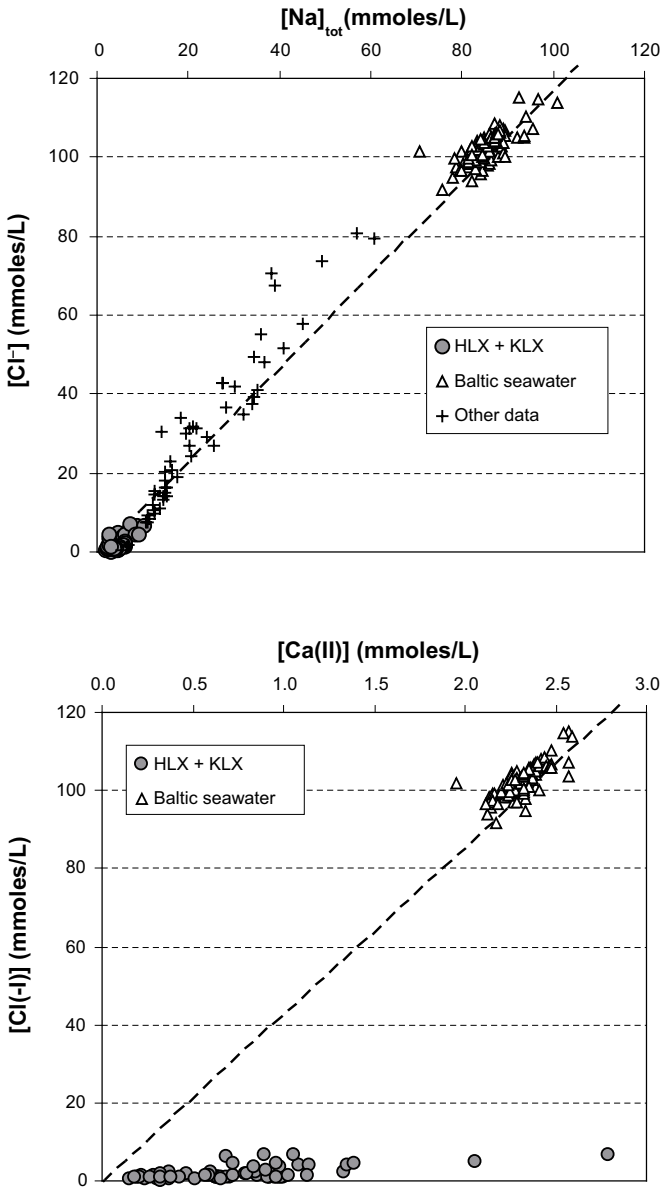

Figure 7. *Cl-Na and Cl-Ca plots for Baltic seawater and deep groundwater samples (dashed line represents Baltic seawater dilution line at constant Na/Cl ratio, not a correlation line). Note that to some extent, the increase in chloride and sodium, matches the mixing line with Baltic seawater, especially when considering samples from Simpevarp with higher salinity but below that of seawater (labelled as other data in the Cl-Na plot). However, the increase in calcium concentration is up to one order of magnitude higher than for pure mixing with seawater, suggesting that there is another source for calcium than seawater.*

is in fact a sum of different processes, mainly the non-congruent dissolution of primary silicates (i.e. feldspars, quartz and biotite) to form secondary silicates (i.e. clay minerals and silica phases as cristobalite). An example of the overall weathering reaction of anorthite can be written as:

$$1.9\ CaAl_2Si_2O_8 + 4.2\ Si(OH)_4 + 3.2\ H^+ \rightarrow 2\ Ca_{0.15}Al_{1.9}Si_4O_{10}(OH)_2 + 1.6\ Ca^{2+} + 8\ H_2O$$

Anorthite Ca-montmorillonite

This reaction lead to a pH increase, as expected, but it also implies an increase of the aqueous calcium concentration. Nevertheless, in the area of study, the dissolving feldspar is likely a solid solution between the three most common end-members: anorthite ($CaAl_2Si_2O_8$), albite ($NaAlSi_3O_8$), and K-feldspar ($KAlSi_3O_8$). The dissolution of such feldspar would lead to a minor increase in

calcium concentration in groundwater. Moreover, calcium in montmorillonite, as in most clay minerals, occupies the interlaminar position which is a weak binding site easily exchangeable by other cations as sodium. Therefore, the behaviour of calcium in the system due to the weathering process would depend on the feldspar composition, the clay mineral formed and its cation exchange capacity (CEC), whose composition will be controlled by that of the groundwater.

The stability diagrams shown in Figure 8 help to assess which are the silicates most likely to form in the area. On the basis, of these diagrams it seems clear that the kinetic dissolution (weathering) of feldspars, biotite and quartz, may lead to the formation of Na-Ca-(± K)-montmorillonite, illite, cristobalite and kaolinite.

Despite, the possible geochemical evolution of the deepest part of the system under consideration, there are still some uncertainties related to the redox state and the behaviour of iron. This is due to the lack of data concerning the Eh of groundwaters. In any case, it is likely that the source of iron is biotite, what can produce a precipitation of Fe(III) oxy-hydroxide, although not definite conclusions can be drawn in the light of the existing data.

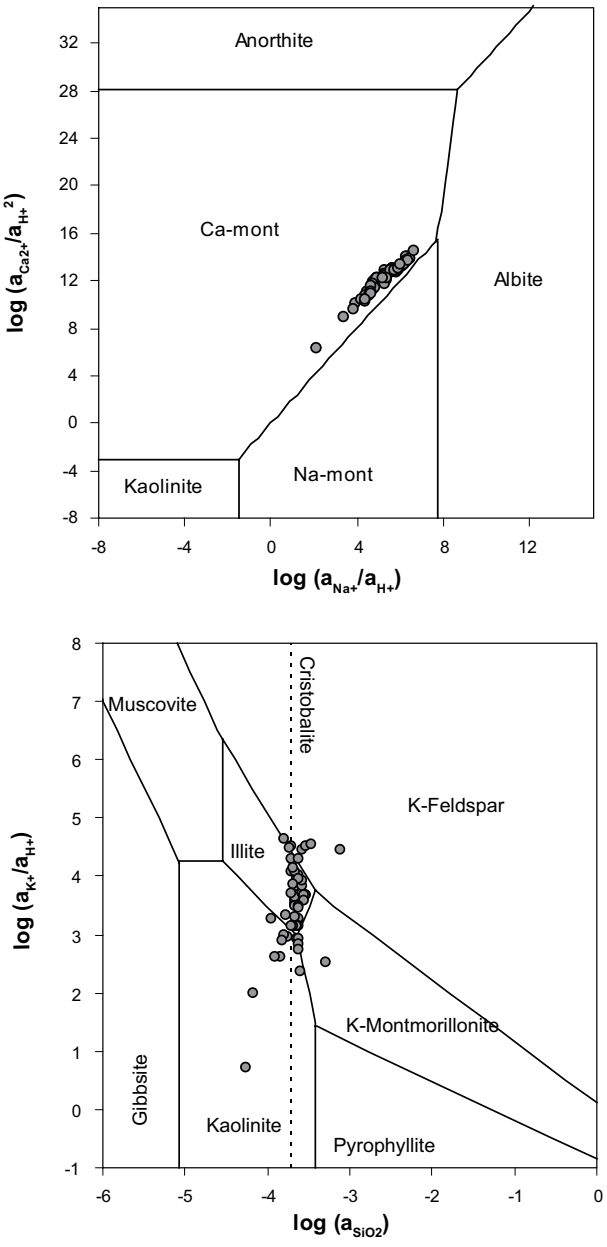

Figure 8. *Log (a_{Ca2+}/a_{H+}^2)-log (aN_{a+}/a_{H+}) and log (a_{Na+}/a_{H+})-log (a_{H4SiO4}) diagrams showing the possible stable clay minerals formed during the alteration of the primary silicates from the granitic rock.*

4 The numerical model

In this section we present a numerical model where the conceptual model previously described is implemented. As we focus on the geochemical evolution of infiltrating water due to water-rock interactions, it is reasonable to conduct a batch calculation, where a pool of granitic minerals (i.e. feldspars) are assumed to be in contact with infiltrating water and dissolve following a kinetic rate law. Simultaneously, the precipitation of secondary minerals is allowed in case they oversaturate in the system.

The geochemical code used for the calculations is PHREEQC /Parkhurst and Appelo 1999/ together with its associated thermodynamic database, with the addition of dissolution-precipitation reactions of illite and montmorillonite using thermodynamic data from /Garrels 1984/.

First of all it is essential to properly select the chemical composition of infiltrating water. The model takes into consideration the geochemical processes affecting the groundwater composition from the deeper part of the system; this is the weathering of primary granitic minerals. Therefore, the selection of a realistic initial water composition is based on the analysis of water evolution from the previous section. The less evolved groundwater in the lower part of the system is the one presenting the lowest pH values. There are a few samples with pH around 6.5 (Figure 6). To select the most convenient initial groundwater composition, additional criteria like high calcium concentration (see previous section) and proximity to surface (that means excluding very deep groundwater samples) have to be considered. The water composition that best fits these requirements is that corresponding to a sample collected in borehole KLX02 at a depth interval (referred to sea level) between –12.5 and –62.3 m (Table 1).

This water composition is simulated to be in contact with granitic primary minerals, as K-feldspar, albite and anorthite which are allowed to dissolve kinetically. The kinetic rate laws for these minerals are based on the work by /Sverdrup 1990/ and /Sverdrup and Warfvinge 1995/, through the following rate expression at 25°C:

$$Rate = \left(k_{H^+} a_{H^+}^{n} + k_{H_2O} + k_{CO_2} \left(10^{SI_{CO_2}}\right)^{m} \right) \times A/V \times \left(1 - 10^{SI_{\min eral}}\right)$$

Where k_i are experimental rate coefficients, a_i are the activities of the i^{th} species, n, m and t are reaction orders, SI refers to the saturation indices, and A/V is the area to volume ration for the mineral in m^{-1}. According to /Sverdrup and Warfvinge 1995/ the parameters to be used are as in Table 2.

According to the above rate expression, some parameters, such as reactive surface area (A/V) can be changed and have been fixed arbitrarily to 1 mm side cubes in order to obtain the results that best fit to the analytical data, being within the range of values typical for systems like the one under study.

Table 1. Chemical composition selected as initial water for the calculations (units in moles/L). This composition corresponds to sampled water from borehole KLX02 at a depth of 37 m.

pH	6.6	C(IV)	$3.31 \cdot 10^{-3}$
Na(I)	$5.83 \cdot 10^{-3}$	Cl(–I)	$4.12 \cdot 10^{-3}$
Ca(II)	$1.14 \cdot 10^{-3}$	S(VI)	$6.05 \cdot 10^{-4}$
K(I)	$1.00 \cdot 10^{-4}$	Si(IV)	$1.42 \cdot 10^{-4}$
Mg(II)	$1.77 \cdot 10^{-4}$	Al(III)	$1.00 \cdot 10^{-6}$

Table 2. Experimental rate coefficients and parameters for the dissolution rate of feldspars according to /Sverdrup and Warfvinge 1995/.

Mineral	pk_{H+}	pk_{H2O}	pk_{CO2}	n	m
K-feldspar	14.7	17.5	16.8	0.5	0.6
Anorthite	14.6	17.2	15.9	0.5	0.6
Albite	14.5	16.7	15.9	0.5	0.6

If supersaturated, a series of minerals are allowed to precipitate, as montmorillonite, illite, calcite, dolomite, and cristobalite. It is known that, at least montmorillonite and illite will follow a kinetic rate for precipitation. However, as the dissolution rate of feldspars is slower than the precipitation of these clay minerals, we can assume that the dissolution of feldspars will be the limiting step in the overall reaction, and thus, we can assume the precipitation of clay minerals driven by thermodynamic equilibrium.

The total modelling time has been set to 200,000 years, although increasing the reactive surface area of feldspars, thus increasing the reaction rate, will get the same results in a shorter simulation time and the contrary is also true.

4.1 Numerical modelling results

The results of the model show that a good agreement between the computed evolution for the chemical composition of groundwater and the selected analytical data. Moreover, the expected increase in pH due to dissolution of feldspars seems to be confirmed (Figure 9). In addition, the decrease in calcium associated to the water-rock interaction can be attributed to the precipitation of a calcium-rich montmorillonite (Figure 10), as pH increases due to the kinetic dissolution of feldspar, the increase in silica and aluminium leads to the precipitation of cristobalite (SiO_2) and clay minerals such as illite and montmorillonite. The precipitation of all these minerals is in agreement with the conceptual model described above.

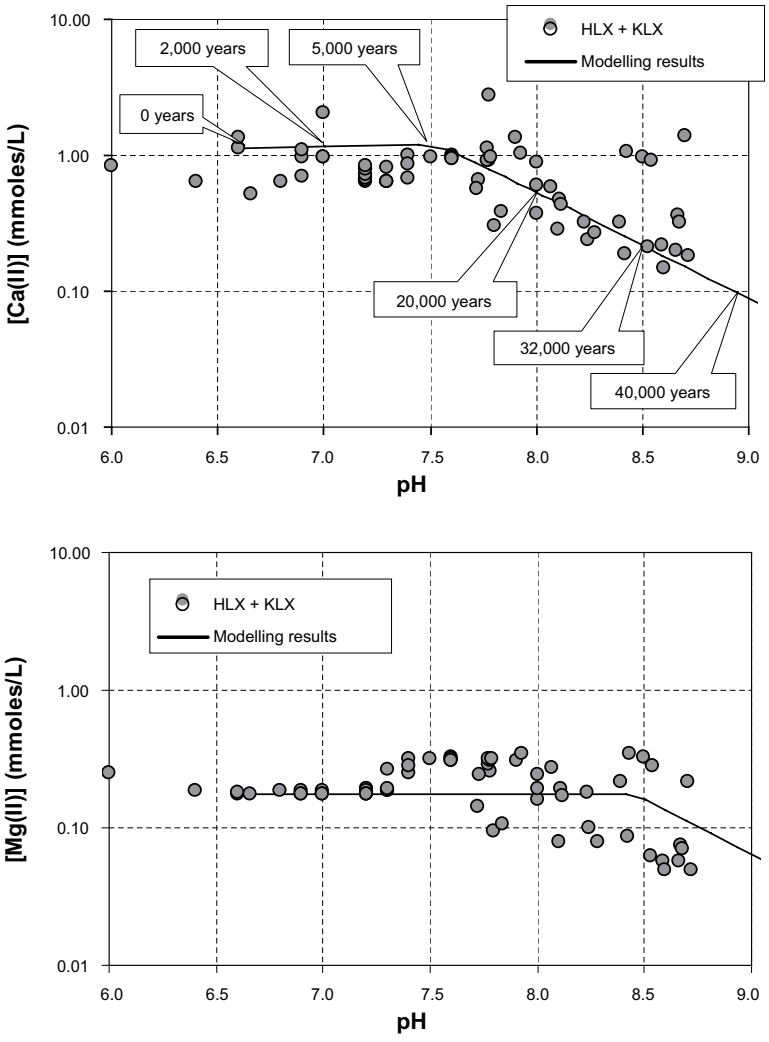

Figure 9. *pH-Ca(II) and pH-Mg(II) diagrams showing the analytical data for deep boreholes together with the modelling results. In the upper graphic the simulation time is also indicated for the modelling results.*

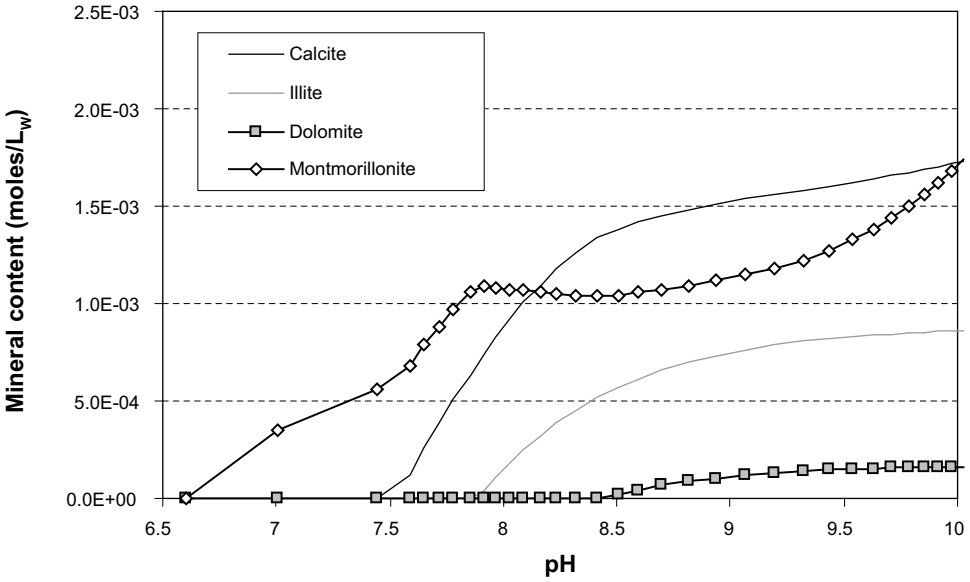

Figure 10. *Predicted precipitation of secondary minerals as a function of pH. Cristobalite is also predicted to precipitate, although it has not been represented in this graphic.*

However, the predicted increase in pH has also an additional effect, the precipitation of carbonate minerals, as calcite and dolomite, which also contribute to the decrease in the concentration of both calcium and magnesium (Figure 9). The precipitation of these phases results in a decrease in aqueous carbonate concentration in groundwater (Figure 11), although this is not reflected in the analytical data of dissolved carbon. Most probably other hydrogeochemical processes can be invoked to explain the behaviour of measured dissolved carbon, such as microbially-mediated degradation (respiration) of dissolved organic matter. Such a process has been proved to have a relevant impact on the hydrochemical compositions of the granitic groundwater in the Äspö site /Banwart et al. 1999, Molinero et al. 2004/. In any case, the predicted decrease in aqueous carbonate concentration is very low and could be within the analytical error of the data.

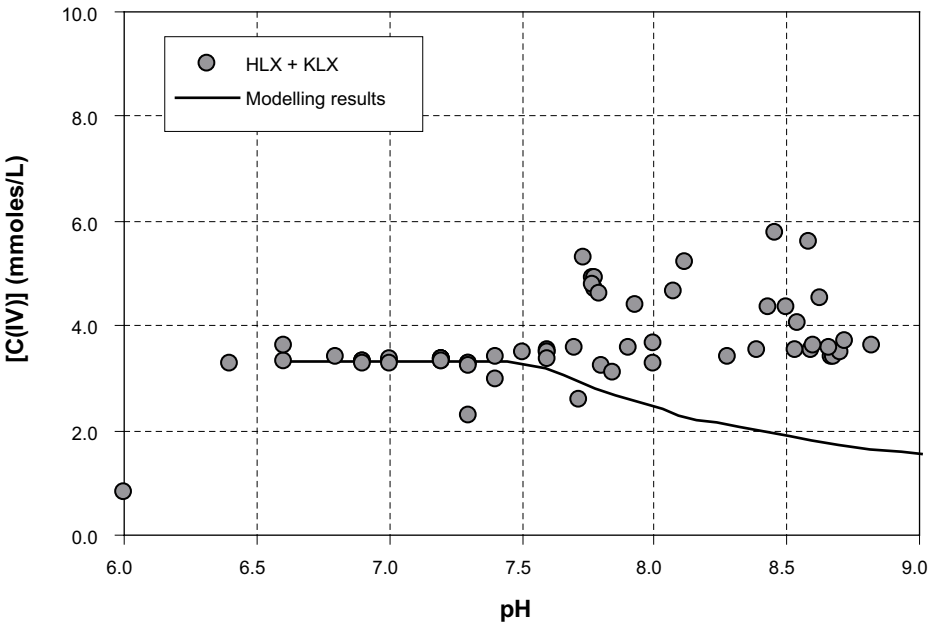

Figure 11. *pH-C(IV) diagram showing the analytical data for bedrock boreholes together with the modelling results.*

5 Conclusions

The existing hydrochemical data for dilute groundwaters indicates that there are two relatively independent hydrogeologically active systems, one corresponding to near surface groundwaters and other represented by the granitic bedrock. For near surface groundwaters there is a clear evolution driven by calcite and/or dolomite dissolution, increasing the concentration of both aqueous calcium (and magnesium) and carbonate and increasing the pH. In the granitic aquifer, the increase in pH can not be attributed to the dissolution of calcite but it seems that silicates weathering play a major role on the observed pH increase. This increase in pH can be properly reproduced by a geochemical model simulating the silicates weathering process through a theoretical flow line. The model can also reproduce the decrease in calcium and magnesium associated to the water-rock interaction processes. However, the detailed geochemical model fails at reproducing the aqueous carbonate behaviour, most probably due to the occurrence of oxidation of organic matter, which would induce an increase on water alkalinity.

6 References

Banwart S, Gustafsson E, Laaksoharju M, 1999. Hydrological and Reactive Processes during Rapid Recharge to Fracture Zones. The Äspö Large Scale Redox Experiment. Applied Geochemistry. 14, 873–892.

Garrels R M, 1984. Montmorillonite/illite stability diagrams. Clays and Clay Minerals, 32,161–166.

Laaksoharju M, Smellie J, Gimeno M, Auqué L, Gómez J, Tullborg E-L, Gurban I, 2004. Hydrogeochemical evaluation of the Simpevarp area, model version 1.1. SKB R-04-16, Svensk Kärnbränslehantering AB.

Molinero J, Raposo J R, 2004. Appendix 6: Coupled hydrogeological and reactive transport modelling, in: Hydrogeochemical evaluation for Simpevarp model version 1.2. Preliminary site description of the Simpevarp area, M. Laaksoharju (ed.), SKB R-04-74, 417–458, Svensk Kärnbränslehantering AB.

Molinero J, Samper F J, Zhang G, Yang C, 2004. Biogeochemical reactive transport model of the redox zone experiment of the Äspö hard rock laboratory in Sweden. Nuclear Technology, 148: 151–165.

Parkhurst D L, Appelo C A J, 1999. User's guide to PHREEQC (version 2) – A computer program for speciation, batch-reaction, one-dimensional transport, and inverse geochemical calculations: U.S. Geological Survey Water-Resources Investigations Report 99-4259.

SKB, 2004. Hydrogeochemical evaluation for Simpevarp model version 1.2. Preliminary site description of the Simpevarp area. SKB R-04-74, Svensk Kärnbränslehantering AB.

Sverdrup H U, 1990. The kinetics of base cation release due to chemical weathering: Lund University Press, Lund, 246 p.

Sverdrup H, Warfinge P, 1995. Critical loads of acidity for Swedish forest ecosystems. Ecol. Bull., 44: 75–89.

15 Appendix 7: Modelling of the interaction beween the salinities in the bedrock fractures and in the rock matrix

Contribution to the model version 2.1

Luis Moreno, KTH

August 2006

Keywords: Fractures, rock matrix, salinity, modelling, interaction

Abstract

Calculations were performed to study the interaction between species dissolved in the pore water in a rock matrix and those dissolved in the water flowing in fractures. In a first set of calculations, the evolution of the concentration in the rock matrix was determined for the case of fresh water intrusion, where the concentration in adjacent fractures becomes negligible. Three different geometries were modelled (matrix/fracture system, rock block surrounded by water-conductive fractures, and a channel embedded in a rock mass). The results show that the depletion of salinity takes several hundreds of years for distances of about one metre to the adjacent fracture. In a second set of calculations, the evolution of the concentration in the adjacent fractures was considered. The change in concentration depends on the surface area contacted by the fresh water (FWS) and the water flow rate Q in the path the water follows from the intrusion point to the studied zone. For large values of $\sum$ (FWS/Q), the depletion time may be very long; thousands of years. Finally, fractures with a large transmissivity intersecting a borehole were studied in detail. The results show that these fractures collect water that has travelled along paths with small and large water flow rates.

Sammanfattning

Beräkningar för att studera samverkan mellan ämnen lösta i bergmatrisens porvatten och ämnen lösta i vattenbärande sprickor har genomförts. I ett första steg bestämdes koncentrationsutvecklingen i bergmatrisen vid inträngning av färskvatten, där koncentrationen i närliggande sprickor är försumbar. Tre olika geometrier modellerades (matris/spricksystem, bergblock omgivet av vattenbärande konduktiva sprickor och en kanal inbäddad i berg). Resultaten visar att det tar hundratals år att utarma saliniteten i matrisen då avståndet till närliggande spricka är ungefär en meter. I ett andra steg togs hänsyn till koncentrationsutvecklingen i närliggande sprickor. Koncentrations-förändringen beror på ytarean i kontakt med färskvatten (FWS) och vattnets flödeshastighet Q längs vattnets flödesväg från inträngningspunkten till den studerade zonen. Tiden för att utarma saliniteten kan bli mycket lång, tusentals år, för stora värden på $\sum$ (FWS/Q). I detalj studerades slutligen sprickor med hög transmissivitet som skär genom borrhål. Resultaten visar att dessa sprickor samlar vatten som transporteras längs flödesvägar med små och stora flödeshastigheter

Executive Summary

Scoping calculations were performed to study the interaction between species dissolved in the pore water in a rock matrix and those dissolved in the water flowing in fractures. These calculations were carried out to show the effect of fresh water intrusion into a zone containing saline water. The saline species migrate by diffusion in the matrix pores and the direction of migration is determined by the direction of the concentration gradient. In the case of fresh water intrusion, ions will migrate from the matrix pore water into the water in the fracture.

In a first set of calculations, the evolution of the concentration in the rock matrix was determined for the case of fresh water intrusion where the concentration in the adjacent fractures becomes negligible. Three different geometries were modelled: a) fracture matrix interaction with diffusion perpendicular to the fracture plane, b) a rock block surrounded by conductive fractures, and c) a narrow channel embedded in a large rock mass. The results show that the time for salinity depletion is of the order of hundreds to thousands of years for a distance of one metre in the matrix. These results could be directly applied to the case of salinity depletion from the rock matrix into a fracture with a very high flow rate.

In a second set of calculations, the evolution of the concentration in the adjacent fractures was considered and the time to depletion of the matrix salinity increased. The time to depletion depends on the surface area contacted by the fresh water (FWS) and on the water flow rate Q in the path followed by the water flowing from the intrusion point to the studied zone. Actually, the depletion time depends on the sum of the ratio FWS/Q along the path followed by the water i.e. $\sum$ (FWS/Q). For large values of $\sum$ (FWS/Q), the depletion time may be very long; thousands of years. However, for small values of this term (e.g. high water flow rate), the concentration in the fracture may decrease very rapidly.

Finally, simulations were carried out to determine the paths followed by the water from the point of intrusion to the zone under study. These simulations were made using the Channel Network Model /Gylling et al. 1999/. Particle tracking was used to determine $\sum$ (FWS/Q) for the several water parcels travelling through the channel network. The results show that fractures with large transmissivity collect water that has travelled through paths where $\sum$ (FWS/Q) varies over a wide interval. The evolution of concentration in a fracture as a function of time is weakly related to the fracture transmissivity.

Contents

1 Introduction

The concentrations of some species dissolved in the pore water in a rock matrix may be used in Site Characterization (SC) to obtain information about the origin and age of the waters that have intruded into a specific site. The impact of fresh water intrusion into zones with saline water could be estimated by studying the salinity (chloride concentration) evolution of the pore water.

The concentrations of solutes in pore water taken from drill-core samples have been determined by /Waber and Smellie 2005/. Since this pore water cannot be sampled by conventional groundwater sampling techniques, an indirect method was used, based on the diffusion of ions dissolved in water in the the pore space between minerals and along grain boundaries in the drill-core material. Accessible, interconnected pore water has been extracted by laboratory out-diffusion experiments. The purpose of these experiments was to characterise the pore water chemically and isotopically and to relate these data to the groundwater evolution in the past and at the present time /Waber and Smellie 2005/. In addition, diffusion coefficients in the bore cores were determined, for subsequent use in transport calculations. In our case, we have devoted our attention to the chloride concentration (salinity). However, the results may be applied to other conservative (non-sorbing) species. The transmissivity of the fractures intersecting the bore hole and the salinity in these fractures have also been determined.

The present concentration of the pore water in the rock matrix is dependent on several factors. One of these is the occasion when water exchange last occurred. Another is the evolution of the concentration of the water flowing in the fractures adjacent to the rock matrix. For fractures with a large water flow, it could be expected that the concentration would change quickly; i.e. the concentration would start to decline a short time after the fresh water intrusion had taken place. On the other hand, in a fracture with a small water flow, it could be expected that the concentration would be unchanged for a very long time.

The aim of this report is to relate the pore water concentration and the concentration in the fracture to the time when the intrusion has taken place.

2 Background

The solute dissolved in water flowing in the fracture interacts with that dissolved in the pore water in the matrix through diffusion. Pore diffusion in crystalline rock is usually very small; of the order of $3.0 \cdot 10^{-12}$–$2 \cdot 10^{-10}$ m^2/s. Therefore, it is expected that the depletion of species dissolved in the pore water in the matrix by diffusion takes a very long time.

2.1 Diffusion

Diffusion is the process by which a solute dissolved in a fluid (gas or liquid) migrates to a location with a lower concentration. As a result of this process, the salt dissolved in the water in the pore space may migrate into the water flowing in adjacent fractures if the concentration in the latter is lower than that in the matrix. The opposite also is valid, if the salinity in the rock matrix is initially lower; the solute may migrate from the fracture into the matrix. Figure 1 shows a schematic picture of a fracture surrounded by a semi-infinite matrix where the solute dissolved in the water in the fracture is migrating into the rock matrix.

The porosity of the rock matrix is defined by the pore space between minerals and along the grain boundaries, as shown in the lower part of Figure 1. For a water-saturated porous medium where diffusion occurs in the pore fluid, the specific mass flow (mass flux) rate is given by

$$n = \frac{N}{A} = D_p \cdot \varepsilon_p \frac{dC_p}{dx} \qquad \text{(Equation 1)}$$

where n is the mass flux ($mol/m^2/s$) and N is the mass flow rate (mol/s). C_p is the solute concentration in the pore water (mol/m^3) and ε_p is the rock matrix porosity accessible for diffusion; the so-called transport porosity. D_p is the diffusivity in the pore water (m^2/s), which takes into account the longer paths along the pores (tortuosity) and the zones with small pore diameter (constrictivity).

The pore diffusivity may then be expressed as a function of the diffusivity in free water D_v:

$$D_p = D_v \frac{\delta_D}{\tau^2} \qquad \text{(Equation 2)}$$

where δ_D is the constrictivity, τ^2 is the tortuosity, and D_v is the diffusivity (m^2/s) in free water (a large volume of water).

The effective diffusivity, D_e (m^2/s) is then defined as the product of the pore diffusivity and the transport porosity,

$$D_e = D_p \varepsilon_p \qquad \text{(Equation 3)}$$

For sorbing species, an apparent diffusivity can be defined as:

$$D_a = \frac{D_e}{\varepsilon_p + K_d \rho} \qquad \text{(Equation 4)}$$

where $K_d \rho_p$ is the volumetric sorption constant. For a non-sorbing species D_a is equal to D_p.

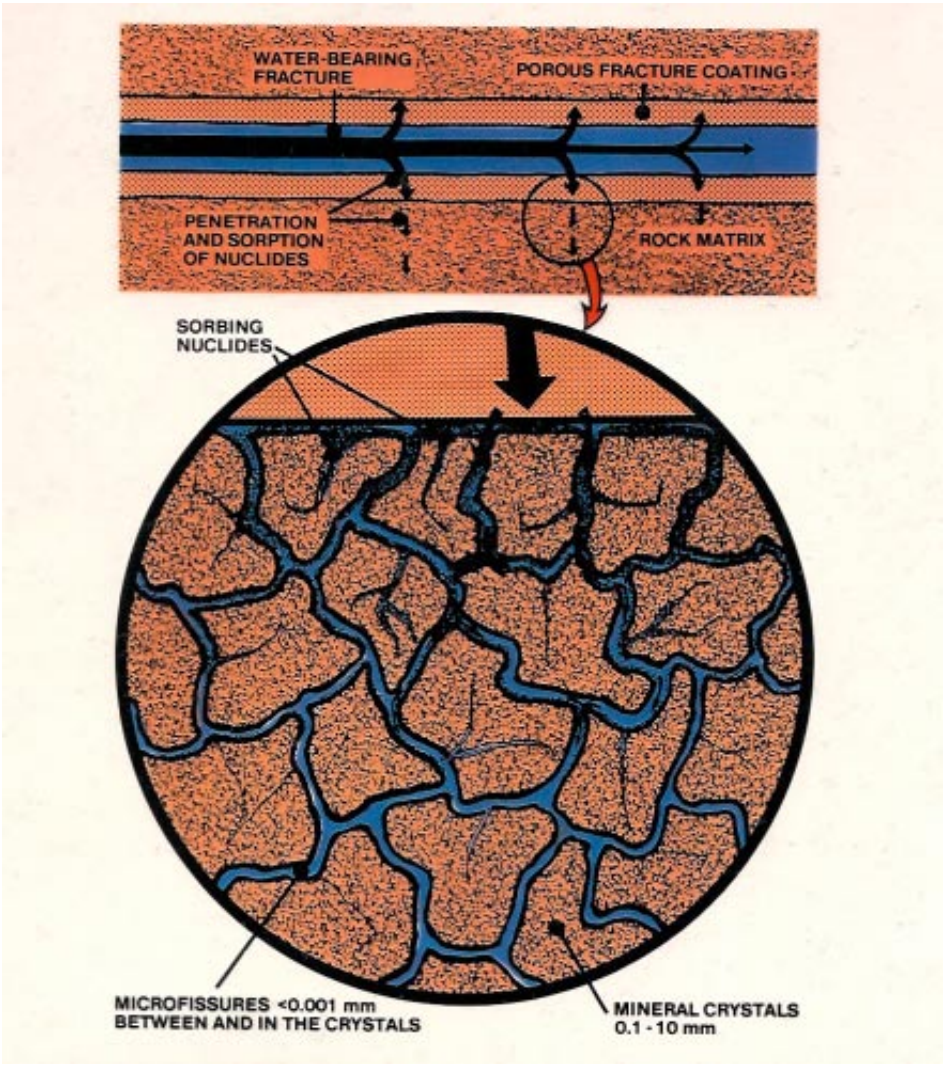

Figure 1. *Schematic picture of diffusion of a solute dissolved in the water flowing in the fracture.*

3 Scoping calculations

In this section, some simple calculations are performed to clarify the interaction between the pore water in the matrix and the water in the fractures. The calculations refer to the salinity, but the results can be applied to other conservative species.

These calculations are based on the case where fresh water intrudes into a zone containing saline water; so-called fresh water intrusion. Initially, fresh water flows through the fractures and the chloride ions in the pore water diffuse into the fracture. The calculation may also be applied to the opposite situation. However, the initial and boundary conditions must then be modified by replacing the concentration C with ($C_{initial}$–C).

The evolution of the concentration in the matrix is calculated assuming a negligible concentration in the fracture. This is a hypothetical case, since the concentration in the fracture is initially similar to the concentration in the rock matrix and decreases with time due to the fresh water intrusion. This calculation shows how the different geometries influence the depletion time, i.e. the time until the salinity decreases to a negligible value.

In Chapter 4, the evolution of the concentration in the fracture is considered.

3.1 Calculations of salinity evolution in the matrix with a negligible concentration in the fracture

In these calculations, salt diffusion in three different geometries is considered

- Diffusion in a plane geometry. This takes place when the fracture is sufficiently wide and diffusion is perpendicular to the fracture plane, from the rock matrix into the fracture.
- Diffusion in a spherical geometry. In a situation where a rock block is totally surrounded by conductive fractures, the water flows through all the faces.
- Diffusion in a cylindrical geometry. If a narrow channel is embedded in a large rock mass, the diffusion is initially perpendicular to the channel plane, but at longer times the diffusion becomes radial.

3.1.1 Diffusion from the matrix perpendicular to the fracture plane

Diffusion from the rock matrix into the fracture is schematically shown in Figure 2. The salinity in the fracture is assumed to be negligible. In addition, it is assumed that all the chloride is dissolved in the pore water.

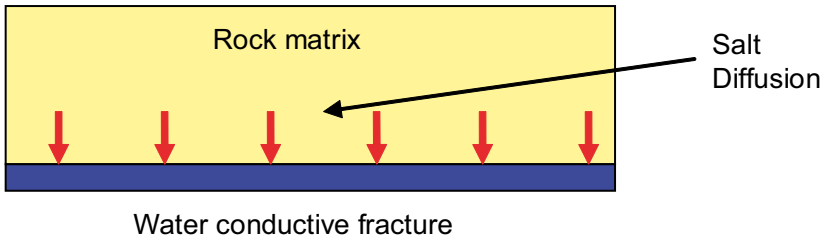

Figure 2. *Schematic picture of diffusion from the matrix into the water in the fracture for a plane geometry.*

For a semi-infinite matrix with an initial concentration of C_o in the pore water and a negligible concentration in the fracture, the concentration in the matrix as a function of the depth and time is /Bird et al. 2002/:

$$\frac{C}{C_0} = 1 - \mathrm{Erfc}\left[\frac{z}{4 \cdot D_p \cdot t}\right] \qquad \text{(Equation 5)}$$

where z is the distance in the matrix measured from the matrix-fracture interface (m), Dp the pore diffusivity (m^2/s), and t the time (s).

3.1.2 Diffusion into fractures surrounded a block of rock.

If a rock mass is totally surrounded totally by conductive fractures and if the distance between the water conductive fractures is the same in the three directions, the rock mass becomes a cube. This is shown in Figure 3, as a two-dimensional section.

Figure 4 shows the concentration in the rock matrix after a given time for a negligible salinity in the fracture.

For the sake of simplicity, the cube is transformed to a sphere with a diameter equal to the cube side. For a sphere with an initial concentration C_o and zero concentration at the surface, the solution /Crank 1975/ is:

$$\frac{C}{Co} = 1 - \frac{a}{r}\sum_{n=0}^{\infty}\left[\mathrm{Erf}\left(\frac{(2n+1)a + r}{2\sqrt{D_p t}}\right) - \mathrm{Erf}\left(\frac{(2n+1)a - r}{2\sqrt{D_p t}}\right)\right] \qquad \text{(Equation 6)}$$

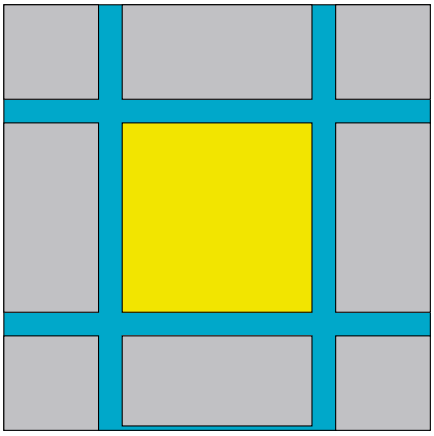

Figure 3. *A rock block surrounded by conductive fractures.*

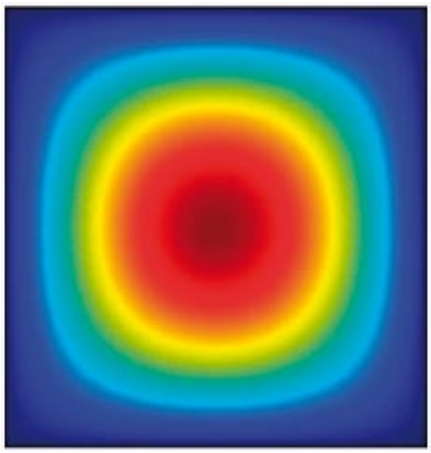

Figure 4. *Salinity in the rock block.*

This relationship is not applicable for small values of the ratio r/a, but it is not a limitation in this case, since we are not interested in the concentration at the centre of the sphere. The concentration profiles may be plotted for different times, or for different values of the product $\frac{D_p \cdot t}{a^2}$, where D_p is the pore diffusivity (m^2/s), t is the time (s), and a is the sphere radius (m).

The amount of mass that diffuses from the rock block may also be calculated by the relationship /Crank 1975/:

$$\frac{M}{M_o} = 1 - \frac{6}{\pi^2}\sum_{n=1}^{\infty}\frac{1}{n^2}\mathrm{Exp}\left[-n^2\pi^2\frac{D_p t}{a^2}\right] \qquad \text{(Equation 7)}$$

3.1.3 Diffusion into a narrow fracture/channel embedded in an infinite rock mass

A schematic picture of the situation where diffusion takes place from an infinite rock mass into a narrow channel/fracture embedded in it is shown in Figure 5 on the left hand side. The infinite rock mass has been omitted; only the channel is shown. On the right hand side, the concentration distribution in the rock mass at a given time is shown. The lines of equal concentration (isoclines) close to the channel are ellipses, but at locations far from the channel they become circles. Although the diffusion is initially perpendicular to the channel/fracture plane, it then becomes radial with time.

For the sake of simplicity, the situation is transformed to the case of diffusion from an infinite rock mass into a cylindrical channel. The radius of the cylinder is chosen so that the perimeter of the cylinder is equal to that of the channel.

The solution may be expressed as a definite integral between zero and infinity, where the integrand is a function of Bessel functions. This solution is very complicated; a solution in series, which may be applied for short times, is therefore used. The concentration profiles in the rock mass for diffusion into a cylindrical channel for short times may be then calculated /Crank 1975/ as:

$$\frac{C}{C_0} = \sqrt{\frac{a}{r}}\mathrm{erfc}\left[\frac{r-a}{2\sqrt{Dt}}\right] + \frac{(r-a)\sqrt{Dt}}{4a^{\frac{1}{2}}r^{\frac{3}{2}}}\mathrm{ierfc}\left[\frac{r-a}{2\sqrt{Dt}}\right] + \qquad \text{(Equation 8)}$$

$$+\frac{Dt\cdot\left(9a^2-2ar-7r^2\right)\sqrt{D\cdot t}}{32a^{\frac{3}{2}}r^{\frac{5}{2}}}\mathrm{i}^2\mathrm{erfc}\left[\frac{r-a}{2\sqrt{D\cdot t}}\right]+\ldots$$

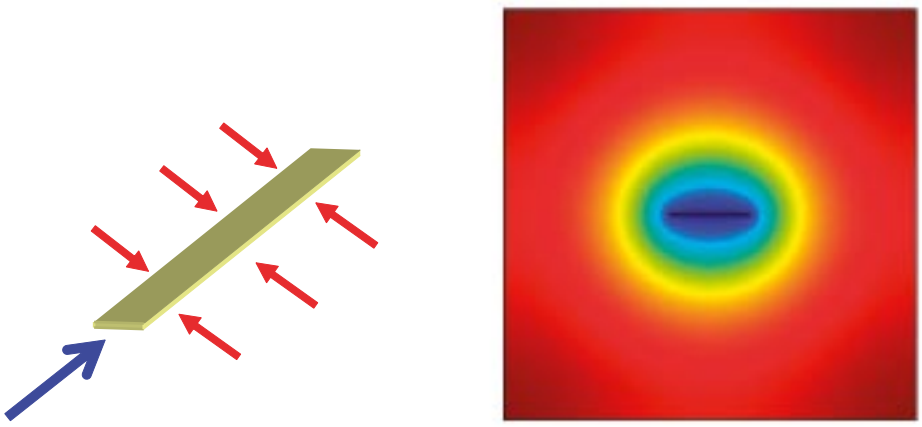

Figure 5. *A schematic view of diffusion into a channel/fracture surrounded by an infinite rock mass (left) and concentration profilesin at the rock mass (right)*

This equation may be expressed as a function of dimensionless terms as:

$$\frac{C}{C_0} = \frac{1}{\sqrt{\frac{r}{a}}}\operatorname{erfc}\left[\frac{\frac{r}{a}-1}{2\sqrt{\frac{Dt}{a^2}}}\right] + \frac{\left(\frac{r}{a}-1\right)\sqrt{\frac{Dt}{a^2}}}{4\left(\frac{r}{a}\right)^{\frac{3}{2}}}\operatorname{ierfc}\left[\frac{\frac{r}{a}-1}{2\sqrt{\frac{Dt}{a^2}}}\right] + \frac{\left(9-2\left(\frac{r}{a}\right)-7\left(\frac{r}{a}\right)^2\right)\left(\frac{Dt}{a^2}\right)}{32\left(\frac{r}{a}\right)^{\frac{5}{2}}}\operatorname{i^2erfc}\left[\frac{\frac{r}{a}-1}{2\sqrt{\frac{Dt}{a^2}}}\right] + \ldots \quad \text{(Equation 9)}$$

This equation is applicable for short times. For longer times, new terms must be added to the series.

3.2 Results of salinity evolution in the matrix with negligible concentration in the fracture

The results are here first presented for the three cases and they are then compared with each other. In general, the results are presented as a function of a relative concentration calculated as the ratio of the actual concentration to the initial concentration.

/Waber and Smellie 2005/ in their out-diffusion experiments found values between $4.0 \cdot 10^{-12}$ and $6.0 \cdot 10^{-12}$ m^2/s for the pore diffusivity. These values are somewhat lower than the values obtained by /Löfgren 2004/, who reported formation factors in the interval from $1.0 \cdot 10^{-5}$ to $5.0 \cdot 10^{-4}$ corresponding to values of pore diffusivity in the interval from $4.0 \cdot 10^{-12}$ to $2.0 \cdot 10^{-10}$ m^2/s. A value of $2.0 \cdot 10^{-11}$ m^2/s for the pore diffusivity has therefore been used in these calculations.

3.2.1 Diffusion from the matrix perpendicular to the fracture plane

The relative concentration in the rock matrix is shown in Figure 6 as a function of the depth from the matrix-fracture interface for several times. The results show that the time for salinity depletion is very long, about a thousand years for a depth of about one metre.

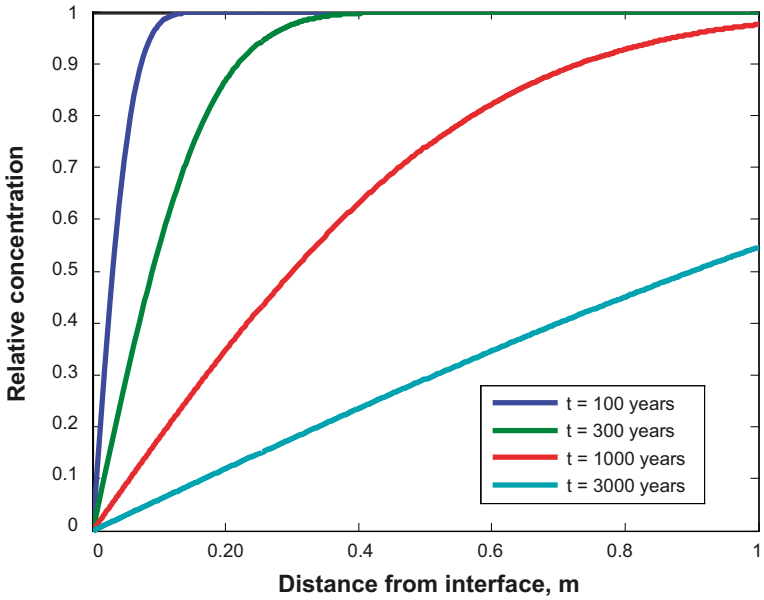

Figure 6. *Concentration in the matrix with a negligible concentration in the fracture.*

3.2.2 Diffusion in a rock block surrounded by conductive fractures

Figure 7 shows the concentration profiles in the sphere for different times for a pore diffusivity of $2.0 \cdot 10^{-11}$ m^2/s. The profiles are shown for different dimensionless times $D_p \cdot t/a^2$, where a is the sphere radius. Figure 8 shows the time to reduce the salinity by 90% as a function of the sphere radius. For a sphere with a diameter of 1 metre, this time is about 300 years. In general, the depletion from the rock block is somewhat shorter than from a fracture matrix system, because the ratio of the contact surface area to the sphere volume is higher.

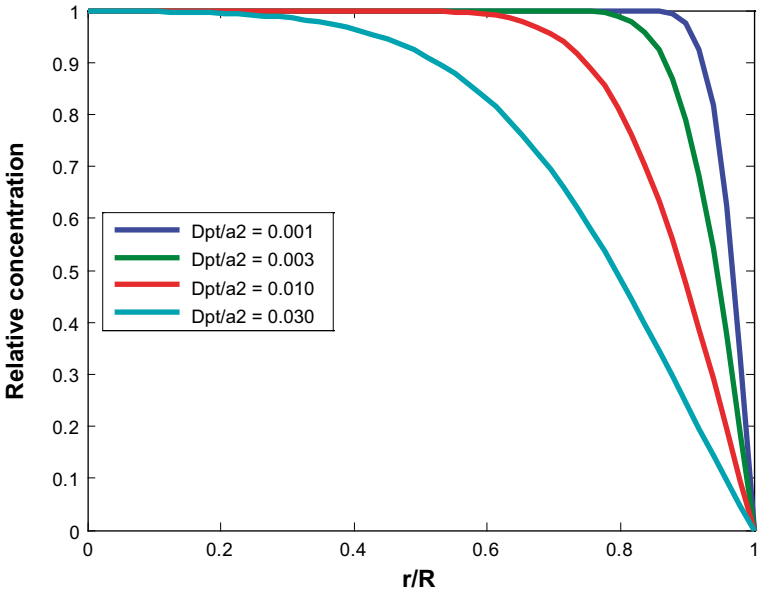

Figure 7. *Concentration profiles in the sphere for different dimensionless times.*

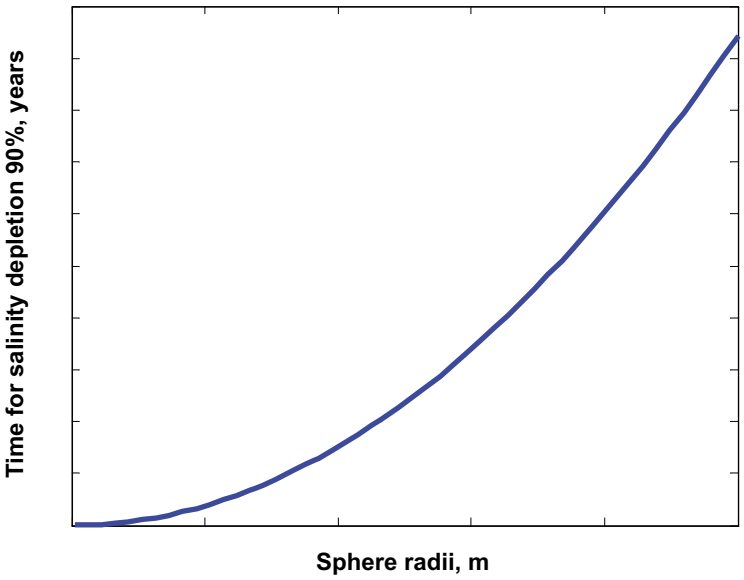

Figure 8. *Time for salinity depletion for different radius.*

3.2.3 Diffusion into a narrow fracture/channel surrounded by an infinite rock mass

Figure 9 shows the relative concentration as a function of the distance from the cylinder centre for different times. The results are plotted only for short times, since the evaluation of the analytical solution is uncertain for longer times, only two terms being taken from the series in the analytical solution.

3.2.4 Comparison between the different geometries

For short times, all the situations are similar, since only a short distance into the matrix is involved. In this case, the diffusion may be considered to take place perpendicular to the fracture-matrix interface. However, for longer times the geometry of the system becomes important.

In the case of a rock block surrounded of conductive fractures, there is a large interface between the conductive fractures and the rock mass. In the case of a narrow channel embedded in a rock mass, the situation is completely the opposite; there is only a small interface between the water flowing in the channel and the rock mass. In the case of a fracture rock mass with diffusion perpendicular to the fracture plane, the situation is intermediate.

The ratio of the interface surface area to the rock volume is used in the comparison. This ratio is largest in the case of a rock block surrounded by conductive fractures. This means that the salinity will be reduced more rapidly in this case. The opposite is true in the case of a narrow channel embedded in a large rock mass, and longer depletion times are found.

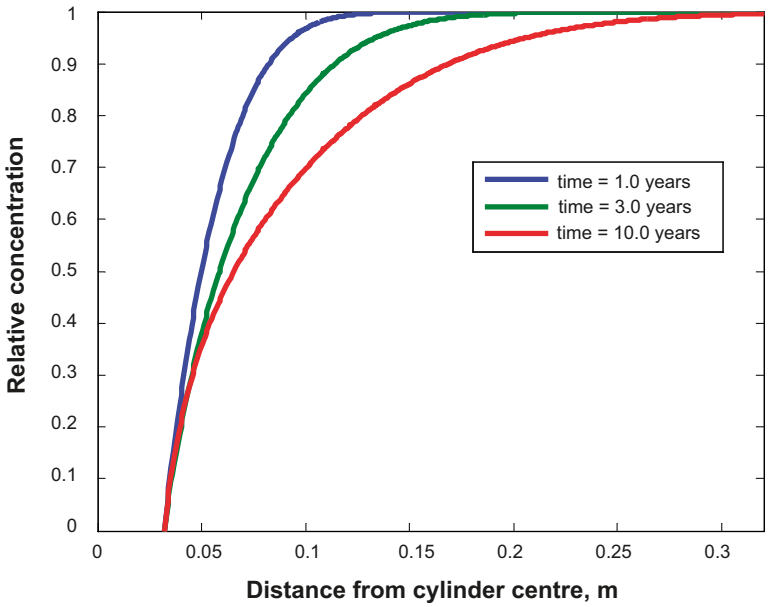

Figure 9. *Concentration profiles in the rock mass around a narrow fracture represented by a cylinder embedded in the rock mass. This solution is valid for short times.*

4 Evolution of the salinity with time

The salinity in the rock matrix is determined by the evolution of the salinity in the nearest conductive fracture. The evolution with time of the salinity in the fracture is determined by the water flow rate in the fracture/channel and the interaction between the water and the rock mass containing saline water. For the sake of simplicity, the calculations consider the case of diffusion into a fracture where diffusion takes place perpendicularly to the fracture plane. Some conclusions relevant for the other cases may be drawn from the results reported in Chapter 3 (Scoping calculations)

The calculations are first made for a simple fracture or channel. Later, the calculations are extended to the case of a large number of channels.

4.1 Salinity evolution in the water flowing in a simple fracture/channel

4.1.1 Governing equation

When fresh water intrudes into a fractured medium containing saline water, salt will diffuse from the rock matrix into the fracture. Initially, saline water is contained in the fracture, but with time the salinity will decrease.

In the simplest case; water is flowing in a channel and diffusion takes place into the rock matrix in the direction perpendicular to the fracture plane. When fresh water is flowing in a fractured medium with an initial concentration C_o in the fracture and in the pore water, the concentration in the channel is given by

$$\frac{C(x,t)}{Co} = Erf\left(\frac{\sqrt{D_e\varepsilon_p}}{2\sqrt{(t-tw)}}\cdot\frac{FWS}{Q}\right) = Erf\left(\frac{\sqrt{D_e\varepsilon_p}}{\sqrt{(t-tw)}}\cdot\frac{x\cdot W}{Q}\right) \qquad \text{(Equation 10)}$$

In the matrix, the concentration is given by

$$\frac{C(x,z,t)}{Co} = Erf\left(\frac{\sqrt{D_e\varepsilon_p}}{\sqrt{(t-tw)}}\cdot\frac{x\cdot W}{Q} + z\cdot\frac{1}{2\sqrt{t-tw}}\sqrt{\frac{1}{D_p}}\right) \qquad \text{(Equation 11)}$$

4.1.2 Calculated cases

In order to show the evolution with time of the fracture and matrix concentrations some simple calculations were performed, assuming an effective diffusivity in the matrix of 1.0E–13 m^2/s and a matrix porosity of 0.005 for a 100 metre long channel.

The concentration at the channel outlet was calculated for three different flow rates. The flow rate is expressed as flow rate per channel width, $m^3/(year\cdot m)$. The flow rates used were: 0.0003, 0.001, and 0.003 $m^3/year/m$.

The concentration in the matrix was determined for the intermediate water flow rate (0.001 $m^3/year/m$) and for the rock mass located at the channel outlet (after a travel distance of 100 metres) at different depths from the fracture surface. The depths used in the calculations were 0.1, 0.3, 1.0, and 3.0 m.

In the third set, the concentration profile in the matrix at the channel outlet was calculated for the intermediate water flow rate (0.001 $m^3/year/m$) for different times. The times used were 100, 1,000, and 10,000 years.

4.1.3 Results

The results for the first set of calculations are shown in Figure 10, for different flow rates. For the largest flow rate (0.003 m^3/year/m), the relative concentration falls to a value of 0.2–0.3 after a few hundreds of years and continues to decrease slowly to a value of 0.1 after 10,000 years. For the smallest flow rate (0.0003 m^3/year/m), the outlet relative concentration decays very slowly, reaching a value of 0.4 only after 10,000 years.

The relative concentration in the matrix, at the outlet of the channel, is shown in Figure 11 as a function of time for different depths in the matrix. The concentration in the matrix decreases slowly at the greatest depth. Even after 10,000 years, the relative concentration in the matrix is higher than 50%. On the other hand, the concentration at a depth of 0.1 m follows the value of the salinity in the fractures with some delay.

The concentration profiles in the matrix, at the channel outlet, at different times are shown in Figure 12. For the shortest time (300 years), the concentration has decreased only at zones close to the fracture. For a time of 30,000 years, the relative concentration is down to almost 0.15 at depth of one metre.

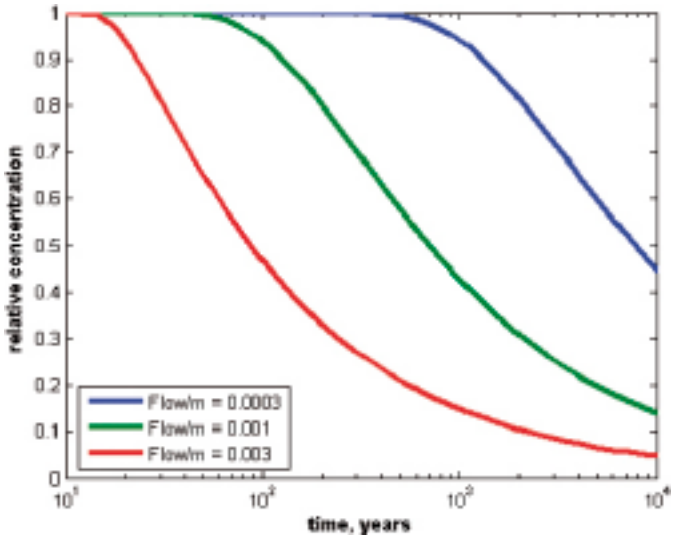

Figure 10. *Concentration at the channel outlet (L = 100 m), for three flow rates (m^3/year/m).*

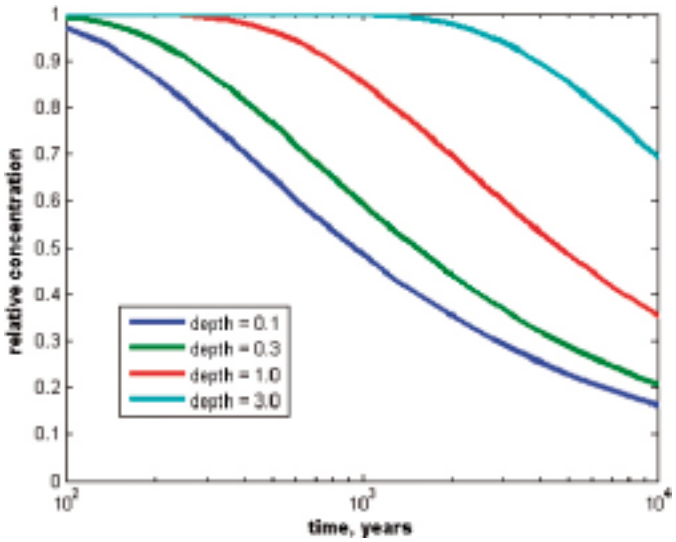

Figure 11. *Relative concentration in the matrix, at the outlet of the channel (L=100m), as a function of time, at different depths.*

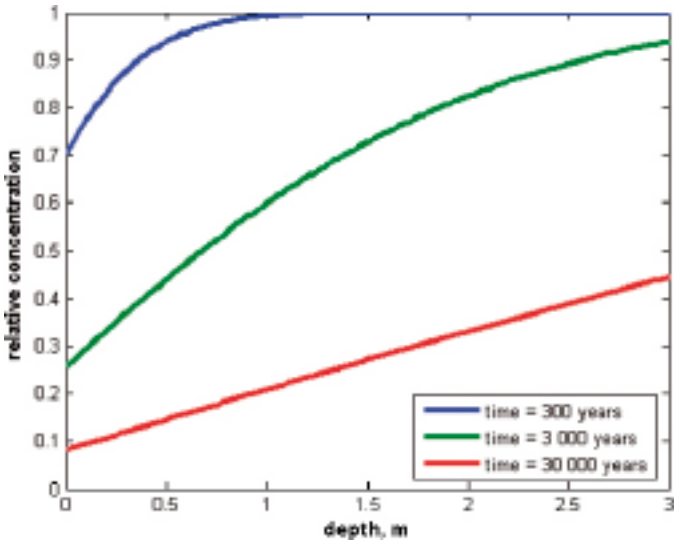

Figure 12. *Relative concentration profiles in the matrix, at the channel outlet, at different times.*

4.2 Salinity evolution in the water flowing in a path formed by different fractures/channels

4.2.1 Governing equation

In crystalline rock, the water flow takes place through fractures in the rock. These fractures or channels form a network in the rock volume. When water flow through this network, it may travel through different paths. The water that reaches a certain location (in our case, the fractures intersecting the borehole where the salinity in the matrix has been measured) has therefore usually travelled through different fractures or channels.

The concentration in these fractures/channels is determined by the flow rate in each of the channels through which the water has travelled, the channel geometry and the properties of the rock matrix (diffusion, porosity). The channel geometry determines the surface area through which the water in the fracture contacts the rock matrix, the so-called Flow Wetted Surface FWS).

The outlet concentration for a channel is determined by the ratio FWS/Q, the water residence time in the channel t_w, and the rock properties. It may be demonstrated that, for transport of a water parcel in a channel network, it is sufficient to obtain the sums of $\sum(FWS/Q)_i$ and $\sum tw_i$ in each channel through which the water parcel has travelled /Moreno et al. 2006/. Equations 10 and 11 may be then rewritten as

$$\frac{C_{path}(x,t)}{Co} = Erf\left(\frac{\sqrt{D_e\varepsilon_p}}{2\sqrt{(t-\sum_i tw_i)}}\cdot\sum_i\left(\frac{FWS}{Q}\right)_i\right) = Erf\left(\frac{\sqrt{D_e\varepsilon_p}}{\sqrt{(t-\sum_i tw_i)}}\cdot\sum_i\left(\frac{x\cdot W}{Q}\right)_i\right) \quad \text{(Equation 12)}$$

and

$$\frac{C(x,z,t)}{Co} = Erf\left(\frac{\sqrt{D_e\varepsilon_p}}{\sqrt{(t-\sum_i tw_i)}}\cdot\sum_i\left(\frac{x\cdot W}{Q}\right)_i + z\cdot\frac{1}{2\sqrt{t-\sum_i tw_i}}\sqrt{\frac{1}{D_p}}\right) \quad \text{(Equation 13)}$$

4.2.2 Calculated cases

The concentration at the channel outlet was calculated for three different values of the ratio FWS/Q, $1.0 \cdot 10^3$, $1.0 \cdot 10^4$, and $1.0 \cdot 10^5$ y/m. The lowest value corresponds to a small FWS (narrow channel) or a channel with large water flow. The largest value corresponds to the opposite situation; a low water flow rate or a large FWS (wide fracture).

In the second set of calculations, a value of $1.0 \cdot 10^4$ y/m was chosen for the ratio FWS/Q and the concentration in the matrix was determined for the rock mass located at the channel outlet at different distances from the fracture surface, 0.1, 0.3, 1.0, and 3.0 m.

In the third set, the concentration profile in the matrix at the channel outlet was calculated at different times; 100, 1,000, and 10,000 years.

4.2.3 Results

The results for the first set of calculations are shown in Figure 13, for different values of the ratio FWS/Q. For the smallest ratio, the relative concentration falls rapidly to a value less than 0.1 and continues to decrease and becomes to be negligible after about 200 years. For the largest ratio, the outlet concentration decays slowly, reaching a relative concentration of 0.2 after 1,000 years.

The concentration in the matrix, at the channel outlet, is shown in Figure 14 for different depths in the matrix. The concentration decreases very slowly for the point located at a depth of 3 m. Even after 1,000 years the relative concentration in the matrix is higher than 80%. At a depth of 0.1 m, the relative concentration decreases rapidly, reaching a value of 0.3 at about 100 years. At longer times the variation in concentration with time follows the value of the salinity in the fracture with a certain delay.

The concentration profiles in the matrix at different times are shown in Figure 15. For the shortest time, the concentration is almost 1.0 at any location in the matrix. Only for locations very close to the fracture, has the salinity been reduced. For a time of 10,000 years the relative concentration is still almost 1.0 at a depth of 5 m, but it is lower at positions closer to the fracture surface.

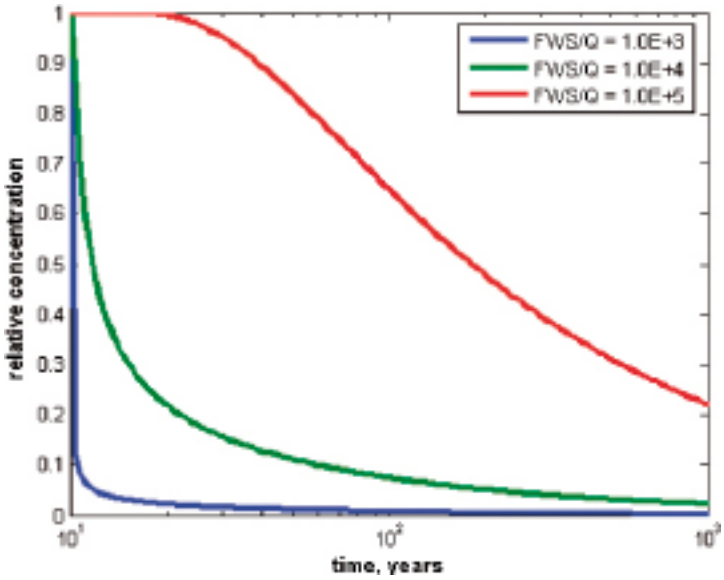

Figure 13. *Concentration at the channel outlet (L = 100 m), for three flow rates (m^3/year/m).*

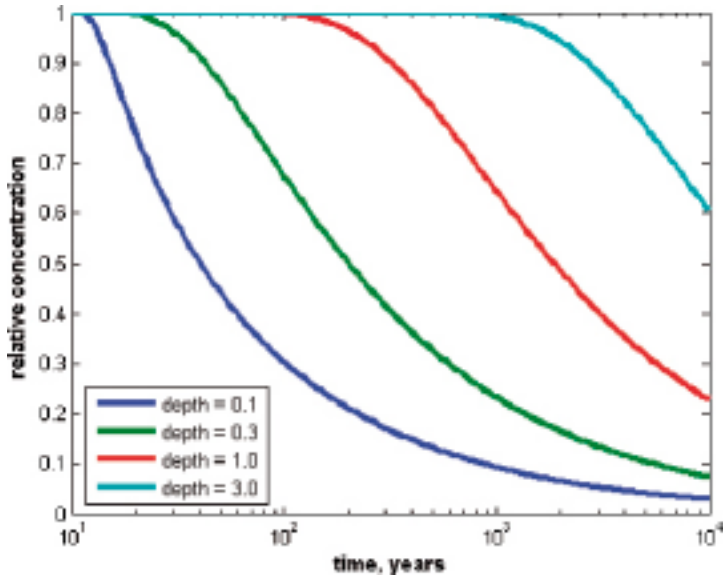

Figure 14. *Concentration in the matrix, at the channel outlet (L = 100 m), at different depths.*

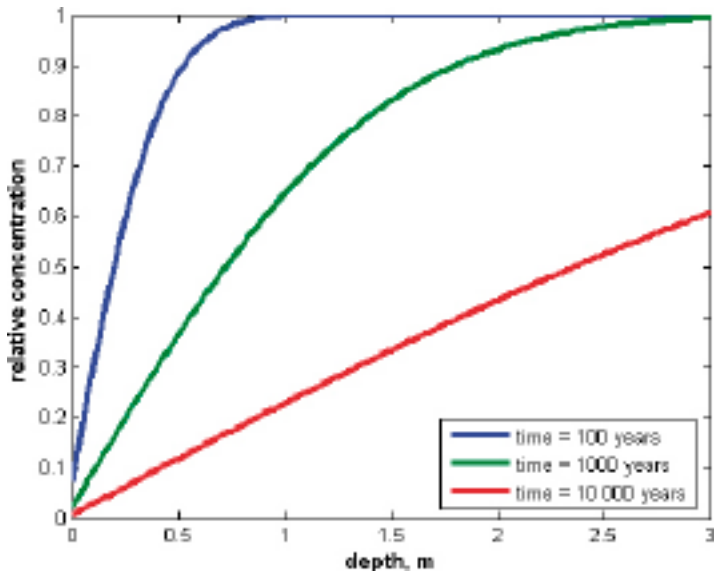

Figure 15. *Concentration profiles in the matrix at different times.*

5 Discussion regarding salinity in the rock matrix

As indicated in Chapter 2, the salinity was determined in a drill core by out-diffusion experiments /Waber and Smellie 2005/. In Chapter 3, the evolution with time of the concentration in the rock matrix was studied for the case of negligible concentration in the fractures. In Chapter 4, the evolution with time of the concentration in the fracture was determined and related to the concentration in the matrix. The important question here is whether the concentration in the matrix, at a given time can related to the water flow rate in the fractures and to the time when the last water intrusion took place. Another important aspect is whether it is possible to predict the variation of the salinity in the matrix (and fracture) after a new fresh water intrusion has taken place.

The evolution of the concentration in the fracture with time can be determined if the path followed by the water parcels from the intrusion point to the fracture is known, but this is not, in practice, possible. Some information can however be obtained by simulation.

The results show that the ratio $\sum$(FWS/Q) has a strong influence on the concentration in the fractures at any given time. For a path with a small value of $\sum$(FWS/Q), the relative concentration of salt in the water in the fracture changes very rapidly. A small value of $\sum$(FWS/Q) is characteristic of a path with a large water flow rate and/or a small FWS value. This corresponds, for example, to a narrow channel with large water flow rate. On the other hand, a path with a large value of the $\sum$(FWS/Q) ratio shows a very slow evolution of the concentration. In this latter case, hundreds of years may pass before there are significant changes in the salinity in the fracture. Therefore, it can be expected that in a fracture with a high transmissivity, the salinity will decrease faster than in a fracture with less transmissivities.

However, water flowing from the intrusion point to the location where the sample is taken travels through different paths. The channels forming these paths may have very different water flow rates and different FWS values. For fresh water intrusion, the concentration in a fracture will decrease rapidly if most of the water has travelled through fractures with a large water flow rate; i.e. a low value of $\sum$(FWS/Q).

5.1 Relationship between the fracture transmissivity and the path followed by the water parcels

Simulations were done in order to study the relation between the transmissivity of the fractures intersecting the borehole and the properties of the channels travelled by the water parcels from the intrusion point, i.e. $\sum$(FWS/Q). A channel network formed by 30 channels in each direction was modelled. The channel length was 5 metres. In each simulation, the evolution of the salinity with time in 30 hypothetical fractures/channels intersecting a hypothetical borehole was determined. The transmissivity of the simulated fractures intersecting the hypothetical borehole vary over a wide interval, as is also found in the field.

In the model, it is assumed that the water in the fractures and in the matrix initially has a concentration, C_o. At a given instant, the concentration of the water intruding the system fracture/rock is changed to zero. The Power Law was used to define the transmissivity of the channels. It was also assumed that the transmissivity of these fractures/channels is proportional to their size (L^2).

The calculations were carried out using the CHAN3D /Gylling et al. 1999/, which was modified for including the Power Law when the size and conductivity of the channels were defined.

The system modelled is very simple, a cubic volume with a side of 150 m. A hydraulic gradient is applied from a side of the cube to the opposite side and no flow condition is applied to the other faces. A borehole is drilled through the channel network and the transmissivity and the water flow rate of these channels are recorded. The water intrusion is simulated through a large number of water parcels (500) released on the upstream side. The water parcels that travel through the fractures intersecting the borehole are studied in detail.

5.1.1 Results of the simulations

The results are shown for a particular simulation. Since, the absolute values are not important, the results are discussed in relative values. Figure 16 shows the number of water parcels (particles in particle tracking procedure) that flow through different fractures, grouped in ranges of fracture transmissivities. Most of the water parcels flow through fractures with high transmissivity. A few water parcels or no water at all flow through the fractures with small transmissivity. The largest and smallest transmissivities differ by several orders of magnitude in both cases.

Figure 17 shows the value of $\sum$(FWS/Q) for the 500 water parcels arriving at the fractures intersecting the borehole distributed as a function of the fracture transmissivity. For each water parcel arriving at a fracture, the value of $\sum$(FWS/Q) is determined and its value is plotted against the fracture transmissivity. The results indicate that the water parcels arriving at the fractures with a large transmissivity have values of $\sum$(FWS/Q) over a wide interval. This means that even in fractures with a large transmissivity, an important fraction of the intruding water has travelled thorough channels with small flow rate. Moreover, there was a slight tendency for fractures with a large transmissivity to show a slight dominance of water parcels with small value of $\sum$(FWS/Q).

The expected relation that the water parcels flowing through fractures with a large transmissivity have travelled through channels/fractures with a large water flow rate was relatively weak.

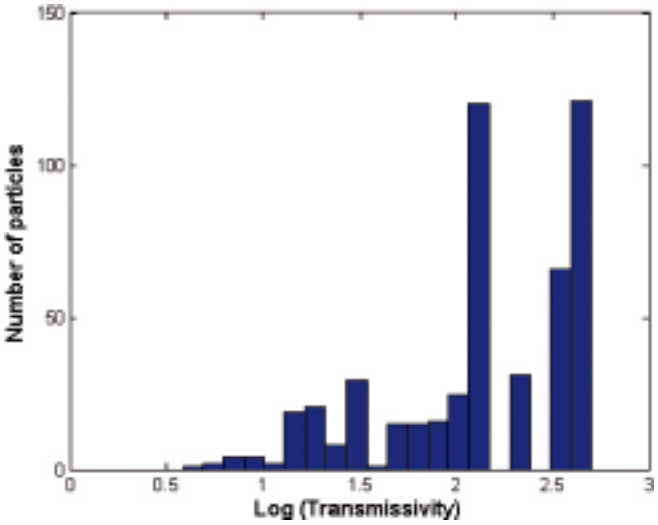

Figure 16. *Numbers of particles (water parcels) arriving at the fractures intersecting the borehole for different fracture transmissivities.*

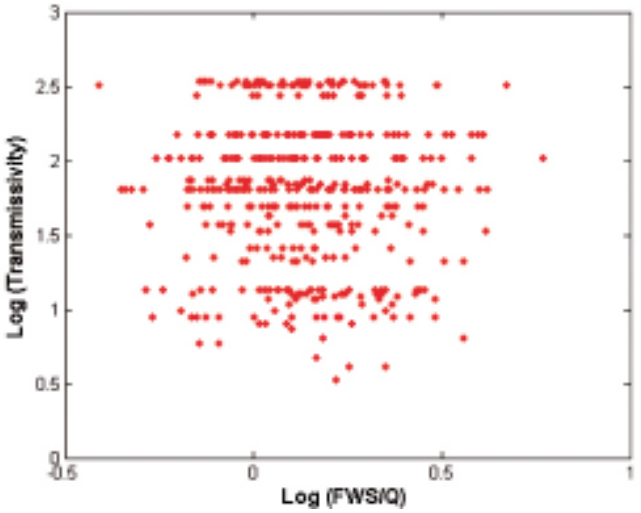

Figure 17. *Value of the term* $\sum$(FWS/Q) *in each of the fractures sorted by fracture transmissivities for the case where the Power Law was used.*

6 Conclusions

The interaction between ions dissolved in the pore water in the rock matrix and ions dissolved in the flowing water in the fractures was studied. To visualise the effect of fresh water intrusion into a zone containing saline water, several calculations were performed with increasing level of difficulty.

In the first set of calculations, the evolution of the concentration in the matrix was studied for the case where the concentration in the adjacent fractures was assumed to be negligible. Three different geometries were modelled: a) a fracture in a rock mass with diffusion perpendicular to the fracture plane, b) a narrow channel embedded in a large rock mass, and c) a rock block surrounded by conductive fractures. The results show that the time for salinity depletion is of the order of hundreds to thousands of years at a distance of one metre in the matrix.

In a second set of calculations, the evolution of the concentration in the water in the fracture was taken into account. The time to deplete the salinity in the fracture depends on $\Sigma(FWS/Q)$ determined along the path followed by the water from the intrusion point. For small values of this term (e.g., large water flow rate) the concentration in the fracture decreases very rapidly. However, for large values of the term $\Sigma(FWS/Q)$, the salinity depletion in the fracture may take thousands of years.

Finally, simulations were carried out to determine the paths followed by the water from the point of intrusion to the zone under study. The results show that fractures with a large transmissivity collect water that has travelled along paths with $\sum(FWS/Q)$ varying over a wide interval. The evolution with time of the concentration in the fracture is weakly related to the transmissivity of the fracture.

7 References

Bird R W, Stewart W E, Lightfoot E N, 2002. "Transport Phenomena," 2nd edition, John Wiley & Sons, Inc, New York.

Crank J, 1975. "The mathematics of diffusion," 2nd Ed, Clarendon Press, Oxford.

Gylling B, Moreno L, Neretnieks I, 1999. The Channel Network Model – A tool for transport simulation in fractured media, Groundwater 37, 367–375.

Löfgren M, 2004. Diffusive properties of granitic rock as measured by in-situ electrical methods. Doctoral thesis at the Royal Institute of Technology, Stockholm, Sweden. ISBN 91-7283-935-X.

Moreno L, Crawford J, Neretnieks I, 2006. Modelling radionuclide transport for time varying flow in a channel network, Journal of Contaminant Hydrology, In press March 2006.

Waber H N, Smellie J A T, 2005. SKB Site Investigations Forsmark, Borehole KFM06: Characterisation of pore water, Part I: Diffusion experiments. SKB P-05-196, Svensk Kärnbränslehantering AB.

16 Appendix 8: Groundwater data for Laxemar 2.1

This data set is stored in the SKB database SIMON.

The loggfile used in SICADA to create the data set is stored in the database SIMON.

17 Appendix 9: Groundwater data from Nordic sites

This data set is stored in the SKB database SIMON.